Etude des mécanismes d'actions de SuperMApo dans un modèle de sclérose en plaques

Thierry Gauthier

« Université de Bourgogne Franche-Comté

UFR des Sciences Médicales et Pharmaceutiques »

Ecole doctorale Environnements-Santé

Etude des mécanismes d'actions de SuperMApo dans un modèle de sclérose en plaques

Thèse

Présentée et soutenue publiquement le 17 Octobre 2017 par

Thierry Gauthier

En vue du grade de **Docteur de l'Université de Bourgogne Franche-Comté**

Spécialité : Sciences de la vie et de la santé

Travaux réalisés au sein de l'UMR1098 Interactions Hôte-Greffon-Tumeur, ingénierie cellulaire et génique (EFS BFC/INSERM) à Besançon

Directeur de thèse : Dr. Sylvain Perruche

Jury :

Pr. Stéphanie Hugues Université de Genève	Rapporteur
Pr. Régis Josien Université de Nantes	Rapporteur
Pr. Christophe Baron (Président du Jury) Université de Tours	Examinateur
Dr. Eric Hervouet Université de Bourgogne Franche-Comté	Examinateur
Dr. Sylvain Perruche Université de Bourgogne Franche-Comté	Examinateur

Remerciements

Je souhaite en premier lieu remercier les Pr Stéphanie Hugues et Régis Josien pour avoir accepté d'évaluer mon manuscrit de thèse ainsi que de faire partie de mon jury de thèse. Je remercie également le Pr Christophe Baron et le Dr Eric Hervouet pour leurs conseils tout au long de ce projet au sein du comité de suivi de thèse et leur participation à mon jury de thèse.

Je tiens tout particulièrement à remercier le Dr Sylvain Perruche pour m'avoir donné la chance de trouver une thèse et m'avoir fait confiance durant ces trois années. Malgré les nombreuses difficultés tu m'as toujours soutenu et relancer lorsque rien ne marchait. Merci pour ton expertise, tes encouragements, ton amitié et m'avoir permis de trouver ma voie (dans la recherche bien sûr pas dans l'enseignement). Et surtout merci pour cette immense opportunité de post-doc que je te dois en grande partie (pour ne pas dire plus). J'espère que nous continuerons à collaborer durant de nombreuses années.

Je remercie aussi le Pr Philippe Saas pour m'avoir accueilli au sein de son équipe de recherche et pour vos conseils toujours précieux.

Je remercie également l'EFS, le LIPSTIC et l'université de Bourgogne Franche-Comté pour leur soutien financier durant ces trois années de thèse.

Je voulais également remercier l'ensemble de membre de l'ex EA3922 (Michaël, Régis, Gilles, Annick, Pascale, Hélène, Jean) pour avoir permis à de nombreuses génération d'étudiants de devenir ce qu'ils sont, pour m'avoir permis d'intégrer votre laboratoire et de découvrir ce qu'était la recherche. Merci à toi Eric pour m'avoir encadré avec Michaël durant ces deux années merveilleuses. Merci pour votre amitié, vos nombreux conseils, votre dynamisme et vos encouragements qui me permettront à n'en pas douter de devenir un grand chercheur (et accessoirement d'être un super lanceur de falcon 15). Merci à Laura et Aurore mes deux thésardes préférées qui ont toujours été d'une gentillesse immense et d'une grande aide au labo (P.S : La team Hervouet…).

A toutes les personnes à l'UMR1098 qui ont été nécessaires à la réalisation de ce travail :

Anna pour ta bonne humeur, tes inventions géniales (à mon goût en tout cas), ton aide matinale et tardive sur mes nombreuses manips et tout simplement d'être Banana. Un jour tu deviendras riche et célèbre grâce à une de tes inventions…

Cécile, Anaïs et Hanane : la dream team du bureau du haut (qui riez toujours à mes blagues… ou pas du tout). Cécile merci pour toutes ces manips où je t'ai levé au petit matin un peu trop tôt, pour les fois innombrables ou tu auras vu une présentation brillante sur le SuperMApo. Et non ne t'inquiète pas tu n'as pas les cheveux de M….. Le P.. Yo Anaïs, ça va ? Un jour tu maniperas une semaine entière sans venir la nuit, un jour. Bon par contre les cicatrices chéloïdes non mais sérieusement ??? Hanane merci pour ta bonne humeur, ta gentillesse et surtout merci d'avoir corrigé ma thèse. Finalement tu es un peu mon co-directeur de thèse maintenant. Ah oui et merci pour tous les midis où tu as mangé avec nous.

Mélanie, toi qui est un peu la Super(women)MApo du laboratoire, merci pour tes nombreux conseils, ta gentillesse, ta bonne humeur et surtout ton supercookie géant. Bonne chance pour ton futur poste de directrice de production de medinn' pharma.

Francis, merci pour tes nombreux conseils qui m'ont été d'un grand secours au laboratoire (tri de pDC ☺). J'espère un jour devenir un aussi grand manipulateur de souris que toi (PRO sans les endormir entre autre).

Martine, ma compagne de recherche, merci pour ton aide précieuse au cours de ces 5 années et ses nombreux sacrifices d'intestin de souris à 7h du matin. Ne déprime pas trop l'Angleterre ça à l'air cool et puis on peut faire des Immunity là bas…

Mymi et Alphonsine, merci pour votre bonne humeur, votre gentillesse, toute votre aide qui ont rendu les difficultés administratives bien plus sympathiques.

Mon petit bichon d'amour (alias Adam Ceroi), que la vie est triste ici sans tes blagues de mauvais goût et ta folie scientifique. En tout cas j'espère que je serai le parrain du petit LymphoJedi qui naîtra un jour avec Laurie. Ah oui et ne la laisse pas partir celle-là tu ne retrouveras une femme jamais d'aussi formidable (déjà que c'est dur à la base mais pour toi…).

Idir, pour sa grande amitié durant ces trois années.

Séverine, Inès, Kiki (la petite jeune), Sami, Anaïs, Dom, François, Emmanuel, Emilie, Pacou, Charline, Sophie et Romain pour avoir partagé votre quotidien et de bons moments avec moi à l'IBCT.

A toutes les personnes travaillant à l'EFS pour leur aide, leur gentillesse et leur amitié : Emilie et Sindy mes dernières camarades survivantes de la licence, Walid, Clémence, Jeanne, Sarah, Clémentine, Anne, Sabeha, Jean-René, Jean-Marie, Jean-Paul, Elodie, Laurie, Caroline, Yann, Olivier.

Je tiens également à remercier chaleureusement ma famille et plus particulièrement mes parents. Merci pour tout (votre éducation, votre amour, votre soutien et votre rôle dans cette thèse). Je ne peux malheureusement pas m'étendre mais sachez que je vous dois tout et que je vous serai à jamais reconnaissant.

Sabrioche, qui est là depuis plus de 10 ans déjà (mais qui m'a quand même abandonné malgré tout…).

Enfin, à mon petit cœur, mon Amour, Ranya. Tu as toujours été là pour moi depuis 5 ans pour me soutenir, m'aider, me rendre heureux même quand j'étais insupportable. Merci de m'avoir donné les 3 enfants les plus merveilleux du monde. J'espère qu'un jour je deviendrai un mari aussi exceptionnel que tu le mérites. Sache que la plus grande réussite de ma vie c'est vous et que cette thèse est d'abord la tienne car elle n'aurait jamais été sans toi.

Liste des abréviations

2-DG : 2-DeoxyGlucose

ADN: Acide Désoxyribonucléique

ARN: Acide Ribonucléique

APC: Antigen Presenting Cell

ATP: Adénosine-Triphosphate

BDCA2: Blood Dendritic Cell Antigen 2

BHE: Barrière Hémato-encéphalique

CD: Cluster of differentiation

CMH-II: Complexe Majeur d'Histocompatibilité de type II

CMKLR1: Chemokine-Like Receptor 1

DAMP: Damage Associated Molecular Pattern

DC (ou cDC): Classical Dendritic Cell

DNMT: DNA MéthylTransférase

EAE: Encéphalomyélite Auto-immune Expérimentale

Foxp3: Forkhead Box P3

GM-CSF: Granulocyte-Macrophage Colony-Stimulating Factor

HLA: Human Leukocyte Antigen

ICAM1: Intercellular Adhesion Molecule 1

IFN: Interferon

IGF-1: Insulin Growth Factor-1

IKK: IκB Kinase

IκB: Inhibitor of kappa B

IL: Interleukine

IRF3: Interferon Regulating Factor 3

LB: Lymphocyte B

LPS: Lipopolysaccharide

LT: Lymphocyte T

LXA: Lipoxine A

LXR: Liver X Receptor

M-CSF: Macrophage Colony-Stimulating Factor

MAPK: Mitogen-Activated Protein Kinases

MBP: Myelin Binding Protein

ME : Moelle épinière

MEC: Matrice Extracellulaire

MICI: Maladies Inflammatoires Chroniques de l'Intestin

MMP: Métalloprotéases

MO: Moelle osseuse

MOG: Myelin Oligodendrocyte Glycoprotein

NET: Neutrophil extracellular trap

NFκB: Nuclear Factor kappa B

NLR: NOD-Like-Receptors

NO: Nitric Oxide

PAMP: Pathogen Activation Molecular Pattern

pDC: Plasmacytoid Dendritic Cells

PGE2: Prostaglandine E2

PLP: Proteolipid Protein

PMN: Polymorphonuclear Neutrophils

PPAR-γ: Peroxisome Proliferator-Activated Receptor-γ

PRR: Pattern Recognition receptor

PtdSer: Phosphatidylsérine

RLR: RIG-I-Like Receptors

ROS: Reactive Oxygen Species

S1P: Sphingosine-1-Phosphate

SEP: Sclérose en plaques

SIGN-R1: SIGN-Related protein 1

SNC: Système Nerveux Central

STAT: Signal Transducers and Activators of Transcription

SuperMApo: Supernatant from Macrophages and Apoptotic cell culture

TCR: T Cell Receptor

TET: Ten-eleven Translocation

TGF-β: Transforming Growth Factor beta

Th: Lymphocyte T helper

TLR: Toll Like Receptor

TNF-α: Tumor Necrosis factor alpha

TNFR1: Tumor Necrosis Factor Receptor 1

Treg: Lymphocytes T régulateurs

TSP-1: Thrombospondine 1

VCAM-1: Vascular Cell Adhesion protein 1

VEGF: Vascular Endothelial Growth Factor

WT: Wild-Type

Résumé

La sclérose en plaques (SEP) est une maladie auto-immmune notamment marquée par une défaillance de la mise en place des mécanismes de réparation tissulaire, ne permettant pas de rétablir l'homéostasie. L'utilisation de la résolution de l'inflammation, médiée par les macrophages phagocytant des cellules apoptotiques, a récemment été évoquée afin de proposer une nouvelle famille de médicaments basée sur cette résolution de l'inflammation. Dans ce cadre, nous proposons de résoudre l'inflammation dans un modèle murin de SEP, à l'aide du surnageant de co-culture de macrophages ayant phagocyté des cellules apoptotiques, induisant la production de facteurs pro-résolutifs (SuperMApo). Nous démontrons ici que l'injection de SuperMApo dans un modèle de SEP permet de contrôler la maladie *via* une reprogrammation des macrophages et des pDC, mais pas des cDC, dans la rate. Ces cellules démontrent en effet une capacité accrue à générer des T régulateurs (Treg) et moins de Th1, et leur présence est nécessaire pour l'effet du SuperMApo. Cette reprogrammation se fait à deux niveaux moléculaires. Premièrement, un contrôle épigénétique de l'expression des gènes induit notamment une modification de la méthylation globale de l'ADN et des promoteurs de miRNA impliqués dans la régulation des réponses immunes. Deuxièmement, une diminution de l'activation des acteurs de la voie de transcription pro-inflammatoire NFκB (*nuclear factor kappa B*) a lieu, résultant d'une baisse de l'activation de ces cellules. Ces travaux démontrent donc que cibler la résolution de l'inflammation est une stratégie intéressante afin de contrôler la SEP.

Abstract

Multiple sclerosis (MS) is an autoimmune disease notably defined by a default of mechanisms of tissue reparation which are insufficient to establish homeostasis. The active resolution of inflammation mediated by macrophage efferocytosis of apoptotic cells has emerged to propose a new branch of pharmacology named "resolution pharmacology". In this study, we propose to resolve inflammation in a murine model of MS, using the supernatant issued from the culture between apoptotic cells and macrophages, inducing efferocytosis and the production of pro-resolutive factors (SuperMApo). Here, we demonstrate that injection of SuperMApo in a model of MS allow the control of the disease correlated with a reduction of the inflammatory infiltrate in the central nervous system. The control of the disease is associated with a reprogramming of macrophages and pDC, but not cDC, in the spleen, demonstrated by a higher capacity to generate Treg and a lower ability to generate Th1, and their presence is necessary to the anti-inflammatory effect of SuperMApo. Reprogramming of macrophages and pDC occurs at two main levels. First, an epigenetic control of gene expression induces a modulation of global DNA methylation and a modulation of DNA methylation at the promoter of miRNA implicated in the regulation of immune responses. Secondly, a decreased activation of NFκB activation pathway is observed resulting to a decreased activation of these cells. Thus, this work demonstrates that targeting the resolution of inflammation is an interesting strategy to treat MS.

Introduction

La réponse inflammatoire

I) Concept général

I.1) Définition

L'inflammation est une réaction physiologique du corps humain face à une agression. Elle se manifeste par des signes cliniques tels qu'un érythème (rougeur), un œdème (gonflement), des chaleurs, des douleurs ainsi qu'une altération du fonctionnement de l'organe touché. Sa description initiale a été faite il y a 2000 ans par Celsus et a été complétée avec la notion d'impotence fonctionnelle par Wirchow en 1858. D'un point de vue immunologique (qui est la définition que nous utiliserons au cours de ce manuscrit), la réponse inflammatoire est un processus naturel de l'organisme déclenché en réponse à des stimuli nocifs, tels qu'une infection ou une blessure, entraînant une rupture de l'homéostasie tissulaire (Medzhitov 2008). L'organisme va alors mettre en place une réponse adaptée mettant en jeu différents composés solubles (réponse humorale) et cellulaires (réponse cellulaire). Les travaux de Metchnikoff et Ehrlich au début du XIX^{ème} siècle ont été les premiers à montrer la mise en place de réponses immunes face aux pathogènes pouvant entrainer une inflammation. Ils ont respectivement démontré le rôle des phagocytes, ainsi que des anticorps et du complément, dans les réponses de l'hôte au pathogène, au niveau du site inflammatoire, et des dommages tissulaires subséquents. Si l'inflammation est un processus bénéfique pour l'organisme, sa non régulation peut entraîner la survenue de différentes pathologies définies comme des maladies inflammatoires chroniques (sclérose en plaques, maladie de Crohn, polyarthrite rhumatoïde…) (Medzhitov 2008; Wallach, Kang et al. 2014). Certaines pathologies inflammatoires démontrent cependant une résolution de l'inflammation sans dommages tissulaires. La pneumonie à streptocoque, par exemple, induit une accumulation de cellules de l'immunité innée au sein des poumons et se résout totalement 3 à 4 jours après les premiers signes cliniques. La réponse inflammatoire apparait alors comme un processus en plusieurs étapes interconnectées et contrôlées (Lawrence, Willoughby et al. 2002).

I.2) La réponse inflammatoire, un processus en deux étapes

La réponse inflammatoire est un système complexe, régulé par de multiples boucles de contrôles positifs et négatifs. L'inflammation est classiquement représentée au cours du temps par une courbe de magnitude croissante, atteignant un plateau suivi par une phase de décroissance. Cette courbe permet de mettre en évidence les deux phases principales de

l'inflammation : la phase d'initiation et la phase de résolution. Ces deux phases mettent en jeu des éléments communs qui se régulent réciproquement et de manière différentielle au cours du temps, mettant en lumière un phénomène dynamique. La phase d'initiation se met en place suite à la libération de médiateurs lipidiques et d'amines vasoactives entraînant la formation d'une exsudation et d'un œdème. Cette réaction va permettre, par l'intermédiaire de chemokines et cytokines, la migration des polynucléaires neutrophiles au site de l'inflammation. Ces cellules constituent la première ligne de défense de l'organisme et assurent principalement la phagocytose et la destruction des agents pathogènes. Après avoir effectués leur travail, ces neutrophiles entrent en apoptose, permettant le recrutement des monocytes, leur différenciation en macrophages et la phagocytose des neutrophiles. Les macrophages, après phagocytose, vont alors moduler leurs fonctions et sécréter des facteurs anti-inflammatoires et pro-résolutifs induisant une réparation tissulaire et un retour à l'homéostasie (**Figure 1**) (Sansbury and Spite 2016). Les étapes d'initiation et de résolution de l'inflammation vont maintenant être détaillées afin de mettre en lumière les mécanismes par lesquels le corps humain répond à une agression et retourne à son état basal.

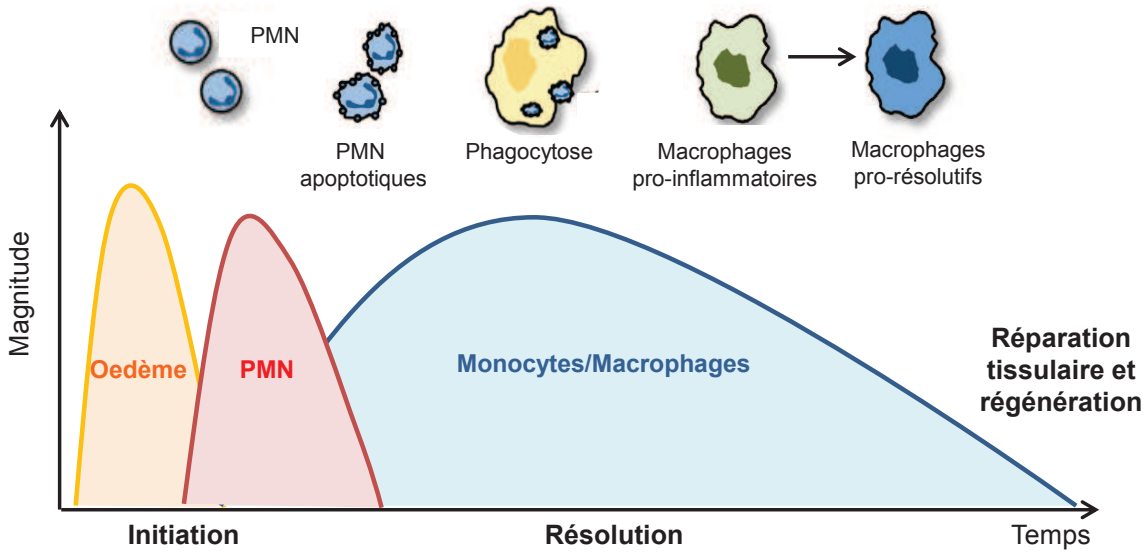

Figure 1. Evénements temporels liés à l'inflammation aiguë. L'inflammation peut se diviser en deux grandes phases. La phase d'initiation débute par une exsudation suivie d'un œdème tissulaire. Les polynucléaires neutrophiles (PMN) sont alors recrutés au site inflammatoire, en réponse à différents stimuli, et permettent la dégradation des pathogènes. Après avoir joué leur rôle, les PMN entrent en apoptose et permettent l'attraction des monocytes au lieu de l'inflammation. Les macrophages présents au site de l'inflammation et les monocytes dérivés en macrophages vont alors phagocyter les PMN apoptotiques et induire la résolution de l'inflammation, la réparation tissulaire et le retour à l'homéostasie. D'après (Sansbury and Spite 2016).

I.3) Initiation de la réponse inflammatoire

L'initiation de la réponse inflammatoire met en jeu un réseau de différents inducteurs, senseurs et médiateurs qui détermineront l'intensité, la spécificité et le type de réponse inflammatoire mise en place. Les inducteurs de la réponse inflammatoire peuvent être d'origine exogène ou endogène (**Figure 2**).

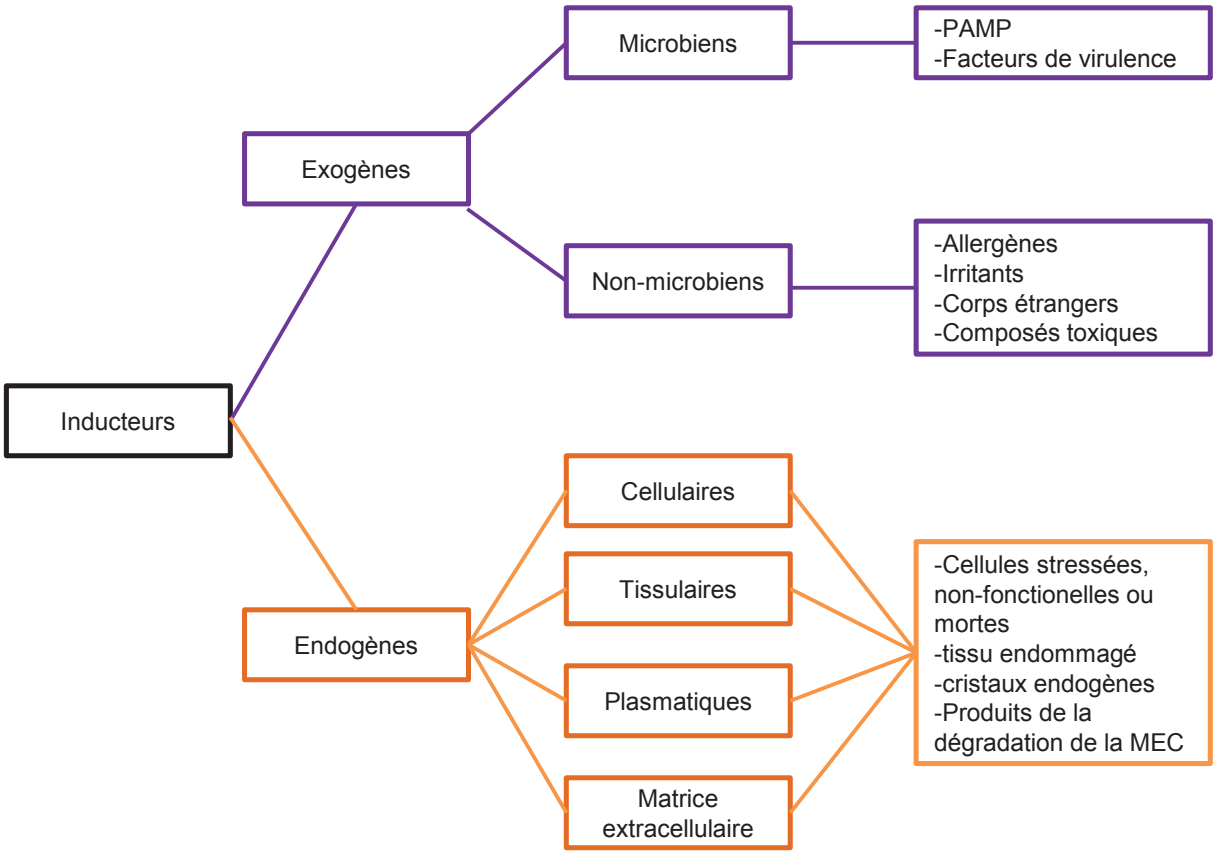

Figure 2. Les inducteurs de la réponse inflammatoire. Les inducteurs de la réponse inflammatoire sont de deux types : exogènes et endogènes. Les exogènes sont composés de facteurs microbiens et non microbiens. Les facteurs endogènes sont peuvent eux provenir de sources cellulaires, tissulaires, plasmatiques et de la matrice extraceullaire. PAMP: *pathogen-associated molecular pattern*. MEC: matrice extracellulaire. D'après (Medzhitov 2008).

I.3.1) Les inducteurs exogènes

Les inducteurs exogènes peuvent être d'origine microbienne ou non (**Figure 2**). Les inducteurs non-microbiens sont composés des allergènes, des irritants, de corps étrangers et de composés toxiques. Les inducteurs microbiens se divisent en motifs moléculaires associés aux pathogènes ou PAMP (*pathogen-associated molecular pattern*), et en facteurs de virulence (**Figure 2**). Les PAMP sont reconnus par les récepteurs PRR (*pathogen recognition*

receptor) majoritairement exprimés sur les cellules de l'immunité innée telles que les cellules dendritiques (DC), les macrophages et les neutrophiles. Les PRR sont capables de détecter différents types de molécules comme les lipides, les protéines, les sucres et les acides nucléiques exogènes. Cette reconnaissance va alors aboutir à l'élimination du pathogène *via* une réponse inflammatoire médiée par les cytokines et chemokines. Les facteurs de virulence, contrairement aux PAMP, ne sont pas reconnus directement par des récepteurs spécifiques. Les exotoxines produites par les bactéries à Gram positif, par exemple, forment un pore membranaire induisant un efflux de potassium qui est alors détecté par l'inflammasome NALP3 (*NACHT-leucine-rich-repeat and pyrin-domain-containing- protein 3*) élicitant une réponse inflammatoire (Mariathasan, Weiss et al. 2006).

I.3.2. Les inducteurs endogènes

Les inducteurs endogènes sont induits suite à différents stress ou dommages au sein des tissus (**Figure 2**). Ils sont également appelés alarmines ou motifs moléculaires associés au dommage (ou DAMP *; damage-asssociated molecular pattern*). Ces motifs, normalement contenus au sein de la cellule (par la membrane plasmique notamment), sont libérés suite à un dommage tissulaire et peuvent ainsi activer une réponse inflammatoire. Les DAMP comprennent divers facteurs comme HMGB1 (*high–mobility group box 1*), les protéines S100 (dont les protéines S100A8, S100A9 et S100A12), les protéines de choc thermique (HSP ; *heat shock protein*), l'acide urique ou encore l'ATP (Adénosine-Triphosphate) (Bianchi 2007). Ces facteurs sont soit libérés de manière passive lors d'une rupture de la membrane cellulaire (nécrose, nécroptose [forme de mort programmée menant à la lyse cellulaire]), soit sécrétés de manière non classique dans le cas des protéines (indépendante du réticulum endoplasmique et de l'appareil de Golgi), activant alors l'inflammasome de manière dépendante de la voie caspase 1 (Keller, Ruegg et al. 2008). Ces inducteurs endogènes seront alors reconnus par les PRR afin d'éliciter une réponse inflammatoire.

I.3.3 Les récepteurs aux inducteurs

Les PRR comprennent différents récepteurs tels que les TLR (*toll-like receptors*), les RLR (*RIG-I-like receptors*), les NLR (*NOD-like-receptors*), les CLR (*C-type lectine receptor*) et les récepteurs à ADN (acide désoxyribonucléique) (Kumar, Kawai et al. 2009; Kumar, Kawai et al. 2011). Les PRR ont différentes localisations cellulaires, les TLR sont transmembranaires ou endosomaux, les RLR intracellulaires, les NLR intracellulaires et les CLR transmembranaires. Ces PRR sont exprimés par les cellules de l'immunité innée comme les cellules dendritiques et les macrophages, mais également par des cellules non-immunitaires

(cellules épithéliales, fibroblastes…). Ils sont responsables de la reconnaissance des PAMP bactériens et viraux mais également des DAMP provenant des cellules du soi et d'induire, *via* différentes voies de signalisation, une réponse inflammatoire.

Les TLR sont la famille de PRR la mieux caractérisée, et contiennent 10 membres chez l'homme (TLR1 à 10) et 12 chez la souris (TLR1 à 13 sauf TLR10). Les TLR reconnaissent une grande variété de PAMP tels que le zymozan (TLR2), l'ARN double brin (TLR3), le lipopolysaccharide (LPS ; TLR4), la flagelline (TLR5), les lipoprotéines (TLR2/6), l'ARN simple brin (TLR7), ou encore les motifs CpG de l'ADN (TLR9) (Jang, Shin et al. 2015).

Les RLR sont composés de RIG-I (*retinoic acid-inducible gene I*), MDA5 (*melanoma differentiation factor-5*) et LGP-2 (*laboratory of genetics and physiology-2*). RIG-I et MDA5 possèdent tous deux un domaine hélicase capable d'ouvrir les hélices ARN (acide ribonucléique)/ADN, permettant ainsi la prise en charge d'ARN et ADN viraux. MDA5 détecte les ADN doubles brins et les ARN doubles brins longs alors que RIG-I va détecter les ARN doubles brins courts (Takeuchi and Akira 2010).

Les NLR contiennent les récepteurs intracellulaires NOD1 et 2 (*nucleotide-binding oligomerization domain-containing protein 1*) ainsi que de l'inflammasome NALP3. NOD1 et 2 vont respectivement reconnaître les bactéries à Gram positif et négatif. NALP3 va quant à lui prendre en charge certains DAMP (acide urique, peptide β-amyloïde, ATP…) (Takeuchi and Akira 2010).

Si tous ces PRR ont des voies de signalisations différentes, ils vont tous aboutir au déclenchement d'une réaction immunitaire innée *via* la transcription de gènes codant pour des protéines de l'inflammation telles que l'IL-1β, l'IL-6, l'IL-8, RANTES (*regulated on activation, normal T cell expressed and secreted*), le TNF-α (*tumor necrosis factor-α*) ou encore l'IFN-γ (*interferon-gamma*). Les PRR reconnaissant des produits viraux (TLR7, TLR9, RIG-I, MDA5) vont quant à eux activer la sécrétion des IFN de type I (IFN-α et β) qui jouent un rôle fondamental dans la réponse antivirale (Kumar, Kawai et al. 2009; Takeuchi and Akira 2010; Jang, Shin et al. 2015). Les différentes voies d'activation des PRR par les PAMP et les DAMP sont schématisées dans les **figures 3** et **4**.

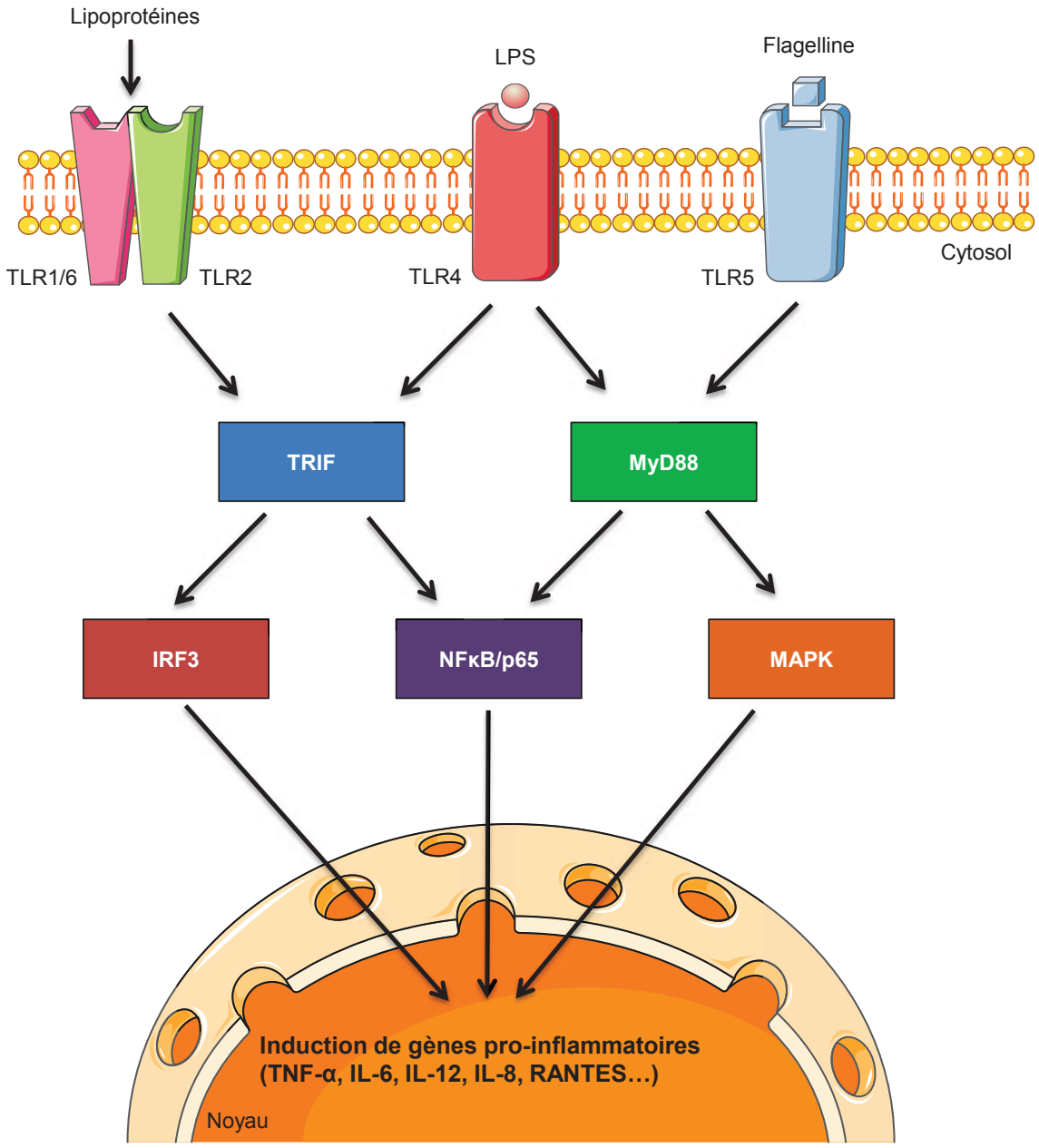

Figure 3. Voies d'activation des TLR membranaires par les PAMP bactériens. L'activation des TLR par des ligands d'origine bactérienne induit l'activation d'une voie de signalisation sous-jacente liée aux adaptateurs TRIF (*TIR-domain-containing adapter-inducing interferon-β*) et Myd88 (*myeloid differentiation primary response gene 88*). Ces adaptateurs vont ensuite activer les facteurs de transcription IRF3, NFκB/p65 ainsi que la voie des MAPK (*mitogen-activated protein kinases*) permettant la transcription de gènes pro-inflammatoires. IL: Interleukine. IRF3: *interferon regulating factor 3*. LPS: Lipopolysaccharide. MAPK: *Mitogen-activated protein kinases*. NFκB: *Nuclear factor kappa B*. RANTES: *Regulated on activation: normal T cell expressed and secreted*. TLR: *Toll like receptor*. TNF-α: *Tumor necrosis factor α.*

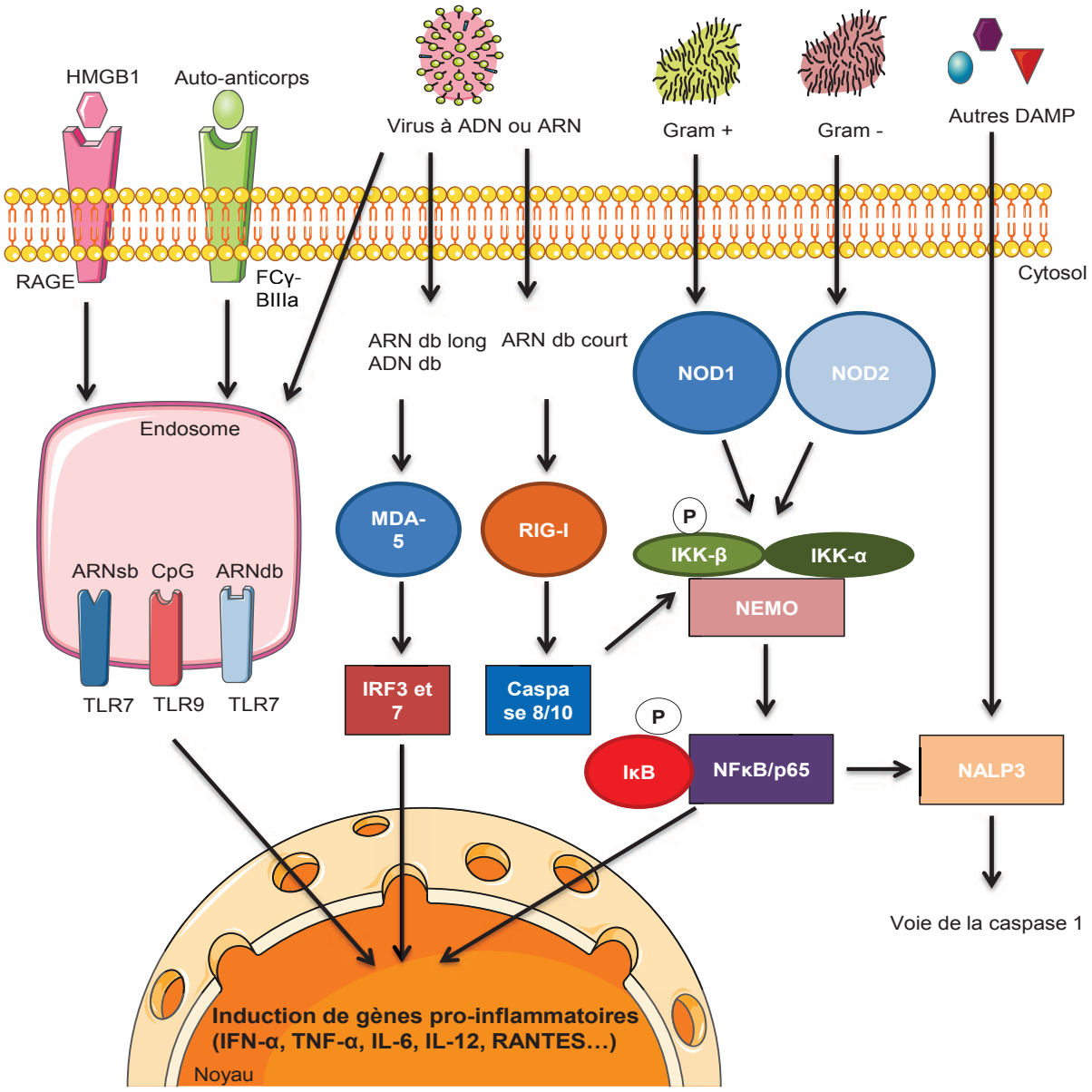

Figure 4. Voies d'activation des différents PRR par les inducteurs de l'inflammation. L'activation des récepteurs RAGE (*receptor for advanced glycation end-products*) et FCγ-BIIA par des inducteurs exogènes, comme certains facteurs viraux, va permettre l'activation de la voie des TLR7/9. Les virus peuvent également, par différents mécanismes dépendants de la structure du virus, activer les RLR MDA-5 et RIG-I. Les bactéries, en plus de l'activation classique par les TLR, peuvent également induire la voie des NLR NOD1 et 2. Enfin, certains DAMP vont activer directement l'inflammasome NALP3, ce qui permettra le clivage de la caspase 1. Toutes ces voies de signalisation vont permettre l'activation des facteurs de transcription NFκB et IRF3/7 notamment et la production de facteurs pro-inflammatoires (cytokines, chémokines, interférons de type I…). ADN: Acide désoxyribonucléique. ARN: Acide ribonucléique. DAMP: *Damage associated molecular pattern*. HMGB1: H*igh–mobility group box 1*. IFN-α*:* Interféron α. IκB: *Inhibitor of kappa B*. IKK: *IκB kinase*. IL: Interleukine. IRF: *Interferon regulating factor*. LPS: Lipopolysaccharide. MDA-5: *Melanoma differentiation factor-5*. NALP3: *NACHT-Leucine-rich-repeat and Pyrin-domain-containing- protein*. NEMO: *NF-kB Essential Modulator*. NFκB: *Nuclear factor kappa B*. NOD: *Nucleotide-binding oligomerization domain-containing protein*. RANTES: *Regulated on activation: normal T cell expressed and secreted.* RIG-I: *Retinoic acid-Inducible Gene I*. TLR: *Toll like receptor*. TNF-α: *Tumor necrosis factor α.*

I.3.4) Les médiateurs solubles de l'inflammation

L'activation des voies de signalisation sous-jacentes des PRR par les différents DAMP et PAMP va conduire à la synthèse de médiateurs de l'inflammation par les cellules cibles. Ces médiateurs vont favoriser le recrutement et l'activation des leucocytes au site inflammatoire permettant la mise en place d'une réponse immunitaire innée. Ces médiateurs peuvent dériver de protéines plasmatiques ou être sécrétés par les cellules, et sont divisés en 7 groupes basés sur leurs propriétés biochimiques : les amines vasoactives, les peptides vasoactifs, les composés du complément, les médiateurs lipidiques, les enzymes protéolytiques, les cytokines et les chémokines.

Les amines vasoactives (histamine et sérotonine) sont produites lors de la dégranulation des plaquettes ou des cellules mastocytaires, et vont moduler la perméabilité vasculaire ainsi que la vasodilatation (ou la vasoconstriction selon les contextes). Leur relargage par les cellules mastocytaires est notamment responsable des manifestations cliniques observées durant un choc anaphylactique chez les patients prédisposés (Mohammad-Zadeh, Moses et al. 2008; Krystal, Richelson et al. 2013).

Les peptides vasoactifs, quant à eux, peuvent être conservés sous forme mature dans des vésicules (tel que la substance P) ou générés par clivage de précurseurs inactifs dans le milieu extracellulaire (tels que les kinines, les fibrinopeptides A ou B). Les peptides vasoactifs favorisent la vasodilatation et une augmentation de la perméabilité vasculaire de manière directe ou indirecte en induisant la dégranulation des cellules mastocytaires (Medzhitov 2008).

Les facteurs du complément C3a, C4a et C5a (aussi connus sous le nom d'anaphylatoxines) sont également considérés comme des médiateurs de l'inflammation. Le complément peut être activé par la voie des lectines, la voie classique ou la voie alternative menant à la synthèse finale de C3a, C4a et C5a. Ces anaphylatoxines vont alors être responsables du recrutement des leucocytes (monocytes, granulocytes et cellules mastocytaires), de la dégranulation des mastocytes et d'une augmentation de la perméabilité vasculaire (Markiewski and Lambris 2007).

Les médiateurs lipidiques (les éicosanoïdes et le facteur activateur des plaquettes [PAF]) dérivent des phospholipides présents à la surface interne des membranes cellulaires. Les principaux précurseurs des éicosanoïdes sont l'acide arachidonique et l'acide

lysophosphatidique, libérés par la phospholipase A2. L'acide arachidonique, *via* les cyclooxygénases, permet la production des prostaglandines (PG) (PGE2, PGI2) et thromboxanes (TBXA4…), ou, *via* les lypoxygénases, des leucotriènes (LTA4, LTB4…) et des lipoxines (LXA4…). Le PAF, quant à lui, est généré par l'acétylation de l'acide lysophosphatidique. Ces médiateurs lipidiques vont activer l'immunité innée, induire le recrutement de leucocytes, la vasodilatation et augmenter la perméabilité vasculaire. Cependant, certains peuvent également avoir un rôle anti-inflammatoire dans certains contextes comme la PGE2 ou les lipoxines (Lawrence, Willoughby et al. 2002).

Les enzymes protéolytiques (élastines, cathepsines et métalloprotéases [MMP]) ont un rôle important dans la régulation de la réparation tissulaire et la migration leucocytaire. Les MMP jouent un rôle dans la dégradation de la MEC et des membranes basales. Elles ont d'ailleurs un rôle pathogénique dans la polyarthrite rhumatoïde, les périodontites ou encore les maladies neuro-inflammatoires (Amalinei, Caruntu et al. 2010). Cependant, les MMP peuvent également diminuer la réponse inflammatoire, comme les MMP1, 2, 3 et 9 qui dégradent l'IL-1β et neutralisent ainsi son activité pro-inflammatoire (Ito, Mukaiyama et al. 1996).

Enfin, les cytokines et chémokines pro-inflammatoires sont deux types de protéines sécrétées par différents types cellulaires immunitaires et non-immunitaires, jouant un rôle fondamental dans la réponse inflammatoire.

La production de ces différents médiateurs inflammatoires va permettre le recrutement et l'activation des cellules de l'immunité au site de l'inflammation, et en premier lieu les neutrophiles, cellules clés de la réponse inflammatoire.

I.3.5) Les médiateurs cellulaires de la réponse inflammatoire

Les neutrophiles : un effecteur essentiel de la réponse inflammatoire

Les neutrophiles sont des cellules immunitaires impliquées dans la protection de l'organisme contre les pathogènes et constituent 40 à 60 % des leucocytes sanguins chez l'Homme. Ils se développent dans la moelle osseuse à partir de cellules souches hématopoïétiques par granulopoïèse et ont une durée de vie dans le sang de 1,5 heures chez la souris et de 8 heures chez l'homme (Kolaczkowska and Kubes 2013). Lors d'une réponse inflammatoire, les différents stimuli produits vont permettre le recrutement des neutrophiles au site de l'inflammation. Cette migration se fait essentiellement *via* les chémokines et leurs récepteurs associés (de Oliveira, Rosowski et al. 2016).

Complément sur les chémokine :

Les chémokines constituent la plus large famille de cytokines (environ 50 membres chez l'Homme et la souris). Leur classification est basée sur la présence de deux résidus cystéine en N-terminal permettant une subdivision en 4 sous-groupes : les CXC, CC, (X)C et CX3C (**Tableau 1**). La famille CX3C ne comprend qu'un seul membre, CX3CL1, nommé également fractalkine. Les chémokines peuvent également être subdivisées suivant leur fonctionnalité. Trois sous-groupes émergent alors : les chémokines inflammatoires (impliquées dans le recrutement leucocytaire au site inflammatoire), les chémokines homéostatiques (exprimées de manière constitutive et impliquées dans la migration des cellules de manière homéostatique) et les chémokines duelles qui peuvent avoir les deux fonctions citées précédemment (Zlotnik and Yoshie 2012).

Chémokine	Source	Récepteur associé	Rôle
CXCL1	Macrophages	CXCR2	Recrutement des neutrophiles
CXCL2	Macrophages	CXCR2	Recrutement des neutrophiles
CXCL5	Macrophages, eosinophiles, cellules épithéliales	CXCR2	Recrutement des neutrophiles
CXCL8	Macrophages, neutrophiles	CXCR2	Recrutement des neutrophiles et des monocytes
CXCL9	Neutrophiles, DC, cellules mastocytaires	CXCR3	Recrutement des Th1, CD8 et NK
CXCL10	Monocytes, cellules endothéliales, fibroblastes	CXCR3	Recrutement des Th1, CD8 et NK
CXCL11	Cellules mastocytaires	CXCR3	Recrutement des Th1, CD8 et NK
CCL2	Macrophages, cellules endothéliales	CCR2	Recrutement des monocytes
CCL3	Macrophages, monocytes, cellules endothéliales	CCR1	Recrutement des monocytes et NK
CCL5	Macrophages	CCR5	Recrutement des monocytes et NK
CCL20	Neutrophiles, macrophages, lymphocytes	CCR6	Recrutement des monocytes et Th17
CX_3CL1	Macrophages, cellules endothéliales	CX_3CR1	Recrutement des monocytes, LT et NK

Tableau 1. Principales chémokines impliquées dans les réponses inflammatoires. LT: lymphocytes T. NK: *natural killer*. Th1: *T helper 1*. Th17: *T helper 17*. D'après (Soehnlein, Drechsler et al. 2013).

Ces chémokines sont les ligands de récepteurs exprimés de manière différentielle sur les leucocytes mais qui possèdent tous 7 domaines transmembranaires. Ces récepteurs peuvent se différencier en deux grands sous-types : les récepteurs couplés aux protéines G et ceux qui signalent de manière indépendante des protéines G. Les récepteurs aux chémokines peuvent également être subdivisés selon leurs ligands en 5 classes : les CXCR, CCR, XCR, CX3CR et atypiques (Zlotnik and Yoshie 2012).

Les neutrophiles sont principalement attirés par les chémokines de la famille CXC telles que CXCL1, 2 ou encore CXCL5 (**Tableau 1**).

Une fois attirés à proximité du site inflammatoire, les neutrophiles vont quitter la circulation sanguine puis pénétrer dans le tissu cible par extravasation. Les neutrophiles migrent ensuite selon un gradient chimiotactique au sein du tissu. Ils seront alors responsables de la production de nombreux médiateurs pro-inflammatoires (IL-8, TNF-α, GM-CSF, LTB4, PGE2, ROS [*reactive oxygen species*]) pouvant activer diverses cellules du système immunitaire. Ils sont également capables d'exprimer les molécules de co-stimulation CD80 et CD86 ainsi que le complexe majeur d'histocompatibilité de classe II (CMH-II) et de présenter l'antigène aux lymphocytes T (Wright, Moots et al. 2010). L'expression du CMH-II sur les neutrophiles peut notamment être induite par le LPS suggérant un rôle dans les réponses antibactériennes (Sandilands, Ahmed et al. 2005). De plus, en présence de différentes cytokines inflammatoires (GM-CSF et IFN-γ), les neutrophiles acquièrent également la capacité d'exprimer le CMH-II et d'activer les lymphocytes T vers un profil Th1/Th17 (Gosselin, Wardwell et al. 1993; Abi Abdallah, Egan et al. 2011). Des neutrophiles exprimant le CMH-II et activant les LT ont été retrouvés dans le liquide synovial de patient atteints de polyarthrite rhumatoïde suggérant que l'acquisition de ces capacités présentatrices d'antigène pourraient avoir un rôle pathologique en cas d'inflammation chronique (Cross, Bucknall et al. 2003). Les neutrophiles peuvent également libérer le contenu de leurs granules (notamment la cathepsine G et la protéine LL37), ce qui permettra le recrutement de monocytes inflammatoires (Soehnlein and Lindbom 2010). Enfin, l'activité antimicrobienne des neutrophiles est basée sur leur capacité de sécrétion de structures formées de chromatine, de peptides antimicrobiens et d'enzymes (neutrophile élastase, cathepsine G et myélopéroxidase). Ces structures sont appelées NET (*neutrophil extracellular trap*) (Brinkmann, Reichard et al. 2004). Les NET limitent la dissémination des microbes en les séquestrant *via* des interactions électrostatiques. De plus, ces complexes inactivent les

protéines microbiennes. Enfin, ces structures sont capables de tuer ou inhiber directement les pathogènes *via* la sécrétion d'enzyme (lyzozyme et protéases), de peptides antimicrobiens (défensines) et de chélateurs d'ions (calgranuline) (Vorobjeva and Pinegin 2014). Cependant, les NET pourraient également avoir un rôle dans le déclenchement des maladies inflammatoires telles que le lupus ou le psoriasis. En effet, certaines molécules impliquées dans la formation des NET sont des auto-antigènes dans les maladies auto-immunes. Par exemple, la protéine LL37 et l'ADN contenus dans les NET peuvent être pris en charge par les cellules dendritiques plasmacytoïdes qui synthétisent de l'interféron de type I qui est délétère dans le lupus et le psoriasis (Kaplan and Radic 2012). Le but de l'initiation de l'inflammation est donc de permettre au corps de lutter contre une agression. Généralement, l'intervention des neutrophiles suffit donc à éliminer la source de l'agression et doit ainsi être limitée pour ne pas devenir délétère pour les tissus sains avoisinants. Les cellules immunitaires vont alors mettre en place d'autres mécanismes afin de basculer vers la phase de résolution de l'inflammation permettant le retour à l'homéostasie et la réparation tissulaire.

II) La résolution de l'inflammation

En conditions normales, l'initiation de l'inflammation se termine par l'entrée en apoptose des neutrophiles après avoir joué leur rôle. Les macrophages présents au sein du tissu enflammé vont alors phagocyter ces neutrophiles apoptotiques et adopter un phénotype anti-inflammatoire leur permettant d'induire la phase de résolution de l'inflammation (Ortega-Gomez, Perretti et al. 2013).

II.1) Les macrophages, acteurs essentiels de la résolution de l'inflammation

Les monocytes, qui sont les précurseurs des macrophages, apparaissent au niveau du foie chez les embryons de 11,5 à 12,5 jours. Les monocytes fœtaux sont ensuite relâchés dans la circulation sanguine à 12,5-13,5 jour de vie embryonnaire puis migrent dans les tissus à 13,5-14,5 jours (Hoeffel, Wang et al. 2012). Les monocytes se différencient alors en macrophages matures une fois dans le tissu comme cela a été démontré dans les poumons et le cœur (Guilliams, De Kleer et al. 2013; Epelman, Lavine et al. 2014). Toutes les populations de macrophages étudiées jusqu'à présent proviennent majoritairement de l'hématopoïèse définitive. Cependant, la microglie fait exception à cette règle car elle se développe à partir du sac de Yolk et de l'hématopoïèse primitive (Ginhoux, Greter et al. 2010).

Si chez l'Homme la classification des monocytes/macrophages fait encore débat, les études récentes chez la souris ont permis de définir des populations de macrophages en fonction de leurs tissus de résidence. Cependant, une grande hétérogénéité aussi bien fonctionnelle que phénotypique est observée (**Tableau 2**) (Lavin, Mortha et al. 2015).

Sous-types de macrophages	Tissu	Fonction homéostatique	Marqueurs spécifiques
Macrophages alvéolaires	Poumons	Clairance des tensioactifs	F4/80^{+}, Siglec-F^{+}, CD11c^{hi}, CD169^{+}
Macrophages de la pulpe rouge	Pulpe rouge de la rate	Clairance des érythrocytes, recyclage du fer	F4/80^{+}, VCAM1^{+}
Macrophages de la zone marginale	Zone marginale de la rate	Piéger les particules circulantes, maintenance des LB	SIGN-R1^{+}, MARCO^{+}
Cellules de Kupffer	Foie, sinusoïdes	Clairance des érythrocytes et des particules antigéniques, métabolisme de la bilirubine	F4/80^{+}, CD169^{+}, CLEC4F^{+}
Cellules de Langerhans	Epiderme	Tolérance et contrôle immunitaire	F4/80^{+}, CX_3CR1^{+}
Macrophages de la *lamina propria*	*Lamina propria* du petit et grand intestin	Tolérance et contrôle immunitaire	F4/80^{+}, CX_3CR1^{+}
Microglie	Système nerveux central (cerveau et moelle épinière)	Formation des synapses, surveillance immunitaire	CX_3CR1^{+}, CD45^{mid}, FCRLS^{+}, Siglec-H^{+}

Tableau 2. Caractéristiques des phagocytes mononuclées résidants des tissus sains. Une forte hétérogénéité des macrophages est observée dans les différents tissus, qu'elle soit fonctionnelle ou phénotypique. Il est à noter que les différentes fonctions des macrophages ne sont pas uniquement associées à des fonctions immunologiques. CLEC4F: *C-type lectin domain family 4 member F*. FCRLS: *Fc receptor-like S*. LB: lymphocyte B. MARCO: *macrophage receptor with collagenous structure*. Siglec: *sialic acid binding IG-like lectins*. SIGN-R1: *DC-SIGN-related protein 1*. Modifié d'après Lavin et al (2015).

La classification des macrophages peut également se faire selon leur profil de maturation. En s'inspirant de la classification Th1/Th2 des lymphocytes T basée sur le profil des molécules sécrétées par ces différentes sous populations de lymphocytes T, une classification en M1/M2 a été établie pour les macrophages ; les M1 représentant des macrophages pro-inflammatoires et les M2 des macrophages anti-inflammatoires. D'une manière générale, les macrophages de type M1 sont impliqués dans les réponses antibactériennes et anti-tumorales. Ils sont responsables de la production de cytokines pro-inflammatoires et vont influencer les LT vers une polarisation Th1. Les macrophages de type M2 sont responsables de la réponse antiparasitaire et ont des fonctions immuno-modulatrices et de réparation tissulaire. De plus, les M2 ont une capacité accrue de phagocytose des cellules apoptotiques (Martinez and Gordon 2014). Les M1 seront donc définis lors de ce manuscrit comme des macrophages pro-inflammatoires et les M2 comme des macrophages anti-inflammatoires et pro-résolutifs. Malgré cela, les macrophages tissulaires étant soumis à des microenvironnements constitués d'une multitude de molécules, leur régulation est un phénomène extrêmement complexe. Une

hétérogénéité très importante est ainsi retrouvée dans ces deux groupes de telle sorte qu'une nouvelle classification a été récemment proposée, basée sur les stimuli nécessaires à leur différenciation : M(IL-4), M(M-CSF), M(IL-10), M(LPS), M(GM-CSF) et M(IFN-γ) (Murray, Allen et al. 2014; Wynn and Vannella 2016) (**Figure 5**).

Complément sur les sous-types de macrophages :

Les macrophages de type M1 comprennent les macrophages stimulés à l'IFN-γ, au LPS et au GM-CSF (**Figure 5**). L'IFN-γ est une cytokine produite par les Th1, les NK ainsi que par les macrophages. La signalisation de cette molécule sur ces récepteurs (IFNGR1 et 2) va aboutir à l'activation de la voie JAK1/2-STAT1-IRF1/8 (Hu and Ivashkiv 2009). Si l'absence de production d'IFN-γ ou de sa signalisation ne modifie pas la génération de macrophages chez la souris, les macrophages ne sont plus capables de produire des produits antimicrobiens et les souris sont susceptibles à des infections (Martinez and Gordon 2014). De manière similaire, chez l'Homme, des mutations induisant un déficit d'expression du récepteur à l'IFN-γ induisent des susceptibilités aux infections démontrant un rôle crucial de l'IFN-γ dans la génération de macrophages de type M1 (Dorman and Holland 2000). Les macrophages de type M1 comprennent également les macrophages générés en présence de LPS qui est un activateur des réponses immune innées. Le LPS signale par le récepteur TLR4 dimérisé au TLR2 ce qui active la voie de signalisation MyD88/TRIF-NFκB/STAT5. Cette voie de signalisation va induire la sécrétion de cytokines (telles que l'IL-6, l'IL-12, le TNF-α) et de chemokines inflammatoires (CCL2, CXCL10, CXCL11). De manière importante, l'IFN-γ et le LPS partagent l'induction de certains gènes en commun par les macrophages et notamment des gènes impliqués dans la mise en place de réponses inflammatoires (Nau, Richmond et al. 2002; Martinez, Gordon et al. 2006). Enfin, les macrophages générés au GM-CSF sont considérés comme des M1 au profil inflammatoire. Le GM-CSF signale par son récepteur CSF2 qui induit la voie de signalisation liée à JAK2-STAT5/NFκB/IRF5 induisant la production de TNF-α, IL-1β, IL-8 et IL-6. De souris déficientes en GM-CSF ont notamment un défaut de maturation des macrophages alvéolaires et développent une protéinose au sein des poumons. (Dranoff and Mulligan 1994). Chez l'Homme, une mutation du GM-CSF mène à un phénotype similaire à celui observée chez la souris (Dirksen, Nishinakamura et al. 1997).

Les macrophages de type M2 comprennent eux les macrophages stimulés à l'IL-4, l'IL-10 et au M-CSF (**Figure 5**). L'IL-4 est produite par les Th2, éosinophiles, basophiles et macrophages. Il signale par son récepteur (IL-4R) et active la voie JAK1/3-STAT6. Cette cytokine étant importante pour la génération de réponses immunes anti-parasitaire, des souris déficientes en IL-4 ont des défauts de réponses à certaines infections notamment contre les nématodes. Chez l'Homme, des mutations dans le gène codant le récepteur à l'IL-4 favorisent l'apparition de l'asthme et d'allergies (Martinez and Gordon 2014). L'IL-10 se lie, elle, à l'IL10R et induit la voie de signalisation JAK1/Tyk2-STAT3 et favorise la sécrétion de chemokines (CXCL4 et CXCL13) mais

également l'expression de récepteurs impliqués dans la phagocytose telle que la protéine MARCO (Park-Min, Antoniv et al. 2005). Des défauts d'expression de l'IL-10 et de son récepteur respectivement chez la souris et l'Homme favorisent la survenue de maladies inflammatoires chroniques de l'intestin (Martinez and Gordon 2014). Enfin, le M-CSF signale par son récepteur CSF1R activant la voie Grb2-SP1. Une déficience de ce gène chez la souris diminue la génération de monocytes et macrophages et favorise la survenue d'ostéopétrose alors que des mutations de son récepteur chez l'Homme favorisent la survenue de syndromes myélodysplasiques et de leucémie myéloïde aigue (Tobal, Pagliuca et al. 1990; Wiktor-Jedrzejczak, Bartocci et al. 1990).

Les études *in vitro* ont donc permis de définir l'induction de réponses spécifiques à différents stimuli par les macrophages et la manière dont ils s'activaient. Cependant, la présence commune de certaines de ces molécules, et plus particulièrement lors de la mise en place de l'inflammation, ne nous permet pas de transposer directement ces résultats *in vivo*. *In vivo*, le phénotype des macrophages est dépendant du type de réponses que doit fournir l'organisme. Lors d'infections bactériennes, de cancers ou de maladies auto-immunes, la présence de macrophages de type M1 est observée. Lors de l'asthme, d'infections parasitaires et de la réparation tissulaire, les macrophages se différencient généralement en M2 (Sica and Mantovani 2012). Cependant, la plasticité importante des macrophages doit être notée car elle jour un rôle dans la modulation des réponses immunes. Par exemple, au sein de cancers de hauts grades, les macrophages dévient leur phénotype de M1 à M2 et l'infiltration de ces macrophages au sein des tumeurs est généralement associée à un mauvais pronostic. Au contraire, lors du démarrage de la phase de résolution de l'inflammation, notamment dans des modèles de péritonite, les macrophages acquièrent un phénotype intermédiaire M1/M2 afin de favoriser la réparation tissulaire et le retour à l'homéostasie (Bystrom, Evans et al. 2008; Stables, Shah et al. 2011).

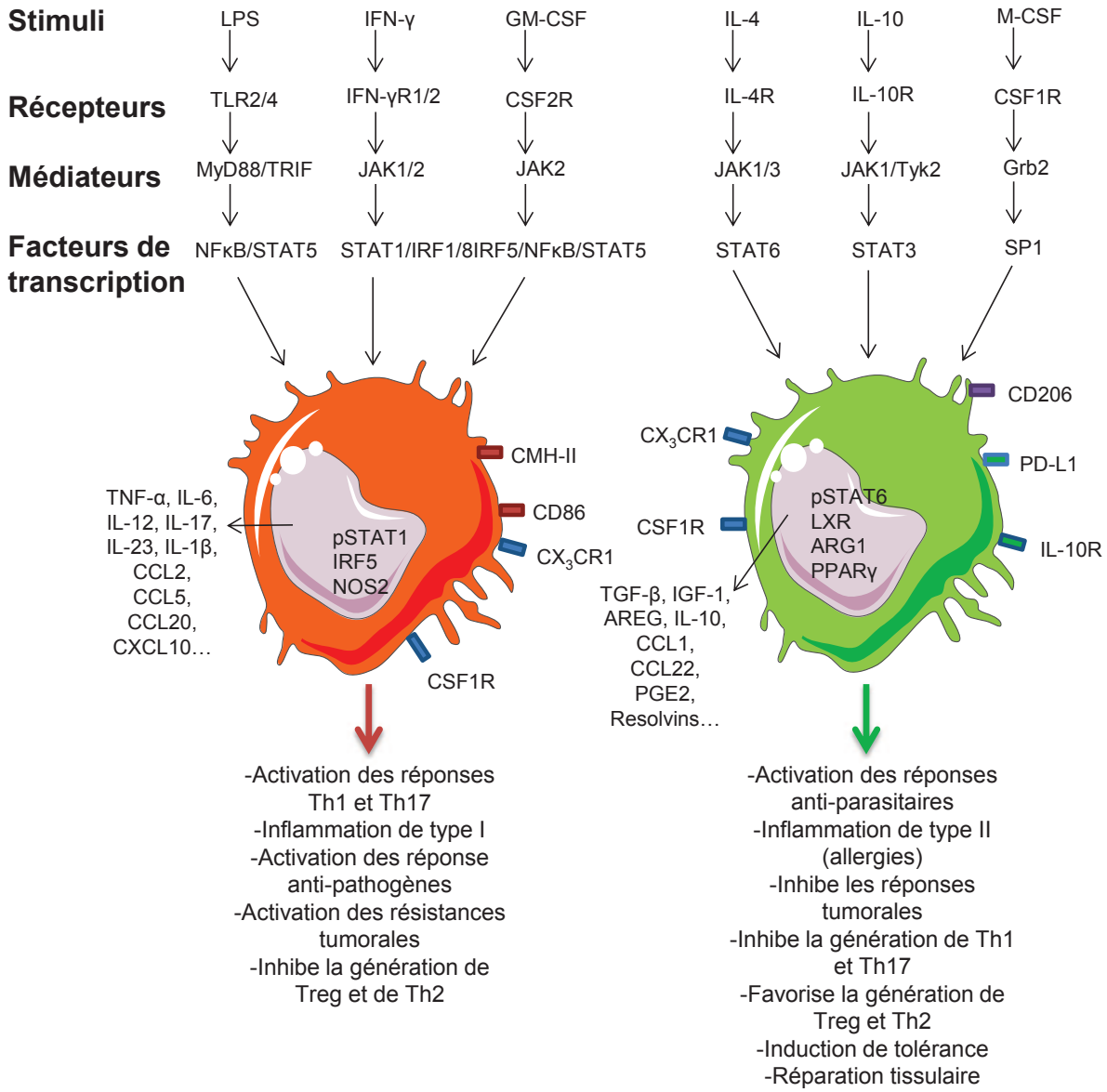

Figure 5. Polarisation des macrophages. La polarisation des macrophages en sous-types pro-inflammatoires (gauche du graphique) et pro-résolutifs (droite du graphique) est influencée par différents stimuli induisant des voies de signalisation variées. Ces voies aboutiront, *via* des facteurs de transcription, à la synthèse de récepteurs et de molécules pro ou anti-inflammatoires selon les stimuli. ARG1: arginase 1. AREG: amphiréguline. CSF1R: *colony stimulating factor 1 receptor*. GM-CSF: *granulocyte-macrophage colony-stimulating factor*. Grb2: *growth factor receptor-bound protein 2*. IGF-1: *insulin growth factor-1*. JAK: *janus kinase*. LXR: *liver X receptor*. M-CSF: *macrophage colony-stimulating factor*. NOS2: *nitric oxyde synthase 2*. PD-L1: *programmed death-ligand 1*. PGE2: prostaglandine E2. PPAR-γ: *peroxisome proliferator-activated receptor-γ*. STAT: *signal transducers and activators of transcription*. SP1: *specificity protein 1*. Tyk2: *tyrosine kinase.* D'après (Murray, Allen et al. 2014; Wynn and Vannella 2016).

II.2) L'efferocytose

Plus de 100 millions de neutrophiles meurent chaque jour par apoptose. Cette mort cellulaire programmée de type I est impliquée dans de nombreux phénomènes tels que le développement, la réparation tissulaire, la tumorigénèse ou encore les infections virales.

L'apoptose, contrairement à la nécrose, permet un contrôle du système immunitaire, qui peut se traduire par une immunomodulation voire l'induction de tolérance. En effet, l'activation des caspases durant l'apoptose empêche la mise en place de réponses immunes innées en inhibant la sécrétion d'IFN de type I ou en oxydant le signal de danger HMGB1 (Kazama, Ricci et al. 2008; Rongvaux, Jackson et al. 2014). De plus, les cellules apoptotiques vont moduler les réponses immunes de manière directe en sécrétant différents facteurs anti-inflammatoires tels que le TGF-β, l'IL-10, l'annexine A1, la thrombospondine-1 ou encore l'adénosine monophosphate. Toutes ces molécules vont principalement favoriser la modulation du phénotype des phagocytes (macrophages et cellules dendritiques) vers un profile tolérogénique (Voll, Roth et al. 1997; Gao, Herndon et al. 1998; Chen, Frank et al. 2001; Krispin, Bledi et al. 2006; Pupjalis, Goetsch et al. 2011; Yamaguchi, Maruyama et al. 2014). L'expression de CCR5 sur les cellules apoptotiques va également permettre la séquestration de chémokines pro-inflammatoires CCL3 et 5 ce qui bloquera la migration des cellules immunitaires (Ariel, Fredman et al. 2006). Enfin, les cellules apoptotiques modulent aussi le système immunitaire *via* leur élimination par les phagocytes, et plus particulièrement les macrophages. La clairance des cellules apoptotiques est assurée par différents types cellulaires appelés phagocytes spécialisés dans cette fonction, dits professionnels, ou par des phagocytes non-professionnels (Hochreiter-Hufford and Ravichandran 2013). L'efferocytose, ou l'élimination des cellules apoptotiques par les phagocytes, est un processus extrêmement régulé qui se déroule en plusieurs étapes. Cette étape est considérée comme l'étape clé de la résolution de l'inflammation permettant le retour à l'homéostasie tissulaire.

II.2.1) Signaux « trouvez-moi »

Des premiers travaux chez *Caenorhabditis elegans* ont permis de mettre en évidence le fait que les cellules apoptotiques pouvaient être reconnues et prises en charge avant leur mort *via* un système de reconnaissance (Reddien, Cameron et al. 2001). Ces données ont été les premières à suggérer que les cellules apoptotiques produisent des facteurs permettant l'attraction de phagocytes appelés signaux « trouvez –moi » ou « *find me* » en anglais. Ces signaux incluent notamment la chémokine CX3CL1, la sphingosine-1-phosphate (S1P), la lysophosphatidylcholine (LPC) ou des nucléotides tels que l'ATP ou l'UTP.

CX3CL1 est une protéine membranaire produite par les lymphocytes B et les neurones apoptotiques et qui attire les macrophages en se fixant sur son récepteur CX3CR1. En effet, au niveau des centres germinatifs, un fort taux d'apoptose est observé ainsi qu'un recrutement des macrophages à cet endroit de manière CX3CL1/CX3CR1 spécifique. Cependant, aucune

augmentation du nombre de cellules apoptotiques n'est observée au niveau de ces centres germinatifs dans des souris déficientes en CX3CR1, démontrant que cet axe n'est pas requis pour la prise en charge des cellules mortes mais uniquement pour l'attraction des macrophages (Truman, Ford et al. 2008).

S1P est un lipide produit par la sphingosine 1 kinase qui une fois sécrété par les cellules apoptotiques attire les macrophages *via* des récepteurs couplés aux protéines G (S1P-R1 à 5) exprimés à la surface des macrophages (Gude, Alvarez et al. 2008).

Le LPC est également un lipide considéré comme un signal « trouvez-moi ». Il est sécrété par les cellules apoptotiques après activation de la phospholipase A2 par la caspase 3 permettant la conversion de phosphatidylcholine en LPC. Sa reconnaissance par le récepteur G2a mène au recrutement des macrophages vers les cellules apoptotiques (Lauber, Bohn et al. 2003; Peter, Waibel et al. 2008).

Enfin, les nucléotides ATP et UTP ont également été découverts comme étant des signaux « trouvez-moi ». Ils sont produits par les cellules apoptotiques et relâchés au travers des canaux pannexines qui sont ouverts après leur clivage par les caspases (Chekeni, Elliott et al. 2010). Ces nucléotides vont alors signaler par les récepteurs P2Y2 et ainsi favoriser l'attraction des monocytes. Le blocage de cette interaction nucléotides/récepteurs *in vivo* dans des souris $P2Y2^{-/-}$ diminue l'efferocytose de thymocytes apoptotiques en limitant le recrutement des phagocytes (Elliott, Chekeni et al. 2009).

II.2.2) Les signaux « mangez-moi »

Une fois attirés par les cellules apoptotiques, les macrophages reconnaissent ces dernières de manière spécifique. Pour cela, les cellules apoptotiques expriment différentes molécules à leur surface permettant leur reconnaissance par les phagocytes *via* des récepteurs spécifiques. Ces signaux sont appelés signaux « mangez-moi ». Les principaux signaux et récepteurs associés sont les suivants : les sucres (comme le mannose ou les sucres liés à des groupements amines) qui sont reconnus par les lectines (Ezekowitz, Sastry et al. 1990), la thrombospondine 1 (TSP1) qui est reconnue par le récepteur CD36 et par les intégrines αvβ3 et αvβ5 (Savill, Dransfield et al. 1990), le complément C1q qui est reconnu par la protéine LRP1 (*low density lipoprotein receptor-related protein 1*) et le CD91 (Ogden, deCathelineau et al. 2001), ICAM3 qui est reconnu par le CD14 (Gregory, Devitt et al. 1998), et les LDL oxydés qui sont reconnus par les récepteurs *scavengers* (Gordon 1999).

Cependant, le signal « mangez-moi » qui est le plus étudié et le mieux défini est l'exposition de la phosphatidylsérine (PtdSer) à la membrane externe des cellules apoptotiques. Les PtdSer sont présentes exclusivement au feuillet interne de la membrane plasmique des cellules vivantes, mais lors de l'entrée en apoptose, les PtdSer passent de la membrane interne à la membrane externe, par un mécanisme non totalement élucidé. Cependant, de récents travaux ont montré que le canal TMEM16F (*transmembrane protein 16 F)* permet ce changement. En effet, une délétion de ce gène dans des plaquettes de souris empêche l'exposition des PtdSer à la surface externe des cellules en réponse à un stimulus pro-apoptotique (Fujii, Sakata et al. 2015). De plus, une mutation dans ce canal est observée chez les patients atteints de syndrome de Scott qui est une maladie liée à une incapacité des cellules sanguines à exprimer les PtdSer (Suzuki, Umeda et al. 2010). Cependant, l'exposition des PtdSer à la surface des plaquettes de patients atteints du syndrome de Scott peut également se faire par un mécanisme indépendant de TMEM16F (van Kruchten, Mattheij et al. 2013). Bien que l'exposition des PtdSer représente un signal « mangez-moi » très important, est-il suffisant pour induire la phagocytose ? Certaines études tendent à démontrer que ce signal est nécessaire et suffisant pour induire la phagocytose des cellules apoptotiques, tandis que d'autres données suggèrent que ce signal n'est pas suffisant, montrant que de nouvelles investigations seront nécessaires afin de répondre à cette question. Notamment, l'exposition de PtdSer sur des cellules viables, de manière naturelle ou artificielle, ne permet pas leur efferocytose (van den Eijnde, van den Hoff et al. 2001; Segawa, Suzuki et al. 2011). Les PdtSer sont reconnues par les phagocytes par deux mécanismes différents, le premier étant une reconnaissance par l'intermédiaire de molécules de pontage. C'est par exemple le cas du récepteur LRP1/CD91 qui se lie aux PtdSer lorsqu'elles co-localisent avec la calréticuline (Gardai, McPhillips et al. 2005). MFG-E8 (*Milk fat globule-EGF factor 8 protein)*, Gas6 (*growth arrest-specific 6)* et la protéine S sont également des molécules de pontage impliquées dans la reconnaissance des PtdSer (Nakano, Ishimoto et al. 1997; Nagata, Hanayama et al. 2010). Le deuxième type de reconnaissance des PtdSer se fait de manière directe *via* un récepteur. C'est le cas notamment du récepteur BAI1 *(brain-specific angiogenesis inhibitor 1*) qui est un récepteur transmembranaire couplé aux protéines G présent à la surface de nombreux types cellulaires (macrophages, cellules épithéliales, neurones…) et permettant la reconnaissance des PtdSer (Park, Tosello-Trampont et al. 2007). Les récepteurs TIM-1 et 4 (*T cell immunoglobulin mucin domain 1 et 4*) sont également impliqués dans la reconnaissance directe des PtdSer à travers leur domaine IgV (Kobayashi, Karisola et al. 2007). Tous ces mécanismes de

reconnaissance de la cellule apoptotique vont permettre aux macrophages d'induire un programme cellulaire de prise en charge et de dégradation de ces cellules.

II.2.3) Elimination des corps apoptotiques

Lorsque la cellule apoptotique se lie au macrophage, une signalisation induisant un réarrangement du cytosquelette va être mise en place afin de permettre la phagocytose de la cellule. Pour ce faire, différentes voies de signalisation vont être mises en place. Leur découverte a d'abord été faite chez *Caenorhabditis elegans* puis étendue à l'Homme. Les principales voies de signalisations sont résumées dans le **tableau 3**.

C. elegans	**Mammifères**	**Rôle**
CED-1	LRP1(CD91)/MEGF10	Récepteur de surface sur les phagocytes reconnaissant un ligand à la surface des cellules apoptotiques
CED-2	CrkII	Adaptateur qui semble co-localisé avec Dock180 et ELMO à la membrane ; son rôle est peu connu
CED-5	Dock180	Facteur d'échange de guanine qui charge Rac de GTP
CED-6	GULP	Adaptateur se liant avec LRP1; son rôle est peu connu
CED-7	ABCA1/ABCA7	Transporteurs ABC impliqués dans l'efflux du cholestérol
CED-10	Rac	Rho GTPase ; régule l'activation d'Arp2/3, la polymérisation de l'actine et le réarrangement du cytosquelette
CED-12	ELMO	Adaptateur se liant à Dock180 et qui facilite son activité

Tableau 3. Protéines impliquées dans la signalisation liée à la prise en charge des cellules apoptotiques. La découverte des protéines impliquées dans le remodelage du cytosquelette a été faite chez *C. elegans* puis étendue à l'Homme mettant en évidence de nombreuses voies de régulation de ce phénomène. ABCA1: *ATP-binding cassette 1*. *C. elegans*: *Caenorhabditis elegans.* CrkII: *CT10 regulator of kinase*. Dock180: *dedicator of cytokinesis*. GULP: *engulfment adaptor PTB domain containing*. Rac: *ras-related C3 botulinum toxin substrate*. ELMO: *engulfment and cell motility*. Modifié d'après (Hochreiter-Hufford and Ravichandran 2013).

Une fois la cellule apoptotique internalisée, l'acidité augmente au sein du phagosome avant la fusion avec les lysosomes permettant la dégradation du contenu phagosomal après l'activation des cathepsines (Lennon-Dumenil, Bakker et al. 2002; Kinchen and Ravichandran 2008). La dégradation des composants cellulaires (ADN, cholestérol, peptides…) est alors prise en charge permettant une stricte régulation de ce processus. Il a par exemple été montré que les fragments d'ADN sont dégradés par la DNAse II. Une délétion de cette protéine chez la souris favorise le développement de la polyarthrite rhumatoïde due à une incapacité du macrophage à dégrader l'ADN issu des cellules apoptotiques induisant une sécrétion de TNF-α (Kawane, Ohtani et al. 2006). Le cholestérol sera lui éliminé *via* une augmentation de l'efflux médié par le transporteur ABCA1 (*ATP-binding cassette 1*) (Kiss, Elliott et al. 2006).

Enfin, les peptides peuvent être présentés par le CMH de classe I aux lymphocytes T afin d'induire des mécanismes de tolérance (Huang, Platt et al. 2000).

II.2.4) Reprogrammation des macrophages et retour à l'homéostasie

Après phagocytose des cellules apoptotiques, les macrophages opèrent un changement phénotypique, d'un profil pro-inflammatoire vers un profil pro-tolérogénique caractérisé notamment par une production d'IL-10 et de TGF-β (Fadok, Bratton et al. 1998). Cette modification de phénotype met en jeu différents facteurs de transcription tels que PPAR-γ *(peroxisome proliferator-activated receptor gamma*) ou LXR (*liver X receptor*) qui favorisent l'acquisition d'un profil tolérogénique (N, Bensinger et al. 2009; Natrajan, de la Fuente et al. 2015). L'analyse transcriptomique des macrophages présents lors de la phase de résolution de l'inflammation a montré une augmentation de l'expression de gènes codant pour des molécules impliquées dans la présentation antigénique (CMH-II, CD86), de molécules chimio-attractantes (XCL1, CCL5, CXCL13) ou encore de facteurs impliqués dans l'arrêt du recrutement cellulaire et la clairance des cellules apoptotiques (Alox15, Timd4) (Stables, Shah et al. 2011). De plus, de nombreux lipides pro-résolutifs sont produits par les macrophages après efferocytose (Serhan, Chiang et al. 2008).

Complément sur les lipides pro-résolutifs :

Les lipides pro-résolutifs sont générés à partir d'acide gras omega 3 polyinsaturé (**Figure 6**). L'omega 3 peut alors donner de l'acide eicosapentaenoique qui via la cyclooxygénase 2 va générer de l'acide hydroxyeicosapentanoique. La 5-lipoxygénase va alors le convertir en résolvine E1 et E2 alors que la 15-lipoxygénase va le convertir en résolvine E3. L'omega 3 peut également donner de l'acide docosahexanoique. La lipoxygénase génèrera alors les marésines (et notamment la marésine 1) alors que la cyclooxygénase 2 génèrera de l'acide 17-hydroxyphospho docosahexanoique. Ce dernier va être à l'origine de la synthèse des protectines et des résolvines D (D1 à 6) par la 5-lipoxygénase (Serhan 2017). Ces lipides pro-résolutifs vont favoriser la mise en place de la résolution de l'inflammation en bloquant l'infiltration des neutrophiles et monocytes, en diminuent la sécretion de cytokines, leucotriènes et prostaglandines ou encore en favorisant l'efferocytose (Serhan and Petasis 2011). Il a par ailleurs été montré que les résolvines E, D1 à 5 et les marésines favorisaient la survie et la résolution de l'inflammation dans des modèles d'infections ou d'inflammations (Serhan 2017). La voie de l'acide arachidonique qui permet la synthèse de lipides pro-inflammatoires (telles que les prostaglandines) mais également la synthèse de lipides anti-inflammatoires (résolvines, protectines et marésines) lors de la reprogrammation des macrophages est également mise en jeu. Les macrophages de type M1 expriment ainsi de manière importante COX2 (cyclo-oxygénase 2) et voient leurs expressions de COX1, leukotriène hydrolase, thromboxane A synthase 1 et arachidonate 5-

lipoxygénase diminuées, favorisant l'acquisition d'un phénotype inflammatoire. En revanche, les macrophages de type M2 voient leurs expressions de COX1 et arachidonate 15-lipoxygénase augmentées favorisant l'acquisition d'un phénotype tolérogénique (Martinez, Gordon et al. 2006). En plus de cette sécrétion de différents facteurs pro-résolutifs et anti-inflammatoires, les macrophages, en réponse à l'efferocytose, ont une capacité moindre à produire de nombreuses cytokines pro-inflammatoires telles que l'IL-1β, l'IL-6, l'IL-8, le GM-CSF, l'IL-12 ou encore l'IL-23 (Saas, Kaminski et al. 2013).

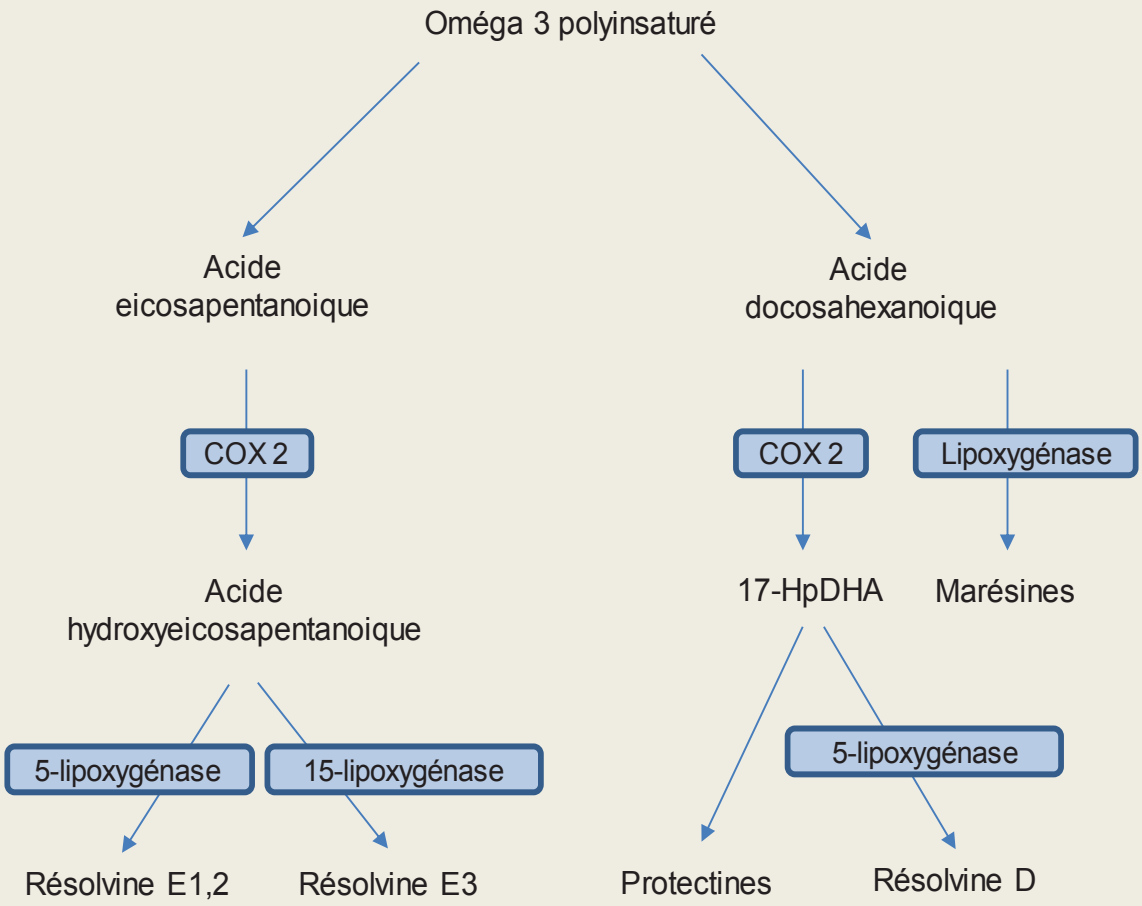

Figure 6. Voie de biosynthèse des lipides pro-résolutifs. La production de lipides pro-résolutifs démarre à partir de la transformation de l'oméga 3 polyinsaturé en acide eicosapentanoique ou docosahexanoique. Le premier donnera comme produits finaux les résolvines E1 et 2 *via* la 5-lipoxygénase et la résolvine E3 *via* la 15-lipoxygénase. La transformation du second acide va permettre la génération de marésines par la lipoxygénase et de 17-HpDHA par COX 2. Finalement, le 17-HpDHA sera à l'origine des résolvines de la série D *via* la 5-lipoxygénase ainsi que des protectines. COX 2 : Cyclooxygénase 2. 17-HpDHA: acide 17-hydroxyphospho docosahexanoique. Modifié d'après (Serhan 2017).

La reprogrammation des macrophages après efferocytose va ensuite induire de nombreux phénomènes immuno-modulateurs sur les cellules de l'immunité innée (**Figure 7**). La lipoxine A4 est un des lipides produits par les macrophages pro-résolutifs. Elle va notamment, *via* son récepteur nommé ALX, diminuer l'attraction des neutrophiles et renforcer celle des

monocytes (Maddox, Hachicha et al. 1997). La famille des résolvines, lipides pro-résolutifs, est également impliquée dans la résolution de l'inflammation. L'interaction de la résolvine E1 avec son récepteur CMKLR1 (*chemokine-like receptor 1*) atténue l'activation du facteur de transcription NFκB et la production de TNF-α subséquente dans différents types cellulaires, dont les monocytes lors de la résolution de l'inflammation (Arita, Bianchini et al. 2005). La résolvine D1 est quant à elle responsable de l'arrêt du recrutement des neutrophiles dans différents contextes inflammatoires (Serhan, Hong et al. 2002). De plus, ces différents lipides pro-résolutifs vont favoriser la phagocytose des cellules apoptotiques par les macrophages permettant d'entretenir l'immuno-modulation tissulaire (Serhan, Chiang et al. 2008).

La reprogrammation des cellules de l'immunité innée va alors permettre de moduler les cellules de l'immunité adaptative et principalement les lymphocytes T (**Figure 7**). En effet, lors de la phagocytose de cellules apoptotiques par les macrophages, une profonde reprogrammation lymphocytaire est observée (Miyake, Asano et al. 2007; Perruche, Zhang et al. 2008). L'efferocytose diminue notamment la production de TNF-α, IL-8, IL-23, GM-CSF ou d'IL-1β, des cytokines impliquées dans la polarisation des LT en Th1 et Th17, et augmente la sécrétion de TGF-β qui est le facteur principal impliqué dans la génération de lymphocytes T régulateurs (Treg) (Fadok, Bratton et al. 1998; Chen, Jin et al. 2003; Stark, Huo et al. 2005). Dans un contexte auto-immun (diabète de type I et sclérose en plaques), la prise en charge de cellules apoptotiques par les macrophages diminue les signes cliniques de la maladie. Cette induction de tolérance est liée à l'efferocytose des cellules apoptotiques par les macrophages qui sécrètent alors du TGF-β induisant la différentiation des lymphocytes T naïfs en Treg spécifiques de l'antigène (Kasagi, Zhang et al. 2014). Chez des souris atteintes d'athérosclérose, le blocage de la phagocytose en utilisant des anticorps anti-TIM1 et 4 mène à une pathologie exacerbée et à une augmentation des réponses Th1 et Th2 et des cytokines associées (Foks, Engelbertsen et al. 2016).

Les cellules non immunes sont également impactées par les produits issus de l'efferocytose permettant la réparation tissulaire et le retour à l'homéostasie (**Figure 7**). Au niveau de la peau, par exemple, les macrophages contrôlent la réparation tissulaire en régulant l'angiogenèse et la différentiation des myofibroblastes en sécrétant du TGF-β et du VEGF (*vascular endothelial growth factor*). Le TGF-β joue également un rôle important dans la régénération tissulaire en facilitant la production d'inhibiteurs des métalloprotéinases (les TIMP) qui régulent le remodelage tissulaire ou encore en favorisant la production de collagène (Lucas, Waisman et al. 2010; Ortega-Gomez, Perretti et al. 2013). Les macrophages

de type M2, et notamment les facteurs qu'ils produisent (VEGF, IL-10, TGF-β1 et 3), favorisent également la prolifération des cellules souches mésenchymateuses et leur motilité permettant la réparation tissulaire dans un modèle de dégradation de la moelle épinière (Anton, Banerjee et al. 2012; Nakajima, Uchida et al. 2012; Freytes, Kang et al. 2013). Enfin, des travaux récents ont démontré que les macrophages après efferocytose sécrètent de l'IGF1 (*insulin growth factor 1*). L'IGF1 interagit alors avec son récepteur présent sur les cellules épithéliales, notamment au niveau des poumons, et diminue l'inflammation démontrant des interactions primordiales entre les macrophages et les cellules non-immunes pour contrôler l'inflammation et induire un retour à l'homéostasie et une réparation tissulaire (Han, Juncadella et al. 2016).

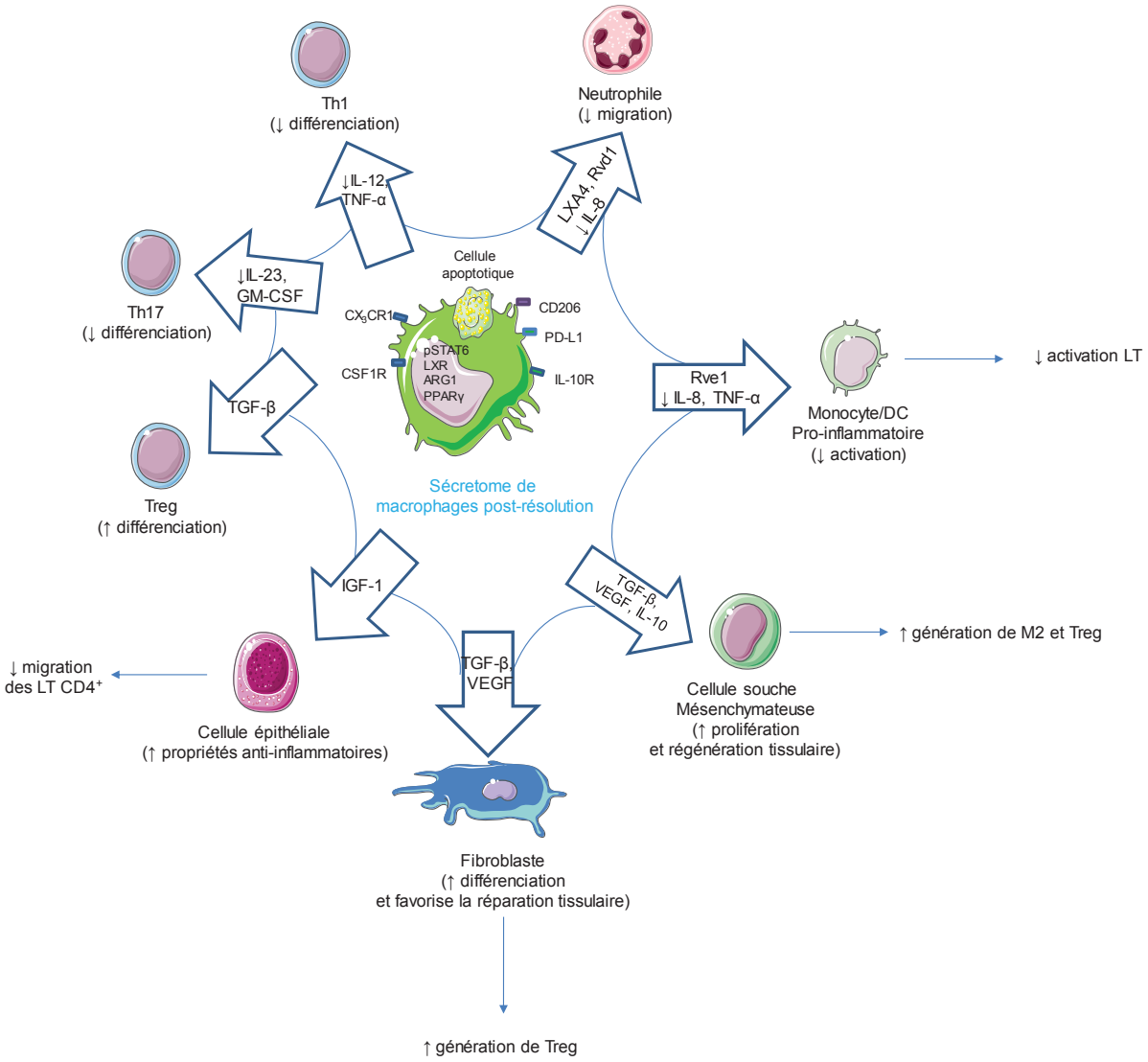

Figure 7. Effet direct et indirect de l'efferocytose sur les cellules du microenvironnement. La production de facteurs anti-inflammatoires (TGF-β, IL-10…) par les macrophages après efferocytose ainsi que la baisse de production de facteurs pro-inflammatoires (GM-CSF, IL12, IL23…) va permettre de modifier les cellules du microenvironnement tissulaire et notamment les cellules de l'immunité innée. En effet, sous l'effet de ce sécretome, les neutrophiles vont acquérir une capacité migratoire moindre alors que l'état d'activation des DC et macrophages sera diminué. Les cellules non immunes seront également modulées par ces macrophages pro-résolutifs. Les cellules souches mésenchymateuses développeront une capacité prolifératives accrue, les fibroblastes se différencieront en myofibroblastes et les cellules épithéliales vont développer un phénotype anti-inflammatoire. Tous ces changements vont alors favoriser la réparation et la régénération tissulaire. Enfin, les cellules de l'immunité adaptative sont également modulées par les macrophages de manière directe ou indirecte. La baisse de sécrétion de cytokines inflammatoires et l'augmentation de la sécrétion de TGF-β vont diminuer la différenciation des LT en Th1 et Th17 et favoriser l'émergence de Treg. De plus, les cellules épithéliales modulées par les macrophages vont moduler la migration des LT CD4+, les fibroblastes induire la génération de Treg et les cellules souches mésenchymateuses vont induire des macrophages anti-inflammatoires et des Treg. Enfin, les APC moduler par le sécretome des macrophages vont alors diminuer l'activation des LT. GM-CSF: Granulocyte-macrophage colony-stimulating factor. IGF-1: Insulin growth factor-1. IL: Interleukine. LXA4: Lipoxine A4. Rv: Résolvine. TGF-β: Transforming growth factor beta. TNF-α: Tumor necrosis factor alpha. VEGF: Vascular endothelial growth factor.

Bien que la mise en place de la réponse inflammatoire soit un mécanisme bénéfique afin de répondre à une agression, cette réponse inflammatoire doit demeurer aiguë et se résoudre d'elle-même. En cas de défaut de résolution de l'inflammation, la persistance de la réponse inflammatoire va favoriser le déclenchement de pathologies inflammatoires chroniques. Il a par exemple été montré que la capacité de phagocytose des macrophages lors de la périodontite (inflammation dentaire) est altérée et que le traitement de ces macrophages avec de la résolvine E1 restaure la phagocytose (Fredman, Oh et al. 2011). Un défaut de phagocytose similaire est observé chez les patients atteints de sclérose en plaques et diminue la capacité de remyélinisation par les oligodendrocytes (Natrajan, de la Fuente et al. 2015). Enfin, les taux de lipides pro-résolutifs sont diminués chez les patients atteints d'Alzheimer ou d'asthme démontrant que la résolution de l'inflammation est défaillante chez les patients atteints de maladies inflammatoires chroniques (Miyata, Fukunaga et al. 2013; Headland and Norling 2015).

Comme nous l'avons vu précédemment, l'inflammation est une réaction naturelle de l'organisme permettant au corps de lutter contre une agression. Cette réaction se résout généralement d'elle-même permettant le retour à l'homéostasie et la réparation tissulaire. Cependant, un défaut de résolution de l'inflammation peut mener au développement de maladies inflammatoires chroniques dont nous allons étudier maintenant l'exemple de la sclérose en plaques.

La sclérose en plaques, une pathologie auto-immune

I) Les maladies inflammatoires à médiation immune

Lors d'une inflammation non-résolue, à cause de facteurs environnementaux non favorables, de mutations génétiques ou encore à cause d'une infection persistante, la réaction inflammatoire peut perdurer et favoriser le développement de maladies auto-immunes inflammatoires chroniques. Environ 80 maladies auto-immunes sont actuellement recensées et constituent la troisième cause de mortalité/morbidité dans le monde, touchant 8% de la population dans les pays développés. Une forte prévalence est observée chez les femmes qui représentent 78% des personnes atteintes de maladie auto-immunes. Ces maladies sont distinguées en premier lieu par l'organe qu'elles affectent : la sclérose en plaques touche le système nerveux central (SNC), le psoriasis la peau, la polyarthrite rhumatoïde se développe au niveau des articulations et les maladies inflammatoires de l'intestin (MICI) affectent le tractus digestif. De plus, ces maladies diffèrent par leur développement. Dans le diabète de type 1 (qui affecte le pancréas), par exemple, d'importants dommages tissulaires sont observés avant le déclenchement de la maladie alors que dans la plupart des autres maladies auto-immunes ces dommages sont proches dans le temps (Cho and Feldman 2015). S'il existe une hétérogénéité importante entre les différents types de maladies auto-immunes, une hétérogénéité est également observée au sein d'une même pathologie. Si l'on prend l'exemple de la polyarthrite rhumatoïde, l'âge de déclenchement, le nombre d'articulations affectées et les complications multi-organes constituent des facteurs de variation interindividuelle (Klareskog, Catrina et al. 2009). Le déclenchement de ces maladies est multifactoriel et encore mal défini. Cependant, les facteurs génétiques ont un rôle certain dans certaines pathologies comme cela a été démontré récemment par différentes études de « *Genome-Wide Association Study* » (GWAS). Cependant, les facteurs génétiques ne suffisent pas à expliquer à eux seuls le développement de ces pathologies. Chez des jumeaux hétérozygotes, la concordance du taux de maladie est de 15% pour la polyarthrite rhumatoïde et de 30% pour le diabète de type 1, suggérant que d'autres facteurs sont mis en jeu (Bogdanos, Smyk et al. 2012). Les infections sont ainsi suspectées de participer au développement des maladies auto-immunes. Par exemple, les infections liées aux périodontites augmentent la susceptibilité à la polyarthrite rhumatoïde (Hajishengallis 2015). Le microbiote et sa dérégulation sont également au cœur du développement des maladies auto-immunes. Des modifications du microbiote dans différents modèles murins de maladies auto-immunes modulent la sévérité de la maladie *via* des modifications des réponses immunes (Mathis and Benoist 2011). Différents

modes d'actions peuvent expliquer les liens entre infections par un pathogène et auto-immunité. Les pathogènes peuvent exprimer certains antigènes possédant une structure proche de celle des antigènes du soi. Des LT ou B autoréactifs vont alors être activés et induire une réaction immunitaire ainsi que des dommages directs contre le tissu cible. Ce phénomène est appelé « mimétisme moléculaire » (Cusick, Libbey et al. 2012). De plus, si la réponse au pathogène persiste au sein du tissu affecté, des dommages tissulaires peuvent avoir lieu menant à la libération d'antigènes du soi qui seront alors pris en charges par les APC initiant une réponse auto-immune. Ce mécanisme est appelé « étalement d'épitope » (Vanderlugt and Miller 2002). Ensuite, une activation des cellules immunes de manière non spécifique par un pathogène peut également mener à activer d'autres cellules du système immunitaire et notamment des LT auto-réactifs. Ce processus est appelé « activation occasionelle » (Boyman 2010). Enfin, la présence persistante d'un pathogène au sein d'un tissu peut créer un environnement inflammatoire activant la production de protéases et le clivage d'antigènes sous-dominants. Ces antigènes sont appelés antigènes cryptiques et ne sont normalement pas reconnus par le système immunitaire. Leur clivage va permettre une présentation antigénique par les APC et à la mise en place d'une auto-immunité (Vanderlugt and Miller 2002).

Enfin, d'autres facteurs environnementaux sont impliqués dans la survenue de maladies auto-immunes tels que l'exposition à des polluants, le régime alimentaire ou une exposition aux ultraviolets (Vojdani 2014).

II) La sclérose en plaques (SEP)

II.1) Généralités

La SEP est une maladie auto-immune démyélinisante affectant le SNC (cerveau et moelle épinière [ME]). La première description de la SEP a été effectuée en 1838 par Robert Carswell qui la décrivit comme « une lésion remarquable de la moelle épinière accompagnée d'atrophie ». Elle est caractérisée par une infiltration des cellules immunes au sein du SNC suivie d'une inflammation et d'une perte des gaines de myéline qui entourent l'axone neuronal affectant ainsi la fonction de ce neurone. Cette maladie touche actuellement environ 3 millions de personnes dans le monde, principalement au sein des pays développés, avec une incidence supérieure chez les femmes. C'est une maladie du jeune adulte dont les premiers signes apparaissent généralement autour de 30 ans et qui provoque une paraplégie chez 50% des patients à 25 ans du diagnostic initial. Ces signes cliniques sont variés et incluent notamment la douleur, la fatigue, des vertiges, des faiblesses, une perte de fonction cognitive

et une perte des fonctions motrices (Compston and Coles 2008). Une hétérogénéité dans les formes de la maladie est cependant observée. Environ 80-85% des patients ont la forme la plus commune qui est la forme récurrente-rémittente (**Figure 8**). Elle est caractérisée par un premier épisode affectant un ou plusieurs sites du SNC (appelé syndrome clinique isolé) suivie par un cycle de phases de rémission et d'épisodes cliniques. Les épisodes de rechute sont marqués notamment par une inflammation et une démyélinisation discernable par IRM (imagerie à résonnance magnétique). Après cette phase récurrente-rémittente, 80% des patients développent une forme de la maladie appelée progressive secondaire (10 à 20 ans après le premier diagnostic) durant laquelle l'évolution est progressive et marquée par une atrophie du cerveau (et donc une perte de volume cérébral). Environ 10% des patients développent une SEP de type progressive primaire qui présente les même symptômes que ceux de la forme progressive secondaire (**Figure 8**) (Dendrou, Fugger et al. 2015). La moyenne de mortalité se situe autour de 30 ans après le début de la maladie ce qui représente 5 à 10 ans de diminution de la durée de vie (Bronnum-Hansen, Koch-Henriksen et al. 2004). Les patients atteints de SEP présentent également un plus grand risque de suicide et de dépression (Minden and Schiffer 1990). D'un point de vue pathologique, la sclérose en plaques est caractérisée par une démyélinisation au niveau de la matière blanche et grise du cerveau et de la ME. Ces aires démyélinisées appelées plaques ou lésions marquent la mort des oligodendrocytes et la disparition de la myéline qu'ils produisent. Avec la progression de la maladie, la perte de myéline va également aboutir à une perte de fonction axonale. L'inflammation est présente tout au long de la maladie mais de manière plus marquée dans les phases aiguës que chroniques. Lors des premiers signes de la maladie, l'infiltrat est constitué principalement de macrophages et de lymphocytes T CD8. L'infiltration des cellules immunitaires est permise par une étanchéité accrue de la barrière hémato-encéphalique (BHE) qui fait du SNC un organe de privilège immun en conditions physiologiques. Au sein des lésions de stades plus avancés, un fort infiltrat de lymphocytes T et B est observé ainsi qu'une activation de la microglie et des astrocytes (Dendrou, Fugger et al. 2015).

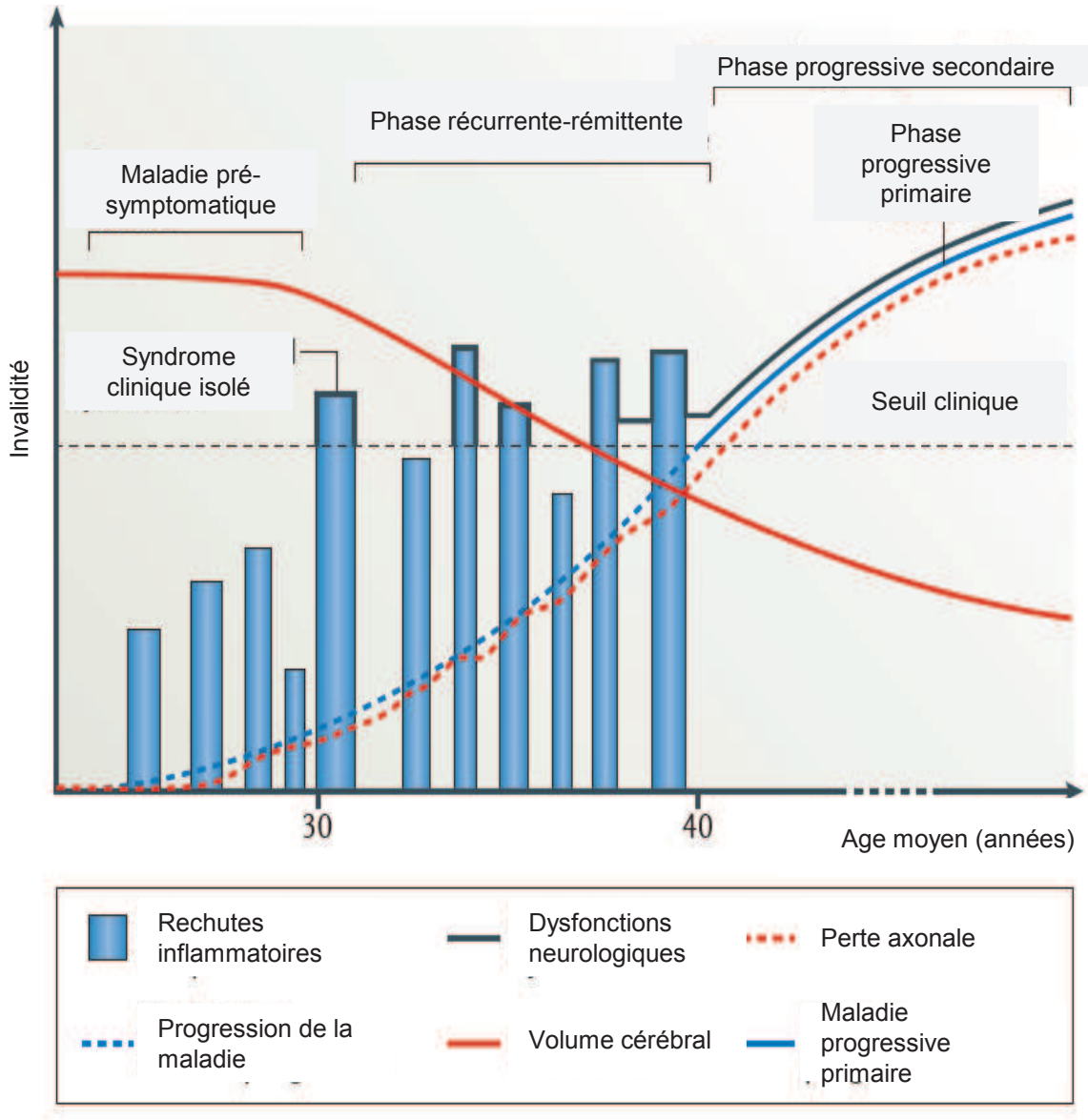

Figure 8. Course clinique de la SEP. Le développement de la maladie est variable suivant les individus. La majorité des personnes atteintes de SEP développent des syndromes cliniques isolés marqués par des épisodes d'affections neurologiques puis des phases de rémission de la maladie. Cette phase est appelée récurrente-rémittente. Elle est généralement suivie d'une phase progressive secondaire marquée par un déclin neurologique progressif. Cependant, une faible proportion de patients (environ 15%) développe directement une phase progressive appelée alors progressive primaire. D'après (Dendrou, Fugger et al. 2015).

II.2) Causes de la SEP

Les causes de déclenchement de la SEP sont encore mal connues mais semblent reposer sur des facteurs génétiques et environnementaux. En effet, cette maladie se développe principalement chez des individus génétiquement susceptibles. La SEP présente notamment un taux de récurrence familial de 20 %. Des études au Canada et aux Etats-Unis ont notamment montré que la concordance clinique était de 25% chez des jumeaux homozygotes (Compston and Coles 2008). Les GWAS ont mis en évidence une centaine de gènes associés au déclenchement de la SEP dont la majorité est impliquée dans la régulation des réponses

immunes. Parmi les gènes mis en cause on note l'IL-2, les interférons (IFN), le récepteur TNFR1 (*tumor necrosis factor receptor 1*), la voie NFκB, l'IL7R ou encore les protéines HLA (Dendrou, Fugger et al. 2015). L'implication de mutations dans les gènes de l'immunité est un caractère commun dans le déclenchement des maladies auto-immunes. Néanmoins, le rôle spécifique de chaque modification génique peut engendrer des effets inverses en fonction de la pathologie. Ainsi, une mutation dans le gène TNFR1 confère une susceptibilité pour la sclérose en plaques mais une résistance à la spondylarthrite, expliquant au moins pour partie les effets positifs des médicaments ciblant la voie du TNFR1 sur la spondylarthrite ankylosante mais délétères sur la SEP (Sawcer, Hellenthal et al. 2011; Gregory, Dendrou et al. 2012).

Cependant, si les facteurs génétiques jouent un rôle certain dans le déclenchement de la SEP, ils ne semblent impliqués que pour 30% dans sa survenue. La survenue de la SEP semble donc liée également à d'autres facteurs comme les facteurs environnementaux. La première catégorie des facteurs environnementaux est composée de facteurs non-infectieux tels que la vitamine D, la cigarette ou encore des modifications du cycle circadien. Des études ont montré une augmentation des taux de SEP dans les pays les plus éloignés de l'équateur, ce qui corrèle inversement avec leur durée d'ensoleillement. Cependant, des populations vivant à des hautes latitudes, mais ayant une forte consommation en vitamines D, voient leur taux de SEP réduit (Westlund 1970; Kurtzke, Beebe et al. 1979). La cigarette est également impliquée dans une exacerbation des réponses immunes et est associée à un risque accru de SEP (Handel, Williamson et al. 2011). De plus, la consommation de cigarettes favorise la mutation de deux gènes, HLA-DRB1 muté en position 15 (HLADRB1*15) et HLA-A muté en position 2 (HLA-A*02) induisant sa non expression, deux gènes considérés comme facteurs de risque de la SEP (Hedstrom, Sundqvist et al. 2011). Enfin, des modifications du rythme circadien peuvent également être en partie responsables du développement de la SEP. En effet, le travail nocturne ou partiellement nocturne favorise l'apparition de SEP chez les sujets de moins de 20 ans en comparaison du travail diurne (Hedstrom, Akerstedt et al. 2011). De plus, un article récent a montré que chez la souris, le rythme circadien modifiait la localisation des LT notamment au niveau des ganglions et que ces changements étaient liés à des variations de la maladie dans un modèle murin de SEP (Druzd, Matveeva et al. 2017).

La deuxième catégorie de facteurs environnementaux sont les facteurs infectieux et notamment les infections virales. Le premier d'entre eux et le plus étudié est le virus d'Epstein-Barr (EBV). Des études épidémiologiques ont montrées que 99,5% des patients

atteints de SEP sont séropositifs pour l'EBV contre 94,2% pour la population totale. De manière encore plus marquante, dans les cas de SEP pédiatrique, 83% des enfants atteints de SEP sont séropositifs pour l'EBV contre 42% pour la population générale (Alotaibi, Kennedy et al. 2004; Goodin 2009). D'autres virus tels que l'*Human herpesvirus-6*, le *Varicella-zoster virus* ou encore le *Torque teno virus* pourraient avoir un rôle dans le déclenchement de la SEP mais leur rôle n'est pas certain et peu défini (Kakalacheva and Lunemann 2011). En plus des virus, le microbiote joue également un rôle fondamental dans le développement de la SEP. Si le rôle exact du microbiote dans la SEP est encore peu étudié, une étude récente a notamment démontré que le microbiote des patients atteints de SEP était modifié tant d'un point de vue des espèces présentes que d'un point de vue fonctionnel (Chen, Chia et al. 2016). Chez la souris, l'absence de microbiote prévient totalement le déclenchement de la maladie (Berer, Mues et al. 2011). De plus, l'administration d'antibiotiques diminue le déclenchement de la maladie dans un modèle murin de SEP appelé EAE (encéphalomyélite auto-immune expérimentale) notamment en modifiant la balance Treg-Th17 (Yokote, Miyake et al. 2008; Ochoa-Reparaz, Mielcarz et al. 2009).

II.3) Pathophysiologie de la SEP

Le SNC a longtemps été considérée comme un organe de privilège immun, donc à l'abri de la réponse immunitaire. Si le SNC est effectivement particulier, il peut être le lieu d'une réponse inflammatoire. Les premières cellules impliquées dans les réponses inflammatoires au sein du SNC sont la microglie et les astrocytes. Les cellules microgliales sont des cellules de l'immunité innée capable de phagocytose, de présenter l'antigène et de sécréter des facteurs cytotoxiques. Les astrocytes sont eux impliqués dans le formation des neurones et leur soutien mais peuvent également induire des réponses inflammatoires *via* la sécrétion de facteurs cytotoxiques et de cytokines inflammatoires (Becher, Spath et al. 2017). Ces deux types cellulaires seront les premiers à s'activer de manière chronique lors de l'inflammation au sein du SNC. La sécrétion des cytokines et chemokines inflammatoires va ensuite permettre d'induire l'expression de molécules d'adhésion au sein du SNC mais également d'activer les cellules immunes en périphérie et de favoriser leur recrutement au sein du SNC. L'infiltration immunitaire au sein du SNC va alors permettre la mise en place de réponses inflammatoires persistantes et induire une dégradation tissulaire (Lucas, Rothwell et al. 2006). Le développement d'une réponse inflammatoire au sein du SNC est donc différent de celle observée dans d'autres organes périphériques et la capacité d'infiltration des leucocytes est un

facteur clé dans le développement de l'inflammation au sein du SNC. Nous allons maintenant détailler le déroulement de la réponse inflammatoire au cours de la SEP.

II.3.1) Les lymphocytes T

Les lymphocytes T $CD4^+$ initient et régulent les réponses immunes adaptatives liées aux infections et au cancer et jouent également un rôle prépondérant dans le développement des allergies et des maladies auto-immunes. Depuis les années 1980, les LT $CD4^+$ ont été classifiés selon leur profil cytokinique (Mosmann, Cherwinski et al. 1986). Les principaux sous-types de T $CD4^+$ ainsi que leurs caractéristiques sont détaillées dans la **figure 8**.

La principale hypothèse de déclenchement de la SEP suggère une activation périphérique des lympthocytes T spécifiques de la myéline qui une fois activés entrent ensuite au niveau du SNC où ils sont réactivés par des cellules présentatrices de l'antigène (APC) (Dendrou, Fugger et al. 2015) (**Figure 9** et **10**). L'activation en périphérie des lymphocytes T implique la présence de protéines dérivées de la myéline, bien que supposées produites strictement au niveau du SNC par les oligodendrocytes. Cependant, certaines observations suggèrent que des protéines telles que la *myelin binding protein* (MBP) ou la protéine protéolipide (PLP) sont constitutivement présentes au niveau systémique. En effet, des souris exprimant un TCR transgénique spécifique de MBP ou PLP développent une EAE spontanée après une activation lymphocytaire au niveau des ganglions cervicaux (Furtado, Marcondes et al. 2008; Zhang, Podojil et al. 2008). L'autre hypothèse majeure pouvant expliquer la survenue de la SEP suggère que le premier évènement inflammatoire est une dégénérescence des oligodendrocytes (Stys, Zamponi et al. 2012). Cette hypothèse est basée sur l'observation du fait que la perte des oligodendrocytes et de la myéline se déroule avant d'observer une inflammation au sein du cerveau de patients atteints de SEP (Seewann, Vrenken et al. 2009). De plus, chez le souris, l'induction de la mort des oligodendrocytes et la subséquente démyélinisation sont des évènements suffisants afin d'induire une infiltration des LT au sein du SNC et une inflammation (Traka, Podojil et al. 2016). Dans ce modèle, l'activation de la microglie, suite à la démyélinisation, permet alors la prise en charge des antigènes myéliniques par les cellules dendritiques qui migrent alors au niveau des organes lymphoïdes périphériques afin d'induire l'activation de LT pathogéniques (Hemmer, Kerschensteiner et al. 2015). Une fois activés, les lymphocytes T vont entrer au sein du SNC par la barrière entre le liquide cérébro-spinal et le sang au niveau de l'espace subarachnoïdien, par cette même barrière au niveau du plexus choroïde et par la BHE au niveau de l'espace périvasculaire (Ransohoff, Kivisakk et al. 2003). Une fois au sein du SNC, les lymphocytes T vont être

réactivés par les APC et notamment les cellules dendritiques (DC) présentant des peptides issus de la myéline. Les lymphocytes T pathogéniques ainsi générés induisent alors une dégradation des gaines de myéline (Bailey, Schreiner et al. 2007).

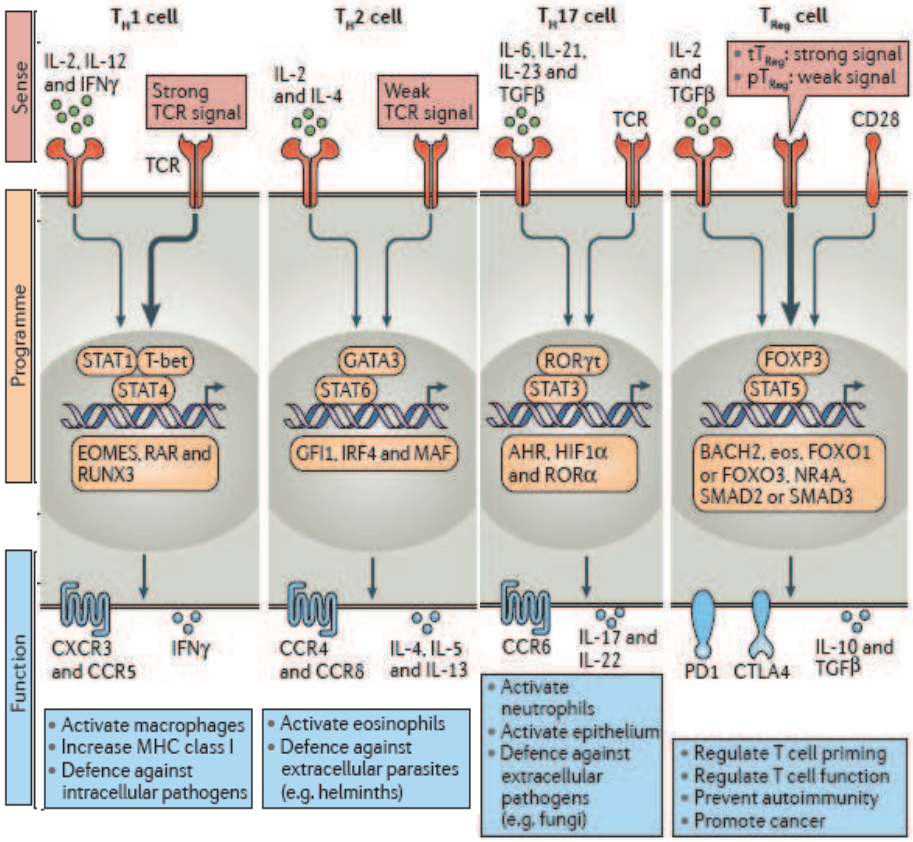

Figure 9. Principaux sous-types de T CD4$^+$. La différenciation en Th1 se fait sous l'action de l'IL-12 et du TNF-α ainsi qu'un fort signal provenant du TCR. Ces signaux activent alors différents facteurs de transcription et notamment le facteur T-bet. Les Th1 sont caractérisés par leur expression des récepteurs CCR5 et CXCR3 ainsi que de la production d'IFN-γ et sont impliqués dans les réponses anti-cancéreuses, la défense contre les pathogènes mais également le développement des maladies auto-immunes. Les Th2 sont générés par la présence d'IL-4 et un faible signal du TCR ce qui aboutira à l'activation des facteurs de transcription GATA3 et STAT6. Ils sont caractérisés par l'expression des récepteurs CCR4, CCR8 et la production d'IL-4, 5 et 13. Ils sont impliqués dans les réponses antiparasitaires et les allergies. La différenciation en Th17 est contrôlée par les cytokines IL-6, IL-21, IL-23 et TGF-β. Le facteur de transcription clé des Th17 est le facteur RORγt qui va permettre l'expression du récepteur CCR6 et des cytokines IL-17 et IL-22. Les Th17 sont impliqués dans les réponses contre les pathogènes, la réparation tissulaire mais également dans les maladies auto-immunes. Enfin, les Treg sont générés sous l'action du TGF-β et le facteur de transcription Foxp3 est essentiel à leur développement. Ils expriment à leur surface les molécules PD-1 et CTLA-4 et sécrètent principalement de l'IL-10 et du TGF-β. Ils sont impliqués dans la régulation des réponses T effectrices et s'ils favorisent la survenue de cancers, ils diminuent le risque de maladies inflammatoires. AHR: *aryl hydrocarbon receptor*. BACH2: *basic leucine zipper transcription factor 2*. CTLA4: *cytotoxic T lymphocyte antigen* 4. EOMES: *eomesodermin*. FOXO: *forkhead box O*. GATA3: *GATA-binding protein 3*. HIF1α: *hypoxia-inducible factor 1α*. IRF4: *interferon-regulatory factor 4*. MAF: *macrophage-activating factor*. NR4A: *nuclear receptor 4A*. PD1: *programmed cell death 1*. pTReg cell*: peripherally derived regulatory T cell*. RAR: *retinoic acid receptor*. ROR: *retinoic acid receptor-related orphan receptor*. RUNX3: *runt-related transcription factor 3*. TCR: *T cell receptor*. SMAD: *SMA and MAD related protein*. tTReg cell: *thymus-derived regulatory T cell*. D'après (DuPage and Bluestone 2016).

Les premières cellules T $CD4^+$ ayant été démontrées comme impliquées dans la SEP sont les Th1. En effet, des observations basées sur le modèle d'EAE ont montré que les LT infiltrant le SNC étaient principalement des cellules productrices d'IFN-γ ainsi que d'IL12p40 (Segal and Shevach 1996). De plus, le transfert de Th1 dans des souris naïves est suffisant pour induire l'EAE (Baron, Madri et al. 1993). Enfin, chez les patients atteints de SEP, l'expression d'IFN-γ et d'IL-12 est corrélée avec l'activité clinique et l'administration d'IFN-γ augmente les signes cliniques (Panitch, Hirsch et al. 1987; Gutcher and Becher 2007). Cependant, des observations plus récentes remettent en cause l'axe Th1 dans la SEP. Premièrement, des souris déficientes en IFN-γ, IL-12 ou TNF-α sont capables de développer une EAE après immunisation (Steinman 2007). Par ailleurs, des souris déficientes en IL-23, une molécule nécessaire pour le développement des Th17, sont totalement résistantes à l'induction d'EAE (Cua, Sherlock et al. 2003). De plus, le transfert de Th17 induit une pathologie plus sévère que le transfert de Th1 et la neutralisation de l'IL-17 par un anticorps améliore les signes de la maladie, suggérant l'implication de cette population dans la SEP (Hofstetter, Ibrahim et al. 2005; Langrish, Chen et al. 2005). Cependant, des souris déficientes en IL-17a et IL-17f sont toujours susceptibles de déclencher une EAE (Haak, Croxford et al. 2009). Toutes ces données montrent que le déclenchement de la SEP ne peut pas être attribué uniquement à un de ces deux types cellulaires mais serait plutôt une combinaison d'effets. Une des molécules clés dans le déclenchement de la SEP pourrait être le GM-CSF. En effet, ce facteur pro-inflammatoire est nécessaire pour le déclenchement de l'EAE (Croxford, Spath et al. 2015). De plus, cette cytokine est nécessaire et suffisante pour l'acquisition d'un profil encéphalitogénique par les LT $CD4^+$ et ce de manière plus marquée que la sécrétion d'IFN-γ ou d'IL-17 (Codarri, Gyulveszi et al. 2011). Les Th1 et Th17 déficients en GM-CSF sont par ailleurs incapables de déclencher l'EAE malgré leur capacité à infiltrer le SNC (El-Behi, Ciric et al. 2011). Enfin, la présence de GM-CSF est accrue dans le liquide cérébro-spinal de patients atteints de SEP démontrant que le marqueur de polarisation des LT clé dans la SEP pourrait être le GM-CSF, plus que l'IL-17 ou l'IFN-γ (Carrieri, Provitera et al. 1998).

Le déclenchement de la SEP est également associé à une défaillance des Treg qui pourrait permettre l'émergence de lymphocytes T auto-réactifs. En effet, les Treg issus des PBMC de patients atteints de SEP ont une fonction suppressive et un phénotype altérés (Venken, Hellings et al. 2008). De plus, certains sous-types de Treg spécifiques tels que les Treg $CD39^+$, qui contrôlent les réponses Th17 voient leur pourcentage et leur phénotype altérés (Fletcher, Lonergan et al. 2009). Les déficiences des Treg peuvent notamment être attribuées

à une diminution de la fréquence de Treg naïfs circulants provenant du thymus, ce qui induit une expansion des Treg mémoires non effective (Venken, Hellings et al. 2008). De plus, ces Treg pourraient également changer de phénotype pour devenir des Th1-*like* qui sécrètent de l'IFN-γ (Fletcher, Lonergan et al. 2009).

Enfin, le rôle des lymphocytes T $CD8^+$ dans la SEP est souligné par la présence de cette population au niveau des lésions démyélinisées de patients ainsi que celle de leurs granules cytotoxiques au niveau des oligodendrocytes et axones des neurones. Ainsi, des lymphocytes T $CD8^+$ de patients atteints de SEP spécifiques de la MBP sont capables de lyser des oligodendrocytes en culture (Friese and Fugger 2005; Goverman, Perchellet et al. 2005). De plus, ces lymphocytes T ont la capacité de sécréter de l'IFN-γ et du TNF-α ainsi que d'acquérir une activité cytotoxique (Zang, Li et al. 2004). Au niveau des lésions de patients atteints de SEP, les $CD8^+$ produisent de l'IL-17 dans plus de 70% des cas et ce de manière équivalente à celle des lymphocytes T $CD4^+$ suggérant un rôle pathogénique de cette population lymphocytaire (Tzartos, Friese et al. 2008). Chez la souris, des lymphocytes T $CD8^+$ stimulés avec le peptide MOG (*myelin oligodendrocyte glycoprotein*) sont capables d'induire la maladie lorsqu'ils sont transférés à des animaux naïfs (Ford and Evavold 2005).

II.3.2) Les cellules dendritiques

Les DC se subdivisent en deux grands groupes : les DC conventionnelles (cDC) et les DC plasmacytoïdes (pDC). Les cDC expriment le marqueur CD11c ainsi que le CMH-II et sont divisées en deux sous-types basés sur l'expression du CD8α chez la souris et du CD1c et CD141 chez l'Homme (Xie, Zhang et al. 2015). Les cDC $CD8\alpha^+$ chez la souris et $CD141c^+$ chez l'Homme présentent les antigènes exogènes et induisent des réponses Th1 *in vitro* tandis que les cDC $CD8^-$ et CD1c induisent des réponses Th2 *in vitro* et semblent être impliquées dans des phénomènes de tolérance (Maldonado-Lopez, De Smedt et al. 1999; Kassianos, Hardy et al. 2012; Xie, Zhang et al. 2015).

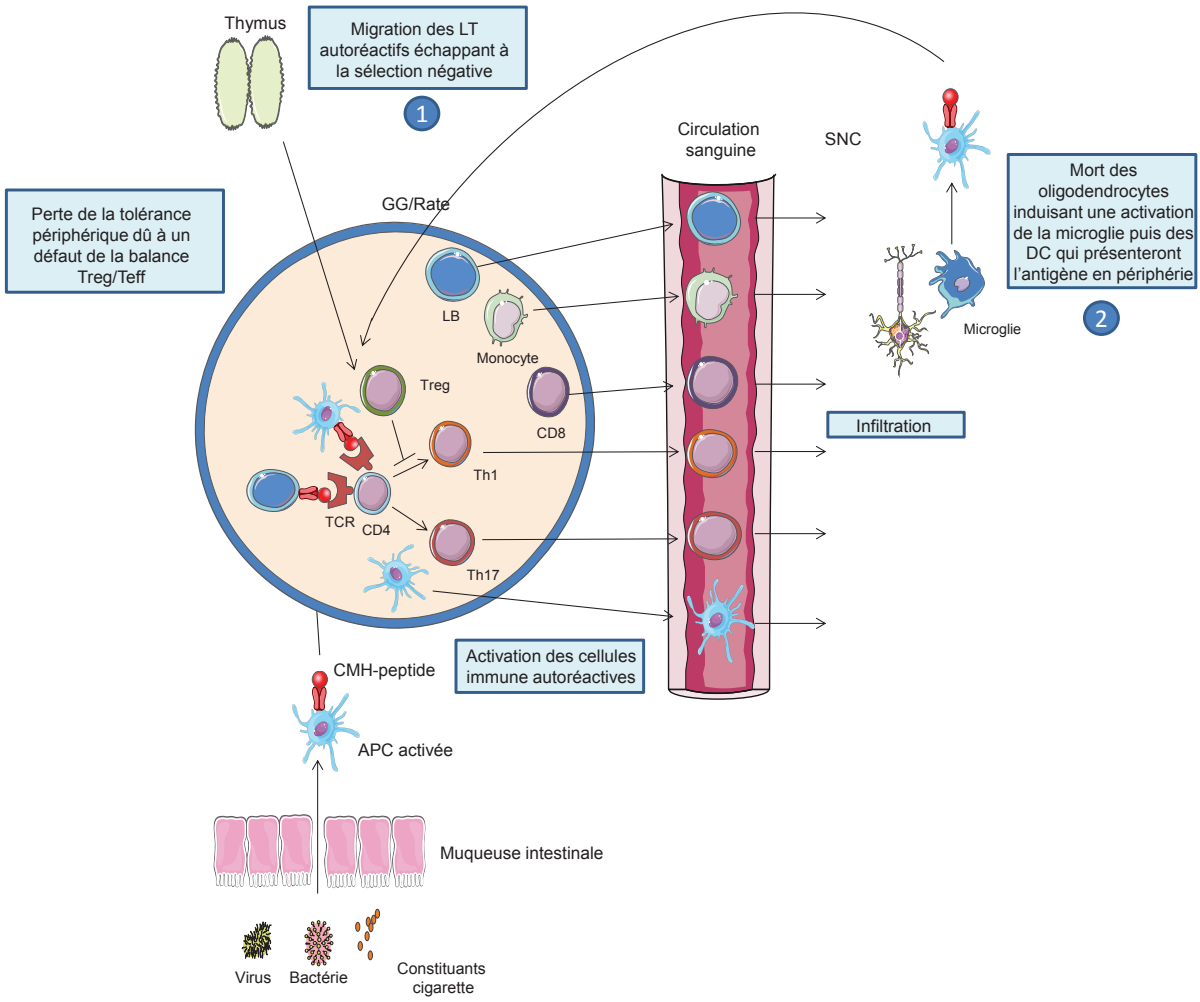

Figure 10. Dérégulation du système immunitaire en périphérie lors de la SEP. Deux hypothèses peuvent expliquer la survenue de la SEP : (1) Au cours de la sélection négative au sein du thymus, certains LT auto-réactifs peuvent échapper à cette sélection et être relargués en périphérie ; (2) Une mort des oligodendrocytes induit une démyélinisation et une activation de la microglie au sein du SNC. Les DC vont alors être activées et vont migrer en périphérie afin de présenter les antigènes myéliniques et d'activer les LT. Chez un individu sain, des mécanismes de tolérance périphérique limitent l'action pathogénique de ces cellules. Cependant, une modification de la balance entre cellules effectrices et régulatrices (notamment au niveau des LT) va permettre l'activation des LT spécifiques de la myéline par une présentation antigénique. Une fois activés, ils vont se différencier, principalement en Th1 et Th17, et migrer au sein du SNC en compagnie des LB et des cellules de l'immunité innée. Des facteurs environnementaux tels que la cigarette, une infection virale ou une modification du microbiote intestinal peuvent également favoriser ces événements. APC: Cellule présentatrice d'antigène. CMH: Complexe majeur d'histocompatibilité. GG: Ganglions. SNC: Système nerveux central. Modifié d'après (Dendrou, Fugger et al. 2015).

Les cDC sont présentes au niveau du SNC sain notamment au sein du plexus choroïde, du parenchyme et des méninges, suggérant un rôle de surveillance immunitaire (Pashenkov and Link 2002). Cependant, elles s'accumulent de manière importante au sein du SNC de patients atteints de SEP (Serafini, Rosicarelli et al. 2006) et présentent un profil pro-inflammatoire avec une augmentation de l'expression des marqueurs de co-stimulation (CD80, CD40), des cytokines pro-inflammatoires (TNF-α, IL-12) et induisent des polarisations de type Th1

également plus de cytokines inflammatoires (Huang, Xiao et al. 1999). Dans le modèle d'EAE, les cDC peuvent induire des Th1 et Th17 au niveau des organes lymphoïdes périphériques et notamment des ganglions (Diebold 2008). Durant le développement de la maladie, les cDC sont suffisantes pour présenter les antigènes et induire la génération de (**Figure 9** et **10**) (Karni, Abraham et al. 2006). De plus, les cDC circulantes produisent lymphocytes T spécifiques de la myéline et l'inflammation au sein du SNC (Greter, Heppner et al. 2005; McMahon, Bailey et al. 2005; Bailey, Schreiner et al. 2007). Cependant, une étude récente a démontré que la présence de cDC n'était pas nécessaire pour l'induction d'EAE et que leur déplétion augmentait le score clinique montrant un rôle régulateur des DC. Cette induction de tolérance passerait par l'induction de Treg *via* un axe PD-1/PD-L1 (Yogev, Frommer et al. 2012).

Les pDC représentent une population cellulaire rare dérivée de la moelle osseuse (0,3 à 0,5 % des PBMC) et qui possède un progéniteur commun avec les cDC exprimant Flt3 (*fms-like tyrosine kinase 3*), CD115 et CD117 (Naik, Sathe et al. 2007). Le développement des pDC requiert l'expression du facteur de transcription E2-2 permettant ainsi l'expression de gènes impliqués dans les fonctions vitales des pDC tels que BDCA2 (*blood dendritic cell antigen 2*), ILT-7 (*immunoglobulin-like transcript 7*) et IRF7 (Cisse, Caton et al. 2008). Les pDC sont les principales cellules responsables de la production d'interférons de type 1 en réponse à une infection virale mais également des cytokines pro-inflammatoires telles que le TNF-α ou l'IL-6 (Liu 2005; O'Keeffe, Grumont et al. 2005). Les médiateurs produits par les pDC semblant exacerber la pathologie, le rôle de cette population a récemment été étudié dans la SEP. En premier lieu, les pDC sont présentes au sein du liquide cérébro-spinal, des leptoméninges et des lésions démyélinisées de patients atteints de SEP (Lande, Gafa et al. 2008). De plus, leur concentration est augmentée durant les phases de rechute (Longhini, von Glehn et al. 2011). Leur phénotype est également modifié au cours de la maladie. En effet, l'expression de la molécule de co-stimulation CD86 est altérée sur les pDC de patients atteints de SEP ainsi que leur capacité à induire des Treg (Stasiolek, Bayas et al. 2006). De plus, une étude récente a montré que plus de 1200 gènes étaient modifiés dans les pDC au cours de la SEP et notamment des gènes impliqués dans la régulation des réponses immunes (Aung, Brooks et al. 2012). Chez la souris, leur rôle est plus controversé et semble dépendant des phases de la maladie. En effet, la déplétion des pDC au jour de l'immunisation diminue le score clinique mais leur déplétion au pic de la maladie exacerbe les symptômes (Bailey-Bucktrout, Caulkins et al. 2008; Isaksson, Ardesjo et al. 2009). Lors du développement de la maladie, les pDC

augmentent les réponses Th1 et Th17 au niveau du SNC et de la rate et diminuent la génération de Treg (Isaksson, Ardesjo et al. 2009). Cependant, l'injection de pDC au cours de la maladie permet de diminuer les réponses Th1 et Th17 ainsi que le score clinique notamment *via* le recrutement de ces pDC au niveau du SNC par un axe chemerine-CMKLR1 (*chemokine like receptor 1*) (Duraes, Lippens et al. 2016). De plus, des souris dont les pDC sont déficientes pour le CMH-II développent une maladie plus forte notamment à cause d'un déficit d'expansion des Treg démontrant un rôle duel des pDC au cours de la SEP (Irla, Kupfer et al. 2010).

II.3.3) Les macrophages/microglie

Les macrophages ont un rôle de « patrouilleurs » au sein du SNC en conditions non pathologiques. Ils sont responsables de la surveillance immunologique du SNC mais jouent également un rôle dans la production des neurones, leur clairance ainsi que la clairance des débris cellulaires. Cependant, une rupture de l'homéostasie au niveau du SNC peut mener à un recrutement de monocytes issus du sang (Bogie, Stinissen et al. 2014). Chez des patients atteints de SEP, les macrophages issus de la moelle osseuse (MO) sont abondamment présents au sein des lésions démyélinisées actives (Trebst, Sorensen et al. 2001). De plus, ils présentent un phénotype activé et notamment une sécrétion de cytokines inflammatoires, de médiateurs toxiques et une augmentation de l'expression des marqueurs de maturation (**Figure 10**) (Kouwenhoven, Teleshova et al. 2001; Hendriks, Teunissen et al. 2005). Si chez l'Homme le rôle des monocytes/macrophages est encore relativement peu décrit, plusieurs études s'y sont consacrées dans le modèle d'EAE. Dans les phases d'induction et de pic, une infiltration massive de macrophages au niveau du SNC est observée notamment au niveau des méninges, du plexus choroïde et de l'espace périvasculaire et ce nombre est diminué durant la phase de résolution de l'inflammation (Ousman and Kubes 2012). Cette augmentation de recrutement des macrophages est notamment liée à une augmentation de production des chémokines CCL2, 3, 4 et 22 au niveau du SNC. Par ailleurs, un blocage de certaines de ces chémokines ou des récepteurs associés diminue la sévérité de la pathologie (Jiang, Jiang et al. 2014). De plus, la déplétion des macrophages chez le rat comme chez la souris atténue fortement la pathologie, démontrant un rôle pathogénique des macrophages dans le déclenchement de la maladie (Huitinga, van Rooijen et al. 1990; Yang, Zheng et al. 2016). De nombreuses études ont démontré que les macrophages exprimant Ly6c de manière forte s'accumulaient dans le sang et infiltraient le SNC de manière dépendante de CCR2 au pic de la maladie (King, Dickendesher et al. 2009; Mildner, Mack et al. 2009; Ajami, Bennett et al.

2011). Ces macrophages présentent une forte expression du CMH-II et du CD11c et le blocage de l'infiltration de ces cellules diminue fortement la pathologie (King, Dickendesher et al. 2009; Ajami, Bennett et al. 2011). Les macrophages, lors de l'EAE, ont donc un profil pro-inflammatoire caractérisé par une sécrétion accrue de TNF-α, IFN-γ, IL-12, IL-6 ou encore de NO et la balance M1/M2 est altérée. Ainsi, de nombreuses études ont montré que rétablir cette balance pouvait être une cible thérapeutique importante dans le traitement de la SEP (Weber, Prod'homme et al. 2007; Mikita, Dubourdieu-Cassagno et al. 2011; Jiang, Milovanovic et al. 2012; Liu, Li et al. 2013).

La microglie est un type cellulaire provenant de la lignée myéloïde, résidant au niveau du parenchyme dans le SNC et jouant un rôle dans la maintenance de son homéostasie. Le rôle joué par la microglie chez les patients atteints de SEP ou dans le modèle d'EAE est encore débattu (Rawji and Yong 2013). La microglie est activée au niveau des lésions et présente une forte expression du CMH-II, des molécules de co-activation, des cytokines inflammatoires et des médiateurs neurotoxiques chez l'Homme et dans le modèle d'EAE (**Figure 10**) (Bogie, Stinissen et al. 2014). L'activation de la microglie dans le modèle d'EAE précède le développement de la maladie et l'inhibition de son activation permet de diminuer l'inflammation au niveau du SNC en altérant la polarisation Th1 (Ponomarev, Shriver et al. 2005; Bhasin, Wu et al. 2007). Cependant, la microglie pourrait également jouer un rôle bénéfique et neuro-protecteur. En effet, la stimulation de l'activation de la microglie avant et au début de la maladie diminue la pathologie et favorise le recouvrement des déficits neurologiques (Bhasin, Wu et al. 2007).

II.3.4) Rôle de la barrière hémato-encéphalique

La barrière hémato-encéphalique (BHE) est une barrière membraneuse qui sépare le SNC du compartiment sanguin. Elle est constituée principalement de cellules endothéliales liées entre elles par des jonctions serrées (formées notamment des protéines *tight junction protein 1* (TJP1), occludine, claudine 5 et *F11 receptor* (F11R)) ainsi que par des astrocytes. Cette barrière joue un rôle important dans le maintien de l'homéostasie du SNC notamment en empêchant l'entrée des xénobiotiques, métabolites toxiques et des cellules immunes (Ortiz, Pacheco-Moises et al. 2014). Une perméabilité accrue de cette barrière est observée chez les patients atteints de SEP sous l'action de cytokines pro-inflammatoires telles que l'IL-17 ou l'IL-22 (Kebir, Kreymborg et al. 2007; Cramer, Simonsen et al. 2014). Dans le modèle d'EAE, une perméabilité de la BHE est observée deux jours avant le début des signes cliniques et semble liée à l'injection de toxine pertussique qui favoriserait l'adhésion et la

migration leucocytaire au sein du SNC (Aube, Levesque et al. 2014). Enfin, l'importance de la perte d'intégrité de la BHE dans la physiopathologie de la SEP est appuyée par l'effet d'un anticorps dirigé contre l'intégrine α4-β1 dans le modèle d'EAE : ce dernier bloque l'accumulation de leucocytes au sein du SNC et prévient la maladie (Yednock, Cannon et al. 1992). Le traitement de patients atteints de SEP par cet anticorps semble prévenir les phases de rechute, les activités lésionnelles et la progression de la maladie (Pucci, Giuliani et al. 2011).

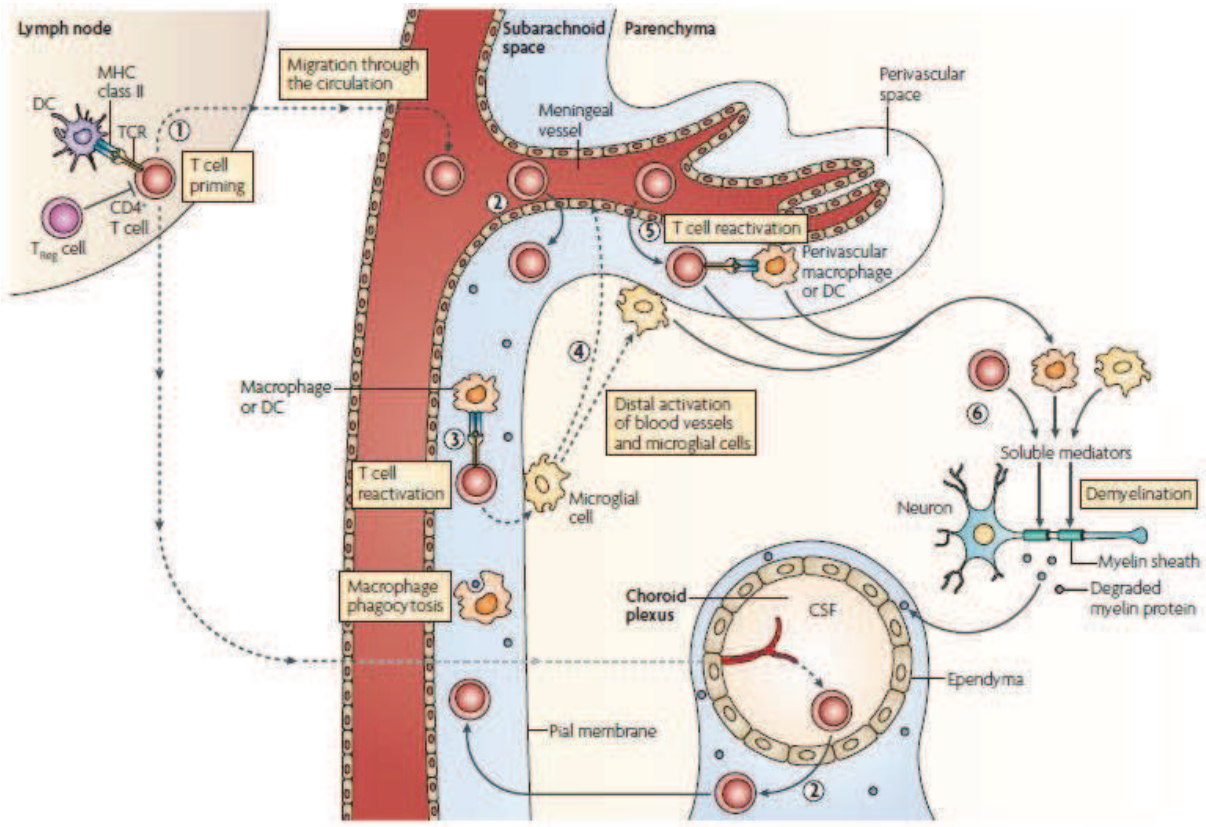

Figure 11. Mécanismes inflammatoires au niveau du SNC lors de la SEP. Une fois les LT activés en périphérie (1) ils entrent au sein du SNC en franchissant la barrière séparant le sang du liquide cérébrospinal au niveau du plexus choroïde ou des méninges (2). Les LT sont alors réactivés par les cellules présentatrices de l'antigène (DC, macrophages, pDC) qui expriment des épitopes myéliniques (3 et 5). Les LT activés vont à leur tour activer les cellules microgliales ainsi que les cellules endothéliales et migrer au sein du SNC en franchissant la BHE perméabilisée (4). Au sein du SNC, les LT, en coopération avec les cellules présentatrices de l'antigène et les LB, vont sécréter des médiateurs solubles induisant la démyélinisation (6). D'après (Goverman 2009).

II.4) Traitements actuels

Actuellement, il n'existe pas de thérapie curative de la SEP, les traitements disponibles permettent uniquement de prévenir ou de retarder la survenue de la phase progressive. Ces approches reposent principalement sur des activités anti-inflammatoires. Les traitements se divisent en deux grandes catégories : les traitements de première ligne qui sont des immuno-modulateurs bien tolérés par les patients mais montrant une efficacité limitée ; les traitements

de seconde ligne qui sont beaucoup plus efficaces mais provoquant d'importants effets secondaires (Michel, Larochelle et al. 2015).

Les traitements de première ligne sont notamment composés de l'IFN-β et de l'acétate de glatiramère. L'IFN-β est une protéine glycosylée de 166 acides aminés qui appartient à la famille des interférons de type I. Le mécanisme d'action exact de l'IFN-β dans le traitement de la SEP n'est pas encore totalement élucidé, cependant il semble exercer un effet majeur sur les lymphocytes T. Il diminue notamment la différenciation des lymphocytes T en Th17 ainsi que leur sécrétion d'IL-17 (Guo, Chang et al. 2008). Il impacte également la capacité des lymphocytes T à adhérer et à migrer à travers la BHE en diminuant leur expression de MMP9 (Stuve, Dooley et al. 1996). En plus de son effet direct sur les lymphocytes T, il diminue la capacité des APC à présenter l'antigène et augmente leur capacité à produire des cytokines anti-inflammatoires telles que l'IL-10 et le TGF-β induisant une génération accrue des lymphocytes T et B régulateurs (Stuart 2004; Meinl, Krumbholz et al. 2006; Guo, Chang et al. 2008). L'acétate de glatiramère est composé d'un mélange de peptide de 40 à 100 acides aminés dont la structure ressemble à celle de la protéine basique de la myéline (MBP). Ce médicament exerce des effets immuno-modulateurs sur les cellules périphériques mais également au niveau du SNC. En périphérie, il va notamment diminuer la génération des lymphocytes Th17 au profit des Treg et des Th2 (Hong, Li et al. 2005; Aharoni, Eilam et al. 2010). Cet effet est notamment dû à la capacité des APC à produire plus d'IL-10 et de TGF-β et moins de TNF-α et d'IL-12 (Vieira, Heystek et al. 2003; Weber, Prod'homme et al. 2007). Au niveau du SNC, l'acétate de glatiramère va favoriser la sécrétion de TGF-β et d'IL-10 par les astrocytes, la microglie et les lymphocytes T et diminuer celle d'IFN-γ par les lymphocytes T (Aharoni 2013).

Les traitements de seconde ligne comprennent le fingolimod, le natalizumab ainsi que des anticorps dirigés contre les marqueurs CD20, CD25 et CD52. Le fingolimod est un antagoniste du récepteur à la sphingosine 1-phosphate (S1P) qui, après avoir été phosphorylé, induit une internalisation de ce récepteur (présent à la surface de nombreuses cellules dont les lymphocytes T) et sa dégradation (Billich, Bornancin et al. 2003). Le rôle principal du fingolimod est d'inhiber la capacité des lymphocytes T auto-réactifs à migrer des ganglions vers le SNC en réponse au gradient de S1P (Chun and Hartung 2010). Le natalizumab, quant à lui, est un anticorps monoclonal dirigé contre l'intégrine α4 présente à la surface des leucocytes humains. Le blocage de ce récepteur entrave l'adhérence des leucocytes au niveau de l'endothélium inflammé, ce qui inhibe leur migration au niveau du SNC (Sellebjerg,

Cadavid et al. 2016). Les anticorps anti-CD20 permettent la déplétion des lymphocytes B qui sont des acteurs importants de la SEP puisqu'ils sont capables de présenter l'antigène et donc d'activer les lymphocytes T mais également de produire des antigènes pathogéniques. Les anticorps monoclonaux anti-CD20 (rituximab, ofatumumab et ocrelizumab) vont permettre la déplétion des lymphocytes B matures et immatures *via* des mécanismes cytotoxiques et dépendants du complément mais également par induction d'apoptose induisant une tolérance (Lehmann-Horn, Kronsbein et al. 2013; Kasagi, Zhang et al. 2014). L'anticorps anti-CD25 (appelé aussi daclizumab) cible lui le récepteur à l'IL-2 (CD25), exprimé à la surface des lymphocytes T, bloquant ainsi la signalisation de l'IL-2 sur son récepteur. Le CD25 étant surexprimé à la surface des lymphocytes T activés il va donc inhiber leur activation (Goebel, Stevens et al. 2000; Dargahi, Katsara et al. 2017). Enfin, un anticorps anti-CD52 a été approuvé dans le traitement de la SEP. Le CD52 est un antigène exprimé sur de nombreux leucocytes tels que les LT, monocytes et certaines cellules dendritiques (Rao, Sancho et al. 2012). L'injection de cet anticorps va donc induire une déplétion des cellules immunes circulantes et principalement des LT et B permettant de moduler les réponses immunes. De plus, une repopulation est ensuite observée au cours de laquelle les proportions de Treg et T mémoires sont augmentées contrairement à celles des LT naïfs. Les différentes populations de LB vont également être modulées en faveur des LB immatures favorisant la mise en place de mécanismes de tolérance (Cox, Thompson et al. 2005; Zhang, Tao et al. 2013; Havrdova, Horakova et al. 2015).

Si les traitements de première ligne présentent des effets secondaires peu importants (grippe, fièvre, douleurs, lymphadénopathies), ils ne diminuent le taux de rechute que de 30% environ et en semble pas influer sur les niveaux de progression d'invalidité lors de la phase progressive. En revanche, les traitements de seconde ligne diminuent le taux de rechute de 50% et les taux d'invalidité de 25 à 50%, ils présentent des effets secondaires importants (infections respiratoires, bradychardies, blocages atrio-ventriculaires, leucoencéphalopathie multifocale progressive). Ces données démontrent donc la nécessité de définir des nouveaux traitements afin de lutter et de moduler cette maladie plus efficacement (Torkildsen, Myhr et al. 2016).

II.5) Les modèles animaux de SEP

Les modèles animaux expérimentaux de SEP ont permis de mettre en lumière les mécanismes de la pathologie et de tester différentes approches thérapeutiques. Le caractère multifactoriel de la SEP a conduit à la mise en place de différents modèles. Ainsi, l'étude de la réponse

immune spécifique est principalement étudiée dans les modèles d'EAE (passifs et actifs) ainsi qu'à l'aide de souris transgéniques, alors que le phénomène de remyélinisation est davantage décrit dans les modèles induits à l'aide de toxines. Enfin, les liens entre SEP et virus ont été étudiés à l'aide de modèle d'infections virales.

Le modèle d'EAE actif est le modèle animal d'étude de la SEP le plus couramment utilisé. Son induction se fait en induisant des réponses immunes dirigées contre des composants de la myéline ce qui permet d'induire une démyélinisation au niveau du SNC. Le premier modèle d'EAE actif a été développé par Koritschoner et Schweinburg en 1925 qui ont montré que l'injection d'un homogénat de moelle épinière humaine chez le lapin permettait de déclencher une inflammation au niveau de la moelle épinière accompagnée d'une paralysie (Stromnes and Goverman 2006). Le fractionnement d'homogénats de moelle épinière a permis de mettre en évidence la présence d'antigènes myéliniques encéphalitogéniques tels que les protéines MBP, PLP et MOG (Kipp, van der Star et al. 2012). Le protocole d'induction d'EAE a été profondément modifié depuis ces débuts et l'immunisation des souris avec différentes protéines ou peptides se fait actuellement en combinaison avec une injection d'adjuvant de Freund complet (qui permet l'induction de réponse Th1 et Th2 *via* l'activation des TLR) et de toxine pertussique (qui induit une perméabilité accrue de la BHE et favorise la génération de Th1) (Kabat, Wolf et al. 1947; Yong, Meininger et al. 1993; Ryan, McCarthy et al. 1998). Dans ces modèles, les signes cliniques sont le reflet de la localisation de l'infiltrat au sein du SNC ainsi que du type d'infiltrat majoritaire (macrophages, lymphocytes T et B) (Berger, Weerth et al. 1997) (Sobel 2000). De plus l'espèce animale, l'âge et le genre influencent le déroulement de la pathologie (Stromnes and Goverman 2006). Les modèles d'EAE les plus couramment utilisés sont déclenchés chez les rongeurs tels que le rat et la souris. Dans la majorité des modèles utilisés chez les rongeurs, les signes cliniques sont marqués par une paralysie progressive de la queue qui atteint les pattes arrières puis avants. Cette forme d'EAE est dite « classique » et reflète une inflammation principalement localisée au niveau de la moelle épinière, atteignant également le nerf optique dans le modèle utilisant le peptide MOG_{35-55}. L'EAE « classique » peut présenter une forme monophasique comme dans le modèle d'injection du peptide MOG_{35-55} dans les souris de fond génétique C57BL/6 ou une forme récurrente-rémittente comme dans le modèle d'injection du peptide $PLP_{139-151}$ dans les souris de fond génétique SJL/J. Leur score clinique est basé sur l'évaluation de la perte de fonctionnalité du train arrière qui s'évalue de la manière suivante: 0: pas de maladie ; 1: paralysie de la queue; 2: faiblesse des pattes arrières; 3: paralysie partielle des pattes arrières;

4: paralysie totale des pattes arrières; 5: état moribond ou mort (Stromnes and Goverman 2006). Au contraire, certains protocoles d'EAE chez les rongeurs provoquent d'autres signes cliniques caractéristiques de la SEP et reflètent une inflammation au niveau du cerveau (Storch, Stefferl et al. 1998). Ces modèles sont dits « atypiques ». La majorité des observations et des mécanismes immunologiques de la SEP ont été faits dans les modèles d'EAE. Brièvement, ces mécanismes reposent sur l'activation de lymphocytes T $CD4^+$ auto-réactifs ayant échappé à la sélection négative au sein du thymus. Leur activation leur permet de franchir la BHE perméabilisée (**Figure 9**). Une fois au sein du SNC, ces lymphocytes T pathogéniques vont être réactivés par des APC locales ou infiltrantes. Les lymphocytes T activés au sein du SNC vont à leur tour alimenter l'attraction de cellules immunitaires telles que les macrophages et la sécrétion de molécules pro-inflammatoires et toxiques comme l'IL-1β, le TNF-α ou encore de dérivés réactifs de l'oxygène (**Figure 10**) (Goverman 2009).

Pharmacologie résolutive : le SuperMApo

La résolution de l'inflammation constitue une cible thérapeutique potentielle dans différentes maladies où l'inflammation est dérégulée. Afin de rétablir cette résolution défaillante, de nombreux groupes ont utilisé les propriétés immuno-modulatrices des cellules apoptotiques afin de contrôler des maladies inflammatoires. L'injection de cellules apoptotiques dans des modèles de diabète, d'EAE, d'arthrite, de MICI ou encore de maladie du greffon contre l'hôte ont permis de mettre en évidence le potentiel thérapeutique de l'injection de cellules apoptotiques (Saas, Daguindau et al. 2016). Dans le contexte de la SEP, il a été démontré que l'injection de cellules apoptotiques surexprimant un fragment de MOG prévenait la progression de l'EAE en réduisant les réponses lymphocytaires spécifiques de l'antigène. L'efficacité de cette approche dépend de la prise en charge des cellules apoptotiques par les macrophages ; leur déplétion entrainant la perte de l'effet tolérogénique (Miyake, Asano et al. 2007). Cependant, une autre étude de la même équipe a montré que les DC $CD8\alpha^{+}CD103^{+}$ étaient également impliquées dans cette induction de tolérance (Qiu, Miyake et al. 2009). L'injection de microparticules couplées à un antigène myélinique permet de diminuer la pathologie chez la souris. Cette induction de tolérance requiert la phagocytose des microparticules par les macrophages de la zone marginale de la rate *via* le récepteur MARCO (*macrophage receptor with collagenous structure*) (Getts, Martin et al. 2012). De plus, l'induction d'apoptose *in vivo* par l'ajout d'anticorps anti-CD3 ou CD20 ou par irradiation permet l'efferocytose par les phagocytes professionnels (DC et macrophages) et la génération de Treg de manière TGF-β dépendante (Perruche, Zhang et al. 2008; Kasagi, Zhang et al. 2014) et le contrôle de la maladie. Enfin, un essai clinique dans la maladie du greffon contre l'hôte a récemment montré que l'injection de cellules apoptotiques était un traitement sans effets secondaires et efficace pour contrôler cette pathologie suggérant que la mise en place de pharmacologies résolutives pourraient être un bon moyen de contrôler les pathologies auto-immunes (Mevorach, Zuckerman et al. 2014).

De nombreuses études ont ainsi permis de mettre en évidence un lien entre dysfonction de la phase de résolution de l'inflammation et survenue et maintien de différentes pathologies inflammatoires chroniques. Au vu de ces observations, un nouveau paradigme a vu le jour au cours de la dernière décennie : la « pharmacologie résolutive » (Perretti, Leroy et al. 2015). Cette pharmacologie résolutive se propose de cibler la phase de résolution de l'inflammation et non plus uniquement la phase inflammatoire. La « pharmacologie résolutive » se propose d'intensifier les processus permettant l'arrêt naturel de la réponse inflammatoire et favoriser

ainsi la réparation tissulaire. Les molécules pro-résolutives ont alors pour but, non pas de supprimer la réponse inflammatoire, mais de rétablir une résolution active de cette dernière. (Serhan, Chiang et al. 2008; Perretti, Leroy et al. 2015). Trois types d'approches peuvent alors être mis en place afin d'établir la résolution de l'inflammation : 1) mimer les médiateurs pro-résolutifs endogènes ; 2) développer des agonistes des récepteurs pro-résolutifs ; 3) favoriser les voies de signalisation menant à la résolution. La première approche a vu un certain nombre de molécules testées lors d'essais cliniques. Des essais cliniques ont notamment testé l'effet de mélanocortines, de la lipoxine A1, de la résolvine E1 ou de l'adénosine dans des pathologies telles que le diabète de type II, la goutte ou encore la polyarthrite rhumatoïde (Perretti, Leroy et al. 2015). La seconde approche cible notamment le récepteur FPR2/ALX (*formyl peptide receptor type 2; lipoxin A4 receptor*) et de nombreux agonistes ont été développés ces dernières années afin de moduler différentes pathologies inflammatoires chroniques. Un des récepteurs ciblés pourrait également être le récepteur MC1 qui est un récepteur à la mélanocortine et dont l'activation a montré un effet bénéfique dans des modèles pré-cliniques d'inflammation vasculaire et de néphropathies (Leoni, Voisin et al. 2010; Lindskog Jonsson, Granqvist et al. 2014). Enfin, la troisième approche peut notamment se faire en favorisant la prise d'oméga-3 (notamment *via* l'alimentation) résultant d'une augmentation de sa conversion et lipides pro-résolutifs par le corps dans des patients atteints de polyarthrite rhumatoïde (Miles and Calder 2012). De plus, la prise d'aspirine ou de statines bloque l'action de la cyclooxygénase ce qui favorise la synthèse de lipoxine A4 et de résolvine D1 en fonction du substrat dans des volontaires sains, des patients atteints d'arthérite à cellule géante ou dans des modèles d'inflammation pulmonaires (Chiang, Bermudez et al. 2004; Planaguma, Pfeffer et al. 2010; Spite and Serhan 2010; Nadkarni, Dalli et al. 2014). Toutes ces études plus ou moins avancées démontrent donc que rétablir la phase de résolution de l'inflammation est une stratégie thérapeutique intéressante.

Basé sur ce concept de « pharmacologie résolutive » et sur les précédents travaux de l'UMR1098 de Besançon sur les cellules apoptotiques, notre équipe a proposé et développé une nouvelle approche pro-résolutive inspiré du processus d'efferocytose. Cette approche propose d'utiliser les facteurs issus de l'efferocytose, processus clé dans la résolution de la réponse inflammatoire. En effet, comme détaillé précédemment, les facteurs produits par les macrophages éliminant les cellules apoptotiques sont capables d'induire un changement pro-tolerogène des cellules immunitaires, de limiter le recrutement lymphocytaire et de permettre l'induction de tolérance. Pour ce faire, des cellules apoptotiques sont cultivées durant 48h *in*

vitro avec des macrophages assurant leur efferocytose et la production de nombreux facteurs pro-résolutifs dans le surnageant cellulaire. Le surnageant de culture compose donc le médicament, appelé SuperMApo pour *supernatant from macrophage and apoptotic cell culture*.

L'injection de ce surnageant dans un modèle de péritonite, permet de favoriser la résolution, de nombreux neutrophiles sont recrutés et leur élimination par les macrophages et également augmentée. En effet, bien que le nombre de macrophages reste constant, ces derniers acquirent une capacité de phagocytose accrue. Dans un modèle d'arthrite induite au collagène, l'injection de SuperMApo à 48h d'intervalle permet de stopper l'arthrite en cours. Cette résolution, qui n'induit pas d'immunosuppression, est associée à l'émergence de Treg spécifiques de l'antigène, dépendante du TGF-β, permettant un maintien à long terme de la résolution (Bonnefoy et al, en préparation). De façon intéressante, en plus de contrôler la réponse inflammatoire, SuperMApo permet également d'augmenter la cicatrisation des tissus. Ces données ont été obtenues dans un modèle expérimental de MICI par transfert de lymphocytes T naïfs chez des animaux immunodéprimés. En effet, l'injection de SuperMAPo permet une régression des lésions coloniques à travers une meilleure prolifération et migration des cellules épithéliales intestinales et des fibroblastes. Cette approche résolutive est donc tout à fait prometteuse dans le traitement de pathologies chroniques inflammatoires. Les stratégies thérapeutiques classiques ayant échoué à réduire efficacement l'inflammation dans les pathologies chroniques telles que la SEP, il apparait nécessaire de développer de nouvelles approches afin de permettre la résolution de l'inflammation et le retour à l'homéostasie accompagnée d'une réparation des tissus lésés.

Objectif des travaux de thèse

La mise en place de la réponse inflammatoire en réponse à une agression est suivie d'une phase de résolution de l'inflammation au cours de laquelle la phagocytose des neutrophiles apoptotiques par les macrophages permet d'induire la réparation tissulaire et le retour à l'homéostasie. Cependant, lorsque cette phase de résolution est défaillante, la persistance de la réponse inflammatoire va aboutir à l'apparition de maladies inflammatoires chroniques telles que la SEP. Au cours de cette maladie, les « chefs d'orchestre » des réponses immunes sont les cellules de l'immunité innée et à leur tête les cellules présentatrices de l'antigène. Ces cellules vont permettre d'induire des réponses adaptatives notamment en favorisant l'émergence de lymphocytes Th1 et Th17 et en diminuant la génération de lymphocytes T régulateurs. Les réponses immunes se développeront d'abord dans les organes lymphoïdes périphériques où la sécrétion de molécules pro-inflammatoires (TNF-α, IL-12, IL-23…) et la présentation de l'antigène pathogénique vont permettre d'induire l'activation de LT auto-réactifs. Une fois activés, ces LT vont alors migrer au sein de l'organe cible (le SNC ici) et être réactivés par ces APC afin de leur permettre de faciliter la destruction des oligodendrocytes producteurs de myéline et la subséquente démyélinisation du SNC.

La régulation de ces APC est donc un facteur clé afin de moduler l'inflammation. De nombreuses publications ont ainsi montrées que la modulation de ces APC lors des maladies inflammatoires chroniques, et particulièrement dans la SEP, permettait de diminuer l'inflammation au sein de l'organe enflammé mais également en périphérie. De plus, cette régulation a été montré récemment comme impliquant des enzymes impliquées dans le contrôle épigénétique de l'expression génique et notamment au niveau de la méthylation de l'ADN. A notre connaissance, l'effet des produits de l'efferocytose sur la régulation de l'inflammation n'a jamais été étudié. De plus, les mécanismes par lesquels l'efferocytose module le phénotype des APC n'ont jamais été décrits. L'objectif de ce travail de thèse sera donc d'étudier l'effet des produits issus de l'efferocytose sur le contrôle de l'inflammation dans un modèle murin de SEP ainsi que les mécanismes qui contrôlent les fonctions des APC.

Résultats

Etude 1 : Implication des macrophages dans l'effet pro-résolutif de SuperMApo

Le surnageant issu de l'élimination des cellules apoptotiques par les macrophages contient de nombreux facteurs pro-résolutifs et permet un contrôle de la réponse inflammatoire et de favoriser la réparation tissulaire. La SEP présente une inflammation du SNC favorisant la destruction de ses composants essentiels, comme la myéline. Nous avons logiquement évalué si les facteurs issus de l'efferocytose pouvaient permettre de terminer l'inflammation en cours et permettre une résolution de la maladie dans le modèle d'EAE.

Dans cette étude, nous montrons que l'injection de SuperMApo chez des souris atteintes d'EAE (score moyen de 1,5/5), permet de contrôler l'évolution du score clinique et de diminuer de façon drastique l'infiltrat inflammatoire au niveau du SNC. Nous avons observé que cette diminution de l'infiltrat au niveau du SNC n'était pas associée à une réparation de la BHE, mais à une moindre capacité des lymphocytes T à migrer au niveau du SNC et à une moindre proportion de lymphocytes T pathogéniques spécifiques du peptide MOG_{35-55} dérivé de la myéline. Alors que les Treg ne semblent pas démontrer d'effets suppressifs spécifiques dans ce modèle après traitement par SuperMApo, les macrophages démontrent *ex vivo* une reprogrammation pro-tolérogène. En effet ces derniers permettent de favoriser une polarisation Treg de lymphocytes naïfs, démontrent une activité NFκB réduite, un profil transcriptomique résolutif et des modifications épigénétiques pro-tolérogènes. Notamment, une baisse de la méthylation globale de l'ADN est observée dans ces macrophages, liée à une augmentation de l'activité TET dépendante de FOXA1, favorisant l'expression du miRNA 127 anti-inflammatoire.

Ces travaux démontrent que les facteurs issus de l'efferocytose sont capables de réprimer une EAE en cours à travers la reprogrammation pro-tolérogénique des macrophages en périphérie. Ces données proposent aussi une nouvelle alternative thérapeutique pro-résolutive dans le traitement de la SEP.

The pro-resolutive factors issued from apoptotic cell phagocytosis by macrophages can control inflammation by inducing tolerogenic macrophages

Thierry Gauthier[1], Omayra Martin-Rodriguez[1], Cécile Chagué[1], Anna Daoui[1,#], Adam Ceroi[1,#], Alexis Varin[1], Francis Bonnefoy[1], Séverine Valmary-Degano[2], Mélanie Couturier[1], Philippe Saas[1], Pierre-François Cartron[3] and Sylvain Perruche[1,#,*]

[1]Université Bourgogne Franche-Comté, INSERM, EFS BFC, UMR1098, Interactions Hôte-Greffon-Tumeur/Ingénierie Cellulaire et Génique, Fédération Hospitalo-Universitaire INCREASE, LabEx LipSTIC, F-25000 Besançon, France ; [2]Besancon University Hospital, Pathology department, F-25000 Besançon, France ; [3]CRCINA-INSERM 1232, Team Apoptose et Progression tumorale - 44 805 Saint Herblain, FR

[#]Current addresses: A.D., Animal Facility, Medical School Department, University of Bourgogne Franche-Comté, Besançon, France; A.C., University of Virginia, Department of Microbiology, Immunology and Cancer Biology, Charlottesville, VA, USA; S.P., MED'INN'Pharma, Besancon, France.

Correspondence should be addressed to S.P. (sylvain.perruche@inserm.fr)

Abstract

Multiple sclerosis is a chronic inflammatory disease of the central nervous system in which resolution is impaired. Here, we proposed to evaluate whether the injection of the factors issued from efferocytosis (i.e. apoptotic cells elimination by macrophages) would permit to reboot resolution and terminate ongoing experimental autoimmune encephalomyelitis (EAE). We demonstrated that treatment with efferocytosis factors (or SuperMApo for supernatant issued from macrophages and apoptotic cell culture) allowed the control of EAE severity, inducing a diminished demyelination and inflammatory cell infiltration. Macrophages played a major role in the control of EAE by SuperMApo, and demonstrated a pro-tolerogenic reprogramming favoring regulatory T cell induction, through NF-κB signaling pathway modulation and epigenetic modifications. Our data demonstrate that efferocytosis factor injection can stop ongoing inflammation by triggering macrophage reprograming and thus propose SuperMApo as a promising therapeutic approach to control multiple sclerosis, and more generally dysregulated chronic inflammatory diseases.

Autoimmune disorders share an altered resolution of inflammation leading to an uncontrolled chronic and pathogenic inflammation causing tissue destruction[1-3]. Recently, innovative approaches triggering the resolution of inflammation have been developed. They can induce short term-immunosuppression, such as apoptotic cell injection, alone[4] or associated with the pathogenic antigen[5], or long term tolerance with cell apoptosis induction *in vivo* in the presence of the pathogenic antigen[6]. The fact that only short term tolerance is achieved or that the pathogen has to be known strongly limit the clinical transfer of these approaches.

However, whereas the therapeutic effect observed in these approaches is associated to efferocytosis, the factors issued from efferocytosis used as a whole has never been evaluated as a therapeutic approach. Resolution of inflammation promotes the return to homeostasis, with tissue healing and repair[7]. Many factors are implicated in this process, notably specialized pro-resolutive lipid mediators which are believe to initiate the shift from inflammation to resolution[8] and anti-inflammatory cytokines which participate to inhibit inflammation and reprogram macrophages[9-11]. Other factors can directly inhibit or degrade inflammatory lipids or molecules in order to limit further inflammatory cell recruitment and over inflammation[11]. Most of these factors are issued from efferocytosis, i.e. apoptotic cell elimination by phagocytes and in particular by tissue-resident and monocyte-derived macrophages. Altogether, efferocytosis factors enhance efferocytosis and tissue cleaning, restore homeostasis and initiate tissue repair[12,13]. This highlights the therapeutic potential of these factors to control resolution and terminate dysregulated inflammation[7,14].

Here we demonstrated that the injection of the efferocytosis factors produced by macrophages eliminating apoptotic cells (called here SuperMApo) can resolve ongoing inflammation in a model of EAE. This effect is mediated by an *in vivo* reprogramming of macrophages toward a tolerogenic profile at different levels. Thus, reintroduction of SuperMApo could be a new therapeutic approach to treat chronic inflammatory diseases.

Results

Injection of SuperMApo modulates ongoing EAE

To determine whether efferocytosis factors injection might control ongoing inflammation, we cultured macrophages with apoptotic cells and collected the supernatant 48 h later. At that time all apoptotic cells have been engulfed by macrophages (data not shown). This supernatant (named SuperMApo) was then injected twice (with 48 h of interval) in mice with ongoing EAE exhibiting a clinical score of 0.5-1 out of 5, and we observed the arrest of EAE progression over the next 10 days after SuperMApo treatment compared to EAE mice receiving vehicle (**Fig. 1a**). Consistent with this, SuperMApo-treated mice demonstrated a lower score of inflammation within the spinal cord with a strongly reduced inflammatory infiltrate and demyelination in the central nervous system (CNS), 72 h after treatment (**Fig. 1b**). Of importance, the control of ongoing EAE was only achieved using efferocytosis factors and not with the factors from apoptotic cell culture plus the factors from macrophage culture (**Fig. 1c**). These data demonstrate that the injection of efferocytosis factors (i.e. SuperMApo) in ongoing EAE is able to stop disease progression and to decrease tissue inflammation.

SuperMApo injection reduces inflammation and modulates macrophage phenotype in the CNS of EAE mice

By further investigating the CNS after SuperMApo treatment, we observed consistently with our immunohistochemistry observations (**Fig. 1b**) that SuperMApo injection strongly decreased the number of leucocytes in the CNS, including Th1, Th17 and Tc1 T cell subsets, dendritic cell (DC) and macrophage numbers as well (**Fig. 2a,b**). The number of Treg within the CNS was not modified **(Fig. 2b**), neither leucocyte subset percentages (**Fig. 2c**). Quantities of the inflammatory cytokines TNF-α, IL-12p70, IFN-γ, IL-6 and IL-10 were not

modified in the CNS after SuperMApo-treatment (**Fig. 2d**). Compared to $CD11b^{med}CD45^{+}$ microglial cell number, in which maturation and cytokine content were not modified by SuperMApo treatment (**Supplementary Fig. 1a-d**), $CD11b^{high}CD45^{+}$ macrophages in the CNS expressed lower levels of CD80 and MHC-II molecules as well as intracellular IL-12 after SuperMApo treatment (**Fig. 2e,f**, **Supplementary Fig. 1d**). The maturation of DC and their content in TNFα, IL-12 and IL-10 was not modified by SuperMApo treatment (not shown). Because SuperMApo lowered pathogenic cell infiltration in the spinal cord, we investigated SuperMApo blood brain barrier (BBB) permeability, which can be damage by inflammation[15,16], first using Evans Blue (EB) dye which pass through the BBB when compromised. The similar quantities of EB dye suggested the absence of BBB repairing 72 h after SuperMApo treatment (**Fig. 2g**) and this was further supported by the mRNA levels of the major genes coding for occludin, claudin-5, tight junction protein 1 and F11 receptor (*Ocln*, *Cldn5*, *Tjp1* and *F11r*, respectively), implicated in the integrity of BBB, which were not increased after SuperMApo treatment (**Fig. 2h**). In addition to the absence of BBB remodeling by SuperMApo, we did not observed modification of chemokine and integrin expression at the CNS level as well (**Fig. 2i,j**). Our results show that the decreased CNS inflammation induced by SuperMApo treatment is not associated with BBB remodeling but might be associated with the peripheral modulation of inflammatory immune cells.

SuperMApo treatment decreases peripheral pathogenic T cell response

To evaluate peripheral modulation, we looked in the spleen and inguinal lymph nodes and observed similar percentages and numbers in terms of $CD4^{+}$ T cells and Th1, Th17 and Treg subsets, as well as $CD8^{+}$ T cells and Tc1 subset (**Fig. 3a,b**). In addition, we did not observed differences in terms of cell apoptosis and proliferation in both lymphoid organs (**Fig. 3c,d**). We then determined pathogenic T cell response by culturing the cells *ex vivo* in the presence

of MOG_{35-55} peptide and observed a lower proliferation of cells issued from SuperMApo-treated EAE mice (**Fig. 3e**). This suggested to us either an immunosuppression of cell proliferation mediated by antigen-specific Treg or a lower proportion of antigen-specific pathogenic T cells. The immunosuppression mediated by Treg was excluded using MOG-specific suppressive assays in which we did not observed antigen-specific Treg immunosuppression (**Fig. 3f**). However, when T cells were submitted to *ex vivo* stimulation by MOG peptide, we observed a reduced response of Th1 and Tc1 subsets (**Fig. 3g**) demonstrating that SuperMApo treatments reduced Th1 and Tc1 pathogenic subsets *in vivo*. This reduction however did not affect total Th1 and Tc1 cell numbers and percentages. Whereas we did not detected any antigen-specific activity of Treg after SuperMApo treatment, our data demonstrate that MOG-specific Th1 and Tc1 pathogenic T cell subsets are invalidated in periphery by the injection of efferocytosis factors.

SuperMApo reprograms macrophages toward a tolerogenic profile

Macrophages have been reported to be involved in the pathogenesis and in the regulation of EAE, notably by modulating the Th1-Th17/Treg balance[17-19]. In addition, macrophages play a key role in resolution and are very plastic cells undergoing reprogramming depending on the microenvironment and the location[11]. Intriguingly, while no Treg increase was observed in SuperMApo-treated EAE mice neither *ex vivo* antigen-specific Treg immunosuppression, macrophages isolated from these mice demonstrated *ex vivo* the capacity to favor Treg rather than Th1 cell polarization of naive T cells (**Fig. 4a**). In addition, naive macrophages submitted to SuperMApo in culture also favored Treg induction rather than Th1 cell polarization from naive T cells (**Fig. 4b**). Thus macrophages underwent a pro-tolerogenic reprogramming in the presence of SuperMApo and they retained their ability to mature after TLR ligand stimulation as they expressed similar levels of co-stimulatory CD40, CD80, CD86 and MHC-II molecules

and produced similar levels of pro-inflammatory cytokines TNF-α and IL-12 than control macrophages (**Supplementary Fig. 2a,b**). Macrophage pro-tolerogenic reprogramming was further confirmed by the adoptive transfer of macrophages from SuperMApo-treated EAE mice into EAE mice where they significantly modulated the severity of the disease compared to macrophages issued from EAE mice receiving vehicle (**Fig. 4c**). This EAE score modulation was associated in the spinal cord with Treg percentage increase and in the iLN with the decrease of IFN-γ^+-producing $CD4^+$ T cell percentages (**Fig. 4d**). Similar data were obtained with the adoptive transfer of naive macrophages cultured with SuperMApo (**Supplementary Fig. 3a,b**). In addition, using clodronate-loaded liposome injection, which depletes phagocytes, EAE resolution by SuperMApo treatment was inhibited (**Fig 4e**). Consistently, T cells from the spleen and the iLN showed the same ability to proliferate after MOG_{35-55} peptide stimulation and similar number of Th1 cells was founded in the spinal cord compared to the EAE plus clodronate liposome control group. (**Fig. 4f,g**). Our data demonstrate that SuperMApo induces *in vitro* and *in vivo* macrophages pro-tolerogenic reprogramming which are therefore mandatory for SuperMApo-induced EAE resolution.

To further explore macrophage reprogramming, a transcriptomic analysis was performed on spleen macrophages from SuperMApo- and vehicle-treated EAE mice 72 h after treatment. Interestingly, among the 571 genes up-regulated in SuperMApo-macrophages, we found the M2-specific markers *Arg1*, *Pparγ*, *Cd226* and *Alox15* which are representative of a pro-tolerogenic macrophage state (**Fig. 5a,b**). In addition among the 810 down regulated genes in SuperMApo-macrophages, we found the pro-inflammatory genes *Fasl*, *Il7*, *Ccr4* and *Ccl22* (**Fig. 5a,b**). Overall, signaling pathway analysis demonstrated the up-regulation of the responses to wounding pathway (a major feature of the resolution of inflammation) (**Fig. 5c,e**). In addition, cellular functions (protein lipidation, regulation of cell cycle phase transition, membrane lipid metabolic process) and exhaustion of immune response pathways

were revealed down-regulated (**Fig. 5d,f**). These results strongly support that SuperMApo induces macrophage reprogramming at the transcriptomic level, giving them pro-resolutive properties to control ongoing EAE.

SuperMApo-induced reprogramming inhibits macrophage pro-inflammatory properties

Because SuperMApo treatment modulated peripheral immune response in EAE setting, we evaluated whether macrophages triggered T cell migration since leukocyte migration into the CNS is one of the major pathogenic feature of EAE development[20,21]. First, we observed that spleen cells from SuperMApo-treated EAE mice demonstrated a decreased migration to the lymphoid organs when transferred into new EAE mice, and that this lower influx was mostly affecting T cells (**Supplementary Fig. 4a-c**). In spleen and lymph node cells from SuperMApo-treated EAE mice only *Cxcr3* expression was observed reduced, but not *Ccr5* and *Ccr6*, compared to controls, and this was observed only in Th1 cells (**Supplementary Fig. 4d,e**). Then, to evaluate whether reprogrammed macrophages influenced CXCR3 expression on Th1 cells, we went back to our coculture experiments and observed that in addition to favor less Th1 polarization, SuperMApo-treated macrophages induced less CXCR3 expression on Th1 cells (**Supplementary Fig. 4f**). In addition, in SuperMApo-treated EAE mice depleted for phagocytes, CXCR3 expression on T cells was not reduced (**Supplementary Fig. 4g**). Together, these data demonstrate that SuperMApo decreases T cell influx within the CNS by targeting the expression of CXCR3 on putative pathogenic Th1 cells through macrophage reprogramming.

Because macrophages treated by SuperMApo displayed a decreased expression of the maturation marker CD40 and a decreased ability to produce the pro-inflammatory cytokine, TNF-α (**Supplementary Fig. 5a,b**) in response to LPS stimulation *in vitro*, we explored the NF-κB pathway in macrophages, which downregulation has been demonstrated to modulate

EAE[22,23]. We observed that macrophages sorted from SuperMApo-treated EAE mice demonstrated a decreased phosphorylation of IKK-β, IκB and p65 subunit, and a decreased percentage of p65 subunit in the nucleus (**Supplementary Fig. 5c,d**). Similar data were observed *in vitro* with SuperMApo and LPS stimulation (**Supplementary Fig. 5e**). Altogether, these data demonstrate that SuperMApo-induced macrophage reprogramming reduced NF-κB pathway signaling in macrophages and reduced Th1 cell migration to the CNS.

Macrophage reprogramming occurs through epigenetic modifications

To further determine whether SuperMApo-induced macrophage reprogramming during the treatment of EAE was an epiphenomenon or a long term modification, we then focused on the regulation of DNA methylation. Macrophages isolated from the spleen of SuperMApo-treated EAE mice displayed a decreased global level of 5-methylcytosine which was associated with both an increase of the ten-eleven translocation (TET) enzyme activity, and particularly of the *de maintenance* methylation activity (but not *de novo* methylation) (**Fig. 6a-d**). Additional experiment performed with antibodies directed against Tet1, Tet2 and Tet3 suggest that TET1 is responsible for the increase of global TET activity since only Tet1 antibody limited the TET activity (**Fig. 6b**). This further supports the long term reprogramming of macrophages by SuperMApo treatment. These methylation modifications by SuperMApo in macrophages increased the anti-inflammatory *miR-223* expression, which was associated with a demethylation of *miR-223* promoter (**Fig. 6e,f**). Then using anti-Foxa1 antibody, the TET conversion activity was modulated, but not with antibodies targeting c-EBPa or EBF1, showing that the Foxa1-TET1 complex was responsible for macrophage DNA decreased methylation of *miR-223* promoter (**Fig. 6g**), and notably of the FOXA1-targeted gene family. In addition, we also observed a decreased expression of the pro-inflammatory *miR-127* while

its promoter was also demethylated, which classically correlate with an increased gene expression (**Fig. 6e,h**). However, *miR-127* promoter demethylation region is close to the CCCTC-binding factor (CTCF) transcriptional repressor binding site, which was observed enriched by ChIP assay after SuperMApo treatment in macrophages (**Fig. 6i**).Thus, macrophages reprogramming by SuperMApo treatment during ongoing EAE occurs through the control of DNA methylation, targeting FOXA1-targeted gene family as well as the repression of the miR-127 and increase of the anti-inflammatory miR-223.

Discussion

Resolution of inflammation is impaired in numerous chronic inflammatory diseases and triggering the resolution of inflammation could be a promising approach to develop new treatment modalities[1,14,24]. Here, we demonstrated that the injection of the factors produced by macrophages clearing apoptotic cells (i.e. SuperMApo) allow the control of EAE progression (a model of MS) by modulating splenic macrophage functions through a deep pro-tolerogenic reprogramming. Hence, this new therapeutic approach could be used as a treatment for MS and more globally to dysregulated inflammatory diseases.

Several conclusions can be drawn from the current study. First, efferocytosis is a key step for inducing a reprogramming of macrophages toward a tolerogenic profile as well as to propagate *in vivo* tolerance (*i.e.*, Treg polarization). Indeed, efferocytosis reprogram macrophages to produce pro-resolutive and healing factors. We were not able to observe any modulation of EAE neither macrophage reprogramming when we used the factors produced by apoptotic cells together with those produced by macrophages.

Second, reduced inflammation and demyelination in spinal cords seem to not be induced directly within the CNS, but is rather due to peripheral immune modulation. Indeed, the factors within SuperMApo did not favor a remodeling of the BBB since we did not observe a decrease of BBB permeability to EB after SuperMApo treatment nor an increase of occludin,

claudin-5, tight junction protein 1 and F11 receptor mRNA levels. In line with these observations, we did not observed accelerated remyelination after SuperMApo treatment after cuprizone chowing (data not shown), which is a model of demyelination secondary to oligodendrocyte death followed by a spontaneous remyelination[25]. Whereas microglial cells, which are local tissue-resident macrophages [26], demonstrated a conserved maturation despite SuperMApo treatment, infiltrating macrophages showed pro-tolerogenic properties. Resolutive macrophages should support tissue repair notably through the action of TGF-β [27-29], but maybe the model we are using do not allow tissue repair, the pertussis toxin is persisting long term and pro-healing factors might not as strong. In addition, the fact pertussis toxin maintains BBB permeability may also contribute to limit SuperMApo therapeutic effect to terminate EAE. Indeed, SuperMApo treatment induced the desertion of the inflammatory infiltrate in the CNS, as well as the strong reduction of pathogenic T cell response to the auto-antigen, attesting of long term immune tolerance induction. Of importance, this has been obtained after only two injections of SuperMApo and in ongoing EAE.

Third, splenic macrophages are mandatory in the control of ongoing inflammation by efferocytosis factors in EAE mice. This is supported by depletion of phagocytes using clodronate-loaded liposome injection which totally abrogated the effect of SuperMApo. Macrophages are reprogrammed toward a tolerogenic profile by SuperMApo and favor the induction of Treg and control disease progression. Our data suggest that macrophages interplayed with T cells after SuperMApo treatment since macrophages depletion restored T cell proliferation to the auto-antigen MOG_{35-55}. Concerning the role of Treg after SuperMApo treatment, whereas we did not observed MOG-specific Treg increase or suppressive activity, the depletion of Treg in Foxp3-DTR EAE mice before SuperMApo treatment abrogated the control of EAE by efferocytosis factors (data not shown). Because SuperMApo-reprogrammed macrophages generated Treg *ex vivo*, our data suggest that tolerogenic

macrophages may favor the emergence of Treg which are necessary to mediate long-term tolerance but to a level undetectable using our assays or in a location (CNS) where Treg numbers are too low to assess suppressive assays. In this line, macrophages modulated by SuperMApo show a decrease activation state *in vitro* and *in vivo*, linked to a down-regulation of the NF-κB pathway. In addition, our transcriptomic data demonstrated a pro-resolutive phenotype of macrophages, with a down regulation of signaling pathways involved in the regulation of immune activation. Interestingly, the pathway "response to wounding" is up-regulated, as well as numerous M2 markers. These data confirm that macrophages are reprogrammed toward a pro-resolutive profile at both the transcriptomic and post-transcriptomic levels. Moreover, this specific control of macrophages by SuperMApo occurs also through epigenetic modifications. The expression of miR-127 and miR-223 is tightly control by DNA methylation through an increase of TET proteins activity in a Foxa1 dependent axis, leading to a skew macrophages polarization toward a tolerogenic profile. Overall, this demonstrates that the factors released during efferocytosis participate in a deep macrophage reprogramming locally but also elsewhere, which will then shape adaptative and innate cell response to induce and maintain tolerance.

Our data strongly demonstrate that efferocytosis factor injection modulate immune responses in an EAE model by a tight control of macrophage functions. After SuperMApo treatment, macrophages reprograms toward a pro-tolerogenic profile and express genes implicated in wounding and down-regulates the expression of genes involved in immune activation. Moreover, the activation of inflammatory NF-κB pathway is impaired resulting in a decrease activation state. These pro-resolutive macrophages are necessary for the anti-inflammatory effect of SuperMApo and able to control T cell migration, as well as stopping EAE clinical score progression. These findings suggest that the injection of SuperMApo could be a new therapy for inflammatory diseases.

Online Methods

Mouse experimentation

Female C57BL/6 mice aged of 6-10 weeks were purchased from Charles River Laboratories. Experimentation (#02831) was approved by the local ethic committee (#58) and the French Ministry of Higher Education and Research (Ministère de l'Enseignement Supérieur et de la Recherche) and was conducted in accordance with the European Union's Directive 2010/63. Mice were housed at the environmentally controlled and germ free UMR1098 animal facility (#D25-056-7) in ventilated cages with cellulose bedding and access ad libitum to pellet food and sterile water pouches (Plexx, The Netherlands).

Production of SuperMApo

Briefly, macrophages were isolated from the peritoneal cavity of C57Bl/6 mice, 48 h after 3% thioglycollate (BD biosciences) mobilization, and then cultured (1.10e6 cells/mL) with apoptotic thymocytes from C57BL/6 mice generated by X-ray irradiation (35 Gy) in 1 mL of X-vivo media (Lonza) at a final ratio of 1 macrophage for 5 apoptotic cells. Supernatant was collected at 48 h and filtered using a 20 µm disposable filter (Greiner bio-one) before storage at -80°C until use. Supernatant of macrophages or apoptotic cells cultured alone were also produced as controls.

EAE induction and SuperMApo treatment

C57BL/6 female mice were injected subcutaneously with 200 µg of MOG_{35-55} peptide (MD Bioproducts) emulsified in IFA with 5 mg/mL of heat-inactivated *Mycobacterium tuberculosis* (Sigma-Aldrich). Pertussis toxin (Calbiochem) was injected i.p. at 0 and 48 h after disease induction (200 ng/mouse). Mice are monitored and scored daily as follows: 0: no disease; 1: flaccid tail; 2: hind limb weakness; 3: partial hind limb paralysis; 4: total hind limb

paralysis; 5: moribund state or death. When mice reached a 0.5-1 clinical score, SuperMApo or vehicle (X-vivo medium) were injected i.p. (1 mL) and reinjected at 48 h.

Cell isolation and staining

Spinal cords were harvested and incubated with type II collagenase (2 mg/ml; Roche). Then, mononuclear cells were separated using a 30% Percoll layered over 70% Percoll (Sigma-aldrich) solution by centrifugation (600 *g*, 20 min). Spleens and inguinal lymph nodes were harvested and cells extracted and stained with a cell viability dye FvS (BD biosciences), as well as labelled monoclonal antibodies against CD45 (BD biosciences, clone 30-F11), CD11b (BD biosciences, clone M1-70), CD11c (BD biosciences, clone HL3), CD19 (BD biosciences, clone 1D3), CXCR3 (BD biosciences, clone CXCR3-173) or F4/80 (BD biosciences, clone T45-2342) after incubation with anti-Fc receptor antibody (clone 24G2). Expression of co-stimulation markers was assessed using CD80 (BD biosciences, clone 16-10A1), CD86 (Biolegend, clone GL-1), CD40 (Biolegend, clone 3/23) and MHC-II (Miltenyi Biotec, clone REA813) antibodies. For intracellular staining, cells were stimulated with 1 µg/mL of LPS (or not) (Sigma-Aldrich, only for *in vitro* stimulation assays) for 6 h and then with 25 ng/mL of phrobol 12-myristate 13-acetate (Sigma-Aldrich) and 1 µg/mL of ionomycin (Sigma-Aldrich) in presence of 10 µg/mL of monencin (BD biosciences) for 4 h at 37°C. Foxp3 (ebiosciences, clone FJK-16S) expression as well as intracellular TNF-α (BD biosciences, clone MP6-XT22), IL-12 (BD biosciences, clone C15.6), IL-10 (BD biosciences, clone JES5-16E3), IL-17A (Miltenyi Biotec, clone REA660), IFN-γ (Miltenyi Biotec, clone REA381) or KI-67 (BD biosciences, Clone B56) staining were performed in $CD3^+$ (BD biosciences, clone 145-2C11), $CD4^+$ (BD biosciences, clone RM4-5), $CD8^+$ (BD biosciences, clone 53-6.7)-gated cells, using a FACS CANTO II cytometer with DIVA v7 software (BD biosciences).

T cell recall responses

Inguinal lymph node and spleen cells were harvested and stimulated with 15 µg of MOG_{35-55} peptide for 72 h. Cell proliferation was evaluated by BrdU incorporation and counting following manufacturer instructions (Perkin Elmer) and T cell polarization was evaluated by FACS.

Suppressive assay

For MOG-specific or *Mycobacterium tuberculosis* (MT)-specific co-cultures, naive $CD4^+CD25^-$ T cells were isolated from EAE mice by MACS (Miltenyi Biotec) and cultured (100.10e3 cells) with $CD11c^+$ dendritic cells (DC) (50.10e3 cells) isolated from naive mice (CD11c MicroBeads, Miltenyi Biotec), in the presence of 15 µg/mL of MOG_{35-55} peptide (MD Bioproducts) or 50 µg/mL MT protein (Difco). For CD3/CD28-stimulated T cell cultures, $CD4^+CD25^-$ naive T cells were isolated from EAE mice and cultured in the presence of coated anti-CD3 (BD biosciences, clone 145-2C11) and soluble anti-CD28 (BD biosciences, clone 37.51) antibodies (2 and 0.5 µg/mL, respectively). After adding sorted Treg and after 4 days of culture, T cell proliferation was assessed by BrdU incorporation and counting.

RNA isolation, cDNA reverse transcription and RT-qPCR

Total RNA from CNS, spleen and iLN cells were isolated using the RNA easy mini kit (Qiagen) according to manufacturer's protocol and used for first-strand cDNA synthesis (Applied Biosystems). Then, mRNA expression levels were quantified by real-time quantitative PCR using Fast SYBR Green Master Mix (Applied Biosystems) with CFX96 system (Biorad). Primers (ThermoFischer) of interest are: *Ccl2* (Mm00441242), *Ccl5* (Mm01302427), *Claudin-5* (Mm01169675_s1), *Cxcl9* (Mm00434946), *Cxcl10* (Mm00445235), *Cxcr3* (Mm99999114), *Ccr5* (Mm01963251), *Ccr6* (Mm99999054), *F11r* (Mm00554113_m1), *Icam* (Mm00516023_m1), *Itga4* (Mm01277951_m1), *Itgb5* (Mm00439825_m1), *Itgb7* (Mm00442916_m1), *Occludin* (Mm00500912_m1), *Tjp1*

(Mm00493699_m1) and *Vcam1* (Mm01320970_m1). Qiagen miScript Primer Assays were used for miR-127 (MI0000154), mir146a (MI0000170), miR-155 (MS00001701) and miR-223(MI0000703).

Histology

Spinal cords were extracted at sacrifice and fixed in 5% formol solution before embedded in paraffin and sectioned. Sections (2 µm) were stained with Luxol fast blue or H&E (Merck) using standard procedures. Inflammation was evaluated by a pathologist blinded to the nature of the mice, and determined using a score system with three levels (0 = no infiltrate, 1 = low mononuclear cell infiltrate, 2 = middle mononuclear cell infiltrate, 3 = dense mononuclear cell infiltrate penetrating in the tissue). Demyelination was also evaluated and determined using a score system with three levels (0 = no demyelination, 1 = few areas of demyelination, 2 = middle areas of demyelination, 3 = large areas of demyelination).

Blood brain barrier permeability evaluation

Evans Blue dye (Sigma-Aldrich) was injected i.v. for 60 min and then mice were sacrificed, the spinal cords removed and weighted. Evans Blue was extracted with 2.5 mL of 60 % trichloroacetic acid, centrifuged for 30 min at 10 000 g and the amount of Evans Blue was quantified at 610 nm by spectrophotometry and normalized to spinal cord weight.

Macrophages evaluation

$CD11b^+$ macrophages were sorted from spleen using CD11b microbeads and autoMACS pro device (Miltenyi Biotec) (purity >90%). Cells were conserved in RLT buffer for RNA extraction, or cultured with naive $CD4^+CD25^-$ T cells issued from $RAG^{-/-}$OT-II mice (50 000 APC for 100 000 T cells) in presence of $OVA_{323-339}$ peptide (2 µg/mL; Invivogen). After 72 h of culture, T cell polarization was analyzed by FACS. In some experiments, home-made clodronate-loaded or PBS-loaded liposomes[30] were injected i.v. 24 h before pRM treatment (2 mg per mouse). For adoptive transfer of macrophages, spleen $CD11b^+$ cells were sorted and

injected in EAE mice (5.10e6 cells per mouse) exhibiting a clinical score of 1-2. In other experiments, spleen $CD11b^+$ cells were sorted from naive mice, treated *ex vivo* with vehicle or SuperMApo for 24 h and injected in EAE mice (1.5.10e6 cells per mouse).

Injection of CFSE stained cells

Spleen from vehicle- or SuperMApo-treated EAE mice were removed 72 h after treatment and stained with CFSE (Thermo Fischer Scientific) during 10 min at 37°C, then washed and injected i.v in EAE mice (50 million per mice). Four h after the injection, percentage of $CFSE^+$ $CD11c^+CD11b^-$ DC, $CD19^+CD3^-$ B cells and $CD3^+CD19^-$ T cells in spinal cord, iLN and spleen was assessed by FACS.

Immunofluorescence

Spleen macrophages were sorted, treated with SuperMApo or vehicle during 24 h and stimulated with LPS for 1 h. Cells were then fixed in 4 % paraformaldehyde (Sigma-Aldrich) and permeabilized with 0.1% triton X-100 (Sigma-Aldrich) at room temperature. Immunofluorescence staining was performed, as previously described[31,32]. Briefly, non-specific sites were blocked with 0.1 % tween-TBS with 5 % BSA for 1 h at 37°C. Incubations with primary antibodies were performed overnight at +4°C, and then cells were rinsed 3 times with 0.1% tween-TBS. Incubations with secondary antibodies were performed for 1 h at 37°C and then cells were rinsed 3 times with 0.1% tween-TBS, stained with 4',6'-diamidino-2-phénylindole (DAPI) and mounted using Vectashield mounting medium (Vector Laboratories). Primary antibodies were against pP65 (cell signaling; 3033S), P65 (cell signaling; 6956P), pIKBα (cell signaling; 9246s), IKBα (abcam; ab76429), pIKKβ (abcam; ab192440), IKKβ (abcam; ab32135) and secondary antibodies were against donkey anti-mouse IgG Alexa Fluor 555-conjugated (Life technologies; A31571) and donkey anti-rabbit IgG NorthernLights493-conjugated (R&D systems; NL006) antibodies. Mean fluorescence intensity (MFI) was determined using image J software as previously described[33].

Immunoblot analysis

Whole-cell protein fraction was obtained by cell lysis in lysis buffer (complete protease inhibitor cocktail [Sigma], EDTA [1 mM], NaF [1 mM], sodium orthovanadate [1 mM], and Dithiothreitol [DTT, 0.5 mM]). Proteins were separated by electrophoresis using 10 % sodium dodecyl sulfate-polyacrylamide gels and transferred to polyvinylidene difluoride membranes (GE Healthcare). Blots were saturated with 5 % nonfat milk in TRIS-buffered saline (TBS)-0.1 % Tween 20 1.5 h at room temperature (RT), then incubated overnight with specific primary antibodies (same as in immunofluorescence staining), followed by HRP-conjugated secondary antibody (peroxidase-conjugated sheep anti-mouse IgG or donkey anti-rabbit IgG; Jackson Immuno Research) staining in 1% BSA-TBS-Tween for 1.5 h at RT. Bioluminescence was analyzed with the clarity western ECL reagent (Biorad) using a CCD camera (Vilber-Lourmat). Relative intensity was determined using Bio 1-D software (Vilber-Lourmat).

Transcriptomic analysis

RNA samples were sent to Integragen for sequencing on NGS platform (Illumina HiSeq 4000) and the resulting raw data (fastq) were sent to the CLIPP platform (Dijon, France) for analysis on their custom pipeline (mouse reference genome alignment was performed using TopHat2 algorithm followed by differential expression of transcripts with Cufflinks algorithms). Resulting RNA-seq data, containing FPKM (Fragments Per Kilobase of exon per million fragments Mapped) values, were $\log_2$ transformed, normalized and mean-centered using Cluster 3.0 software and data visualization was performed using GiTools and TreeView 3 for the different Heatmaps, and Cytoscape 3.2 for network analysis of the associated pathways.

Epigenetic studies

DNA extract was performed using QIAamp DNA Mini QIAcube Kit and QIAcube (Qiagen, France). 5-methylcytosine ELISA was performed using 5mC ELISA (Ozyme/Zymo, France). TET activity was determined using eth 5mC-Hydroxylase TET Activity/Inhibition Assay Kit (Euromedex, France).

DNMTs magnetic bead (DMB) assays were performed as described by Yokochi and Robertson (PMID: 15273420). A typical methylation reaction contained 30 nM of the respective DNMT protein (Methylation Ltd, Port Orange, Florida or Tebu-Bio, France), 125 nM DNA oligonucleotides, and 900 nM tritium-labeled AdoMet (Amersham Bioscience, 1 mCi/mL), in reaction buffer (50 mM Tris, pH 8.0, 5 mM EDTA, 10% glycerol, 0.5 mM phenylmethylsulfonyl fluoride). After incubation at 37 C for 1 h, the reaction was quenched with an equal volume of magnetic beads suspension, and incubated for 15 min at room temperature. Next, the beads were magnetically isolated from the reaction mix, and tritium incorpo- ration was measured by scintillation counting. Unmethylated double stranded oligonucleotides were used to estimate the de novo MTase activity, and hemimethylated double stranded oligonucleotides were used to estimate the maintenance MTase activity.

miRNA extraction was perfomed using miRNeasy Mini Kit and QIAcube (Qiagen, France). miScript II RT Kit (Qiagen, France), miScript SYBR Green PCR Kit (Qiagen, France) and miScript Primer Assay were used to quantify the miRNA expression. MSRE methodology was adaptated from the OneStep qMethylTM Kit (Ozyme, ZYMO, France). A typical digestion of genomic DNA contained 20ng of DNA and 5 units of considered enzyme (New England Biolab, France). For the non-enzyme control, distilled water was added instead of *considered enzyme*. Except for certain enzyme, all prepared samples were incubated at 37℃ for 12 hours, follow by heat inactivation at 65℃ for 20 minutes. qPCR were performed using SYBR Green PCR Kit (Qiagen, France). The methylation level for any amplified region was determined using the following equation $\%methylation=100x2^{-\Delta Ct}$. Primers used are:

miR127#1: GCGATGGAACTGAGTTTTGTC and TCCTGGTCTACTCAATGAG, miR127#2: GCTCAGAGGGCTCTGATTCAGAAA and ATGAGACTTCCGACCAGCCAA, miR-223#1: ACCAGGGTAAACAGAGCATACAAG and GTGGCCCAAGCCTCAATTAACTCT, and miR-223#2 : ACACGAAACGTAACACTACA and CCAACTCAACTTATCAAATACACG.

Chromatin ImmunoPrecipitation (ChIP) experiments were performed with teh LowCell#ChIP kit (Diagenode, France). Bioruptor (Diagenode, France) was used for the sonication step (3 runs of 8 cycles (30seconds“ON”, 30 seconds “OFF”) at high power setting). 6 µg of antibody (Anti-CTCF antibody (ab70303) Abcam, France) were used and IP tubes were incubated at 40 rpm on a rotating wheel for 4 hours at 4°C. qPCR were performed using SYBR Green PCR Kit (Qiagen, France).

Typically, TET conversion activity was determined by measuring the 5mC level (ELISA) in a methylated oligonucleotide probe mimicking a DNA region of interest. Biotinylated probe was incubated with 10ng of Nuclear Extraction Kit (ab113474, Abcam, France) for 90min at 37°C in presence of not of 10µg of considered antibody (cEBPα: sc- sc-9314, Santa Cruz, France, EBF1 (clone 1G8, Abnova, France), and FOXA1 Abcam ab24738). After isolation and washes, reageants issue to the MethylFlashTM Global DNA Methylation (5-mC) ELISA Easy Kit (Colorimetric) were used to detect the 5mC on probe.

Statistical analysis

All data were analyzed for statistical significance using GraphPad Prism version 5.00 (GraphPad Software, San Diego, CA, USA) by adapted student t test or one or two-way ANOVA test including multiple comparison post-tests, as indicated.

Acknowledgements

We thank Helena Paidassi (Centre International de Recherche en Infectiologie) for providing us with OTII/RAG–/– mice and Jean-Paul Remy-Martin for his expertise in making liposomes and blotting. We also thank Dominique Paris, Francois Coulon and Emmanuel Salvado for taking care of the mice.

The work was funded by the Etablissement Français du Sang (2016-02 to S.P.), the Conseil Régional de Franche-Comté ("Soutien au LabEX LipSTIC" 2014/2015 to P.S. and AAP 2013-2017 to S.P.), and by the Agence Nationale de la Recherche (ANR-11-LABX-0021 to Labex LipSTIC). T.G. is supported by a doctoral fellowship from the Etablissement Français du Sang and from the Labex LipSTIC, O.M.R. and C.C. by a doctoral fellowship from the Ministère de l'Education Nationale, de l'Enseignement Supérieur et de la Recherche.

Author contributions

T.G. designed and performed most of the experiments, analyzed and interpreted the data. O.M.R., C.C., A.D., A.C., F.B. and M.C. contributed to some experiments. A.V. participated to transcriptomic analysis. S.V.D. performed the histological analysis and scoring of the tissues. P.F.C. designed and performed epigenetic experiments. T.G., P.S. and S.P. wrote the manuscript. All authors discussed the results and the manuscript. S.P. supervised the study.

Competing financial interests

The authors declare no competing financial interest.

References

1. Natrajan, M.S.*, et al.* Retinoid X receptor activation reverses age-related deficiencies in myelin debris phagocytosis and remyelination. *Brain : a journal of neurology* **138**, 3581-3597 (2015).
2. Lee, C.S.*, et al.* Boosting Apoptotic Cell Clearance by Colonic Epithelial Cells Attenuates Inflammation In Vivo. *Immunity* **44**, 807-820 (2016).
3. Perretti, M. The resolution of inflammation: New mechanisms in patho-physiology open opportunities for pharmacology. *Seminars in immunology* **27**, 145-148 (2015).
4. Bonnefoy, F.*, et al.* Apoptotic cell infusion treats ongoing collagen-induced arthritis, even in the presence of methotrexate, and is synergic with anti-TNF therapy. *Arthritis research & therapy* **18**, 184 (2016).
5. Lutterotti, A.*, et al.* Antigen-specific tolerance by autologous myelin peptide-coupled cells: a phase 1 trial in multiple sclerosis. *Science translational medicine* **5**, 188ra175 (2013).
6. Kasagi, S.*, et al.* In vivo-generated antigen-specific regulatory T cells treat autoimmunity without compromising antibacterial immune response. *Science translational medicine* **6**, 241ra278 (2014).
7. Ortega-Gomez, A., Perretti, M. & Soehnlein, O. Resolution of inflammation: an integrated view. *EMBO molecular medicine* **5**, 661-674 (2013).
8. Serhan, C.N. Pro-resolving lipid mediators are leads for resolution physiology. *Nature* **510**, 92-101 (2014).
9. Serhan, C.N., Chiang, N. & Van Dyke, T.E. Resolving inflammation: dual anti-inflammatory and pro-resolution lipid mediators. *Nature reviews. Immunology* **8**, 349-361 (2008).
10. Fadok, V.A.*, et al.* Macrophages that have ingested apoptotic cells in vitro inhibit proinflammatory cytokine production through autocrine/paracrine mechanisms

involving TGF-beta, PGE2, and PAF. *The Journal of clinical investigation* **101**, 890-898 (1998).

11. Fullerton, J.N. & Gilroy, D.W. Resolution of inflammation: a new therapeutic frontier. *Nature reviews. Drug discovery* **15**, 551-567 (2016).
12. Dalli, J. & Serhan, C.N. Specific lipid mediator signatures of human phagocytes: microparticles stimulate macrophage efferocytosis and pro-resolving mediators. *Blood* **120**, e60-72 (2012).
13. Poon, I.K., Lucas, C.D., Rossi, A.G. & Ravichandran, K.S. Apoptotic cell clearance: basic biology and therapeutic potential. *Nature reviews. Immunology* **14**, 166-180 (2014).
14. Perretti, M., Leroy, X., Bland, E.J. & Montero-Melendez, T. Resolution Pharmacology: Opportunities for Therapeutic Innovation in Inflammation. *Trends in pharmacological sciences* **36**, 737-755 (2015).
15. Kebir, H.*, et al.* Human TH17 lymphocytes promote blood-brain barrier disruption and central nervous system inflammation. *Nature medicine* **13**, 1173-1175 (2007).
16. Bennett, J.*, et al.* Blood-brain barrier disruption and enhanced vascular permeability in the multiple sclerosis model EAE. *Journal of neuroimmunology* **229**, 180-191 (2010).
17. Zhang, H.*, et al.* Silencing c-Rel in macrophages dampens Th1 and Th17 immune responses and alleviates experimental autoimmune encephalomyelitis in mice. *Immunology and cell biology* **95**, 593-600 (2017).
18. Weber, M.S.*, et al.* Type II monocytes modulate T cell-mediated central nervous system autoimmune disease. *Nature medicine* **13**, 935-943 (2007).
19. Croxford, A.L.*, et al.* The Cytokine GM-CSF Drives the Inflammatory Signature of CCR2+ Monocytes and Licenses Autoimmunity. *Immunity* **43**, 502-514 (2015).

20. Renner, K.*, et al.* IL-3 promotes the development of experimental autoimmune encephalitis. *JCI insight* **1**, e87157 (2016).

21. Sporici, R. & Issekutz, T.B. CXCR3 blockade inhibits T-cell migration into the CNS during EAE and prevents development of adoptively transferred, but not actively induced, disease. *European journal of immunology* **40**, 2751-2761 (2010).

22. Yang, Q.*, et al.* Spermidine alleviates experimental autoimmune encephalomyelitis through inducing inhibitory macrophages. *Cell death and differentiation* **23**, 1850-1861 (2016).

23. Andreakos, E.*, et al.* Distinct pathways of LPS-induced NF-kappa B activation and cytokine production in human myeloid and nonmyeloid cells defined by selective utilization of MyD88 and Mal/TIRAP. *Blood* **103**, 2229-2237 (2004).

24. Nathan, C. & Ding, A. Nonresolving inflammation. *Cell* **140**, 871-882 (2010).

25. Torkildsen, O., Brunborg, L.A., Myhr, K.M. & Bo, L. The cuprizone model for demyelination. *Acta neurologica Scandinavica. Supplementum* **188**, 72-76 (2008).

26. Bogie, J.F., Stinissen, P. & Hendriks, J.J. Macrophage subsets and microglia in multiple sclerosis. *Acta neuropathologica* **128**, 191-213 (2014).

27. Lucas, T.*, et al.* Differential roles of macrophages in diverse phases of skin repair. *J Immunol* **184**, 3964-3977 (2010).

28. Anton, K., Banerjee, D. & Glod, J. Macrophage-associated mesenchymal stem cells assume an activated, migratory, pro-inflammatory phenotype with increased IL-6 and CXCL10 secretion. *PloS one* **7**, e35036 (2012).

29. Freytes, D.O., Kang, J.W., Marcos-Campos, I. & Vunjak-Novakovic, G. Macrophages modulate the viability and growth of human mesenchymal stem cells. *Journal of cellular biochemistry* **114**, 220-229 (2013).

30. Kleinclauss, F.*, et al.* Intravenous apoptotic spleen cell infusion induces a TGF-beta-dependent regulatory T-cell expansion. *Cell Death Differ* **13**, 41-52 (2006).

31. Gauthier, T., Claude-Taupin, A., Delage-Mourroux, R., Boyer-Guittaut, M. & Hervouet, E. Proximity Ligation In situ Assay is a Powerful Tool to Monitor Specific ATG Protein Interactions following Autophagy Induction. *PloS one* **10**, e0128701 (2015).

32. Ceroi, A.*, et al.* LXR agonist treatment of blastic plasmacytoid dendritic cell neoplasm restores cholesterol efflux and triggers apoptosis. *Blood* **128**, 2694-2707 (2016).

33. Burgess, A.*, et al.* Loss of human Greatwall results in G2 arrest and multiple mitotic defects due to deregulation of the cyclin B-Cdc2/PP2A balance. *Proceedings of the National Academy of Sciences of the United States of America* **107**, 12564-12569 (2010).

Figure Legends

FIGURE 1 SuperMApo attenuates ongoing EAE in C57BL/6 mice. (**a**) Clinical score of EAE mice treated twice (black arrows) with SuperMApo (n = 6 mice) or with vehicle (n = 5 mice). Data representative of 3 independent experiments. (**b**) H&E and Luxol Fast Blue staining of spinal cords 72 h after the first injection of SuperMApo or vehicle. Degree of inflammation in mice is depicted by inflammatory index and scored in H&E sections. Demyelination is scored in Luxol Fast Blue sections. Demyelinated areas are pointed out by black arrows. Scale bar, 80 μM. Data pooled from 3 independent experiments (n= 5 mice). (**c**) Clinical score of EAE mice treated twice (black arrows) with supernatant of apoptotic cells added to the supernatant of macrophages (1 mL) (n= 5 mice). Data representative of 2 independent experiments. Mean

± SEM. Statistical significance was assessed by using anova two-way and Bonferroni post test (a,c) or unpaired two tailed Student's t test (b) (*p<0.05 ***p<0.001).

FIGURE 2 SuperMApo decreases spinal cord inflammation in EAE mice. (**a**) Total number of leukocytes in spinal cords 72h after the first SuperMApo (n= 5 mice) or vehicle (n= 5 mice) treatment. Data representative of 3 independent experiments. (**b**) Absolute number of Th1 (IFN-γ^+CD4$^+$CD3$^+$), Th17 (CD3$^+$CD4$^+$IL-17$^+$), Tc1 (CD3$^+$CD8$^+$IFN-γ^+), dendritic cells (DC) (CD11c$^+$CD11b$^-$) and macrophages (CD11b^{hi}CD45$^+$). Data representative of 3 independent experiments. (**c**) Percentages of cells depicted in (b). (**d**) Analysis by Cytometric Bead Array of TNF-α, IL-12p70, IFN-γ, IL-6 and IL-10 concentrations in spinal cord lysate (n= 5 mice). Data representative of 3 independent experiments. (**e**) Leukocytes isolated from spinal cords were analyzed by FACS and Mean Fluorescence Intensity (MFI) of CD86, CD80, MHC-II and CD40 in macrophages are given (n= 4 mice). Data representative of 3 independent experiments. (**f**) Frequency of TNF-α, IL-12 and IL-10 positive cells gated on macrophages in spinal cords of mice (n= 5 mice). Data representative of 2 independent experiments. (**g**) Evan's Blue (EB) was injected i.v 72h after the first injection of SuperMApo and extracted 1h after dye injection (n= 5 mice). Data given in ng EB/mg of tissue (refer to Materials and Methods section). Data representative of 3 independent experiments. (**h**) Analysis by qRT-PCR for expression of *Occludin*, *Claudin5*, *Tjp1*and *F11r* in total spinal cord extracts (n= 5 mice). Data are representative of 3 independent experiments. (**i**) Analysis by qRT-PCR for expression of *Ccl2*, *Ccl5*, *Cxcl9* and *Cxcl10* in total spinal cord extracts (n= 5 mice). Data are representative of 3 independent experiments. (**j**) Analysis by qRT-PCR for expression of *Itgβ5*, *Itgβ7*, *Vla-4*, *Icam-1* and *Vcam* in total spinal cord extracts (n= 5 mice). Data are representative of 3 independent experiments. Mean ± SEM. *= p<0.05 **=p<0.01 ***=p<0.005, unpaired two-tailed Student's T test.

FIGURE S1 SuperMApo does not modulate microglia phenotype. (**a**) Absolute number of microglia ($CD11b^{med}CD45^{+}$) in spinal cords of EAE mice 72h after the first SuperMApo treatment (n= 5 mice). Data representative of 3 independent experiments. (**b**) Mean Fluorescence Intensity (MFI) of CD80, CD86, CD40 and MHC-II in microglia (n= 4 mice). Data representative of 3 independent experiments. (**c**) Frequency of TNF-α, IL-12 and IL-10 positive cells gated on microglia in spinal cords of mice (n= 5 mice). Data representative of 2 independent experiments. (**d**) Cytometric representation illustrating (c) and figure 2.f. Mean ± SEM, unpaired two-tailed Student's t test.

FIGURE 3 SuperMApo decreases peripheral T cell responses in peripheral lymphoid organ. Percentage of CD4, Th1, Th17, Treg (**a**) or CD8 and Tc1 (**b**) in spleen and iLN 72 h after the first SuperMApo treatment (n= 5 mice). Data representative of 3 independent experiments. (**c**) Percentage of activated caspases was assessed by FACS in $CD4^{+}CD3^{+}$, $CD8^{+}CD3^{+}$ or total cells in the spleen (n= 3 mice). Data representative of 3 independent experiments. (**d**) Percentage of ki67 positive cells was assessed by FACS in $CD4^{+}CD3^{+}$, $CD8^{+}CD3^{+}$, $IL17^{+}CD4^{+}$ $CD3^{+}$, IFN-$\gamma^{+}CD4^{+}$ $CD3^{+}$ and IFN-$\gamma^{+}CD8^{+}$ $CD3^{+}$ in the spleen and iLN (n= 5 mice). Data representative of 2 independent experiments. (**e**) Spleen or iLN from SuperMApo- (n= 5 mice) or vehicle-treated mice (n= 4 mice) were restimulated with MOG_{35-55} peptide (15 µg/mL) and proliferation was assessed by BrdU incorporation. Data representative of 3 independent experiments. (**f**) Naive OT-II T cells sorted from the spleen of EAE mice were cultured in presence of DC and $OVA_{323-339}$, *Mycobacterium tuberculosis* or CD3/CD28 and different ratio of Treg sorted from the spleen of EAE mice treated with SuperMApo or vehicle. Data representative of two independent experiments. (**g**) Spleen and iLN from SuperMApo- or vehicle-treated mice were restimulated with MOG peptide (15

μg/mL) and frequencies of $IL17^+CD4^+$, IFN-γ^+CD4^+ and IFN-γ^+CD8^+ were determined by FACS (n= 4 mice). Data representative of 3 independent experiments. Mean ± SEM. *=p<0.05 **=p<0.01 ***=p<0.005, unpaired two tailed Student's t test.

FIGURE 4 SuperMApo decreases immune responses in EAE mice by inducing pro-tolerogenic macrophages. (**a**) Macrophages sorted from vehicle- or SuperMApo-treated mice were co-cultured during 96 h with naive $CD25^-CD4^+$ OT-II T cells in presence of OVA peptide (2 μg/mL). Frequencies of $IL17^+CD4^+$, IFN-γ^+CD4^+ and $Foxp3^+CD25^+CD4^+$ were determined by FACS (left panels show representative staining of these $CD4^+$ T cells cultured with macrophages from a vehicle-treated EAE mouse [EAE] or macrophages from a SuperMApo-treated EAE mouse [+SuperMApo]). Data representative of 3 independent experiments (triplicate from a pool of 5 mice, right panel). (**b**) Macrophages isolated from the spleen of naive C57BL/6 mice were pre-treated with SuperMApo or vehicle during 24 h, and then co-cultured during 96 h with naive $CD25^-CD4^+$ OT-II T cells in presence of OVA peptide (2 μg/mL). Frequencies of $CD4^+IL17^+$, $CD4^+$IFN-γ^+ and $CD4^+CD25^+Foxp3^+$ were determined by FACS (same gating strategy as in a). Data representative of 2 independent experiments. (**c**) Clinical score of mice treated with macrophages sorted from vehicle- or SuperMApo-treated mice (n= 4 mice). Data representative of 2 independent experiments. (**d**) Percentage of T cell subset was analyzed by FACS in the spinal cord (left) and inguinal lymph node (iLN) (right) seven days after treatment of mice in (c) (n= 4 mice) (same gating strategy as in a). Data pooled from 2 independent experiments. (**e**) Clinical score of mice treated with clodronate loaded- or PBS loaded-liposomes infused i.v. at day 6, 8 and 10, and then treated with vehicle or SuperMApo at day 9 and 11 (n= 3-4 mice). Data representative of 2 independent experiments. (**f**) Splenocytes (left) or iLN (right) from mice (described in e) were restimulated with MOG_{35-55} peptide (15 μg/mL) and proliferation was assessed by BrdU

incorporation (n= 4-5 mice). Data pooled from 2 independent experiments. (**g**) Leukocytes from spinal cord of mice (described in e) were sorted 7 days after treatment and analyzed by FACS. Data pooled from 2 independent experiments. Mean ± SEM. *=p<0.05 **=p<0.01 ***=p<0.005, unpaired two-tailed Student's T test (a, c, d, f, h, i), Anova two-way with Bonferroni post test (b) or Anova one-way with Tukey post test (e and g).

FIGURE S2 SuperMApo does not modulate *in vivo* macrophage response to LPS restimulation *in vitro*. Maturation markers (**a**) and pro-inflammatory cytokines (**b**) were analyzed on macrophages from the spleen of vehicle- or SuperMApo-treated EAE mice after ex vivo LPS stimulation (1 µg/mL) during 24 h compared to not treated cells (n= 5 mice). Data representative of at least 2 independent experiments. Mean ± SEM. Unpaired two-tailed Student's t test.

FIGURE S3 SuperMApo induces pro-tolerogenic macrophages *in vitro* which are able to control EAE. (**a**) Macrophages sorted from naive mice were treated with vehicle or SuperMApo during 24 h, and then injected in EAE mice (n= 5 mice). Clinical score is depicted. Data representative of 2 independent experiments. (f) T cells from spinal cord (left) or iLN (right) were sorted 7 days after treatment and analyzed by FACS (n= 3-5 mice). Data pooled from 2 independent experiments. Mean ± SEM. Anova two-way with Bonferroni post test (a) or Anova one-way with Tukey post test (b).

Figure 5 SuperMApo reprogramms macrophages toward a pro-tolerogenic profile. (**a**) Gene expression (log2 FPKM transformed) of macrophages from EAE mice treated with vehicle or SuperMApo. Genes are ordered and colored based on their fold change, with (a) 357 genes with a change in expression of 1.5-fold or more, (b) 569 genes with a fold change of 0.67 or

below, (c) 214 genes expressed only in macrophages from SuperMApo-treated mice, and (d) 241 genes expressed only in macrophages from vehicle-treated mice. (**b**) Expression (log2 FPKM transformed, normalized, mean centered) of all 12049 genes in mouse macrophages, clustered from lowest fold change (top) to highest (bottom). (**c**) Network analysis of gene-ontology pathway enrichment on all 357 genes with a fold change of 1.5 or more and all 214 genes only expressed in macrophages from SuperMApo-treated mice with a $P< 0.05$. (**d**) Network analysis of gene-ontology pathway enrichment on all 569 genes with a fold change of 0.67 or below and all 241 genes only expressed in macrophages from vehicle-treated mice. (**e**) Expression (log2 FPKM transformed, normalized, mean centered) of genes corresponding to selected pathways found in the network analysis enrichment on all 357 genes with a fold change of 1.5 or more and all 214 genes only expressed in macrophages from SuperMApo-treated mice. (**f**) Expression (log2 FPKM transformed, normalized, mean centered) of selected genes corresponding to selected pathways found in the network analysis enrichment on all 569 genes with a fold change of 0.67 or below and all 241 genes only expressed in macrophages from vehicle-treated mice. Data obtained from 2 independent experiments from a pool of 5 mice.

FIGURE S4 Macrophages modulate expression of CXCR3 on Th1 cells. (**a**) Experimental scheme of the EAE splenocytes transfer. (**b**) Spleen of vehicle- (n= 5 mice) or SuperMApo-treated (n= 4 mice) EAE mice were removed, stained with CFSE, and then reinjected in EAE mice (50*10e6 cells/mice). Four hour after injection, spleen, inguinal lymph node (iLN) and spinal cord (SC) were sorted and analyzed by FACS for expression of CFSE. Data pooled from two independent experiments. (**c**) Percentage of CFSE-positive B cells, T cells and dendritic cells (DC) from the spleen and iLN of (a). (**d**) Analysis by qRT-PCR for expression of Cxcr3, Ccr5 and Ccr6 in spleen and iLN of vehicle- or SuperMApo-treated mice (n= 4

mice). Data representative of 3 independent experiments. (**e**) Splenocytes removed from vehicle- or SuperMApo-treated EAE mice and analyzed by FACS for the expression of CXCR3 on Th1, Th17, Tc1, and DC (n= 5 mice). Data representative of three independent experiments. (**f**) Macrophages isolated from spleen of naive mice were pre-treated with SuperMApo or vehicle during 24 h, and then co-cultured during 96 h with naive $CD25^{-}CD4^{+}$ OTII T cells in presence of 2 µg/mL of OVA peptide. Data representative of 2 independent experiments from triplicate measurements. (**g**) Analysis of CXCR3 expression on Th1 cells from the spleen of mice treated with vehicle (n= 4 mice) or SuperMApo (n= 5 mice) and with an i.v. injection of clodronate-loaded or control PBS-loaded liposomes. Data pooled from two independent experiments. Mean ± SEM. *=$p<0.05$ **=$p<0.01$ ***=$p<0.005$.

FIGURE S5 SuperMApo decreases macrophage inflammatory state by blocking NF-κB activation. Expression of co-stimulatory molecules (**a**) and pro-inflammatory cytokines (**b**) were analyzed on macrophages sorted from naive mice after SuperMApo or vehicle treatment, and then stimulated for 24 h by LPS (1 µg/mL). Data representative of 3 independent experiments. (**c**) Immunofluorescence staining of p-IKKb, p-IκB, p-P65 and P65 subunits on $CD11b^{+}$ macrophages sorted from SuperMApo- or vehicle-treated EAE mice. Data pooled from three independent experiments (**d**) P-P65, p-IκB (S473), as well as unphosphorylated corresponding protein expression was assessed by western blotting on $CD11b^{+}$ macrophages sorted from SuperMApo- or vehicle-treated EAE mice. The expression of these proteins was compared with actin. Data representative of three independent experiments. (**e**) p65 NF-κB subunit localization was assessed by immunofluorescence on $CD11b^{+}$ macrophages sorted from the spleen of naive mice and treated during 24 h with SuperMApo or vehicle, and then stimulated with LPS during 1 h. Data representative of three independent experiments. Mean ± SEM. *=$p<0.05$ ***=$p<0.005$, unpaired two-tailed Student's T test.

Figure 6 Macrophage reprogramming by SuperMApo occurs through an epigenetic-dependent manner. (**a**) Total level of 5-methylcytosine observed on macrophages sorted from EAE mice 72 h after the first SuperMApo treatment. TET activity (**b**), de maintenance (**c**) and de novo (**d**) methyltransferase activity on macrophages sorted from EAE mice 72 h after the first SuperMApo treatment. (**e**) TET conversion was assessed using antibodies directed against c-EBPa, EBF1 and FOXA1. (**f**) Analysis by qRT-PCR for expression of miRNA-155, -127, -146a and 223. (**g**) Local methylation level on genes coding miR-223 (left) and miR-127 (right) observed by qMSRE. (**h**) CHIP of CTCF enrichment on region 1 on the promoter of miR-127. Data pooled from three independent experiments from a pool of five mice. Mean ± SEM. **=$p<0.01$ ***=$p<0.005$, unpaired two-tailed Student's T test.

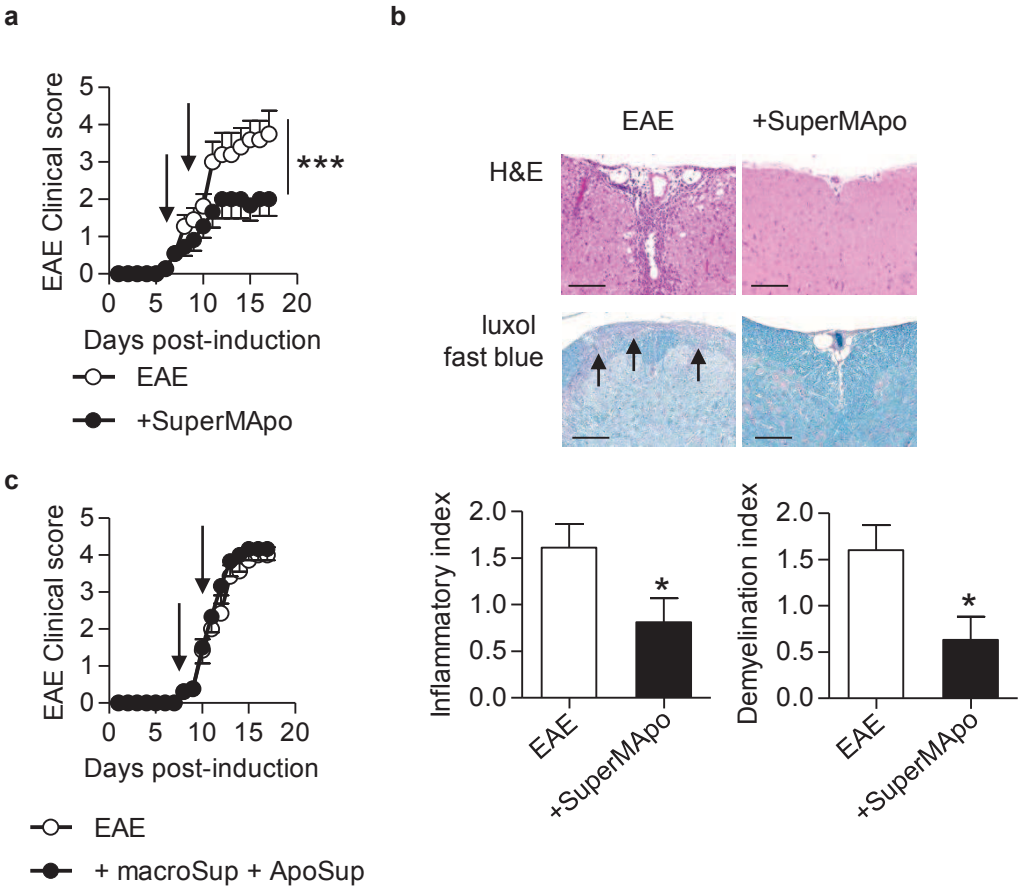
a
EAE Clinical score
Days post-induction
***
EAE
+SuperMApo
b
EAE
+SuperMApo
H&E
luxol
fast blue
Inflammatory index
Demyelination index
*
*
EAE
+SuperMApo
c
EAE Clinical score
Days post-induction
EAE
+ macroSup + ApoSup

Fig 1

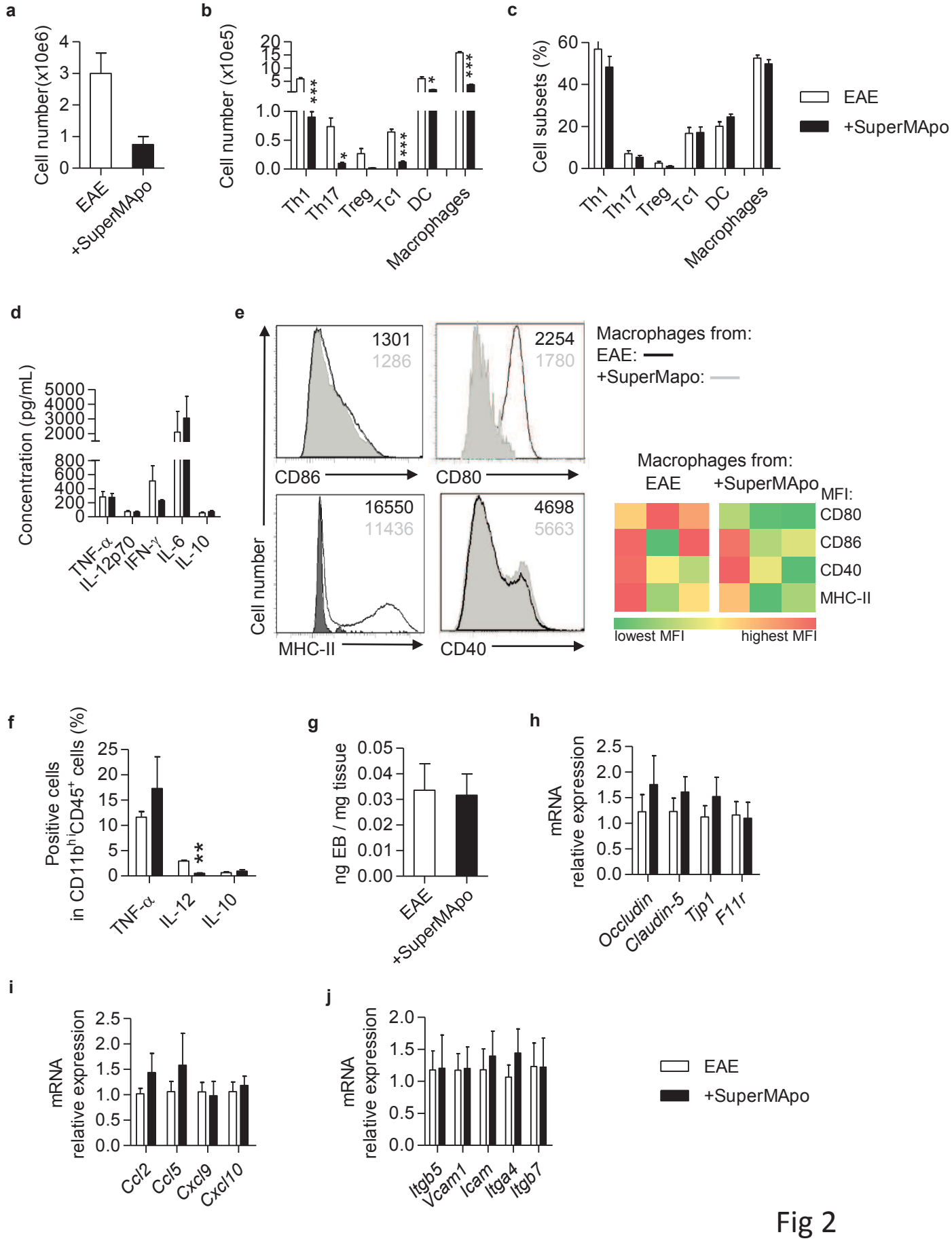
a
Cell number(x10e6)
EAE
+SuperMApo
b
Cell number (x10e5)
Th1
Th17
Treg
Tc1
DC
Macrophages
c
Cell subsets (%)
EAE
+SuperMApo
d
Concentration (pg/mL)
TNF-α
IL-12p70
IFN-γ
IL-6
IL-10
e
Macrophages from:
EAE:
+SuperMapo:
1301
1286
2254
1780
CD86
CD80
16550
11436
4698
5663
Cell number
MHC-II
CD40
Macrophages from:
EAE
+SuperMApo
MFI:
CD80
CD86
CD40
MHC-II
lowest MFI
highest MFI
f
Positive cells in CD11b^hiCD45^+ cells (%)
TNF-α
IL-12
IL-10
g
ng EB / mg tissue
EAE
+SuperMApo
h
mRNA relative expression
Occludin
Claudin-5
Tjp1
F11r
i
mRNA relative expression
Ccl2
Ccl5
Cxcl9
Cxcl10
j
mRNA relative expression
Itgb5
Vcam1
Icam
Itga4
Itgb7
EAE
+SuperMApo

Fig 2

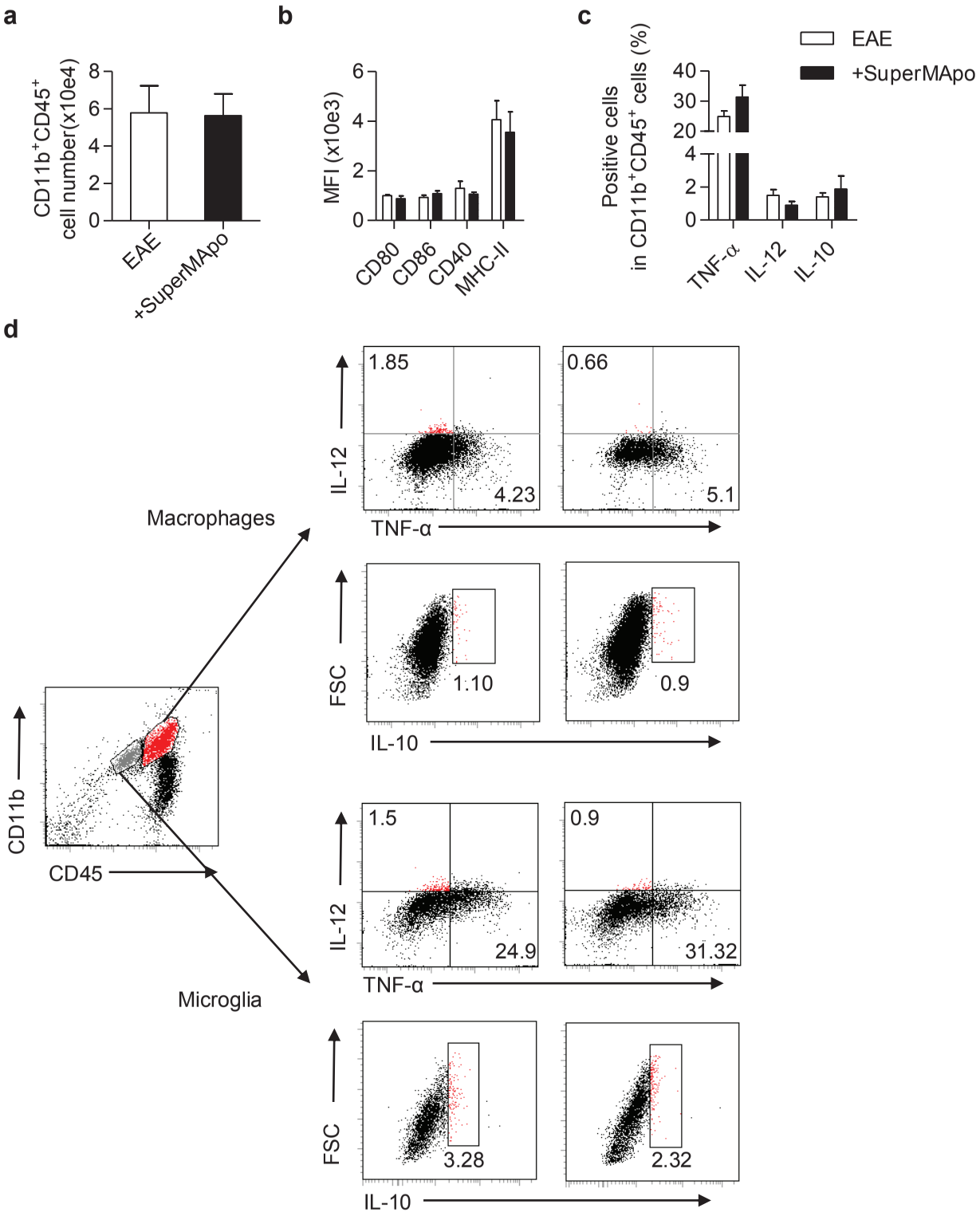
a
CD11b+CD45+ cell number(x10e4)
EAE
+SuperMApo
b
MFI (x10e3)
CD80
CD86
CD40
MHC-II
c
EAE
+SuperMApo
Positive cells in CD11b+CD45+ cells (%)
TNF-α
IL-12
IL-10
d
Macrophages
CD11b
CD45
Microglia
IL-12
TNF-α
1.85
4.23
0.66
5.1
FSC
IL-10
1.10
0.9
1.5
24.9
0.9
31.32
3.28
2.32

Fig S1

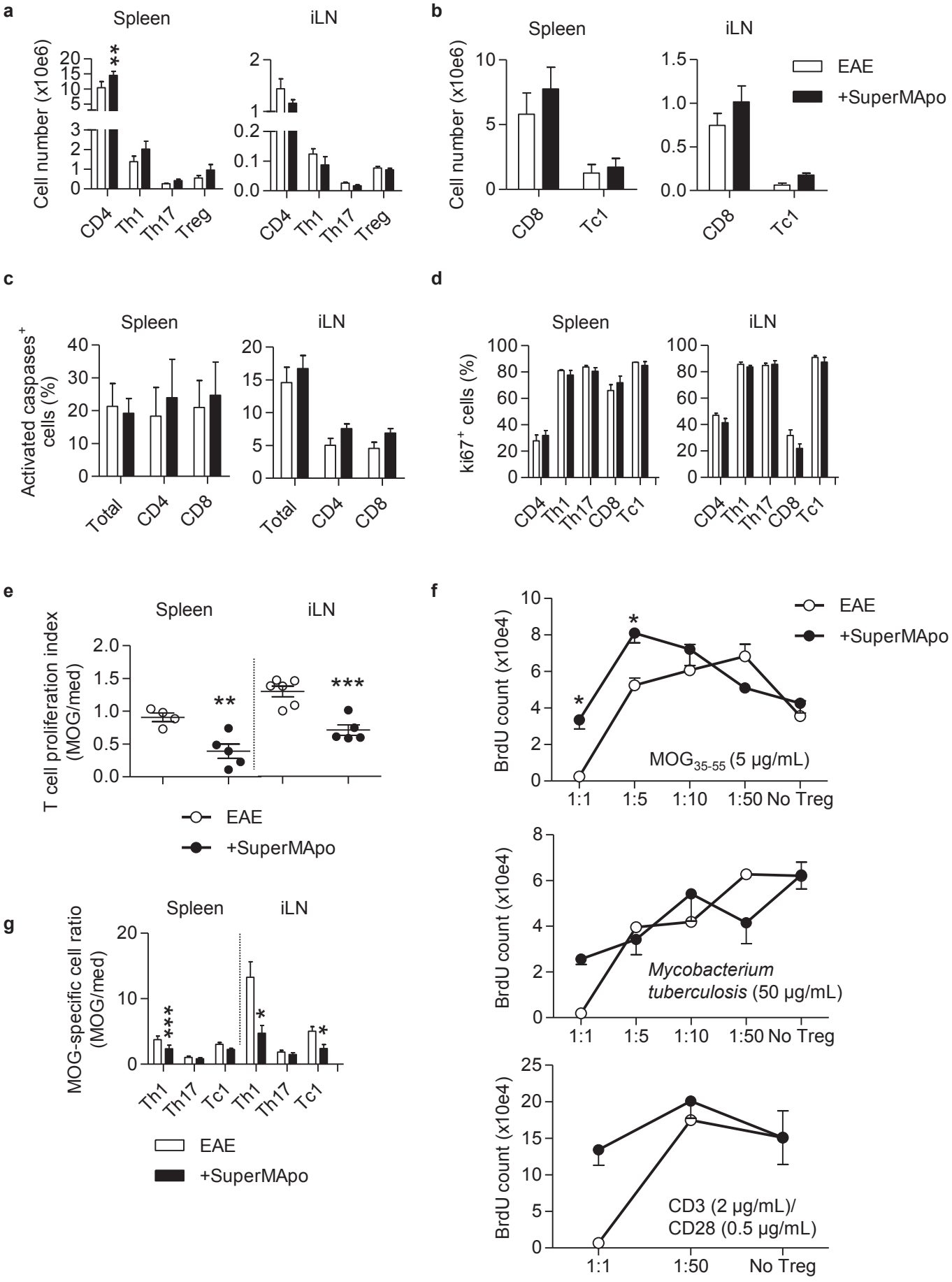
a
Spleen
iLN
Cell number (x10e6)
CD4
Th1
Th17
Treg
b
Spleen
iLN
Cell number (x10e6)
CD8
Tc1
EAE
+SuperMApo
c
Spleen
iLN
Activated caspases+ cells (%)
Total
CD4
CD8
d
Spleen
iLN
ki67+ cells (%)
CD4
Th1
Th17
CD8
Tc1
e
Spleen
iLN
T cell proliferation index (MOG/med)
EAE
+SuperMApo
f
BrdU count (x10e4)
EAE
+SuperMApo
MOG35-55 (5 µg/mL)
1:1
1:5
1:10
1:50
No Treg
Mycobacterium tuberculosis (50 µg/mL)
CD3 (2 µg/mL)/ CD28 (0.5 µg/mL)
g
Spleen
iLN
MOG-specific cell ratio (MOG/med)
Th1
Th17
Tc1
EAE
+SuperMApo

Fig 3

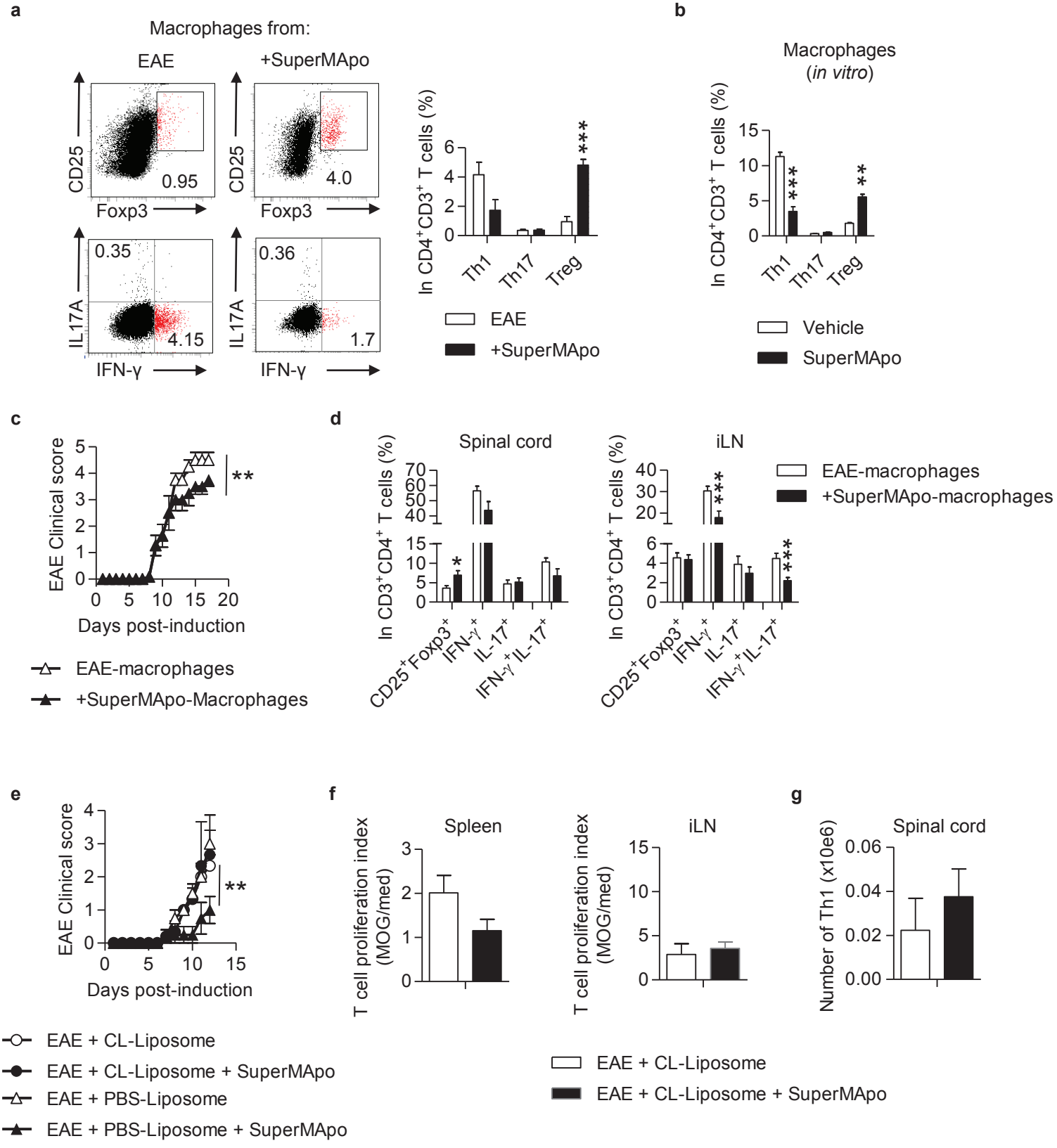
a
Macrophages from:
EAE
+SuperMApo
CD25
Foxp3
0.95
4.0
IL17A
IFN-γ
0.35
4.15
0.36
1.7
ln CD4+CD3+ T cells (%)
Th1
Th17
Treg
***
EAE
+SuperMApo
b
Macrophages
(in vitro)
ln CD4+CD3+ T cells (%)
***
**
Vehicle
SuperMApo
c
EAE Clinical score
Days post-induction
**
EAE-macrophages
+SuperMApo-Macrophages
d
Spinal cord
iLN
ln CD3+CD4+ T cells (%)
*
***
CD25+Foxp3+
IFN-γ+
IL-17+
IFN-γ+IL-17+
EAE-macrophages
+SuperMApo-macrophages
e
EAE Clinical score
Days post-induction
**
EAE + CL-Liposome
EAE + CL-Liposome + SuperMApo
EAE + PBS-Liposome
EAE + PBS-Liposome + SuperMApo
f
Spleen
iLN
T cell proliferation index
(MOG/med)
EAE + CL-Liposome
EAE + CL-Liposome + SuperMApo
g
Spinal cord
Number of Th1 (x10e6)

Fig 4

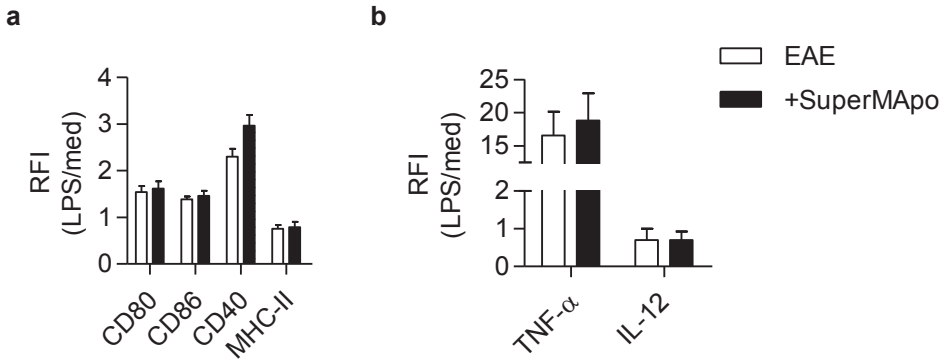
a
b
RFI
(LPS/med)
4
3
2
1
0
CD80
CD86
CD40
MHC-II
25
20
15
2
1
0
TNF-α
IL-12
EAE
+SuperMApo

Fig S2

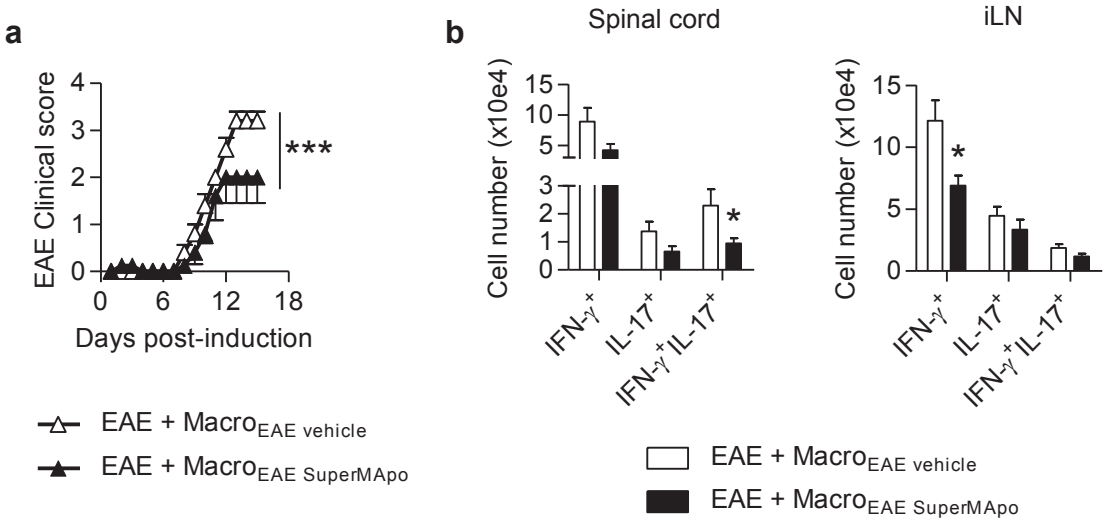
a
EAE Clinical score
4
3
2
1
0
0
6
12
18
Days post-induction
***
EAE + Macro EAE vehicle
EAE + Macro EAE SuperMApo
b
Spinal cord
iLN
Cell number (x10e4)
15
10
5
3
2
1
0
*
IFN-γ+
IL-17+
IFN-γ+IL-17+
EAE + Macro EAE vehicle
EAE + Macro EAE SuperMApo

Fig S3

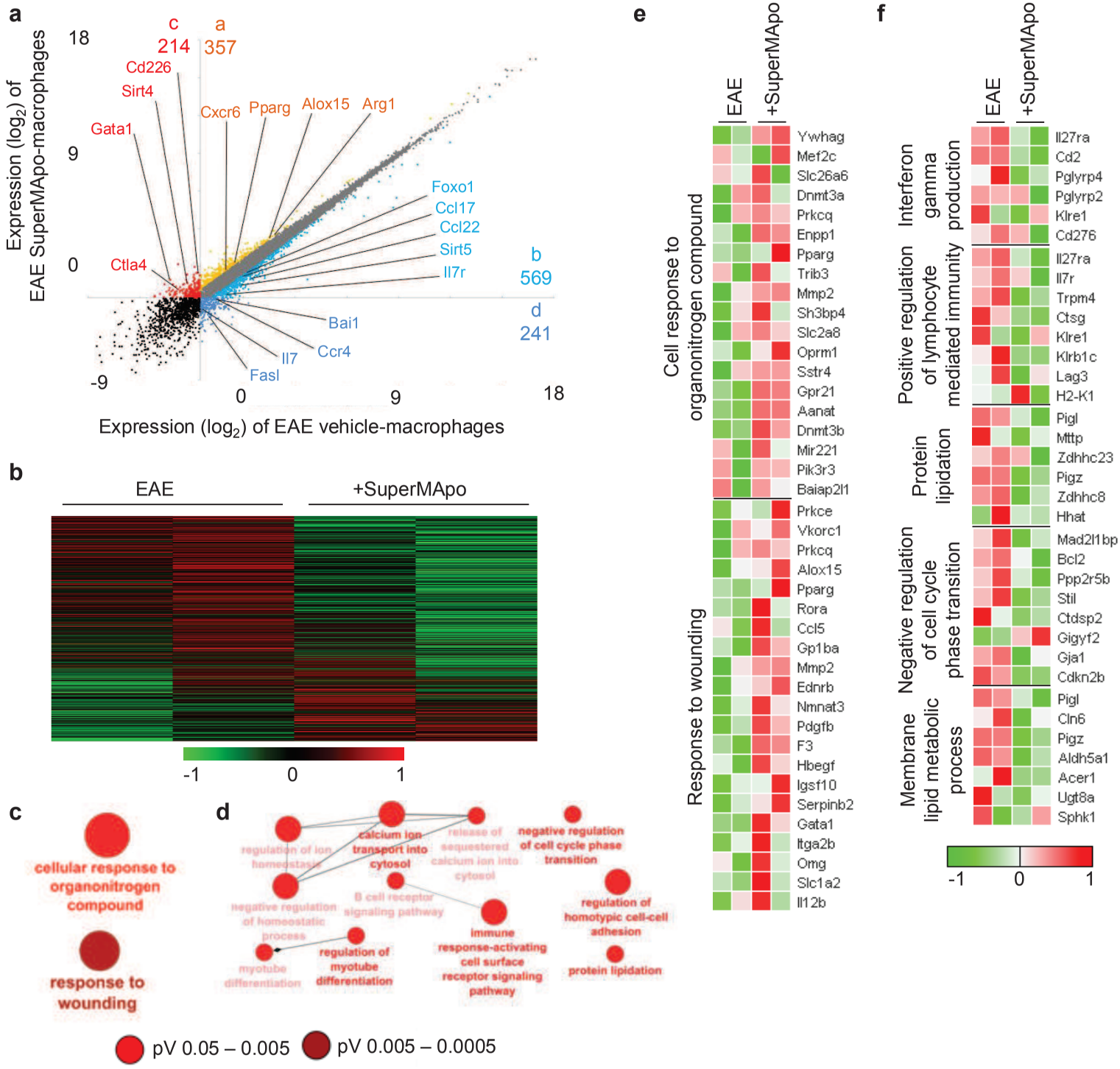
a
c
214
a
357
Cd226
Sirt4
Cxcr6
Pparg
Alox15
Arg1
Gata1
Foxo1
Ccl17
Ccl22
Sirt5
Il7r
Ctla4
b
569
d
241
Bai1
Ccr4
Il7
Fasl
18
9
0
-9
Expression (log2) of EAE SuperMApo-macrophages
Expression (log2) of EAE vehicle-macrophages
b
EAE
+SuperMApo
-1
0
1
c
cellular response to organonitrogen compound
response to wounding
d
calcium ion transport into cytosol
release of sequestered calcium ion into cytosol
negative regulation of cell cycle phase transition
regulation of ion homeostasis
negative regulation of homeostatic process
B cell receptor signaling pathway
regulation of homotypic cell-cell adhesion
immune response-activating cell surface receptor signaling pathway
myotube differentiation
regulation of myotube differentiation
protein lipidation
pV 0.05 – 0.005
pV 0.005 – 0.0005
e
EAE
+SuperMApo
Cell response to organonitrogen compound
Ywhag
Mef2c
Slc26a6
Dnmt3a
Prkcq
Enpp1
Pparg
Trib3
Mmp2
Sh3bp4
Slc2a8
Oprm1
Sstr4
Gpr21
Aanat
Dnmt3b
Mir221
Pik3r3
Baiap2l1
Response to wounding
Prkce
Vkorc1
Prkcq
Alox15
Pparg
Rora
Ccl5
Gp1ba
Mmp2
Ednrb
Nmnat3
Pdgfb
F3
Hbegf
Igsf10
Serpinb2
Gata1
Itga2b
Omg
Slc1a2
Il12b
f
EAE
+SuperMApo
Interferon gamma production
Il27ra
Cd2
Pglyrp4
Pglyrp2
Klre1
Cd276
Positive regulation of lymphocyte mediated immunity
Il27ra
Il7r
Trpm4
Ctsg
Klre1
Klrb1c
Lag3
H2-K1
Protein lipidation
Pigl
Mttp
Zdhhc23
Pigz
Zdhhc8
Hhat
Negative regulation of cell cycle phase transition
Mad2l1bp
Bcl2
Ppp2r5b
Stil
Ctdsp2
Gigyf2
Gja1
Cdkn2b
Membrane lipid metabolic process
Pigl
Cln6
Pigz
Aldh5a1
Acer1
Ugt8a
Sphk1
-1
0
1

Fig 5

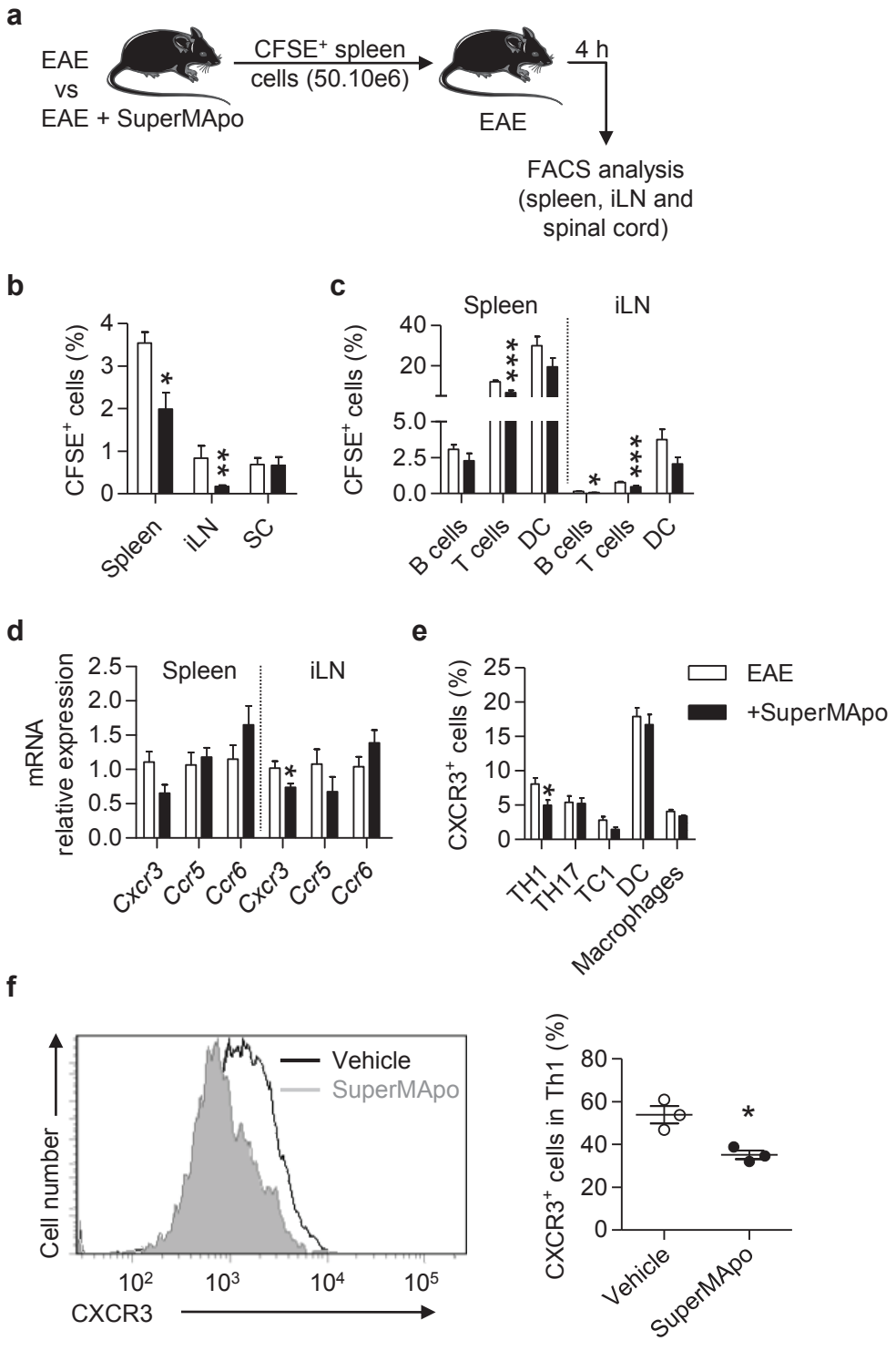
a
EAE
vs
EAE + SuperMApo
CFSE+ spleen
cells (50.10e6)
EAE
4 h
FACS analysis
(spleen, iLN and
spinal cord)
b
CFSE+ cells (%)
Spleen
iLN
SC
c
Spleen
iLN
CFSE+ cells (%)
B cells
T cells
DC
B cells
T cells
DC
d
mRNA
relative expression
Spleen
iLN
Cxcr3
Ccr5
Ccr6
Cxcr3
Ccr5
Ccr6
e
CXCR3+ cells (%)
EAE
+SuperMApo
TH1
TH17
TC1
DC
Macrophages
f
Vehicle
SuperMApo
Cell number
CXCR3
CXCR3+ cells in Th1 (%)
Vehicle
SuperMApo
g
CXCR3+ cells
in Th1 cells (%)
EAE + CL-Liposome
EAE + CL-Liposome + SuperMApo

Fig S4

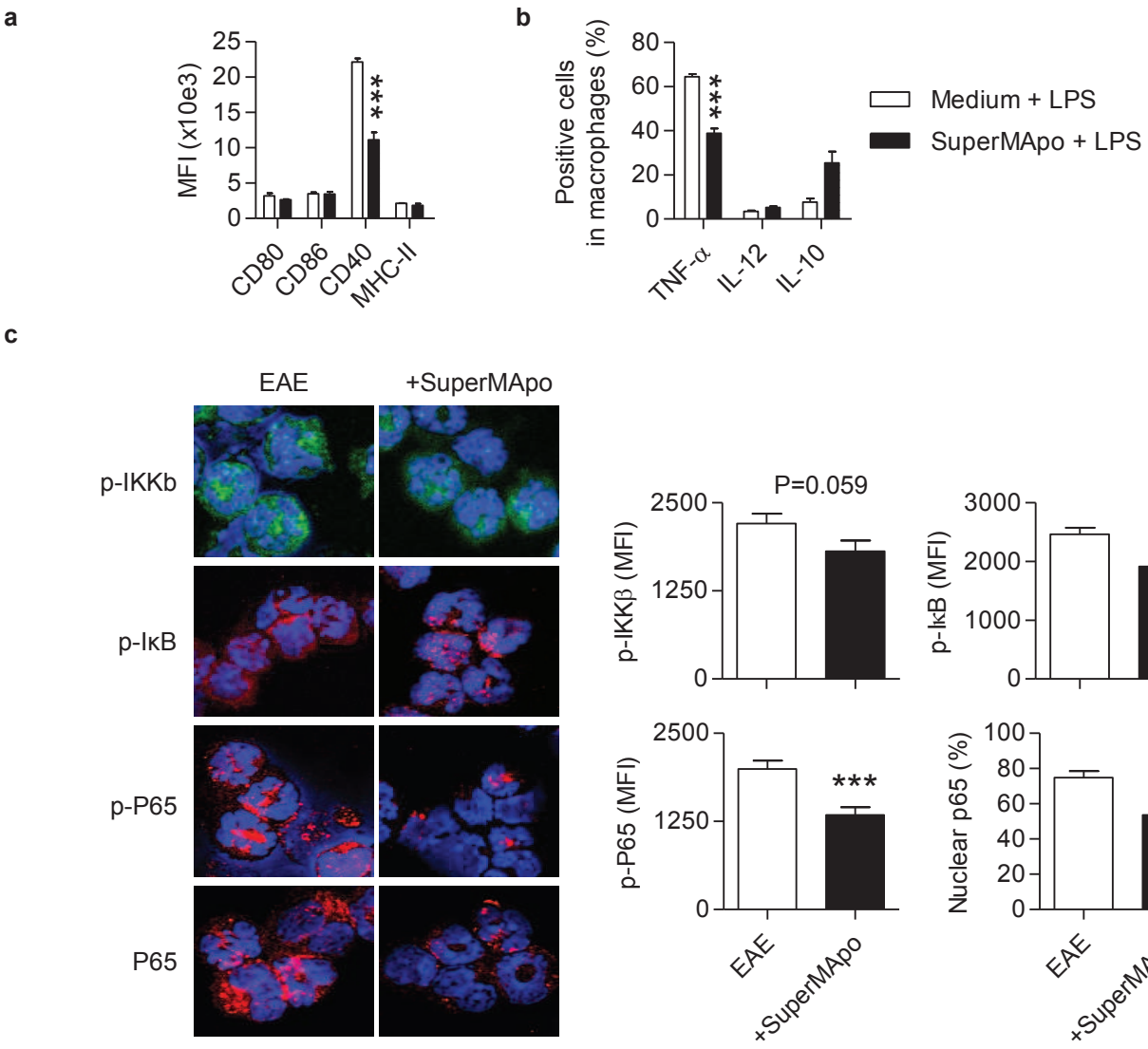
a
MFI (x10e3)
25
20
15
10
5
0
***
CD80
CD86
CD40
MHC-II
b
Positive cells in macrophages (%)
80
60
40
20
0
***
TNF-α
IL-12
IL-10
Medium + LPS
SuperMApo + LPS
c
EAE
+SuperMApo
p-IKKb
p-IκB
p-P65
P65
P=0.059
p-IKKβ (MFI)
2500
1250
0
p-κB (MFI)
3000
2000
1000
*
p-P65 (MFI)
***
Nuclear p65 (%)
100
80
60
40
20
EAE
+SuperMApo
d
EAE
+SuperMApo
pP65 (65 kDa)
P65 (65 kDa)
pIkB (37 kDa)
IkB (37 kDa)
Actine (42 kDa)
Relative intensity
1.2
0.8
0.4
0.0
pP65
pIkB
P65
IkB
Actin
e
p65
DAPI
Merged
Med+ LPS
SuperMApo + LPS
Nuclear p65 (%)
***
Med +LPS
SuperMApo +LPS
Total p65 (MFI)
1000
800
600
400
200

Fig S5

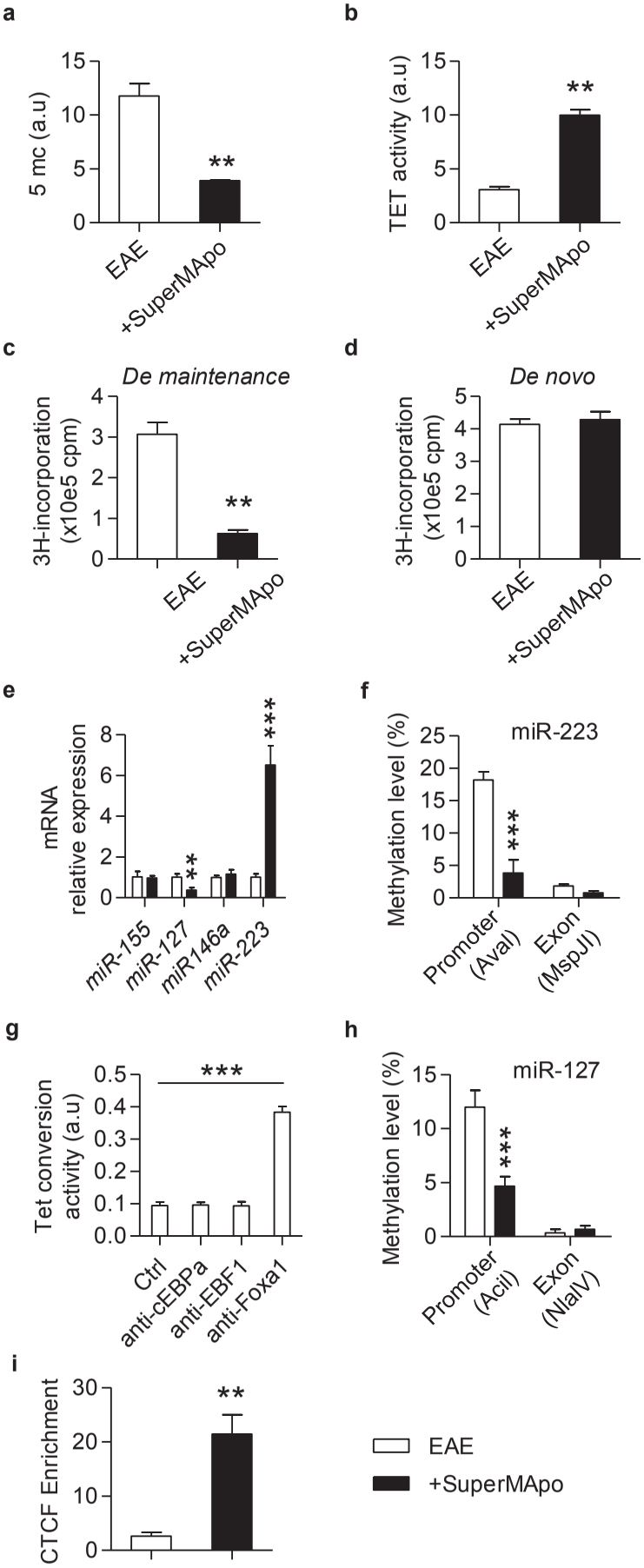
a
5 mc (a.u)
15
10
5
0
**
EAE
+SuperMApo
b
TET activity (a.u)
15
10
5
0
**
EAE
+SuperMApo
c
De maintenance
3H-incorporation (x10e5 cpm)
4
3
2
1
0
**
EAE
+SuperMApo
d
De novo
3H-incorporation (x10e5 cpm)
5
4
3
2
1
0
EAE
+SuperMApo
e
mRNA relative expression
8
6
4
2
0
**
***
miR-155
miR-127
miR146a
miR-223
f
miR-223
Methylation level (%)
25
20
15
10
5
0
***
Promoter (AvaI)
Exon (MspJI)
g
Tet conversion activity (a.u)
0.5
0.4
0.3
0.2
0.1
0.0
***
Ctrl
anti-cEBPa
anti-EBF1
anti-Foxa1
h
miR-127
Methylation level (%)
15
10
5
0
***
Promoter (AciI)
Exon (NlaIV)
i
CTCF Enrichment
30
20
10
0
**
EAE
+SuperMApo

Fig 6

Etude 2 : Effet de SuperMApo sur la reprogrammation des cDC et pDC

Nos premières données ont montré que le traitement SuperMApo diminuait le score clinique dans un modèle d'EAE par la reprogrammation des macrophages. Cependant, d'autres cellules présentatrices de l'antigène sont impliquées dans la modulation des réponses immunes dans l'EAE. De plus, l'effet de l'efferocytose sur la modulation des différents sous-types de cellules dendritiques est totalement inconnu à ce jour. Les cDC et les pDC, bien que partageant des fonctions communes, divergent dans leurs fonctions immunes et les facteurs qui les contrôlent. Au cours de cette seconde étude, nous avons donc cherché à évaluer l'effet de SuperMApo sur ces cellules dans le modèle d'EAE. Premièrement, nous avons observé l'effet du traitement sur le phénotype des cDC et pDC au sein de l'organe inflammatoire qui est la ME. Puis, étant donné leur rôle dans l'activation des LT au sein des organes lymphoïdes périphériques, nous avons étudié leur modulation au sein de la rate. Afin de poursuivre cette étude, nous nous sommes intéressés à la modulation de leur expression génique en réponse à SuperMApo. Enfin, nous avons étudié par quels mécanismes d'actions, notamment épigénétique, ces cellules étaient régulées.

Nos résultats ont montré que l'injection de SuperMApo ne modifiait pas le phénotype pro-inflammatoire des cDC et pDC au sein du SNC. Cependant, une diminution du nombre de ces cellules est observée. Dans la rate, les cDC et pDC ont la même expression des marqueurs de maturation et cytokines pro-inflammatoires mais les pDC, contrairement au cDC, ont une capacité accrue de générer des Treg et une capacité moindre à générer des Th1. Les données de transcriptomique ont alors permis de mettre en évidence une certaine proximité entre ces deux types cellulaires. Cependant, les pDC présentent un profil tolérogénique alors que les cDC ont un profil plus mitigé puisqu'elles expriment des facteurs de tolérance en combinaison avec des facteurs inflammatoires. La modulation différentielle de ces deux types cellulaires peut notamment s'expliquer par une régulation différente au niveau épigénétique. En effet, les cDC ont une baisse de la méthylation globale de l'ADN (qui s'explique par une augmentation de l'expression et de l'activité de TET1) alors que les pDC ont une augmentation de la méthylation globale de l'ADN (qui s'explique par une augmentation de l'expression de DNMT1 et 3B). De plus, les pDC, contrairement aux cDC, ont démontré une baisse de l'expression du miR-214 qui est associé avec l'induction d'un profil tolérogénique.

Enfin, afin de confirmer le rôle des pDC dans l'effet résolutif de SuperMApo, nous avons déplété ce type cellulaire à l'aide de souris BDCA2-DTR. La déplétion des pDC entraîne une perte de l'effet de SuperMApo démontrant un rôle clé des pDC dans la résolution de l'inflammation dans ce modèle.

Ces données nous ont donc permis de mettre en évidence que les produits de l'efferocytose régulent de manière différentielle les cDC et pDC, mettant en lumière un rôle important de la reprogrammation des pDC dans l'effet résolutif de ces facteurs.

Pro-resolutive factors issued from efferocytosis modulate differentially cDC and pDC in an epigenetic manner during EAE

Gauthier T[1], Martin-Rodriguez O[1], Bonnefoy F[1], Chagué C[1], Ceroi A[1], Varin A[1], Missey A[1], Adda-Rezzig H[1], Saas P[1],Couturier M[1] Cartron PF[2], Perruche S[1]

[1]Université Bourgogne Franche-Comté, INSERM, EFS BFC, UMR1098, Interactions Hôte-Greffon-Tumeur/Ingénierie Cellulaire et Génique, Fédération Hospitalo-Universitaire INCREASE, LabEx LipSTIC, F-25000 Besançon, France ; [2]CRCINA-INSERM 1232, Team Apoptose et Progression tumorale - 44 805 Saint Herblain, FR

Abstract

Background: Experimental autoimmune encephalomyelitis (EAE) is the most common used MS model. It has been shown that classical dendritic cells (cDC) and plasmacytoid dendritic cells (pDC) in EAE are dysregulated toward a pro-inflammatory profile. Moreover, resolution of inflammation is failing during multiple sclerosis leading to investigate new therapies targeting the resolution of inflammation. To this aim, we used *ex vivo* phagocytosis of apoptotic cells by macrophages (i.e efferocytosis) to induce pro-resolutive mediators (here named SuperMApo for Supernatant issued from Macrophages Apoptotic cell culture) production to resolve inflammation in EAE.

Methods: EAE MOG_{35-55} mouse model was used to monitor the effect of SuperMApo on resolution of inflammation. Flow cytometry staining was used to observe the effect of SuperMApo on cDC and pDC inflammatory profile in the spinal cord and the spleen or after lipopolysaccharide (LPS) restimulation. The ability of cDC and pDC after SuperMApo treatment to polarize T cells was observed by coculture with $CD4^+$ naive T cells from $RAG^{-/-}$ OT-II mice. The gene expression profile of cDC and pDC was assessed in the spleen by transcriptomic analysis after cell sorting using magnetic beads or FACS cell sorting.

Epigenetics modification of DNA methylation was performed using qRT-PCR and qMSRE experiments. Finally, depletion of pDC was performed using BDCA2-DTR mice.

Results: EAE mice receiving SuperMApo at the first days of clinical appearance demonstrated a decreased clinical score correlated with a decreased infiltrate in the spinal cord. While cDC and pDC seemed to not be modulated by SuperMApo in the spinal cord, pDC in the spleen, contrary to cDC, displayed a tolerogenic profile *in vivo* or after LPS exposure *in vitro*. Moreover, pDC demonstrated a totally reprogrammed profile toward a resolutive phenotype as attested by their expression of genes implied in axon regeneration which was not observed on cDC. We also demonstrated that pDC and cDC reprogramming was modulated in an epigenetic manner toward differential phenotype. Finally, the depletion of pDC led to lose SuperMApo effects demonstrating their role in inducing tolerance after SuperMApo treatment.

Conclusion: This study reveals a previously unrecognized role of targeting the resolution of inflammation to control EAE. Our results also demonstrate that pDC, but not cDC, are a major target of factors issued from efferocytosis which induces a tolerogenic profile in these cells through modulation of DNA methylation.

Keywords: Experimental autoimmune encephalomyelitis (EAE), multiple sclerosis (MS), pro-resolutive factors (SuperMApo), classical dendritic cells (cDC), plasmacytoid DC (pDC), DNA methylation

Background

Multiple sclerosis (MS) is an autoimmune disorder characterized by demyelination in the central nervous system (CNS). It affects about 3 millions of people worldwide with primary clinical course occurring in young adults[1]. Currently, no potent therapy for MS is

available, and several investigations of new therapeutic approaches are in progress[2]. These last mainly used mouse model namely Experimental autoimmune encephalomyelitis (EAE) allowing a better understanding of pathological mechanistic underlying, and the *in vivo* investigation of therapeutic drug effects[3]. While the pathogenesis of MS remains poorly understood, several evidences suggest the involvement of autoreactive Th1 and Th17 cells[4]. Indeed, antigen presenting cells (APC) such as classical dendritic cells (cDC) and plasmacytoid DC (pDC) were described to prime myelin specific T cells in peripheral organs, inducing their migration into inflammatory area where they would be re-stimulated by the previously infiltrated APC[1,5]. The evidence of cDC and pDC involvement was proven in several experiments in EAE mice. Indeed, pDC depletion leads to a decrease clinical score in the MOG_{35-55} (Myelin Oligodendrocyte Protein 35-55) model and a decrease percentage of MOG-specific Th17 cells into the spleen[6]. Similar effects were demonstrated with DC, showing a decrease of clinical score induced by cell depletion and that MHC II expression in DC is sufficient to induce pathological events[7,8]. In another hand, APC were described to control pathogenesis of EAE. It was demonstrated that MOG-presenting DC can control the pathology through PD-1 involvement[9]. Moreover, injection of resting pDC, but not CpG activated pDC, inhibits EAE in a MOG-dependent fashion[10]. Thus, the expression of MHC-II during EAE on pDC decreases the clinical course of the disease by modulating the priming of $CD4^+$ T cells and the generation of Treg cells[11].

While autoimmune diseases are characterized by chronic inflammatory responses, several mechanisms occur in physiological circumstances to maintain homeostasis and promote tissular reparation[12]. The paradigm of active resolution of inflammation mediated by macrophages has emerged and been detailed in terms of actors and mechanisms, as well as to propose a new branch of pharmacology called “resolution pharmacology”[13]. Among these,

production of anti-inflammatory factors (e.g. IL-10, PGE2, TGF-β, adenosine, retinoids…) by apoptotic cells/bodies phagocytosized-macrophages is widely accepted as a key step of inflammation resolution[14,15]. In MS, CNS infiltrating macrophages during flairs were described as inflammatory M1 macrophages, contributing to pathogenesis through pro-inflammatory cytokines secretion and damaging CNS tissue. However, it was interestingly demonstrated that after flairs, same macrophages presente a similar profile compared to activated M2 macrophages, releasing anti-inflammatory cytokines which was associated to resolution of inflammation and tissue repair[16]. This suggests that physiological mechanisms of inflammation control are available, but insufficient in MS to prevent autoimmune disease[17]. Several approaches were investigated to promote resolutive activity of macrophages in autoimmune disease. One of them is the promotion of apoptotic body phagocytosis, namely efferocytosis[18]. This concept was illustrated through apoptotic cells injection [19]. Interestingly, apoptotic cells were also demonstrated to reverse the inflammatory response induced by a specific antigen[20]. Then, our group showed that *in vivo* induction of apoptosis using CD3-specific antibody in EAE mice reduced MOG-induced and diminished ongoing PLP-induced EAE severity. Involvement of efferocytosis was demonstrated in these effects, involving the induction of antigen-specific regulatory T cells (Treg)[21]. However, the factors issued from efferocytosis have never been investigated to modulate MS and their effect on different APC populations is totally unknown.

In this study we investigated another approach to resolve inflammation in EAE mouse model. This last includes the *ex vivo* efferocytosis of apoptotic cells by macrophages to induce the pro-resolutive factors production, which could be isolated for subsequent therapeutic use. This resolution-based medicinal drug is named SuperMApo. We found that SuperMApo injection decreased the clinical score of EAE mice and the inflammation in the spinal cord.

Since the effect of resolution of inflammation on cDC and pDC has not been previously investigated, we focused on these cell types. We observed that their phenotypes were not altered after SuperMApo treatment in the spinal cord. However, in the spleen, while their expression of co-stimulation markers and cytokines remained stable, the ability of pDC, but not cDC, to prime Treg cells and to inhibit Th1 differentiation was enhanced. We also demonstrated that pDC had a decreased ability to respond to TLR activation *in vitro*. This differential behavior was explained by a differential gene expression pattern due to a differential DNA methylation status and a modulation of miRNA expression. Finally, we observed that the pro-resolutive effect of SuperMApo in EAE was dependent on pDC because their depletion leads to lose SuperMApo effect. Thus, our experiments demonstrated new insights on the mechanisms by which resolution of inflammation could modulate MS.

Methods

Mice

Female C57BL/6 mice aged of 6-10 weeks were purchased from Charles River Laboratories (L'Arbresle, France). Experimentation (#02831) was approved by the local ethic committee (#58) and the French Ministry of Higher Education and Research (Ministère de l'Enseignement Supérieur et de la Recherche) and was conducted in accordance with the European Union's Directive 2010/63. Mice were housed at the environmentally controlled and germ free UMR1098 animal facility (#D25-056-7) in ventilated cages with cellulose bedding and access ad libitum to pellet food and sterile water pouches (Plexx, The Netherlands).

Production of SuperMApo

Briefly, macrophages were isolated from the peritoneal cavity of C57BL/6 mice, 48 h after thioglycollate (3%, BD biosciences) mobilization, and then cultured (1.10e6 cells/mL) with apoptotic thymocytes from C57BL/6 mice generated by X-ray irradiation (35 Gy) in 1 mL of X-vivo media for a final ratio of 1 macrophage for 5 apoptotic cells. Supernatant was collected at 48 h and filtered using a 20 µm disposable filter (Greiner bio-one) before storage at -80°C until use. Supernatant of macrophages or apoptotic cells cultured alone were also produced as controls.

EAE induction and SuperMApo treatment

C57BL/6 female mice were injected subcutaneously with 200 µg of MOG_{35-55} peptide (Mb bioproducts, Zurich, Switzerland) emulsified in IFA and 5 mg/mL of heat-inactivated *Mycobacterium tuberculosis* (Sigma-Aldrich). Pertussis toxin (Merck Millipore, Billerica, MA) was injected i.p. at 0 and 48 h after disease induction (200 ng/ mouse). . Mice were monitored and scored daily as follows: 0, no disease; 1, flaccid tail; 2, hind limb weakness; 3, partial hind limb paralysis; 4, total hind limb paralysis; 5, moribund state. When mice reached a clinical score ranged between 0.5 and 1, SuperMApo or X-vivo medium (Lonza, Basel, Switzerland) alone used as vehicle control (vehicle) were injected twice i.p. (1 mL, each 48 h). To deplete pDC in BDCA2-DTR mice, 1 µg of diphtheria toxin (Sigma-Aldrich) was injected the 2 days before and the day after the first injection of SuperMApo

Isolation of CNS-infiltrating leukocytes

Spinal cords were extracted 72 h after the first SuperMApo treatment, excised and digested using 2 mg/mL of collagenase II (Roche Diagnostics, Indianapolis, IN) for 35 min at 37°C. Cells were washed with Roswell Park Memorial Institute medium containing 10 % Fetal Bovine Serum, then resuspended on 30 % Percoll (Sigma-Aldrich) solution. The 30 % Percoll

141 homogenate was layered over 70 % Percoll followed by centrifugation for 20 min at room
142 temperature. Leukocytes were collected from the interface and washed twice as previously
143 described.

144 **Flow cytometry analysis**

145 For surface staining, cells were incubated with anti-CD16/CD32 (24G2, BD biosciences, Le
146 pont de Claix, France) during 10 min at 4°C with Fixable Viability Stain (V510, BD
147 biosciences). Then, cells were stained with anti-CD11c-PECy7 (clone N418), CD19-APCCy7
148 (clone 6D5), mPDCA-APC (JF05-1C2.4.1), Siglec-H-PE (REA819), MHC-II-VioBlue (clone
149 REA813) (Miltenyi Biotec, Bergisch Gladbach, Deutschland), CD80-FITC (clone 16-10A1)
150 (BD biosciences), CD86-PerCP (clone GL-1) and CD40 PECy7 (clone 3/23) (Biolegend, San
151 Diego, CA) at 4°C during 20 min. For intracellular staining, cells were stimulated with 1
152 µg/mL of LPS (Sigma-Aldrich, only for *in vitro* stimulation assays) followed by a stimulation
153 with 25 ng/mL of phrobol 12-myristate 13-acetate (Sigma-Aldrich) and 1 µg/mL of
154 ionomycin (Sigma-Aldrich) in presence of 10 µg/mL of monensin (BD biosciences) 4 h at
155 37°C. Cells were then washed and stained with surface antibodies as described previously.
156 After a wash in Phosphate Buffer Saline (PBS, Life technologies, Carlsbad, CA), cells were
157 fixed with Cytofix/Cytoperm (BD biociences) 20 min at 4°C, rinced with permeabilization
158 buffer (ThermoFischer Scientific, Waltham, MA) and stained with anti-TNF-PerCPCy5.5
159 (clone MP6-XT22), IL-12-PE (clone C15.6) and IL-10-FITC (clone JES5-16E3) (BD
160 biosciences) for 40 min at 4°C. FACS analysis was performed using LSR Fortessa X-20
161 system (BD biosciences). cDC were considered as $CD11c^{+}CD19^{-}$ and pDC as
162 $mPDCA^{+}Siglec\text{-}H^{+}$ (or $mPDCA^{+}CD11c^{int}$ when indicated).

163 **T cell polarization**

To assess the effect of cDC and pDC on T cell polarization, splenocytes from EAE mice at 72 h after the first SuperMApo treatment or splenocytes from naïve C57BL/6 mice were harvested. cDC were isolated using CD11c magnetic beads (Miltenyi Biotec, following the manufacturer's instructions) and pDC using FACS cell sorting (pDC were considered as Siglec-H^+mPDCA$^+$$CD19^-$ gated on live cells). Cells from naive mice were then cultured with SuperMApo during 18 h followed by TLR stimulation during 6 h (1 µg/mL of LPS (Sigma-Aldrich) for cDC and 12 µg/mL of CpG ODN 2216 (Invivogen, San Diego, CA) for pDC). cDC and pDC were then cultured with $CD4^+CD25^-$ naïve T cells sorted from $RAG^{-/-}$/OT-II mice (50 000 APCs for 100 000 T cells) in presence of ovalbumine peptide (323-339) (2 µg/mL, Invivogen). After 96 h of culture, T cell polarization was analyzed using CD3-APCCy7 (clone 145-2C11), CD4-V450 (clone RM4-5) (BD biosciences), CD25-PECy7 (clone 7D4), IFN-γ-FITC (clone REA381), IL-17-APC (clone REA660) (Miltenyi Biotec) and Foxp3 PE (ebiosciences, clone FJK-16S) as described previously for intracellular staining.

Transcriptomic analysis

cDC and pDC were isolated using cell sorting as previously described. RNA samples were sent to Integragen (Evry, France) for sequencing on their NGS platform (Illumina HiSeq 4000) and resulting raw data (fastq.gz) were sent to Plateforme CLIPP (Dijon, France) for data processing on their custom pipeline (alignment on mouse reference genome was performed using TopHat2 algorithm followed by differential expression of transcripts with Cufflinks algorithms). Resulting RNA-seq data, containing FPKM (Fragments Per Kilobase of exon per million fragments Mapped) values, were $\log_2$ transformed, normalized and mean-centered using Cluster 3.0 software and data visualization was performed using GiTools and

TreeView 3 for the different Heatmaps, and Cytoscape 3.2 for network analysis of the associated pathways.

Epigenetic analysis

DNA extract was performed using QIAamp DNA Mini QIAcube Kit and QIAcube (Qiagen, France). 5-methylcytosine ELISA was performed using 5mC ELISA (Ozyme/Zymo, France).

DNMTs magnetic bead (DMB) assays were performed as described by Yokochi and Robertson (PMID: 15273420). A typical methylation reaction contained 30 nM of the respective DNMT protein (Methylation Ltd, Port Orange, Florida or Tebu-Bio, France), 125 nM DNA oligonucleotides, and 900 nM tritium-labeled AdoMet (Amersham Bioscience, 1 mCi/mL), in reaction buffer (50 mM Tris, pH 8.0, 5 mM EDTA, 10% glycerol, 0.5 mM phenylmethylsulfonyl fluoride). After incubation at 37 C for 1 h, the reaction was quenched with an equal volume of magnetic beads suspension, and incubated for 15 min at room temperature. Next, the beads were magnetically isolated from the reaction mix, and tritium incorpo- ration was measured by scintillation counting. Unmethylated double stranded oligonucleotides were used to estimate the de novo MTase activity, and hemimethylated double stranded oligonucleotides were used to estimate the maintenance MTase activity.

miRNA extraction was perfomed using miRNeasy Mini Kit and QIAcube (Qiagen, France). miScript II RT Kit (Qiagen, France), miScript SYBR Green PCR Kit (Qiagen, France) and miScript Primer Assay were used to quantify the miRNA expression. MSRE methodology was adaptated from the OneStep qMethylTM Kit (Ozyme, ZYMO, France). A typical digestion of genomic DNA contained 20ng of DNA and 5 units of considered enzyme (New England Biolab, France). For the non-enzyme control, distilled water was added instead of *considered enzyme*. Except for certain enzyme, all prepared samples were incubated at 37℃

for 12 hours, follow by heat inactivation at 65℃ for 20 minutes. Primers (ThermoFischer) of interest are: *Dnmt1* (Mm01151063_m1), *Dnmt3a* (Mm00432881_m1), *Dnmt3b* (Mm01240113_m1), *Uhrf1* (Mm00477872_m1), *Tet1* (Mm01169087_m1), *Tet2* (Mm00524395_m1), *Tet3* (Mm00805756_m1) and *Tdg* (Mm02602088_g1). Qiagen miScript Primer Assays were used for *miR-22* (MS00001330), *mi-34a* (MS00001428), *miR-146a* (MI0000170), *miR-155* (MS00001701) and *miR-214* (MS00032571). The methylation level for any amplified region was determined using the following equation %methylation=100x$2^{-\Delta Ct}$.

Chromatin ImmunoPrecipitation (ChIP) experiments were performed with the LowCell#ChIP kit (Diagenode, France). Bioruptor (Diagenode, France) was used for the sonication step (3 runs of 8 cycles (30seconds"ON", 30 seconds "OFF") at high power setting). 6 µg of antibody (Anti-CTCF antibody (ab70303) Abcam, France) were used and IP tubes were incubated at 40 rpm on a rotating wheel for 4 hours at 4°C. qPCR were performed using SYBR Green PCR Kit (Qiagen, France).

Typically, TET conversion activity was determined by measuring the 5mC level (ELISA) in a methylated oligonucleotide probe mimicking a DNA region of interest. Biotinylated probe was incubated with 10ng of Nuclear Extraction Kit (ab113474, Abcam, France) for 90min at 37°C in presence of not of 10µg of considered antibody (GATA1: sc-265, Santa Cruz, France, RXRa (clone 1C1, Abnova, France), and FOXM1 (clone 3A9, Abnova). After isolation and washes, reageants issue to the MethylFlashTM Global DNA Methylation (5-mC) ELISA Easy Kit (Colorimetric) were used to detect the 5mC on probe.

Statistical analysis

Data were expressed as mean ± sem. Statistical differences among groups were assessed by ANOVA followed by Bonferroni post test (for clinical score analysis) or unpaired two-tailed Student's T test. Values of $p < 0.05$ were considered statistically significant.

Results

SuperMApo modulates ongoing EAE and reduces cellular infiltrate in the CNS

To evaluate the therapeutic properties of effercoytosis factors we cultured macrophages with apoptotic cells during 48 h and collected the supernatant (SuperMApo). EAE mice demonstrating an ongoing disease (clinical score between 0.5 and 1) received SuperMApo twice (1 mL) in i.p as indicated by the black arrows (**Fig. 1a**). We observed that SuperMApo treatment modulated significantly the pathology compared to vehicle X-vivo during the ten days following injection ($p<0.005$) (**Fig. 1a**). While the CNS inflammatory cytokine content (TNF-α, IL-12, IL-6, IFN-γ) was not modulated by the treatment (**Fig. 1b**), the number of total leukocytes was dramatically decreased after SuperMApo treatment at 72 h ($p<0.01$) (**Fig. 1c**). We then focused on cDC and pDC which are major immune player during EAE but in which the effect of efferocytosis is not understood. Among the leukocytes, the number of cDC and pDC was dramatically diminished 72 h after the first SuperMApo treatment (**Fig. 1d**). Analysis by FACS of their expression of co-stimulation markers (CD80, CD86, CD40 and MHC-II) as well as their production of cytokines in the spinal cord was not altered after SuperMApo treatement (**Fig. 1e-f**). Together, these results demonstrated that SuperMApo treatment modulates an ongoing EAE by inducing a decrease infiltration of immune cells in the CNS.

SuperMApo influences spleen pDC, but not cDC toward a tolerogenic profile

APC like cDC and pDC are key players of inflammation notably by activating immune responses in lymphoid organs[4,6]. Having established that SuperMApo modulated the infiltration of these cells into the CNS, we questioned whether SuperMApo could modulate their phenotype in peripheral lymphoid organs. The number of cDC and pDC was increased

of about three in the spleen 72 h after SuperMApo treatment in EAE mice (**Fig. 2a**). pDC demonstrated a slight, but not significant, decreased expression of IL-12, but the expression of co-stimulation markers and cytokines was not altered after treatment (**Fig. 2b-c**). Since these cell types could modulate T cell responses *in vivo*, we hypothesized that cDC and pDC after SuperMApo treatment could influence T cell polarization. While cDC (upper panel) had the same ability to generate T cell responses after SuperMApo treatment, pDC (lower panel) demonstrated a decreased ability to generate Th1 responses and an increased ability to generate Treg (**Fig. 2d**). In line with these observations, SuperMApo did not modulate the response of cDC to TLR ligand *in vitro* but impaired the ability of pDC to express maturation markers (**Fig. 2e**). When we co-cultured these APC with naïve $CD4^+$ OT-II T cells as described previously, cDC displayed the same T cell responses, but interestingly pDC had a stronger capacity to generate Treg cells (**Fig. 2f**). These results demonstrated that SuperMApo impact the functionnality of pDC, but not cDC, *in vivo* and *in vitro* allowing them to acquire a pro-tolerogenic phenotype.

SuperMApo modulates the transcriptome of cDC and pDC in a differential manner

To further investigate the regulation of these cells by SuperMApo treatment, transcriptomic analysis was performed on splenic cDC and pDC from SuperMApo- and vehicle-treated EAE mice. 328 genes were upregulated in cDC after SuperMApo treatment and 482 genes were down-regulated (**Fig. 3a,c**). Similarly, 336 genes were upregulated in pDC treated by SuperMApo and 513 were downregulated (**Fig. 3b,d**). Interestingly, cDC and pDC share common genes upregulated as the immunoregulatory genes *Ido1*, *Arg1* or *Sirt4* as well as common genes downregulated as pro-inflammatory factors *Mmp9* and *Rarres1* (**Fig. 3a-b**). Interestingly, pDC overexpressed only genes implicated on tolerogenicity and downregulated genes implied on maturation and inflammation. However, cDC while expressing tolerogenic

genes (Ido1 and Arg1) also expressed the pro-inflammatory chemokine *Ccl22*[22] and downregulated the tolerogenic enzyme *Arg2*[23]. Moreover, pDC overexpressed a pathway implicated on alpha amino acid catabolic process containing the genes *Arg1* and *Ido1* and also a pathway implicated on axon regeneration which is a key feature of resolution of inflammation in the pathology of MS and which was not overexpressed on cDC (**Fig. 3e-l**). Thus, these results confirmed that pDC and cDC were differentially regulated by SuperMApo treatment allowing pDC to express pro-tolerogenic genes.

Modulation of the epigenome of pDC and cDC by SuperMApo

To further determine the mechanisms by which SuperMApo regulates differentially cDC and pDC, we focused on DNA methylation which play a role on DC immune responses[24,25]. First, cDC from the spleen of EAE mice 72 h after the first SuperMApo treatment demonstrated a decreased level of global methylation while pDC demonstrated an increased level of global methylation (**Fig. 4a**). These changes were accompanied by an increased expression and activity of the demethylase TET1 in cDC and an increased expression of the methyltransferases DNMT1 and DNMT3B (**Fig. 4b**). Thus, we focused on miRNA which exert a tight control on immune cells during different inflammatory context[26,27]. We observed that the anti-inflammatory *miR-146a* expression was increased after SuperMApo treatment in cDC while the pro-inflammatory *miR-214* expression was decreased after SuperMApo treatment in pDC (**Fig. 4c**). In cDC, the increased expression of *mir-146a* was due to a decrease methylation level on its promoter (Fig. 4e) and in pDC the *miR-214* was hypermethylated (**Fig. 4d,e**). Using blocking anti-RXRa antibody, the demethylating activity on promoter of *miR-146a* has been lost in cDC however, the hypermethylating activity on promoter of *miR-214* was dependent on GATA1 in pDC (**Fig. 4f**).

SuperMApo resolutive effect is dependent on pDC

309 Since pDC were modulated by SuperMApo toward a tolerogenic profile in our EAE model,
310 we questioned whether the effect of SuperMApo was mediated by pDC. To this aim, pDC
311 were depleted before SuperMApo treatment in BDCA2-DTR mice by injecting diphtheria
312 toxin at day 6, 7 and 9 to ensure a complete depletion of pDC during SuperMApo treatment
313 (at day 8 and 10). As expected, SuperMApo decreased the clinical score compared to vehicle
314 control ($p<0.01$). However, the depletion of pDC leads to totally lose SuperMApo effect (**Fig.**
315 **5**). Thus, the pro-resolutive factors issued from effereocytosis induce the reprogramming of
316 pDC toward a tolerogenic profile which allow them to control EAE.

317

Discussion

Resolution of inflammation is impaired in several inflammatory diseases and new insights suggest that targeting the resolution of inflammation could be a promising therpeutic way[13,17]. The role of cDC and pDC cells in the pathogenesis of EAE is well defined but remains still controversial. In fact, cDC were found to prime Th1 and Th17 responses in the lymph nodes and be sufficient to induce antigen specific pathogenic T cells *via* antigen presentation[8]. However, a recent publication demonstrated that their depletion could lead to an exacerbated pathology because they were able to prime Treg responses in a PD-1/PD-L1 axis[9]. pDC depletion leads to decrease clinical score in EAE mice suggesting a pathogenic role of these cells notably by modulating the balance between pathogenic Th1/Th17 cells and Treg cells[6]. However, their injection into EAE mice induces their recruitment through a chemerin/CMKLR1 axis into the SNC leading to decreased pathology[10]. Moreover, mice deficient for MHC-II specifically on pDC lead to an increased disease due to lower Treg generation[11]. These facts suggest that modulating the phenotype of cDC and pDC during EAE could be a good way to establish tolerance. Indeed, the effect of the resolution of inflammation, notably in the context of EAE, is largely undescribed leading us to focus on the effect of SuperMApo on these cells.

Here, we have demonstrated that reintroducing pro-resoliving factors issued from the resolution of inflammation permits to control the disease in an EAE model (Fig. 1a). We observed that number of cDC and pDC was dramatically decreased in the spinal cord of EAE mice after SuperMApo treatment while their inflammatory markers remained stable (Fig. 1d-f). However, in the spleen, pDC but not cDC were reprogrammed toward a tolerogenic profile. They are able to generate higher levels of Treg cells but lower level of Th1 cells demonstrating that targeting pDC is a promising way to re-establish the balance between Treg

342 and Th1 which is broken during EAE (Fig. 2d). Moreover, in response to TLR ligand, which
343 mimick an inflammation *in vitro*, pDC demonstrated also a tolerogenic phenotype (Fig. 2e-f).
344 It is particularly intriguing to observe that SuperMApo exert a differential effect on these cells
345 type. An explanation could be the expression of the receptor CMKLR1 which is expressed
346 both on cDC and pDC[28]. However, a study have been demonstrated a differential expression
347 of this receptor on cDC and pDC on human blood and an ability of chemerin (a ligand of
348 CMKLR1) to attract pDC[29]. Moreover, in the EAE model, injection of pDC leads to their
349 recruitment in the SNC in a CMKLR1/chemerin dependent manner which permits to control
350 the disease[10]. Interestingly, the CMKLR1 receptor is able to transduce the pro-resolutive
351 lipids resolvin D1 and E1 which are produced during efferocytosis suggesting that the
352 differential effect of SuperMApo on cDC and pDC may be partly due to their differential
353 CMKLR1 expression[15].

354 Further analysis of cDC and pDC transcriptome demonstrated also a differential pattern
355 between these cells (Fig. 3). Interestingly, pDC and cDC overexpressed genes implied on
356 resolution of inflammation as *Arg1* and *Ido1* and expressed lower amount of pro-
357 inflammatory genes as *Mmp9* and *Raress1* (Fig. 3a-b). However, cDC expressed also more
358 levels of the pro-inflammatory chemokines *Ccl22* which is implied on the pathogenesis of
359 EAE by recruiting inflammatory macrophages[22]. Moreover, they displayed also a decrease
360 expression of *Arg2* which has recently been demonstrated to permit the suppression of T cell
361 responses by fetal cDC[23]. Indeed, pDC overexpressed a pathway relying on axon regeneration
362 which is a key feature of resolution of inflammation in the model of EAE demonstrating a
363 strong resolutive phenotype in this model[30]. Interestingly, the presence of two different
364 pathways implicated on cellular metabolism could indicate that metabolism in cDC and pDC

365 is regulated differently after SuperMApo treatment. Thus, pDC are pro-tolerogenic but cDC
366 expressed a “mixed” phenotype composed of pro-tolerogenic and pro-inflammatory genes.

367 To further address the underlying cause of reprogrammation observed on pDC but not on
368 cDC, we focused on the regulation of these cells by epigenetic counterparts. As observed
369 during this study, the methylation profile of cDC and pDC is differently regulated. In cDC,
370 the global level of DNA methylation is decreased due to an increase of TET1 expression (Fig.
371 4). However, in pDC the global level of DNA methylation is increased due to an higher
372 expression of DNMT1 and DNMT3B which is link with a decrease of miR-214 not observed
373 on cDC which overexpressed the miR-146a (Fig. 4). Interestingly, miR-214 has been found
374 down-regulated on tolerogenic cDC (treated with TGF-β and IL-10)[26]. Moreover, the
375 inhibition of this miRNA led to decrease the activation of cDC *in vitro* and *in vivo*, their
376 production of pro-inflammatory cytokines and enhance their capacity to generate Treg cells[31].
377 Although the role of miR-214 in pDC is not known, our data suggest that it plays the same
378 function as in cDC because pDC treated with SuperMApo demonstrated a decrease activation
379 and an increased ability to generate Treg cells which is correlated to a decrease expression of
380 miR-214. While the anti-inflammatory miR-146a[32,33] is overexpressed on cDC it’s not
381 sufficient to induce a tolerogenic profile in these cells suggesting that other factors
382 counterbalance this effect.

383 Finally, we observed that depletion of pDC lead to lose SuperMApo pro-resolutive effect
384 demonstrating that they are key cells in the control of EAE. This effect seemed to be due to an
385 increase ability to generate Treg cells in peripheral organs and to induce tolerance more than
386 by decreasing immune response in periphery directly in the spinal cord. Thus, our data
387 strongly demonstrate that reintroduction of pro-resolutive mediators issued from efferocytosis
388 is an interesting way to treat inflammatory diseases.

Abbreviations

APC: Antigen Presenting Cells; cDC: classical Dendritic Cells; CNS: Central Nervous System; DT: Diphteria Toxin; EAE: Experimental Autoimmune Encephalomyelitis; LPS: Lipopolysaccharide; MOG: Myelin Oligodendrocyte Glycoprotein; MS: Multiple Sclerosis; pDC: plasmacytoid Dendritic Cells; SuperMApo: Supernatant issued from Macrophages Apoptotic cell culture

Acknowledgements

We thank Helena Paidassi (Centre International de Recherche en Infectiologie) for providing us with OTII/RAG–/– mice and Jean-Paul Remy-Martin for his expertise in making liposomes and blotting. We also thank Dominique Paris, Francois Coulon and Emmanuel Salvado for taking care of the mice.

The work was funded by the Etablissement Français du Sang (2016-02 to S.P.), the Conseil Régional de Franche-Comté ("Soutien au LabEX LipSTIC" 2014/2015 to P.S. and AAP 2013-2017 to S.P.), and by the Agence Nationale de la Recherche (ANR-11-LABX-0021 to Labex LipSTIC). T.G. is supported by a doctoral fellowship from the Etablissement Français du Sang and from the Labex LipSTIC, O.M.R. and C.C. by a doctoral fellowship from the Ministère de l'Education Nationale, de l'Enseignement Supérieur et de la Recherche.

Author contributions

T.G. designed and performed most of the experiments, analyzed and interpreted the data. O.M.R., F.B., C.C., A.C., A.M and H.AD contributed to some experiments. A.V. participated to transcriptomic analysis. P.F.C. designed and performed epigenetic experiments. T.G., P.S. and S.P. wrote the manuscript. All authors discussed the results and the manuscript. S.P. supervised the study.

413

414 **Competing financial interests**

415 The authors declare no competing financial interest.

416 **Availability of data and materials**

417 The datasets used and/or analayzed during the current study are available from the
418 corresponding author on reasonable request.

419

1. Dendrou, C.A., Fugger, L. & Friese, M.A. Immunopathology of multiple sclerosis. *Nature reviews. Immunology* **15**, 545-558 (2015).
2. Franklin, R.J. & Ffrench-Constant, C. Remyelination in the CNS: from biology to therapy. *Nature reviews. Neuroscience* **9**, 839-855 (2008).
3. Stromnes, I.M. & Goverman, J.M. Active induction of experimental allergic encephalomyelitis. *Nature protocols* **1**, 1810-1819 (2006).
4. Goverman, J. Autoimmune T cell responses in the central nervous system. *Nature reviews. Immunology* **9**, 393-407 (2009).
5. Berger, T.*, et al.* Experimental autoimmune encephalomyelitis: the antigen specificity of T lymphocytes determines the topography of lesions in the central and peripheral nervous system. *Laboratory investigation; a journal of technical methods and pathology* **76**, 355-364 (1997).
6. Isaksson, M.*, et al.* Plasmacytoid DC promote priming of autoimmune Th17 cells and EAE. *European journal of immunology* **39**, 2925-2935 (2009).
7. Paterka, M.*, et al.* Gatekeeper role of brain antigen-presenting CD11c+ cells in neuroinflammation. *The EMBO journal* **35**, 89-101 (2016).
8. Bailey, S.L., Schreiner, B., McMahon, E.J. & Miller, S.D. CNS myeloid DCs presenting endogenous myelin peptides 'preferentially' polarize CD4+ T(H)-17 cells in relapsing EAE. *Nature immunology* **8**, 172-180 (2007).
9. Yogev, N.*, et al.* Dendritic cells ameliorate autoimmunity in the CNS by controlling the homeostasis of PD-1 receptor(+) regulatory T cells. *Immunity* **37**, 264-275 (2012).
10. Duraes, F.V.*, et al.* pDC therapy induces recovery from EAE by recruiting endogenous pDC to sites of CNS inflammation. *Journal of autoimmunity* **67**, 8-18 (2016).
11. Irla, M.*, et al.* MHC class II-restricted antigen presentation by plasmacytoid dendritic cells inhibits T cell-mediated autoimmunity. *The Journal of experimental medicine* **207**, 1891-1905 (2010).
12. Poon, I.K., Lucas, C.D., Rossi, A.G. & Ravichandran, K.S. Apoptotic cell clearance: basic biology and therapeutic potential. *Nature reviews. Immunology* **14**, 166-180 (2014).
13. Perretti, M., Leroy, X., Bland, E.J. & Montero-Melendez, T. Resolution Pharmacology: Opportunities for Therapeutic Innovation in Inflammation. *Trends in pharmacological sciences* **36**, 737-755 (2015).
14. Chen, W., Frank, M.E., Jin, W. & Wahl, S.M. TGF-beta released by apoptotic T cells contributes to an immunosuppressive milieu. *Immunity* **14**, 715-725 (2001).
15. Fullerton, J.N. & Gilroy, D.W. Resolution of inflammation: a new therapeutic frontier. *Nature reviews. Drug discovery* **15**, 551-567 (2016).
16. Jiang, Z., Jiang, J.X. & Zhang, G.X. Macrophages: a double-edged sword in experimental autoimmune encephalomyelitis. *Immunology letters* **160**, 17-22 (2014).
17. Nathan, C. & Ding, A. Nonresolving inflammation. *Cell* **140**, 871-882 (2010).
18. Hochreiter-Hufford, A. & Ravichandran, K.S. Clearing the dead: apoptotic cell sensing, recognition, engulfment, and digestion. *Cold Spring Harbor perspectives in biology* **5**, a008748 (2013).
19. Saas, P., Kaminski, S. & Perruche, S. Prospects of apoptotic cell-based therapies for transplantation and inflammatory diseases. *Immunotherapy* **5**, 1055-1073 (2013).
20. Miyake, Y.*, et al.* Critical role of macrophages in the marginal zone in the suppression of immune responses to apoptotic cell-associated antigens. *The Journal of clinical investigation* **117**, 2268-2278 (2007).

21. Perruche, S., *et al.* CD3-specific antibody-induced immune tolerance involves transforming growth factor-beta from phagocytes digesting apoptotic T cells. *Nature medicine* **14**, 528-535 (2008).
22. Dogan, R.N., *et al.* CCL22 regulates experimental autoimmune encephalomyelitis by controlling inflammatory macrophage accumulation and effector function. *Journal of leukocyte biology* **89**, 93-104 (2011).
23. McGovern, N., *et al.* Human fetal dendritic cells promote prenatal T-cell immune suppression through arginase-2. *Nature* **546**, 662-666 (2017).
24. Zhang, X., *et al.* DNA methylation dynamics during ex vivo differentiation and maturation of human dendritic cells. *Epigenetics & chromatin* **7**, 21 (2014).
25. Pacis, A., *et al.* Bacterial infection remodels the DNA methylation landscape of human dendritic cells. *Genome research* **25**, 1801-1811 (2015).
26. Stumpfova, Z., Hezova, R., Meli, A.C., Slaby, O. & Michalek, J. MicroRNA profiling of activated and tolerogenic human dendritic cells. *Mediators of inflammation* **2014**, 259689 (2014).
27. Smyth, L.A., Boardman, D.A., Tung, S.L., Lechler, R. & Lombardi, G. MicroRNAs affect dendritic cell function and phenotype. *Immunology* **144**, 197-205 (2015).
28. Yoshimura, T. & Oppenheim, J.J. Chemokine-like receptor 1 (CMKLR1) and chemokine (C-C motif) receptor-like 2 (CCRL2); two multifunctional receptors with unusual properties. *Experimental cell research* **317**, 674-684 (2011).
29. Zabel, B.A., Silverio, A.M. & Butcher, E.C. Chemokine-like receptor 1 expression and chemerin-directed chemotaxis distinguish plasmacytoid from myeloid dendritic cells in human blood. *J Immunol* **174**, 244-251 (2005).
30. Nikic, I., *et al.* A reversible form of axon damage in experimental autoimmune encephalomyelitis and multiple sclerosis. *Nature medicine* **17**, 495-499 (2011).
31. Gu, C., *et al.* MicroRNA-214 induces dendritic cell switching from tolerance to immunity by targeting beta-Catenin signaling. *International journal of clinical and experimental pathology* **8**, 10050-10060 (2015).
32. Stickel, N., *et al.* MicroRNA-146a reduces MHC-II expression via targeting JAK/STAT signaling in dendritic cells after stem cell transplantation. *Leukemia* (2017).
33. Park, H., Huang, X., Lu, C., Cairo, M.S. & Zhou, X. MicroRNA-146a and microRNA-146b regulate human dendritic cell apoptosis and cytokine production by targeting TRAF6 and IRAK1 proteins. *The Journal of biological chemistry* **290**, 2831-2841 (2015).

Figure 1 SuperMApo modulates EAE by decreasing CNS infiltration.

(**a**) Clinical score of EAE mice treated twice (black arrows) with SuperMApo (n= 5 mice) or vehicle (n= 3 mice). Data representative of 3 independent experiments. (**b**) Analysis by qRT-PCR of TNF-α, Il-12p70, Il-6 and IFN-γ relative gene expressions in spinal cord lysate 72 h after the first SuperMApo treatment (n= 4 mice). Data representative of 2 independent experiments. (**c**) Absolute number of leukocytes in spinal cord of SuperMApo- (n= 5 mice) or vehicle- (n= 3 mice) treated EAE mice 72 h after treatment. Data representative of 3 independent experiments. (**d**) Absolute number of conventional DC (cDC) and plasmacytoid DC (pDC) in the spinal cord (n= 5 mice). Data representative of 3 independent experiments. (**e**) Costimulatory (CD80, CD86, CD40) and MHC-II mean florescence intensity (MFI) expressions evaluated in cDC and pDC from the spinal cord by FACS (n= 4-5 mice). Data representative of 3 independent experiments. (**f**) Cytokines (TNF-α, IL-12 and IL-10) expressions evaluated in cDC and pDC from the spinal cord (n= 5-6 mice). Data representative of 2 independent experiments. Mean $\pm$ SEM. *= $p<0.05$, **=$p<0.01$ ***=$p<0.005$, unpaired two-tailed Student's T test (b-f) or Anova two-way followed by Bonferroni post test (a).

Figure 2 SuperMApo modulates splenic pDC, but not DC, toward a tolerogenic profile *in vivo* and *in vitro*.

(**a**) Absolute number of conventional DC (cDC) and plasmacytoid DC (pDC) in the spleen of EAE mice 72 h after the first SuperMApo (or vehicle) treatment (n= 5 mice). Data representative of 3 independent experiments. (**b**) Costimulatory (CD80, CD86, CD40) and MHC-II mean florescence intensity (MFI) expressions evaluated in cDC and pDC from the spleen 72 h after the first SuperMApo treatment by FACS (n= 5 mice). Data representative of 3 independent experiments. (**c**) Cytokine (TNF-α, IL-12 and IL-10) expressions evaluated in

cDC and pDC from the spleen (n= 5 mice). Data representative of 2 independent experiments. (**d**) cDC (upper panel) and pDC (lower panel) sorted from vehicle- or SuperMApo-treated mice were co-cultured during 96 h with $CD4^+CD25^-$ OT-II naive T cells in presence of OVA peptide (2 µg/mL). Frequencies of $CD4^+IL17^+$, $CD4^+IFN\text{-}\gamma^+$ and $CD4^+CD25^+Foxp3^+$ were determined by FACS. Data representative of 3 independent experiments (triplicate from a pool of 5 mice). (**e**) Splenocytes from naive mice were treated with SuperMApo or vehicle and then restimulated with TLR ligand (LPS for cDC and CpG for pDC). Costimulatory (CD80, CD80 and CD40) and MHC-II mean fluorescence intensity (MFI) expressions were evaluated by FACS. Mean of triplicate. Data representative of 2 independent experiments. (**f**) cDC and pDC from the spleen of naive mice were isolated, treated with SuperMApo or vehicle, restimulated with TLR ligand (LPS for cDC and CpG for pDC) and then co-cultured during 96 h with $CD4^+CD25^-$ OT-II naive T cells in presence of OVA peptide (2 µg/mL). Frequencies of $CD4^+IL17^+$, $CD4^+IFN\text{-}\gamma^+$ and $CD4^+CD25^+Foxp3^+$ were determined by FACS. Data representative of 3 independent experiments. Mean $\pm$ SEM. *= $p<0.05$, **=$p<0.01$ ***=$p<0.005$, unpaired two-tailed Student's T test.

Figure 3 SuperMApo modulates differentially the transcriptome of cDC and pDC. (**a,b**) Gene expression (log_2 FPKM transformed) of conventional DC (cDC) (a) and plasmacytoid DC (pDC) (b) from EAE mice treated with vehicle or SuperMApo. Genes are ordered and colored based on their fold change, with (a) 231 (pDC) and 229 (cDC) genes with a change in expression of 1.5-fold or more, (b) 379 (pDC) and 366 (DC) genes with a fold change of 0.67 or below, (c) 105 (pDC) and 99 (cDC) genes expressed only in SuperMApo-treated mice, and (d) 134 (pDC) and 116 (cDC) genes expressed only in vehicle-treated mice. (**c,d**) Expression (log_2 FPKM transformed, normalized, mean centered) of all 12348 (cDC) (c) and 12382 (pDC) (d) genes expressed, clustered from lowest fold change (top) to highest (bottom). (**e,f**)

Network analysis of gene-ontology pathway enrichment on all 229 (cDC) (e) and 231 (pDC) (f) genes with a fold change of 1.5 or more and all 99 (cDC) and 105 (pDC) genes only expressed in SuperMApo treated mice with a $P< 0.05$. (**g,h**) Network analysis of gene-ontology pathway enrichment on all 366 (cDC) (g) and 379 (pDC) (h) genes with a fold change of 0.67 or below all 116 (cDC) and 134 (pDC) genes only expressed in vehicle treated mice. (**i,j**) Expression (log_2 FPKM transformed, normalized, mean centered) of genes corresponding to selected pathways found in the network analysis enrichment on all 229 (cDC) (i) and 231 (pDC) (j) genes with a fold change of 1.5 or more and all 105 (pDC) and 99 (cDC) genes only expressed in SuperMApo treated mice. (**k,l**) Expression (log_2 FPKM transformed, normalized, mean centered) of selected genes corresponding to selected pathways found in the network analysis enrichment on all 366 (cDC) (k) and 379 (pDC) (l) genes with a fold change of 0.67 or below and all 134 (pDC) and 116 (cDC) genes only expressed in vehicle treated mice. Data obtained from 3 independent experiments from a pool of 5 mice.

Figure 5 pDC were responsible of SuperMApo tolerogenic effect. Clinical score of EAE BDCA2-DTR mice treated with 1 µg of diphtheria toxin (DT) (or PBS) i.p at day 6, 7 and 9 and vehicle or SuperMApo at day 8 and 10 (n=4-5 mice). Data representative of 2 independent experiments. Mean $\pm$ SEM. *= $p<0.05$, **=$p<0.01$, Anova one-way followed by Bonferroni post test.

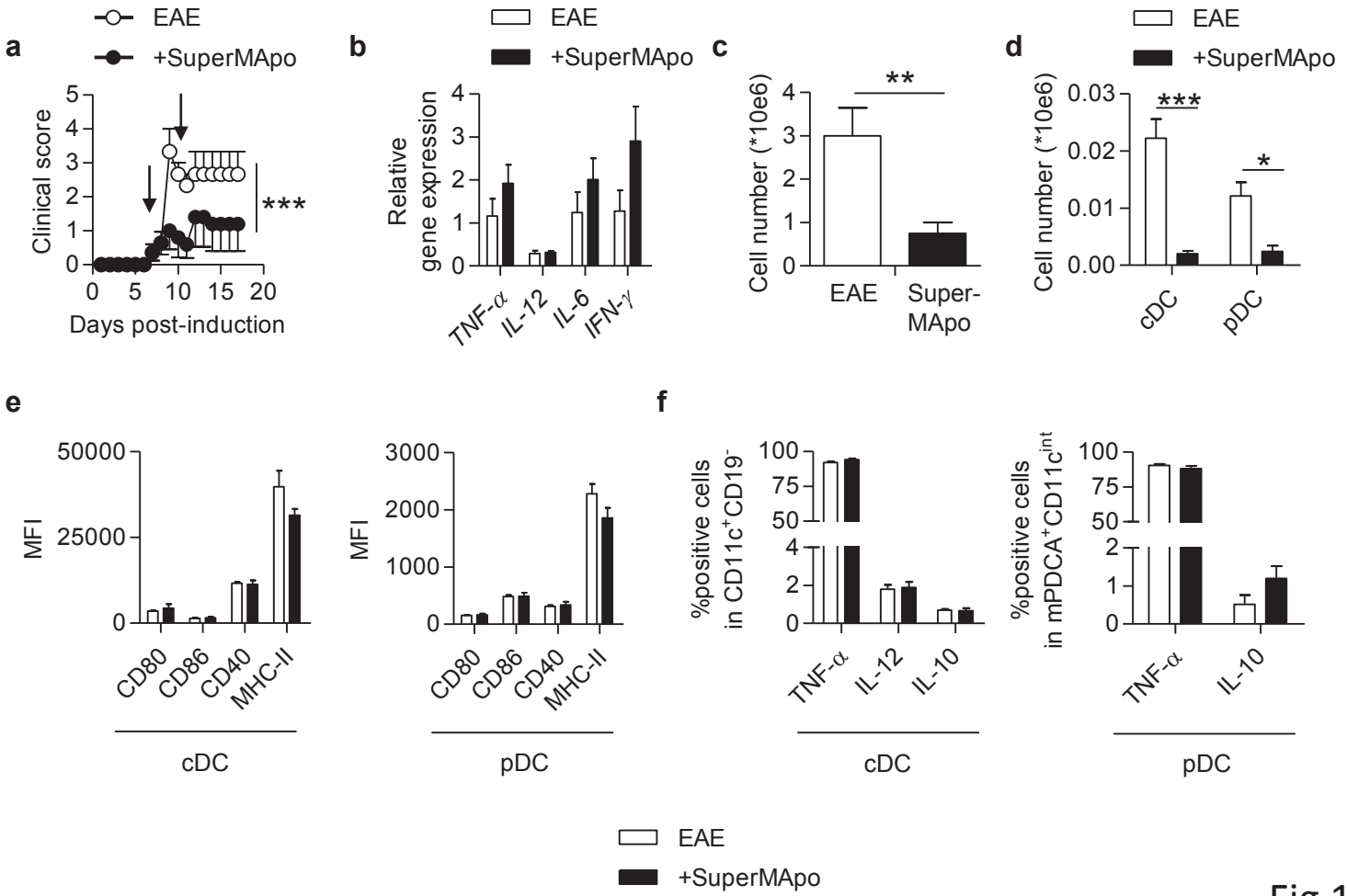
a
EAE
+SuperMApo
Clinical score
Days post-induction
***
b
Relative gene expression
TNF-α
IL-12
IL-6
IFN-γ
c
Cell number (*10e6)
**
EAE
Super-MApo
d
Cell number (*10e6)
***
*
cDC
pDC
e
MFI
CD80
CD86
CD40
MHC-II
cDC
pDC
f
%positive cells in CD11c+CD19-
%positive cells in mPDCA+CD11cint
TNF-α
IL-12
IL-10
cDC
pDC

Fig 1

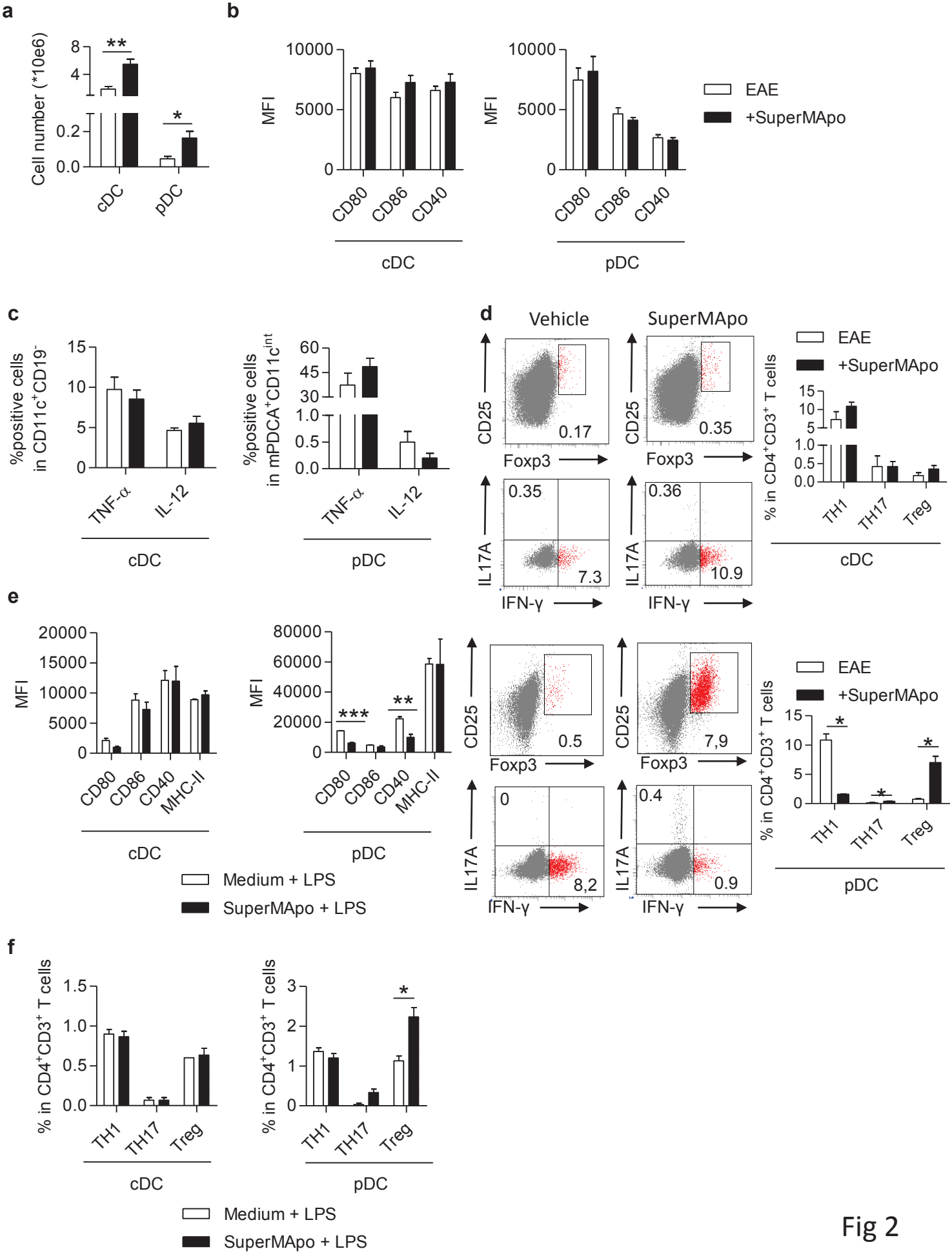
a
b
c
d
e
f
Cell number (*10e6)
cDC
pDC
MFI
CD80
CD86
CD40
EAE
+SuperMApo
%positive cells in CD11c+CD19-
%positive cells in mPDCA+CD11cint
TNF-α
IL-12
Vehicle
SuperMApo
CD25
Foxp3
IL17A
IFN-γ
% in CD4+CD3+ T cells
TH1
TH17
Treg
MHC-II
Medium + LPS
SuperMApo + LPS

Fig 2

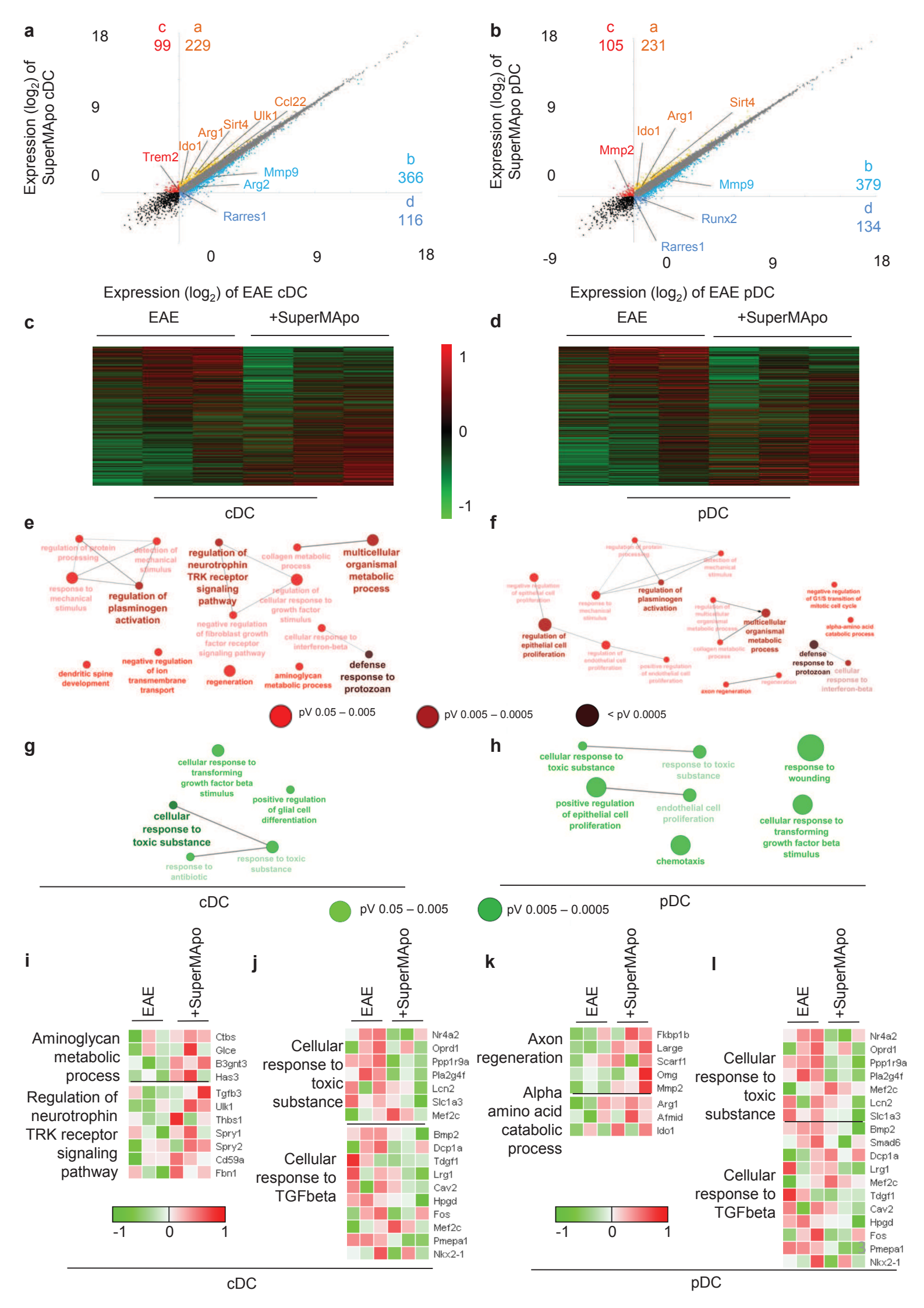
a
c 99
a 229
b 366
d 116
Expression (log2) of SuperMAPo cDC
Expression (log2) of EAE cDC
Ccl22
Ulk1
Sirt4
Arg1
Ido1
Trem2
Mmp9
Arg2
Rarres1
b
c 105
a 231
b 379
d 134
Expression (log2) of SuperMAPo pDC
Expression (log2) of EAE pDC
Sirt4
Arg1
Ido1
Mmp2
Mmp9
Runx2
Rarres1
c
EAE
+SuperMAPo
cDC
d
EAE
+SuperMAPo
pDC
e
regulation of protein processing
detection of mechanical stimulus
response to mechanical stimulus
regulation of plasminogen activation
regulation of neurotrophin TRK receptor signaling pathway
collagen metabolic process
multicellular organismal metabolic process
regulation of cellular response to growth factor stimulus
negative regulation of fibroblast growth factor receptor signaling pathway
cellular response to interferon-beta
dendritic spine development
negative regulation of ion transmembrane transport
regeneration
aminoglycan metabolic process
defense response to protozoan
f
regulation of protein processing
detection of mechanical stimulus
negative regulation of epithelial cell proliferation
response to mechanical stimulus
regulation of plasminogen activation
negative regulation of G1/S transition of mitotic cell cycle
regulation of multicellular organismal metabolic process
multicellular organismal metabolic process
alpha-amino acid catabolic process
regulation of epithelial cell proliferation
collagen metabolic process
defense response to protozoan
regulation of endothelial cell proliferation
positive regulation of endothelial cell proliferation
cellular response to interferon-beta
axon regeneration
regeneration
pV 0.05 – 0.005
pV 0.005 – 0.0005
< pV 0.0005
g
cellular response to transforming growth factor beta stimulus
positive regulation of glial cell differentiation
cellular response to toxic substance
response to antibiotic
response to toxic substance
cDC
h
cellular response to toxic substance
response to toxic substance
response to wounding
positive regulation of epithelial cell proliferation
endothelial cell proliferation
cellular response to transforming growth factor beta stimulus
chemotaxis
pDC
pV 0.05 – 0.005
pV 0.005 – 0.0005
i
EAE
+SuperMAPo
Aminoglycan metabolic process
Ctbs
Glce
B3gnt3
Has3
Regulation of neurotrophin TRK receptor signaling pathway
Tgfb3
Ulk1
Thbs1
Spry1
Spry2
Cd59a
Fbn1
-1 0 1
cDC
j
EAE
+SuperMAPo
Cellular response to toxic substance
Nr4a2
Oprd1
Ppp1r9a
Pla2g4f
Lcn2
Slc1a3
Mef2c
Cellular response to TGFbeta
Bmp2
Dcp1a
Tdgf1
Lrg1
Cav2
Hpgd
Fos
Mef2c
Pmepa1
Nkx2-1
k
EAE
+SuperMAPo
Axon regeneration
Fkbp1b
Large
Scarf1
Omg
Mmp2
Alpha amino acid catabolic process
Arg1
Afmid
Ido1
-1 0 1
pDC
l
EAE
+SuperMAPo
Cellular response to toxic substance
Nr4a2
Oprd1
Ppp1r9a
Pla2g4f
Mef2c
Lcn2
Slc1a3
Cellular response to TGFbeta
Bmp2
Smad6
Dcp1a
Lrg1
Mef2c
Tdgf1
Cav2
Hpgd
Fos
Pmepa1
Nkx2-1

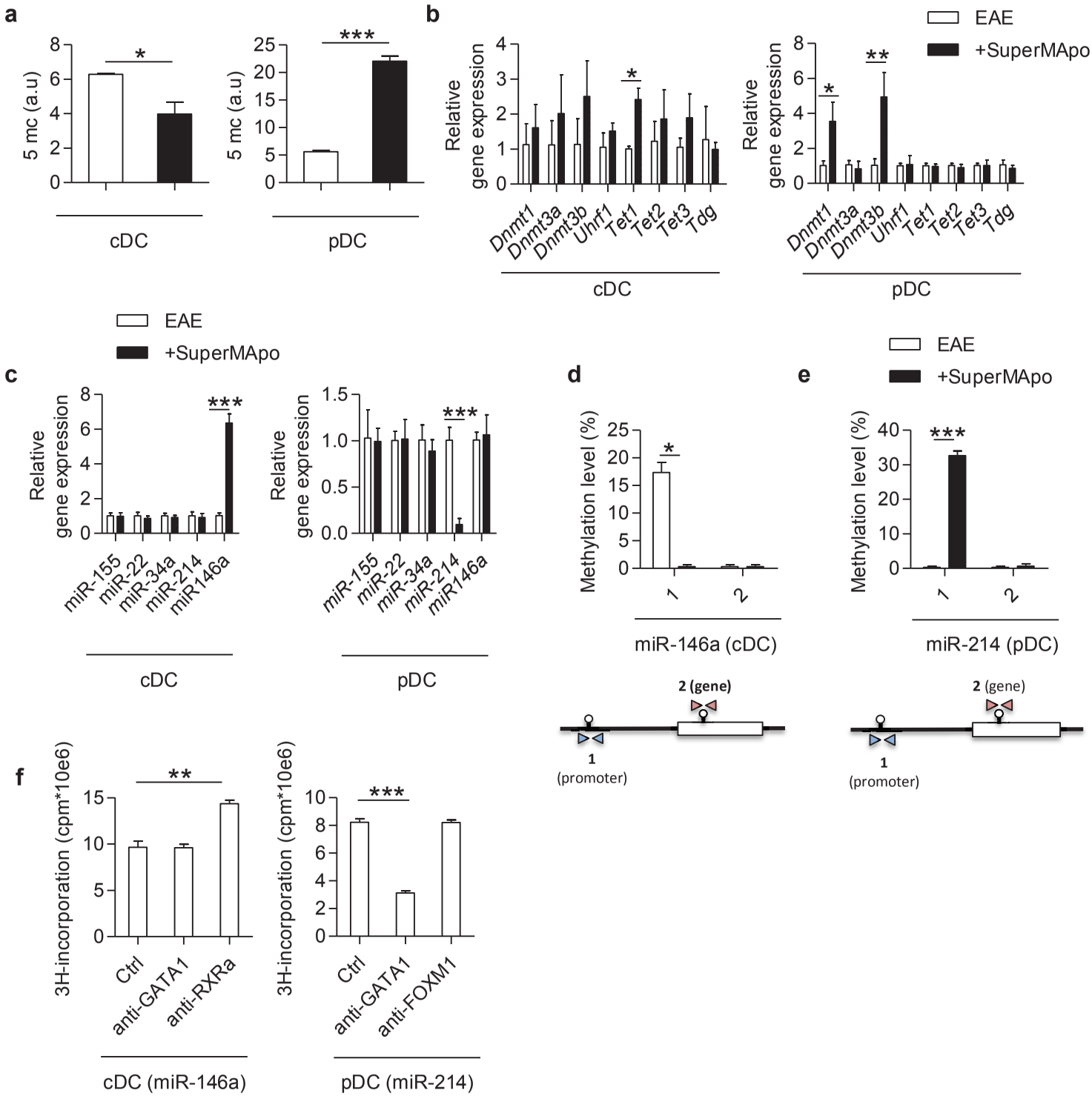
a
5 mc (a.u)
cDC
pDC
b
EAE
+SuperMAPo
Relative gene expression
Dnmt1
Dnmt3a
Dnmt3b
Uhrf1
Tet1
Tet2
Tet3
Tdg
cDC
pDC
c
miR-155
miR-22
miR-34a
miR-214
miR146a
d
Methylation level (%)
miR-146a (cDC)
2 (gene)
1
(promoter)
e
miR-214 (pDC)
f
3H-incorporation (cpm*10e6)
Ctrl
anti-GATA1
anti-RXRa
anti-FOXM1
cDC (miR-146a)
pDC (miR-214)

Fig 4

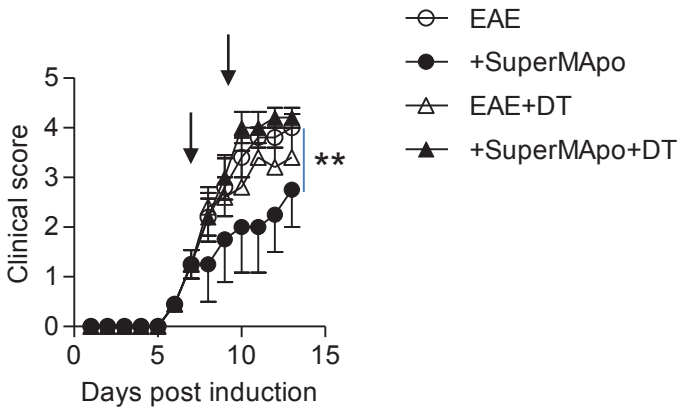
EAE
+SuperMApo
EAE+DT
+SuperMApo+DT
Clinical score
Days post induction
0
1
2
3
4
5
0
5
10
15
**

Fig 5

Résultats complémentaires

D'autres résultats nous ont permis au cours de cette thèse d'orienter notre recherche mais ils ne sont pas inclus dans les résultats précédents soumis pour publication ou en cours de préparation. Ces travaux sont détaillés ici, après une section « matériel et méthodes » récapitulant les techniques utilisées et non décrites précédemment.

Matériel et méthodes

Western blotting

Des pDCs triées (Miltenyi Biotech, pureté supérieure à 80%) de la rate de souris naïves (ou de souris EAE traitées par SuperMApo) ont été incubées pendant 24h avec SuperMApo ou son contrôle X-vivo (Lonza), suivie d'une activation au CpG durant 1 h (12 µg/mL, invivoGen). Les cellules ont alors été rincées en PBS puis les protéines ont été extraites à l'aide d'un tampon Laemmli. Les protéines ont été déposées sur un gel d'acrylamide à 8,5 % suivi d'un transfert sur membrane de polyvinlydène difluoride. La membrane a été bloquée avec du PBS-Tween 20 0,01 % régilait 5 % durant 1,5 h puis incubée sur la nuit avec des anticorps anti-pP65, p-STAT1, pIκB, P65, IκB ou actine (Cell signaling). La détection a été réalisée 2 h à température ambiante à l'aide d'anticorps anti-IgG couplé à la peroxidase suivie d'une révélation à l'ECL (BioRad).

Etude de la glycolyse in vivo

Des souris C57BL/6 ont été mises à la diète 3h avant l'injection i.p. d'1 mL de SuperMApo ou 1 mL de X-vivo. La glycémie a été mesurée avant injection puis à 1, 3, 6 et 24 h à l'aide d'un *Freestyle Accu check* (Freestyle).

Etude de la glycolyse in vitro

Après extraction, des splénocytes ont été prétraitées 12 h avec SuperMApo ou du X-vivo en présence ou non de 2-déoxyglucose (2-DG, 2mM ; Sigma-aldrich) puis activées avec du

LPS (1 µg/mL ; Sigma-Aldrich) ou du CpG (12 µg/mL) pendant 24 h. Après rinçage, les cellules ont été bloquées pour les récepteurs Fc puis marquées avec des anticorps anti-CD11c, CD11b, CD19, F4/80, mPDCA, Siglec-H, CD80, CD86, CD40 et MHC-II (BD biosciences) pendant 20 min à +4°C à l'abri de la lumière. Les cellules mortes ont été exclues avec un marquage FVS (BD biosciences). Enfin, les cellules ont été rincées et analysées en cytométrie de flux à l'aide d'un FACS canto II (BD biosciences).

SPR et spectrométrie de masse

Une puce d'or (Femto-ST, Besançon, France) a été activée durant 30 min avec de l'EDC-S (1-Ethyl-3-(3-Dimethylaminopropyl)-sulfo-N-hydroxysuccinimide) puis l'anticorps anti-TGF-β (clone 2G7 ; gracieusement fourni par L Chatenoud, Hôpital Necker-Enfants Malades, Paris) ou son isotype (Biolegend) ont été greffés durant 35 min sous ultrason. Après saturation de la puce avec de l'albumine de sérum de rat (Sigma-Aldrich), le surnageant SuperMApo a été injecté pendant 90 min en recirculation à 200 µL/min. La puce a alors été envoyée pour analyse en spectrométrie de masse à la plateforme CLIPP (G. Lucchi, Dijon, France). Des expériences identiques ont été réalisées avec un anticorps anti-LAP (clone TW7-16B4 ; Biolegend) et son isotype (Biolegend).

Résultats

En complément de ces travaux, nous avons étudié plus en amont les voies de régulation des différentes APC qui pouvaient expliquer ces changements observés après l'action de SuperMApo. La voie NFκB a été montrée comme sous-exprimée dans les macrophages *in vivo* et *in vitro*. De plus, la voie d'activation classique de NFκB est impliquée dans la mise en place de l'activation des pDC notamment lors de leur activation par le ligand TLR9 CpG (Volpi, Fallarino et al. 2013; Ceroi, Delettre et al. 2016). Nous avons donc cherché à déterminer l'effet du traitement par SuperMApo sur la voie NFκB dans les pDC. Pour se faire, des pDC ont été isolées de la rate de souris EAE traitées ou non par SuperMApo 72 h après traitement. Nous avons alors étudié la phosphorylation des acteurs de la voie NFκB, IκB et p65. Une diminution de la phosphorylation de p65 et de son régulateur IκB a été observée démontrant que cette voie est modulée par le traitement SuperMApo dans les pDC (**Figure 11a**). De plus, le traitement de pDC *in vitro* avec SuperMApo suivie d'une stimulation par le ligand TLR CpG permet aussi de diminuer la phosphorylation de p65 et du facteur de transcription pro-inflammatoire STAT1 (**Figure 11b**) (Takauji, Iho et al. 2002). Ces données

montrent que SuperMApo modulent le phénotype pro-inflammatoire des pDC en modulant l'activation de la voie NFκB.

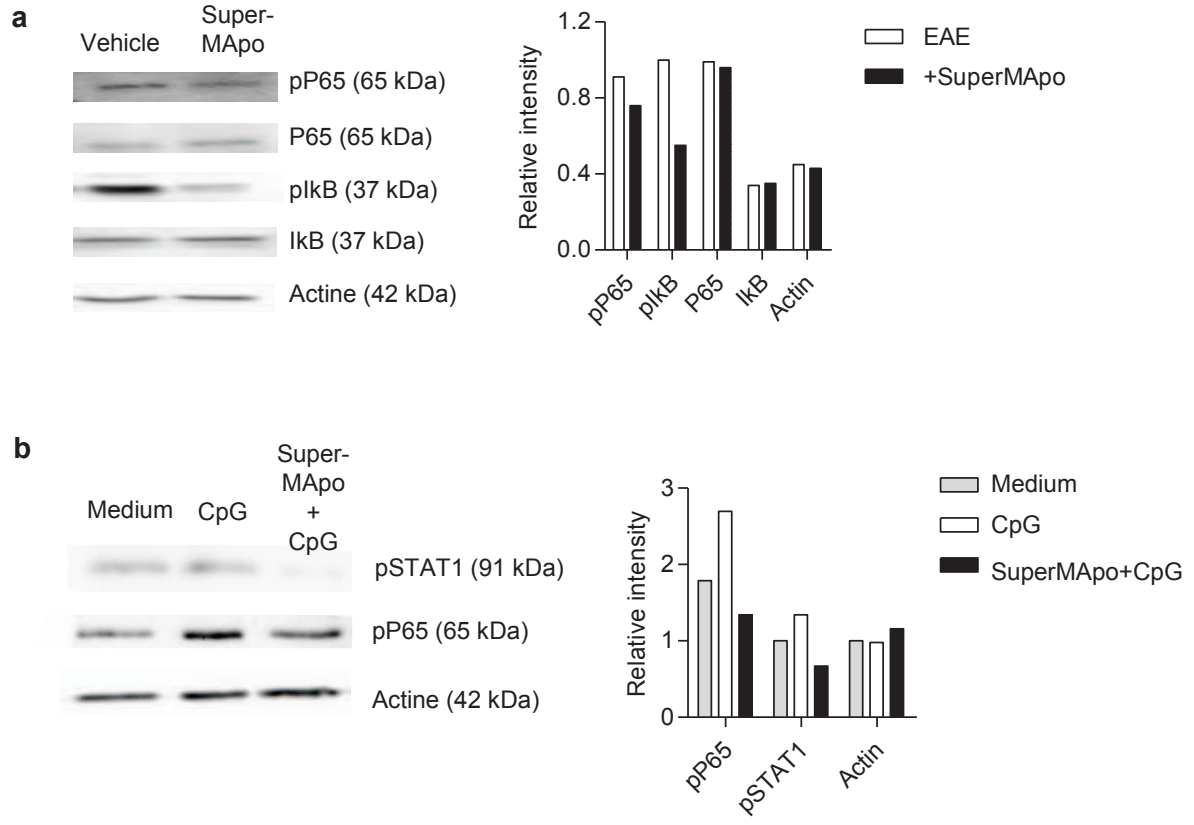

Figure 12. Etude de l'activation de la voie NFκB dans les pDC. (**a**) Des pDC ont été isolées de la rate de souris EAE, 72 h après avoir été traitées ou non par SuperMApo. L'activation de la voie NFκB a été évaluée par Western blotting. (**b**) Des pDC ont été isolées de la rate de souris naïves, traitées durant 24 h par SuperMApo ou son contrôle (med) puis activées par CpG (ligand du TLR9) pendant 1 h. L'activation de la voie NFκB et de la phosphorylation de STAT1 a été étudiée par Western blotting. Données représentatives de 3 expériences indépendantes.

Le rôle du métabolisme dans la reprogrammation des cellules immunitaires a été décrit récemment comme étant un facteur essentiel de la réponse immunitaire (Kelly and O'Neill 2015; Buck, Sowell et al. 2017). De manière étonnante, l'analyse par spectrométrie de masse de SuperMApo démontre qu'il contient des enzymes de la glycolyse (7 sur 10) alors que les surnageants de cellules apoptotiques ou de macrophages n'en contiennent pas (**Figure 12a**). Ces données nous ont donc incités à évaluer si SuperMApo pouvait affecter le métabolisme. Tout d'abord, l'injection de SuperMApo dans des souris C57BL/6 WT diminue le taux de glucose dans les souris de manière significative ($p<0,005$) dans l'heure suivant le traitement puis ce taux revient au taux basal dès 3 h (**Figure 12b**). Cependant, le même phénomène est observé dans les souris traitées avec le contrôle X-vivo (qui contient de l'insuline) démontrant

que cette baisse de la glycémie n'est pas liée à l'injection de SuperMApo. Afin de poursuivre l'étude de la reprogrammation métabolique des APC par SuperMApo, nous avons observé l'effet du blocage de la glycolyse sur la capacité d'activation des APC en réponse à un ligand TLR après traitement par SuperMApo *in vitro*. L'activation des différents types d'APC par un ligand TLR (LPS pout les DC et macrophages et CpG pour les pDC) induit une augmentation de l'expression des marqueurs de co-stimulation CD40, CD80 et CD86 (**Figure 12c**). Cette activation est prévenue lorsque les cellules ont été prétraitées par SuperMApo confirmant l'effet immunomodulateur des SuperMApo sur les APC. Afin d'étudier le rôle de la glycolyse sur l'effet de SuperMApo, les cellules ont été incubées en présence de 2-deoxyglucose (2-DG) (inhibiteur de la glycolyse) lors du traitement par SuperMApo ou son contrôle. L'ajout de 2-DG dans les cultures diminue les niveaux d'activation basale des APC ainsi que leur capacité de réponse au ligand TLR ce qui est cohérent avec la littérature (Jantsch, Chakravortty et al. 2008; Chiba, Hisamatsu et al. 2017). Cependant, le 2-DG ne bloque pas l'effet anti-inflammatoire de SuperMApo puisque SuperMApo en présence de 2-DG diminue toujours la capacité d'activation des APC. De manière intéressante, l'insuline présente dans le X-vivo ne semble pas avoir d'effets sur l'activation des cellules et l'inhibition de cette activation par le 2-DG suggérant que l'insuline modifie principalement le taux de glucose *in vivo* par l'action de cellules non immunes qui ne sont pas présentes dans la rate. Ces données démontrent que l'effet de SuperMApo n'est pas dépendant de la glycolyse et que d'autres mécanismes de modulations métaboliques, s'ils existent, pourraient être mis en jeu.

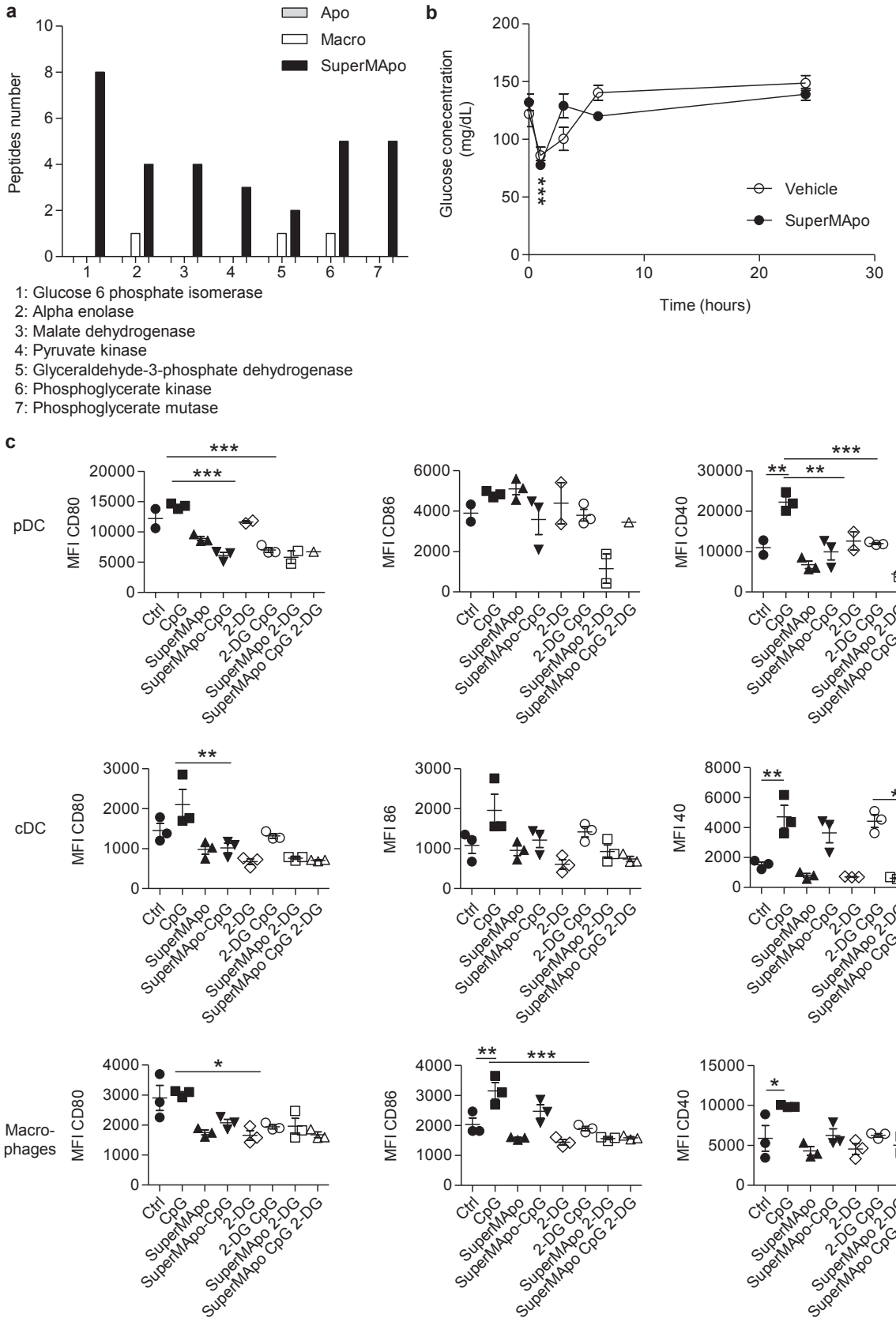
a
Apo
Macro
SuperMApo
Peptides number
1: Glucose 6 phosphate isomerase
2: Alpha enolase
3: Malate dehydrogenase
4: Pyruvate kinase
5: Glyceraldehyde-3-phosphate dehydrogenase
6: Phosphoglycerate kinase
7: Phosphoglycerate mutase
b
Glucose conecentration (mg/dL)
Vehicle
SuperMApo
Time (hours)
c
pDC
cDC
Macro-phages
MFI CD80
MFI CD86
MFI CD40
MFI 86
MFI 40
Ctrl
CpG
SuperMApo
SuperMApo-CpG
2-DG
2-DG CpG
SuperMApo 2-DG
SuperMApo CpG 2-DG

Figure 13. L'effet immunodmodulateur de SuperMApo n'est pas dépendant de la glycolyse. (**a**) Analyse par spectrométrie de masse des enzymes de la voie glycolytique dans le surnageant SuperMApo, de cellules apoptotiques (Apo) et de macrophages (Macro). (**b**) Taux de glucose dans le sang chez des souris C57BL/6 naïves injectées par SuperMApo ou son contrôle X-vivo (1 mL en i.p à 0 h). (c) Les splénocytes de souris C57BL/6 naïves ont été cultivés durant 24 h en présence de SuperMApo ou son contrôle combiné ou non à du 2-DG (2 deoxyglucose), puis stimulés pendant 24 h avec un ligand TLR (CpG pour les pDC et LPS pour les DC et macrophages). Les cellules ont ensuite été analysées par cytométrie de flux pour l'expression (MFI ou *Mean Fluoresence Intensity*) des marqueurs CD80, CD86 et CD40. Données représentatives de 2 expériences indépendantes. Moyenne ± SEM de 5 souris/groupe (b) ou de triplicat (c).

L'immunomodulation observée après traitement par SuperMApo, que ce soit celle des macrophages dans le modèle d'EAE ou l'induction de Treg dans le modèle d'arthrite induite au collagène nous a amené à étudier plus précisément le TGF-β au sein de SuperMApo. En effet, les résultats dans le modèle d'arthrite ont montré que SuperMApo déplété en TGF-β n'était plus actif, que le TGF-β recombinant n'était pas capable de mimer l'effet de SuperMApo et que l'injection de TGF-β recombinant dans du SuperMApo déplété en TGF-β restaurait l'activité résolutive du médicament. Ces travaux suggèrent que le TGF-β requiert des partenaires pour médier et potentialiser son effet. Afin d'étudier cette hypothèse, nous avons réalisé des expériences de résonnance plasmonique de surface (SPR) couplée à de la spectrométrie de masse. Cette technique a consisté à greffer un anticorps anti-TGF-β sur une puce d'or. Cette puce a été placée dans un système de fluidique permettant à SuperMApo de passer de manière continue sur la puce. Lors d'une interaction entre l'anticorps anti-TGF-β et un ligand, le faisceau optique était décalé, signe d'interaction (**Figure 13a**). L'injection de SuperMApo permet de visualiser un signal d'interaction de l'anticorps (mais pas de l'isotype contrôle) démontrant que SuperMApo contient le ligand spécifique de l'anticorps, du TGF-β (**Figure 13b,c**). L'analyse par spectrométrie de masse a ensuite mise en évidence d'autres molécules ayant été captées par la puce, grâce à leur interaction avec le TGF-β et notamment l'apolipoproteine E (ApoE), le composant du complément C1q, la macrophage métalloélastase MMP12, la thrombospondine 1 (Thbs1) et la transthyretine (Ttr). En revanche, sur trois essais indépendants, le peptide de latence associé au TGF- (*latency-associated peptide* ; LAP) et Ltbp3 (*latent-transforming growth factor beta-binding protein 3*) n'ont été détectés que de façon aléatoire. Ensuite, grâce au couplage d'un anticorps anti-LAP, nous avons pu détecter à nouveau ApoE, MMP12, Thbs1 et Ttr en plus de l'Annexin-A2 et de la lipoprotéine lipase. Ces protéines sont pour la plupart impliquées dans l'induction de tolérance (**Figure 13d,e**) (Mendez, Fernandez-Luna et al. 1986; Beppu, Nakamura et al. 2001; Bellac, Dufour et al. 2014; Spivia, Magno et al. 2014). Toutes ces protéines doivent donc être impliquées dans l'effet du TGF-β, notamment en potentialisant son effet immunomodulateur.

De manière très intéressante, la thrombospondine a été montrée comme étant un activateur du TGF-β sous sa forme non-active (qui est la forme présente dans SuperMApo) (Murphy-Ullrich and Poczatek 2000). Ces données nécessitent d'autres expériences afin d'étudier le rôle de l'interaction du TGF-β et de ses différents partenaires dans l'effet de SuperMApo.

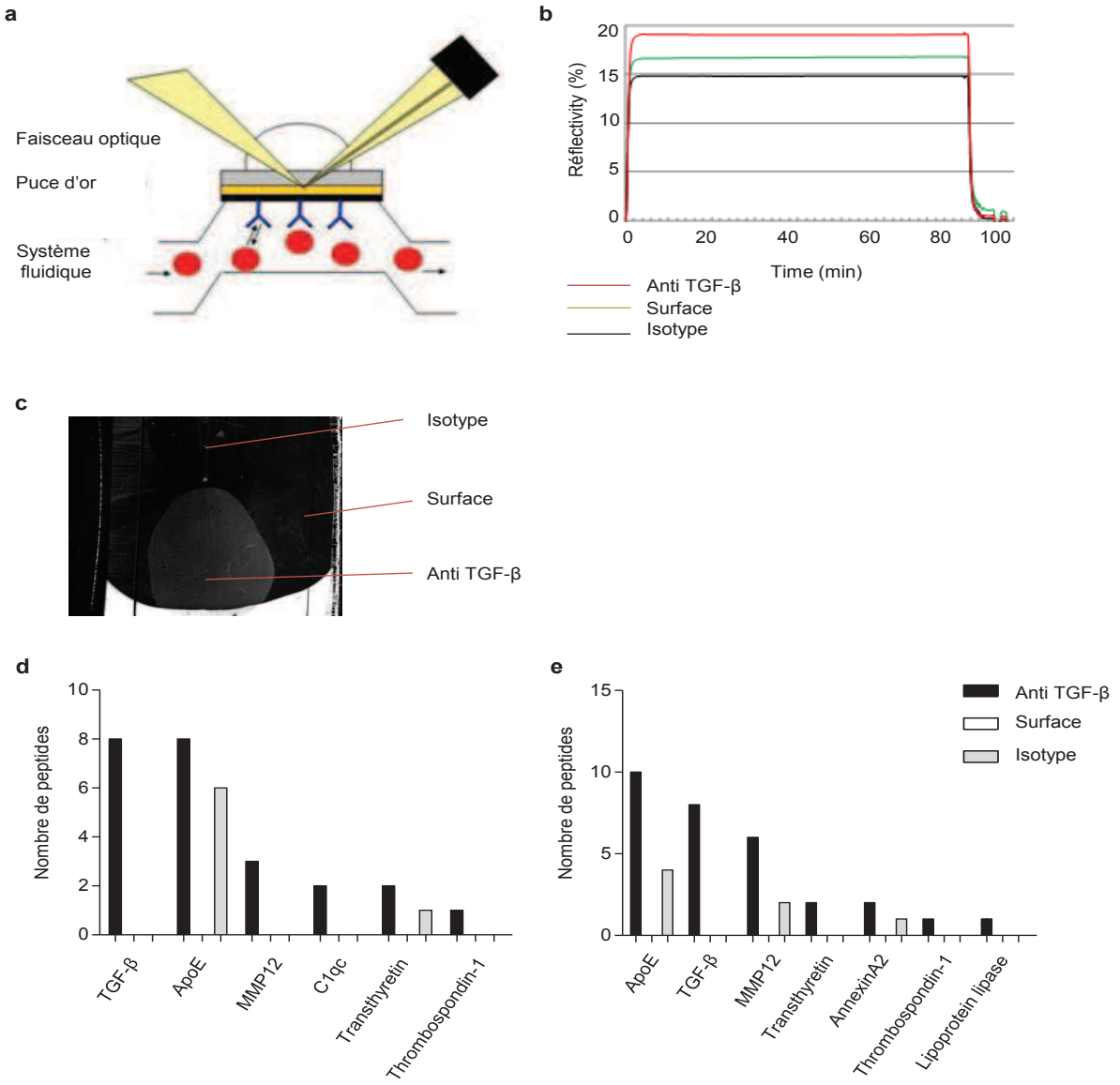

Figure 14. Le TGF-β est complexé à différentes protéines dans le surnageant SuperMApo. (**a**) Principe de la SPR. (**b**) Sensorgramme représentant la capture de TGF-β par un anticorps anti-TGF-β, son isotype ou la surface d'immobilisation seule. (**c**) Image différentielle du canal correspondant au graphique (b). (**d**) Analyse par spectrométrie de masse des partenaires du TGF-β à l'aide d'un anticorps anti-TGF-β. (**e**) Analyse par spectrométrie de masse des partenaires du TGF-β à l'aide d'un anticorps anti-LAP. Données représentatives de 3 expériences indépendantes. ApoE: Apolipoprotéine E. MMP12: Métalloprotéinase 12.

Discussion

Lors de ce travail de thèse, nous nous sommes intéressés à l'effet des facteurs pro-résolutifs issus de l'efferocytose sur la modulation de la sclérose en plaques dans un modèle murin et les mécanismes qui y étaient associés. L'efferocytose est un mécanisme bien décrit permettant l'induction de tolérance *via* la synthèse de nombreux facteurs anti-inflammatoires et pro-résolutifs par les macrophages tels que le TGF-β, la PGE2, l'IL-10 et les lipides pro-résolutifs (Résolvines, Marésines, Lipoxine A4…). Cependant, l'effet des facteurs produits lors de ce processus sur la modulation des maladies inflammatoires chroniques n'avaient jamais été étudiées à ce jour.

Transfert de l'approche SuperMApo dans le traitement de la SEP

Des données parallèles à ce travail ont montré que l'injection de SuperMApo dans des modèles d'arthrite induite au collagène et d'IBD permettait de diminuer la pathologie en favorisant la réparation tissulaire ainsi qu'en modulant les réponses immunes. Lors de cette étude, nous avons démontré que l'injection de SuperMApo aux premiers signes cliniques de la maladie permettait de contrôler l'EAE démontrant que SuperMApo pourrait être efficace dans les traitements des maladies inflammatoires chroniques. Il est à noter que le choix de la posologie du médicament (1 mL à deux reprises en i.p) a été fait sur la base des données préliminaires dans l'arthrite démontrant que cette posologie permettait de contrôler l'inflammation. Cependant, il serait intéressant d'étudier différentes posologies et voies d'injections du médicament afin de déterminer les paramètres optimaux. En effet, la production de SuperMApo s'effectue *via* la phagocytose d'un millions de macrophages pour 5 millions de cellules apoptotiques ce qui correspond à la dose moyenne utilisée dans les études ayant montrées l'effet tolérogénique des cellules apoptotiques *in vivo* (Saas, Kaminski et al. 2013). Cependant, un nombre supérieur de cellules apoptotiques ont déjà été injectées avec succès chez la souris suggérant que d'autres doses de SuperMApo pourraient être injectées dans notre modèle afin d'obtenir une rémission complète de la maladie (Saas, Kaminski et al. 2013). De plus, l'injection de SuperMApo a été réalisée en i.p se basant sur des études précédentes démontrant que l'injection de cellules apoptotiques en i.v ou en i.p ne modifiait pas la réponse obtenue mais il paraît intéressant de confirmer que l'injection de SuperMApo en i.v démontre les mêmes effets (Gray, Miles et al. 2007). L'injection de SuperMApo dans le modèle d'EAE MOG_{35-55} a été réalisée aux premiers signes cliniques de la maladie afin d'être dans les conditions les plus proches de ce qui se fait chez l'Homme. Cependant, il serait également pertinent de tester l'effet de SuperMApo dans la phase chronique de l'EAE. Pour cela, un modèle d'EAE dans les souris SJL/J est actuellement mis en place au laboratoire afin

de déterminer l'effet de l'injection de SuperMApo lors des phases de « rémissions/récurrences ». Les premières données préliminaires montrent que l'injection de SuperMApo lors des phases de « récurrences » permet de contrôler la maladie à long terme (données non montrées). A terme, il sera également important de tester l'effet de SuperMApo dans des modèles d'EAE chez d'autres animaux tels que le rat ou encore le singe Callithrix (Adelmann, Wood et al. 1995; Jagessar, Dijkman et al. 2016). Enfin, SuperMApo est actuellement en cours de développement chez l'Homme où des études pré-cliniques ont débuté chez des patients atteints de différentes maladies inflammatoires (notamment les MICI, la polyartrite rhumatoïde ou encore la fibrose pulmonaire). A la différence de la souris, les macrophages sont générés à partir de cellules mononuclées sanguines à l'aide de M-CSF et les cellules apoptotiques proviennent également de cellules mononuclées sanguines. Pour cela, les cellules mononuclées sont issues de couches leuco-plaquettaires (45 mL par prélèvement) qui nous permettent d'obtenir un volume final de 30 mL de SuperMApo. Nous évaluons actuellement la quantité de SuperMApo à injecter chez l'Homme à 500 mL en intrapéritonéal lors des premières phases de la maladie en combinaison ou non avec des traitements de fond (notamment des immunomodulateurs). Ces données font que le passage du SuperMApo souris au SuperMApo humain nécessitent encore des ajustements notamment liés à la provenance des macrophages (péritonéaux chez la souris et dérivés de cellules monuclées sanguines chez l'Homme) mais également à la quantité de SuperMApo obtenue (une souris prélevée pour 10 injectées contre 10 humains prélevés contre 1 injecté). Malgré ces difficultés, les derniers avancements pré-cliniques nous font espérer pouvoir démarrer des essais cliniques au cours des 2 à 3 prochaines années.

SuperMApo et réparation de la BHE

Nos travaux ont ensuite démontré que l'injection de SuperMApo dans un modèle murin d'EAE contrôlait la maladie en diminuant l'inflammation et la démyélinisation au sein du système nerveux central. Dans le but de montrer que SuperMApo pouvait induire une réparation tissulaire, nous nous sommes intéressés à l'effet de SuperMApo sur la BHE. Cependant, le traitement par SuperMApo n'induit pas de réparation de la BHE. Ces données sont différentes de celles obtenues dans un modèle de MICI au cours duquel nous avons observé un réparation accrue de la barrière intestinale due notamment à une augmentation des propriétés réparatrices des fibroblastes et cellules épithéliales. Ces données suggèrent que SuperMApo influe uniquement sur les réponses immunes en périphérie dans ce modèle ou qu'il n'est pas accessible au SNC et ne peut donc pas moduler directement cet organe. Il serait

intéressant afin de confirmer ces données de tester l'effet de SuperMApo sur la réparation de cette BHE et la migration cellulaire dans des modèles *in vitro* de BHE (Czupalla, Liebner et al. 2014). Au vu des données préliminaires dans le modèle de MICI et de données montrant une baisse de la démyélinisation au sein du SNC, il semble également intéressant d'étudier l'effet direct de SuperMApo sur cette démyélinisation. Pour cela, nous sommes en train de mettre en place un modèle de destruction chimique basé sur l'ingestion de cuprizone au sein du laboratoire. Cependant, les premières données suggèrent que SuperMApo ne module pas directement la remyélinisation au sein du SNC ce qui confirme que SuperMApo joue plutôt un rôle d'immunomodulateur périphérique au cours de la pathologie et ne module pas directement la pathologie au niveau du SNC.

SuperMApo et migration cellulaire

Nos travaux ont démontré que l'injection de SuperMApo dans un modèle murin d'EAE contrôlait la maladie en diminuant l'inflammation et la démyélinisation au sein du système nerveux central. De nombreux facteurs peuvent favoriser l'infiltration des cellules immunes au sein du SNC. Parmi eux, on compte la perméabilité de la BHE ainsi que l'expression de chemokines et d'intégrines au niveau du SNC (Jain, Coisne et al. 2010; Steiner, Coisne et al. 2010; Schlager, Korner et al. 2016; Wang, Li et al. 2016). Cependant, l'injection de SuperMApo ne permet pas de moduler ces facteurs mais semble plutôt agir en périphérie. Nous nous sommes donc intéressés à l'effet de SuperMApo sur la capacité migratoire des cellules immunitaires depuis la périphérie, et notamment les lymphocytes T. En effet, les cellules de la rate provenant de souris traitées par SuperMApo démontrent une baisse de capacité migratoire au niveau de différents organes (rate et ganglions inguinaux) qui est liée à une baisse d'expression du récepteur CXCR3 qui est le récepteur des chemokines pro-inflammatoires CXCL9, 10 et 11 (Groom and Luster 2011). Ce récepteur est exprimé principalement par les Th1 et joue un rôle dans le contrôle de l'EAE (Sporici and Issekutz 2010). De plus, sa modulation, notamment au niveau des Th1, impacte différentes maladies inflammatoires telles que l'IBD ou la maladie de Kawasaki (Altara, Mallat et al. 2016; Wadwa, Klopfleisch et al. 2016). De manière très intéressante, cette baisse de l'expression de CXCR3 sur les Th1 est dépendante des macrophages (qui semble être une des cellules clés dans l'effet de SuperMApo) puisque leur déplétion mène à perdre cette baisse. Cependant, les facteurs produits par les macrophages qui sont responsables de cette baisse d'expression devront être déterminés et notamment le rôle de l'IL-10 dans cet effet (Wadwa, Klopfleisch et al. 2016). De manière particulièrement intéressante, les macrophages diminuent également la

polarisation Th1 *in vivo* et *in vitro* démontrant une régulation fine de ce type cellulaire par les macrophages qui diminuent leur différenciation mais également leur capacité migratoire suggérant un profil « semi-mature ». Ces résultats n'excluent pas la contribution d'autres mécanismes dans le contrôle de la migration par SuperMApo. Comme nous l'avons montré figure 10.b, SuperMApo contient un certain nombre de chémokines qui pourraient attirer les cellules immunitaires dans un lieu autre que le SNC dans notre modèle. De plus, l'expression de CXCR3 peut expliquer la baisse d'infiltration des LT ; cependant une baisse d'infiltration générale est observée et pourrait être due à la sous-expression d'autres récepteurs de chémokines que nous n'avons pas étudiés ici. Une rétention au niveau des organes lymphoïdes secondaires empêchant la sortie des cellules immunitaires pourrait également expliquer la baisse de capacité migratoire observée. Ces données suggèrent donc que SuperMApo contrôle la migration cellulaire depuis la périphérie, notamment *via* un rôle fondamental des APC qui sera décrit dans le paragraphe ci-dessous.

SuperMApo, cellules dendritiques et macrophages

Dans le cadre de la SEP, les lymphocytes T pathogéniques sont activés par les APC en périphérie avant de migrer au sein du SNC (Figure 15). Notre étude a également permis de montrer que l'effet pro-résolutif de SuperMApo dans le modèle d'EAE était dû à une reprogrammation des APC permettant une modulation des lymphocytes T CD4 et CD8 au niveau des organes périphériques (ganglions inguinaux et rate). Il est intéressant de noter que les réponses immunes sont modulées au niveau des ganglions inguinaux, considérés comme les ganglions drainants dans ce modèle, mais pas au niveau des ganglions brachiaux (données non montrées) qui sont des ganglions non-drainants. Ces observations sont à mettre en regard du fait que les réponses T affectées sont celles induites par le peptide MOG et que les APC sont toujours sensibles à une restimulation TLR au niveau de la rate suggérant que l'effet de SuperMApo est spécifique de notre antigène et n'entraîne pas une immunosuppression globale. De plus, des données préliminaires ont montré que l'injection de SuperMApo dans un modèle d'infection bactérienne ou de tumorigénèse n'altérait pas les réponses immunes ainsi que la survie (données non montrées). SuperMApo n'entraîne donc pas d'immunosuppression mais bien une tolérance immunitaire.

De manière intéressante, les macrophages et les pDC démontrent un profil tolérogénique alors que ce n'est pas le cas pour les cDC. Ceci pourrait s'expliquer par un profil moins « plastique » des cDC qui ne seraient pas capables d'être reprogrammées suffisament par

SuperMApo, ce que suggèrent nos données de transcriptomique montrant une reprogrammation seulement partielle des cDC vers un profil tolérogénique. De plus, les cDC se divisent en différentes catégories selon l'expression notamment du CD11b et du CD8α. Or, dans cette étude, la stratégie d'étude des cDC est basée uniquement sur l'expression du CD11c sans avoir étudier les différents sous-types de cDC. De plus, les cDC $CD8\alpha^+$ ont tendance à générer des Th1 *via* la synthèse d'IL-12 et qui sont pathogéniques dans le cadre de l'EAE tandis que les cDC $CD11b^+$ ont tendance à générer des Th2 qui sont bénéfiques pour la pathologie (Maldonado-Lopez, De Smedt et al. 1999; Weber, Prod'homme et al. 2007; Grifka-Walk, Giles et al. 2015). Le rôle exact des cDC doit donc être étudié plus en profondeur.

L'étude du rôle des pDC et macrophages dans l'effet pro-résolutif de SuperMApo a mis en évidence que leur déplétion menait à la perte de son effet. Ces données viennent confirmer des travaux précedents de notre laboratoire démontrant que l'injection de cellules apoptotiques permettait la prise de greffe de moelle osseuse de manière dépendante des macrophages qui induisaient des pDC tolérogéniques nécessaire à l'effet observé. Ces pDC étaient alors capable d'induire la génération de Treg de manière TGF-β dépendante (Bonnefoy, Perruche et al. 2011). Nos travaux suggèrent donc que ce sont les facteurs issus de l'efferocytose qui seraient responsables de cet effet. Les macrophages et pDC semblent donc coopérer afin d'induire un contrôle de l'activation des LT au niveau des organes périphériques. Il serait donc intéressant de déterminer l'influence d'un type cellulaire sur l'autre et de savoir quel type cellulaire joue l'effet premier dans notre modèle d'EAE et notamment de déterminer si les pDC en l'absence de macrophages induisent toujours des Treg sous l'effet de SuperMApo. De plus, l'injection de macrophages modulés par SuperMApo *in vitro* ou *in vivo* module l'EAE. Cependant, ce contrôle n'est pas aussi marqué qu'avec l'injection de SuperMApo directe suggérant que les macrophages ne sont pas les seuls responsables de l'effet résolutif de SuperMApo. Il paraît donc intéressant d'injecter des pDC reprogrammé par SuperMApo en synergie avec des macrophages afin de déterminer si l'effet cumulé de ces deux types cellulaires permet de récapituler l'effet de SuperMApo. Ces résultats suggèrent que les cellules de l'immunité innée sont en première ligne afin d'induire une immunomodulation globale. Des travaux du laboratoire ont également montré que l'injection de SuperMApo dans un modèle de MICI chez la souris induisait non seulement une modulation du phénotype des APC mais également une modulation des cellules du microenvironnement (cellules épithéliales et fibroblastes) et favorisaient la réparation tissulaire (Omayra Martin-Rodriguez et al., en préparation). Dans ce contexte, des

macrophages présentant un profil réparateur sont retrouvés au sein des colons de souris après traitement par SuperMApo. Nous proposons donc un modèle au cours duquel SuperMApo module premièrement les macrophages, leur permettant d'acquérir un phénotype pro-réparateur et pro-tolérogénique. Ces macrophages modulent alors les réponses immunes innées, et notamment les pDC, ainsi que la réparation tissulaire en les cellules de l'environnement tissulaire. Tous ces types cellulaires favoriseront alors la modulation de l'immunité adaptative permettant d'établir une tolérance à long terme, une réparation tissulaire et un retour à l'homéostasie.

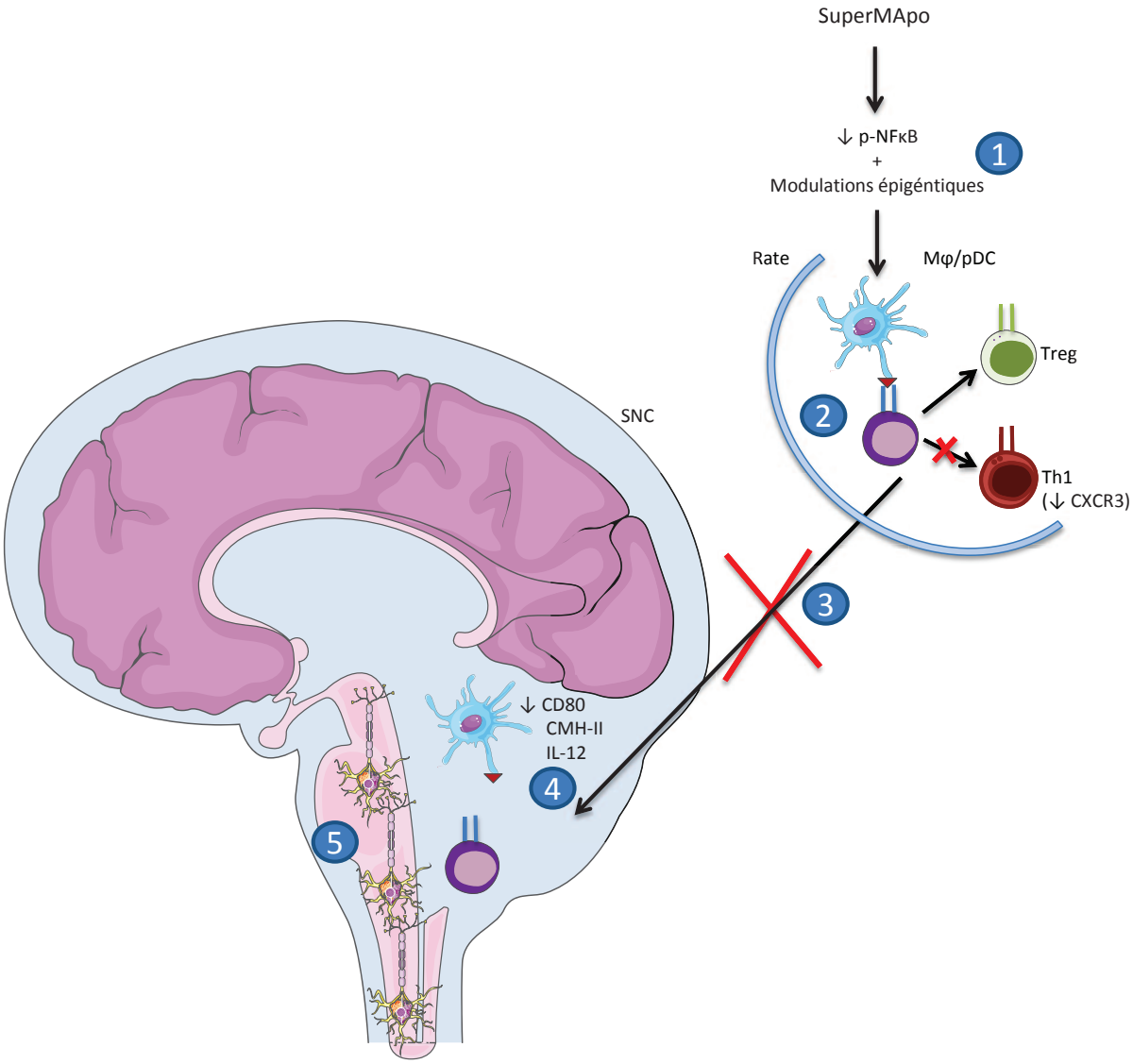

Figure 15. Mécanisme général d'action de SuperMApo. 1 : L'injection de SuperMApo dans un modèle d'EAE induit une baisse de l'activation de la voie NFκB ainsi que des modulations épigénétiques dans les macrophages et pDC au sein de la rate. 2 : Ces modifications permettent à ces cellules d'acquérir un profil tolérogénique et de favoriser la génération de Treg et d'inhiber la génération de Th1. Les Th1, sous l'effet des macrophages, voient également leur expression du récepteur CXCR3 diminué. 3 : La diminution de l'expression de CXCR3 sur les Th1, ainsi que l'induction générale de tolérance, diminue les capacités migratoires des cellules immunes de la périphérie vers le SNC induisant une diminution de l'infiltrat inflammatoire au sein de cet organe. 4 : Les macrophages, au sein du SNC, possèdent également un profil moins inflammatoire (baisse de l'expression du CD80, CMH-II et de l'IL-12) suggérant une capacité moindre à réactiver les LT. 5 : La diminution de l'inflammation au sein du SNC diminue la démyélinisation neuronale ce qui entraîne une amélioration des signes cliniques de la maladie. Mφ : Macrophages.

De manière particulièrement intéressante, les trois types cellulaires ne sont pas du tout réguler de la même manière au niveau génique. En effet, les macrophages sur-expriment principalement des marqueurs de type M2 tels que Arg1, Alox15, Pparg ou Cd226 et sous-expriment des gènes impliqués dans les réponses inflammatoires tels que Ccl17, Ccl22, l'IL-

7, Foxo1 ou Ccr4. De plus, les voies modulées de manière négatives sont impliquées dans les réponses immunes et la régulation de processus cellulaires alors qu'une des deux seules voies sur-exprimées est impliquée dans la réparation tissulaire démontrant que ce type cellulaire est profondément remodelé par SuperMApo et qu'il acquiert un phénotype pro-résolutif. Les pDC sont également modulées vers un profil tolérogénique alors que les cDC acquièrent un profil plus mitigé puisqu'elles sur-expriment des molécules impliquées dans les réponses inflammatoires. De plus les pDC surexpriment la voie « *axon regeneration* » renforçant l'idée qu'elles possèdent un profil résolutif. Une question reste cependant à élucider, les pDC et macrophages expriment des voies impliquées dans la réparation tissulaire qui a lieu au sein du SNC dans notre modèle. Or, ces cellules sont présentes en moins grand nombre au sein de cet organe ce qui pose la question de leur mécanisme d'action afin de favoriser la remyélinisation. Une explication pourrait être l'induction de Treg par ces deux types cellulaires. En effet, les pDC et macrophages ont une capacité accrue de produire des Treg. Ces observations sont à mettre en lien avec une étude récente démontrant que les Treg favorisent de manière directe la remyélinisation au sein du SNC de manière CCN3 dépendante, suggérant que les pDC et macrophages pourraient favoriser la réparation tissulaire en induisant des Treg (Dombrowski, O'Hagan et al. 2017). De plus, bien qu'aucune augmentation du nombre de Treg spécifique de l'antigène ne soit observée dans nos souris après injection de SuperMApo, la déplétion de Treg inhibe l'effet de SuperMApo démontrant un rôle dans le contrôle de la maladie (données non montrées). Ces données suggèrent que des Treg spécifiques de l'antigène pourraient être présents dans d'autres organes et notamment au sein des ganglions inguinaux et de la moelle épinière. Les pDC et macrophages semblent donc jouer un rôle important dans l'effet de SuperMApo qui devra être confirmé par des données pré-cliniques chez l'Homme.

SuperMApo et modulations épigénétiques

Les APC étant reprogrammées vers un profil tolérogénique, nous nous sommes intéressés à l'étude des mécanismes impliqués dans cette reprogrammtion. Nous avons démontré que la modulation des APC *in vivo* par SuperMApo implique une modulation épigénétique différentielle qui pourrait notamment expliquer en partie les différences de comportement entre ces trois types cellulaires. Les macrophages présentent un profil de méthylation globale diminué qui est lié à une augmentation de l'activité TET et une baisse de l'activité DNMT de maintien. Cette déméthylation globale est associée à une déméthylation au niveau du promoteur de gènes impliqués dans la synthèse de miRNA tels que les miR-223 (qui est sur-

exprimé) et -127 (qui est sous-exprimé). De manière intéressante, la déméthylation du miR-127 est associée à une augmentation du facteur de transcription CTCF qui est un répresseur transcriptionnel (Holwerda and de Laat 2013). Le miR-223 a été décrit récemment comme étant un régulateur des réponses immunes dans les macrophages et sa déplétion augmente la colite induite au dextran sulfate sodium (Zhou, Xiao et al. 2015; Neudecker, Haneklaus et al. 2017). Cette régulation se fait notamment via une modulation de l'activité du facteur de transcription PPARγ, facteur qui est sur-exprimé dans les macrophages modulés par SuperMApo (Ying, Tseng et al. 2015). Le miR-127 favorise la génération de macrophages de type M1 et réprime la génération des M2 et son inhibition protège d'une inflammation pulmonaire induite au LPS en induisant la génération de M2 (Ying, Kang et al. 2015). Cependant, sa régulation par des facteurs épigénétiques et par le répresseur transcriptionnel CTCF n'avaient jamais été démontrées à ce jour. Chez les cDC et pDC, une régulation différentielle a lieu comme celle observée au niveau fonctionnel et génique. En effet, les cDC présentent une baisse de la méthylation globale de l'ADN alors que les pDC présentent une augmentation de cette méthylation. La baisse de méthylation des cDC s'explique par une augmentation de l'expression de TET1 alors que chez les pDC, une augmentation de l'expression de DNMT1 et DNMT3 est observée. La régulation des APC par SuperMApo passe donc par un contrôle épigénétique de ces cellules suggérant que la modulation épigénétique, de manière ciblée, de la SEP pourrait être un moyen intéressant de contrôle de la maladie.

SuperMApo et signalisation cellulaire

La régulation des APC par SuperMApo induit également une baisse de l'activation de la voie de transcription pro-inflammatoire NFκB mais aussi, chez les macrophages, une diminution de l'expression du facteur de transcription p65. Il serait également intéressant d'étudier d'autres voies de signalisations impliquées dans la reprogrammation des APC telles que les voies AKT/PI3K/mTOR, JAK/STAT, MAPK ou encore la voie NFκB non canonique. Des données chez la souris ont mis en évidence que le TGF-β (qui est une molécule présente dans le surnageant SuperMApo) induisait la production de l'enzyme IDO1 (qui est surexprimée dans nos pDC traitées par SuperMApo *in vivo*) ce qui activait la voie NFκB non-canonique résultant un profil tolérogénique au niveau des pDC (Pallotta, Orabona et al. 2011). De plus, cette voie a été montrée comme impliquée dans la génération de macrophages de type M2, permettant d'induire la tolérance dans un modèle d'inflammation lié à la réaction de Schwartzmann (Porta, Rimoldi et al. 2009). La voie PI3K/AKT/mTOR est également une

cible intéressante. En effet, elle est impliquée dans la génération de macrophages de type M2 (Vergadi, Ieronymaki et al. 2017). De plus, le blocage de mTOR inhibe la génération de M2 en permettant notamment l'activation de la voie NFκB (Weichhart, Haidinger et al. 2011; Zhu, Yang et al. 2014). Des récents travaux ont démontré l'importance de la régulation du métabolisme au sein des cellules immunitaires ainsi que le rôle important de la voie PI3K/AKT/mTOR. De manière générale, les cellules lors de leur activation (notamment par les agonistes des TLR) ont besoin de mettre en place une glycolyse accrue due à des besoins énergétiques croissants. Les cellules régulatrices ont tendances à favoriser l'utilisation de la β-oxidation des acides gras (Kelly and O'Neill 2015). *In vitro*, l'effet de SuperMApo ne semble pas dépendant de la glycolyse puisque les APC sont toujours capables de démontrer un profil moins inflammatoire lorsque la glycolyse est bloquée à l'aide de 2-DG. Cependant, nous n'avons pas étudié le rôle de la β-oxidation des acides gras dans l'effet de SuperMApo notamment en bloquant cette voie avec l'etomoxir. L'étude de la reprogrammation métabolique des APC par SuperMApo semble d'autant plus importante que des données préliminaires suggèrent que la culture de macrophages avec SuperMApo suivie d'une activation au LPS modifie les besoins métaboliques de la cellule (données non montrées). De plus, la présence d'enzyme de la glycolyse renforce l'idée que la reprogrammation métabolique possède un rôle important dans l'effet de SuperMApo qui devra être étudié en profondeur.

Les acteurs essentiels de SuperMApo

S'il semble important d'étudier les différentes voies métaboliques mises en jeu (glycolyse, β-oxidation des acides gras, cholestérol…), il semble aussi important de définir les différentes molécules présentes dans le surnageant SuperMApo. La présence de TGF-β dans notre surnageant est particulièrement intéressante. En effet, des articles récents ont démontré que cette molécule favorisait la génération de M2 et diminuait la génération de M1 mais modulait également les cDC et pDC vers un profil tolérogénique (Speck, Lim et al. 2014; Chalise, Pallotta et al. 2016; Zhang, Wang et al. 2016). De plus, une étude récente à montrer que le mannose permettait la différenciation en Treg *via* une augmentation de l'activation du TGF-β de manière intégrine β8 et ROS dépendante (Zhang, Chia et al. 2017). Or, le TGF-β présent dans notre surnageant de SuperMApo se trouve sous sa forme non active et une activation est nécessaire afin d'obtenir une molécule active. Nos travaux suggèrent que si le TGF-β est important pour l'effet pro-résolutif de SuperMApo, il n'est pas la seule molécule importante et qu'il pourrait interagir avec d'autres protéines (Apolipoprotéine E, TSP-1, C1qc,

transthyrétine, Annexine A2, Lipoprotéines lipase et MMP12). Il est notamment intéressant de retrouver la TSP-1 parmi ces interactants possibles car cette protéine permet l'activation du TGF-β latent (Murphy-Ullrich and Poczatek 2000). L'apolipoprotéine E a également été montrée comme modulant les réponses immunes en ciblant les cellules présentatrices de l'antigène (Tenger and Zhou 2003). De plus, sa production est sous le contrôle du TGF-β (Braesch-Andersen, Paulie et al. 2013). Enfin, la MMP12 a été montrée récemment comme favorisant la résolution de l'inflammation et la réparation tissulaire dans un modèle d'arthrite (Bellac, Dufour et al. 2014). La présence de TGF-β et de MMP12 dans SuperMApo suggère que SuperMApo en plus de moduler les réponses immunes pourrait également affecter directement la réparation tissulaire. Des données obtenues dans un modèle de MICI ont notamment montrées que le TGF-β, le VEGF et l'IGF-1 présents dans le SuperMApo favorisaient l'acquisition d'un phénotype pro-réparateur par les fibroblastes et les cellules épithéliales. Or, ces protéines ont été montrées comme impliquées dans la réparation tissulaire et le contrôle de l'inflammation confirmant que SuperMApo pourrait avoir un rôle direct sur la phase de réparation tissulaire (Bao, Kodra et al. 2009; Finnson, McLean et al. 2013; Han, Juncadella et al. 2016). Il parait également important d'étudier la présence d'autres molécules (lipides, sucres…) favorisant l'effet résolutif de SuperMApo. Le mannose est une piste d'autant plus intéressante que son récepteur CD206 est impliqué dans la génération de macrophages de type M2 et est un marqueur important de ce type de polarisation (Kambara, Ohashi et al. 2015). Des travaux récents ont également montré que l'α-ketoglutarate favorisait la génération de macrophages de type M2 en modulant notamment la voie NFκB et des acteurs épigénétiques (Liu, Wang et al. 2017). Enfin, il faudra définir la présence ou non de lipides au sein du surnageant de SuperMApo. En effet, de nombreuses études ont démontrées la présence de lipides pro-résolutifs (Résolvine D1 et 2,PGE2, lipoxine B4, marésine 1, protectine D1, thromboxane B2 et lipoxine A4) au sein du sécretome de macrophages lors de la phagocytose de cellules apoptotiques (Dalli and Serhan 2016). La protectine D1 favorise notamment l'acquisition de macrophages pro-réparateurs au niveau de la peau dans des souris diabétiques (Hong, Tian et al. 2014). De plus, la lipoxine A4 diminue la capacité de sécrétion de l'IL-12 par les DC (Aliberti, Serhan et al. 2002). Enfin, la résolvine D1 diminue l'infiltration de cellules inflammatoires au sein des articulations de souris arthtritiques favorisant la réparation tissulaire et la diminution de la pathologie (Norling, Headland et al. 2016). Ces lipides ont donc des effets sur l'inhibition de la migration cellulaire, de la sécrétion de cytokines pro-inflammatoires, de signaux pro-inflammatoires ou encore la favorisation de macrophages de type M2 qui sont tous des phénotypes retrouvés dans notre modèle d'EAE

(Fullerton and Gilroy 2016). En conséquence, si le TGF-β semble être une molécule importante pour l'effet de SuperMApo, la caractérisation des molécules essentielles à l'effet pro-résolutif de SuperMApo (et notamment les lipides) devra être étudiée plus en détails.

Données pré-cliniques humaines

Enfin, des données préliminaires suggèrent que la reprogrammation des APC observée dans notre modèle avait aussi lieu chez l'Homme. En effet, des APC issus de cellules mononuclées sanguines de donneurs sains notamment démontrent une diminution de la sécrétion de cytokines pro-inflammatoires et une augmentation à générer des Treg (données non montrées). Nous sommes actuellement en train de confirmer la reprogrammation des APC chez des donneurs sains mais également chez des patients atteints de SEP au cours de leur premier épisode clinique et n'ayant donc jamais été traités.

L'inflammation est un processus finement régulé qui permet au corps de répondre à une agression. Ce processus aboutit de manière naturelle à une résolution permettant le retour à l'homéostasie et à la réparation tissulaire. Cependant, un défaut de résolution de l'inflammation est à l'origine de maladies inflammatoire chroniques. Les travaux présentés ici ont permis de montrer que les facteurs pro-résolutifs issus de l'efferocytose (un des processus clés de la résolution de l'inflammation) permettaient de diminuer la maladie dans un modèle de SEP. Nous avons ensuite pu montrer que le contrôle de la maladie était lié à une reprogrammation des macrophages et pDC en périphérie afin de contrôler les réponses T pathogéniques. Par ailleurs, cette induction de tolérance ne semble pas affecter le profil des cDC. Enfin, ces régulations mettent en jeu des mécanismes de régulations épigénétiques différentiels entre ces trois types cellulaire expliquant leur rôle dans le contrôle de la maladie (**Figure 15**). Ces travaux démontrent donc que les produits issus de l'efferocytose modulent les cellules de l'immunité innée en premier lieu induisant une tolérance générale et suggèrent que SuperMApo pourrait être une approche thérapeutique intéressante afin de contrôler les pathologies inflammatoires chroniques.

Références bibliographiques

Abi Abdallah, D. S., C. E. Egan, B. A. Butcher and E. Y. Denkers (2011). "Mouse neutrophils are professional antigen-presenting cells programmed to instruct Th1 and Th17 T-cell differentiation." Int Immunol **23**(5): 317-326.

Adelmann, M., J. Wood, I. Benzel, P. Fiori, H. Lassmann, J. M. Matthieu, M. V. Gardinier, K. Dornmair and C. Linington (1995). "The N-terminal domain of the myelin oligodendrocyte glycoprotein (MOG) induces acute demyelinating experimental autoimmune encephalomyelitis in the Lewis rat." J Neuroimmunol **63**(1): 17-27.

Aharoni, R. (2013). "The mechanism of action of glatiramer acetate in multiple sclerosis and beyond." Autoimmun Rev **12**(5): 543-553.

Aharoni, R., R. Eilam, A. Stock, A. Vainshtein, E. Shezen, H. Gal, N. Friedman and R. Arnon (2010). "Glatiramer acetate reduces Th-17 inflammation and induces regulatory T-cells in the CNS of mice with relapsing-remitting or chronic EAE." J Neuroimmunol **225**(1-2): 100-111.

Ajami, B., J. L. Bennett, C. Krieger, K. M. McNagny and F. M. Rossi (2011). "Infiltrating monocytes trigger EAE progression, but do not contribute to the resident microglia pool." Nat Neurosci **14**(9): 1142-1149.

Aliberti, J., C. Serhan and A. Sher (2002). "Parasite-induced lipoxin A4 is an endogenous regulator of IL-12 production and immunopathology in Toxoplasma gondii infection." J Exp Med **196**(9): 1253-1262.

Alotaibi, S., J. Kennedy, R. Tellier, D. Stephens and B. Banwell (2004). "Epstein-Barr virus in pediatric multiple sclerosis." JAMA **291**(15): 1875-1879.

Altara, R., Z. Mallat, G. W. Booz and F. A. Zouein (2016). "The CXCL10/CXCR3 Axis and Cardiac Inflammation: Implications for Immunotherapy to Treat Infectious and Noninfectious Diseases of the Heart." J Immunol Res **2016**: 4396368.

Amalinei, C., I. D. Caruntu, S. E. Giusca and R. A. Balan (2010). "Matrix metalloproteinases involvement in pathologic conditions." Rom J Morphol Embryol **51**(2): 215-228.

Anton, K., D. Banerjee and J. Glod (2012). "Macrophage-associated mesenchymal stem cells assume an activated, migratory, pro-inflammatory phenotype with increased IL-6 and CXCL10 secretion." PLoS One **7**(4): e35036.

Ariel, A., G. Fredman, Y. P. Sun, A. Kantarci, T. E. Van Dyke, A. D. Luster and C. N. Serhan (2006). "Apoptotic neutrophils and T cells sequester chemokines during immune response resolution through modulation of CCR5 expression." Nat Immunol **7**(11): 1209-1216.

Arita, M., F. Bianchini, J. Aliberti, A. Sher, N. Chiang, S. Hong, R. Yang, N. A. Petasis and C. N. Serhan (2005). "Stereochemical assignment, antiinflammatory properties, and receptor for the omega-3 lipid mediator resolvin E1." J Exp Med **201**(5): 713-722.

Aube, B., S. A. Levesque, A. Pare, E. Chamma, H. Kebir, R. Gorina, M. A. Lecuyer, J. I. Alvarez, Y. De Koninck, B. Engelhardt, A. Prat, D. Cote and S. Lacroix (2014). "Neutrophils mediate blood-spinal cord barrier disruption in demyelinating neuroinflammatory diseases." J Immunol **193**(5): 2438-2454.

Aung, L. L., A. Brooks, S. A. Greenberg, M. L. Rosenberg, S. Dhib-Jalbut and K. E. Balashov (2012). "Multiple sclerosis-linked and interferon-beta-regulated gene expression in plasmacytoid dendritic cells." J Neuroimmunol **250**(1-2): 99-105.

Bailey-Bucktrout, S. L., S. C. Caulkins, G. Goings, J. A. Fischer, A. Dzionek and S. D. Miller (2008). "Cutting edge: central nervous system plasmacytoid dendritic cells regulate the severity of relapsing experimental autoimmune encephalomyelitis." J Immunol **180**(10): 6457-6461.

Bailey, S. L., B. Schreiner, E. J. McMahon and S. D. Miller (2007). "CNS myeloid DCs presenting endogenous myelin peptides 'preferentially' polarize CD4+ T(H)-17 cells in relapsing EAE." Nat Immunol **8**(2): 172-180.

Bao, P., A. Kodra, M. Tomic-Canic, M. S. Golinko, H. P. Ehrlich and H. Brem (2009). "The role of vascular endothelial growth factor in wound healing." J Surg Res **153**(2): 347-358.

Baron, J. L., J. A. Madri, N. H. Ruddle, G. Hashim and C. A. Janeway, Jr. (1993). "Surface expression of alpha 4 integrin by CD4 T cells is required for their entry into brain parenchyma." J Exp Med **177**(1): 57-68.

Becher, B., S. Spath and J. Goverman (2017). "Cytokine networks in neuroinflammation." Nat Rev Immunol **17**(1): 49-59.

Bellac, C. L., A. Dufour, M. J. Krisinger, A. Loonchanta, A. E. Starr, U. Auf dem Keller, P. F. Lange, V. Goebeler, R. Kappelhoff, G. S. Butler, L. D. Burtnick, E. M. Conway, C. R. Roberts and C. M. Overall (2014). "Macrophage matrix metalloproteinase-12 dampens inflammation and neutrophil influx in arthritis." Cell Rep **9**(2): 618-632.

Beppu, R., K. Nakamura, H. Miyajima-Uchida, M. Kuroki, P. D. Khare, Y. Yamauchi, Y. Yamashita and T. Shirakusa (2001). "Soluble thrombospondin-1 suppresses T cell proliferation and enhances IL-10 secretion by antigen presenting cells stimulated with phytohemagglutinin." Immunol Invest **30**(2): 143-156.

Berer, K., M. Mues, M. Koutrolos, Z. A. Rasbi, M. Boziki, C. Johner, H. Wekerle and G. Krishnamoorthy (2011). "Commensal microbiota and myelin autoantigen cooperate to trigger autoimmune demyelination." Nature **479**(7374): 538-541.

Berger, T., S. Weerth, K. Kojima, C. Linington, H. Wekerle and H. Lassmann (1997). "Experimental autoimmune encephalomyelitis: the antigen specificity of T lymphocytes determines the topography of lesions in the central and peripheral nervous system." Lab Invest **76**(3): 355-364.

Bhasin, M., M. Wu and S. E. Tsirka (2007). "Modulation of microglial/macrophage activation by macrophage inhibitory factor (TKP) or tuftsin (TKPR) attenuates the disease course of experimental autoimmune encephalomyelitis." BMC Immunol **8**: 10.

Bianchi, M. E. (2007). "DAMPs, PAMPs and alarmins: all we need to know about danger." J Leukoc Biol **81**(1): 1-5.

Billich, A., F. Bornancin, P. Devay, D. Mechtcheriakova, N. Urtz and T. Baumruker (2003). "Phosphorylation of the immunomodulatory drug FTY720 by sphingosine kinases." J Biol Chem **278**(48): 47408-47415.

Bogdanos, D. P., D. S. Smyk, E. I. Rigopoulou, M. G. Mytilinaiou, M. A. Heneghan, C. Selmi and M. E. Gershwin (2012). "Twin studies in autoimmune disease: genetics, gender and environment." J Autoimmun **38**(2-3): J156-169.

Bogie, J. F., P. Stinissen and J. J. Hendriks (2014). "Macrophage subsets and microglia in multiple sclerosis." Acta Neuropathol **128**(2): 191-213.

Bonnefoy, F., S. Perruche, M. Couturier, A. Sedrati, Y. Sun, P. Tiberghien, B. Gaugler and P. Saas (2011). "Plasmacytoid dendritic cells play a major role in apoptotic leukocyte-induced immune modulation." J Immunol **186**(10): 5696-5705.

Boyman, O. (2010). "Bystander activation of CD4+ T cells." Eur J Immunol **40**(4): 936-939.

Braesch-Andersen, S., S. Paulie, C. Smedman, S. Mia and M. Kumagai-Braesch (2013). "ApoE production in human monocytes and its regulation by inflammatory cytokines." PLoS One **8**(11): e79908.

Brinkmann, V., U. Reichard, C. Goosmann, B. Fauler, Y. Uhlemann, D. S. Weiss, Y. Weinrauch and A. Zychlinsky (2004). "Neutrophil extracellular traps kill bacteria." Science **303**(5663): 1532-1535.

Bronnum-Hansen, H., N. Koch-Henriksen and E. Stenager (2004). "Trends in survival and cause of death in Danish patients with multiple sclerosis." Brain **127**(Pt 4): 844-850.

Buck, M. D., R. T. Sowell, S. M. Kaech and E. L. Pearce (2017). "Metabolic Instruction of Immunity." Cell **169**(4): 570-586.

Bystrom, J., I. Evans, J. Newson, M. Stables, I. Toor, N. van Rooijen, M. Crawford, P. Colville-Nash, S. Farrow and D. W. Gilroy (2008). "Resolution-phase macrophages possess a unique inflammatory phenotype that is controlled by cAMP." Blood **112**(10): 4117-4127.

Carrieri, P. B., V. Provitera, T. De Rosa, G. Tartaglia, F. Gorga and O. Perrella (1998). "Profile of cerebrospinal fluid and serum cytokines in patients with relapsing-remitting multiple sclerosis: a correlation with clinical activity." Immunopharmacol Immunotoxicol **20**(3): 373-382.

Ceroi, A., F. A. Delettre, C. Marotel, T. Gauthier, A. Asgarova, S. Biichle, A. Duperrier, G. Mourey, S. Perruche, L. Lagrost, D. Masson and P. Saas (2016). "The anti-inflammatory effects of platelet-derived microparticles in human plasmacytoid dendritic cells involve liver X receptor activation." Haematologica **101**(3): e72-76.

Chalise, J. P., M. T. Pallotta, S. C. Narendra, B. Carlsson, A. Iacono, J. Namale, L. Boon, U. Grohmann and M. Magnusson (2016). "IDO1 and TGF-beta Mediate Protective Effects of IFN-alpha in Antigen-Induced Arthritis." J Immunol **197**(8): 3142-3151.

Chekeni, F. B., M. R. Elliott, J. K. Sandilos, S. F. Walk, J. M. Kinchen, E. R. Lazarowski, A. J. Armstrong, S. Penuela, D. W. Laird, G. S. Salvesen, B. E. Isakson, D. A. Bayliss and K. S. Ravichandran (2010). "Pannexin 1 channels mediate 'find-me' signal release and membrane permeability during apoptosis." Nature **467**(7317): 863-867.

Chen, J., N. Chia, K. R. Kalari, J. Z. Yao, M. Novotna, M. M. Soldan, D. H. Luckey, E. V. Marietta, P. R. Jeraldo, X. Chen, B. G. Weinshenker, M. Rodriguez, O. H. Kantarci, H. Nelson, J. A. Murray and A. K. Mangalam (2016). "Multiple sclerosis patients have a distinct gut microbiota compared to healthy controls." Sci Rep **6**: 28484.

Chen, W., M. E. Frank, W. Jin and S. M. Wahl (2001). "TGF-beta released by apoptotic T cells contributes to an immunosuppressive milieu." Immunity **14**(6): 715-725.

Chen, W., W. Jin, N. Hardegen, K. J. Lei, L. Li, N. Marinos, G. McGrady and S. M. Wahl (2003). "Conversion of peripheral CD4+CD25- naive T cells to CD4+CD25+ regulatory T cells by TGF-beta induction of transcription factor Foxp3." J Exp Med **198**(12): 1875-1886.

Chiang, N., E. A. Bermudez, P. M. Ridker, S. Hurwitz and C. N. Serhan (2004). "Aspirin triggers antiinflammatory 15-epi-lipoxin A4 and inhibits thromboxane in a randomized human trial." Proc Natl Acad Sci U S A **101**(42): 15178-15183.

Chiba, S., T. Hisamatsu, H. Suzuki, K. Mori, M. T. Kitazume, K. Shimamura, S. Mizuno, N. Nakamoto, K. Matsuoka, M. Naganuma and T. Kanai (2017). "Glycolysis regulates LPS-induced cytokine production in M2 polarized human macrophages." Immunol Lett **183**: 17-23.

Cho, J. H. and M. Feldman (2015). "Heterogeneity of autoimmune diseases: pathophysiologic insights from genetics and implications for new therapies." Nat Med **21**(7): 730-738.

Chun, J. and H. P. Hartung (2010). "Mechanism of action of oral fingolimod (FTY720) in multiple sclerosis." Clin Neuropharmacol **33**(2): 91-101.

Cisse, B., M. L. Caton, M. Lehner, T. Maeda, S. Scheu, R. Locksley, D. Holmberg, C. Zweier, N. S. den Hollander, S. G. Kant, W. Holter, A. Rauch, Y. Zhuang and B. Reizis (2008). "Transcription factor E2-2 is an essential and specific regulator of plasmacytoid dendritic cell development." Cell **135**(1): 37-48.

Codarri, L., G. Gyulveszi, V. Tosevski, L. Hesske, A. Fontana, L. Magnenat, T. Suter and B. Becher (2011). "RORgammat drives production of the cytokine GM-CSF in helper T cells, which is essential for the effector phase of autoimmune neuroinflammation." Nat Immunol **12**(6): 560-567.

Compston, A. and A. Coles (2008). "Multiple sclerosis." Lancet **372**(9648): 1502-1517.

Cox, A. L., S. A. Thompson, J. L. Jones, V. H. Robertson, G. Hale, H. Waldmann, D. A. Compston and A. J. Coles (2005). "Lymphocyte homeostasis following therapeutic lymphocyte depletion in multiple sclerosis." Eur J Immunol **35**(11): 3332-3342.

Cramer, S. P., H. Simonsen, J. L. Frederiksen, E. Rostrup and H. B. Larsson (2014). "Abnormal blood-brain barrier permeability in normal appearing white matter in multiple sclerosis investigated by MRI." Neuroimage Clin **4**: 182-189.

Cross, A., R. C. Bucknall, M. A. Cassatella, S. W. Edwards and R. J. Moots (2003). "Synovial fluid neutrophils transcribe and express class II major histocompatibility complex molecules in rheumatoid arthritis." Arthritis Rheum **48**(10): 2796-2806.

Croxford, A. L., S. Spath and B. Becher (2015). "GM-CSF in Neuroinflammation: Licensing Myeloid Cells for Tissue Damage." Trends Immunol **36**(10): 651-662.

Cua, D. J., J. Sherlock, Y. Chen, C. A. Murphy, B. Joyce, B. Seymour, L. Lucian, W. To, S. Kwan, T. Churakova, S. Zurawski, M. Wiekowski, S. A. Lira, D. Gorman, R. A. Kastelein and J. D. Sedgwick (2003). "Interleukin-23 rather than interleukin-12 is the critical cytokine for autoimmune inflammation of the brain." Nature **421**(6924): 744-748.

Cusick, M. F., J. E. Libbey and R. S. Fujinami (2012). "Molecular mimicry as a mechanism of autoimmune disease." Clin Rev Allergy Immunol **42**(1): 102-111.

Czupalla, C. J., S. Liebner and K. Devraj (2014). "In vitro models of the blood-brain barrier." Methods Mol Biol **1135**: 415-437.

Dalli, J. and C. Serhan (2016). "Macrophage Proresolving Mediators-the When and Where." Microbiol Spectr **4**(3).

Dargahi, N., M. Katsara, T. Tselios, M. E. Androutsou, M. de Courten, J. Matsoukas and V. Apostolopoulos (2017). "Multiple Sclerosis: Immunopathology and Treatment Update." Brain Sci **7**(7).

de Oliveira, S., E. E. Rosowski and A. Huttenlocher (2016). "Neutrophil migration in infection and wound repair: going forward in reverse." Nat Rev Immunol **16**(6): 378-391.

Dendrou, C. A., L. Fugger and M. A. Friese (2015). "Immunopathology of multiple sclerosis." Nat Rev Immunol **15**(9): 545-558.

Diebold, S. S. (2008). "Determination of T-cell fate by dendritic cells." Immunol Cell Biol **86**(5): 389-397.

Dirksen, U., R. Nishinakamura, P. Groneck, U. Hattenhorst, L. Nogee, R. Murray and S. Burdach (1997). "Human pulmonary alveolar proteinosis associated with a defect in GM-CSF/IL-3/IL-5 receptor common beta chain expression." J Clin Invest **100**(9): 2211-2217.

Dombrowski, Y., T. O'Hagan, M. Dittmer, R. Penalva, S. R. Mayoral, P. Bankhead, S. Fleville, G. Eleftheriadis, C. Zhao, M. Naughton, R. Hassan, J. Moffat, J. Falconer, A. Boyd, P. Hamilton, I. V. Allen, A. Kissenpfennig, P. N. Moynagh, E. Evergren, B. Perbal, A. C. Williams, R. J. Ingram, J. R. Chan, R. J. M. Franklin and D. C. Fitzgerald (2017). "Regulatory T cells promote myelin regeneration in the central nervous system." Nat Neurosci **20**(5): 674-680.

Dorman, S. E. and S. M. Holland (2000). "Interferon-gamma and interleukin-12 pathway defects and human disease." Cytokine Growth Factor Rev **11**(4): 321-333.

Dranoff, G. and R. C. Mulligan (1994). "Activities of granulocyte-macrophage colony-stimulating factor revealed by gene transfer and gene knockout studies." Stem Cells **12 Suppl 1**: 173-182; discussion 182-174.

Druzd, D., O. Matveeva, L. Ince, U. Harrison, W. He, C. Schmal, H. Herzel, A. H. Tsang, N. Kawakami, A. Leliavski, O. Uhl, L. Yao, L. E. Sander, C. S. Chen, K. Kraus, A. de Juan, S. M. Hergenhan, M. Ehlers, B. Koletzko, R. Haas, W. Solbach, H. Oster and C. Scheiermann (2017). "Lymphocyte Circadian Clocks Control Lymph Node Trafficking and Adaptive Immune Responses." Immunity **46**(1): 120-132.

DuPage, M. and J. A. Bluestone (2016). "Harnessing the plasticity of CD4(+) T cells to treat immune-mediated disease." Nat Rev Immunol **16**(3): 149-163.

Duraes, F. V., C. Lippens, K. Steinbach, J. Dubrot, D. Brighouse, N. Bendriss-Vermare, S. Issazadeh-Navikas, D. Merkler and S. Hugues (2016). "pDC therapy induces recovery from EAE by recruiting endogenous pDC to sites of CNS inflammation." J Autoimmun **67**: 8-18.

El-Behi, M., B. Ciric, H. Dai, Y. Yan, M. Cullimore, F. Safavi, G. X. Zhang, B. N. Dittel and A. Rostami (2011). "The encephalitogenicity of T(H)17 cells is dependent on IL-1- and IL-23-induced production of the cytokine GM-CSF." Nat Immunol **12**(6): 568-575.

Elliott, M. R., F. B. Chekeni, P. C. Trampont, E. R. Lazarowski, A. Kadl, S. F. Walk, D. Park, R. I. Woodson, M. Ostankovich, P. Sharma, J. J. Lysiak, T. K. Harden, N. Leitinger and K. S.

Ravichandran (2009). "Nucleotides released by apoptotic cells act as a find-me signal to promote phagocytic clearance." Nature **461**(7261): 282-286.

Epelman, S., K. J. Lavine, A. E. Beaudin, D. K. Sojka, J. A. Carrero, B. Calderon, T. Brija, E. L. Gautier, S. Ivanov, A. T. Satpathy, J. D. Schilling, R. Schwendener, I. Sergin, B. Razani, E. C. Forsberg, W. M. Yokoyama, E. R. Unanue, M. Colonna, G. J. Randolph and D. L. Mann (2014). "Embryonic and adult-derived resident cardiac macrophages are maintained through distinct mechanisms at steady state and during inflammation." Immunity **40**(1): 91-104.

Ezekowitz, R. A., K. Sastry, P. Bailly and A. Warner (1990). "Molecular characterization of the human macrophage mannose receptor: demonstration of multiple carbohydrate recognition-like domains and phagocytosis of yeasts in Cos-1 cells." J Exp Med **172**(6): 1785-1794.

Fadok, V. A., D. L. Bratton, A. Konowal, P. W. Freed, J. Y. Westcott and P. M. Henson (1998). "Macrophages that have ingested apoptotic cells in vitro inhibit proinflammatory cytokine production through autocrine/paracrine mechanisms involving TGF-beta, PGE2, and PAF." J Clin Invest **101**(4): 890-898.

Finnson, K. W., S. McLean, G. M. Di Guglielmo and A. Philip (2013). "Dynamics of Transforming Growth Factor Beta Signaling in Wound Healing and Scarring." Adv Wound Care (New Rochelle) **2**(5): 195-214.

Fletcher, J. M., R. Lonergan, L. Costelloe, K. Kinsella, B. Moran, C. O'Farrelly, N. Tubridy and K. H. Mills (2009). "CD39+Foxp3+ regulatory T Cells suppress pathogenic Th17 cells and are impaired in multiple sclerosis." J Immunol **183**(11): 7602-7610.

Foks, A. C., D. Engelbertsen, F. Kuperwaser, N. Alberts-Grill, A. Gonen, J. L. Witztum, J. Lederer, P. Jarolim, R. H. DeKruyff, G. J. Freeman and A. H. Lichtman (2016). "Blockade of Tim-1 and Tim-4 Enhances Atherosclerosis in Low-Density Lipoprotein Receptor-Deficient Mice." Arterioscler Thromb Vasc Biol **36**(3): 456-465.

Ford, M. L. and B. D. Evavold (2005). "Specificity, magnitude, and kinetics of MOG-specific CD8+ T cell responses during experimental autoimmune encephalomyelitis." Eur J Immunol **35**(1): 76-85.

Fredman, G., S. F. Oh, S. Ayilavarapu, H. Hasturk, C. N. Serhan and T. E. Van Dyke (2011). "Impaired phagocytosis in localized aggressive periodontitis: rescue by Resolvin E1." PLoS One **6**(9): e24422.

Freytes, D. O., J. W. Kang, I. Marcos-Campos and G. Vunjak-Novakovic (2013). "Macrophages modulate the viability and growth of human mesenchymal stem cells." J Cell Biochem **114**(1): 220-229.

Friese, M. A. and L. Fugger (2005). "Autoreactive CD8+ T cells in multiple sclerosis: a new target for therapy?" Brain **128**(Pt 8): 1747-1763.

Fujii, T., A. Sakata, S. Nishimura, K. Eto and S. Nagata (2015). "TMEM16F is required for phosphatidylserine exposure and microparticle release in activated mouse platelets." Proc Natl Acad Sci U S A **112**(41): 12800-12805.

Fullerton, J. N. and D. W. Gilroy (2016). "Resolution of inflammation: a new therapeutic frontier." Nat Rev Drug Discov **15**(8): 551-567.

Furtado, G. C., M. C. Marcondes, J. A. Latkowski, J. Tsai, A. Wensky and J. J. Lafaille (2008). "Swift entry of myelin-specific T lymphocytes into the central nervous system in spontaneous autoimmune encephalomyelitis." J Immunol **181**(7): 4648-4655.

Gao, Y., J. M. Herndon, H. Zhang, T. S. Griffith and T. A. Ferguson (1998). "Antiinflammatory effects of CD95 ligand (FasL)-induced apoptosis." J Exp Med **188**(5): 887-896.

Gardai, S. J., K. A. McPhillips, S. C. Frasch, W. J. Janssen, A. Starefeldt, J. E. Murphy-Ullrich, D. L. Bratton, P. A. Oldenborg, M. Michalak and P. M. Henson (2005). "Cell-surface calreticulin initiates clearance of viable or apoptotic cells through trans-activation of LRP on the phagocyte." Cell **123**(2): 321-334.

Getts, D. R., A. J. Martin, D. P. McCarthy, R. L. Terry, Z. N. Hunter, W. T. Yap, M. T. Getts, M. Pleiss, X. Luo, N. J. King, L. D. Shea and S. D. Miller (2012). "Microparticles bearing encephalitogenic peptides induce T-cell tolerance and ameliorate experimental autoimmune encephalomyelitis." Nat Biotechnol **30**(12): 1217-1224.

Ginhoux, F., M. Greter, M. Leboeuf, S. Nandi, P. See, S. Gokhan, M. F. Mehler, S. J. Conway, L. G. Ng, E. R. Stanley, I. M. Samokhvalov and M. Merad (2010). "Fate mapping analysis reveals that adult microglia derive from primitive macrophages." Science **330**(6005): 841-845.

Goebel, J., E. Stevens, K. Forrest and T. L. Roszman (2000). "Daclizumab (Zenapax) inhibits early interleukin-2 receptor signal transduction events." Transpl Immunol **8**(3): 153-159.

Goodin, D. S. (2009). "The causal cascade to multiple sclerosis: a model for MS pathogenesis." PLoS One **4**(2): e4565.

Gordon, S. (1999). "Macrophage-restricted molecules: role in differentiation and activation." Immunol Lett **65**(1-2): 5-8.

Gosselin, E. J., K. Wardwell, W. F. Rigby and P. M. Guyre (1993). "Induction of MHC class II on human polymorphonuclear neutrophils by granulocyte/macrophage colony-stimulating factor, IFN-gamma, and IL-3." J Immunol **151**(3): 1482-1490.

Goverman, J. (2009). "Autoimmune T cell responses in the central nervous system." Nat Rev Immunol **9**(6): 393-407.

Goverman, J., A. Perchellet and E. S. Huseby (2005). "The role of CD8(+) T cells in multiple sclerosis and its animal models." Curr Drug Targets Inflamm Allergy **4**(2): 239-245.

Gray, M., K. Miles, D. Salter, D. Gray and J. Savill (2007). "Apoptotic cells protect mice from autoimmune inflammation by the induction of regulatory B cells." Proc Natl Acad Sci U S A **104**(35): 14080-14085.

Gregory, A. P., C. A. Dendrou, K. E. Attfield, A. Haghikia, D. K. Xifara, F. Butter, G. Poschmann, G. Kaur, L. Lambert, O. A. Leach, S. Promel, D. Punwani, J. H. Felce, S. J. Davis, R. Gold, F. C. Nielsen, R. M. Siegel, M. Mann, J. I. Bell, G. McVean and L. Fugger (2012). "TNF receptor 1 genetic risk mirrors outcome of anti-TNF therapy in multiple sclerosis." Nature **488**(7412): 508-511.

Gregory, C. D., A. Devitt and O. Moffatt (1998). "Roles of ICAM-3 and CD14 in the recognition and phagocytosis of apoptotic cells by macrophages." Biochem Soc Trans **26**(4): 644-649.

Greter, M., F. L. Heppner, M. P. Lemos, B. M. Odermatt, N. Goebels, T. Laufer, R. J. Noelle and B. Becher (2005). "Dendritic cells permit immune invasion of the CNS in an animal model of multiple sclerosis." Nat Med **11**(3): 328-334.

Grifka-Walk, H. M., D. A. Giles and B. M. Segal (2015). "IL-12-polarized Th1 cells produce GM-CSF and induce EAE independent of IL-23." Eur J Immunol **45**(10): 2780-2786.

Groom, J. R. and A. D. Luster (2011). "CXCR3 ligands: redundant, collaborative and antagonistic functions." Immunol Cell Biol **89**(2): 207-215.

Gude, D. R., S. E. Alvarez, S. W. Paugh, P. Mitra, J. Yu, R. Griffiths, S. E. Barbour, S. Milstien and S. Spiegel (2008). "Apoptosis induces expression of sphingosine kinase 1 to release sphingosine-1-phosphate as a "come-and-get-me" signal." FASEB J **22**(8): 2629-2638.

Guilliams, M., I. De Kleer, S. Henri, S. Post, L. Vanhoutte, S. De Prijck, K. Deswarte, B. Malissen, H. Hammad and B. N. Lambrecht (2013). "Alveolar macrophages develop from fetal monocytes that differentiate into long-lived cells in the first week of life via GM-CSF." J Exp Med **210**(10): 1977-1992.

Guo, B., E. Y. Chang and G. Cheng (2008). "The type I IFN induction pathway constrains Th17-mediated autoimmune inflammation in mice." J Clin Invest **118**(5): 1680-1690.

Gutcher, I. and B. Becher (2007). "APC-derived cytokines and T cell polarization in autoimmune inflammation." J Clin Invest **117**(5): 1119-1127.

Haak, S., A. L. Croxford, K. Kreymborg, F. L. Heppner, S. Pouly, B. Becher and A. Waisman (2009). "IL-17A and IL-17F do not contribute vitally to autoimmune neuro-inflammation in mice." J Clin Invest **119**(1): 61-69.

Hajishengallis, G. (2015). "Periodontitis: from microbial immune subversion to systemic inflammation." Nat Rev Immunol **15**(1): 30-44.

Han, C. Z., I. J. Juncadella, J. M. Kinchen, M. W. Buckley, A. L. Klibanov, K. Dryden, S. Onengut-Gumuscu, U. Erdbrugger, S. D. Turner, Y. M. Shim, K. S. Tung and K. S. Ravichandran (2016). "Macrophages redirect phagocytosis by non-professional phagocytes and influence inflammation." Nature **539**(7630): 570-574.

Handel, A. E., A. J. Williamson, G. Disanto, R. Dobson, G. Giovannoni and S. V. Ramagopalan (2011). "Smoking and multiple sclerosis: an updated meta-analysis." PLoS One **6**(1): e16149.

Havrdova, E., D. Horakova and I. Kovarova (2015). "Alemtuzumab in the treatment of multiple sclerosis: key clinical trial results and considerations for use." Ther Adv Neurol Disord **8**(1): 31-45.

Headland, S. E. and L. V. Norling (2015). "The resolution of inflammation: Principles and challenges." Semin Immunol **27**(3): 149-160.

Hedstrom, A. K., T. Akerstedt, J. Hillert, T. Olsson and L. Alfredsson (2011). "Shift work at young age is associated with increased risk for multiple sclerosis." Ann Neurol **70**(5): 733-741.

Hedstrom, A. K., E. Sundqvist, M. Baarnhielm, N. Nordin, J. Hillert, I. Kockum, T. Olsson and L. Alfredsson (2011). "Smoking and two human leukocyte antigen genes interact to increase the risk for multiple sclerosis." Brain **134**(Pt 3): 653-664.

Hemmer, B., M. Kerschensteiner and T. Korn (2015). "Role of the innate and adaptive immune responses in the course of multiple sclerosis." Lancet Neurol **14**(4): 406-419.

Hendriks, J. J., C. E. Teunissen, H. E. de Vries and C. D. Dijkstra (2005). "Macrophages and neurodegeneration." Brain Res Brain Res Rev **48**(2): 185-195.

Hochreiter-Hufford, A. and K. S. Ravichandran (2013). "Clearing the dead: apoptotic cell sensing, recognition, engulfment, and digestion." Cold Spring Harb Perspect Biol **5**(1): a008748.

Hoeffel, G., Y. Wang, M. Greter, P. See, P. Teo, B. Malleret, M. Leboeuf, D. Low, G. Oller, F. Almeida, S. H. Choy, M. Grisotto, L. Renia, S. J. Conway, E. R. Stanley, J. K. Chan, L. G. Ng, I. M. Samokhvalov, M. Merad and F. Ginhoux (2012). "Adult Langerhans cells derive predominantly from embryonic fetal liver monocytes with a minor contribution of yolk sac-derived macrophages." J Exp Med **209**(6): 1167-1181.

Hofstetter, H. H., S. M. Ibrahim, D. Koczan, N. Kruse, A. Weishaupt, K. V. Toyka and R. Gold (2005). "Therapeutic efficacy of IL-17 neutralization in murine experimental autoimmune encephalomyelitis." Cell Immunol **237**(2): 123-130.

Holwerda, S. J. and W. de Laat (2013). "CTCF: the protein, the binding partners, the binding sites and their chromatin loops." Philos Trans R Soc Lond B Biol Sci **368**(1620): 20120369.

Hong, J., N. Li, X. Zhang, B. Zheng and J. Z. Zhang (2005). "Induction of CD4+CD25+ regulatory T cells by copolymer-I through activation of transcription factor Foxp3." Proc Natl Acad Sci U S A **102**(18): 6449-6454.

Hong, S., H. Tian, Y. Lu, J. M. Laborde, F. A. Muhale, Q. Wang, B. V. Alapure, C. N. Serhan and N. G. Bazan (2014). "Neuroprotectin/protectin D1: endogenous biosynthesis and actions on diabetic macrophages in promoting wound healing and innervation impaired by diabetes." Am J Physiol Cell Physiol **307**(11): C1058-1067.

Hu, X. and L. B. Ivashkiv (2009). "Cross-regulation of signaling pathways by interferon-gamma: implications for immune responses and autoimmune diseases." Immunity **31**(4): 539-550.

Huang, F. P., N. Platt, M. Wykes, J. R. Major, T. J. Powell, C. D. Jenkins and G. G. MacPherson (2000). "A discrete subpopulation of dendritic cells transports apoptotic intestinal epithelial cells to T cell areas of mesenteric lymph nodes." J Exp Med **191**(3): 435-444.

Huang, Y. M., B. G. Xiao, V. Ozenci, M. Kouwenhoven, N. Teleshova, S. Fredrikson and H. Link (1999). "Multiple sclerosis is associated with high levels of circulating dendritic cells secreting pro-inflammatory cytokines." J Neuroimmunol **99**(1): 82-90.

Huitinga, I., N. van Rooijen, C. J. de Groot, B. M. Uitdehaag and C. D. Dijkstra (1990). "Suppression of experimental allergic encephalomyelitis in Lewis rats after elimination of macrophages." J Exp Med **172**(4): 1025-1033.

Irla, M., N. Kupfer, T. Suter, R. Lissilaa, M. Benkhoucha, J. Skupsky, P. H. Lalive, A. Fontana, W. Reith and S. Hugues (2010). "MHC class II-restricted antigen presentation by plasmacytoid dendritic cells inhibits T cell-mediated autoimmunity." J Exp Med **207**(9): 1891-1905.

Isaksson, M., B. Ardesjo, L. Ronnblom, O. Kampe, H. Lassmann, M. L. Eloranta and A. Lobell (2009). "Plasmacytoid DC promote priming of autoimmune Th17 cells and EAE." Eur J Immunol **39**(10): 2925-2935.

Ito, A., A. Mukaiyama, Y. Itoh, H. Nagase, I. B. Thogersen, J. J. Enghild, Y. Sasaguri and Y. Mori (1996). "Degradation of interleukin 1beta by matrix metalloproteinases." J Biol Chem **271**(25): 14657-14660.

Jagessar, S. A., K. Dijkman, J. Dunham, B. A. t Hart and Y. S. Kap (2016). "Experimental Autoimmune Encephalomyelitis in Marmosets." Methods Mol Biol **1304**: 171-186.

Jain, P., C. Coisne, G. Enzmann, R. Rottapel and B. Engelhardt (2010). "Alpha4beta1 integrin mediates the recruitment of immature dendritic cells across the blood-brain barrier during experimental autoimmune encephalomyelitis." J Immunol **184**(12): 7196-7206.

Jang, J. H., H. W. Shin, J. M. Lee, H. W. Lee, E. C. Kim and S. H. Park (2015). "An Overview of Pathogen Recognition Receptors for Innate Immunity in Dental Pulp." Mediators Inflamm **2015**: 794143.

Jantsch, J., D. Chakravortty, N. Turza, A. T. Prechtel, B. Buchholz, R. G. Gerlach, M. Volke, J. Glasner, C. Warnecke, M. S. Wiesener, K. U. Eckardt, A. Steinkasserer, M. Hensel and C. Willam (2008). "Hypoxia and hypoxia-inducible factor-1 alpha modulate lipopolysaccharide-induced dendritic cell activation and function." J Immunol **180**(7): 4697-4705.

Jiang, H. R., M. Milovanovic, D. Allan, W. Niedbala, A. G. Besnard, S. Y. Fukada, J. C. Alves-Filho, D. Togbe, C. S. Goodyear, C. Linington, D. Xu, M. L. Lukic and F. Y. Liew (2012). "IL-33 attenuates EAE by suppressing IL-17 and IFN-gamma production and inducing alternatively activated macrophages." Eur J Immunol **42**(7): 1804-1814.

Jiang, Z., J. X. Jiang and G. X. Zhang (2014). "Macrophages: a double-edged sword in experimental autoimmune encephalomyelitis." Immunol Lett **160**(1): 17-22.

Kabat, E. A., A. Wolf and A. E. Bezer (1947). "The Rapid Production of Acute Disseminated Encephalomyelitis in Rhesus Monkeys by Injection of Heterologous and Homologous Brain Tissue with Adjuvants." J Exp Med **85**(1): 117-130.

Kakalacheva, K. and J. D. Lunemann (2011). "Environmental triggers of multiple sclerosis." FEBS Lett **585**(23): 3724-3729.

Kambara, K., W. Ohashi, K. Tomita, M. Takashina, S. Fujisaka, R. Hayashi, H. Mori, K. Tobe and Y. Hattori (2015). "In vivo depletion of CD206+ M2 macrophages exaggerates lung injury in endotoxemic mice." Am J Pathol **185**(1): 162-171.

Kaplan, M. J. and M. Radic (2012). "Neutrophil extracellular traps: double-edged swords of innate immunity." J Immunol **189**(6): 2689-2695.

Karni, A., M. Abraham, A. Monsonego, G. Cai, G. J. Freeman, D. Hafler, S. J. Khoury and H. L. Weiner (2006). "Innate immunity in multiple sclerosis: myeloid dendritic cells in secondary progressive multiple sclerosis are activated and drive a proinflammatory immune response." J Immunol **177**(6): 4196-4202.

Kasagi, S., P. Zhang, L. Che, B. Abbatiello, T. Maruyama, H. Nakatsukasa, P. Zanvit, W. Jin, J. E. Konkel and W. Chen (2014). "In vivo-generated antigen-specific regulatory T cells treat autoimmunity without compromising antibacterial immune response." Sci Transl Med **6**(241): 241ra278.

Kassianos, A. J., M. Y. Hardy, X. Ju, D. Vijayan, Y. Ding, A. J. Vulink, K. J. McDonald, S. L. Jongbloed, R. B. Wadley, C. Wells, D. N. Hart and K. J. Radford (2012). "Human CD1c (BDCA-1)+ myeloid dendritic cells secrete IL-10 and display an immuno-regulatory phenotype and function in response to Escherichia coli." Eur J Immunol **42**(6): 1512-1522.

Kawane, K., M. Ohtani, K. Miwa, T. Kizawa, Y. Kanbara, Y. Yoshioka, H. Yoshikawa and S. Nagata (2006). "Chronic polyarthritis caused by mammalian DNA that escapes from degradation in macrophages." Nature **443**(7114): 998-1002.

Kazama, H., J. E. Ricci, J. M. Herndon, G. Hoppe, D. R. Green and T. A. Ferguson (2008). "Induction of immunological tolerance by apoptotic cells requires caspase-dependent oxidation of high-mobility group box-1 protein." Immunity **29**(1): 21-32.

Kebir, H., K. Kreymborg, I. Ifergan, A. Dodelet-Devillers, R. Cayrol, M. Bernard, F. Giuliani, N. Arbour, B. Becher and A. Prat (2007). "Human TH17 lymphocytes promote blood-brain barrier disruption and central nervous system inflammation." Nat Med **13**(10): 1173-1175.

Keller, M., A. Ruegg, S. Werner and H. D. Beer (2008). "Active caspase-1 is a regulator of unconventional protein secretion." Cell **132**(5): 818-831.

Kelly, B. and L. A. O'Neill (2015). "Metabolic reprogramming in macrophages and dendritic cells in innate immunity." Cell Res **25**(7): 771-784.

Kinchen, J. M. and K. S. Ravichandran (2008). "Phagosome maturation: going through the acid test." Nat Rev Mol Cell Biol **9**(10): 781-795.

King, I. L., T. L. Dickendesher and B. M. Segal (2009). "Circulating Ly-6C+ myeloid precursors migrate to the CNS and play a pathogenic role during autoimmune demyelinating disease." Blood **113**(14): 3190-3197.

Kipp, M., B. van der Star, D. Y. Vogel, F. Puentes, P. van der Valk, D. Baker and S. Amor (2012). "Experimental in vivo and in vitro models of multiple sclerosis: EAE and beyond." Mult Scler Relat Disord **1**(1): 15-28.

Kiss, R. S., M. R. Elliott, Z. Ma, Y. L. Marcel and K. S. Ravichandran (2006). "Apoptotic cells induce a phosphatidylserine-dependent homeostatic response from phagocytes." Curr Biol **16**(22): 2252-2258.

Klareskog, L., A. I. Catrina and S. Paget (2009). "Rheumatoid arthritis." Lancet **373**(9664): 659-672.

Kobayashi, N., P. Karisola, V. Pena-Cruz, D. M. Dorfman, M. Jinushi, S. E. Umetsu, M. J. Butte, H. Nagumo, I. Chernova, B. Zhu, A. H. Sharpe, S. Ito, G. Dranoff, G. G. Kaplan, J. M. Casasnovas, D. T. Umetsu, R. H. Dekruyff and G. J. Freeman (2007). "TIM-1 and TIM-4 glycoproteins bind phosphatidylserine and mediate uptake of apoptotic cells." Immunity **27**(6): 927-940.

Kolaczkowska, E. and P. Kubes (2013). "Neutrophil recruitment and function in health and inflammation." Nat Rev Immunol **13**(3): 159-175.

Kouwenhoven, M., N. Teleshova, V. Ozenci, R. Press and H. Link (2001). "Monocytes in multiple sclerosis: phenotype and cytokine profile." J Neuroimmunol **112**(1-2): 197-205.

Krispin, A., Y. Bledi, M. Atallah, U. Trahtemberg, I. Verbovetski, E. Nahari, O. Zelig, M. Linial and D. Mevorach (2006). "Apoptotic cell thrombospondin-1 and heparin-binding domain lead to dendritic-cell phagocytic and tolerizing states." Blood **108**(10): 3580-3589.

Krystal, A. D., E. Richelson and T. Roth (2013). "Review of the histamine system and the clinical effects of H1 antagonists: basis for a new model for understanding the effects of insomnia medications." Sleep Med Rev **17**(4): 263-272.

Kumar, H., T. Kawai and S. Akira (2009). "Pathogen recognition in the innate immune response." Biochem J **420**(1): 1-16.

Kumar, H., T. Kawai and S. Akira (2011). "Pathogen recognition by the innate immune system." Int Rev Immunol **30**(1): 16-34.

Kurtzke, J. F., G. W. Beebe and J. E. Norman, Jr. (1979). "Epidemiology of multiple sclerosis in U.S. veterans: 1. Race, sex, and geographic distribution." Neurology **29**(9 Pt 1): 1228-1235.

Lande, R., V. Gafa, B. Serafini, E. Giacomini, A. Visconti, M. E. Remoli, M. Severa, M. Parmentier, G. Ristori, M. Salvetti, F. Aloisi and E. M. Coccia (2008). "Plasmacytoid dendritic cells in multiple sclerosis: intracerebral recruitment and impaired maturation in response to interferon-beta." J Neuropathol Exp Neurol **67**(5): 388-401.

Langrish, C. L., Y. Chen, W. M. Blumenschein, J. Mattson, B. Basham, J. D. Sedgwick, T. McClanahan, R. A. Kastelein and D. J. Cua (2005). "IL-23 drives a pathogenic T cell population that induces autoimmune inflammation." J Exp Med **201**(2): 233-240.

Lauber, K., E. Bohn, S. M. Krober, Y. J. Xiao, S. G. Blumenthal, R. K. Lindemann, P. Marini, C. Wiedig, A. Zobywalski, S. Baksh, Y. Xu, I. B. Autenrieth, K. Schulze-Osthoff, C. Belka, G. Stuhler and S. Wesselborg (2003). "Apoptotic cells induce migration of phagocytes via caspase-3-mediated release of a lipid attraction signal." Cell **113**(6): 717-730.

Lavin, Y., A. Mortha, A. Rahman and M. Merad (2015). "Regulation of macrophage development and function in peripheral tissues." Nat Rev Immunol **15**(12): 731-744.

Lawrence, T., D. A. Willoughby and D. W. Gilroy (2002). "Anti-inflammatory lipid mediators and insights into the resolution of inflammation." Nat Rev Immunol **2**(10): 787-795.

Lehmann-Horn, K., H. C. Kronsbein and M. S. Weber (2013). "Targeting B cells in the treatment of multiple sclerosis: recent advances and remaining challenges." Ther Adv Neurol Disord **6**(3): 161-173.

Lennon-Dumenil, A. M., A. H. Bakker, R. Maehr, E. Fiebiger, H. S. Overkleeft, M. Rosemblatt, H. L. Ploegh and C. Lagaudriere-Gesbert (2002). "Analysis of protease activity in live antigen-presenting cells shows regulation of the phagosomal proteolytic contents during dendritic cell activation." J Exp Med **196**(4): 529-540.

Leoni, G., M. B. Voisin, K. Carlson, S. Getting, S. Nourshargh and M. Perretti (2010). "The melanocortin MC(1) receptor agonist BMS-470539 inhibits leucocyte trafficking in the inflamed vasculature." Br J Pharmacol **160**(1): 171-180.

Lindskog Jonsson, A., A. Granqvist, J. Elvin, M. E. Johansson, B. Haraldsson and J. Nystrom (2014). "Effects of melanocortin 1 receptor agonists in experimental nephropathies." PLoS One **9**(1): e87816.

Liu, C., Y. Li, J. Yu, L. Feng, S. Hou, Y. Liu, M. Guo, Y. Xie, J. Meng, H. Zhang, B. Xiao and C. Ma (2013). "Targeting the shift from M1 to M2 macrophages in experimental autoimmune encephalomyelitis mice treated with fasudil." PLoS One **8**(2): e54841.

Liu, P. S., H. Wang, X. Li, T. Chao, T. Teav, S. Christen, G. Di Conza, W. C. Cheng, C. H. Chou, M. Vavakova, C. Muret, K. Debackere, M. Mazzone, H. D. Huang, S. M. Fendt, J. Ivanisevic and P. C. Ho (2017). "alpha-ketoglutarate orchestrates macrophage activation through metabolic and epigenetic reprogramming." Nat Immunol.

Liu, Y. J. (2005). "IPC: professional type 1 interferon-producing cells and plasmacytoid dendritic cell precursors." Annu Rev Immunol **23**: 275-306.

Longhini, A. L., F. von Glehn, C. O. Brandao, R. F. de Paula, F. Pradella, A. S. Moraes, A. S. Farias, E. C. Oliveira, J. G. Quispe-Cabanillas, C. H. Abreu, A. Damasceno, B. P. Damasceno, K. E. Balashov and L. M. Santos (2011). "Plasmacytoid dendritic cells are increased in cerebrospinal fluid of untreated patients during multiple sclerosis relapse." J Neuroinflammation **8**(1): 2.

Lucas, S. M., N. J. Rothwell and R. M. Gibson (2006). "The role of inflammation in CNS injury and disease." Br J Pharmacol **147 Suppl 1**: S232-240.

Lucas, T., A. Waisman, R. Ranjan, J. Roes, T. Krieg, W. Muller, A. Roers and S. A. Eming (2010). "Differential roles of macrophages in diverse phases of skin repair." J Immunol **184**(7): 3964-3977.

Maddox, J. F., M. Hachicha, T. Takano, N. A. Petasis, V. V. Fokin and C. N. Serhan (1997). "Lipoxin A4 stable analogs are potent mimetics that stimulate human monocytes and THP-1 cells via a G-protein-linked lipoxin A4 receptor." J Biol Chem **272**(11): 6972-6978.

Maldonado-Lopez, R., T. De Smedt, P. Michel, J. Godfroid, B. Pajak, C. Heirman, K. Thielemans, O. Leo, J. Urbain and M. Moser (1999). "CD8alpha+ and CD8alpha- subclasses of dendritic cells direct the development of distinct T helper cells in vivo." J Exp Med **189**(3): 587-592.

Mariathasan, S., D. S. Weiss, K. Newton, J. McBride, K. O'Rourke, M. Roose-Girma, W. P. Lee, Y. Weinrauch, D. M. Monack and V. M. Dixit (2006). "Cryopyrin activates the inflammasome in response to toxins and ATP." Nature **440**(7081): 228-232.

Markiewski, M. M. and J. D. Lambris (2007). "The role of complement in inflammatory diseases from behind the scenes into the spotlight." Am J Pathol **171**(3): 715-727.

Martinez, F. O. and S. Gordon (2014). "The M1 and M2 paradigm of macrophage activation: time for reassessment." F1000Prime Rep **6**: 13.

Martinez, F. O., S. Gordon, M. Locati and A. Mantovani (2006). "Transcriptional profiling of the human monocyte-to-macrophage differentiation and polarization: new molecules and patterns of gene expression." J Immunol **177**(10): 7303-7311.

Mathis, D. and C. Benoist (2011). "Microbiota and autoimmune disease: the hosted self." Cell Host Microbe **10**(4): 297-301.

McMahon, E. J., S. L. Bailey, C. V. Castenada, H. Waldner and S. D. Miller (2005). "Epitope spreading initiates in the CNS in two mouse models of multiple sclerosis." Nat Med **11**(3): 335-339.

Medzhitov, R. (2008). "Origin and physiological roles of inflammation." Nature **454**(7203): 428-435.

Meinl, E., M. Krumbholz and R. Hohlfeld (2006). "B lineage cells in the inflammatory central nervous system environment: migration, maintenance, local antibody production, and therapeutic modulation." Ann Neurol **59**(6): 880-892.

Mendez, E., J. L. Fernandez-Luna, A. Grubb and F. Leyva-Cobian (1986). "Human protein HC and its IgA complex are inhibitors of neutrophil chemotaxis." Proc Natl Acad Sci U S A **83**(5): 1472-1475.

Mevorach, D., T. Zuckerman, I. Reiner, A. Shimoni, S. Samuel, A. Nagler, J. M. Rowe and R. Or (2014). "Single infusion of donor mononuclear early apoptotic cells as prophylaxis for graft-versus-host disease in myeloablative HLA-matched allogeneic bone marrow transplantation: a phase I/IIa clinical trial." Biol Blood Marrow Transplant **20**(1): 58-65.

Michel, L., C. Larochelle and A. Prat (2015). "Update on treatments in multiple sclerosis." Presse Med **44**(4 Pt 2): e137-151.

Mikita, J., N. Dubourdieu-Cassagno, M. S. Deloire, A. Vekris, M. Biran, G. Raffard, B. Brochet, M. H. Canron, J. M. Franconi, C. Boiziau and K. G. Petry (2011). "Altered M1/M2 activation patterns of monocytes in severe relapsing experimental rat model of multiple sclerosis. Amelioration of clinical status by M2 activated monocyte administration." Mult Scler **17**(1): 2-15.

Mildner, A., M. Mack, H. Schmidt, W. Bruck, M. Djukic, M. D. Zabel, A. Hille, J. Priller and M. Prinz (2009). "CCR2+Ly-6Chi monocytes are crucial for the effector phase of autoimmunity in the central nervous system." Brain **132**(Pt 9): 2487-2500.

Miles, E. A. and P. C. Calder (2012). "Influence of marine n-3 polyunsaturated fatty acids on immune function and a systematic review of their effects on clinical outcomes in rheumatoid arthritis." Br J Nutr **107 Suppl 2**: S171-184.

Minden, S. L. and R. B. Schiffer (1990). "Affective disorders in multiple sclerosis. Review and recommendations for clinical research." Arch Neurol **47**(1): 98-104.

Miyake, Y., K. Asano, H. Kaise, M. Uemura, M. Nakayama and M. Tanaka (2007). "Critical role of macrophages in the marginal zone in the suppression of immune responses to apoptotic cell-associated antigens." J Clin Invest **117**(8): 2268-2278.

Miyata, J., K. Fukunaga, R. Iwamoto, Y. Isobe, K. Niimi, R. Takamiya, T. Takihara, K. Tomomatsu, Y. Suzuki, T. Oguma, K. Sayama, H. Arai, T. Betsuyaku, M. Arita and K. Asano (2013). "Dysregulated synthesis of protectin D1 in eosinophils from patients with severe asthma." J Allergy Clin Immunol **131**(2): 353-360 e351-352.

Mohammad-Zadeh, L. F., L. Moses and S. M. Gwaltney-Brant (2008). "Serotonin: a review." J Vet Pharmacol Ther **31**(3): 187-199.

Mosmann, T. R., H. Cherwinski, M. W. Bond, M. A. Giedlin and R. L. Coffman (1986). "Two types of murine helper T cell clone. I. Definition according to profiles of lymphokine activities and secreted proteins." J Immunol **136**(7): 2348-2357.

Murphy-Ullrich, J. E. and M. Poczatek (2000). "Activation of latent TGF-beta by thrombospondin-1: mechanisms and physiology." Cytokine Growth Factor Rev **11**(1-2): 59-69.

Murray, P. J., J. E. Allen, S. K. Biswas, E. A. Fisher, D. W. Gilroy, S. Goerdt, S. Gordon, J. A. Hamilton, L. B. Ivashkiv, T. Lawrence, M. Locati, A. Mantovani, F. O. Martinez, J. L. Mege, D. M. Mosser, G. Natoli, J. P. Saeij, J. L. Schultze, K. A. Shirey, A. Sica, J. Suttles, I. Udalova, J. A. van Ginderachter, S. N. Vogel and T. A. Wynn (2014). "Macrophage activation and polarization: nomenclature and experimental guidelines." Immunity **41**(1): 14-20.

N, A. G., S. J. Bensinger, C. Hong, S. Beceiro, M. N. Bradley, N. Zelcer, J. Deniz, C. Ramirez, M. Diaz, G. Gallardo, C. R. de Galarreta, J. Salazar, F. Lopez, P. Edwards, J. Parks, M. Andujar, P. Tontonoz and A. Castrillo (2009). "Apoptotic cells promote their own clearance and immune tolerance through activation of the nuclear receptor LXR." Immunity **31**(2): 245-258.

Nadkarni, S., J. Dalli, J. Hollywood, J. C. Mason, B. Dasgupta and M. Perretti (2014). "Investigational analysis reveals a potential role for neutrophils in giant-cell arteritis disease progression." Circ Res **114**(2): 242-248.

Nagata, S., R. Hanayama and K. Kawane (2010). "Autoimmunity and the clearance of dead cells." Cell **140**(5): 619-630.

Naik, S. H., P. Sathe, H. Y. Park, D. Metcalf, A. I. Proietto, A. Dakic, S. Carotta, M. O'Keeffe, M. Bahlo, A. Papenfuss, J. Y. Kwak, L. Wu and K. Shortman (2007). "Development of plasmacytoid and conventional dendritic cell subtypes from single precursor cells derived in vitro and in vivo." Nat Immunol **8**(11): 1217-1226.

Nakajima, H., K. Uchida, A. R. Guerrero, S. Watanabe, D. Sugita, N. Takeura, A. Yoshida, G. Long, K. T. Wright, W. E. Johnson and H. Baba (2012). "Transplantation of mesenchymal stem cells promotes an alternative pathway of macrophage activation and functional recovery after spinal cord injury." J Neurotrauma **29**(8): 1614-1625.

Nakano, T., Y. Ishimoto, J. Kishino, M. Umeda, K. Inoue, K. Nagata, K. Ohashi, K. Mizuno and H. Arita (1997). "Cell adhesion to phosphatidylserine mediated by a product of growth arrest-specific gene 6." J Biol Chem **272**(47): 29411-29414.

Natrajan, M. S., A. G. de la Fuente, A. H. Crawford, E. Linehan, V. Nunez, K. R. Johnson, T. Wu, D. C. Fitzgerald, M. Ricote, B. Bielekova and R. J. Franklin (2015). "Retinoid X receptor activation reverses age-related deficiencies in myelin debris phagocytosis and remyelination." Brain **138**(Pt 12): 3581-3597.

Nau, G. J., J. F. Richmond, A. Schlesinger, E. G. Jennings, E. S. Lander and R. A. Young (2002). "Human macrophage activation programs induced by bacterial pathogens." Proc Natl Acad Sci U S A **99**(3): 1503-1508.

Neudecker, V., M. Haneklaus, O. Jensen, L. Khailova, J. C. Masterson, H. Tye, K. Biette, P. Jedlicka, K. S. Brodsky, M. E. Gerich, M. Mack, A. A. B. Robertson, M. A. Cooper, G. T. Furuta, C. A. Dinarello, L. A. O'Neill, H. K. Eltzschig, S. L. Masters and E. N. McNamee (2017). "Myeloid-derived miR-223 regulates intestinal inflammation via repression of the NLRP3 inflammasome." J Exp Med **214**(6): 1737-1752.

Norling, L. V., S. E. Headland, J. Dalli, H. H. Arnardottir, O. Haworth, H. R. Jones, D. Irimia, C. N. Serhan and M. Perretti (2016). "Proresolving and cartilage-protective actions of resolvin D1 in inflammatory arthritis." JCI Insight **1**(5): e85922.

O'Keeffe, M., R. J. Grumont, H. Hochrein, M. Fuchsberger, R. Gugasyan, D. Vremec, K. Shortman and S. Gerondakis (2005). "Distinct roles for the NF-kappaB1 and c-Rel transcription factors in the differentiation and survival of plasmacytoid and conventional dendritic cells activated by TLR-9 signals." Blood **106**(10): 3457-3464.

Ochoa-Reparaz, J., D. W. Mielcarz, L. E. Ditrio, A. R. Burroughs, D. M. Foureau, S. Haque-Begum and L. H. Kasper (2009). "Role of gut commensal microflora in the development of experimental autoimmune encephalomyelitis." J Immunol **183**(10): 6041-6050.

Ogden, C. A., A. deCathelineau, P. R. Hoffmann, D. Bratton, B. Ghebrehiwet, V. A. Fadok and P. M. Henson (2001). "C1q and mannose binding lectin engagement of cell surface calreticulin and CD91 initiates macropinocytosis and uptake of apoptotic cells." J Exp Med **194**(6): 781-795.

Ortega-Gomez, A., M. Perretti and O. Soehnlein (2013). "Resolution of inflammation: an integrated view." EMBO Mol Med **5**(5): 661-674.

Ortiz, G. G., F. P. Pacheco-Moises, M. A. Macias-Islas, L. J. Flores-Alvarado, M. A. Mireles-Ramirez, E. D. Gonzalez-Renovato, V. E. Hernandez-Navarro, A. L. Sanchez-Lopez and M. A. Alatorre-Jimenez (2014). "Role of the blood-brain barrier in multiple sclerosis." Arch Med Res **45**(8): 687-697.

Ousman, S. S. and P. Kubes (2012). "Immune surveillance in the central nervous system." Nat Neurosci **15**(8): 1096-1101.

Pallotta, M. T., C. Orabona, C. Volpi, C. Vacca, M. L. Belladonna, R. Bianchi, G. Servillo, C. Brunacci, M. Calvitti, S. Bicciato, E. M. Mazza, L. Boon, F. Grassi, M. C. Fioretti, F. Fallarino, P. Puccetti and U. Grohmann (2011). "Indoleamine 2,3-dioxygenase is a signaling protein in long-term tolerance by dendritic cells." Nat Immunol **12**(9): 870-878.

Panitch, H. S., R. L. Hirsch, A. S. Haley and K. P. Johnson (1987). "Exacerbations of multiple sclerosis in patients treated with gamma interferon." Lancet **1**(8538): 893-895.

Park-Min, K. H., T. T. Antoniv and L. B. Ivashkiv (2005). "Regulation of macrophage phenotype by long-term exposure to IL-10." Immunobiology **210**(2-4): 77-86.

Park, D., A. C. Tosello-Trampont, M. R. Elliott, M. Lu, L. B. Haney, Z. Ma, A. L. Klibanov, J. W. Mandell and K. S. Ravichandran (2007). "BAI1 is an engulfment receptor for apoptotic cells upstream of the ELMO/Dock180/Rac module." Nature **450**(7168): 430-434.

Pashenkov, M. and H. Link (2002). "Dendritic cells and immune responses in the central nervous system." Trends Immunol **23**(2): 69-70; author reply 70.

Perretti, M., X. Leroy, E. J. Bland and T. Montero-Melendez (2015). "Resolution Pharmacology: Opportunities for Therapeutic Innovation in Inflammation." Trends Pharmacol Sci **36**(11): 737-755.

Perruche, S., P. Zhang, Y. Liu, P. Saas, J. A. Bluestone and W. Chen (2008). "CD3-specific antibody-induced immune tolerance involves transforming growth factor-beta from phagocytes digesting apoptotic T cells." Nat Med **14**(5): 528-535.

Peter, C., M. Waibel, C. G. Radu, L. V. Yang, O. N. Witte, K. Schulze-Osthoff, S. Wesselborg and K. Lauber (2008). "Migration to apoptotic "find-me" signals is mediated via the phagocyte receptor G2A." J Biol Chem **283**(9): 5296-5305.

Planaguma, A., M. A. Pfeffer, G. Rubin, R. Croze, M. Uddin, C. N. Serhan and B. D. Levy (2010). "Lovastatin decreases acute mucosal inflammation via 15-epi-lipoxin A4." Mucosal Immunol **3**(3): 270-279.

Ponomarev, E. D., L. P. Shriver, K. Maresz and B. N. Dittel (2005). "Microglial cell activation and proliferation precedes the onset of CNS autoimmunity." J Neurosci Res **81**(3): 374-389.

Porta, C., M. Rimoldi, G. Raes, L. Brys, P. Ghezzi, D. Di Liberto, F. Dieli, S. Ghisletti, G. Natoli, P. De Baetselier, A. Mantovani and A. Sica (2009). "Tolerance and M2 (alternative) macrophage polarization are related processes orchestrated by p50 nuclear factor kappaB." Proc Natl Acad Sci U S A **106**(35): 14978-14983.

Pucci, E., G. Giuliani, A. Solari, S. Simi, S. Minozzi, C. Di Pietrantonj and I. Galea (2011). "Natalizumab for relapsing remitting multiple sclerosis." Cochrane Database Syst Rev(10): CD007621.

Pupjalis, D., J. Goetsch, D. J. Kottas, V. Gerke and U. Rescher (2011). "Annexin A1 released from apoptotic cells acts through formyl peptide receptors to dampen inflammatory monocyte activation via JAK/STAT/SOCS signalling." EMBO Mol Med **3**(2): 102-114.

Qiu, C. H., Y. Miyake, H. Kaise, H. Kitamura, O. Ohara and M. Tanaka (2009). "Novel subset of CD8{alpha}+ dendritic cells localized in the marginal zone is responsible for tolerance to cell-associated antigens." J Immunol **182**(7): 4127-4136.

Ransohoff, R. M., P. Kivisakk and G. Kidd (2003). "Three or more routes for leukocyte migration into the central nervous system." Nat Rev Immunol **3**(7): 569-581.

Rao, S. P., J. Sancho, J. Campos-Rivera, P. M. Boutin, P. B. Severy, T. Weeden, S. Shankara, B. L. Roberts and J. M. Kaplan (2012). "Human peripheral blood mononuclear cells exhibit heterogeneous CD52 expression levels and show differential sensitivity to alemtuzumab mediated cytolysis." PLoS One **7**(6): e39416.

Rawji, K. S. and V. W. Yong (2013). "The benefits and detriments of macrophages/microglia in models of multiple sclerosis." Clin Dev Immunol **2013**: 948976.

Reddien, P. W., S. Cameron and H. R. Horvitz (2001). "Phagocytosis promotes programmed cell death in C. elegans." Nature **412**(6843): 198-202.

Rongvaux, A., R. Jackson, C. C. Harman, T. Li, A. P. West, M. R. de Zoete, Y. Wu, B. Yordy, S. A. Lakhani, C. Y. Kuan, T. Taniguchi, G. S. Shadel, Z. J. Chen, A. Iwasaki and R. A. Flavell (2014). "Apoptotic caspases prevent the induction of type I interferons by mitochondrial DNA." Cell **159**(7): 1563-1577.

Ryan, M., L. McCarthy, R. Rappuoli, B. P. Mahon and K. H. Mills (1998). "Pertussis toxin potentiates Th1 and Th2 responses to co-injected antigen: adjuvant action is associated with enhanced regulatory cytokine production and expression of the co-stimulatory molecules B7-1, B7-2 and CD28." Int Immunol **10**(5): 651-662.

Saas, P., E. Daguindau and S. Perruche (2016). "Concise Review: Apoptotic Cell-Based Therapies-Rationale, Preclinical Results and Future Clinical Developments." Stem Cells **34**(6): 1464-1473.

Saas, P., S. Kaminski and S. Perruche (2013). "Prospects of apoptotic cell-based therapies for transplantation and inflammatory diseases." Immunotherapy **5**(10): 1055-1073.

Sandilands, G. P., Z. Ahmed, N. Perry, M. Davison, A. Lupton and B. Young (2005). "Cross-linking of neutrophil CD11b results in rapid cell surface expression of molecules required for antigen presentation and T-cell activation." Immunology **114**(3): 354-368.

Sansbury, B. E. and M. Spite (2016). "Resolution of Acute Inflammation and the Role of Resolvins in Immunity, Thrombosis, and Vascular Biology." Circ Res **119**(1): 113-130.

Savill, J., I. Dransfield, N. Hogg and C. Haslett (1990). "Vitronectin receptor-mediated phagocytosis of cells undergoing apoptosis." Nature **343**(6254): 170-173.

Sawcer, S., G. Hellenthal, M. Pirinen, C. C. Spencer, N. A. Patsopoulos, L. Moutsianas, A. Dilthey, Z. Su, C. Freeman, S. E. Hunt, S. Edkins, E. Gray, D. R. Booth, S. C. Potter, A. Goris, G. Band, A. B. Oturai, A. Strange, J. Saarela, C. Bellenguez, B. Fontaine, M. Gillman, B. Hemmer, R. Gwilliam, F. Zipp, A. Jayakumar, R. Martin, S. Leslie, S. Hawkins, E. Giannoulatou, S. D'Alfonso, H. Blackburn, F. Martinelli Boneschi, J. Liddle, H. F. Harbo, M. L. Perez, A. Spurkland, M. J. Waller, M. P. Mycko, M. Ricketts, M. Comabella, N. Hammond, I. Kockum, O. T. McCann, M. Ban, P. Whittaker, A. Kemppinen, P. Weston, C. Hawkins, S. Widaa, J. Zajicek, S. Dronov, N. Robertson, S. J. Bumpstead, L. F. Barcellos, R. Ravindrarajah, R. Abraham, L. Alfredsson, K. Ardlie, C. Aubin, A. Baker, K. Baker, S. E. Baranzini, L. Bergamaschi, R. Bergamaschi, A. Bernstein, A. Berthele, M. Boggild, J. P. Bradfield, D. Brassat, S. A. Broadley, D. Buck, H. Butzkueven, R. Capra, W. M. Carroll, P. Cavalla, E. G. Celius, S. Cepok, R. Chiavacci, F. Clerget-Darpoux, K. Clysters, G. Comi, M. Cossburn, I. Cournu-Rebeix, M. B. Cox, W. Cozen, B. A. Cree, A. H. Cross, D. Cusi, M. J. Daly, E. Davis, P. I. de Bakker, M. Debouverie, B. D'Hooghe M, K. Dixon, R. Dobosi, B. Dubois, D. Ellinghaus, I. Elovaara, F. Esposito, C. Fontenille, S. Foote, A. Franke, D. Galimberti, A. Ghezzi, J. Glessner, R. Gomez, O. Gout, C. Graham, S. F. Grant, F. R. Guerini, H. Hakonarson, P. Hall, A. Hamsten, H. P. Hartung, R. N. Heard, S. Heath, J. Hobart, M. Hoshi, C. Infante-Duarte, G. Ingram, W. Ingram, T. Islam, M. Jagodic, M. Kabesch, A. G. Kermode, T. J. Kilpatrick, C. Kim, N. Klopp, K. Koivisto, M. Larsson, M. Lathrop, J. S. Lechner-Scott, M. A. Leone, V. Leppa, U. Liljedahl, I. L. Bomfim, R. R. Lincoln, J. Link, J. Liu, A. R. Lorentzen, S. Lupoli, F. Macciardi, T. Mack, M. Marriott, V. Martinelli, D. Mason, J. L. McCauley, F. Mentch, I. L. Mero, T. Mihalova, X. Montalban, J. Mottershead, K. M. Myhr, P. Naldi, W. Ollier, A. Page, A. Palotie, J. Pelletier, L. Piccio, T. Pickersgill, F. Piehl, S. Pobywajlo, H. L. Quach, P. P. Ramsay, M. Reunanen, R. Reynolds, J. D. Rioux, M. Rodegher, S. Roesner, J. P. Rubio, I. M. Ruckert, M. Salvetti, E. Salvi, A. Santaniello, C. A. Schaefer, S. Schreiber, C. Schulze, R. J. Scott, F. Sellebjerg, K. W. Selmaj, D. Sexton, L. Shen, B. Simms-Acuna, S. Skidmore, P. M. Sleiman, C. Smestad, P. S. Sorensen, H. B. Sondergaard, J. Stankovich, R. C. Strange, A. M. Sulonen, E. Sundqvist, A. C. Syvanen, F. Taddeo, B. Taylor, J. M. Blackwell, P. Tienari, E. Bramon, A. Tourbah, M. A. Brown, E. Tronczynska, J. P. Casas, N. Tubridy, A. Corvin, J. Vickery, J. Jankowski, P. Villoslada, H. S. Markus, K. Wang, C. G. Mathew, J. Wason, C. N. Palmer, H. E. Wichmann, R. Plomin, E. Willoughby, A. Rautanen, J. Winkelmann, M. Wittig, R. C. Trembath, J. Yaouanq, A. C. Viswanathan, H. Zhang, N. W. Wood, R. Zuvich, P. Deloukas, C. Langford, A. Duncanson, J. R. Oksenberg, M. A. Pericak-Vance, J. L. Haines, T. Olsson, J. Hillert, A. J. Ivinson, P. L. De Jager, L. Peltonen, G. J. Stewart, D. A. Hafler, S. L. Hauser, G. McVean, P. Donnelly and A. Compston (2011). "Genetic risk and a primary role for cell-mediated immune mechanisms in multiple sclerosis." Nature **476**(7359): 214-219.

Schlager, C., H. Korner, M. Krueger, S. Vidoli, M. Haberl, D. Mielke, E. Brylla, T. Issekutz, C. Cabanas, P. J. Nelson, T. Ziemssen, V. Rohde, I. Bechmann, D. Lodygin, F. Odoardi and A. Flugel (2016). "Effector T-cell trafficking between the leptomeninges and the cerebrospinal fluid." Nature **530**(7590): 349-353.

Seewann, A., H. Vrenken, P. van der Valk, E. L. Blezer, D. L. Knol, J. A. Castelijns, C. H. Polman, P. J. Pouwels, F. Barkhof and J. J. Geurts (2009). "Diffusely abnormal white matter in chronic multiple sclerosis: imaging and histopathologic analysis." Arch Neurol **66**(5): 601-609.

Segal, B. M. and E. M. Shevach (1996). "IL-12 unmasks latent autoimmune disease in resistant mice." J Exp Med **184**(2): 771-775.

Segawa, K., J. Suzuki and S. Nagata (2011). "Constitutive exposure of phosphatidylserine on viable cells." Proc Natl Acad Sci U S A **108**(48): 19246-19251.

Sellebjerg, F., D. Cadavid, D. Steiner, L. M. Villar, R. Reynolds and D. Mikol (2016). "Exploring potential mechanisms of action of natalizumab in secondary progressive multiple sclerosis." Ther Adv Neurol Disord **9**(1): 31-43.

Serafini, B., B. Rosicarelli, R. Magliozzi, E. Stigliano, E. Capello, G. L. Mancardi and F. Aloisi (2006). "Dendritic cells in multiple sclerosis lesions: maturation stage, myelin uptake, and interaction with proliferating T cells." J Neuropathol Exp Neurol **65**(2): 124-141.

Serhan, C. N. (2017). "Discovery of specialized pro-resolving mediators marks the dawn of resolution physiology and pharmacology." Mol Aspects Med.

Serhan, C. N., N. Chiang and T. E. Van Dyke (2008). "Resolving inflammation: dual anti-inflammatory and pro-resolution lipid mediators." Nat Rev Immunol **8**(5): 349-361.

Serhan, C. N., S. Hong, K. Gronert, S. P. Colgan, P. R. Devchand, G. Mirick and R. L. Moussignac (2002). "Resolvins: a family of bioactive products of omega-3 fatty acid transformation circuits initiated by aspirin treatment that counter proinflammation signals." J Exp Med **196**(8): 1025-1037.

Serhan, C. N. and N. A. Petasis (2011). "Resolvins and protectins in inflammation resolution." Chem Rev **111**(10): 5922-5943.

Sica, A. and A. Mantovani (2012). "Macrophage plasticity and polarization: in vivo veritas." J Clin Invest **122**(3): 787-795.

Sobel, R. A. (2000). "Genetic and epigenetic influence on EAE phenotypes induced with different encephalitogenic peptides." J Neuroimmunol **108**(1-2): 45-52.

Soehnlein, O., M. Drechsler, Y. Doring, D. Lievens, H. Hartwig, K. Kemmerich, A. Ortega-Gomez, M. Mandl, S. Vijayan, D. Projahn, C. D. Garlichs, R. R. Koenen, M. Hristov, E. Lutgens, A. Zernecke and C. Weber (2013). "Distinct functions of chemokine receptor axes in the atherogenic mobilization and recruitment of classical monocytes." EMBO Mol Med **5**(3): 471-481.

Soehnlein, O. and L. Lindbom (2010). "Phagocyte partnership during the onset and resolution of inflammation." Nat Rev Immunol **10**(6): 427-439.

Speck, S., J. Lim, S. Shelake, M. Matka, J. Stoddard, A. Farr, V. Kuchroo and Y. Laouar (2014). "TGF-beta signaling initiated in dendritic cells instructs suppressive effects on Th17 differentiation at the site of neuroinflammation." PLoS One **9**(7): e102390.

Spite, M. and C. N. Serhan (2010). "Novel lipid mediators promote resolution of acute inflammation: impact of aspirin and statins." Circ Res **107**(10): 1170-1184.

Spivia, W., P. S. Magno, P. Le and D. A. Fraser (2014). "Complement protein C1q promotes macrophage anti-inflammatory M2-like polarization during the clearance of atherogenic lipoproteins." Inflamm Res **63**(10): 885-893.

Sporici, R. and T. B. Issekutz (2010). "CXCR3 blockade inhibits T-cell migration into the CNS during EAE and prevents development of adoptively transferred, but not actively induced, disease." Eur J Immunol **40**(10): 2751-2761.

Stables, M. J., S. Shah, E. B. Camon, R. C. Lovering, J. Newson, J. Bystrom, S. Farrow and D. W. Gilroy (2011). "Transcriptomic analyses of murine resolution-phase macrophages." Blood **118**(26): e192-208.

Stark, M. A., Y. Huo, T. L. Burcin, M. A. Morris, T. S. Olson and K. Ley (2005). "Phagocytosis of apoptotic neutrophils regulates granulopoiesis via IL-23 and IL-17." Immunity **22**(3): 285-294.

Stasiolek, M., A. Bayas, N. Kruse, A. Wieczarkowiecz, K. V. Toyka, R. Gold and K. Selmaj (2006). "Impaired maturation and altered regulatory function of plasmacytoid dendritic cells in multiple sclerosis." Brain **129**(Pt 5): 1293-1305.

Steiner, O., C. Coisne, R. Cecchelli, R. Boscacci, U. Deutsch, B. Engelhardt and R. Lyck (2010). "Differential roles for endothelial ICAM-1, ICAM-2, and VCAM-1 in shear-resistant T cell

arrest, polarization, and directed crawling on blood-brain barrier endothelium." J Immunol **185**(8): 4846-4855.

Steinman, L. (2007). "A brief history of T(H)17, the first major revision in the T(H)1/T(H)2 hypothesis of T cell-mediated tissue damage." Nat Med **13**(2): 139-145.

Storch, M. K., A. Stefferl, U. Brehm, R. Weissert, E. Wallstrom, M. Kerschensteiner, T. Olsson, C. Linington and H. Lassmann (1998). "Autoimmunity to myelin oligodendrocyte glycoprotein in rats mimics the spectrum of multiple sclerosis pathology." Brain Pathol **8**(4): 681-694.

Stromnes, I. M. and J. M. Goverman (2006). "Active induction of experimental allergic encephalomyelitis." Nat Protoc **1**(4): 1810-1819.

Stuart, W. H. (2004). "Clinical management of multiple sclerosis: the treatment paradigm and issues of patient management." J Manag Care Pharm **10**(3 Suppl B): S19-25.

Stuve, O., N. P. Dooley, J. H. Uhm, J. P. Antel, G. S. Francis, G. Williams and V. W. Yong (1996). "Interferon beta-1b decreases the migration of T lymphocytes in vitro: effects on matrix metalloproteinase-9." Ann Neurol **40**(6): 853-863.

Stys, P. K., G. W. Zamponi, J. van Minnen and J. J. Geurts (2012). "Will the real multiple sclerosis please stand up?" Nat Rev Neurosci **13**(7): 507-514.

Suzuki, J., M. Umeda, P. J. Sims and S. Nagata (2010). "Calcium-dependent phospholipid scrambling by TMEM16F." Nature **468**(7325): 834-838.

Takauji, R., S. Iho, H. Takatsuka, S. Yamamoto, T. Takahashi, H. Kitagawa, H. Iwasaki, R. Iida, T. Yokochi and T. Matsuki (2002). "CpG-DNA-induced IFN-alpha production involves p38 MAPK-dependent STAT1 phosphorylation in human plasmacytoid dendritic cell precursors." J Leukoc Biol **72**(5): 1011-1019.

Takeuchi, O. and S. Akira (2010). "Pattern recognition receptors and inflammation." Cell **140**(6): 805-820.

Tenger, C. and X. Zhou (2003). "Apolipoprotein E modulates immune activation by acting on the antigen-presenting cell." Immunology **109**(3): 392-397.

Tobal, K., A. Pagliuca, B. Bhatt, N. Bailey, D. M. Layton and G. J. Mufti (1990). "Mutation of the human FMS gene (M-CSF receptor) in myelodysplastic syndromes and acute myeloid leukemia." Leukemia **4**(7): 486-489.

Torkildsen, O., K. M. Myhr and L. Bo (2016). "Disease-modifying treatments for multiple sclerosis - a review of approved medications." Eur J Neurol **23 Suppl 1**: 18-27.

Traka, M., J. R. Podojil, D. P. McCarthy, S. D. Miller and B. Popko (2016). "Oligodendrocyte death results in immune-mediated CNS demyelination." Nat Neurosci **19**(1): 65-74.

Trebst, C., T. L. Sorensen, P. Kivisakk, M. K. Cathcart, J. Hesselgesser, R. Horuk, F. Sellebjerg, H. Lassmann and R. M. Ransohoff (2001). "CCR1+/CCR5+ mononuclear phagocytes accumulate in the central nervous system of patients with multiple sclerosis." Am J Pathol **159**(5): 1701-1710.

Truman, L. A., C. A. Ford, M. Pasikowska, J. D. Pound, S. J. Wilkinson, I. E. Dumitriu, L. Melville, L. A. Melrose, C. A. Ogden, R. Nibbs, G. Graham, C. Combadiere and C. D. Gregory (2008). "CX3CL1/fractalkine is released from apoptotic lymphocytes to stimulate macrophage chemotaxis." Blood **112**(13): 5026-5036.

Tzartos, J. S., M. A. Friese, M. J. Craner, J. Palace, J. Newcombe, M. M. Esiri and L. Fugger (2008). "Interleukin-17 production in central nervous system-infiltrating T cells and glial cells is associated with active disease in multiple sclerosis." Am J Pathol **172**(1): 146-155.

van den Eijnde, S. M., M. J. van den Hoff, C. P. Reutelingsperger, W. L. van Heerde, M. E. Henfling, C. Vermeij-Keers, B. Schutte, M. Borgers and F. C. Ramaekers (2001). "Transient expression of phosphatidylserine at cell-cell contact areas is required for myotube formation." J Cell Sci **114**(Pt 20): 3631-3642.

van Kruchten, R., N. J. Mattheij, C. Saunders, M. A. Feijge, F. Swieringa, J. L. Wolfs, P. W. Collins, J. W. Heemskerk and E. M. Bevers (2013). "Both TMEM16F-dependent and TMEM16F-independent pathways contribute to phosphatidylserine exposure in platelet apoptosis and platelet activation." Blood **121**(10): 1850-1857.

Vanderlugt, C. L. and S. D. Miller (2002). "Epitope spreading in immune-mediated diseases: implications for immunotherapy." Nat Rev Immunol **2**(2): 85-95.

Venken, K., N. Hellings, T. Broekmans, K. Hensen, J. L. Rummens and P. Stinissen (2008). "Natural naive CD4+CD25+CD127low regulatory T cell (Treg) development and function are disturbed in multiple sclerosis patients: recovery of memory Treg homeostasis during disease progression." J Immunol **180**(9): 6411-6420.

Vergadi, E., E. Ieronymaki, K. Lyroni, K. Vaporidi and C. Tsatsanis (2017). "Akt Signaling Pathway in Macrophage Activation and M1/M2 Polarization." J Immunol **198**(3): 1006-1014.

Vieira, P. L., H. C. Heystek, J. Wormmeester, E. A. Wierenga and M. L. Kapsenberg (2003). "Glatiramer acetate (copolymer-1, copaxone) promotes Th2 cell development and increased IL-10 production through modulation of dendritic cells." J Immunol **170**(9): 4483-4488.

Vojdani, A. (2014). "A Potential Link between Environmental Triggers and Autoimmunity." Autoimmune Dis **2014**: 437231.

Voll, R. E., E. A. Roth, I. Girkontaite, H. Fehr, M. Herrmann, H. M. Lorenz and J. R. Kalden (1997). "Histone-specific Th0 and Th1 clones derived from systemic lupus erythematosus patients induce double-stranded DNA antibody production." Arthritis Rheum **40**(12): 2162-2171.

Volpi, C., F. Fallarino, M. T. Pallotta, R. Bianchi, C. Vacca, M. L. Belladonna, C. Orabona, A. De Luca, L. Boon, L. Romani, U. Grohmann and P. Puccetti (2013). "High doses of CpG oligodeoxynucleotides stimulate a tolerogenic TLR9-TRIF pathway." Nat Commun **4**: 1852.

Vorobjeva, N. V. and B. V. Pinegin (2014). "Neutrophil extracellular traps: mechanisms of formation and role in health and disease." Biochemistry (Mosc) **79**(12): 1286-1296.

Wadwa, M., R. Klopfleisch, A. Adamczyk, A. Frede, E. Pastille, K. Mahnke, W. Hansen, R. Geffers, K. S. Lang, J. Buer, J. Buning and A. M. Westendorf (2016). "IL-10 downregulates CXCR3 expression on Th1 cells and interferes with their migration to intestinal inflammatory sites." Mucosal Immunol **9**(5): 1263-1277.

Wallach, D., T. B. Kang and A. Kovalenko (2014). "Concepts of tissue injury and cell death in inflammation: a historical perspective." Nat Rev Immunol **14**(1): 51-59.

Wang, D., S. P. Li, J. S. Fu, S. Zhang, L. Bai and L. Guo (2016). "Resveratrol defends blood-brain barrier integrity in experimental autoimmune encephalomyelitis mice." J Neurophysiol **116**(5): 2173-2179.

Weber, M. S., T. Prod'homme, S. Youssef, S. E. Dunn, C. D. Rundle, L. Lee, J. C. Patarroyo, O. Stuve, R. A. Sobel, L. Steinman and S. S. Zamvil (2007). "Type II monocytes modulate T cell-mediated central nervous system autoimmune disease." Nat Med **13**(8): 935-943.

Weichhart, T., M. Haidinger, K. Katholnig, C. Kopecky, M. Poglitsch, C. Lassnig, M. Rosner, G. J. Zlabinger, M. Hengstschlager, M. Muller, W. H. Horl and M. D. Saemann (2011). "Inhibition of mTOR blocks the anti-inflammatory effects of glucocorticoids in myeloid immune cells." Blood **117**(16): 4273-4283.

Westlund, K. (1970). "Distribution and mortality time trend of multiple sclerosis and some other diseases in Norway." Acta Neurol Scand **46**(4): 455-483.

Wiktor-Jedrzejczak, W., A. Bartocci, A. W. Ferrante, Jr., A. Ahmed-Ansari, K. W. Sell, J. W. Pollard and E. R. Stanley (1990). "Total absence of colony-stimulating factor 1 in the macrophage-deficient osteopetrotic (op/op) mouse." Proc Natl Acad Sci U S A **87**(12): 4828-4832.

Wright, H. L., R. J. Moots, R. C. Bucknall and S. W. Edwards (2010). "Neutrophil function in inflammation and inflammatory diseases." Rheumatology (Oxford) **49**(9): 1618-1631.

Wynn, T. A. and K. M. Vannella (2016). "Macrophages in Tissue Repair, Regeneration, and Fibrosis." Immunity **44**(3): 450-462.

Xie, Z. X., H. L. Zhang, X. J. Wu, J. Zhu, D. H. Ma and T. Jin (2015). "Role of the immunogenic and tolerogenic subsets of dendritic cells in multiple sclerosis." Mediators Inflamm **2015**: 513295.

Yamaguchi, H., T. Maruyama, Y. Urade and S. Nagata (2014). "Immunosuppression via adenosine receptor activation by adenosine monophosphate released from apoptotic cells." Elife **3**: e02172.

Yang, Q., C. Zheng, J. Cao, G. Cao, P. Shou, L. Lin, T. Velletri, M. Jiang, Q. Chen, Y. Han, F. Li, Y. Wang, W. Cao and Y. Shi (2016). "Spermidine alleviates experimental autoimmune encephalomyelitis through inducing inhibitory macrophages." Cell Death Differ **23**(11): 1850-1861.

Yednock, T. A., C. Cannon, L. C. Fritz, F. Sanchez-Madrid, L. Steinman and N. Karin (1992). "Prevention of experimental autoimmune encephalomyelitis by antibodies against alpha 4 beta 1 integrin." Nature **356**(6364): 63-66.

Ying, H., Y. Kang, H. Zhang, D. Zhao, J. Xia, Z. Lu, H. Wang, F. Xu and L. Shi (2015). "MiR-127 modulates macrophage polarization and promotes lung inflammation and injury by activating the JNK pathway." J Immunol **194**(3): 1239-1251.

Ying, W., A. Tseng, R. C. Chang, A. Morin, T. Brehm, K. Triff, V. Nair, G. Zhuang, H. Song, S. Kanameni, H. Wang, M. C. Golding, F. W. Bazer, R. S. Chapkin, S. Safe and B. Zhou (2015). "MicroRNA-223 is a crucial mediator of PPARgamma-regulated alternative macrophage activation." J Clin Invest **125**(11): 4149-4159.

Yogev, N., F. Frommer, D. Lukas, K. Kautz-Neu, K. Karram, D. Ielo, E. von Stebut, H. C. Probst, M. van den Broek, D. Riethmacher, T. Birnberg, T. Blank, B. Reizis, T. Korn, H. Wiendl, S. Jung, M. Prinz, F. C. Kurschus and A. Waisman (2012). "Dendritic cells ameliorate autoimmunity in the CNS by controlling the homeostasis of PD-1 receptor(+) regulatory T cells." Immunity **37**(2): 264-275.

Yokote, H., S. Miyake, J. L. Croxford, S. Oki, H. Mizusawa and T. Yamamura (2008). "NKT cell-dependent amelioration of a mouse model of multiple sclerosis by altering gut flora." Am J Pathol **173**(6): 1714-1723.

Yong, T., G. A. Meininger and D. S. Linthicum (1993). "Enhancement of histamine-induced vascular leakage by pertussis toxin in SJL/J mice but not BALB/c mice." J Neuroimmunol **45**(1-2): 47-52.

Zang, Y. C., S. Li, V. M. Rivera, J. Hong, R. R. Robinson, W. T. Breitbach, J. Killian and J. Z. Zhang (2004). "Increased CD8+ cytotoxic T cell responses to myelin basic protein in multiple sclerosis." J Immunol **172**(8): 5120-5127.

Zhang, D., C. Chia, X. Jiao, W. Jin, S. Kasagi, R. Wu, J. E. Konkel, H. Nakatsukasa, P. Zanvit, N. Goldberg, Q. Chen, L. Sun, Z. J. Chen and W. Chen (2017). "D-mannose induces regulatory T cells and suppresses immunopathology." Nat Med.

Zhang, F., H. Wang, X. Wang, G. Jiang, H. Liu, G. Zhang, R. Fang, X. Bu, S. Cai and J. Du (2016). "TGF-beta induces M2-like macrophage polarization via SNAIL-mediated suppression of a pro-inflammatory phenotype." Oncotarget **7**(32): 52294-52306.

Zhang, H., J. R. Podojil, X. Luo and S. D. Miller (2008). "Intrinsic and induced regulation of the age-associated onset of spontaneous experimental autoimmune encephalomyelitis." J Immunol **181**(7): 4638-4647.

Zhang, X., Y. Tao, M. Chopra, M. Ahn, K. L. Marcus, N. Choudhary, H. Zhu and S. Markovic-Plese (2013). "Differential reconstitution of T cell subsets following immunodepleting treatment with alemtuzumab (anti-CD52 monoclonal antibody) in patients with relapsing-remitting multiple sclerosis." J Immunol **191**(12): 5867-5874.

Zhou, H., J. Xiao, N. Wu, C. Liu, J. Xu, F. Liu and L. Wu (2015). "MicroRNA-223 Regulates the Differentiation and Function of Intestinal Dendritic Cells and Macrophages by Targeting C/EBPbeta." Cell Rep **13**(6): 1149-1160.

Zhu, L., T. Yang, L. Li, L. Sun, Y. Hou, X. Hu, L. Zhang, H. Tian, Q. Zhao, J. Peng, H. Zhang, R. Wang, Z. Yang and Y. Zhao (2014). "TSC1 controls macrophage polarization to prevent inflammatory disease." Nat Commun **5**: 4696.

Zlotnik, A. and O. Yoshie (2012). "The chemokine superfamily revisited." Immunity **36**(5): 705-716.

Annexes: Publications obtenues lors de la thèse

PLOS | ONE

RESEARCH ARTICLE

Proximity Ligation *In situ* Assay is a Powerful Tool to Monitor Specific ATG Protein Interactions following Autophagy Induction

Thierry Gauthier, Aurore Claude-Taupin, Régis Delage-Mourroux, Michaël Boyer-Guittaut, Eric Hervouet*

Université de Franche-Comté, Laboratoire de Biochimie, EA3922 « Estrogènes, Expression Génique et Pathologies du Système Nerveux Central », SFR IBCT FED4234, UFR Sciences et Techniques, France

* eric.hervouet@univ-fcomte.fr

Citation: Gauthier T, Claude-Taupin A, Delage-Mourroux R, Boyer-Guittaut M, Hervouet E (2015) Proximity Ligation *In situ* Assay is a Powerful Tool to Monitor Specific ATG Protein Interactions following Autophagy Induction. PLoS ONE 10(6): e0128701. doi:10.1371/journal.pone.0128701

Academic Editor: Maasaki Komatsu, Niigata University School of Medicine, JAPAN

Received: March 17, 2015

Accepted: April 29, 2015

Published: June 2, 2015

Data Availability Statement: All relevant data are within the paper and its Supporting Information files.

Funding: This work was supported by 1) the University of Franche-Comté, 2) "Ministère de l'Enseignement Supérieur et de la Recherche" (MESR) and fundings from 1) "Région de Franche-Comté" 2013 : EH 2) fellowship of "Région de Franche-Comté". : ACT 3) Conférence de Coordination Interrégional du Grand-Est "Ligue Contre le Cancer" 2014 (#007.Y-2014) : EH. The funders had no role in study design, data collection

Abstract

Macroautophagy is a highly regulated intracellular degradation process which has been extensively studied over the last decade. This pathway has been initially described as a non selective process inducing the degradation of parts of the cytoplasm as well as organelles at random. Nevertheless, over the last few years, new research highlighted the existence of a more selective autophagy pathway specifically recruiting some organelles or aggregates to the autophagosomes in order to induce their degradation. These selective autophagy pathways such as aggrephagy, mitophagy, pexophagy or xenophagy, involve the intervention of a cargo, the material to be degraded, cargo adapters, the molecules allowing the recruitment of the cargo to the autophagosome, and the proteins of the ATG8 family which link the cargo adapters to the autophagosome. One of the main questions which now remain is to develop new techniques and protocols able to discriminate between these different types of induced autophagy. In our work, we studied the possibility to use the P-LISA technique, which has been recently developed to study endogenous *in vivo* protein interactions, as a new technique to characterize the ATG proteins specifically involved in bulk or selective autophagy. In this manuscript, we indeed demonstrate that this technique allows the study of endogenous ATG protein interactions in cells following autophagy induction, but more interestingly that this technique might be used to characterize the ATG proteins involved in selective autophagy.

Introduction

Macroautophagy (hereafter called autophagy) is a catabolic process that leads to the identification, transport and the degradation of cytosolic constituents to the lysosome. More than 40 ATG proteins are related to the initiation, elongation and maturation of a double membrane vesicle, referred as autophagosome, during autophagy. One family has been described to be particularly important for vesicle formation in yeast as well as mammals, the ATG8 family. In mammals, these homologues of the only yeast ATG8 are divided in two subfamilies: the LC3

and analysis, decision to publish, or preparation of the manuscript.

Competing Interests: The authors have declared that no competing interests exist.

family (LC3A, LC3B, LC3C) required in the early phases of autophagosome formation and the GABARAP family (GABARAP, GEC1/GABARAPL1 (GL1), GATE-16/GABARAPL2) which seems to be more involved in the elongation and closure of autophagosomes.[1] The ATG8 members are synthetized as cytosolic pro-proteins and cleaved by ATG4 enzymes at a C-terminal Glycine to give the mature form of these proteins (form I) before their conjugation onto phospholipids to give the lipidated form of ATG8s (form II). Starvation or hypoxic stress have been described to induce autophagy in a non selective manner and induce the degradation and/or recycling of damaged cellular components in order to regulate cellular homeostasis. More recently, a selective autophagy leading to the specific degradation of intracellular components (ubiquitinylated proteins, damaged mitochondria, endoplasmic reticulum, peroxysomes, ribosomes) has been described. This selective process requires the interaction of specific protein cargo adapters with the ATG8 proteins, linked to the membrane of the autophagosome as an anchor point to recruit the cargo into the autophagosome. These cargo adapters, such as SQSTM1/P62, NBR1, NIX/BNIP3L or NDP52/CALCOCO2, all interact with LC3-II *via* a LIR domain (LC3 interacting domain) and with their ligand to be degraded, the cargo using an UBA domain (ubiquitin associated).[2] NIX/BNIP3L is required for the selective degradation of mitochondria, called mitophagy, while NBR1 is indispensable for the selective degradation of peroxisomes, called pexophagy.[3] NDP52 regulates the selective degradation of DICER and AGO2 and thus regulates miRNA activity [4] whereas SQSTM1/P62 is implicated in the selective degradation of ubiquitinylated proteins.[5] These different autophagy cargo adapters can then interact with different ATG8 proteins through an AIM WXXL-like motif (ATG8-family interacting motif).[6] This high number of putative interactions between cargo adapters and ATG8s might explain the existence of numerous types of selective autophagy in the cells. This hypothesis has been confirmed by a recent *in vitro* study performed by Berhends and collaborators in order to characterize the cellular autophagy network which revealed a complex network of interactions between autophagy proteins.[7]

Autophagy deregulation has been associated with numerous human pathological disorders even if the mechanism still remains unknown. For example, inactivation or modulation of the expression of several autophagy genes have been reported in cancer cells. Indeed, *BECLIN-1*, *BIF-1* and *UVRAG*, three essential autophagy genes have been classified as tumor suppressor genes and are frequently inactivated in cancer cells leading to the promotion of cell proliferation and aggressiveness.[8,9,10] Defects and mutations in autophagy genes have also been frequently observed in neurodegenerative disorders such as Alzheimer's disease, or familial Parkinson's disease.[11] Since then, the development of techniques to efficiently monitor autophagy levels in cell and tissue models became a challenge to better characterize autophagy protein expression, function and deregulation in these pathologies. This information will be essential in the future to characterize autophagy levels or autophagy gene and protein expressions as potential diagnostic markers or therapeutic targets.

Several techniques currently used to quantify autophagy levels in cells and tissues are based on the detection of proteins associated to the autophagosomes. Therefore, the ATG8 proteins, and in particular LC3, are the preferential targets for autophagy level quantification. SQSTM1/P62 has also been extensively studied by the autophagy community since this protein was defined as a specific substrate of autophagy.[12] Nevertheless, more recent studies demonstrated that the levels of SQSTM1/P62 are highly regulated by different cellular stresses and cannot be considered anymore as exclusively correlated to autophagy levels. Therefore, western blotting experiments are used to quantify both the LC3-II and LC3-I forms and the amounts of SQSTM1/P62 protein, and *in situ* analysis of GFP-LC3 vesicles in transfected cells are frequently performed. An improved version of the latter approach has been obtained by the expression of a double fusion protein mRFP-GFP-LC3B which allows the identification and

quantification of both autophagosomes (in yellow) and lysosomes (in red). Indeed, it has been described a loss of GFP fluorescence, but not red fluorescence, in acidic compartments (*e.g.* lysosomes).[13] In spite of their highly informative power on autophagosome formation, these techniques are not adapted to study bulk versus selective autophagy. Regarding selective autophagy, researchers concentrate on the study of localization and quantification of cargo adapters such as GFP-P62 or GFP-NBR1.[14] However, due to high levels of aggregation following protein overexpression,[15] variable levels of expression of exogenous GFP or the difficulty to accurately quantify the number of GFP vesicles in transfected cells, in particular when willing to perform co-localization quantification, these models remain difficult and problematic to use. Here, we propose the use of a recently new described technique, called proximity ligation *in situ* assay (P-LISA) (S1 Fig), to monitor endogenous ATG8/cargo adapters interactions to accurately analyze and quantify non selective and selective autophagy in cells.

In this publication, we demonstrate that SQSTM1/LC3B, SQSTM1/GL1, NIX/LC3B and NIX/GL1 interactions can be quantified using P-LISA and are effectively correlated to autophagy levels as shown by the comparison with former techniques. Moreover, our work shows that SQSTM1/LC3B interaction is increased following different autophagy inducers whereas NIX/LC3B and NIX/GL1 interactions are mainly regulated by mitochondria stressors. Altogether, our data describe for the first time, the use of P-LISA in order to easily and efficiently discriminate between different types of autophagy targeting endogenous non overexpressed autophagy proteins.

Material and Methods

Antibodies and reagents

The following antibodies were used: monoclonal anti-P62/SQSTM1 (Santa Cruz, sc-28359; dilutions: IF/P-LISA 1/200, WB 1/1000), polyclonal anti-LC3B (Sigma, L8918; dilutions: IF/P-LISA 1/100, WB 1/3000), polyclonal anti-GABARAPL1 (Proteintech, 11010-AP, dilution: IF/P-LISA 1/100), monoclonal anti-NIX (Santa Cruz, sc-166332; dilution: IF/P-LISA 1/100), polyclonal anti-rabbit-HRP conjugate (P.A.R.I.S, BI2407; dilution: 1/10 000), polyclonal anti-mouse-HRP conjugate (P.A.R.I.S.; dilution: 1/10 000), polyclonal anti-rabbit-Alexa 488 (Life Technologies, BI2413C; dilution 1/1 000), and polyclonal anti-mouse-Alexa 555 (Life Technlogies; dilution: 1/1000). Cell culture reagents were purchased from Invitrogen. EBSS (E3024), BafA1 (B1793), Rapa (R8781) and CCCP (C2759) were purchased from Sigma-Aldrich. Rot (AC13237) was purchased from Acros organics.

Cell culture

MDA-MB-436 and MCF-7 cells were obtained from ATCC (HTB-130 and HTB-22). Cells were cultured at 37°C with 5% CO_2 atmosphere in DMEM 1g/L glucose (Dominique Dutscher, L0066) supplemented with 5% SVF (Dominique Dutscher, S1810), 1% penicillin/streptomycin (Dominique Dutscher, L0018) and 0.1% Fungizone (PAA, P11-001). MCF-7 control and MCF-7 overexpressing FLAG-GABARAPL1-6His were available in the laboratory and cultured as described above with the exception of 10% SVF.[16]

Plasmids and transfection

The pGFP-LC3 vector was kindly provided by Dr. Elazar (The Weizmann Institute of Science, Rehovot, Israel). The pEGFP-NIX was kindly provided by Dr. Xiao-Ming Yin[17] and the pGFP-mRFP-LC3B (ptf-LC3) vector was purchased from Addgene (21074). Transient

transfections were performed in 24-well plates using 0.5 μg of DNA and 1μL of JetPrime reagent (Polyplus Transfection, 114–07) according to manufacturer's protocol.

Western blotting

Cells were scraped, harvested and lysed in RIPA buffer (50 mM Tris-HCl, pH 8, 150 mM NaCl, 1% Triton X 100, 0.5% DOCA, 0.1% SDS) supplemented with 0.1% protease inhibitors (104 mM AEBSF, 1.5 mM pepstatin A, 1.4 mM E-64, 4 mM bestatin, 2 mM leupeptin, 80 μM aprotinin). Lysates were sonicated ten times for 5 sec. 40μg of protein were loaded and separated on a 12.5% sodium dodecyl sulfate-polyacrylamide gel electrophoresis (SDS-PAGE) before being transferred onto a polyvinylidenedifluoride (PVDF) membrane (Bio-Rad, 162–0177). Membrane was blocked with 5% nonfat milk in Tris-buffered saline supplemented with Tween 20 (TBS-T) (20 mM Tris-HCl, pH 7.6, 137 mM NaCl, 0.1% Tween 20) and incubated with primary antibodies overnight at 4°C under gentle agitation. Immunoreactive bands were detected using goat horseradish peroxidase (HRP)-coupled secondary (anti-mouse or anti-rabbit antibodies) and the *p*-coumaric acid-enhanced chemiluminescent (PCA-ECL) solution. Signals were acquired using the ChemiDocXRS+ (Biorad, France) and quantified using the Biorad Image Lab software (version 4.0) (Biorad, France).

Immunofluorescence and Proximity Ligation in situ Assay (P-LISA)

Cells were cultured for 24 h on coverslips and then fixed with 4% paraformaldehyde pH 7.4 in PBS (137 mM NaCl, 2.7 mM KCl, 10 mM Na_2HPO_4, 2 mM KH_2PO_4) during 15 min at room temperature. Permeabilization was performed in cold methanol for 20 min at 4°C.

For immunofluorescence, blocking was realized with 0.1% tween-TBS with 5% BSA for 1h at 37°C. Incubations with primary antibodies were performed overnight at 4°C, and then cells were rinsed 3 times with 0.1% tween-TBS. Incubations with secondary antibodies were performed for 1 h at 37°C and then cells were rinsed 3 times with 0.1% tween-TBS, stained with DAPI (4',6'-diamidino-2-phénylindole) and mounted using Vectashield Hardset mounting medium (Vector Laboratories, H-1400).

For P-LISA, all incubations were performed in a humidity chamber and according the OlinkBioscience's recommendations using Duolink In Situ Detection Reagents Red kit (DUO92008, Sigma-Aldrich, France). Briefly, coverslips were blocked with Blocking solution (82007, Olinkbioscience) for 45 min at 37°C and then incubated with primary antibodies previously diluted in Antibody diluent (82008, Olinkbioscience) overnight at 4°C. Coverslips were washed 3 times for 5 min in T-PBS buffer under gentle shaking and then incubated with PLA probes MINUS and PLUS corresponding to the primary antibodies using Duolink In Situ PLA Probe Anti-Goat MINUS (DUO92006, Sigma-Aldrich, France), Duolink In Situ PLA Probe Anti-Mouse PLUS (DUO92001, Sigma-Aldrich, France), Duolink In Situ PLA Probe Anti-Mouse MINUS (DUO92004, Sigma-Aldrich, France) and Duolink In Situ PLA Probe Anti-Rabbit MINUS (DUO92005, Sigma-Aldrich, France) for 2 h at 37°C. Then, coverslips were washed 3 times for 5 min in T-PBS buffer under gentle shaking and then incubated with a DNA ligase previously diluted in Ligation buffer for 30 min at 37°C. Coverslips were washed 3 times for 5 min in T-PBS buffer under gentle shaking and incubated with a DNA polymerase previously diluted in Amplification buffer for 90 min at 37°C. Finaly, coverslips were rinsed for 10 min in presence of DAPI under gentle shaking and then washed 2 min with (0.02X, 0.2X, or 2X (30 mM sodium citrate; 300 mM sodium chloride) SCC buffer, and then 2 min in 70% ethanol. Dried coverslips were mounted with Vectashield Mounting Medium (Vector Laboratories, H-1000). Fluorescence was visualized with an Olympus IX81 confocal microscope (Olympus, France) and pictures acquisition was realized using a DP75 camera.

Finally, immunofluorescence images were analyzed using the "ImageJ" software while P-LISA images were analyzed using the "BlobFinder"software available for download from www.cb.uu.se/~amin/BlobFinder. Interactions were quantified by counting the number of dots per cell as well as the intensity of signal per dot. An increase of intensity is the consequence of a concentration of interactions in the same cellular dots. [18] In the different figures, each bar (Mean ± SEM) represents the mean obtained from the quantification of signals observed in about 200 cells chosen randomly in 5 different fields from 3 independent experiments.

Statistical Analysis

Differences between means were analyzed using t-test with GraphPad Prism 5 software. Co-localization experiments were analyzed using Pearson and the Image J (plug-in Coloc-2) software. * ($p<0.05$), ** ($p<0.01$), *** ($p<0.001$) and **** ($p<0.0001$)

Results

P-LISA can be used for the detection of autophagy protein interactions in breast cancer cell models

Previous reports described the importance of multiple interactions between autophagy proteins during the course of autophagosome formation.[2,5,6,7,19] Moreover, recent data suggested that specific interactions between members of the ATG8 family (LC3B, GABARAP or GABARAPL1) and cargo adapters, such as SQSTM1/P62 or NIX, were essential to induce the selective degradation of target proteins or organelles during a new processus called selective autophagy. For example, SQSTM1/LC3B interaction has been previously reported in cells over-expressing GFP-LC3B, and the authors demonstrated that this interaction favored the SQSTM1 localization in autophagosomes.[19,20,21] Moreover, additional interactions of SQSTM1 with other ATG8 proteins (LC3A, LC3B, LC3C, GABARAP, GABARAPL1 and GABARAPL2) have been reported in ATG8-overexpressing cell models [7]. Unfortunately, these data were mostly observed in transfected cells and it is known that overexpression of exogenous proteins might lead to non specific interactions or the formation of GFP aggregates as already pointed out.[15] Therefore, we decided to develop a specific P-LISA protocol to quantify *in cellulo* endogenous autophagy protein interactions.

P-LISA is a multi-step technique leading to the detection of specific fluorescent dots linked to close proximity protein interactions (range below 40 nm) (S1 Fig). This technique is based on the use of two different primary antibodies of different species which are specific of two proteins supposed to interact in the cells. The advantage of this technique is the detection of endogenous proteins in the cellular context without the need of overexpression. Moreover, the maximal distance between the two proteins to get a signal should not exceed 40 nm, a distance which is below the sensitivity of confocal microscopy used for co-localization experiments.

First, we compared the possibility to use P-LISA in breast cancer cells (MDA-MB-436) to detect the interaction between LC3B (an ATG8 family member) and SQSTM1 (a cargo adapter). Immunofluorescence (IF) experiments confirmed the expression of these proteins and their partial co-localization in the MDA-MB-436 cells (Fig 1A left panel). However, co-localization of proteins detected by IF does not necessarily mean interaction. Moreover, co-localization quantification of ATG proteins in immunostained cells is difficult to analyze due to the large distribution of these proteins in the cell. Since our LC3 antibody seemed to present a rather low specificity and induced the detection of non specific nuclear signals, which has already been described by others,[22] we wondered whether P-LISA would give a

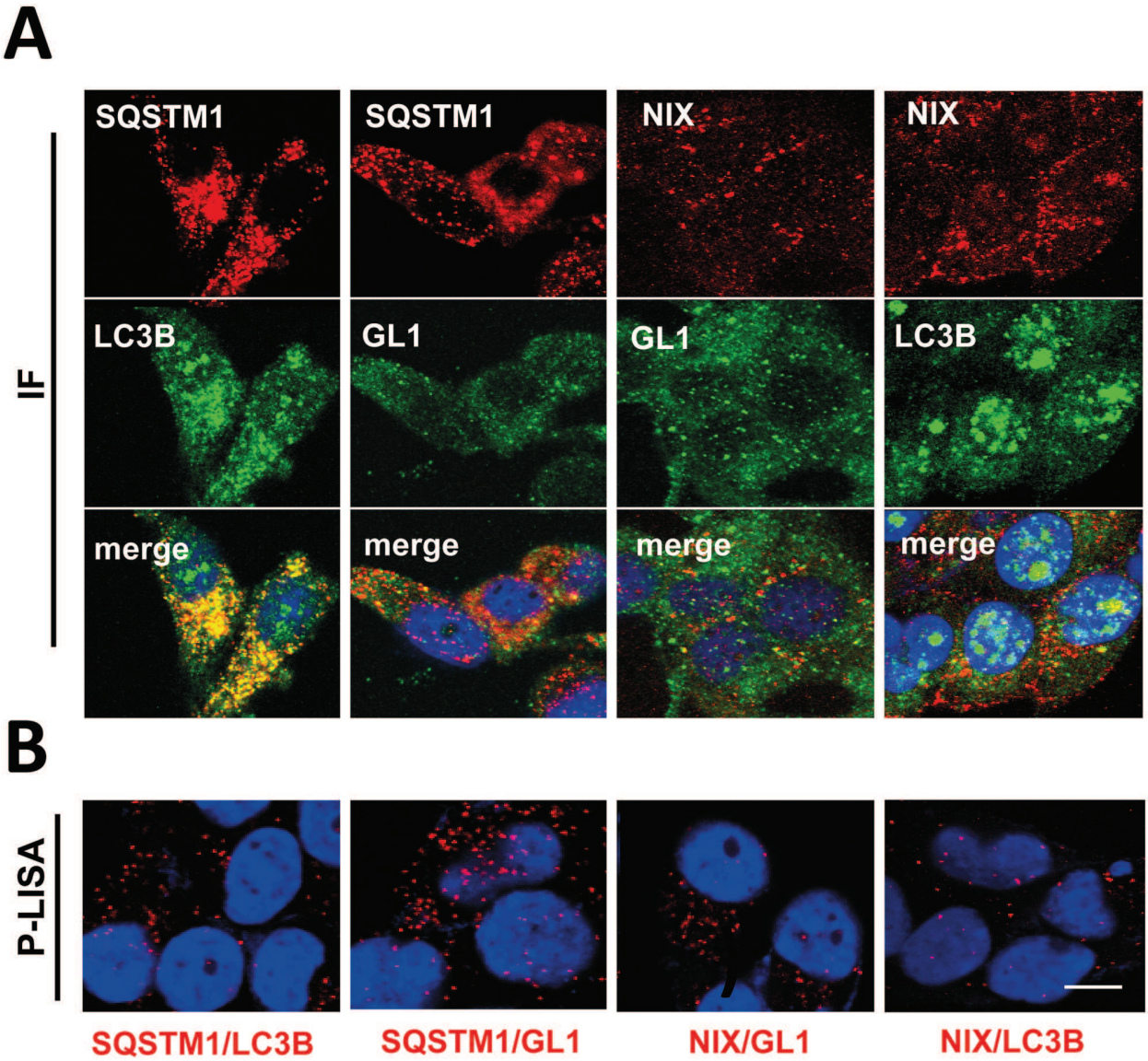

Fig 1. Detection of SQSTM1/LC3B, SQSTM1/GL1, NIX/GL1 and NIX/LC3B interactions by P-LISA. (**A**) MDA-MB-436 cells were cultured for 24 h at 37°C and 5% CO_2, fixed, permeabilized, blocked with 5% BSA, incubated with rabbit anti-LC3B, rabbit anti-GL1, mouse anti-SQSTM1 or/and mouse anti-NIX antibodies overnight at 4°C and then with an Alexa Fluor 488 goat anti-rabbit and an Alexa Fluor 555 goat anti-mouse, respectively, for 1 h. The cells were then analyzed using a confocal microscope. (**B**) For P-LISA, the protocol was performed according to the manufacturer's recommendations using the same antibodies as described above. Nuclei were stained with DAPI. Each picture is representative of a typical cell staining observed in 10 fields chosen at random. Scale bars: 20μm.

doi:10.1371/journal.pone.0128701.g001

more specific result in our model. Therefore, we developed a specific P-LISA protocol to quantify *in cellulo* endogenous SQSTM1 and LC3B interactions. During these P-LISA experiments, using two specific primary antibodies directed against SQSTM1 and LC3B, we detected quantifiable specific P-LISA dots corresponding to the interaction of endogenous LC3B and SQSTM1 in MDA-MB-436 cells without the need to overexpress these proteins (Fig 1B left panel). We then asked whether this protocol could be used for the study of other

autophagy-related protein interactions and therefore targeted the interactions between SQSTM1 and GABARAPL1 (GL1, another ATG8 family member) or interactions of a second cargo adapter NIX with LC3B or GL1 in MDA-MB-436 cells (Fig 1). Immunofluorescence experiments confirmed the expression of NIX and LC3 proteins in our models and their partial co-localization in MDA-MB-436 cells (Fig 1A). Then, the use of NIX/GL1 P-LISA revealed the presence of dots (a mean of 11.6 dots/cell) in MDA-MB-436 which quantification was facilitated thanks to the specificity of P-LISA staining. We obtained similar results regarding the interaction between LC3B and NIX (a mean of 18.9 dots/cell) (Fig 1B).

To confirm that these signals observed in MDA-MB-436 cells were indeed specific, we performed several technical controls (Fig 2). First, we performed P-LISA controls without primary antibodies (Fig 2A left panel) or using one secondary PLA probe antibody incompatible with the primary antibodies used. As expected, both controls did not produce any P-LISA signals in the cells (Fig 2A). Second, we used siRNA targeting *LC3B* expression in our models (Fig 2B top panel). We also observed that the specific *LC3B* siRNA also strongly decreased the number of SQSTM1/LC3B P-LISA fluorescent dots, data which demonstrated the specificity of the technique (Fig 2B bottom panel). To confirm these data, we performed a control using murine cells since the murine SQSTM1 protein does not contain the human epitope recognized by the anti-SQSTM1 antibody used in our P-LISA experiments. Once again, we confirmed the specificity of our technique since we observed no SQSTM1/LC3B P-LISA signal in murine cells but showed the restoration of P-LISA signals when these cells were transfected with a vector coding the human HA-SQSTM1 protein (Fig 2C). At last, we performed NIX/GL1 P-LISA in MDA-MB-436 cells stably expressing a shRNA targeting *GABARAPL1*.[16] Absence of GL1 in these cells was confirmed using westen blotting (Fig 2D). Our data confirmed that the cells which did not express GL1 following shRNA expression did not present any P-LISA staining (Fig 2E).

Since a decreased expression of GL1, a member of the ATG8 family, has been frequently observed in breast cancer (BC) cells, we decided to use the MCF-7 cell line, which has been described to present an undetectable expression of GL1 in western blotting and a weak basal signal in IF, to validate the specificity of the SQSTM1/GL1 and NIX/GL1 P-LISA (Fig 3). Western blotting (Fig 3A) and immunofluorescence experiments (Fig 3B) indeed confirmed the low GL1 expression in MCF-7 control cells (stably transfected with an empty vector) and the presence of this protein in MCF-7 cells stably overexpressing FLAG-GL1-6His, as previously described.[16] These data also showed an increase in the co-localization of GL1 and SQSTM1 in overexpressing cells compared to non-expressing cells (Fig 3B top panel). Regarding SQSTM1/GL1 P-LISA staining, as expected, few fluorescent dots were observed in MCF-7 control cells (3.9 dots per cell) while a significant increase of SQSTM1/GL1 P-LISA signals was quantified in MCF-7 stably overexpressing FLAG-GL1-6His (15.4 dots per cell) ($p<0.0001$, Fig 3B bottom panel). MCF-7 cells stably overexpressing FLAG-GL1-6His cells expressed a very low level of NIX protein associated with a low signal of NIX/GL1 P-LISA signals in these cells (Fig 3C). Nevertheless, the transfection of the pEGFP-NIX vector and the overexpression of GFP-NIX in these cells, increased NIX/GL1 P-LISA signals confirming that these interactions are NIX-dependent (Fig 3C).

Altogether, these data demonstrated the feasibility and the specificity of P-LISA to detect specific autophagy protein interactions in BC cell models. Moreover, we showed that, in our models, the quantification of P-LISA signals is easier and more accurate than the quantification of co-localization signals in IF experiments.

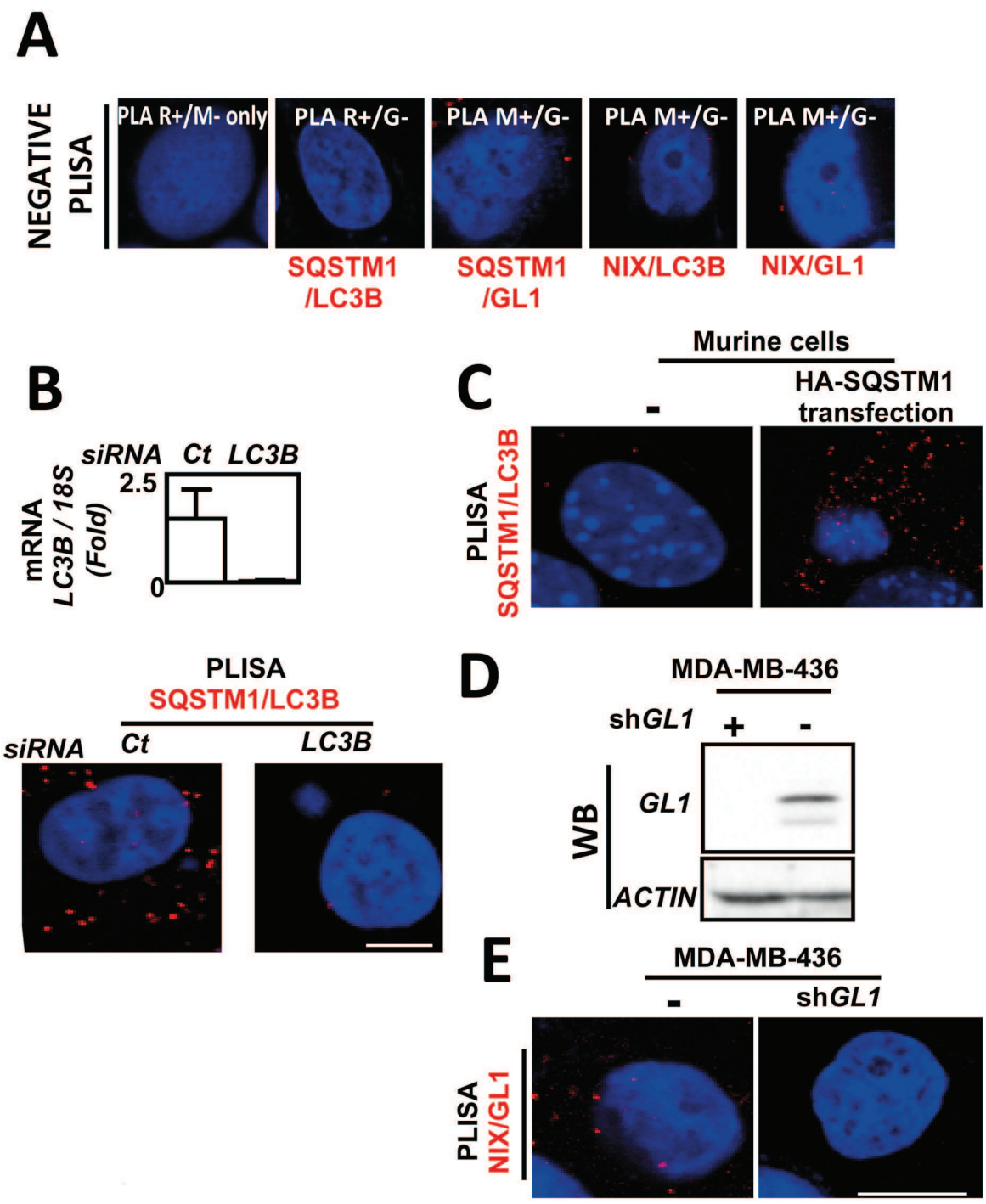

Fig 2. Technical controls demonstrating the specificity of P-LISA signals. (**A**) MDA-MB-436 cells were cultured for 24 h at 37°C and 5% CO_2. P-LISA were performed according to the manufacturer's recommendations. No primary antibodies were added before performing P-LISA with PLA R+ (anti-rabbit) and PLA M- (anti-mouse) (left panel); P-LISA SQSTM1/LC3B was also performed with PLA R+ (anti-rabbit) against LC3B and with PLA G- (anti-goat) unable to recognize SQSMT1 (left panel). Similar controls were performed for P-LISA SQSTM1/GL1, P-LISA LC3B/NIX and P-LISA GL1/NIX. (**B**) Quantification of *LC3B* mRNA expression in MDA-MB-436 cells following *LC3B* siRNA transfection analyzed using qRT-PCR (top panel). Quantification of SQSTM1/LC3 interactions detected by P-LISA in MDA-MB-436 cells transfected or not with *LC3B* siRNA (bottom panel) according to the manufacturer's recommendations using rabbit anti-LC3B and mouse anti-SQSTM1 antibodies. (**C**) Absence of SQSTM1/LC3B P-LISA signals in murine cells since the anti-SQSTM1 antibody is specific of the human SQSTM1 protein and restoration of P-LISA signals when these cells were transfected with a vector coding the human HA-SQSTM1 protein. (**D**) Absence of GL1 protein was validated using western blotting in MDA-MB-436 cells expressing or not a *GABARAPL1* shRNA (**E**) Quantification of

NIX/GL1 interactions was performed by P-LISA in MDA-MB-436 cells expressing or not a *GABARAPL1* shRNA using rabbit anti-GL1 and mouse anti-NIX antibodies.

doi:10.1371/journal.pone.0128701.g002

Quantification of SQSTM1/LC3B, SQSTM1/GL1, NIX/LC3B and NIX/GL1 specific interactions using P-LISA following autophagy flux inhibition

In order to analyze whether the autophagy protein interactions could be detected following autophagy induction using P-LISA and whether they were indeed associated to the formation of autophagosomes, we asked whether the signals obtained with SQSTM1/LC3B P-LISA, SQSTM1/GL1 P-LISA, NIX/LC3B P-LISA, or NIX/GL1 P-LISA co-localized with the fusion protein GFP-LC3 overexpressed in MDA-MB-436 cells. As expected, GFP-LC3 puncta significantly colocalized with all four P-LISA signals suggesting that these signals were related to autophagosomes (Fig 4A–4D). These conclusions were confirmed by the significant correlation index determined between the number of GFP-LC3B puncta and the SQSTM1/LC3B P-LISA signals ($p = 0.025$) (Fig 4A). However, due to the overexpression of GFP-LC3B in transfected cells, the strong increase of SQSTM1/LC3B P-LISA signals linked to large puncta in the cells was influenced by GFP-LC3 overexpression and not only by autophagy induction since expression of GFP-LC3B significantly increased SQSTM1/LC3B P-LISA signals in both the absence or presence of EBSS/BafA1 treatment in MDA-MB-436 cells (S2 Fig). Indeed, it has already been demonstrated that the overexpression of LC3B can induce the formation of cellular aggregates which could also include SQSTM1.[15] Taken together, these observations suggest that SQSTM1/LC3B P-LISA quantification of endogenous proteins interactions may be more accurate than overexpressed GFP-LC3B quantification for autophagy flux analysis. Similar experiments performed using SQSTM1/GL1 P-LISA revealed a very strong correlation between the number of GFP-LC3B vesicles and P-LISA signals ($p<0.0001$) (Fig 4B). These experiments were also performed using NIX/LC3B P-LISA or NIX/GL1 P-LISA and, once more, a significant co-localization between GFP-LC3-positive puncta and P-LISA signals were observed (Fig 4C, $p = 0.016$ and Fig 4D, $p = 0.005$).

P-LISA can be used to monitor selective autophagy

Following the demonstration that P-LISA can quantify differences in autophagosome formation, we next asked whether this technique might also help discriminating between responses to different autophagy inducers. Indeed, until now, none of the current techniques used to quantify autophagy may specifically and undoubtedly discriminate between non selective and selective autophagy. To do so, we decided to use P-LISA protocols including cargo adapters (such as NIX or SQSTM1) and ATG8 proteins (LC3B or GABARAPL1) since these proteins have been described to play an essential role in autophagy selectivity.[2,5]

In this assay, we treated MDA-MB-436 cells, described to express endogenous SQSTM1, LC3B, NIX and GL1, with different modulators of autophagy: i) rapamycin (Rapa), an autophagy inducer inhibiting mTOR activity; ii) rotenone (Rot), an inhibitor of oxidative phosphorylation complex I or, iii) CCCP (carbonyl cyanide m-chloro-phenyl hydrazone), an uncoupling agent. The two latter chemicals have been described to induce a mitochondrial stress and mitophagy.[23,24,25] As expected, using western-blotting, an increase of the autophagosome-linked LC3B form (LC3B-II) was observed following treatment with Rapa, BafA1, CQ, Rot and CCCP but we were unable to detect any significant differences in autophagy induction following these treatments using this technique (S3 Fig). To determine whether SQSTM1/LC3B, SQSTM1/GL1, NIX/LC3B and NIX/GL1 interactions are differentially modulated by these treatments,

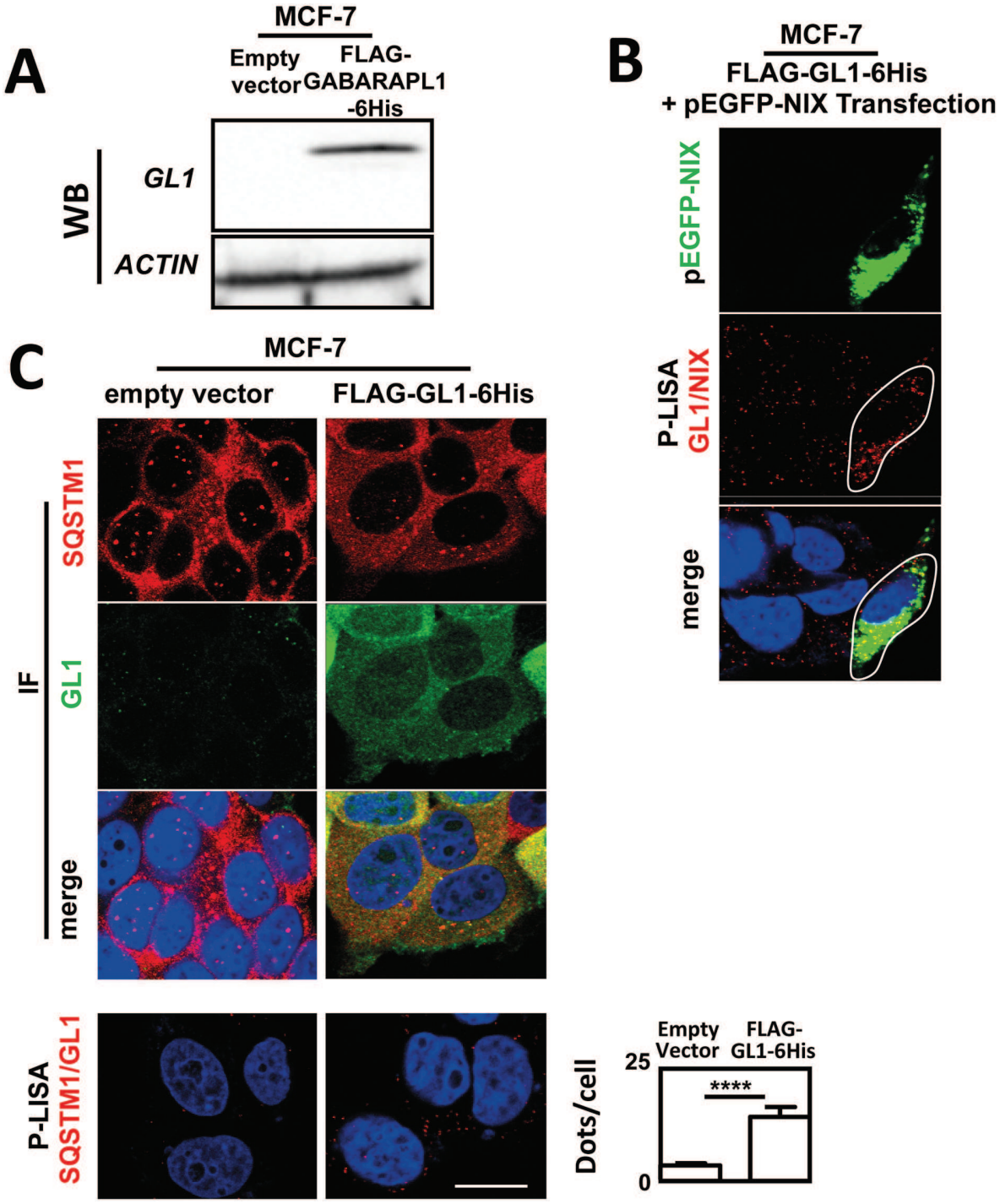

Fig 3. Increase of SQSTM1/GL1 and NIX/GL1 interactions quantified by P-LISA in MCF-7 overexpressing FLAG-GABARAPL1-6His and GFP-NIX. (A) Expression of GL1 protein was analyzed using western blotting in MCF-7 expressing or not FLAG-GL1-6His. (**B**) MCF-7 Control or MCF-7 FLAG-GL1-6His cells were cultured for 24 h at 37°C and 5% CO_2, fixed, permeabilized, blocked with 5% BSA, incubated with mouse anti-SQSTM1 and rabbit anti-GL1 antibodies antibodies overnight at 4°C and then with an Alexa Fluor 555 goat anti-mouse and an Alexa Fluor 488 goat anti-rabbit, respectively, for 1 h. The cells were then analyzed using a confocal microscope (top panel). For P-LISA, the protocol was performed according to the manufacturer's recommendations using mouse anti-SQSTM1 and rabbit anti-GL1 antibodies (bottom panel). (**C**) MCF-7 FLAG-GL1-6His cells were cultured for 24 h at 37°C and 5% CO_2 and transfected with pEGFP-NIX plasmid and then fixed and permeabilized. P-LISA was performed as precognized by the manufacturer using rabbit anti-GL1 and mouse anti-NIX antibodies. Nuclei were stained with DAPI. Each picture is representative of a typical cell staining observed in 10 fields chosen at random. Scale bar: 20μm.

doi:10.1371/journal.pone.0128701.g003

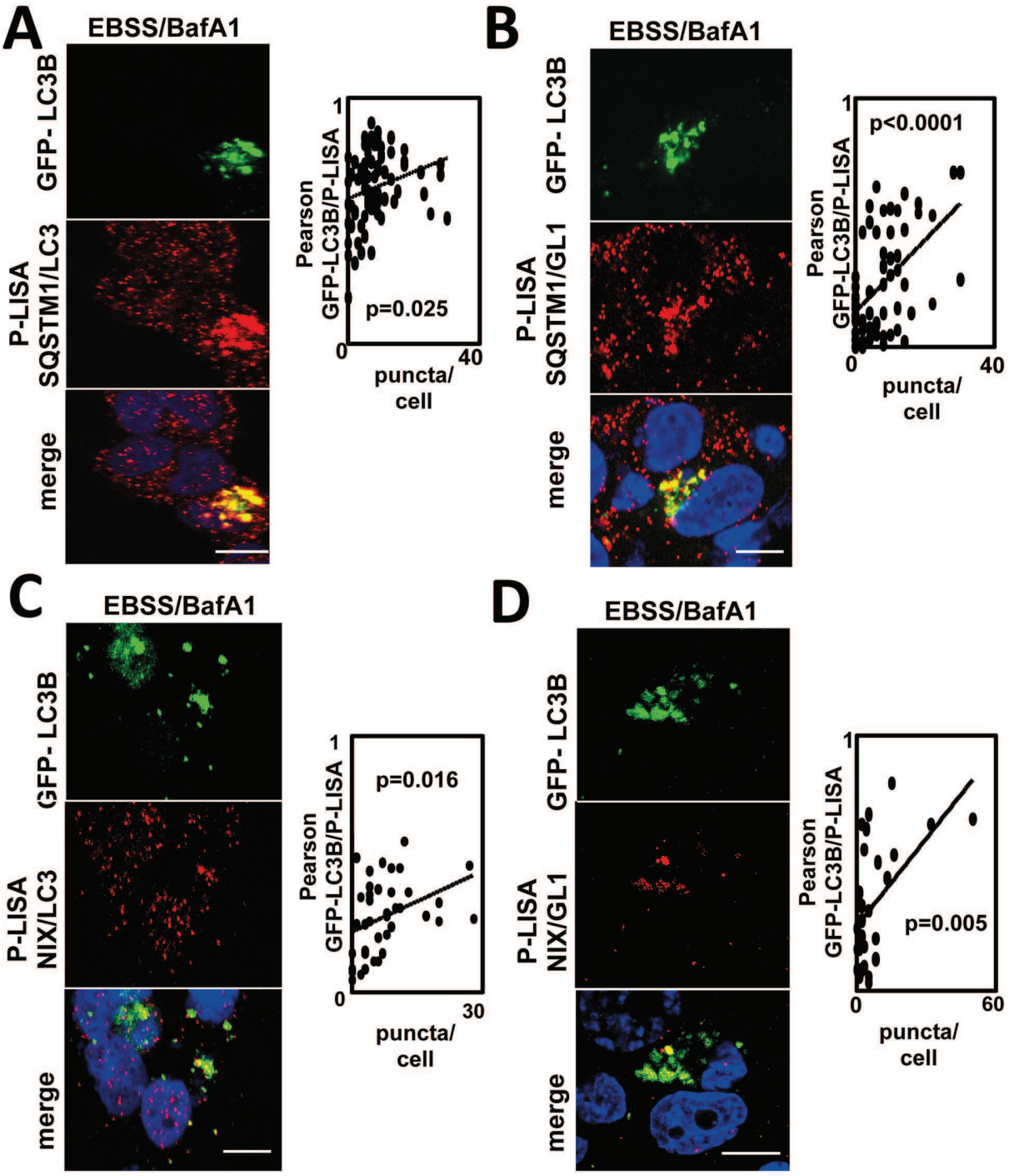

Fig 4. Co-localization of SQSTM1/LC3B, SQSTM1/GL1, NIX/LC3B and NIX/GL1 P-LISA signals with the GFP-LC3B protein. MDA-MB-436 cells were transfected with the pEGFP-LC3B vector then cultured with EBSS and BafA1 (100 nM) for 2 h. (**A**) Co-localization of SQSTM1/LC3B P-LISA signal and GFP-LC3B fluorescence. (**B**) Co-localization of SQSTM1/GL1 P-LISA signal and GFP-LC3B fluorescence. (**C**) Co-localization of NIX/LC3B P-LISA signal and GFP-LC3B fluorescence. (**D**) Co-localization of NIX/GL1 P-LISA signal and GFP-LC3B fluorescence. Co-localization of P-LISA signal and GFP-LC3B puncta was determined in at least 30 cells using the imageJ software. Nuclei were stained with DAPI. ****: $p \leq 0.0001$ and ***: $p \leq 0.001$, vs control (n = 3). Scale bar: 20μm.

doi:10.1371/journal.pone.0128701.g004

we quantified both the number of P-LISA signals as well as the intensity per dot in untreated and treated MDA-MB-436 cells (Fig 5). Since autophagic vesicles frequently accumulate in clusters, the result is a partial or total overlap of the P-LISA signals. This explains why close interactions could not be independently quantified. However, this concentration of signals in the same area of the cell led to the increase of intensity per dot and this parameter is therefore useful to quantify autophagy since a strong increase of intensity per dot, without an apparent increase of dots per cell, also corresponds to a significant increase in ATG/cargo adapter interactions which are preferentially concentrated in specific punctates.

All treatments significantly increased SQSTM1/LC3B P-LISA signals (Fig 5A and 5E) suggesting an accumulation of autophagosomes in the cells. Moreover, SQSTM1/LC3B PLISA intensity per dot was also increased following exposure to the three autophagy inducers suggesting a relocalization of SQSTM1/LC3B interactions in these vesicles. Although the increase of intensity per dot is quite similar (about 1.5 to 2 fold) following treatment with the different autophagy inducers, the highest increase in intensity per dot and the lowest increase in dots per cell was obtained after Rapa treatment whereas the lowest increase in intensity per dot and the highest increase in dots per cell was induced by CCCP. These results suggest that these three autophagy inducers increased SQSTM1/LC3B interactions but that SQSTM1/LC3B interactions are more concentrated in specific areas of the cells following Rapa treatment.

CCCP and Rot treatments led to the highest increase in SQSTM1/LC3B P-LISA signals. As expected, transfection of *LC3B* siRNA extinguished SQSTM1/LC3B P-LISA signals in cells treated with CCCP demonstrating, once again, the specificity of these signals (S4 Fig). On the opposite, no variations in the number of SQSTM1/GL1 P-LISA signals were observed following the different treatments (Fig 5B and 5E). Interestingly, when we analyzed the interactions involving NIX, an autophagy adaptor described to be involved in mitophagy, we only observed an increase in P-LISA signals following treatments using specific mitochondrial stress inducers (Fig 5C, 5D and 5E).

Altogether, our P-LISA experiments led to the conclusion that NIX/GL1 and LC3B/NIX P-LISA can be used to specifically monitor mitophagy while SQSTM1/LC3B P-LISA, but not SQSTM1/GL1 P-LISA, is more suitable to study overall autophagy levels.

Discussion

Whereas autophagy quantification is a crucial point when studying autophagy or biological pathways regulating autophagy, end-points analysis remain often difficult to interpret due to the dynamic autophagy flux which corresponds to the sum of initiation and degradation. Several methods have been developed by the "autophagy community" to quantify autophagy but western-blotting of SQSTM1 and LC3B-II moieties still remains the most popular experiment to estimate autophagy.[12] However, some recent data showing the frequent transcriptional up-regulation of *SQSTM1* following different autophagy-inducing stresses have demonstrated that the levels of this protein cannot exclusively be linked to autophagy degradation anymore.[26]

Quantification of fluorescent vesicles following pGFP-LC3B or pmRFP-LC3B expression is also considered as a powerful tool useful for autophagy quantification but is limited to cells in culture. Moreover, fluorescence intensities of the GFP or mRFP reporter proteins are difficult to quantify due to variable levels of expression in transfected cells. In addition, some cells remain difficult to transfect and autophagy flux could not be analyzed using this protocol. Moreover, it has been shown that overexpression of GFP-LC3B can induce the formation of aggregates independent of its role in autophagy.[15,27] More recently, the development of a new vector called ptf-LC3B leading to the expression of a double-tagged GFP-RFP-LC3B

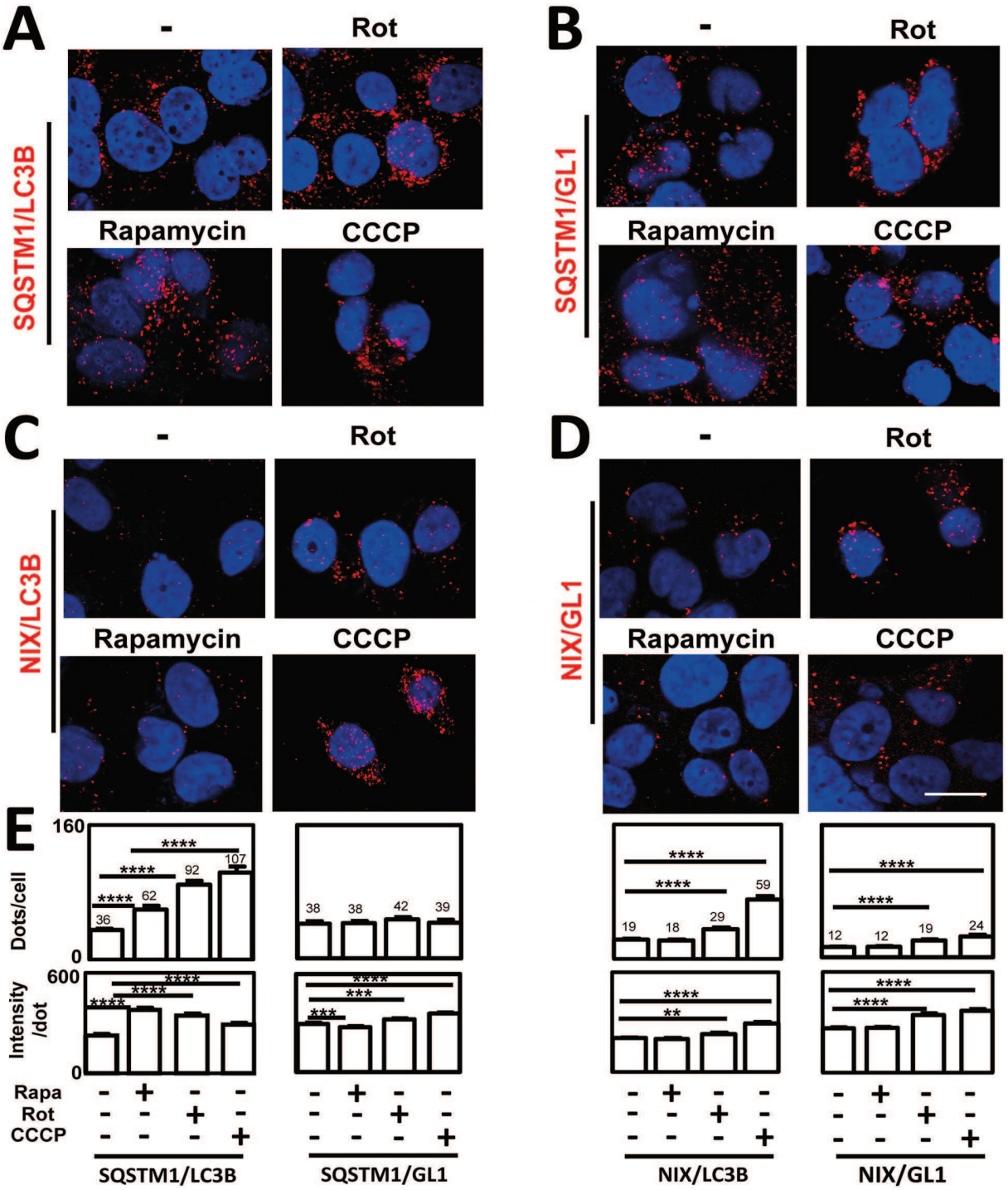

Fig 5. Effects of Rapamycin, Rotenone and CCCP on ATG8/cargo adapter interactions. MDA-MB436 cells were cultured for 24 h at 37°C and 5% CO_2 then with Rapa (10 μM for 5h), Rot (50 μM for 24h) or CCCP (100 μM for 24h). (**A**) SQSTM1/LC3B, (**B**) SQSTM1/GL1, (**C**) NIX/LC3B and (**D**) NIX/GL1 P-LISA were performed according to the manufacturer's recommendations using mouse anti-NIX or anti-SQSTM1 and rabbit anti-GL1 or anti-LC3B antibodies. Nuclei were stained with DAPI. Each picture is representative of a typical cell staining observed in 10 fields chosen at random. (**E**) Quantification of P-LISA signals (dots/cell and intensity per dot) was performed using the Blobfinder software. Each bar (Mean ± SEM) represents the mean obtained from the quantification of signals observed in about 200 cells chosen randomly in 5 different fields from 3 independent experiments. ****: $p \leq 0.0001$, ***: $p \leq 0.0001$, and **: $p \leq 0.001$, vs control. Scale bar: 20μm.

doi:10.1371/journal.pone.0128701.g005

protein has helped in the study of autophagy flux. Indeed, this recombinant protein allows to distinguish between autophagosomes and autophagolysosomes. Nevertheless, the quantification of red and yellow dots still remains difficult to perform in cells and this protocol is still linked to the necessity of high transfection rates. Moreover, co-localization of this double fluorescent protein with other ATG proteins remains almost impossible to interpret. These data strongly suggest that autophagy should be analyzed by a combination of protocols and techniques.

Recent new data have also demonstrated that autophagy can be non selective or selective and that these two processes might require different autophagy proteins in the cells. For example, some specific ATGs or autophagy-related proteins, such as NIX, have been described to be specifically involved in selective autophagy of mitochondria, called mitophagy. Therefore, in order to improve the quantification of autophagy and to better discriminate between non selective or selective autophagy, we developed a P-LISA protocol to specifically monitor ATG8/cargo adapter interactions. First we asked whether this technique could be used to quantify cellular autophagy levels and, then, to discriminate between different types of induced autophagy. Indeed, the currently available techniques are preferentially used to quantify autophagic flux (WB, IF) and are not always sensitive enough to quantify slight modifications of autophagy levels. Our data confirmed that the SQSTM1/LC3B and SQTSM1/GL1 P-LISA signals detected in the cells were indeed specifically related to autophagy as demonstrated by their strong co-localization with GFP-LC3B vesicles in autophagy-induced cells following an EBSS/BafA1 treatment. Then, our data led to the conclusion that SQSTM1/LC3B interactions measured by P-LISA were increased in all treatments described to induce autophagy and might be used to quantify overall autophagy rates. On the opposite, NIX/GL1 and NIX/LC3B P-LISA appeared to be useful to discriminate between rapa-induced autophagy and specific degradation of mitochondria and therefore might be used to quantify selective mitophagy.

In conclusion, our work proves that P-LISA can be used as a new tool for autophagy quantification and for the discrimination between different induced selective autophagy. Moreover, since this technique can be adapted to the study of protein interactions in parrafine-included tissue samples or *in vivo* biological tissues, this technique could become an useful tool to perform diagnostic test targeting endogenous autophagy proteins.[28]

Supporting Information

S1 Fig. Schematic representation of the P-LISA protocol. (A) Two primary antibodies issued from distinct species recognize specific endogenous ATG proteins supposed to interact. (B) Secondary antibodies called Proximity Ligation Assay (PLA) probes, each coupled to an oligonucleotide + or an oligonucleotide—, recognize the two primary antibodies. (C) A circular probe targets the PLA + and—, only if the distance between these probes is less than 40nm. (D) Circular DNA is amplified by a DNA polymerase. (E) DNA probes coupled to fluorochromes hybridize to amplicons and lead to the formation of intracellular fluorescent dots specific to the interaction of the two ATG proteins.
(TIF)

S2 Fig. Effect of EBSS/BafA1 treatment and influence of GFP-LC3B expression on SQSTM1/LC3B P-LISA signals. MDA-MB-436 cells were transfected with the pEGFP-LC3B vector then treated or not with EBSS and BafA1 (100 nM) for 2 h (left panel). SQSTM1/LC3B P-LISA signals were quantified in about 20 cells (right panel). Nuclei were stained with DAPI. ****: $p \leq 0.0001$ and **: $p \leq 0.01$.
(TIF)

S3 Fig. Effects of Rapamycin, BafA1, CQ, Rotenone and CCCP on LC3B-II levels. MDA-MB436 cells were cultured for 24 h at 37°C and 5% CO_2 then treated with Rapa (10 μM for 5h, BafA1 (100 nM for 2h), Chloroquin (40 μM for 2h)), Rot (50 μM for 24h), or CCCP (100 μM for 24h). Accumulation of the LC3B-II form was determined by western blotting using an anti-LC3B antibody.
(TIF)

S4 Fig. SQSTM1/LC3B P-LISA in cells transfected with *siLC3B* and treated with CCCP. MDA-MB-436 cells were cultured for 24 h at 37°C and 5% CO_2 and treated with CCCP (100 μM for 24h). P-LISA was performed according to the manufacturer's recommendations. Inhibition of SQSTM1/LC3B P-LISA signals was observed in cells previously transfected with *siLC3B* compared to cells transfected with a *siRNA* control, Nuclei were stained with DAPI. Each picture is a representative image of a typical cell staining observed in 10 fields chosen at random.
(TIF)

Acknowledgments

This work was suported by the University of Franche-Comté, "Ministère de l'Enseignement Supérieur et de la Recherche" (MESR) and fundings from "Région de Franche-Comté" 2013 and CCIR-GE "Ligue Contre le Cancer" 2014 (#007.Y-2014). AT was supported by a fellowship of "Région de Franche-Comté".

Author Contributions

Conceived and designed the experiments: EH MBG. Performed the experiments: TG ACT EH. Analyzed the data: TG ACT EH MBG RDM. Wrote the paper: EH MBG.

References

1. Weidberg H, Shvets E, Shpilka T, Shimron F, Shinder V, et al. (2010) LC3 and GATE-16/GABARAP subfamilies are both essential yet act differently in autophagosome biogenesis. EMBO J 29: 1792–1802. doi: 10.1038/emboj.2010.74 PMID: 20418806
2. Novak I, Kirkin V, McEwan DG, Zhang J, Wild P, et al. (2010) Nix is a selective autophagy receptor for mitochondrial clearance. EMBO Rep 11: 45–51. doi: 10.1038/embor.2009.256 PMID: 20010802
3. Deosaran E, Larsen KB, Hua R, Sargent G, Wang Y, et al. (2013) NBR1 acts as an autophagy receptor for peroxisomes. J Cell Sci 126: 939–952. doi: 10.1242/jcs.114819 PMID: 23239026
4. Gibbings D, Mostowy S, Jay F, Schwab Y, Cossart P, et al. (2012) Selective autophagy degrades DICER and AGO2 and regulates miRNA activity. Nat Cell Biol 14: 1314–1321. PMID: 23143396
5. Kirkin V, Lamark T, Johansen T, Dikic I (2009) NBR1 cooperates with p62 in selective autophagy of ubiquitinated targets. Autophagy 5: 732–733. PMID: 19398892
6. Noda NN, Ohsumi Y, Inagaki F (2010) Atg8-family interacting motif crucial for selective autophagy. FEBS Lett 584: 1379–1385. doi: 10.1016/j.febslet.2010.01.018 PMID: 20083108
7. Behrends C, Sowa ME, Gygi SP, Harper JW (2010) Network organization of the human autophagy system. Nature 466: 68–76. doi: 10.1038/nature09204 PMID: 20562859
8. Takahashi Y, Young MM, Serfass JM, Hori T, Wang HG (2013) Sh3glb1/Bif-1 and mitophagy: acquisition of apoptosis resistance during Myc-driven lymphomagenesis. Autophagy 9: 1107–1109. doi: 10.4161/auto.24817 PMID: 23680845
9. Liang C, Feng P, Ku B, Dotan I, Canaani D, et al. (2006) Autophagic and tumour suppressor activity of a novel Beclin1-binding protein UVRAG. Nat Cell Biol 8: 688–699. PMID: 16799551
10. Liang XH, Jackson S, Seaman M, Brown K, Kempkes B, et al. (1999) Induction of autophagy and inhibition of tumorigenesis by beclin 1. Nature 402: 672–676. PMID: 10604474
11. Nixon RA (2013) The role of autophagy in neurodegenerative disease. Nat Med 19: 983–997. doi: 10.1038/nm.3232 PMID: 23921753

12. Klionsky DJ, Abdalla FC, Abeliovich H, Abraham RT, Acevedo-Arozena A, et al. (2012) Guidelines for the use and interpretation of assays for monitoring autophagy. Autophagy 8: 445–544. PMID: 22966490
13. Nyfeler B, Bergman P, Wilson CJ, Murphy LO (2012) Quantitative visualization of autophagy induction by mTOR inhibitors. Methods Mol Biol 821: 239–250. doi: 10.1007/978-1-61779-430-8_14 PMID: 22125069
14. Larsen KB, Lamark T, Overvatn A, Harneshaug I, Johansen T, et al. (2010) A reporter cell system to monitor autophagy based on p62/SQSTM1. Autophagy 6: 784–793. PMID: 20574168
15. Ciechomska IA, Tolkovsky AM (2007) Non-autophagic GFP-LC3 puncta induced by saponin and other detergents. Autophagy 3: 586–590. PMID: 17786021
16. Boyer-Guittaut M, Poillet L, Liang Q, Bole-Richard E, Ouyang X, et al. (2014) The role of GABARAPL1/GEC1 in autophagic flux and mitochondrial quality control in MDA-MB-436 breast cancer cells. Autophagy 10: 986–1003. doi: 10.4161/auto.28390 PMID: 24879149
17. Ding WX, Ni HM, Li M, Liao Y, Chen X, et al. (2010) Nix is critical to two distinct phases of mitophagy, reactive oxygen species-mediated autophagy induction and Parkin-ubiquitin-p62-mediated mitochondrial priming. J Biol Chem 285: 27879–27890. doi: 10.1074/jbc.M110.119537 PMID: 20573959
18. Allalou A, Wahlby C (2009) BlobFinder, a tool for fluorescence microscopy image cytometry. Comput Methods Programs Biomed 94: 58–65. doi: 10.1016/j.cmpb.2008.08.006 PMID: 18950895
19. Pankiv S, Clausen TH, Lamark T, Brech A, Bruun JA, et al. (2007) p62/SQSTM1 binds directly to Atg8/LC3 to facilitate degradation of ubiquitinated protein aggregates by autophagy. J Biol Chem 282: 24131–24145. PMID: 17580304
20. Shvets E, Abada A, Weidberg H, Elazar Z (2011) Dissecting the involvement of LC3B and GATE-16 in p62 recruitment into autophagosomes. Autophagy 7: 683–688. PMID: 21460636
21. Pankiv S, Lamark T, Bruun JA, Overvatn A, Bjorkoy G, et al. (2010) Nucleocytoplasmic shuttling of p62/SQSTM1 and its role in recruitment of nuclear polyubiquitinated proteins to promyelocytic leukemia bodies. J Biol Chem 285: 5941–5953. doi: 10.1074/jbc.M109.039925 PMID: 20018885
22. Buckingham EM, Carpenter JE, Jackson W, Grose C (2014) Nuclear LC3-positive puncta in stressed cells do not represent autophagosomes. Biotechniques 57: 241–244. doi: 10.2144/000114226 PMID: 25399676
23. Joselin AP, Hewitt SJ, Callaghan SM, Kim RH, Chung YH, et al. (2012) ROS-dependent regulation of Parkin and DJ-1 localization during oxidative stress in neurons. Hum Mol Genet 21: 4888–4903. doi: 10.1093/hmg/dds325 PMID: 22872702
24. Chu CT, Bayir H, Kagan VE (2014) LC3 binds externalized cardiolipin on injured mitochondria to signal mitophagy in neurons: implications for Parkinson disease. Autophagy 10: 376–378. doi: 10.4161/auto.27191 PMID: 24351649
25. Park S, Choi SG, Yoo SM, Son JH, Jung YK (2014) Choline dehydrogenase interacts with SQSTM1/p62 to recruit LC3 and stimulate mitophagy. Autophagy 10: 1906–1920. doi: 10.4161/auto.32177 PMID: 25483962
26. (2014) p62 Loss Reprograms Stromal Metabolism to Promote Tumor Growth. Cancer Discov 4: OF17. doi: 10.1158/2159-8290.CD-RW2014-196 PMID: 25367958
27. Korkhov VM (2009) GFP-LC3 labels organised smooth endoplasmic reticulum membranes independently of autophagy. J Cell Biochem 107: 86–95. doi: 10.1002/jcb.22103 PMID: 19259979
28. Soderberg O, Gullberg M, Jarvius M, Ridderstrale K, Leuchowius KJ, et al. (2006) Direct observation of individual endogenous protein complexes in situ by proximity ligation. Nat Methods 3: 995–1000. PMID: 17072308

Hervouet et al. BMC Cancer (2015) 15:729
DOI 10.1186/s12885-015-1761-4

BMC Cancer

RESEARCH ARTICLE Open Access

The autophagy *GABARAPL1* gene is epigenetically regulated in breast cancer models

Eric Hervouet[1*], Aurore Claude-Taupin[1], Thierry Gauthier[1], Valérie Perez[1], Annick Fraichard[1], Pascale Adami[1], Gilles Despouy[1], Franck Monnien[2], Marie-Paule Algros[2], Michèle Jouvenot[1], Régis Delage-Mourroux[1] and Michaël Boyer-Guittaut[1]

Abstract

Background: The GABARAP family members (GABARAP, GABARAPL1/GEC1 and GABARAPL2 /GATE-16) are involved in the intracellular transport of receptors and the autophagy pathway. We previously reported that *GABARAPL1* expression was frequently downregulated in cancer cells while a high *GABARAPL1* expression is a good prognosis marker for patients with lymph node-positive breast cancer.

Methods: In this study, we asked using qRT-PCR, western blotting and epigenetic quantification whether the expression of the *GABARAP* family was regulated in breast cancer by epigenetic modifications.

Results: Our data demonstrated that a specific decrease of *GABARAPL1* expression in breast cancers was associated with both DNA methylation and histone deacetylation and that CREB-1 recruitment on *GABARAPL1* promoter was required for *GABARAPL1* expression.

Conclusions: Our work strongly suggests that epigenetic inhibitors and CREB-1 modulators may be used in the future to regulate autophagy in breast cancer cells.

Keywords: Autophagy, GABARAP, GABARAPL1, GABARAPL2, Breast cancer, CREB-1, DNA methylation, Epigenetics

Background

Autophagy is a cell process which regulates cell homeostasis and survival by inducing the degradation and recycling of intracellular components like protein aggregates or organelles (such as damaged mitochondria) [1]. This mechanism involves more than 40 proteins required for : i) the formation of autophagosomes, ii) the fusion of autophagosomes with lysosomes and/or, iii) the regulation of autophagy flux. The role of autophagy in tumorigenesis is controversial, even though evidence indicated that autophagy is often downregulated in cancer cells. On one hand, autophagy might protect against transformation of non tumoral cells into cancer cells and in the other hand, a loss of autophagy might help the cancer cells to escape from type II cell death (also called autophagy cell death) [2, 3]. Since induction of autophagy in cancer cells has also been described to confer resistance to chemotherapeutive agents, the co-administration of both alkyling agents and autophagy inhibitors (such as hydroxychloroquine) could improve the anti-tumoral response in these resistant cells [4]. Among the proteins involved in autophagy, two subfamilies of homologs of the yeast Atg8 (Autophagy-related 8) have been described in mammals: i) the MAP-LC3s (Microtubule-associated protein Light Chain 3) including LC3A, LC3B and LC3C and, ii) the GABARAP ($GABA_A$-receptor-associated protein) family. The latter comprises 3 members: GABARAP, GABARAPL1/GEC1/ATG8L (GABARAP-like protein 1/guinea-pig endometrial glandular epithelial cells-1/Atg8-like protein) and GABARAPL2/GATE-16 (GABARAP-like protein 2/Golgi-associated ATPase enhancer of 16 kDa).

* Correspondence: eric.hervouet@univ-fcomte.fr
[1]Université de Franche-Comté, Laboratoire de Biochimie, EA3922 « Estrogènes, Expression Génique et Pathologies du Système Nerveux Central », SFR IBCT FED4234, UFR Sciences et Techniques, 16 route de Gray, 25030 Besançon Cedex, France
Full list of author information is available at the end of the article

GABARAP, *GABARAPL1* and *GABARAPL2* genes are located on the human chromosomes, 17p13.12, 12p12.3 and 16q22.3 respectively, and are differentially expressed in normal and pathological tissues. The *GABARAP* gene has been described to be highly expressed in endocrine tissues while the *GABARAPL1* gene is predominantly expressed in the central nervous system but they both are underexpressed in a large variety of cancer cell lines [5]. Nevertheless, the analysis of *GABARAPL1* expression in a cohort of 256 breast adenocarcinoma revealed that a low *GABARAPL1* expression was correlated with a high risk of metastasis, in particular for lymph node-positive patients [6]. Despite these recent studies, the regulation of the *GABARAP* family is still poorly understood and the origin of their decreased expression in tumor models remains unknown.

It is now recognized that epigenetic modifications control the expression of numerous genes *via* the regulation of promoter accessibility to transcriptional factors. Both DNA methylation and histone modifications affect the level of chromatin compaction and it has been described that epigenetically-mediated aberrant silencing of genes are an important factor in the pathogenesis of cancers including breast cancers (BC) [7, 8] Indeed, epigenetic modifications can regulate the expression of a large panel of genes involved in the hallmarks of cancer, such as apoptosis, cell signaling, invasion and proliferation. For example, the detection of the promoter methylation of the tumor suppressor gene *BRCA1*, which is frequent in BC and is associated with a decrease of *BRCA1* expression, can help to predict the response to conventional chemotherapies in triple negative BC patients [9]. DNA methylation consists on the addition of a methyl group on a cytosine in CpG islands. It is catalyzed by DNA methyl transferases (DNMTs) and is unfavorable to transcription. Following DNA replication and formation of hemi-methylated DNA, the conservation of DNA methylation on the neo-synthesized strand, is mainly processed by DNMT1 using the parental strand as a model. This DNA methylation conservation is called maintaining or inheritance DNA methylation. On the opposite, *de novo* DNA methylation referred to the addition of DNA methylation on both strands of DNA on previously unmethylated loci is catalyzed by both DNMT3A and DNMT3B.

Besides DNA methylation, post-translational modifications of histones are also frequently associated to the regulation of gene expression in cancers. Histones are associated as octamers in nucleosomes (dimer of H2A, H2B, H3 and H4 and a loop of 126 pb DNA) whose compaction is regulated by post-translational modifications such as phosphorylation, methylation or acetylation. The local sum of these modifications is called the histone code and determine the status of local chromatin compaction (for a review see [10]). Histone methyl transferases (HMTs) or histone demethylases (HDMs) respectively catalyze the methylation or demethylation of histones leading to different effects on transcription. For example, H3K9me or K3K27me are negative marks while H3K4me is favorable to transcription. Acetylation, the most studied histone modification, is processed by histone acetyl transferases (HATs) and is associated with a local relaxed chromatin and is therefore favorable to gene expression. On the opposite, the removal of acetyl groups from histones, which is catalyzed by histone deacetylases (HDACs), contributes to gene silencing.

Some recent studies also revealed that epigenetic modifications can regulate autophagy gene expression as well as autophagy levels in both normal and cancer cells. For example, HDACs play an essential role in the regulation of autophagy: HDAC1 inhibition favors the conversion of the soluble LC3B form (LC3B-I) to the membrane-bound form of LC3B (LC3B-II), while the presence of H4K16ac (catalyzed by hMOF (human ortholog of drosophila males absent in the first)) in some *ATGs* genes, is associated to a decrease of expression of these genes [11, 12]. Moreover, HDAC6, an HDAC mainly localized in the cytosol, has also been described to be involved in the transport and maturation of autophagosomes [13]. DNA methylation is also involved in autophagy regulation as hypermethylation of several *ATG* genes has been described in various cancers [13, 14]. For example, methylation of *BECN-1*, a tumor suppressor gene, has been observed in BC, while methylation of *ATG16L2*, *LC3A*, *ULK2*, or *BNIP3* has been suggested to be involved in the down-regulation of autophagy in other cancers [15–19].

In order to characterize the regulation of *GABARAP* gene family expression in cancer cells, we analyzed their expression and the epigenetic modifications in the promoters of these genes in *in vitro* human BC cell models. Our data demonstrated that *GABARAPL1* expression is decreased in BC patients and BC cell line models. Moreover, both DNA methylation and deacetylation of histone H3 in *GABARAPL1* promoter were observed in these BC cell line models while the inhibition of DNMTs and HDACs using specific inhibitors restored *GABARAPL1* expression in these cells. These data suggest that DNMTi (DNMT inhibitors) and HDACi (HDAC inhibitors) could be used in the future to modulate autophagy levels in BC cells.

Methods

Ethic statement

Human samples were collected according to French laws and the recommendations of the French National Committee of Ethics. Indeed, this study has been approved by of the scientific committee of "the tumorothèque régionale de Franche-Comté BB-0033-00024". The samples and the medical history of patients were encoded to protect

patients confidentiality and used under protocols approved by the recommendations of the French national Committee of Ethics. All human samples were collected by Pr. Severine Valmary-Degano (Centre Hospitalo-Universitaire, Besançon, France) at the "Tumorothèque régionale de Franche-Comté BB-0033-00024". Collection of samples and their use (AC-2010-1163) for studies (approved by the scientific committee of "the tumorothèque régionale de Franche-Comté BB-0033-00024") have been approved by the French "ministère de la recherché" and by the CPP EST II.We obtained all necessary consents from any patients involved in the study.

Quantitative RT-PCR

RNA was isolated from cells and frozen tissues using Tri Reagent (Molecular Research Center, TR-118) as described by the manufacturer. Reverse transcription were performed using M-MLV (Sigma-Aldrich, M-1302) reverse transcriptase and 1.5 μg total RNA according to manufacturer's instructions (Sigma-Aldrich). Quantitative PCR (qPCR) were done in duplicate using the Step one Real-Time PCR system (Applied Biosystems), Power SYBR Green PCR Master Mix (Applied Biosystems, 4367659), according to manufacturer's instructions and primers specific of *GABARAP* (F: 5′-GCCTTTCCCATCCTGCTGTA-3′ and R: 5′-AGGAGGGGATTGCTGGGTTCT-3′) ; *GABARAPL1* (F: 5′-CCCTCCCTTGGTTATCATCCA-3′ and R: 5′-ACTCCCACCCCACAAAATCC-3′) and *GABARAPL2* (F: 5′-AAATATCCCGACAGGGTTCC-3′ and R: 5′-CAG GAAGATCGCCTTTTCAG-3′). *H3B2* was used as an housekeeping gene (F: 5′-GCTAGCTGGATGTCTTTT GG-3′ and R: 5′-GTGGTAAAGCACCCAGGAA-3′) as previously described [20].

Cell culture

MCF-7 and MDA-MB-453 cell lines were obtained from ATCC (HTB-130 and HTB-22) and grown in DMEM 1 g/L glucose (Dominique Dutscher, L0066) containing fetal calf serum (5 %) (Dominique Dutscher, S1810), penicillin (50 U/ml) (Dominique Dutscher, L0018), streptomycin (50 μg/ml), and amphotericin B (1.25 μg/ml) (PAA, P11-001) at 37 °C in 5 % CO_2, and routinely used at 70–80 % confluence. When indicated, cells were exposed to 2 μM 5-aza-CdR (A3656, Sigma-Aldrich) for 48 h and 400 nM TSA (T8552, Sigma-Aldrich) for 16 h.

Luciferase activity

GABARAPL1 promoter fragments were obtained by PCR using the following primers–336 F: 5′-GCTGGATCCC AACCAGCAGGA-3′, –659 F: 5′-GTCAGGCTGGTCTC GAACTC-3′ and +241 R: 5′-GGGATGCACCGCAGGG CTTCC-3′ and then cloned into the pGL3 basic plasmid. 5000 cells were seeded in 96 multiwell dishes and cells were transfected with pGL3 plasmids, co-transfected with the pCDNA3.1-CREB-1 vector (kindly provided by Vincent Coulon, Montpellier, France) or treated with 10 μM forskolin. Luciferase expression was measured using the Luciferase Assay System kit (E1500, Promega) according to the manufacturer's recommendations.

Epigenetics

gDNA was extracted using the NucleoSpin® Tissue kit (740952, Macherey Nagel). Global DNA methylation was quantified using the MethylFlash methylated DNA quantification kit (P-1034, Epigentek, France). Methyl DNA collection were performed using the "Methyl-Collector Ultra kit" (55005, Active Motif). Histone 3 acetylation was quantified using the EpiQuik Tissue Acetyl-Histone H3 ChIP Kit (P-2012, Epigentek). ChIP was performed using the ChIP-IT High Sensitivity kit (53040, Active Motif) with ChIP grade antibodies (Table 1). All these kits were used according to the manufacturer's instructions. Primers used in this study were designed with the primer3 software [21]: *GABARAP* (F: 5′-AAAGCCAACC GTCTTTGCTA-3′ and R: 5′-GCCACTTCCCTATTCAC-CAA-3′), *GABARAPL1* (MC1 F: 5′-GTCAGGCTGGTC TCGAACTC-3′ and R: 5′-CGCTCCTGAACAGCAACA TA-3′) and *GABARAPL1* (MC2 F: 5′-AAGGAAACGCA GTGAGACAGA-3′ and R: 5′-AGCTGGGAGCACAAAA ACAG-3′), *GABARAPL2* (F: 5′AATTCCCCAGACTTCCC CTA-3′ and R: 5′-GGTGGCGAAGAAGTTGGTTA-3′).

Western-blotting

Cells were scraped, harvested and lysed in RIPA buffer (50 mM Tris–HCl, pH 8, 150 mM NaCl, 1 % Triton ×100, 0.5 % DOCA, 0.1 % SDS) supplemented with protease inhibitors (104 mM AEBSF, 1.5 mM pepstatin A,

Table 1 List of antibodies

Antibody	Application	Dilution	Manufacturer	Ref
GABARAP/GABARAPL1	WB	1:3000	(Millipore, France)	#AB15278
GABARAPL2	WB	1:1000	(Proteintech, France)	#18727-AP
ACTIN	WB	1:3000	(Sigma-Aldrich, France)	#A5060
CREB-1	IF/ChIP	1:50/1 μg	(Santa-Cruz Biotechnology, France)	#sc-374227
DNMT1	ChIP	1 μg	(Active Motif, Belgium)	#39204
HDAC1	ChIP	1 μg	(Active Motif, Belgium)	#40967

1.4 mM E-64, 4 mM bestatin, 2 mM leupeptin, 80 μM aprotinin) for 30 min on ice, sonicated for 15 sec and centrifuged at 10 000 g for 10 min at 4 °C. Supernatant was used for protein quantification using the Bradford method [22] and then proteins (40 μg) were separated using SDS-PAGE gels and transferred to PVDF membranes (Bio-Rad, 162–0177) for 2 h in Tris-Glycine buffer as previously described [23]. Membranes were saturated in 0.1 % TBS-Tween 20 and 5 % nonfat milk for 1 h and then incubated with primary antibodies (Table 1) overnight at 4 °C. Membranes were washed 3 times with TBS-Tween 20 0.1 %, incubated with secondary anti-rabbit HRP conjugate or anti-mouse HRP conjugate antibody according to manufacturer's instructions (P.A.R.I.S., BI2407 and BI2413C). The membrane was washed 3 times with TBS-0.1 % Tween 20 incubated with ECL revelation buffer (Pierce) and cheluminescence was monitored using a ChemiDoc^{TM}XRS+ (Biorad).

Immunofluorescence

CREB-1 IF was performed as precognized by the manufacturer. Briefly, cells were seeded on coverslips in 24 multiwell-plates, fixed and permeabilized for 20 min with cold methanol at−20 °C, washed 3 times with cold PBS (Phosphate buffer saline : 137 mM NaCl, 2.7 mM KCl, 10 mM Na_2HPO_4, 2 mM KH_2PO_4), incubated with 1 % BSA-PBS for 1 h at 37 °C and incubated overnight with the CREB-1 antibody (Table 1). The coverslips were washed 3 times for 5 min with 0.1 % Tween-PBS (T-PBS), incubated for 1 h with a goat secondary anti-mouse Alexa 555 antibody (Life technology, France) and washed 3 times for 5 min with (T-PBS). Cells were then mounted in Vectashield Hardset mounting medium (Vector Laboratories, H-1000) and analyzed using an Olympus IX81 confocal microscope (Olympus, France).

Statistics

Mean's comparison were analyzed using a Student t-test with GraphPad Prism5 software (USA). Correlation indexes were measured using a Spearman test with ImageJ software. Significant values were highlighted in bold in each figure.

Results

GABARAP family genes are differentially expressed in human breast cancer biopsies

We first analyzed *GABARAP*, *GABARAPL1* or *GABARAPL2* mRNA expression in human BC biopsies using qRT-PCR (Fig. 1). The different BC subtypes are classified in regard of their molecular marker expression. Luminal BC, which represent 50 % of total BC and generally associated with a good prognosis, are divided in Luminal A and Luminal B BC. Both Luminal A and B BC express ERα (estrogen receptor: ER+) whereas the expression of the *HER2* (HER+) (human epidermal growth factor receptor) gene was only observed in Luminal B BC. HER+ BC subtype, which represents 17 % of BC, presents an amplification of the *HER2* gene without the expression of ERα (ER-). The triple negative BC (ER-/PR-/HER-) do not express ERα, PR (progesterone receptor) and HER2 and cannot be treated with specific therapies (for a review, see [24]). Our cohort comprised 5 grade I BC (ER+/PR+/HER-) and 8 grade III BC (5 ER-/PR-/HER-and 3 ER+/PR+/HER+). Our results revealed an insignificant decrease of both *GABARAP* and *GABARAPL2* mRNA levels in grade III BC compared to non tumoral tissue (NT). More interestingly, *GABARAPL1* expression was strongly decreased in BC grade III tissues ($p = 0.004$) versus non tumoral tissues. An inverse correlation ($r = -0.57$) was also observed between *GABARAPL1* mRNA and tumor stage while a very poor correlation was determined between *GABARAP* or *GABARAPL2*

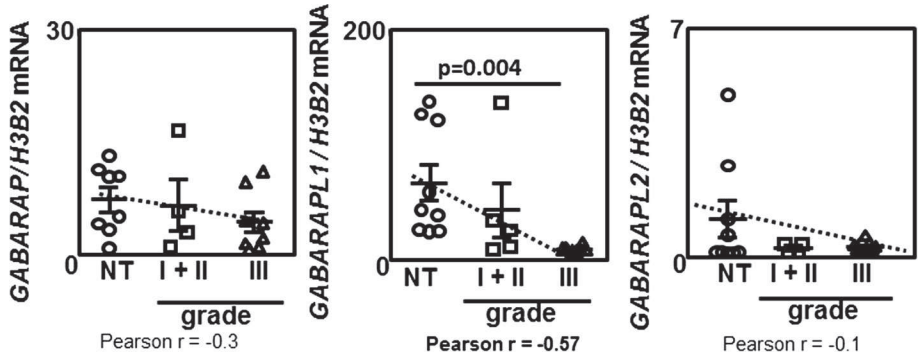

Fig. 1 *GABARAP* family expression is deregulated in breast cancers. Quantification of *GABARAP*, *GABARAPL1*, *GABARAPL2* expression using qRT-PCR, in grade I + II and grade III BC biopsies compared to normal adjacent tissue. Circle: NT (non tumoral), square: grade II, triangle: grade III. Difference of expression were quantified using a t-test. The correlation between the tumor grade and gene expression was measured using a Spearman test

expression levels and the tumor grade (respectively $r = -0.3$ and $r = -0.1$).

Study of global and local epigenetic modifications in *GABARAPL1* promoter and *GABARAPL1* expression in BC tissues and cell models

Since tumors are frequently associated with aberrant DNA methylation content, we quantified global DNA methylation levels using ELISA in gDNA issued from both grade III BC samples (associated with the lowest expression of *GABARAPL1* mRNA, as previously described in Fig. 1 and NT tissues (Fig. 2a).[7] [25, 26] As expected, several gDNA issued from grade III BC presented a lower global DNA methylation compared to gDNA issued from NT tissues. These results suggested that epigenetic modifications might occur in these tumors. To determine whether local DNA methylation was also altered in these BC samples, methylation of *XIST*, a X-linked gene known to be methylated in women, and *GAPDH*, a gene constitutively active and unmethylated, were analyzed by precipitation of methylated DNA using the methylCollector Ultra kit. As expected, methylation of *XIST* was observed in 100 % of both gDNA issued from NT and grade I-II BC tissues tested but lost in 3 out of 5

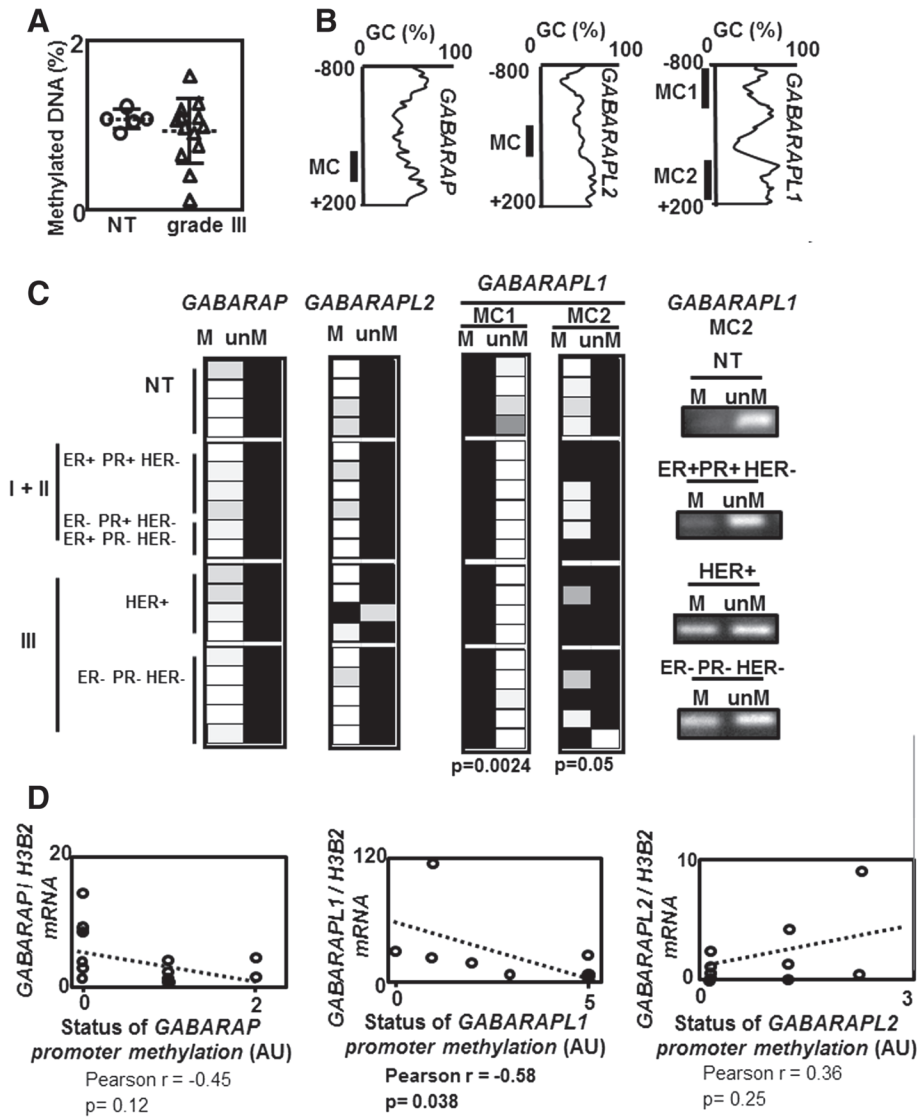

Fig. 2 Detection of DNA methylation in *GABARAP* family promoters **a** Global DNA methylation quantification in BC and non tumoral biopsies using methylFlash ELISA kit. **b** Scheme describing the *GABARAP* family gene promoter structure (Methprimer) and primer localization. **c** Left: Descriptive of *GABARAP* family gene methylation using methylCollector kit ; right : examples of methylation signal observed using *GABARAPL1* MC2 primers. White : absence of signal of methylation; black : signal of methylation. **d** Correlations (Spearman test) between expression and methylation of *GABARAP*, *GABARAPL1* and *GABARAPL2* genes. NT: non tumoral, ER +/−: status of expression of estrogen receptor α, PR+/−: status of expression of progesterone receptor, HER+/−: status of expression of Human epidermal growth factor receptor; I-III: BC grade

triple negative BC biopsies (Grade III) (Additional file 1: Figure S1). On the contrary, *GAPDH* was never found to be methylated in NT gDNA but was surprisingly frequently methylated in gDNA issued from BC samples (Additional file 1: Figure S1). Loss of global DNA methylation in several tissues (Fig. 2a 4 out 13 samples) and aberrant status of methylation of *XIST* and *GAPDH* (Additional file 1: Figure S1) strongly suggested that DNA methylation was deregulated in BC samples.

We next analyzed whether epigenetic regulation of the *GABARAPL1* might explain its specific down-regulation in BC. *GABARAP*, *GABARAPL1* and *GABARAPL2* present CpG rich areas in their promoter (−800/+200) as predicted using the methPrimer software [27], so we analyzed the methylation status of these promoters using the methylCollector Ultra kit (Fig. 2b and c). A low methylation signal was observed in both *GABARAP* and *GABARAPL2* promoters (MC primers) both in tumors and NT tissues while primers designed in the−800 region of *GABARAPL1* (MC1) (Fig. 2c) revealed a strong signal of methylation in both NT and BC tissues. Regarding *GABARAPL1*, a low signal of unmethylation was also measured in NT samples but not in BC samples suggesting that hemi-methylation was lost in cancer cells ($p = 0.0024$) (Fig. 2c). To confirm the higher level of methylation in the *GABARAPL1* promoter in BC, the same experiment was repeated using primers (MC2) designed to detect the 5′-UTR region of this gene. Results obtained with MC2 primers showed that *GABARAPL1* was not or weakly methylated in NT samples but highly methylated in BC tissues ($p = 0.05$) (Fig. 2c). Pearson correlation analysis revealed that *GABARAP* or *GABARAPL2* expression was not correlated with methylation status (r = −0.45, $p = 0.12$ and r = 0.36, $p = 0.25$ Fig. 2d), while *GABARAPL1* expression was indeed correlated with the methylation status of the gene (r = −0.58, $p = 0.03$ suggesting that methylation of the *GABARAPL1* promoter may explain the downregulation of *GABARAPL1* expression in BC (Fig. 2d).

In order to characterize the pathway allowing epigenetic modifications to control *GABARAP* family expression, we first analyzed *GABARAP*, *GABARAPL1* and *GABARAPL2* mRNA levels using qRT-PCR in MCF-7 and MDA-MB-453 (BC cell lines) and MCF-10A (Breast immortalized but non tumoral cell line) cell lines (Fig. 3a). Both *GABARAP* ($p = 0.039$), *GABARAPL1* ($p = 0.013$) and *GABARAPL2* ($p = 0.039$) expression were decreased in MCF-7 compared to MCF-10A but while the loss of *GABARAP* or *GABARAPL2* expression was weak (0.5-2 fold), *GABARAPL1* expression was about 100-fold lower in MCF-7 compared to MCF-10A (Fig. 3a). Similar results were obtained for *GABARAP*, *GABARAPL1* and *GABARAPL2* in MDA-MB-453 cells but *GABARAP* did not show any significant differences in this cell line (Fig. 3a). Methylation of the *GABARAP* family promoters was then assessed using the MethylCollector kit in both MCF-7 and MDA-MB-453 cell lines presenting a low expression of *GABARAPL1*. First, a signal of methylation of *GABARAP* promoter was observed in MCF-7 cells but not in MDA-MB-453 cells (Fig. 3b). Regarding *GABARAPL2* promoter, no methylation was detected in both cell lines. A high signal of methylation was detected in the *GABARAPL1* promoter in MCF-7 and MDA-MB-453 cells using MC1 primers confirming that the region of MC1 is highly frequently methylated. As expected *GABARAPL1* promoter methylation was lost in MCF-7 cells treated with 5-aza-CdRdeoxycytidine (5-aza-CdR), a DNMTi (Fig. 3b). A high signal of methylation was also detected using MC2 primers in MCF-7 cells but not in MCF-10A cells suggesting, as observed before in human BC biopsies, that *GABARAPL1* methylation is predominantly observed in BC cell lines (Fig. 3c)

As local DNA methylation is frequently associated to histone deacetylation, the acetylation status of histone H3 (H3-ac) was analyzed by ChIP in MCF-7 and MDA-MB-453 cells previously treated or not with trichostatin A (TSA), an inhibitor of HDACs (Fig. 3d). ChIP analysis revealed that H3 acetylation was detected in the *GABARAP* promoter in MCF-7 cells but not in MDA-MB-453 cells. A very low level of H3 acetylation was also observed in *GABARAPL2* promoter in these both cell lines. These signals were increased following TSA treatment in MCF-7 and MDA-MB-453 cells. Similarly, no H3 acetylation signal could be detected in the *GABARAPL1* promoter of BC cells but this signal was increased after TSA treatment, particularly in the MDA-MB-453 cells (Fig. 3d).

All these data (Figs. 1, 2 and 3) suggest that *GABARAPL1* is the most regulated gene of the *GABARAP* family and that require promoter deacetylation and DNA methylation. Interestingly, both DNMT1, which predominantly catalyzes inheritance DNA methylation, and HDAC1 were detected on *GABARAPL1* promoter in MCF-7 cells using ChIP experiments (Fig. 3e).

We next asked whether 5-aza-CdR or TSA could restore *GABARAPL1* expression in BC cell lines. To do so, MCF-7 and MDA-MB-453 cells were treated with 5-aza-CdR or TSA and the levels of *GABARAP*, *GABARAPL1* and *GABARAPL2* mRNA were measured using qRT-PCR (Fig. 4a) while protein levels were quantified by western-blotting (Fig. 4b). All cells were also treated with MG-132, before protein extraction, to prevent the fast proteasomal degradation of GABARAPL1 which has been previously reported [28]. First we observed a not significant increase of *GABARAP* mRNA ($p = 0.07$) but a significant increase of the corresponding protein GABARAP ($p = 0.007$ and $p = 0.02$) following TSA treatment in MCF-7 and MDA-MB-453 cells. Both *GABARAPL2* mRNA ($p = 0.05$ and $p = 0.05$ respectively) and GABARAPL2 protein ($p = 0.045$ and $p = 0.0003$ respectively) were increased in MCF-7 and

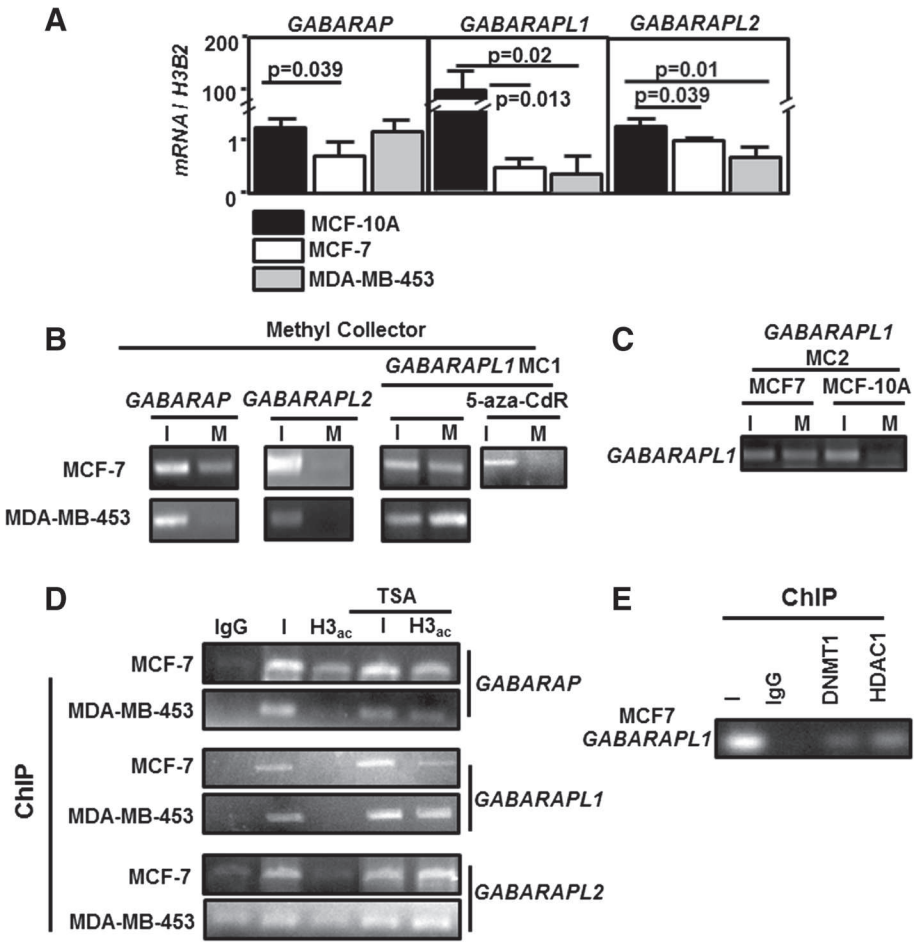

Fig. 3 Epigenetic modifications in *GABARAP* family gene promoters. **a** Quantification of *GABARAP*, *GABARAPL1*, *GABARAPL2* expression using qRT-PCR in BC MCF-7 and MDA-MB-453 cancer cells and MCF-10A immortalized cells. **b** and **c** *GABARAP* family gene methylation using methylCollector kit in MCF-7, MDA-MB-453 and MCF-10A cells. (I: input; M: methylated fraction). **d** Visualization of H3 deacetylation using ChIP experiment and anti-H3 acetylated (H3-ac) antibody in the *GABARAP* family gene in MCF-7 and MDA-MB-453 cells (I: input; IgG: negative control of IP). **e** Detection of DNMT1 and HDAC1 recruitment on *GABARAPL1* promoter using ChIP experiment and anti-DNMT1 or anti-HDAC1 antibody (I: input; IgG : negative control)

MDA-MB-453 cells treated with TSA. No significant effect of 5-aza-CdR could be observed on *GABARAP* and *GABARAPL2* expression (Fig. 4a). On the opposite, 5-aza-CdR treatment increased *GABARAPL1* mRNA level (about 2 fold) in both cell lines ($p = 0.004$ and $p < 0.0001$ respectively) while TSA treatment increased *GABARAPL1* expression of 10 to 25 fold (Fig. 4a). Moreover, GABARAPL1 expression, which was undetectable in non treated MCF-7 cells or 5-aza-CdR-treated cells, was increased following TSA treatment (Fig. 4b). A weak and diffuse band signal corresponding to the GABARAPL1 protein was also in over-exposed western-blotting using lysates of MDA-MB-453 cells treated with TSA, suggesting that GABARAPL1 might also be slightly increased in these cells after TSA treatment.

Altogether these results confirm that *GABARAPL1* is the gene of the *GABARAP* family whose expression is the most sensitive to epigenetic regulation in BC cell lines. Since 5-aza-CdR and TSA treatments restored GABARAPL1 content, we next asked whether these compounds modulate autophagy and cell proliferation in MCF-7 cells (Additional file 2: Figure S2). Both an increase of LC3B-II (form associated to the autophagosomes) (Additional file 2: Figure S2A) and of cells with GFP-LC3 puncta (Additional file 2: Figure S2B) were observed in respectively 5-aza-CdR/ TSA treated cells and in GFP-LC3 transfected and TSA treated cells compared to control cells. Moreover, both an decrease of cell proliferation and clonogenecity were also observed in MCF-7 treated cells (Additional file 2: Figure S2C and D). These results suggest that restoration of GABARAPL1 expression might be linked to these processes although some pleiotropic effects of 5-aza-CdR and TSA treatment could also be involved [29].

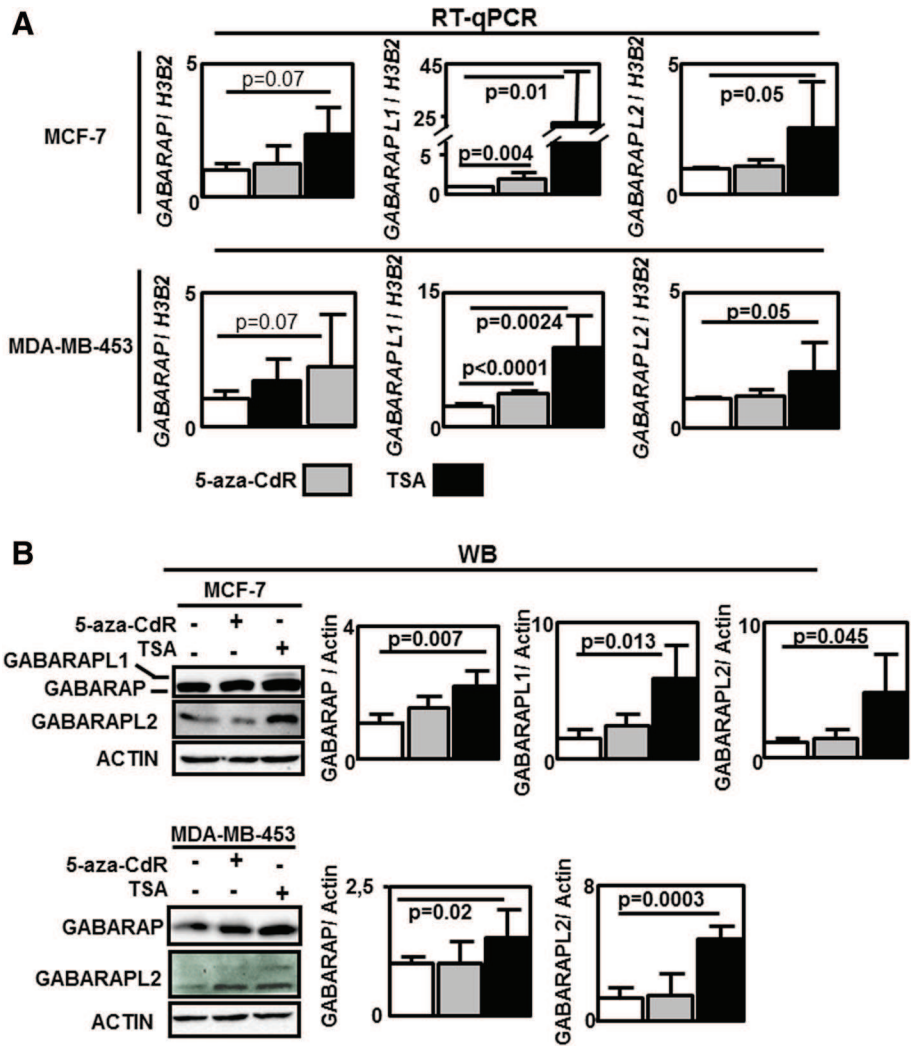

Fig. 4 Effects of epigenetic modulators on the *GABARAP* family gene expression. **a** Effects of 5-aza-deoxycytidine (5-aza-CdR) or trichostatin A (TSA) on *GABARAP* family gene expression using qRT-PCR analysis. **b** Effects of 5-aza-CdR or TSA on GABARAP family protein expression using WB (anti-GABARAP/GABARAPL1, anti-GABARAPL2 and anti-ACTIN antibodies) in cells previously treated with MG-132. Differences were quantified using a t-test

GABARAPL1 expression is regulated by CREB-1

Behind epigenetic modifications of the promoter, the second step of gene regulation is the recruitment of transcriptional factors (TF). Therefore, in order to characterize the mechanisms governing *GABARAPL1* expression in these cells, we cloned two fragments of the *GABARAPL1* promoter (−659/+241 and −336/+241) in the pGL3 luciferase reporter plasmid. As suggested by 3 different softwares (TESS http://www.cbil.upenn.edu/tess, Cister http://zlab.bu.edu/~mfrith/cister.shtml and Patch http://www.gene-regulation.com/pub/programs.html#patch) used to predict TF binding sites, several putative CRE (cAMP Response Element) elements were identified in *GABARAPL1* promoter (Fig. 5a). Indeed, following transfection of our constructions in MCF-7 cells, we observed a significant increase of luciferase signal in cells transfected with the−336/+241-*GABARAPL1*-promoter-pGL3 plasmid compared to the empty pGL3 vector suggesting the presence of functional regulatory elements in this region. Moreover, luciferase activity was strongly increased when cells were transfected with the−659/+241-*GABARAPL1*−promoter-pGL3 vector compared to the basal−336/+241-*GABARAPL1*-promoter-pGL3 vector suggesting that the region −659/-336 is also important for *GABARAPL1* regulation (Fig. 5b). Both treatment of MCF-7 cells with forskolin, a compound known to activate CREB-1 (CRE binding protein-1), or transfection with a plasmid expressing the CREB-1 protein significantly increased luciferase activity linked to the construction−659/+241-*GABARAPL1*−promoter-pGL3, suggesting that CREB-1 is indeed involved in *GABARAPL1* expression (Fig. 5c). The increase of luciferase activity in cells

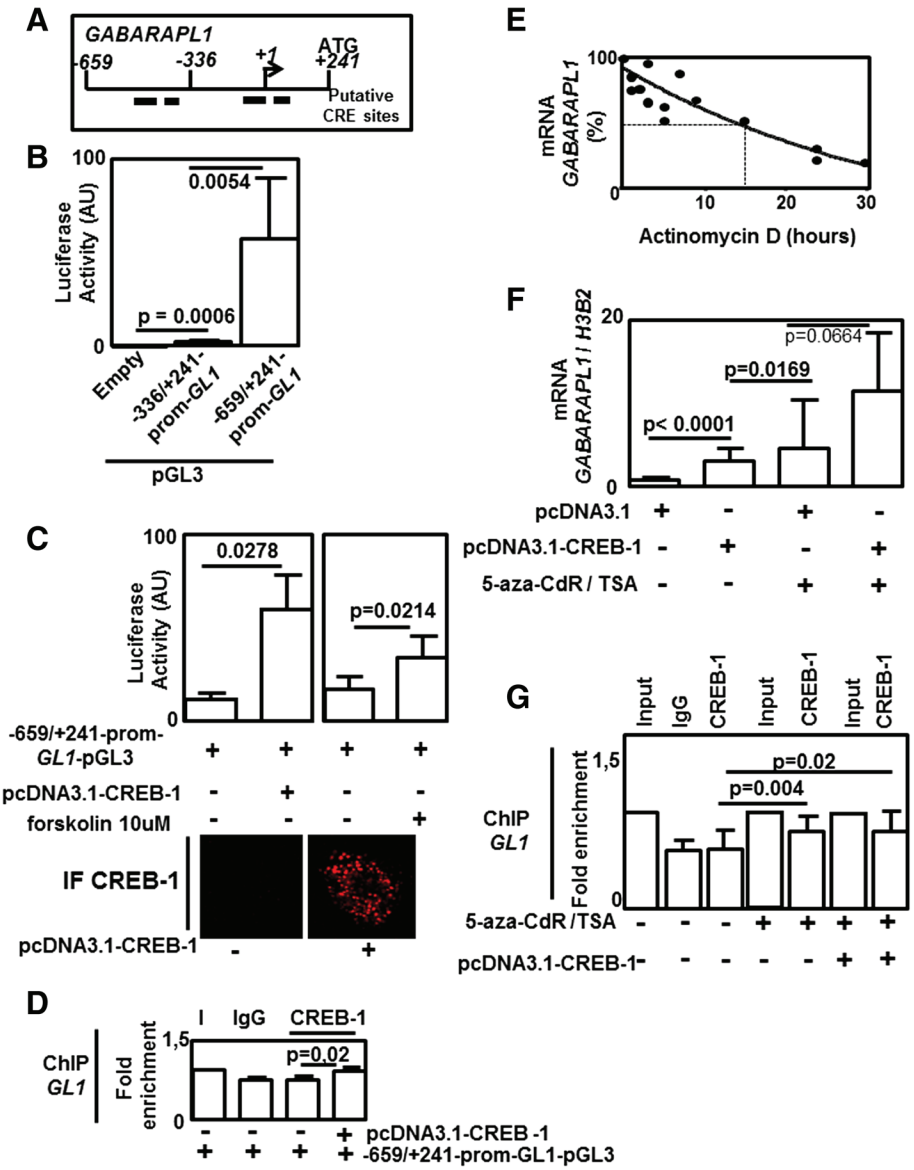

Fig. 5 *GABARAPL1* expression I controlled by CREB-1. **a** Scheme describing the position of primers used (in regard of the putative initial transcription site (+1)) and putative CRE (CREB-1 response elements) sites in the *GABARAPL1* promoter. **b** and **c** Luciferase activity measured using a Luciferase assay System Kit in MCF-7 cells transfected with empty pGL3 plasmid,–336/+241-*GABARAPL1*-promoter-pGL3 plasmid,–659/+241-*GABARAPL1*-promoter-pGL3 plasmid, pCDNA3.1-CREB-1 or treated with (10 μM) forskolin. **c** Bottom : expression of CREB-1 using IF in cells transfected or not with the pCDN3A.1-CREB-1 vector. **d** Recruitment of CREB-1 on–659/+241-*GABARAPL1*-promoter-pGL3 plasmid using ChIP experiment and anti-CREB-1 antibody in MCF-7 cells transfected with–659/+241-*GABARAPL1*-promoter-pGL3 and pCDNA3.1-CREB-1 plasmids (I: input; IgG : negative control of IP). **e** Half-life of *GABARAPL1* mRNA using qRT-PCR following Actinomycin D treatment in MCF-7 cells. **f** Effects of CREB-1 overexpression (following pCDNA3.1-CREB-1 plasmid transfection) and/or 5-aza-CdR /TSA treatment on *GABARAPL1* expression using qRT-PCR in MCF-7 cells. **g** Effects of CREB-1 overexpression (following pCDNA3.1-CREB-1 plasmid transfection) and/or 5-aza-CdR/TSA treatment on CREB-1 recruitment in *GABARAPL1* promoter using ChIP experiment and an anti-CREB-1 antibody (I: input; IgG : negative control). Differences were quantified using a t-tests. GL1: GABARAPL1

transfected with the pcDNA3.1-CREB-1 vector might be explained by the low level of endogenous CREB-1 in MCF-7 cells as observed in IF experiments (Fig. 5c) and ChIP experiment also confirmed the recruitment of CREB-1 on the–659/+241-*GABARAPL1*-promoter in spite of the presence of a high background noise that may be provoked by the presence of–659/+241-*GABARAPL1*-promoter plasmid (Fig. 5d). We next asked whether endogenous *GABARAPL1* expression may be regulated by CREB-1. Treatment of MCF-7 cells with Actinomycin D revealed that the half-life of *GABARAPL1* mRNA was high (about 17 h) suggesting that regulation of *GABARAPL1* mRNA content is more dependent on transcription that mechanisms affecting mRNA stability (Fig. 5e)

[30, 31]. Moreover, overexpression of CREB-1 in MCF-7 cells significantly increased *GABARAPL1* expression but at a lower level than the ones observed in cells treated with 5-aza-CdR/TSA (Fig. 5f). Moreover, a non-significant ($p = 0.066$) further increase of *GABARAPL1* expression was observed in cells transfected with the CREB-1 plasmid and treated with 5-aza-CdR/TSA compared to cells with 5-aza-CdR/TSA treatment alone.

These data suggest that epigenetic modifications may be an initial predominant factor allowing the recruitment of CREB-1 on *GABARAPL1* promoter. These observations were partly confirmed by ChIP experiments showing an increase of CREB-1 recruitment on *GABARAPL1* promoter in MCF-7 cells previously treated with 5-aza-CdR/TSA. But no significant difference could be observed between 5-aza-CdR/TSA treated cells transfected or not with the vector encoding CREB-1 (Fig. 5g).

Discussion

While the role of autophagy in tumorigenesis is still controversial, it is currently admitted that autophagy is generally reduced in cancer cells. Whereas the origin of the autophagy disruption is still unknown, mutations or loss of heterozygosity-dependent autophagy gene silencing (*LC3*, *ATGs*, *UVRAG*, *BECN-1*) have been reported in many different cancers, such as colorectal, gastric carcinoma or breast cancers [32–36]. Besides mutations, epigenetic modifications frequently occur in cancers, such as global DNA hypomethylation and/or both local hypo and hypermethylations in specific loci [37–39]. Hypermethylation of five autophagy-related genes, *BECN-1*, *ATG16L2*, *ULK2*, *BNIP3* and a variant of *LC3A*, were previously reported respectively in BC, leukemia, astrocytoma, colorectal cancer and esophageal carcinoma and these data demonstrated that this hypermethylation was correlated to tumor grade [15–19]. Moreover, inhibition of the HMT EZH2 or G9a promotes autophagy in cancer cells while the use of HDACi gave contradictory results on autophagy levels in cancer cells [12, 40].

Despite a high homology between the different members of the GABARAP family (GABARAPL1 shows 87 % identity with GABARAP and 61 % with GABARAPL2), these proteins are differentially expressed during development and in adult tissues (for review see [41]) and these proteins have been described to be involved in several molecular pathways, including receptor transport and autophagy. Previous studies revealed that GABARAP and GABARAPL1 may have redundant functions in transport but experiments of invalidation/overexpression of GABARAP and GABARAPL1 showed that both are required for autophagy [42, 43]. *GABARAPL1* expression has been described to be decreased in cancer cell lines. MCF-7 cells stably expressing exogenous Flag-GABARAPL1-6His presents a significantly reduced proliferation rate compared to control cells [6]. Other studies described that a high expression of this gene is associated with a positive outcome in metastatic BC [5, 6] while a low expression of *GABARAPL1* was also associated with a poor outcome in kidney carcinoma patients [44]. Our results presented in this study confirmed these data by showing an inverse correlation between *GABARAPL1* expression and BC grade (Fig. 1). While *GABARAP* and *GABARAPL2* expression are also reduced in the tumor samples, this decrease was not significant. Similar differences were observed between non tumoral MCF-10A cells and MCF-7 BC cells since we showed a significant decrease of *GABARAP* and *GABARAPL2* expression in MCF-7 cells but the highest decrease was observed for *GABARAPL1*. Based on previous data reporting an epigenetic regulation of *BECN-1* in BC and our data showing a deregulation of DNA methylation in our BC samples (Fig. 2a, and Additional file 1: Figure S1), we hypothesized that the loss of *GABARAPL1* expression in BC might be linked to epigenetic modifications. Indeed, DNA methylation dependent gene silencing is frequent in BC and is highly related to BC tumor genotypes (*e.g.* hypermethylation of *ESR1* in ERα negative patients), and may be essential to determine the good treatment [45]. We report here that the *GABARAPL1* gene is highly methylated in both−600 (MC1) and +200 (MC2) promoter regions but the 5′-UTR +200 region presents the more significant difference between non tumoral tissues/cells promoter regions and tumoral/cancer cells since this region is poorly methylated in normal tissue and frequently methylated in tumors (Fig. 2). As described in previous studies, a correlation between local DNA methylation and histone modifications is frequently observed in epigenetic-mediated gene silencing [46, 47]. Our results confirm these observations, since we observed that the promoter of *GABARAPL1* presented a high level of methylated DNA and deacetylated histone H3 (Fig. 3). On the other hand, DNA methylation seemed poorly involved in *GABARAP* and *GABARAPL2* expression while the inhibition of HDACs by TSA increased H3 acetylation and increased *GABARAP* and *GABARAPL2* expression (Figs. 3 and 4).

Since the control of transcription factor accessibility in the region close to the transcription initiation site is often crucial for gene expression, we wondered whether it might be important for the regulation of *GABARAPL1* expression. According to transcription binding site prediction softwares, our data indeed revealed that *GABARAPL1* expression is controlled by CREB-1 and that inhibition of epigenetic repressive marks increased CREB-1-recruitment on the *GABARAPL1* promoter. Since CREB-1 has been previously involved in the regulation of autophagy, the role of this transcriptional factor may be crucial in this process. Indeed, neuron protection mediated by CREB-1 activation and associated with an increase of BECN-1 and LC3

expression, was observed following rapamycin administration in ischemic neonatal rats [48]. On the opposite, CREB-1 activation together with mTOR inhibitors has also been described to potentiate chemotherapies in renal cancers [49]. Nevertheless, the mechanism by which CREB-1 can regulate autophagy and pro-survival signals in cancer cells will require further studies.

Conclusion

The current use of epigenetic drugs in clinical trials provides new options for personalized adjuvant therapies in cancers. Indeed, HDACi, such as Entinostat or valproic acid efficiently increase ERα expression in ER-BC tumors and considerably improve the efficiency of anti-estrogen signaling therapies [50, 51]. 5-aza-CdR treatment has also been previously reported to increase autophagy by inducing LC3B-II in myeloid cells and myeloid cells resistant to 5-aza-CdR presented an increase of basal autophagy [52]. An increase of GABARAP family protein expression, following 5-aza-CdR/TSA treatment, might at least partly explain this increase of autophagy levels. Indeed, GABARAP/GABARAPL1 overexpression in BC has been described to decrease cell proliferation and tumorigenesis in nude mice [53, 54]. All these data strongly support the idea that autophagy regulation may be a focal point for the design of combined anti-cancer therapies in the future. Mahalingam *et al*. recently proposed the evaluation of a combination of HDACi (vorinostat) and autophagy inhibitor (hydroxychloroquine) in a phase I study in patients with solid tumors [55]. However, identification of the molecular mechanisms governing gene silencing in autophagy impairment in cancer will definitely help to develop future specific drugs, and decrease the important side effects. Indeed, while DNMTi efficiently restore *ERα* or *BECN-1* expression in methylated tumors, these compounds also reduce global DNA methylation and local methylation [56]. DNMTi also strongly induce metalloproteinase expression in lymphoma and pancreatic cancers suggesting an increase of metastatic potential [57]. Similarly, urokinase, a marker of invasiveness associated with the most aggressive BC and with prostate cancers is increased after DNMTi treatment [58, 59].. In agreement with previous studies on different autophagy related-genes, our work demonstrated for the first time that the *GABARAP* family genes, and particularly *GABARAPL1*, are regulated by epigenetic modifications in BC and that epigenetic inhibitors might be used in combination with classical anti-chemotherapeutive drugs for futures anti-cancer therapies.

Additional files

Additional file 1: Figure S1. *XIST* and *GAPDH* methylation status in BC. *XIST* and *GAPDH* methylation was quantified using methylCollector kit. NT: non tumoral, ER +/−: status of expression of estrogen receptor α, PR+/−: status of expression of progesterone receptor, HER+/−: status of expression of Human epidermal growth factor receptor. White : absence of signal ; black : signal of methylation. (TIFF 77 kb)

Additional file 2: Figure S2. Effects of *5-aza-CdR/TSA treatment on autophagy and cell proliferation*. Increase of both cytosolic LC3-I and autophagosome associated LC3-II forms detected by western blotting using lysates of MCF-7 cells treated with 5-aza-CdR/TSA (antibody anti-LC3: L8918, Sigma-Aldrich). (B) Increase of the number of cells presenting vesicles in GFP-LC3 positive MCF-7 cells transfected with GFP-LC3 and treated with 5-aza-CdR or TSA. (C) A decrease of cell proliferation was observed in MCF-7 cells treated with 5-aza-CdR/TSA using the crystal violet/acid acetic method as previously described [61]. (D) A decrease of clonogenecity was observed in MCF-7 treated with 5-aza-CdR/TSA using the crystal violet method as previously described [62]. (TIFF 122 kb)

Abbreviations

ATG: Autophagy-related protein; BECN-1: BECLIN-1; BC: Breast Cancer; ChIP: Chromatin immunoprecipitation; CREB-1: cAMP response element binding protein; DNMT: DNA methyl transferase; DNMTi: DNMT inhibitor; ER: Estrogen receptor; GABARAP: $GABA_A$-receptor associated protein; GABARAPL1/GEC1: GABARAP like protein 1/Glandular Epithelial Cells 1; GL1: GABARAPL1; GABARAPL2/GATE-16: GABARAP like protein 2/golgi-associated ATPase enhancer of 16 kDa; HDAC: Histone deacetylase; HDACi: HDAC inhibitor; HDM: Histone demethylase; HER: Human epidermal growth factor; hMOF: Human ortholog of drosophila males absent in the first; HMT: Histone methyl transferase; IF: Immunofluorescence; MAP-LC3: Microtubule associated protein-Light chain 3; PBS: Phosphate buffer saline; PBS-T: PBS-triton-×100; PFA: Paraformaldehyde; PR: Progesterone receptor; PVDF: Polyvinylidene difluoride; SDS: Sodium dodecylsulfate; TBS-T: Tris buffer saline tween 20; TSA: Trichostatin A; 5aza-CdR: 5-aza-deoxycytidine.

Competing interest

The authors declare that they have no competing interests

Authors' contributions

EH, ACT, TG, VP carried out the molecular studies. FM and MPA participated in the selection of samples and their validation. EH and MBG wrote the manuscript. AF, PA, GD and RDM helped draft the manuscript. All authors have read and approved the final version of the manuscript

Acknowledgements

We thank Dr. Vincent Coulon (Montpellier, France) for providing the pCDNA3.1-CREB-1 plasmid [60]. This work was supported by the Université de Franche-Comté, and funding from "BQR Jeunes chercheurs" of Université de Franche-Comté, Ministère de l'Enseignement Supérieur de la Recherche (MESR), Région de Franche-Comté 2013 and Ligue Contre le Cancer (#007. Y-2014). ACT was supported by a fellowship from Région de Franche-Comté.

Author details

[1]Université de Franche-Comté, Laboratoire de Biochimie, EA3922 « Estrogènes, Expression Génique et Pathologies du Système Nerveux Central », SFR IBCT FED4234, UFR Sciences et Techniques, 16 route de Gray, 25030 Besançon Cedex, France. [2]Department of Pathology, University Hospital Jean-Minjoz, 25030 Besançon, France.

Received: 5 May 2015 Accepted: 9 October 2015
Published online: 17 October 2015

References

1. Behrends C, Sowa ME, Gygi SP, Harper JW. Network organization of the human autophagy system. Nature. 2010;466(7302):68–76.
2. Galluzzi L, Pietrocola F, Bravo-San Pedro JM, Amaravadi RK, Baehrecke EH, Cecconi F, et al. Autophagy in malignant transformation and cancer progression. EMBO J. 2015;34(7):856–80.
3. Shimizu S, Kanaseki T, Mizushima N, Mizuta T, Arakawa-Kobayashi S, Thompson CB, et al. Role of Bcl-2 family proteins in a non-apoptotic programmed cell death dependent on autophagy genes. Nat Cell Biol. 2004;6(12):1221–8.

4. Yu L, Gu C, Zhong D, Shi L, Kong Y, Zhou Z, et al. Induction of autophagy counteracts the anticancer effect of cisplatin in human esophageal cancer cells with acquired drug resistance. Cancer Lett. 2014;355(1):34–45.
5. Nemos C, Mansuy V, Vernier-Magnin S, Fraichard A, Jouvenot M, Delage-Mourroux R. Expression of gec1/GABARAPL1 versus GABARAP mRNAs in human: predominance of gec1/GABARAPL1 in the central nervous system. Brain Res Mol Brain Res. 2003;119(2):216–9.
6. Berthier A, Seguin S, Sasco AJ, Bobin JY, De Laroche G, Datchary J, et al. High expression of gabarapl1 is associated with a better outcome for patients with lymph node-positive breast cancer. Br J Cancer. 2010;102(6):1024–31.
7. Byler S, Goldgar S, Heerboth S, Leary M, Housman G, Moulton K, et al. Genetic and epigenetic aspects of breast cancer progression and therapy. Anticancer Res. 2014;34(3):1071–7.
8. Vaissiere T, Sawan C, Herceg Z. Epigenetic interplay between histone modifications and DNA methylation in gene silencing. Mutat Res. 2008;659(1–2):40–8.
9. Sharma P, Stecklein SR, Kimler BF, Sethi G, Petroff BK, Phillips TA, et al. The prognostic value of promoter methylation in early stage triple negative breast cancer. J Cancer Ther Res. 2014;3(2):1–11.
10. Guil S, Esteller M. DNA methylomes, histone codes and miRNAs: tying it all together. Int J Biochem Cell Biol. 2009;41(1):87–95.
11. Fullgrabe J, Lynch-Day MA, Heldring N, Li W, Struijk RB, Ma Q, et al. The histone H4 lysine 16 acetyltransferase hMOF regulates the outcome of autophagy. Nature. 2013;500(7463):468–71.
12. Oh M, Choi IK, Kwon HJ. Inhibition of histone deacetylase1 induces autophagy. Biochem Biophys Res Commun. 2008;369(4):1179–83.
13. Lee JY, Koga H, Kawaguchi Y, Tang W, Wong E, Gao YS, et al. HDAC6 controls autophagosome maturation essential for ubiquitin-selective quality-control autophagy. EMBO J. 2010;29(5):969–80.
14. Yan J, Seibenhener ML, Calderilla-Barbosa L, Diaz-Meco MT, Moscat J, Jiang J, et al. SQSTM1/p62 interacts with HDAC6 and regulates deacetylase activity. PLoS One. 2013;8(9):e76016.
15. Bai H, Inoue J, Kawano T, Inazawa J. A transcriptional variant of the LC3A gene is involved in autophagy and frequently inactivated in human cancers. Oncogene. 2012;31(40):4397–408.
16. Dunwell T, Hesson L, Rauch TA, Wang L, Clark RE, Dallol A, et al. A genome-wide screen identifies frequently methylated genes in haematological and epithelial cancers. Mol Cancer. 2010;9:44.
17. Li Z, Chen B, Wu Y, Jin F, Xia Y, Liu X. Genetic and epigenetic silencing of the beclin 1 gene in sporadic breast tumors. BMC Cancer. 2010;10:98.
18. Shukla S, Patric IR, Patil V, Shwetha SD, Hegde AS, Chandramouli BA, et al. Methylation silencing of ULK2, an autophagy gene, is essential for astrocyte transformation and tumor growth. J Biol Chem. 2014;289(32):22306–18.
19. Swiderek E, Kalas W, Wysokinska E, Pawlak A, Rak J, Strzadala L. The interplay between epigenetic silencing, oncogenic KRas and HIF-1 regulatory pathways in control of BNIP3 expression in human colorectal cancer cells. Biochem Biophys Res Commun. 2013;441(4):707–12.
20. Pernodet N, Hermetet F, Adami P, Vejux A, Descotes F, Borg C, et al. High expression of QSOX1 reduces tumorogenesis, and is associated with a better outcome for breast cancer patients. Breast Cancer Res. 2012;14(5):R136.
21. Rozen S, Skaletsky H. Primer3 on the WWW for general users and for biologist programmers. Methods Mol Biol. 2000;132:365–86.
22. Bradford MM. A rapid and sensitive method for the quantitation of microgram quantities of protein utilizing the principle of protein-dye binding. Anal Biochem. 1976;72:248–54.
23. Hervouet E, Demont J, Pecina P, Vojtiskova A, Houstek J, Simonnet H, et al. A new role for the von Hippel-Lindau tumor suppressor protein: stimulation of mitochondrial oxidative phosphorylation complex biogenesis. Carcinogenesis. 2005;26(3):531–9.
24. Claude-Taupin A, Boyer-Guittaut M, Delage-Mourroux R, Hervouet E. Use of epigenetic modulators as a powerful adjuvant for breast cancer therapies. Methods Mol Biol. 2015;1238:487–509.
25. Hon GC, Hawkins RD, Caballero OL, Lo C, Lister R, Pelizzola M, et al. Global DNA hypomethylation coupled to repressive chromatin domain formation and gene silencing in breast cancer. Genome Res. 2012;22(2):246–58.
26. Tryndyak VP, Kovalchuk O, Pogribny IP. Loss of DNA methylation and histone H4 lysine 20 trimethylation in human breast cancer cells is associated with aberrant expression of DNA methyltransferase 1, Suv4-20 h2 histone methyltransferase and methyl-binding proteins. Cancer Biol Ther. 2006;5(1):65–70.
27. Li LC, Dahiya R. MethPrimer: designing primers for methylation PCRs. Bioinformatics. 2002;18(11):1427–31.
28. Seguin-Py S, Lucchi G, Croizier S, Chakrama FZ, Despouy G, Le Grand JN, et al. Identification of HSP90 as a new GABARAPL1 (GEC1)-interacting protein. Biochimie. 2012;94(3):748–58.
29. Zou CF, Jia L, Jin H, Yao M, Zhao N, Huan J, et al. Re-expression of ARHI (DIRAS3) induces autophagy in breast cancer cells and enhances the inhibitory effect of paclitaxel. BMC Cancer. 2011;11:22.
30. Mahmoud L, Al-Enezi F, Al-Saif M, Warsy A, Khabar KS, Hitti EG. Sustained stabilization of Interleukin-8 mRNA in human macrophages. RNA Biol. 2014;11(2):124–33.
31. Sharova LV, Sharov AA, Nedorezov T, Piao Y, Shaik N, Ko MS. Database for mRNA half-life of 19 977 genes obtained by DNA microarray analysis of pluripotent and differentiating mouse embryonic stem cells. DNA Res. 2009;16(1):45–58.
32. Gao X, Zacharek A, Salkowski A, Grignon DJ, Sakr W, Porter AT, et al. Loss of heterozygosity of the BRCA1 and other loci on chromosome 17q in human prostate cancer. Cancer Res. 1995;55(5):1002–5.
33. Kang MR, Kim MS, Oh JE, Kim YR, Song SY, Kim SS, et al. Frameshift mutations of autophagy-related genes ATG2B, ATG5, ATG9B and ATG12 in gastric and colorectal cancers with microsatellite instability. J Pathol. 2009;217(5):702–6.
34. Kim MS, Jeong EG, Ahn CH, Kim SS, Lee SH, Yoo NJ. Frameshift mutation of UVRAG, an autophagy-related gene, in gastric carcinomas with microsatellite instability. Hum Pathol. 2008;39(7):1059–63.
35. Russell SE, Hickey GI, Lowry WS, White P, Atkinson RJ. Allele loss from chromosome 17 in ovarian cancer. Oncogene. 1990;5(10):1581–3.
36. Saito H, Inazawa J, Saito S, Kasumi F, Koi S, Sagae S, et al. Detailed deletion mapping of chromosome 17q in ovarian and breast cancers: 2-cM region on 17q21.3 often and commonly deleted in tumors. Cancer Res. 1993;53(14):3382–5.
37. Hervouet E, Hulin P, Vallette FM, Cartron PF. Proximity ligation in situ assay for monitoring the global DNA methylation in cells. BMC Biotechnol. 2011;11:31.
38. Hervouet E, Lalier L, Debien E, Cheray M, Geairon A, Rogniaux H, et al. Disruption of Dnmt1/PCNA/UHRF1 interactions promotes tumorigenesis from human and mice glial cells. PLoS One. 2010;5(6):e11333.
39. Hervouet E, Vallette FM, Cartron PF. Impact of the DNA methyltransferases expression on the methylation status of apoptosis-associated genes in glioblastoma multiforme. Cell Death Dis. 2010;1:e8.
40. He G, Wang Y, Pang X, Zhang B. Inhibition of autophagy induced by TSA sensitizes colon cancer cell to radiation. Tumour Biol. 2014;35(2):1003–11.
41. Le Grand JN, Chakrama FZ, Seguin-Py S, Fraichard A, Delage-Mourroux R, Jouvenot M, et al. GABARAPL1 (GEC1): original or copycat? Autophagy. 2011;7(10):1098–107.
42. Cook JL, Re RN, DeHaro DL, Abadie JM, Peters M, Alam J. The trafficking protein GABARAP binds to and enhances plasma membrane expression and function of the angiotensin II type 1 receptor. Circ Res. 2008;102(12):1539–47.
43. Mansuy V, Boireau W, Fraichard A, Schlick JL, Jouvenot M, Delage-Mourroux R. GEC1, a protein related to GABARAP, interacts with tubulin and GABA (A) receptor. Biochem Biophys Res Commun. 2004;325(2):639–48.
44. Liu C, Xia Y, Jiang W, Liu Y, Yu L. Low expression of GABARAPL1 is associated with a poor outcome for patients with hepatocellular carcinoma. Oncol Rep. 2014;31(5):2043–8.
45. Hervouet E, Cartron PF, Jouvenot M, Delage-Mourroux R. Epigenetic regulation of estrogen signaling in breast cancer. Epigenetics. 2013;8(3):237–45.
46. Ali MW, Cacan E, Liu Y, Pierce JY, Creasman WT, Murph MM, et al. Transcriptional suppression, DNA methylation, and histone deacetylation of the regulator of G-protein signaling 10 (RGS10) gene in ovarian cancer cells. PLoS One. 2013;8(3):e60185.
47. Cartron PF, Blanquart C, Hervouet E, Gregoire M, Vallette FM. HDAC1-mSin3a-NCOR1, Dnmt3b-HDAC1-Egr1 and Dnmt1-PCNA-UHRF1-G9a regulate the NY-ESO1 gene expression. Mol Oncol. 2012;7(3):452–63.
48. Carloni S, Girelli S, Scopa C, Buonocore G, Longini M, Balduini W. Activation of autophagy and Akt/CREB signaling play an equivalent role in the neuroprotective effect of rapamycin in neonatal hypoxia-ischemia. Autophagy. 2010;6(3):366–77.
49. Wang Y, Hu Z, Liu Z, Chen R, Peng H, Guo J, et al. MTOR inhibition attenuates DNA damage and apoptosis through autophagy-mediated suppression of CREB1. Autophagy. 2013;9(12):2069–86.

50. Fortunati N, Bertino S, Costantino L, De Bortoli M, Compagnone A, Bandino A, et al. Valproic acid restores ER alpha and antiestrogen sensitivity to ER alpha-negative breast cancer cells. Mol Cell Endocrinol. 2010;314(1):17–22.
51. Sabnis GJ, Goloubeva O, Chumsri S, Nguyen N, Sukumar S, Brodie AM. Functional activation of the estrogen receptor-alpha and aromatase by the HDAC inhibitor entinostat sensitizes ER-negative tumors to letrozole. Cancer Res. 2011;71(5):1893–903.
52. Cluzeau T, Robert G, Puissant A, Jean-Michel K, Cassuto JP, Raynaud S, et al. Azacitidine-resistant SKM1 myeloid cells are defective for AZA-induced mitochondrial apoptosis and autophagy. Cell Cycle. 2011;10(14):2339–43.
53. Klebig C, Seitz S, Arnold W, Deutschmann N, Pacyna-Gengelbach M, Scherneck S, et al. Characterization of {gamma}-aminobutyric acid type A receptor-associated protein, a novel tumor suppressor, showing reduced expression in breast cancer. Cancer Res. 2005;65(2):394–400.
54. Liang XH, Jackson S, Seaman M, Brown K, Kempkes B, Hibshoosh H, et al. Induction of autophagy and inhibition of tumorigenesis by beclin 1. Nature. 1999;402(6762):672–6.
55. Mahalingam D, Mita M, Sarantopoulos J, Wood L, Amaravadi RK, Davis LE, et al. Combined autophagy and HDAC inhibition: a phase I safety, tolerability, pharmacokinetic, and pharmacodynamic analysis of hydroxychloroquine in combination with the HDAC inhibitor vorinostat in patients with advanced solid tumors. Autophagy. 2014;10(8):1403–14.
56. Cheray M, Pacaud R, Nadaradjane A, Vallette FM, Cartron PF. Specific inhibition of one DNMT1-including complex influences tumor initiation and progression. Clin Epigenetics. 2013;5(1):9.
57. Sato N, Maehara N, Su GH, Goggins M. Effects of 5-aza-2′-deoxycytidine on matrix metalloproteinase expression and pancreatic cancer cell invasiveness. J Natl Cancer Inst. 2003;95(4):327–30.
58. Ateeq B, Unterberger A, Szyf M, Rabbani SA. Pharmacological inhibition of DNA methylation induces proinvasive and prometastatic genes in vitro and in vivo. Neoplasia. 2008;10(3):266–78.
59. Pakneshan P, Xing RH, Rabbani SA. Methylation status of uPA promoter as a molecular mechanism regulating prostate cancer invasion and growth in vitro and in vivo. FASEB J. 2003;17(9):1081–8.
60. Coulon V, Chebli K, Cavelier P, Blanchard JM. A novel mouse c-fos intronic promoter that responds to CREB and AP-1 is developmentally regulated in vivo. PLoS One. 2010;5(6):e11235.
61. Arrigo AP, Firdaus WJ, Mellier G, Moulin M, Paul C, Diaz-latoud C, et al. Cytotoxic effects induced by oxidative stress in cultured mammalian cells and protection provided by Hsp27 expression. Methods. 2005;35(2):126–38.
62. Hervouet E, Debien E, Campion L, Charbord J, Menanteau J, Vallette FM, et al. Folate supplementation limits the aggressiveness of glioma via the remethylation of DNA repeats element and genes governing apoptosis and proliferation. Clin Cancer Res. 2009;15(10):3519–29.

www.impactjournals.com/oncotarget/ Oncotarget, 2017, Vol. 8, (No. 34), pp: 55998-56020

Research Paper: Autophagy and Cell Death

GABARAPL1 tumor suppressive function is independent of its conjugation to autophagosomes in MCF-7 breast cancer cells

Laura Poillet-Perez[1,3,*] Marine Jacquet[1,*] Eric Hervouet[1], Thierry Gauthier[1], Annick Fraichard[1], Christophe Borg[1], Jean-René Pallandre[1], Bruno J. Gonzalez[2], Yasmina Ramdani[2], Michaël Boyer-Guittaut[1], Régis Delage-Mourroux[1] and Gilles Despouy[1]

[1] Unité Mixte de Recherche, Interactions Hôte-Greffon-Tumeur, Ingénierie Cellulaire et Génique, Université Bourgogne Franche-Comté, Besançon, France

[2] Microvascular Endothelium and Neonatal Brain Lesions, Université de Normandie, UFR de Médecine et de Pharmacie, Rouen, France

[3] Rutgers Cancer Institute of New Jersey, New Brunswick, New Jersey, USA

[*] These authors have contributed equally to this work

Correspondence to: *Gilles Despouy*, ***email***: *gilles.despouy@univ-fcomte.fr*

Keywords: autophagy, breast cancer, GABARAPL1, LC3, MCF-7

Received: *August 02, 2016* ***Accepted***: *July 18, 2017* ***Published***: *July 27, 2017*

ABSTRACT

The GABARAPL1 protein belongs to the ATG8 family whose members are involved in autophagy. Our laboratory previously demonstrated that GABARAPL1 associates with autophagic vesicles, regulates autophagic flux and acts as a tumor suppressor protein in breast cancer. In this study, we aimed to determine whether GABARAPL1 conjugation to autophagosomes is necessary for its tumor suppressive functions using the MCF-7 breast cancer cell line overexpressing GABARAPL1 or a G116A mutant, which is unable to be lipidated and associated to autophagosomes. We show that the G116A mutation impaired GABARAPL1 function in autophagosome/lysosome fusion and inhibited lysosome activity but did not alter MTOR and ULK1 activities or tumor growth *in vivo*. Our results demonstrate for the first time that GABARAPL1 plays different regulatory functions during early and late stages of autophagy, independently or not of its conjugation to autophagosomes, but its tumor suppressive function appeared to be independent of its conjugation to autophagic vesicles.

INTRODUCTION

Macroautophagy (hereafter called autophagy) is a cellular degradation process in which damaged proteins, organelles and other cytoplasmic constituents are degraded and recycled to provide nutrients and energy [1, 2]. This process is characterized by the engulfment of portions of the cytosol, soluble proteins and/or organelles into a unique double-membrane structure called the phagophore. The phagophore elongates and closes to generate a double-membrane organelle called the autophagosome which then fuses with the lysosome to form the autophagolysosome, leading to the degradation of its content by lysosomal hydrolases [3, 4]. This mechanism occurs at low basal levels to maintain cellular homeostasis but can be induced by different stresses such as hypoxia or nutrient starvation to allow cell survival. These stresses induce different signaling pathways involving MTORC1 (mechanistic target of rapamycin complex), an autophagy inhibitor, or AMPK (AMP-activated protein kinase), an inducer of autophagy. MTORC1 and AMPK then phosphorylate the same protein called ULK1 (unc-51 like autophagy activating kinase 1), the yeast homolog of Atg1, to modulate autophagy following nutrient or energy starvation. During nutrient-rich conditions, MTORC1 associates with the ULK1 complex and inhibits autophagy through the phosphorylation of ULK1 at Ser 757. Nutrient starvation leads to the inhibition of MTORC1, activation of ULK1 and subsequent induction of autophagy [5, 6]. During nutrient or energy starvation, AMPK can inhibit MTORC1 and activate ULK1 through phosphorylation

at Ser 317, 555 and 777 leading to the induction of autophagy [7-9].

The autophagy process is mediated by more than 30 autophagy-related (ATG) proteins. Among these proteins, GABARAPL1/GEC1 ($GABA_A$ receptor-associated protein-like 1/Glandular epithelial cells 1), which was first described by our group as an estrogen regulated gene, belongs to the ATG8 family [10], composed of 2 subfamilies the MAP-LC3 (microtubule-associated light chain-3) subfamily and the GABARAP subfamily. The latter includes GABARAPL1, GABARAP and GABARAPL2/GATE-16 (GABARAP like-2 protein/ Golgi-associated ATPase enhancer of 16 kDa), which share 87% and 61% identity with GABARAPL1, respectively [11-13]. GABARAPL1 is composed of 117 amino acids and is involved in protein intracellular transport due to its interaction with the $GABA_A$ receptor, the κ opioid receptor and TUBULIN [14, 15]. GABARAPL1 also interacts with HSP-90 (Heat shock protein 90) which prevents its degradation by the proteasome [16].

The members of the ATG8 family possess a conserved C-terminal glycine at position 116 (GABARAP family) or 120 (LC3 family) which is essential for their conjugation to autophagosomes and their role in autophagy [17]. Indeed, during autophagy, GABARAPL1, like the other members of ATG8 family, is cleaved by the protease ATG4B which exposes its C-terminal glycine, and give the cytosolic mature form called GABARAPL1-I [18]. During phagophore elongation, this cytosolic form is linked to phosphatidylethanolamine, by the ATG7 (E1-like) and ATG3 (E2-like) enzymes, to give rise to the membrane-associated form, called GABARAPL1-II [19-23].

Despite their homology, GABARAP and LC3 subfamily members are suspected to be involved at different stages of the autophagic process. Indeed, the LC3 subfamily is thought to be necessary for the elongation of the phagophore whereas the GABARAP subfamily has been suggested to be necessary for the maturation of the autophagosome [24]. In a previous study, we demonstrated that a cellular knock-down of GABARAPL1 decreased autophagic flux and lysosome number in the breast cancer cell line MDA-MB-436 [25]. This knock-down also led to an increase in glutathione and ATP level, basal respiration and accumulation of damaged mitochondria, suggesting a function of GABARAPL1 in mitochondrial homeostasis and metabolic reprogramming. Moreover, GABARAPL1 has been shown to interact with AMPK (unpublished data) and ULK1 suggesting a potential involvement of this protein during the early stages of autophagy, as well [26, 27].

The ATG8 family is also involved in "selective autophagy" which targets defined cargos for degradation [28]. Cargo adaptor proteins interact with ATG8 proteins via their LIR motif (LC3-interacting region) to deliver ubiquitinated proteins or organelles to the autophagosomes for their degradation [29, 30]. For example, GABARAPL1 interacts with the cargo receptors SQSTM1 (sequestosome 1) or NBR1 (neighbor of BRCA1 gene 1) to induce the degradation of ubiquitinated protein aggregates (cargos) and with NIX to activate the degradation of damaged mitochondria during the selective process called mitophagy [31-33].

Deregulation of autophagy is thought to be involved in various diseases including cancer [34]. However, autophagy presents a double edge-sword in cancer since it can act as a tumor-suppressing or a tumor-promoting process depending on tumor type and stage [35-37]. During the early stages of tumorigenesis, autophagy acts as a tumor suppressor mechanism by limiting DNA damage, chromosome instability, oxidative stress and inflammation which are oncogenic stimuli [38, 39]. Moreover, the expression of proteins involved in autophagy such as BECN1 (BECLIN-1), ATG5, UVRAG (UV radiation resistance-associated gene), GABARAP and LC3 has been described to be reduced or lost in several types of cancers [40-44]. On the contrary, during the later stages of tumorigenesis, some cancer cells present elevated autophagy levels allowing them to survive against metabolic stress. Indeed, the microenvironment of cancer cells presents reduced levels of nutrients, oxygen and growth factors leading to an altered metabolism and an impairment of ATP production [45, 46].

Several studies have highlighted a role of GABARAPL1 as a tumor suppressor protein. We have previously shown in our laboratory that cancer cell lines present a reduced *GABARAPL1* expression compared to normal cells and that a high *GABARAPL1* expression is correlated with a good prognosis in breast cancer patients [47, 48]. Moreover, we have demonstrated that GABARAPL1 overexpression inhibits cell proliferation, colony formation and invasion of breast cancer cells *in vitro* [25, 47]. These results are consistent with those recently demonstrating that GABARAPL1 expression is decreased in hepatocellular carcinoma (HCC) compared to adjacent liver tissue and that GABARAPL1 inhibits cell growth of HCC cancer cell lines [49]. It has also been shown that GABARAPL1 overexpression inhibits tumor growth *in vivo* and mediate the degradation of DVL2 (Dishevelled 2) through selective autophagy leading to the inhibition of the Wnt pathway whose deregulation has been described to be involved in various diseases such as cancer [50].

Given the function of GABARAPL1 in autophagy and cancer, the purpose of our study was to: i) study the role of GABARAPL1 during early and late stages of autophagy and, ii) determine the involvement of GABARAPL1 conjugation to autophagosomes in its tumor suppressive function. To do so, we used the breast cancer cell line MCF-7 overexpressing GABARAPL1 or GABARAPL1 G116A mutant protein in which the essential C-terminal glycine at position 116 has been replaced by an alanine.

RESULTS

The G116A mutation impaired the conjugation of GABARAPL1 to phospholipids and its recruitment to autophagosomes

In order to determine the importance of the GABARAPL1 conjugation to autophagosomes on its tumor suppressive function, we designed MCF-7 breast cancer cell lines overexpressing either Flag:GABARAPL1:6His (GABARAPL1) or Flag:GABARAPL1-G116A:6His mutant (clone 1 and clone 2 ; GABARAPL1 G116A c1 and c2) (Figure 1A). First, we analyzed GABARAPL1 protein and mRNA expression levels in our cell models. As expected, GABARAPL1 and GABARAPL1 G116A expression were detected in MCF-7 GABARAPL1, GABARAPL1 G116A c1 and c2 cells but not in control cells transfected with the empty vector (Figures 1B-1C). Interestingly, we noted that MCF-7 GABARAPL1 G116A c1 cells showed a GABARAPL1 protein expression similar to the one observed in MCF-7 GABARAPL1 cells whereas MCF-7 GABARAPL1 G116A c2 cells presented a lower GABARAPL1 protein expression. We next wanted to check whether overexpression of GABARAPL1 modified the expression of its homologue GABARAP using an antibody which detects both proteins. Overexpression of GABARAPL1 or GABARAPL1 G116A in MCF-7 cells did not modify the expression of its homologue, GABARAP (Supplementary Figure S1A).

Our laboratory has previously reported that, during autophagy, GABARAPL1 needs to be cleaved, depending on its C-terminal glycine, before being associated to autophagic vesicles in HEK-293 cells [23]. We therefore wanted to know whether the G116A mutation impaired lipidation of GABARAPL1 and its localization to autophagosomes in MCF-7 cells. To do so, we studied GABARAPL1 expression in our different cell models following treatment with NH_4Cl, a lysosomal activity inhibitor, which led to the accumulation of autophagosomes and the lipidated form of GABARAPL1 called GABARAPL1-II [23]. Without treatment, only the mature soluble GABARAPL1-I form (19 kDa) was detected in MCF-7 GABARAPL1 or GABARAPL1 G116A c1 and c2 cells (Figure 1D). As expected, in MCF-7 GABARAPL1 cells, NH_4Cl treatment led to the appearance of the GABARAPL1-II form (16 kDa) but this treatment had no effect on MCF-7 GABARAPL1 G116A c1 and c2 cells. These results clearly demonstrate that the G116A mutation impaired the lipidation of GABARAPL1. In order to confirm that GABARAPL1 G116A cannot be cleaved, we transfected MCF-7 cells with three different vectors coding either GFP, GFP fused to the C-terminus of GABARAPL1 (GABARAPL1-GFP) or to the C-terminus of GABARAPL1 G116A (GABARAPL1-G116A-GFP) (Figure 1E). When GABARAPL1-GFP is expressed the anti-GFP antibody recognized the truncated GFP protein due to the cleavage of GABARAPL1 at G116 (lane 2). The difference in size between the native GFP (lane 1) and the cleaved GFP (lane 2) was probably due to a supplementary linker sequence added in the EGFP-C1 commercial vector. These results were confirmed by probing with the anti-GABARAPL1 antibody which detected GABARAPL1 alone (lane 5). When GABARAPL1-G116A-GFP was expressed, we did not observe the truncated form of GFP (lane 3) or GABARAPL1 (lane 6). These results confirmed that the G116A mutation impaired the cleavage of the GABARAPL1 protein in the MCF7 cells. Since GABARAP is also cleaved during autophagy to give the membrane-associated form called GABARAP-II, we wanted to verify that overexpression of GABARAPL1 or GABARAPL1 G116A did not alter the lipidation of GABARAP. As expected, NH_4Cl led to an increase in the GABARAP-II form in MCF-7 C, GABARAPL1, GABARAPL1 G116A c1 and c2 cells (Supplementary Figure S1B). However, this increase appeared similar in our different cell lines confirming that overexpression of GABARAPL1 or GABARAPL1 G116A did not modify expression or lipidation of the GABARAP protein.

Next, we studied the cellular localization of GABARAPL1 and GABARAPL1 G116A after treatment with BafilomycinA1 (BafA1), an inhibitor of autophagosome/lysosome fusion. Without treatment, MCF-7 GABARAPL1 or GABARAPL1 G116A cells presented a diffuse GABARAPL1 staining in the cytoplasm (Figure 1F top panel). As expected, the treatment with BafA1 led to an accumulation of GABARAPL1 puncta around the nucleus in MCF-7 GABARAPL1 cells, indicating a relocalization of GABARAPL1 to autophagosomes. On the contrary, treatment of MCF-7 GABARAPL1 G116A cells with BafA1 did not lead to any accumulation of GABARAPL1 puncta, confirming that GABARAPL1 G116A was unable to conjugate to autophagic vesicles (Figure 1F top panel). Similar results were obtained after treatment with EBSS, an inducer of autophagy, in the presence or absence of BafA1 (Figure 1F bottom panel). Indeed, treatment with EBSS increased the intensity of GABARAPL1 staining and GABARAPL1 puncta in MCF-7 GABARAPL1 but only increased the intensity of GABARAPL1 staining in GABARAPL1 G116A c1 and c2 cells. As shown above, addition of BafA1 led to an accumulation of GABARAPL1 puncta in MCF-7 GABARAPL1 cells but not in MCF-7 GABARAPL1 G116A c1 and c2 cells.

In order to study the effect of the G116A mutation on other functions of GABARAPL1 (those suggested to be independent of its conjugation to autophagosomes), we studied the impact of this mutation on the interaction of GABARAPL1 with TUBULIN and the degradation of GABARAPL1 by the proteasome [14, 16]. Firstly,

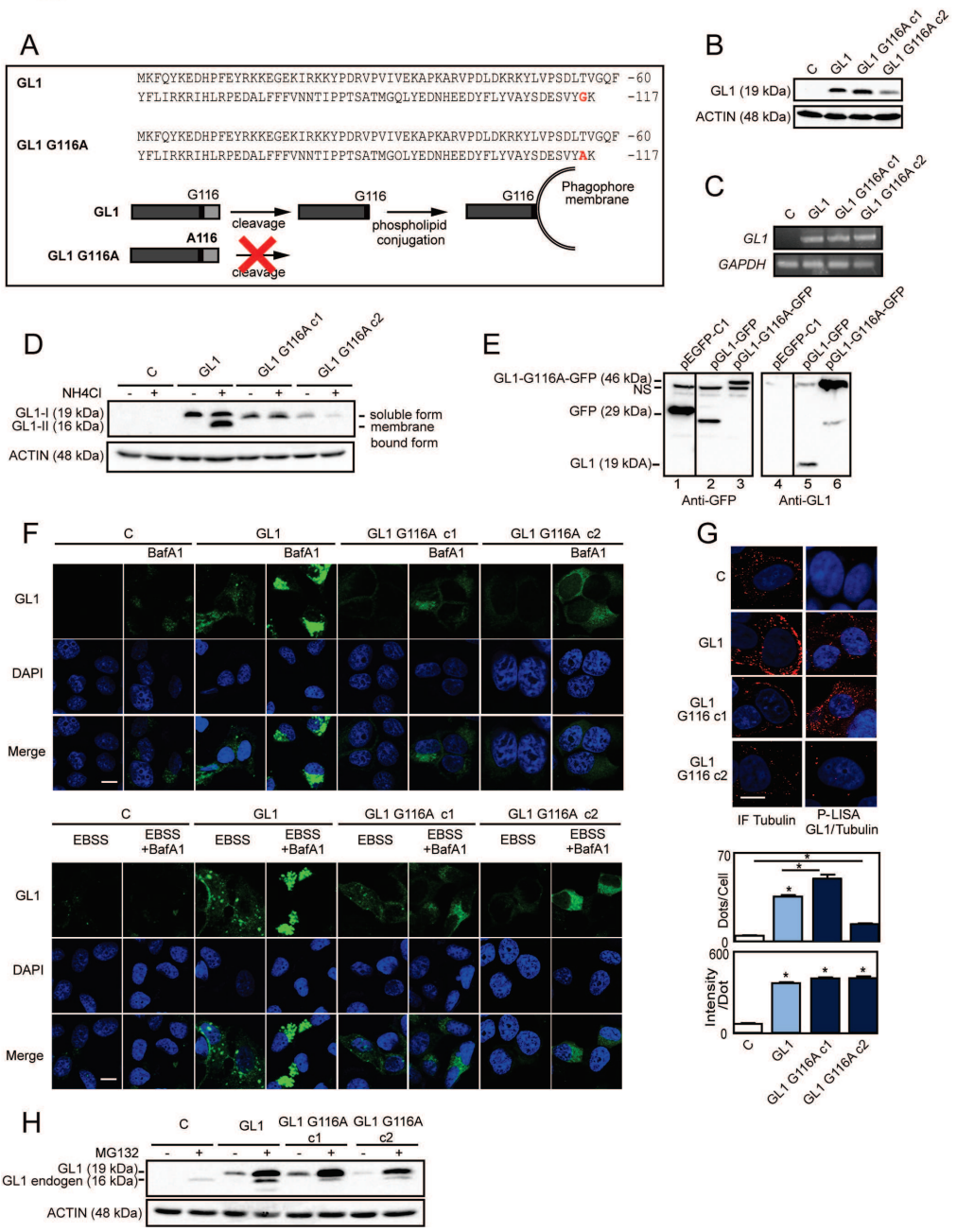

Figure 1: Characterization of MCF-7 overexpressing GABARAPL1 or GABARAPL1 G116A. A. Alignment of the amino acid sequences of GABARAPL1 and GABARAPL1 G116A (Top). Schema representing the cleavage and lipidation of GABARAPL1 during autophagy (Bottom). **B.** Western blotting analysis of GABARAPL1 in MCF-7 C, GABARAPL1 and GABARAPL1 G116A cells. Data are representative of three independent experiments. **C.** qRT-PCR analysis of GABARAPL1 mRNA expression. Representative data of two independent experiments performed in duplicate are shown. **D.** Western blotting analysis of GABARAPL1 in MCF-7 C, GABARAPL1 and GABARAPL1 G116A cells cultured in medium with or without 50 mM NH_4Cl for 2h. Data are representative of three independent experiments. **E.** Western blotting analysis of GFP and GABARAPL1 in MCF-7 cells transfected with the pGFP, pGABARAPL1-GFP and pGABARAPL1-G116A-GFP vectors. Data are representative of three independent experiments. **F.** Immunofluorescence analysis of GABARAPL1 in MCF-7 C, GABARAPL1 and GABARAPL1 G116A cells cultured in medium or EBSS with or without 100 nM BafA1 for 8 h. A representative image of two independent experiments performed in duplicate is shown. Scale bar represents 10 µm. **G.** P-LISA signals analysis of TUBULIN/GABARAPL1 interaction (red) and nuclei (blue) in MCF-7 C, GABARAPL1 and GABARAPL1 G116A cells. A representative image of three independent experiments is shown. The number of red dots and the intensity per dots were counted using the Blobfinder software. 200 cells were randomly selected in 5 fields. Data are means ± S.E.M. *P <0.05 compared to the control. Scale bar represents 5 µm. (H) Western blotting analysis of GABARAPL1 in MCF-7 C, GABARAPL1 and GABARAPL1 G116A cells cultured in medium with or without 2 µM MG132 for 16h. Data are representative of three independent experiments.

we studied the interaction between GABARAPL1 and TUBULIN using the P-LISA protocol (Proximity Ligation In Situ Assay), which allows the quantification of stable and transient interactions of endogenous proteins *in situ* [51]. Our experiments showed that GABARAPL1 G116A exhibited a similar level of interaction with TUBULIN compared to GABARAPL1 suggesting that the G116A mutation did not impair GABARAPL1/TUBULIN interaction (Figure 1G). Next, we studied endogenous or exogenous GABARAPL1 expression [Flag:GABARAPL1:6His and Flag:GABARAPL1-G116A:6His expression (19 kDa) or GABARAPL1 expression (16 kDa)] in our different cell models after treatment with MG132, a proteasome inhibitor (Figure 1H). As previously described, MG132 treatment led to an increase in both exogenous and endogenous GABARAPL1 expression levels in MCF-7 GABARAPL1 cells. Similar results were obtained in MCF-7 GABARAPL1 G116A cells, suggesting that the G116A mutation did not impair its degradation by the proteasome. On the contrary, MG132 treatment did not modify GABARAP expression levels in MCF-7 C, GABARAPL1, GABARAPL1 G116A c1 and c2 cells (Supplementary Figure S1C). These results therefore suggest that the G116A mutation specifically alters GABARAPL1 conjugation to autophagosomes without affecting other functions of this protein.

The G116A mutation impaired the function of GABARAPL1 during induced but not basal autophagy

We then investigated, in a qualitative study, the effect of GABARAPL1 or GABARAPL1 G116A overexpression on autophagy by identifying autophagic vesicles using electron microscopy (Figure 2A). Overexpression of GABARAPL1 and GABARAPL1 G116A appears to lead to an increase in autophagic vesicles (Av) and lysosomes (Lys) compared to the control cells. Surprisingly, these results suggested that GABARAPL1 G116A, like GABARAPL1 might regulate autophagy induction.

Given these results, we next wanted to study the effect of GABARAPL1 or GABARAPL1 G116A expression on autophagic flux. Indeed, our laboratory has previously shown that knocking down GABARAPL1 decreased autophagic flux in MDA-MB-436 cells [25]. During autophagy, LC3B is cleaved and linked to a phospholipid at the autophagosome to form the membrane-associated form LC3-II. The amount of this protein is directly correlated with the number of autophagosomes [20]. We therefore analyzed the effect of GABARAPL1 or GABARAPL1 G116A overexpression on LC3-II levels. Without treatment, overexpression of GABARAPL1 led to an increase in LC3-II levels compared to the control cell lines. On the contrary, overexpression of GABARAPL1 G116A did not regulate the levels of LC3-II (Figure 2B, lanes 1-4-7-10). Since the amount of LC3-II is not directly related to the autophagic flux but represents the number of autophagosomes at a particular time point, an increase in LC3-II might either indicate an increase in autophagic flux or a decrease in autophagolysosome degradation. In order to study autophagic flux, we compared the amount of LC3-II in the presence or absence of BafA1 (Figure 2B, lanes 2-5-8-11) or Chloroquine (CQ) (Figure 2B, lanes 3-6-9-12), two inhibitors of autophagosome/lysosome fusion. Treatments with BafA1 and CQ led to a greater increase in LC3-II protein levels in MCF-7 GABARAPL1 and GABARAPL1 G116A cells compared to the control cells, suggesting an increased autophagic flux in these cells. These results suggested that GABARAPL1 might increase basal autophagic flux independently of its conjugation to autophagosomes. The effect of GABARAPL1 and GABARAPL1 G116A on induced autophagy, following treatment with EBSS, was then studied (Figure 2C). After treatment with EBSS, overexpression of GABARAPL1 led to an increase in LC3-II levels compared to the control cells whereas overexpression of GABARAPL1 G116A did not (Figure 2C, lanes 1-3-5-7). Combination of EBSS with BafA1 led to a greater increase in LC3-II levels in MCF-7 GABARAPL1 cells compared to the control cells (Figure 2C, lanes 2-4), suggesting increased autophagic flux. Interestingly, after treatment with EBSS and BafA1, MCF-7 GABARAPL1 G116A cells exhibited LC3-II levels similar to those observed in control cells (Figure 2C, lanes 2-6-8), suggesting that GABARAPL1 increased induced autophagic flux depending on its conjugation to autophagosomes.

In order to confirm these results, we used a double-tagged GFP-RFP-LC3 construct and studied the effect of GABARAPL1 or GABARAPL1 G116A overexpression on autophagosome and autophagolysosome numbers [52]. Since GFP fluorescence is sensitive to acidic and proteolytic conditions found in lysosomes but RFP fluorescence is not, this construct allows the discrimination of autophagosomes (RFP+/GFP+, yellow) and autophagolysosomes (RFP+/GFP-, red). Therefore, an increase in autophagic flux would result in a concomitant increase of red and yellow puncta. We used CQ as a negative control of this experiment. Indeed, the use of CQ led to an increase in yellow puncta but not red puncta specific of a blockade of autophagic flux (Supplementary Figure S2A). Without treatment, overexpression of GABARAPL1 and GABARAPL1 G116A increased the number of autophagosomes as well as autophagolysosomes compared to the levels observed in control cells (Figure 2D left panel). These results suggested that GABARAPL1 and GABARAPL1 G116A increased the basal autophagic flux. We next studied the number of autophagosomes and autophagolysosomes during induced autophagy. After treatment with EBSS, overexpression of GABARAPL1 led to a greater increase in autophagic flux, characterized by

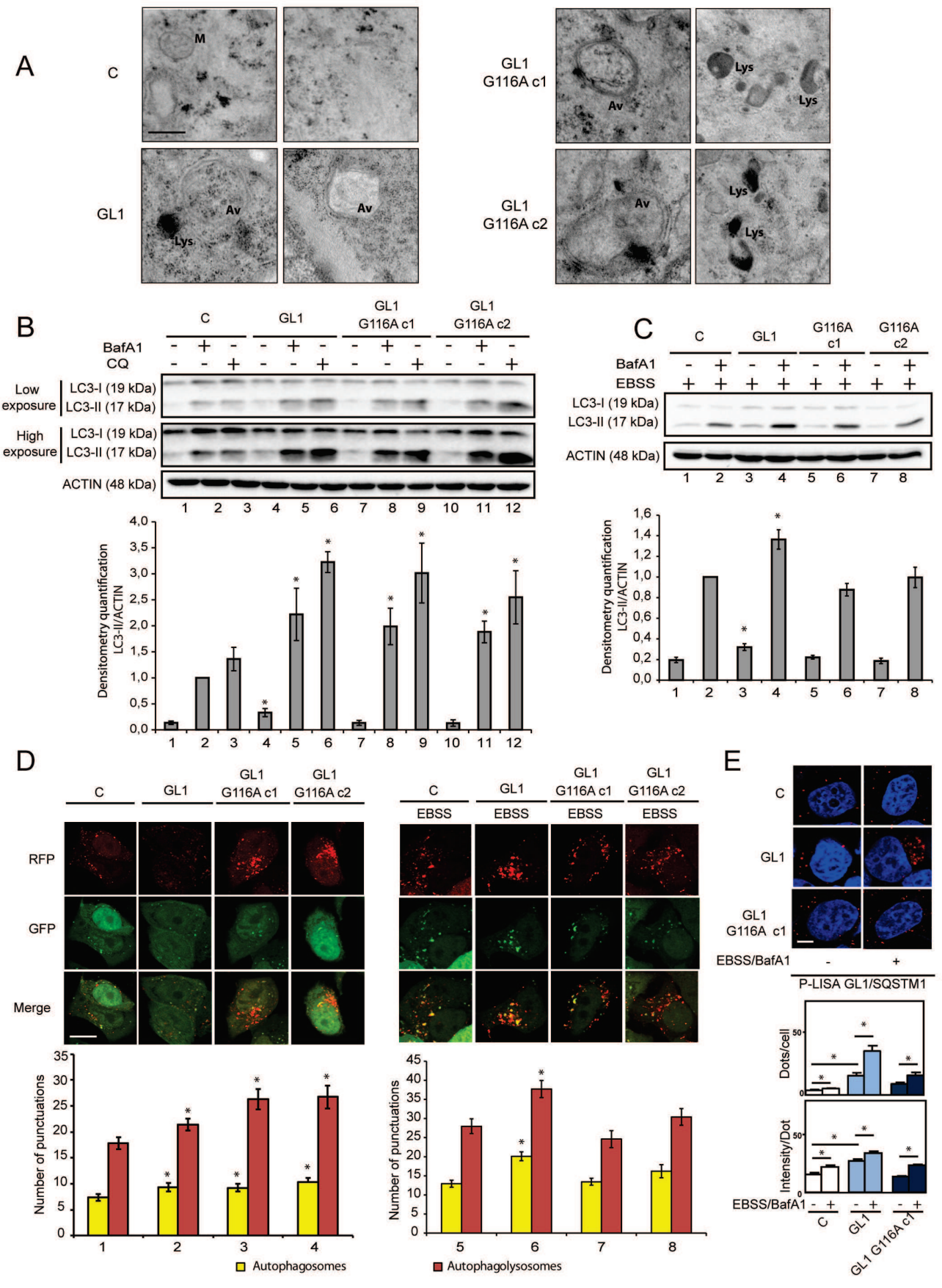
A
C
GL1
GL1 G116A c1
GL1 G116A c2
M
Av
Lys
B
C
GL1
GL1 G116A c1
GL1 G116A c2
BafA1
CQ
Low exposure
High exposure
LC3-I (19 kDa)
LC3-II (17 kDa)
ACTIN (48 kDa)
Densitometry quantification LC3-II/ACTIN
C
GL1
G116A c1
G116A c2
BafA1
EBSS
LC3-I (19 kDa)
LC3-II (17 kDa)
ACTIN (48 kDa)
Densitometry quantification LC3-II/ACTIN
D
C
GL1
GL1 G116A c1
GL1 G116A c2
EBSS
RFP
GFP
Merge
Number of punctuations
Autophagosomes
Autophagolysosomes
E
C
GL1
GL1 G116A c1
EBSS/BafA1
P-LISA GL1/SQSTM1
Dots/cell
Intensity/Dot
EBSS/BafA1
C
GL1
GL1 G116A c1

Figure 2: The G116A mutation impaired the effect of GABARAPL1 on induced but not basal autophagy. A. Electron microscopy of MCF-7 C, GABARAPL1, GABARAPL1 G116A cells. Av: Autophagic vesicles; Lys: Lysosomes and M: Mitochondria. Scale bar represents 0.25 µm. A representative image of 60 pictures for each cell lines is shown. **B.** Western blotting analysis of LC3 in MCF-7 C, GABARAPL1 and GABARAPL1 G116A cells cultured in medium with or without 100 nM BafA1 or 40 µM Chloroquine (CQ) for 2h. A representative image of ten independent experiments is shown. LC3-II levels were quantified using the Image Lab software. Data are means ± S.E.M. of ten independent experiments. *P <0.05 compared to the associated control. **C.** Western blotting analysis of LC3 in MCF-7 C, GABARAPL1 and GABARAPL1 G116A cells cultured in EBSS for 4h with or without 100 nM BafA1 for 2h. A representative image of ten independent experiments is shown. LC3-II levels were quantified using the Image Lab. Data are means ± S.E.M. of ten independent experiments. *P <0.05 compared to the associated control. **D.** GFP-RFP-LC3 puncta analysis in MCF-7 C, GABARAPL1 and GABARAPL1 G116A cells transfected with the ptf-LC3 vector and cultured in medium or EBSS. Each picture is representative of a typical cell staining observed in 20 fields chosen at random. Red and yellow puncta were counted using the ImageJ software (Green and Red puncta colocalization tool). In each group, 20 cells were randomly selected. Data are means ± S.E.M. of three independent experiments. *P <0.05 compared to the control. Scale bar represents 10 µm. **E.** P-LISA signals analysis of SQSTM1/GABARAPL1 interaction (red) and nuclei (blue) in MCF-7 C, GABARAPL1 and GABARAPL1 G116A cells cultured in complete medium or EBSS for 4h with 100 nM BafA1 for 2h. A representative image of three independent experiments is shown. The number of red dots and the intensity per dots were counted using the Blobfinder software. 200 cells were randomly selected in 5 fields. Data are means ± S.E.M. *P <0.05 compared to the control. Scale bar represents 5 µm.

an increase in autophagosomes and autophagolysosomes number (Figure 2D right panel). On the contrary, after treatment with EBSS, overexpression of GABARAPL1 G116A led to a similar number of autophagosomes and autophagolysosomes compared to the one observed in control cells suggesting that GABARAPL1 increased induced autophagic flux depending on its conjugation to autophagosomes. Altogether, results obtained by western blotting and GFP-RFP-LC3 transfection suggested that GABARAPL1 seemed to present different functions in basal or induced autophagy, which are dependent or independent of its conjugation to autophagosomes.

It has been previously shown that GABARAPL1, like the other members of ATG8 family, interacts with SQSTM1 during selective autophagy [29]. In fact, SQSTM1 recognizes ubiquitinylated aggregates or organelles and then interacts with ATG8 proteins localized at the autophagosome membrane to direct their degradation. Moreover, it has been shown that the G120A mutation in LC3 or the G116A mutation in GABARAP or GABARAPL2/GATE-16 impaired their interaction with SQSTM1 [19, 21, 53]. Therefore we next wanted to confirm wether the G116A mutation also impaired the interaction of GABARAPL1 with SQSTM1. We therefore analyzed the interaction between SQSTM1 and GABARAPL1 in MCF-7 GABARAPL1 or GABARAPL1 G116A cells using P-LISA (Figure 2E). First, we observed that the overexpression of GABARAPL1 increased its interaction with SQTM1. As expected, treatment with EBSS and BafA1 led to an increased interaction of SQSTM1 with GABARAPL1. Without treatment, GABARAPL1 G116A did not interact with SQSTM1 since the signals observed were similar to the ones quantified for the interaction between endogenous GABARAPL1 and SQSTM1 in MCF-7 control cells. When MCF7 GABARAPL1 G116A cells were treated with EBSS and BafA1, we observed an increase in cellular dots but to a lower extent than the one quantified for GABARAPL1, suggesting that SQSTM1 interacts preferentially with GABARAPL1 when it is localized in autophagosomes. We confirmed these results by studying the colocalization between SQSTM1 and GABARAPL1 or GABARAPL1 G116A (Supplementary Figure S2B). Our results showed that, GABARAPL1 G116A can still interact with SQSTM1 but to a lesser extent than the interaction observed between GABARAPL1 and SQSTM1. Altogether, these results suggested that the G116A mutation, which prevented the conjugation of GABARAPL1 onto the autophagosomes, might impair its interaction with the cargo adaptor SQSTM1 and consequently its function in selective autophagy.

The G116A mutation impaired GABARAPL1 functions during late stages of autophagy

During the later stages of autophagy, a mature autophagosome fuses with a lysosome, a digestive organelle with an acidic lumen, to allow protein degradation and turnover. We previously reported that a knock-down of GABARAPL1 in MDA-MB-436 cells led to a decreased number of lysosomes compared to the control cells [25]. The effect of GABARAPL1 and GABARAPL1 G116A overexpression on lysosome acidification was then studied using Lysotracker, a fluorescent dye which specifically label acidic compartments including lysosomes. Confocal microscopy analysis showed that overexpression of GABARAPL1 led to an increase in Lysotracker fluorescence suggesting an increase in lysosomal acidification (Figure 3A). On the contrary, overexpression of GABARAPL1 G116A did not change the Lysotracker fluorescence levels compared to control cells. Treatment with EBSS led to an increase in Lysotracker fluorescence in control cells and cells overexpressing GABARAPL1 G116A. Interestingly, treatment with EBSS did not modify Lysotracker fluorescence in cells overexpressing GABARAPL1, probably because the levels in non-treated cells are already

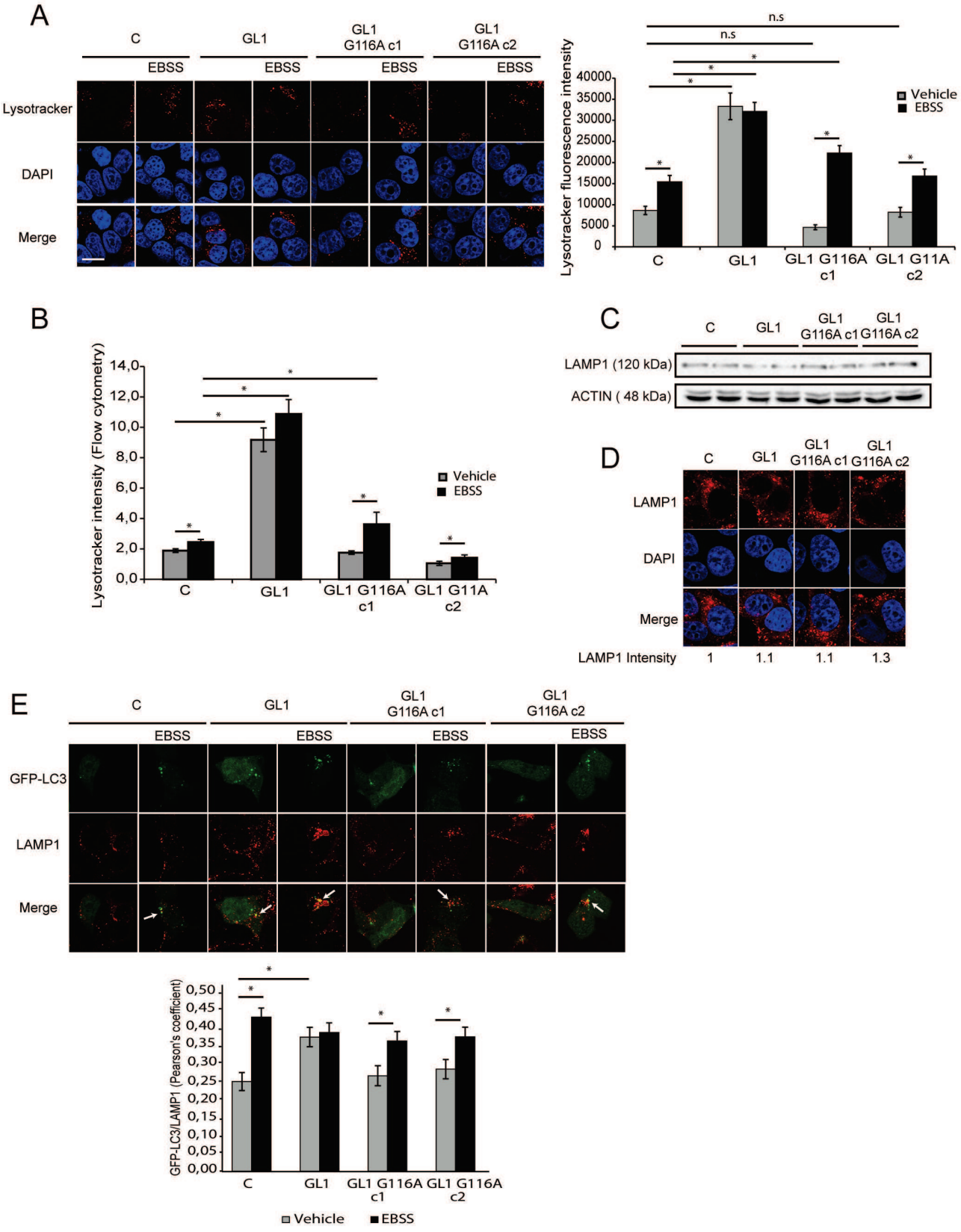
A
C
GL1
GL1 G116A c1
GL1 G116A c2
EBSS
Lysotracker
DAPI
Merge
Lysotracker fluorescence intensity
n.s
Vehicle
EBSS
C
GL1
GL1 G116A c1
GL1 G11A c2
B
Lysotracker intensity (Flow cytometry)
C
C
GL1
GL1 G116A c1
GL1 G116A c2
LAMP1 (120 kDa)
ACTIN (48 kDa)
D
LAMP1
DAPI
Merge
LAMP1 Intensity
1
1.1
1.1
1.3
E
GFP-LC3
LAMP1
Merge
GFP-LC3/LAMP1 (Pearson's coefficient)
Vehicle
EBSS

Figure 3: The G116A mutation impaired GABARAPL1 functions during late stages of autophagy. A. Lysotracker staining in MCF-7 C, GABARAPL1 and GABARAPL1 G116A cultured in medium or EBSS for 4h observed with confocal microscope and quantified with the Blobfinder software. For each group, 100 cells were randomly selected. The data representative of three independent experiments are shown. Data are means ± S.E.M. *P <0.05 compared to the control. Scale bar represents 10 µm. **B.** Intensity of Lysotracker fluorescence analyzed by flow cytometry using the flowing software. Data are means ± S.E.M. of four independent experiments performed in duplicate. *P <0.05 compared to the control. **C.** Western blotting analysis of LAMP1 in MCF-7 C, GABARAPL1 and GABARAPL1 G116A cells. Data representative of three independent experiments performed in duplicate are shown **D.** Immunofluorescence analysis of LAMP1 in MCF-7 C, GABARAPL1 and GABARAPL1 G116A cells. A representative image of three independent experiments is shown. Scale bar represents 10 µm. **E.** Colocalization of LC3 and LAMP1 in MCF-7 C, GABARAPL1 and GABARAPL1 G116A cells transfected with the pGFP-LC3 vector and immunostained for LAMP1. Colocalization of the autophagosome marker GFP-LC3 and the lysosomal marker LAMP1 was analyzed using a confocal microscope and the Pearson's coefficient using coloc_2 (ImageJ software). For each group, 25 cells were randomly selected. The data representative of two independent experiments are shown. Data are means ± S.E.M. *P <0.05 compared to the control.

elevated. Furthermore, we did not detect any change in the percentage of Lysotracker-positive vesicules following overexpression of GABARAPL1 or GABARAPL1 G116A (Supplementary Figure S3A). These results suggested that GABARAPL1 increased the acidification of lysosome depending on its conjugation to autophagosomes. These results were confirmed by the quantification of Lysotracker fluorescence using a flow cytometer (Figure 3B). Since an increase in lysosomal acidification could be linked to an increase in lysosomal number, we then studied the effect of GABARAPL1 or GABARAPL1 G116A overexpression on LAMP1 (Lysosome associated membrane protein 1) protein expression, a lysosomal marker. Our results showed that overexpression of GABARAPL1 and GABARAPL1 G116A did not significantly modify the levels of LAMP1 compared to those observed in control cells (Figure 3C). This result was confirmed by the observation of LAMP1 immunostaining using confocal microscopy. Indeed, overexpression of GABARAPL1 or GABARAPL1 G116A did not modify the fluorescence intensity of LAMP1 (Figure 3D).

The lysosome is a digestive organelle with an acidic lumen containing hydrolases such as cathepsins which are involved in the intracellular degradation and turnover of proteins. We next studied the activity of CATHEPSIN B during basal and induced autophagy using MagicRed (MR) (Supplementary Figure S3B). Without EBSS treatment, overexpression of GABARAPL1 led to an increase in MR fluorescence whereas overexpression of GABARAPL1 G116A did not. Moreover, during EBSS treatment, overexpression of GABARAPL1 led to a further increase in MR fluorescence compared to the one observed in the other cell lines (Supplementary Figure S3B). These preliminary results could suggest that the increase in lysosomal acidification observed in MCF-7 GABARAPL1 cells led to an increase in CATHEPSIN B activity. An increased lysosomal acidification and activity could be due to an increased autophagosome/lysosome fusion [54]. In order to verify this hypothesis, we then studied the effect of GABARAPL1 or GABARAPL1 G116A overexpression on GFP-LC3/LAMP1 colocalization, an event correlated with autophagosome/lysosome fusion (Figure 3E). Overexpression of GABARAPL1 led to an increase in GFP-LC3/LAMP1 colocalization compared to control cells whereas overexpression of GABARAPL1 G116A did not. EBSS treatment led to an increase in GFP-LC3/LAMP1 colocalization in control cells and cells overexpressing GABARAPL1 G116A compared to non-treated cells. In cells overexpressing GABARAPL1, treatment with EBSS did not modify GFP-LC3/LAMP1 colocalization, probably because, as described for Lysotracker fluorescence, the levels in non-treated cells are already elevated. These results suggested that GABARAPL1 increased autophagosome/lysosome fusion depending on its conjugation to autophagosomes. In order to examine whether GABARAPL1 or GABARAPL1 G116A localized at the autophagolysosome, we studied colocalization between GABARAPL1 or GABARAPL1 G116A and LAMP1 (Supplementary Figure S2C). We observed that GABARAPL1 but not GABARAPL1 G116A colocalized with LAMP1 during autophagy, suggesting that the G116A mutation impaired the localization of GABARAPL1 to lysosomes, which is consistent with the fact that this protein could not be linked to autophagosomes anymore. These results suggested that GABARAPL1 might increase autophagosome/lysosome fusion depending on its conjugation to autophagosomes, which could then also explain the increased lysosomal acidification observed in MCF-7 GABARAPL1 cells.

The G116A mutation did not impair GABARAPL1 function during early stages of autophagy

Since it has been previously shown that GABARAPL1 interacts with ULK1 [26, 27], a protein involved in initial events of autophagosome formation, we then studied the effect of GABARAPL1 and GABARAPL1 G116A overexpression during the induction of autophagy and particularly MTOR, a well-known ULK1 inhibitor and autophagy inhibitor [26, 27]. Without treatment overexpression of GABARAPL1 or GABARAPL1 G116A did not significantly modify MTOR phosphorylation (Figure 4A, lanes 1-3-5-7). Moreover, treatment with EBSS led to the same decrease in MTOR phosphorylation

in MCF-7 GABARAPL1, GABARAPL1 G116A c1 or c2 cells (Figure 4A, lanes 2-4-6-8). We therefore studied the effect of GABARAPL1 and GABARAPL1 G116A overexpression on the phosphorylation of P70S6K (p70S6 kinase), a cellular MTOR target (Figure 4B). Without treatment, overexpression of GABARAPL1 and GABARAPL1 G116A led to a decreased phosphorylation of P70S6K compared to control cells suggesting that GABARAPL1 inhibited MTOR activity and consequently P70S6K phosphorylation independently

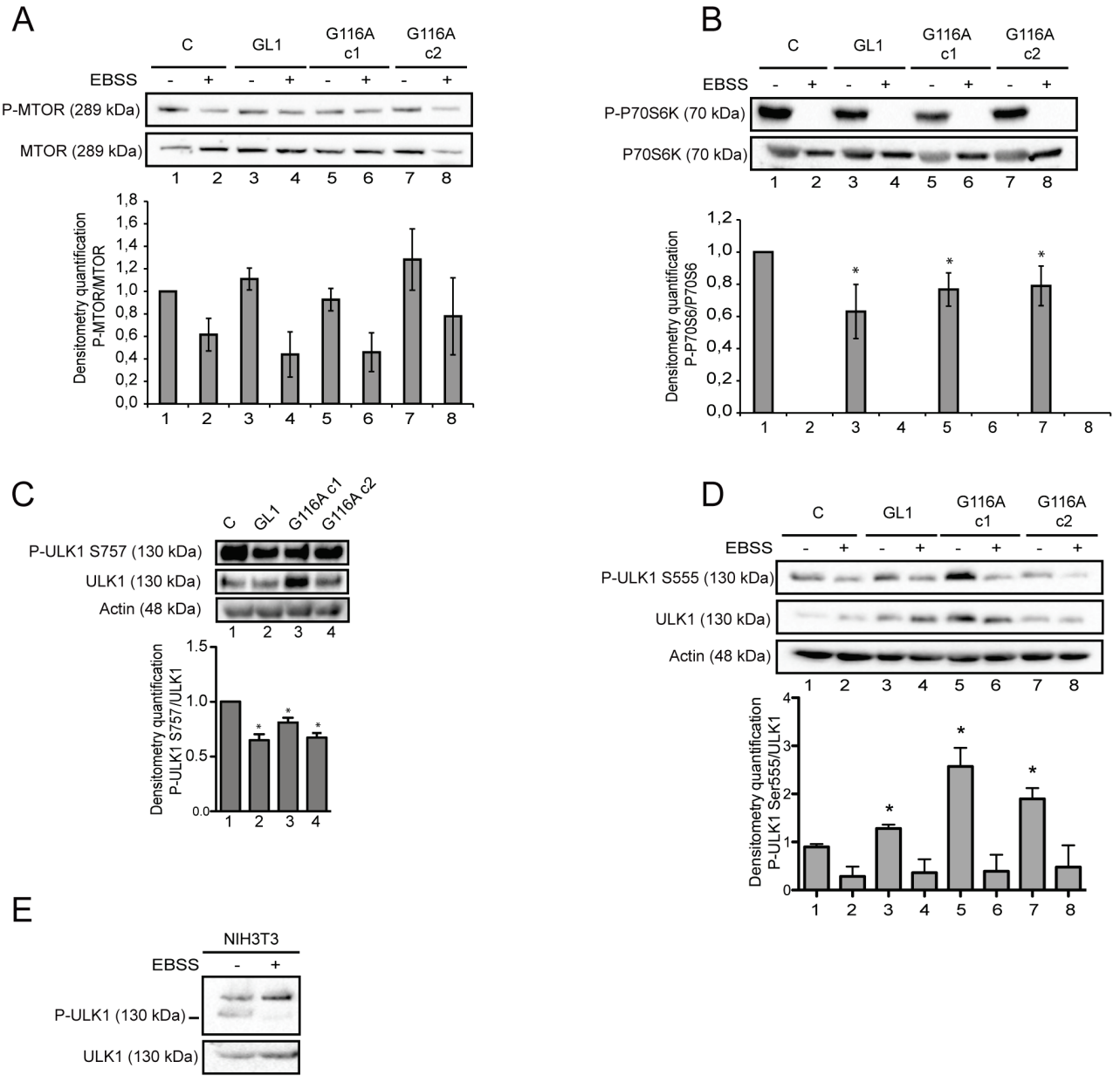

Figure 4: The G116A mutation did not impair GABARAPL1 functions during early stages of autophagy. Western blotting analysis of MTOR phosphorylation **A.** P70S6 phosphorylation **B.** and ULK1 phosphorylation at Ser555 **D.** in MCF-7 C, GABARAPL1 and GABARAPL1 G116A cells cultured in medium or EBSS for 4h. Protein levels were quantified using the Image Lab. Representative image of four independent experiments is shown. Data are means ± S.E.M. of four independent experiments. *P <0.05 compared to the control. **C.** Western blotting analysis of ULK1 phosphorylation at Ser757 in MCF-7 C, GABARAPL1, and GABARAPL1 G116A cells. Protein levels were quantified using the Image Lab. Representative image of three independent experiments is shown. Data are means ± S.E.M. of three independent experiments. *P <0.05 compared to the control. **E.** Western blotting analysis of ULK1 phosphorylation at Ser555 in NIH3T3 cells cultured in medium or EBSS for 4h. Protein levels were quantified using the Image Lab. Representative image of two independent experiments is shown.

of its conjugation to autophagosomes. Treatment with EBSS led to total loss of P70S6K phosphorylation in our cell lines (Figure 4B). Since ATG8 family members and more particularly GABARAP family proteins have been described to interact with ULK1 and allow its conjugation to autophagosomes [26], we wanted to analyze the effect of GABARAPL1 and GABARAPL1 G116A overexpression on the phosphorylation of ULK1 at Ser757, which is a direct target of MTOR and is associated with an inhibition of autophagy [7]. Overexpression of GABARAPL1 and GABARAPL1 G116A c1 led to a decreased phosphorylation of ULK1 at Ser757 (Figure 4C), confirming that GABARAPL1 indeed inhibited MTOR activity and ULK1 phosphorylation at Ser757 independently of its conjugation to the autophagosomes. We then examined another phosphorylation site of ULK1 at Ser555, a phosphorylation event which has been described to be necessary for autophagy induction [8]. Without treatment, overexpression of GABARAPL1 and GABARAPL1 G116A led to an increased phosphorylation of ULK1 at Ser555 (Figure 4D, lanes 1-3-5-7). It is interesting to note that overexpression of GABARAPL1 and GABARAPL1 G116A also increased total levels of the ULK1 protein. It has been previously shown in NIH3T3 cell lines that starvation induced by Krebs-Henseleit medium deprived of amino acids led to an increase in phosphorylation of ULK1 at Ser 555 [55]. On the contrary, in an MCF7 cells, treatment with EBSS led to a complete decrease in ULK1 phosphorylation. So, we repeated our experiment in NIH3T3 cells (Figure 4E) and demonstrated that treatment with EBSS also led to a decrease in Ser555 phosphorylation of ULK1 in NIH3T3 cell line. The use of different starvation medium may therefore explain these contradictory results.

Altogether, these results suggested that GABARAPL1 could regulate early induction autophagy steps independently of its conjugation to autophagosomes.

The G116A mutation modified the function of GABARAPL1 for some cancer cell phenotypes *in vitro* but not tumor growth *in vivo*

Since *GABARAPL1* has been previously described as a tumor suppressor gene [47, 48], we wondered whether the role of GABARAPL1 in cancer was dependent of its conjugation to autophagosomes. To answer this question, we examined the effect of GABARAPL1 or GABARAPL1 G116A overexpression on cancer cell phenotypes. As previously shown, overexpression of GABARAPL1 led to a decrease in cell proliferation [47]. However, overexpression of GABARAPL1 G116A led to cell proliferation rates similar to those obtained in control cells (Figure 5A). This conclusion was the same regarding other *in vitro* cancer cell phenotypes such as clonogenicity, cell adhesion, anchorage independent-cell proliferation and invasion (Figures 5B-5E). However, different results were obtained regarding cell migration. Indeed, overexpression of GABARAPL1 decreased cell migration in a transwell assay, but surprisingly, overexpression of GABARAPL1 G116A also led to a decrease in cell migration (Figure 5F). In order to confirm these results, we studied cell migration using a wound healing assay. This experiment led to similar results suggesting that overexpression of GABARAPL1 and GABARAPL1 G116A decreased migration rates (Figure 5G). We next wanted to confirm the effects of GABARAPL1 and GABARAPL1 G116A on cell cancer phenotype in a second breast cancer cell lines. To do so, the luminal BT474 breast cancer cell lines was first subjected to transient transfection with the Ctrl, the Flag:GABARAPL1:6His (GABARAPL1) or the Flag:GABARAPL1-G116A:6His (G116A)-expressing vectors (Supplementary Figure S4A) and then analyzed using proliferation and migration assays (Supplementary Figure S4B and C). As already observed for cell migration in the MCF-7 cells, overexpression of GABARAPL1 and GABARAPL1 G116A in BT474 cells led to a decrease in cell proliferation and migration. These results suggested that GABARAPL1 conjugation to autophagosomes may not be necessary for its role in cancer cell regulation *in vitro*.

In order to conclude about the effect of GABARAPL1 and GABARAPL1 G116A in cancer, we studied *in vivo* the tumor growth after injection of MCF-7 C, GABARAPL1 or GABARAPL1 G116A cells into Rag γ/c mice. The tumor size was monitored for two months following injection. According to previously published data [50], overexpression of GABARAPL1 decreased the size and inhibited the growth of the tumors *in vivo* (Figure 6A). Overexpression of GABARAPL1 G116A also led to a significant decrease in tumor growth. In order to confirm the overexpression of GABARAPL1 and GABARAPL1 G116A in the respective tumor, we next wanted to analyze levels of these proteins in tumors by IHC (Figure 6B). MCF-7 GABARAPL1 G116A c1 cells showed a GABARAPL1 staining similar to those observed in MCF-7 GABARAPL1 cells whereas MCF-7 GABARAPL1 G116A c2 cells presented a lower GABARAPL1 staining. These results were consistent with those described *in vitro* by western blotting (Figure 1B). Interestingly, we noted that GABARAPL1 expression levels seemed to be inversely correlated with tumor growth, but we cannot exclude that there are other intrinsic differences which may influence tumor growth unrelated to GABARAPL1 expression. Moreover, only MCF-7 GABARAPL1 cells showed a GABARAPL1 vesicular staining in tissue sections from tumors. These results suggested that GABARAPL1 could inhibit tumor growth independently of its conjugation to autophagosomes.

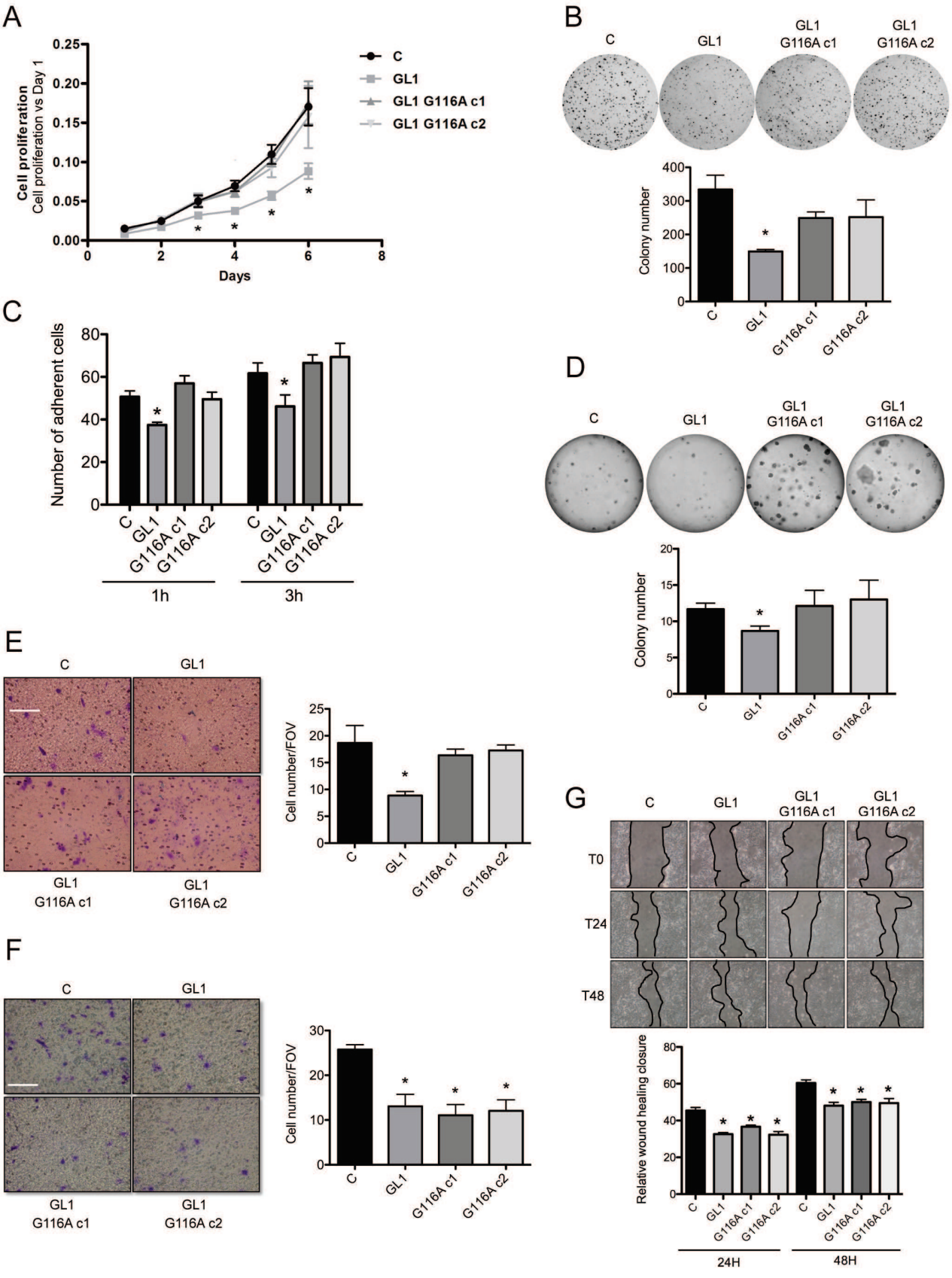
A
Cell proliferation
Cell proliferation vs Day 1
0.25
0.20
0.15
0.10
0.05
0.00
0
2
4
6
8
Days
C
GL1
GL1 G116A c1
GL1 G116A c2
B
C
GL1
GL1 G116A c1
GL1 G116A c2
Colony number
400
300
200
100
0
C
GL1
G116A c1
G116A c2
C
Number of adherent cells
80
60
40
20
0
C
GL1
G116A c1
G116A c2
1h
3h
D
C
GL1
GL1 G116A c1
GL1 G116A c2
Colony number
20
15
10
5
0
C
GL1
G116A c1
G116A c2
E
C
GL1
GL1 G116A c1
GL1 G116A c2
Cell number/FOV
25
20
15
10
5
0
C
GL1
G116A c1
G116A c2
F
C
GL1
GL1 G116A c1
GL1 G116A c2
Cell number/FOV
30
20
10
0
C
GL1
G116A c1
G116A c2
G
C
GL1
GL1 G116A c1
GL1 G116A c2
T0
T24
T48
Relative wound healing closure
80
60
40
20
0
C
GL1
G116A c1
G116A c2
24H
48H

Figure 5: The G116A mutation modified the effect of GABARAPL1 on some cancer cell phenotypes *in vitro*. A. Growth rate of MCF-7 C, GABARAPL1 and GABARAPL1 G116A cells using MTT assay. The data representative of three independent experiments performed in 24 replicates are shown. Data are means ± S.E.M of three independent experiments. *P <0.05 compared to the control. **B.** Clonogenic assay of MCF-7 C, GABARAPL1 and GABARAPL1 G116A cells. The colony numbers were evaluated by counting using Vision Capt software. The data representative of three independent experiments performed in duplicate are shown. Data are means ± S.E.M of three independent experiments. *P <0.05 compared to the control. **C.** Adhesion of MCF-7 C, GABARAPL1 and GABARAPL1 G116A cells. The data representative of three independent experiments performed in triplicate are shown. Data are means ± S.E.M of three independent experiments. *P <0.05 compared to the control. **D.** Colonies formation in soft agar of MCF-7 C, GABARAPL1 and GABARAPL1 G116A cells. Representative cell colonies in soft agar are shown. Data representative of three independent experiments performed in duplicate are shown. Data are means ± S.E.M of three independent experiements. *P <0.05 compared to the control. **E.** Invasion of MCF-7 C, GABARAPL1, GABARAPL1 G116A c1 and c2 cells in Boyden-modified chamber. A representative image of ten fields of view (FOV) of each membrane is shown. 10 FOV were randomly selected and the number of invasive cells was determined. Data representative of three independent experiments performed in duplicate are shown. Data are means ± S.E.M of three independent experiments. *P <0.05 compared to the control. Scale bar represents 10 µm. **F.** Migration of MCF-7 C, GABARAPL1 and GABARAPL1 G116A cells in Boyden-modified chamber. A representative image of ten fields of view (FOV) of each membrane is shown. 10 FOV were randomly selected and the number of migrative cells was determined. Data representative of three independent experiments performed in duplicate are shown. Data are means ± S.E.M of three independent experiments. *P <0.05 compared to the control. Scale bar represents 10 µm. **G.** Migration of MCF-7 C, GABARAPL1 and GABARAPL1 G116A cells using wound healing assay. Data representative of two independent experiments performed in 8 replicates are shown. The wound area was quantified using imageJ software. Data are means ± S.D of two independent experiments. *P <0.05 compared to the control.

DISCUSSION

GABARAPL1 belongs to the ATG8 family whose function in autophagy has been far less studied than the one linked to the members of the LC3 family. During autophagy, GABARAPL1 is associated with autophagic vesicles and acts with other GABARAP family members to regulate autophagosome maturation [23, 24] and autophagosome-lysosome fusion [56]. Moreover, several studies have highlighted a role of GABARAPL1 as a tumor suppressor protein [25, 47, 50]. This tumor suppressive function has been suggested to be dependent on selective autophagy degradation and its interaction with SQSTM1 [50].

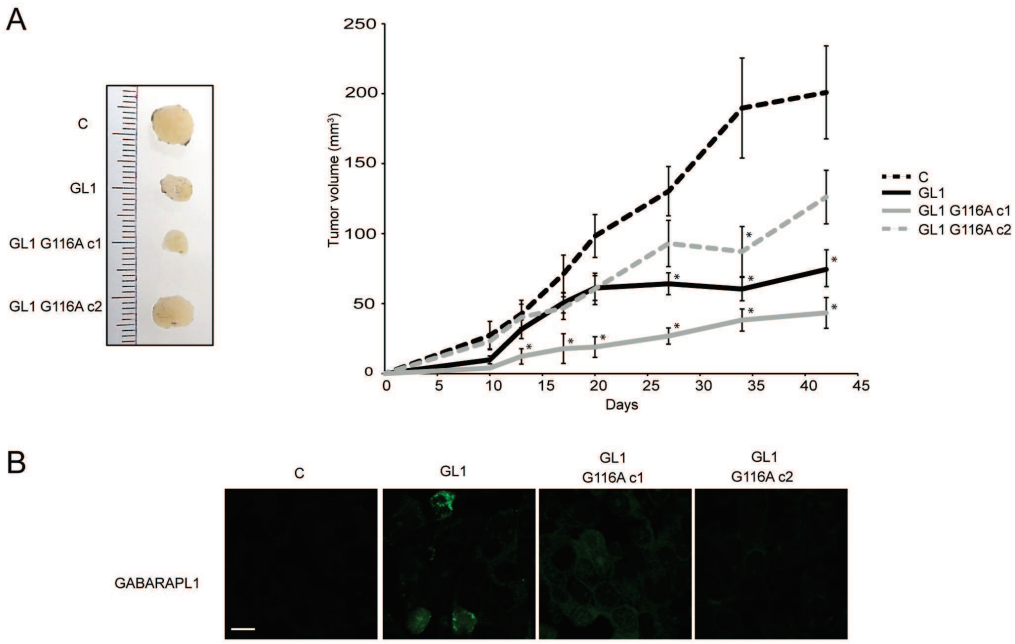

Figure 6: The G116A mutation did not modify the effect of GABARAPL1 on tumor growth *in vivo*. Growth of MCF-7 C, GABARAPL1 and GABARAPL1 G116A cells injected subcutaneously in Rag γ/c mice (n = 12 per group). One week prior to cell inoculation and until the end of the experiment, estrogen was administrated at 1 µg/ml in drinking water. **A.** 13 days after injection, the tumor volume was measured twice a week and the tumor volume was calculated using the formula: $V = ½ (a \times b^2)$, where a is the longest tumor axis, and b is the shortest tumor axis. 42 days after injection, tumors were fixed in formol and photographed. Data are means ± S.E.M. of three independent experiments, *P <0.05, compared to the control. **B.** Immunofluorescence analysis of GABARAPL1 in tissue sections from tumors fixed in formol. A representative image of 2 independent experiments is shown. Scale bar represents 10 µm.

In this study, we demonstrated that GABARAPL1 plays a major role during late stages of autophagy, but can regulate earlier steps of autophagy, as well. More importantly, we showed that these two functions do not necessarily require the conjugation of GABARAPL1 to autophagosomes and significantly, we demonstrated that the tumor suppressive function of GABARAPL1 seems to be independent of its conjugation to autophagosomes (see model in Figure 7).

To investigate the role of GABARAPL1 conjugation to autophagosomes on its tumor suppressive function, we designed two *in vitro* models: one MCF-7 cell line stably overexpressing GABARAPL1 and two stably overexpressing the GABARAPL1 G116A mutant protein which is no longer able to be linked onto phospholipids [23]. In our models, the G116A mutation indeed impaired the cleavage, and subsequently the lipidation and conjugaison of GABARAPL1 to autophagosomes (Figures

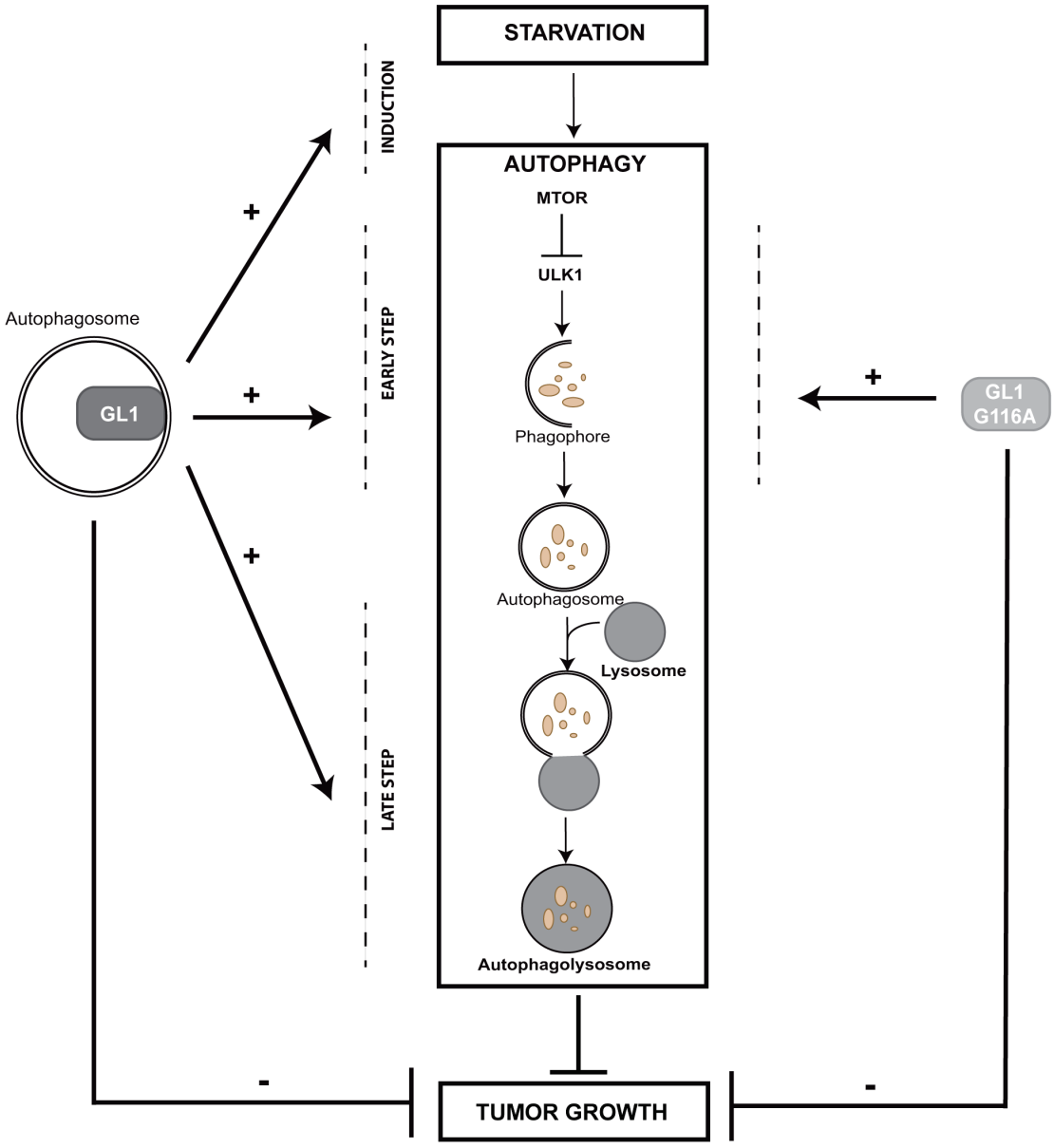

Figure 7: GABARAPL1 functions in autophagy and cancer. Our results demonstrated that GABARAPL1, which is linked to the autophagosome, enhances basal and induced autophagy. GABARAPL1 also increases early stages of autophagy through regulation of MTOR or ULK1 activity and late stages of this process through regulation of lysosome activity and autophagosome/lysosome fusion. GABARAPL1 G116A, which is not linked to the autophagosome, can only enhance basal autophagy through regulation of the early stages of this process. However, GABARAPL1 and GABARAPL1 G116A both inhibit tumor growth *in vivo* suggesting that GABARAPL1 conjugation to autophagosomes as well as its functions during late stages of autophagy is not required for its tumor suppressive functions.

1D-1E). Our data are consistent with previous studies describing similar results for the G120A mutation in LC3 or the G116A mutation in GABARAP or GABARAPL2/GATE-16 [19, 21, 53]. Nevertheless, these previous studies have only investigated the requirement for the C-terminal processing of GABARAP family members on their function in intracellular transport.

GABARAPL1, like the other members of the ATG8 family, can interact with SQSTM1 to enhance the degradation of ubiquitinylated aggregates through selective autophagy [29]. In our models, the G116A mutation impaired the interaction of GABARAPL1 with SQSTM1 (Figure 2E), suggesting that this protein only interacts with GABARAPL1 when it is localized at the surface of the autophagosomes and that the processing of GABARAPL1 is required for its function during selective autophagy with SQSTM1. These results are consistent with data demonstrating that an ATG4B mutant or the mutant LC3 G120A, which both impaired the maturation and lipidation of LC3, inhibited the interaction of LC3 with SQSTM1; suggesting that SQSTM1 preferentially interacted with LC3-II, the lipidated form of LC3, to be efficiently recruited to the autophagosomes and transported into autophagolysosomes [57, 58]. Interestingly, it has been also demonstrated that the mutation of the LC3-binding site in SQSTM1 inhibited the SQSTM1-LC3 interaction and inhibited the degradation of specific substrates through selective autophagy without affecting overall autophagy [59]. Our data are consistent with these results and confirm that the processing of GABARAPL1, like those of other ATG8 family members, could be important for its conjugation to autophagosomes, its interaction with SQSTM1 and its function in selective autophagy.

Previously, we have demonstrated that a knock-down of GABARAPL1 led to a decrease in basal autophagic flux which was suggested to be linked to a decrease in lysosome number [25]. As expected, overexpression of GABARAPL1 in MCF-7 led to an increase in basal autophagic flux. Surprisingly, overexpression of the GABARAPL1 G116A mutant led to a similar result suggesting that the function of GABARAPL1 in basal autophagy might be independent of its conjugation to autophagosomes (Figures 2B and 2D). We have shown that GABARAPL1 and GABARAPL1 G116A both reduced MTOR activation, inhibited ULK1 phosphorylation (Ser757) mediated by MTOR and increased ULK1 phosphorylation (Ser555) mediated by AMPK during the early steps of autophagy (Figure 4). It has been described that ULK1 inhibits MTOR through the phosphorylation of RAPTOR inducing a positive regulatory loop of autophagy induction [60]. We therefore suggested that GABARAPL1, through its interaction with ULK1 [26, 27], could activate this protein leading to the subsequent inhibition of MTOR. In a recent study, Tooze and colleagues have shown that, in HEK293 cells, GABARAP knock-down decreases ULK1 activation demonstrated by the reduction of the phosphorylation in one of its target, ATG13. They also showed that GABARAPL1 interacts with ULK1 *via* its LIR motif but independently of its lipidation [61]. Moreover, it has also been shown in our laboratory, that GABARAPL1 can interact with the energy sensor AMPK (unpublished data), which has been previously shown to inhibit MTOR and activate ULK1 by phosphorylation (Ser555) [5, 8, 62]. Our results are therefore in agreement with previous studies suggesting a link between basal autophagy and MTOR activity [63]. One hypothesis would be that, in fed condition, GABARAPL1 could recruit AMPK in close proximity of the ULK1 complex leading to the increased ULK1 activation, decreased MTOR activity and the induction of basal autophagy.

During induced autophagy following EBSS treatment, overexpression of GABARAPL1, but not GABARAPL1 G116A, led to an increase in autophagic flux suggesting that the role of GABARAPL1 during induced autophagy requires its conjugation to autophagosomes (Figures 2C-2D). This function could be associated with its role in late stages of autophagy. Indeed, overexpression of GABARAPL1, but not GABARAPL1 G116A, led to an increased lysosomal activity and autophagosome/lysosome fusion (Figure 3). These results are in agreement with the recent literature which identified GABARAP family members as primary contributors to starvation-induced autophagy by the regulation of autophagosome-lysosome fusion [56]. Recently, it has been demonstrated that ATG8 family members, localized on the surface of the autophagosomes, could favor autophagosome/lysosome fusion through their interaction with the protein PLEKHM1 (pleckstrin homology domain containing, family M [with RUN domain] member 1) at the lysosomal surface [64, 65]. It has been also demonstrated that the members of the GABARAP family can recruit PI4KIIα (Phosphatidylinositol 4-kinase IIα) to the autophagosomes leading to the generation of PI4P (Phosphatidylinositol 4-phosphate) which favor autophagosome/lysosome fusion [66]. These observations could explain the increase in lysosome activity and autophagosome/lysosome fusion observed in the presence of the membrane-bound GABARAPL1 but not the cytosolic GABARAPL1 G116A. Moreover, GABARAPL1 is known to interact with microtubules and favor their polymerization [14], and microtubules have been shown to regulate autophagosome/lysosome fusion by relocalizing these organelles to the juxta-nuclear region during autophagy [67, 68]. We could then hypothesize that GABARAPL1, but not GABARAPL1 G116A, could improve microtubule polymerization and therefore facilitate the transport of autophagosomes and lysosomes to the juxta-nuclear region to lead to increased autophagosome/lysosome fusion. Moreover, during autophagy, lysosome activation has been described

to require two mechanisms: MTOR inhibition and autophagosome/lysosome fusion [54]. In fact, MTOR not only inhibits ULK1 during early stages of autophagy but also reduces late stages of autophagy through the inhibition of lysosomal function. These data could explain the increased lysosome activity observed in GABARAPL1 overexpressing cells which might present both MTOR inhibition and increased autophagosome/lysosome fusion whereas GABARAPL1 G116A overexpressing cells would only display MTOR inhibition.

Altogether, our results therefore suggest that GABARAPL1 could act during early and late steps of autophagy, functions which are either dependent or independent of its conjugation to autophagosomes. Since GABARAPL1 has also been described as a tumor suppressor protein in breast cancer, we then wondered whether the tumor suppressive function of GABARAPL1 require its conjugation to autophagosomes. *In vitro*, overexpression of GABARAPL1 led to an inhibition of cancer cell phenotypes (proliferation, clonogenicity, adhesion and invasion) which confirmed previous data obtained in the laboratory (Figures 5A-5E) [25, 47]. Interestingly, the G116A mutation inhibited GABARAPL1 tumor suppressive function on several phenotypes apart from migration in MCF7 cells *in vitro* (Figures 5F-5G). Furthermore, the G116A mutation did not alter the effect of GABARAPL1 on cell proliferation and migration phenotypes in another breast cancer cell line BT474 *in vitro* (Figures S4). These data therefore suggest that GABARAPL1 conjugation to autophagosomes may not be necessary for its function in cancer cells *in vitro*.

In order to characterize the effect of GABARAPL1 conjugation to autophagosomes on cancer progression *in vivo*, we studied tumor growth following injection of GABARAPL1 and GABARAPL1 G116A-overexpressing cells into Rag γ/c mice (Figure 6A). Overexpression of GABARAPL1 led to a decrease in tumor size confirming previous results obtained in *nude* mice [50]. Overexpression of GABARAPL1 G116A also led to a decrease in tumor growth suggesting that GABARAPL1 conjugation to autophagosomes could not be necessary for its tumor suppressive function *in vitro* as well as *in vivo*. Moreover, given that GABARAPL1 G116A, which predominately cannot conjugate to autophagosomes and interacts less with SQSTM1, still presented a tumor suppressor role, we might think that GABARAPL1 function in selective autophagy is not essential for its tumor suppressive function. GABARAPL1 and GABARAPL1 G116A could present a tumor suppressor role through the inhibition of MTOR which has been previously shown to be involved in cell proliferation and tumor progression [69-71]. But, we cannot exclude that GABARAPL1 might present a tumor suppressor role through functions independent of its role in autophagy. For example, BECN1, which is a protein involved in the initiation of autophagy and previously described as a tumor suppressor gene frequently deleted or downregulated in cancer [42, 72, 73], can inhibit tumorigenesis through the inhibition of MCL-1 stabilization or WNT1 (wingless-type MMTV integration site family, member 1) activation, two mechanisms independent of autophagy [74, 75].

Our results demonstrate that GABARAPL1 can act during early and late steps of autophagy, independently or not of its conjugation to autophagosomes, respectively. We also showed that its conjugation to autophagosomes as well as its function during late stages of autophagy and selective autophagy is probably not required for its tumor suppressive function *in vivo* (Figure 7).

MATERIALS AND METHODS

Reagents and antibodies

Earle's balanced salt solution (EBSS, E3024), bafilomycin A1 (B1793), chloroquine (C6628), MG132 (C2211) and NH_4Cl (A0171) were purchased from Sigma-Aldrich. For the western blotting experiments, the following antibodies were used: polyclonal anti-GABARAPL1 (Proteintech, 11010-1-AP, 1:1000), monoclonal anti-GABARAPL1/GABARAP (Millipore, AB15278, 1:1000), polyclonal anti-LC3 (Sigma-Aldrich, L8918, 1:3000), monoclonal anti-LAMP1 (Abcam, Ab25630, 1:1000), monoclonal anti-MTOR (Cell signaling, #2983, 1:1000), polyclonal anti-phospho-MTOR (Cell signaling, #2974, 1:1000), polyclonal anti-P70S6K (Cell signaling, #9202, 1:1000), polyclonal anti-phospho-P70S6K (Cell signaling, #9205, 1:1000), monoclonal anti-phospho-ULK1 (Ser555) (Cell signaling, #5869, 1:1000), monoclonal anti-phospho-ULK1 (Ser757) (Cell signaling, #14202, 1:1000), monoclonal anti-ULK1 (Cell signaling, #8054, 1:1000), polyclonal anti-GFP (Chemicon Millipore, AB3080, 1:1000), polyclonal anti-ACTIN (Sigma-Aldrich, A5060, 1:15000), polyclonal anti-rabbit (P.A.R.I.S, BI2407, 1:10000) and polyclonal anti-mouse (P.A.R.I.S, BI24130, 1:10000). For the immunofluorescence and P-LISA experiments, the following antibodies were used: polyclonal anti-GABARAPL1 (Proteintech, 11010-1-AP, 1:200), monoclonal anti-LAMP1 (Abcam, Ab25630, 1:100), monoclonal anti-SQSTM1 (Santa Cruz, sc-28359, 1:250), Alexa Fluor 555 goat anti-mouse (Life technologies, A-21422, 1:800), Alexa Fluor 488 goat anti-rabbit (Life technologies, A-11008, 1:800) and polyclonal anti-rabbit FITC (P.A.R.I.S, BI2107, 1:200).

Cell culture and treatment

MCF-7 control cells (C) and MCF-7 Flag:GABARAPL1:6His (GABARAPL1) cells were obtained previously in our laboratory following

transfection with pcDNA3.1 control, pcDNA3.1-Flag-GABARAPL1-(His)6 [47]. MCF-7-Flag:GABARAPL1-G116A:6his (GABARAPL1 G116A c1 and c2) cells were obtained in the same way following transfection with pcDNA3.1-Flag-GABARAPL1-G116A-(His)6 vectors. The cells were cultured in Dulbecco's minimum essential medium (DMEM) (PAA, E15-891) supplemented with 100 µg/ml penicillin/streptomycin (PAA, P11-010) and 10% fetal bovine serum (FBS) (PAA, A15-101) in a 5 % CO_2 incubator at 37°C. To inhibit autophagosome/lysosome fusion, cells were incubated for 2 h in complete medium supplemented with 100 nM bafilomycin A1, 40 µM chloroquine or 50 mM NH_4Cl. To induce autophagy, cells were incubated in EBSS for 4h at 37°C. To inhibit proteasome degradation, cells were cultured in complete medium supplemented with 2 µM MG132 for 16 h.

For transient transfection, 2 µg of pGFP, pGABARAPL1-GFP, pGABARAPL1-G116A-GFP, 200 µl Jetprime Buffer and 4 µl Jetprime reagent (Polyplus transfection, 114-07) were used per reaction according to the manufacturer's protocol.

Western blotting

Cells were scraped, harvested and lysed in SB1X. Protein lysates were sonicated for 5 s before loading (Sonics and Materials), separated on a 10 or 12.5 % sodium dodecyl sulfate-polyacrylamide gel electrophoresis (SDS-PAGE) before being transferred onto a polyvinylidene difluoride (PVDF) membrane (Bio-Rad, 162-0177). The membrane was blocked with 5 % nonfat milk in Tris-buffered saline with Tween 20 (TBS-T) (20 mM Tris-HCl, pH 7.6, 137 mM NaCl, 0.1 % Tween 20) and incubated with primary antibodies at the previously indicated dilutions. Immunoreactive bands were detected using secondary goat horseradish peroxidase (HRP)-coupled anti-mouse or anti-rabbit antibodies and the *p*-coumaric acid-enhanced chemiluminescent (PCA-ECL) solution [76] and were analyzed using the ChemiDoc XRS+ system (Biorad). Protein levels were quantified using the Image Lab software.

RT-PCR

Total RNAs were extracted as previously described [77]. For RT-PCR analysis, 2 µg of total RNAs were reverse transcribed using the RevertAid M-MulV Reverse Transcriptase to obtain cDNA (Sigma, M1302). The exogenous *GABARAPL1* primer sequences (Flag:GABARAPL1:6His) were: T7 sens 5'-TAAATACGACTCACTATAGGG-3' and BamH1 reverse 5'-CGCGGATCCGCCTTTCCCATAGACACTCTC-3' and the following primer sequences were used for *GAPDH*: GAPDH S 5'-GCGAGATCCCTCCAAAATCA-3' and GAPDH R 5'-TGTGGTCATGAGTCCTTCCA-3'. The DreamTaq DNA polymerase (Life technologies, EP0711) was used to amplify *GABARAPL1* and *GAPDH* from the template cDNA. *GAPDH* was used as an internal control. Polymerase chain reaction was performed for 35 cycles: initial denaturation at 94°C for 5 min, denaturation at 94°C for 30 seconds, annealing at 52°C for 30 seconds, extension at 72°C for 1 min and final extension at 72°C for 10 min. All PCR products were analysed by electrophoresis on a 2% agarose gel and signals were visualized using a Gel doc EZ imager (Biorad).

Immunofluorescence and confocal microscopy

MCF-7 cells were plated on coverslips in 24-well plates at a density of 10^5 cells/well. For transient transfection, the GFP-LC3 (green fluorescent protein-microtubule-associated protein light chain 3) plasmid was kindly provided by Dr. Elazar (Weizmann Institute, Israël) and the ptf-LC3 vector was purchased from Addgene (137624). Plasmids were transfected using the Jetprime reagent (Polyplus transfection, 114-07) according to the manufacturer's protocol. After the designated treatments, cells were washed with phosphate-buffered saline (PBS), fixed with 4 % PFA (paraformaldehyde) in PBS for 15 min at room temperature and mounted in Vectashield Hardset (Vector laboratories, H1400). The cells were then examined and photographed using a confocal microscope (Olympus Fluoview FV1000). For ptf-LC3, green, red and yellow puncta were counted using the "Green and Red puncta colocalization tool" designed for ImageJ. For each experiment, 20 cells were randomly selected.

For Lysotracker staining, cells duplicate were stained with 500 nM of LysoTracker® Red DND-99 (Life technologies, L-7528) for 1 h. Cells were then washed with PBS, fixed with 4 % PFA in PBS for 15 min at room temperature and mounted with Vectashield Hardset. The cells were then examined and photographed using a confocal microscope (Olympus Fluoview FV1000). For each group, 100 cells were randomly selected.

For GABARAPL1, LAMP1 and SQSTM1 immunostaining, cells were washed with PBS and fixed with 4 % PFA in PBS for 15 min at room temperature. Cells were then permeabilized with 0.2 % Triton-X100 in PBS for 5 min, washed with PBS, blocked with 5 % BSA (bovine serum albumin) in PBS for 45 min, incubated with primary antibodies overnight at 4°C, at the previously indicated dilutions, and finally with a secondary goat anti-rabbit-FITC or an Alexa Fluor 555 goat anti-mouse for 1 h. The cells were then mounted with Vectashield Hardset and analyzed using a confocal microscope. Each picture is representative of a typical cell staining observed in 10 fields chosen at random. Colocalization of the autophagosome marker GFP-LC3 and the lysosomal marker LAMP1 was analyzed using a confocal microscope and the Pearson's coefficient using

coloc_2 (ImageJ software). For each group, 25 cells were randomly selected.

For immunofluorescence staining of tumor tissue, tumors were embeded in Tissue-Tek (Microm microtek, F/62550-1) and sliced using a Cryostat (Microm microtech, HM560) (Plateau technique d'histopatholigie, DImaCell platform). The slides were incubated at 95°C for 40 min in sodium citrate buffer (10 mM sodium citrate, pH 6), overnight with the previously described GABARAPL1 antibody and 1 h at room temperature with an Alexa Fluor 488 goat anti-rabbit secondary antibody at previously indicated dilutions. After each incubation, the slides were rinsed thrice in 1% PBS-Triton X-100. After being mounted in PBS-glycerol mounting medium, the slides were observed and analyzed using a confocal microscope (Olympus Fluoview FV1000). Two independent experiments were performed.

Cell migration and invasion assays

10^5 cells were diluted in 250 µl serum-free medium, added to the upper chamber of the Boyden modified chamber™ (SPL Life Sciences) and incubated for 24 h at 37°C. For the cell invasion assay, 50 µl of extra cellular matrix (ECM) gel (Sigma-Aldrich, E1270, 1 mg/ml) were added to the upper chamber 5 h before cell seeding. The invasive cells were fixed, stained with 2 % crystal violet and images of each membrane were acquired. Finally, the invasive cells located in the lower chamber were counted manually. 10 FOV were randomly selected and the number of invasive and migrative cells was determined. Three independent experiments were performed in duplicate.

Cell proliferation

Cells were plated in 96-well plates at a density of 1.5 x 10^3 cells/well and cell proliferation experiments were conducted over a 7-day period using MTT [3-(4,5-dimethylthiazol-2-yl)-2,5- diphenyl tetrazolium bromide] (Sigma-Aldrich, M2128). Each day, 100 µl of 100 mM MTT solution in Hank's were added to the cells after the removal of the supernatant. After a 2 h incubation, the formazan crystals were dissolved in 50 µl of DMSO (dimethyl sulfoxide) (Euromedex, UD8050-A) and the absorbance was quantified at 549 nm using a microplate reader (Multiskan FC, ThermoScientific). For each clone, three independent experiments were performed in 24 wells of a 96 well-plate.

Colony formation assay

Cells were plated duplicate in 6-well plates at a density of 2 x 10^3 cells/well. After 15 days, colonies were fixed with 100% ethanol for 10 min and stained with 2% crystal violet for 10 min. The dye in excess was rinced with water and the colony number was imaged using a ChemiDoc XRS+ and Image Lab 2.0 software (Biorad). Quantitative changes in clonogenicity were determined by counting the colonies, using Bio-Rad Vision-Capt software. Three independent experiments were performed in duplicate.

Cell-matrix adhesion assay

Cells were plated in 24-well plates at a density of 4 × 10^5 cells/well in serum-free DMEM for 1 h and 3 h at 37°C (three wells/cell line: one well to control the number of seeded cells and the two others for the two different times after seeding). After washing, adherent cells were collected and pelleted. Then, cells were counted using a Malassez cell. Results were expressed as the ratio of adherent cells versus total seeded cells. Three independent experiments were performed in triplicate.

Anchorage independent cell proliferation

Cells were seeded in 6-well plates at a density of 5 × 10^5 cells/well in 0.3% agar (Fisher Scientific, 10776644). Before seeding, 0.6% agar was added into each well. The cell layers were then covered with complete medium and cultured for 25 days at 37°C. Images from four representative fields of each well were taken and analyzed. Three independent experiments were performed in duplicate.

Wound healing assay

Cells were seeded in 6-well plates at a density of 5 x 10^5 cells/well. Following confluency, two artificial wound per well were performed into the monolayers using a micropipette tip. After wounding, the tissue culture medium was removed, and cells were washed at least twice in PBS to eliminate detached cells. Wound closure was monitored after 24 h, 48 h and 72 h using image J software. The migration of cells was expressed as the percentage of wound closure: % of wound closure = $[(A_{t=0\ h} - A_{t=\Delta h})/A_{t=0\ h}] \times 100\%$. $A_{t=0h}$ is the wound area measured immediately after scratching, and $A_{t=\Delta\ h}$ is the wound area measured at 24 h, 48 h and 72 h after scratching. Two independent experiments were performed in 8 replicates.

Xenograft experiments

Rag γ/c mice were obtained from Taconic (Germantown, NY, USA) and maintained in the UMR1098 animal facility (agreement number #C25-056-7). Approval for animal experimentation and care was received from the "Services Vétérinaires de la Santé et de la Protection

Animale" delivered by the "Ministère de l'Agriculture", Paris, France and experimental procedures were approved by a local ethic committee. One week prior to cell inoculation and until the end of the experiment, estrogens were administrated at 1 µg/ml in drinking water. A total of 1.5×10^6 cells of the different cell lines resuspended in 100 µL of PBS were inoculated subcutaneously in RAGg/c mice (n = 9 per group) and tumor growth was monitored two times a week in each group. Tumor volume was calculated by the formula $V = ½ (a \times b^2)$, where a is the longest tumor axis and b is the shortest tumor axis. When tumors reached 1 cm in diameter, mice were sacrified and each tumor was fixed in formol and photographed.

Proximity ligation *in situ* assay (P-LISA)

MCF-7 cells were cultured for 24 h on coverslips and then fixed and permeabilized using cold methanol for 20 min at -20°C. P-LISA staining was performed according to the OlinkBioscience's recommendations using Duolink® In Situ Detection Reagents Red kit (Sigma-Aldrich, DUO92008) and as previously described [51]. The number of red dots and the intensity per dots were counted using the Blobfinder software. 200 cells were randomly selected in 5 fields.

Transmission Electron microscopy

MCF-7 cells were washed in 0.1M Sörensen buffer, pH 7.3. Then, cells were fixed with 2% glutaraldehyde (Sigma Aldrich, G5882) in 0.1M Sörensen buffer, pH 7.3 for 1 h at 4°C, and post-fixed in the mixture 1% osmium tetroxide (Sigma Aldrich, 75632) and 1.5% potassium ferricyanide (Sigma Aldrich, 702587) in 0.2M Sörensen buffer, pH 7.3 for 1 h at 4°C. The cells cultures were dehydrated through a graded series of ethanol to 100%, embedded in Poly/Bed 812 resin (Polysciences, 21844-1) and polymerized for 48h at 60°C. Ultrathin sections were collected on 100 mesh nickel grids coated formvar-carbon (Delta microscopy), stained with uranyl acetate (Polysciences, 21447-25) and lead citrate. Then, they were imaged using a Technaï 12 Biotwin TEM microscope (Primacen Platform, University of Rouen). Representative image of 60 pictures for each cell lines is shown.

Flow cytometry

Cells were plated in 24-well plates at a concentration of 2×10^5 cells/well and incubated at 37°C overnight following the different treatments. Cells were stained with MagicRed (Immunochemistry technologies) according to the manufacturer's protocol or 50 nM LysoTracker® Green DND-26 (Life technologies, L-7526) for 45 min. After two PBS washes, cells were then trypsinized and resuspended with 500 µl complete medium before being harvested at 5,000 g for 5 min and resuspended in 250 µl PBS. Cells (10,000 events) were then examined using a FC500 Beckman Coulter flow cytometer. Data were acquired and analyzed using the Flowing software.

Statistical analysis

Statistical analyses were carried out using a Student's t test. A p value <0.05 was considered as statistically significant.

ACKNOWLEDGMENTS

We thank Pierre-Yves Risold for his help and advices during immunofluorescence experiments and Christophe Houdayer for his technical help and advices during the preparation of tumor tissue slides (Plateau technique d'histopathologie, DImaCell, Besançon). Authors also thank Sophie Launay (Plateau technique Imagerie Cellulaire et Tissulaire, DImaCell, Besançon) and Valérie Perez for their technical help. We thank Dr. Elazar for kindly providing the pGFP-LC3 vector and Dr. Mehul Vora for critically reading of our manuscript. Laura Poillet-Perez was supported by a fellowship from the "Région de Franche-Comté" and this work was supported by a fellowship from the "Ligue contre le cancer" (Conférence de Coordination Inter Régionale Grand Est). We thank D.J. Shiwarski, R.K. Dagda, C.T. Chu for providing the "Green and Red puncta colocalization tool" designed for ImageJ.

CONFLICTS OF INTEREST

There are no financial disclosures from any authors.

REFERENCES

1. Yang Z, Klionsky DJ. Mammalian autophagy: core molecular machinery and signaling regulation. Curr Opin Cell Biol. 2010; 22: 124-31. doi: 10.1016/j.ceb.2009.11.014 S0955-0674(09)00228-2.
2. Rubinsztein DC, Shpilka T, Elazar Z. Mechanisms of autophagosome biogenesis. Curr Biol. 2012; 22: R29-34. doi: 10.1016/j.cub.2011.11.034 S0960-9822(11)01316-9.
3. Xie Z, Klionsky DJ. Autophagosome formation: core machinery and adaptations. Nat Cell Biol. 2007; 9: 1102-9. doi: ncb1007-1102 10.1038/ncb1007-1102.
4. Feng Y, He D, Yao Z, Klionsky DJ. The machinery of macroautophagy. Cell Res. 2014; 24: 24-41. doi: 10.1038/cr.2013.168 cr2013168
5. Gwinn DM, Shackelford DB, Egan DF, Mihaylova MM, Mery A, Vasquez DS, Turk BE, Shaw RJ. AMPK phosphorylation of raptor mediates a metabolic

checkpoint. Mol Cell. 2008; 30: 214-26. doi: 10.1016/j.molcel.2008.03.003 S1097-2765(08)00169-X.

6. Dunlop EA, Tee AR. mTOR and autophagy: a dynamic relationship governed by nutrients and energy. Semin Cell Dev Biol. 2014; 36: 121-9. doi: 10.1016/j.semcdb.2014.08.006 S1084-9521(14)00242-0.

7. Kim J, Kundu M, Viollet B, Guan KL. AMPK and mTOR regulate autophagy through direct phosphorylation of Ulk1. Nat Cell Biol. 2011; 13: 132-41. doi: 10.1038/ncb2152.

8. Egan DF, Shackelford DB, Mihaylova MM, Gelino S, Kohnz RA, Mair W, Vasquez DS, Joshi A, Gwinn DM, Taylor R, Asara JM, Fitzpatrick J, Dillin A, et al. Phosphorylation of ULK1 (hATG1) by AMP-activated protein kinase connects energy sensing to mitophagy. Science. 2011; 331: 456-61. doi: 10.1126/science.1196371 science.1196371.

9. Egan D, Kim J, Shaw RJ, Guan KL. The autophagy initiating kinase ULK1 is regulated via opposing phosphorylation by AMPK and mTOR. Autophagy. 2011; 7: 643-4. doi:

10. Pellerin I, Vuillermoz C, Jouvenot M, Ordener C, Royez M, Adessi GL. Identification and characterization of an early estrogen-regulated RNA in cultured guinea-pig endometrial cells. Mol Cell Endocrinol. 1993; 90: R17-21. doi:

11. Wang H, Bedford FK, Brandon NJ, Moss SJ, Olsen RW. GABA(A)-receptor-associated protein links GABA(A) receptors and the cytoskeleton. Nature. 1999; 397: 69-72. doi: 10.1038/16264.

12. Sagiv Y, Legesse-Miller A, Porat A, Elazar Z. GATE-16, a membrane transport modulator, interacts with NSF and the Golgi v-SNARE GOS-28. EMBO J. 2000; 19: 1494-504. doi: 10.1093/emboj/19.7.1494.

13. Vernier-Magnin S, Muller S, Sallot M, Radom J, Musard JF, Adami P, Dulieu P, Remy-Martin JP, Jouvenot M, Fraichard A. A novel early estrogen-regulated gene gec1 encodes a protein related to GABARAP. Biochem Biophys Res Commun. 2001; 284: 118-25. doi: 10.1006/bbrc.2001.4908 S0006-291X(01)94908-3.

14. Mansuy V, Boireau W, Fraichard A, Schlick JL, Jouvenot M, Delage-Mourroux R. GEC1, a protein related to GABARAP, interacts with tubulin and GABA(A) receptor. Biochem Biophys Res Commun. 2004; 325: 639-48. doi: S0006-291X(04)02315-0 10.1016/j.bbrc.2004.10.072.

15. Chen C, Li JG, Chen Y, Huang P, Wang Y, Liu-Chen LY. GEC1 interacts with the kappa opioid receptor and enhances expression of the receptor. J Biol Chem. 2006; 281: 7983-93. doi: M509805200 10.1074/jbc.M509805200.

16. Seguin-Py S, Lucchi G, Croizier S, Chakrama FZ, Despouy G, Le Grand JN, Ducoroy P, Boireau W, Boyer-Guittaut M, Jouvenot M, Fraichard A, Delage-Mourroux R. Identification of HSP90 as a new GABARAPL1 (GEC1)-interacting protein. Biochimie. 2012; 94: 748-58. doi: 10.1016/j.biochi.2011.11.006 S0300-9084(11)00422-6.

17. Tanida I, Ueno T, Kominami E. LC3 conjugation system in mammalian autophagy. Int J Biochem Cell Biol. 2004; 36: 2503-18. doi: 10.1016/j.biocel.2004.05.009 S1357272504002110.

18. Betin VM, Lane JD. Caspase cleavage of Atg4D stimulates GABARAP-L1 processing and triggers mitochondrial targeting and apoptosis. J Cell Sci. 2009; 122: 2554-66. doi: 10.1242/jcs.046250 jcs.046250.

19. Tanida I, Komatsu M, Ueno T, Kominami E. GATE-16 and GABARAP are authentic modifiers mediated by Apg7 and Apg3. Biochem Biophys Res Commun. 2003; 300: 637-44. doi: S0006291X02029078.

20. Tanida I, Ueno T, Kominami E. Human light chain 3/MAP1LC3B is cleaved at its carboxyl-terminal Met121 to expose Gly120 for lipidation and targeting to autophagosomal membranes. J Biol Chem. 2004; 279: 47704-10. doi: 10.1074/jbc.M407016200.

21. Kabeya Y, Mizushima N, Yamamoto A, Oshitani-Okamoto S, Ohsumi Y, Yoshimori T. LC3, GABARAP and GATE16 localize to autophagosomal membrane depending on form-II formation. J Cell Sci. 2004; 117: 2805-12. doi: 10.1242/jcs.01131 117/13/2805.

22. Tanida I, Sou YS, Ezaki J, Minematsu-Ikeguchi N, Ueno T, Kominami E. HsAtg4B/HsApg4B/autophagin-1 cleaves the carboxyl termini of three human Atg8 homologues and delipidates microtubule-associated protein light chain 3- and GABAA receptor-associated protein-phospholipid conjugates. J Biol Chem. 2004; 279: 36268-76. doi: 10.1074/jbc.M401461200 M401461200.

23. Chakrama FZ, Seguin-Py S, Le Grand JN, Fraichard A, Delage-Mourroux R, Despouy G, Perez V, Jouvenot M, Boyer-Guittaut M. GABARAPL1 (GEC1) associates with autophagic vesicles. Autophagy. 2010; 6: 495-505. doi: 10.4161/auto.6.4.11819 11819.

24. Weidberg H, Shvets E, Shpilka T, Shimron F, Shinder V, Elazar Z. LC3 and GATE-16/GABARAP subfamilies are both essential yet act differently in autophagosome biogenesis. EMBO J. 2010; 29: 1792-802. doi: 10.1038/emboj.2010.74 emboj201074.

25. Boyer-Guittaut M, Poillet L, Liang Q, Bole-Richard E, Ouyang X, Benavides GA, Chakrama FZ, Fraichard A, Darley-Usmar VM, Despouy G, Jouvenot M, Delage-Mourroux R, Zhang J. The role of GABARAPL1/GEC1 in autophagic flux and mitochondrial quality control in MDA-MB-436 breast cancer cells. Autophagy. 2014; 10: 986-1003. doi: 10.4161/auto.28390 28390.

26. Alemu EA, Lamark T, Torgersen KM, Birgisdottir AB, Larsen KB, Jain A, Olsvik H, Overvatn A, Kirkin V, Johansen T. ATG8 family proteins act as scaffolds for assembly of the ULK complex: sequence requirements for LC3-interacting region (LIR) motifs. J Biol Chem. 2012; 287: 39275-90. doi: 10.1074/jbc.M112.378109 M112.378109.

27. Kraft C, Kijanska M, Kalie E, Siergiejuk E, Lee SS, Semplicio G, Stoffel I, Brezovich A, Verma M, Hansmann I, Ammerer G, Hofmann K, Tooze S, et al. Binding of

the Atg1/ULK1 kinase to the ubiquitin-like protein Atg8 regulates autophagy. EMBO J. 2012; 31: 3691-703. doi: 10.1038/emboj.2012.225 emboj2012225.

28. Weidberg H, Shvets E, Elazar Z. Biogenesis and cargo selectivity of autophagosomes. Annu Rev Biochem. 2011; 80: 125-56. doi: 10.1146/annurev-biochem-052709-094552.
29. Pankiv S, Clausen TH, Lamark T, Brech A, Bruun JA, Outzen H, Overvatn A, Bjorkoy G, Johansen T. p62/SQSTM1 binds directly to Atg8/LC3 to facilitate degradation of ubiquitinated protein aggregates by autophagy. J Biol Chem. 2007; 282: 24131-45. doi: M702824200 10.1074/jbc.M702824200.
30. Kirkin V, Lamark T, Sou YS, Bjorkoy G, Nunn JL, Bruun JA, Shvets E, McEwan DG, Clausen TH, Wild P, Bilusic I, Theurillat JP, Overvatn A, et al. A role for NBR1 in autophagosomal degradation of ubiquitinated substrates. Mol Cell. 2009; 33: 505-16. doi: 10.1016/j.molcel.2009.01.020 S1097-2765(09)00064-1.
31. Rozenknop A, Rogov VV, Rogova NY, Lohr F, Guntert P, Dikic I, Dotsch V. Characterization of the interaction of GABARAPL-1 with the LIR motif of NBR1. J Mol Biol. 2011; 410: 477-87. doi: 10.1016/j.jmb.2011.05.003 S0022-2836(11)00524-9.
32. Novak I, Kirkin V, McEwan DG, Zhang J, Wild P, Rozenknop A, Rogov V, Lohr F, Popovic D, Occhipinti A, Reichert AS, Terzic J, Dotsch V, et al. Nix is a selective autophagy receptor for mitochondrial clearance. EMBO Rep. 2010; 11: 45-51. doi: 10.1038/embor.2009.256 embor2009256.
33. Pankiv S, Lamark T, Bruun JA, Overvatn A, Bjorkoy G, Johansen T. Nucleocytoplasmic shuttling of p62/SQSTM1 and its role in recruitment of nuclear polyubiquitinated proteins to promyelocytic leukemia bodies. J Biol Chem. 2010; 285: 5941-53. doi: 10.1074/jbc.M109.039925 M109.039925.
34. Choi AM, Ryter SW, Levine B. Autophagy in human health and disease. N Engl J Med. 2013; 368: 651-62. doi: 10.1056/NEJMra1205406.
35. White E, DiPaola RS. The double-edged sword of autophagy modulation in cancer. Clin Cancer Res. 2009; 15: 5308-16. doi: 10.1158/1078-0432.CCR-07-5023 1078-0432.CCR-07-5023.
36. Morselli E, Galluzzi L, Kepp O, Vicencio JM, Criollo A, Maiuri MC, Kroemer G. Anti- and pro-tumor functions of autophagy. Biochim Biophys Acta. 2009; 1793: 1524-32. doi: 10.1016/j.bbamcr.2009.01.006 S0167-4889(09)00024-X.
37. Poillet-Perez L, Despouy G, Delage-Mourroux R, Boyer-Guittaut M. Interplay between ROS and autophagy in cancer cells, from tumor initiation to cancer therapy. Redox Biol. 2014; 4C: 184-92. doi: S2213-2317(14)00127-X 10.1016/j.redox.2014.12.003.
38. Mathew R, Kongara S, Beaudoin B, Karp CM, Bray K, Degenhardt K, Chen G, Jin S, White E. Autophagy suppresses tumor progression by limiting chromosomal instability. Genes Dev. 2007; 21: 1367-81. doi: gad.1545107 10.1101/gad.1545107.
39. Karantza-Wadsworth V, Patel S, Kravchuk O, Chen G, Mathew R, Jin S, White E. Autophagy mitigates metabolic stress and genome damage in mammary tumorigenesis. Genes Dev. 2007; 21: 1621-35. doi: 21/13/1621 10.1101/gad.1565707.
40. Klebig C, Seitz S, Arnold W, Deutschmann N, Pacyna-Gengelbach M, Scherneck S, Petersen I. Characterization of {gamma}-aminobutyric acid type A receptor-associated protein, a novel tumor suppressor, showing reduced expression in breast cancer. Cancer Res. 2005; 65: 394-400. doi: 65/2/394.
41. Bai H, Inoue J, Kawano T, Inazawa J. A transcriptional variant of the LC3A gene is involved in autophagy and frequently inactivated in human cancers. Oncogene. 2012; 31: 4397-408. doi: 10.1038/onc.2011.613 onc2011613.
42. Liang XH, Jackson S, Seaman M, Brown K, Kempkes B, Hibshoosh H, Levine B. Induction of autophagy and inhibition of tumorigenesis by beclin 1. Nature. 1999; 402: 672-6. doi: 10.1038/45257.
43. Liang C, Feng P, Ku B, Dotan I, Canaani D, Oh BH, Jung JU. Autophagic and tumour suppressor activity of a novel Beclin1-binding protein UVRAG. Nat Cell Biol. 2006; 8: 688-99. doi: ncb1426 10.1038/ncb1426.
44. Kang MR, Kim MS, Oh JE, Kim YR, Song SY, Kim SS, Ahn CH, Yoo NJ, Lee SH. Frameshift mutations of autophagy-related genes ATG2B, ATG5, ATG9B and ATG12 in gastric and colorectal cancers with microsatellite instability. J Pathol. 2009; 217: 702-6. doi: 10.1002/path.2509.
45. Brahimi-Horn MC, Bellot G, Pouyssegur J. Hypoxia and energetic tumour metabolism. Curr Opin Genet Dev. 2011; 21: 67-72. doi: 10.1016/j.gde.2010.10.006 S0959-437X(10)00173-5.
46. Harris AL. Hypoxia—a key regulatory factor in tumour growth. Nat Rev Cancer. 2002; 2: 38-47. doi: 10.1038/nrc704.
47. Berthier A, Seguin S, Sasco AJ, Bobin JY, De Laroche G, Datchary J, Saez S, Rodriguez-Lafrasse C, Tolle F, Fraichard A, Boyer-Guittaut M, Jouvenot M, Delage-Mourroux R, et al. High expression of gabarapl1 is associated with a better outcome for patients with lymph node-positive breast cancer. Br J Cancer. 2010; 102: 1024-31. doi: 10.1038/sj.bjc.6605568.
48. Nemos C, Mansuy V, Vernier-Magnin S, Fraichard A, Jouvenot M, Delage-Mourroux R. Expression of gec1/GABARAPL1 versus GABARAP mRNAs in human: predominance of gec1/GABARAPL1 in the central nervous system. Brain Res Mol Brain Res. 2003; 119: 216-9. doi: S0169328X03004339.
49. Liu C, Xia Y, Jiang W, Liu Y, Yu L. Low expression of GABARAPL1 is associated with a poor outcome for

patients with hepatocellular carcinoma. Oncol Rep. 2014; 31: 2043-8. doi: 10.3892/or.2014.3096.

50. Zhang Y, Wang F, Han L, Wu Y, Li S, Yang X, Wang Y, Ren F, Zhai Y, Wang D, Jia B, Xia Y, Chang Z. GABARAPL1 negatively regulates Wnt/beta-catenin signaling by mediating Dvl2 degradation through the autophagy pathway. Cell Physiol Biochem. 2011; 27: 503-12. doi: 10.1159/000329952000329952.
51. Gauthier T, Claude-Taupin A, Delage-Mourroux R, Boyer-Guittaut M, Hervouet E. Proximity Ligation In situ Assay is a Powerful Tool to Monitor Specific ATG Protein Interactions following Autophagy Induction. PLoS One. 2015; 10: e0128701. doi: 10.1371/journal.pone.0128701PONE-D-15-11618.
52. Kimura S, Noda T, Yoshimori T. Dissection of the autophagosome maturation process by a novel reporter protein, tandem fluorescent-tagged LC3. Autophagy. 2007; 3: 452-60. doi: 4451.
53. Kabeya Y, Mizushima N, Ueno T, Yamamoto A, Kirisako T, Noda T, Kominami E, Ohsumi Y, Yoshimori T. LC3, a mammalian homologue of yeast Apg8p, is localized in autophagosome membranes after processing. EMBO J. 2000; 19: 5720-8. doi: 10.1093/emboj/19.21.5720.
54. Zhou J, Tan SH, Nicolas V, Bauvy C, Yang ND, Zhang J, Xue Y, Codogno P, Shen HM. Activation of lysosomal function in the course of autophagy via mTORC1 suppression and autophagosome-lysosome fusion. Cell Res. 2013; 23: 508-23. doi: 10.1038/cr.2013.11cr201311.
55. Ghislat G, Patron M, Rizzuto R, Knecht E. Withdrawal of essential amino acids increases autophagy by a pathway involving Ca2+/calmodulin-dependent kinase kinase-beta (CaMKK-beta). J Biol Chem. 2012; 287: 38625-36. doi: 10.1074/jbc.M112.365767.
56. Nguyen TN, Padman BS, Usher J, Oorschot V, Ramm G, Lazarou M. Atg8 family LC3/GABARAP proteins are crucial for autophagosome-lysosome fusion but not autophagosome formation during PINK1/Parkin mitophagy and starvation. J Cell Biol. 2016. doi: 10.1083/jcb.201607039.
57. Lim J, Kim HW, Youdim MB, Rhyu IJ, Choe KM, Oh YJ. Binding preference of p62 towards LC3-ll during dopaminergic neurotoxin-induced impairment of autophagic flux. Autophagy. 2011; 7: 51-60. doi: 13909.
58. Gao W, Kang JH, Liao Y, Ding WX, Gambotto AA, Watkins SC, Liu YJ, Stolz DB, Yin XM. Biochemical isolation and characterization of the tubulovesicular LC3-positive autophagosomal compartment. J Biol Chem. 2010; 285: 1371-83. doi: 10.1074/jbc.M109.054197 M109.054197.
59. Tung YT, Hsu WM, Lee H, Huang WP, Liao YF. The evolutionarily conserved interaction between LC3 and p62 selectively mediates autophagy-dependent degradation of mutant huntingtin. Cell Mol Neurobiol. 2010; 30: 795-806. doi: 10.1007/s10571-010-9507-y.
60. Dunlop EA, Hunt DK, Acosta-Jaquez HA, Fingar DC, Tee AR. ULK1 inhibits mTORC1 signaling, promotes multisite Raptor phosphorylation and hinders substrate binding. Autophagy. 2011; 7: 737-47. doi: 15491.
61. Joachim J, Jefferies HB, Razi M, Frith D, Snijders AP, Chakravarty P, Judith D, Tooze SA. Activation of ULK Kinase and Autophagy by GABARAP Trafficking from the Centrosome Is Regulated by WAC and GM130. Mol Cell. 2015; 60: 899-913. doi: 10.1016/j.molcel.2015.11.018.
62. Inoki K, Zhu T, Guan KL. TSC2 mediates cellular energy response to control cell growth and survival. Cell. 2003; 115: 577-90. doi: S0092867403009292.
63. Musiwaro P, Smith M, Manifava M, Walker SA, Ktistakis NT. Characteristics and requirements of basal autophagy in HEK 293 cells. Autophagy. 2013; 9: 1407-17. doi: 10.4161/auto.25455.
64. McEwan DG, Dikic I. PLEKHM1: Adapting to life at the lysosome. Autophagy. 2015: 0. doi: 10.1080/15548627.2015.1034419.
65. McEwan DG, Popovic D, Gubas A, Terawaki S, Suzuki H, Stadel D, Coxon FP, Miranda de Stegmann D, Bhogaraju S, Maddi K, Kirchof A, Gatti E, Helfrich MH, et al. PLEKHM1 regulates autophagosome-lysosome fusion through HOPS complex and LC3/GABARAP proteins. Mol Cell. 2015; 57: 39-54. doi: 10.1016/j.molcel.2014.11.006S1097-2765(14)00871-5.
66. Wang H, Sun HQ, Zhu X, Zhang L, Albanesi J, Levine B, Yin H. GABARAPs regulate PI4P-dependent autophagosome:lysosome fusion. Proc Natl Acad Sci U S A. 2015; 112: 7015-20. doi: 10.1073/pnas.1507263112.
67. Mackeh R, Perdiz D, Lorin S, Codogno P, Pous C. Autophagy and microtubules - new story, old players. J Cell Sci. 2013; 126: 1071-80. doi: 10.1242/jcs.115626126/5/1071.
68. Fass E, Shvets E, Degani I, Hirschberg K, Elazar Z. Microtubules support production of starvation-induced autophagosomes but not their targeting and fusion with lysosomes. J Biol Chem. 2006; 281: 36303-16. doi: M607031200.
69. Laplante M, Sabatini DM. mTOR signaling in growth control and disease. Cell. 2012; 149: 274-93. doi: 10.1016/j.cell.2012.03.017S0092-8674(12)00351-0.
70. Cornu M, Albert V, Hall MN. mTOR in aging, metabolism, and cancer. Curr Opin Genet Dev. 2013; 23: 53-62. doi: 10.1016/j.gde.2012.12.005S0959-437X(12)00149-9.
71. Mamane Y, Petroulakis E, LeBacquer O, Sonenberg N. mTOR, translation initiation and cancer. Oncogene. 2006; 25: 6416-22. doi: 10.1038/sj.onc.1209888.
72. Aita VM, Liang XH, Murty VV, Pincus DL, Yu W, Cayanis E, Kalachikov S, Gilliam TC, Levine B. Cloning and genomic organization of beclin 1, a candidate tumor suppressor gene on chromosome 17q21. Genomics. 1999; 59: 59-65. doi: 10.1006/geno.1999.5851 S0888-7543(99)95851-2.

73. Qu X, Yu J, Bhagat G, Furuya N, Hibshoosh H, Troxel A, Rosen J, Eskelinen EL, Mizushima N, Ohsumi Y, Cattoretti G, Levine B. Promotion of tumorigenesis by heterozygous disruption of the beclin 1 autophagy gene. J Clin Invest. 2003; 112: 1809-20. doi: 10.1172/JCI20039.

74. Elgendy M, Ciro M, Abdel-Aziz AK, Belmonte G, Dal Zuffo R, Mercurio C, Miracco C, Lanfrancone L, Foiani M, Minucci S. Beclin 1 restrains tumorigenesis through Mcl-1 destabilization in an autophagy-independent reciprocal manner. Nat Commun. 2014; 5: 5637. doi: 10.1038/ncomms6637.

75. Cicchini M, Chakrabarti R, Kongara S, Price S, Nahar R, Lozy F, Zhong H, Vazquez A, Kang Y, Karantza V. Autophagy regulator BECN1 suppresses mammary tumorigenesis driven by WNT1 activation and following parity. Autophagy. 2014; 10: 2036-52. doi: 10.4161/auto.34398.

76. Haan C, Behrmann I. A cost effective non-commercial ECL-solution for Western blot detections yielding strong signals and low background. J Immunol Methods. 2007; 318: 11-9. doi: S0022-1759(06)00294-8 10.1016/j.jim.2006.07.027.

77. Morel C, Adami P, Musard JF, Duval D, Radom J, Jouvenot M. Involvement of sulfhydryl oxidase QSOX1 in the protection of cells against oxidative stress-induced apoptosis. Exp Cell Res. 2007; 313: 3971-82. doi: S0014-4827(07)00428-4 10.1016/j.yexcr.2007.09.003.

The anti-inflammatory effects of platelet-derived microparticles in human plasmacytoid dendritic cells involve liver X receptor activation

Innate immune responses play a critical role in atherosclerosis progression. Beside the well-known implication of macrophages,[1] plasmacytoid dendritic cells (PDC) emerge as cells present in atherosclerotic lesions that may participate in or regulate atherosclerosis.[2] These cells can exert both pro- and anti-inflammatory functions.[3] This is the case of other cellular messengers, namely microparticles (MP),[4] also implicated in atherosclerosis.[4] Depending on their cellular origin, MP could either activate or inhibit PDC inflammatory responses.[5] However, signaling pathways involved in these PDC responses still have to be identified. As membrane-derived by-products, MP after internalization can be a source of intracellular cholesterol derivatives[6] that trigger liver X receptors (LXR).[7] LXR are nuclear receptors regulating innate immune responses,[8] including cell-derived by-product internalization, such as apoptotic bodies[9] that belong together with MP to extracellular vesicles. Here, implication of the LXR pathway in MP engulfment by PDC and the subsequent PDC inflammatory responses were investigated.

Human PDC were isolated by magnetic cell separation (Diamond PDC Isolation Kit II, Miltenyi Biotec) from blood of healthy donors after the signature of informed consent and were stimulated with 3 different LXR agonists: 22-R-Hydroxycholesterol (22RHC), T0901317 and GW3965, LXR antagonist 22-S-Hydroxycholesterol (22SHC, Sigma Aldrich), MP or toll-like receptor (TLR)7 ligand, R848 (1 μg/mL, or TLR9 ligand, CpG-ODN2216 [class A CpG-containing oligodeoxynucleotides (ODN), 2 μmol/L; Invivogen]. Endothelial-derived MP (EMP) were isolated from a TNF-α-stimulated endothelial cell line and platelet-derived MP (PMP) from platelet concentrate supernatants of healthy donors as described in the *Online Supplementary Methods*. Microparticle size (using Megamix plus™ microbeads, BioCytex), count (using Cytocount® microbeads, Dako) and phenotype [(CD31, CD41, CD235a expression or Annexin V (AnxV) staining)] were determined by cytometry (Navios cytometer with the CXP software, and analyzed with the Kaluza 1.2 software (Beckman Coulter). PDC expression of CD123, BDCA-2/CD303, BAI-1 (brain-specific angiogenesis inhibitor-1) and intracellular TNF-α, as well as detection of eFluor+ PDC after incubation with eFluor-labeled MP, were determined by cytometry (FACS Canto II cytometer with DIVA 6.1 software, BD Biosciences). Unconjugated monoclonal antibodies and their control isotypes were used to block BAI-1 or detect CD123, ABCA1 (ATP-binding cassette transporter A1) and phosphorylated NF-κB subunit RelA (pRelA) after staining with a fluorochrome-conjugated anti-Ig secondary antibody (Life Technologies). Fluorescent images were acquired on an Olympus FV1000 confocal microscope and analyzed with Olympus FV-viewer software. Culture supernatants were collected after PDC treatment to measure the following cytokines: TNF-α, IL-6 and IL-8 (DIAplex technology, Diaclone), or interferon (IFN)-α (Platinum ELISA kit; eBioscience). Expression of LXR target gene, cytokine or endocytic receptor mRNA was assessed by quantitative reverse transcription polymerase chain reaction (qRT-PCR) using either the Power SYBR Green PCR Master Mix or Taqman Universal Buffer II (Applied Biosystems) on a CFX96 Real-Time System (Biorad). Further details are available in the *Online Supplementary Appendix*.

Freshly isolated PDC were treated with either LXR agonists (T0901317, GW3965, 22RHC) or LXR antagonist (22SHC) for 24 h, and expression of LXR target genes (*srebp1c* and *abca1*) was assessed by qRT-PCR. 22SHC inhibited *srebp1c* mRNA expression, while LXR agonists increased both *srepb1c* and *abca1* mRNA (Figure 1A), suggesting LXR pathway activation in PDC. LXR (*lxra* and *lxrb*) isoform mRNA expression was assessed by qRT-PCR in freshly isolated PDC. Preferential expression of the ubiquitous *lxrb* isoform mRNA by PDC was shown (*Online Supplementary Figure S1*). Increased expression of ABCA1 at protein level after LXR agonist treatment was confirmed by induction of ABCA1 expression on PDC membrane, as assessed by confocal microscopy (Figure 1B). In other immune cells, LXR activation has been described to alter TLR stimulation[8,10] and promote phosphatidylserine (PtdSer) positive apoptotic body internalization.[9] We evaluated whether LXR stimulation modulates PDC responses to TLR signaling. PDC were first treated with LXR agonists for 24 h, and stimulated with TLR ligands, R848 (TLR7) and CpG-ODN2216 (TLR9) for 18 h. Secretion of TNF-α and IL-6 was significantly reduced when PDC were pre-treated with LXR agonists (Figure 1C). PDC CAL-1 cells expressed reduced intracellular TNF-α levels when pre-treated with LXR agonists before TLR7 stimulation (Figure 1C). However, LXR agonist pre-treatment did not affect TLR9-induced cytokine production by PDC (Figure 1C). In contrast to TLR9, TLR7 stimulation involves predominantly the canonical NF-κB signaling pathway in PDC.[11] Pre-treatment of PDC for 24 h with LXR agonists, T0901317 or GW3965 followed by R848 stimulation for 45 min significantly decreased pRelA staining analyzed by confocal microscopy (Figure 1D). This demonstrates that the LXR pathway is fully functional in human PDC and its activation inhibits TLR7-mediated NF-κB activation and pro-inflammatory cytokine secretion. This was shown using three different LXR agonists, including GW3965 considered as a pure LXRα/β agonist.[12] As described in macrophages or conventional DC,[8,10] LXR triggering in PDC blocks TLR signaling pathway. NF-κB inhibition by LXR triggering involves stabilization of a corepressor/NF-κB complex in target gene promoter,[8] or prevention of NF-κB p50 subunit nuclear translocation.[10] Here, we observed an inhibition of RelA phosphorylation.

Despite the fact that PDC are not professional phagocytes participating in apoptotic cell/body removal like macrophages,[13] PDC are able to internalize membrane-derived MP.[5] We then evaluated the role of LXR in PtdSer-dependent MP internalization by PDC. After showing that MP uptake by PDC was PtdSer-dependent using AnxV, we observed that LXR stimulation significantly increased eFluor-labeled MP internalization by PDC (Figure 1E). T0901317 treatment showed a concentration-dependent upregulation of *bai1* mRNA levels. The same effect was obtained with the two other LXR agonists, while 22SHC did not change *bai1* mRNA expression (Figure 1F). Increased BAI-1 membrane expression on PDC was confirmed after T0901317 or GW3965 treatment by cytometry (Figure 1G). Finally, blockade of BAI-1 using an anti-BAI-1 antibody significantly reduced MP uptake by LXR-stimulated PDC (Figure 1H). While LXR activation in macrophages induces Mer-tk expression,[9] neither *stabilin2, tim1, tim4* nor *mertk* PtdSer receptor mRNA expression were modulated in PDC after LXR

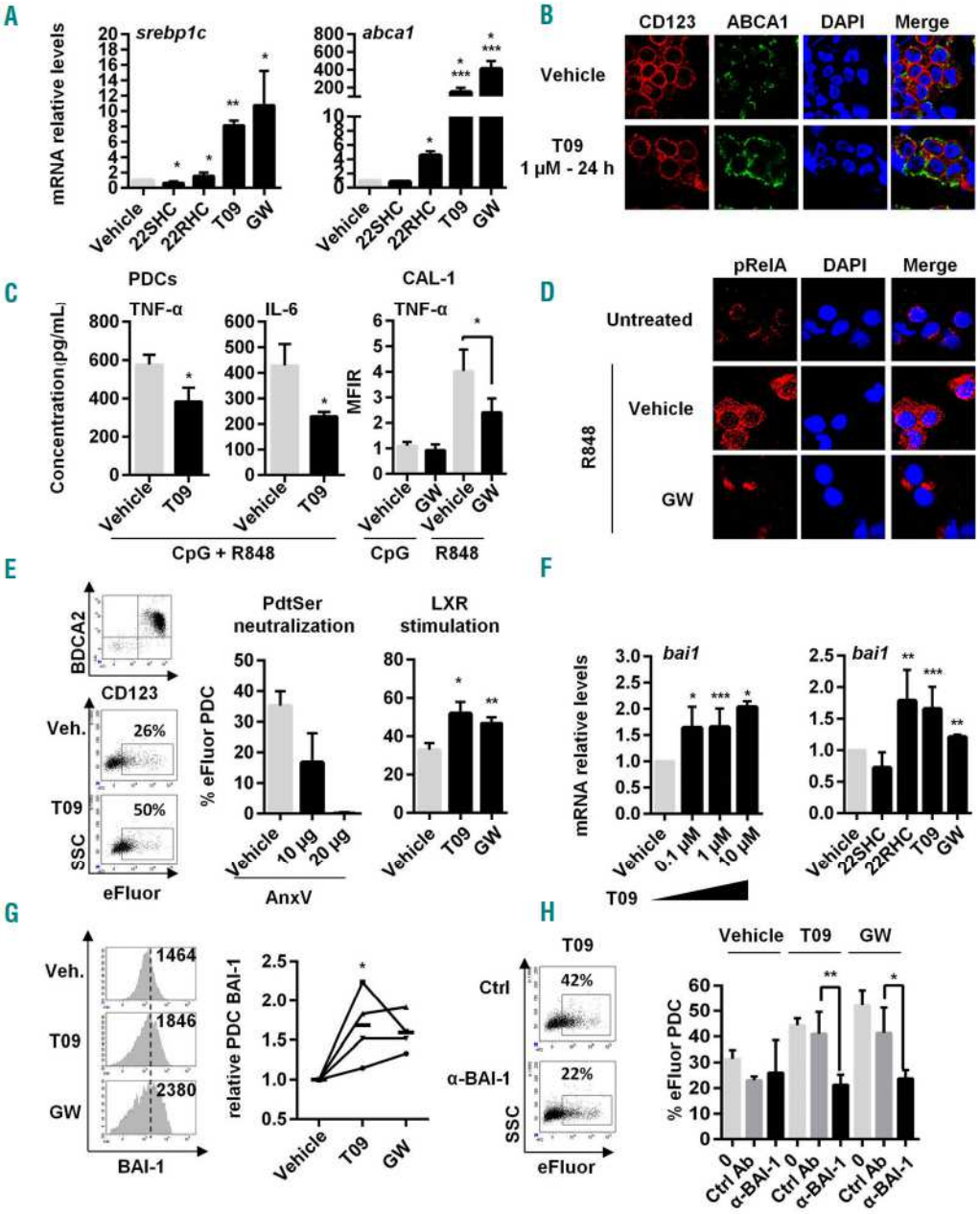

Figure 1. Stimulation of LXR pathway in PDC inhibits TLR7-induced NF-κB activation, pro-inflammatory cytokine secretion and up-regulates MP internalization *via* BAI-1. (A) Different LXR agonists, T0901317 (T09), GW3965 (GW), 22RHC or LXR antagonist 22SHC were added (1 µM) to PDC from healthy donors for 24 h and LXR target gene *(srebp1c, abca1, lxra [not depicted] data not shown)* expression was assessed by qRT-PCR (n=7, meaning PDC isolated from 7 different donors). (B) Freshly isolated PDC were stimulated with 1 µM of T0901317 (T09) for 24 h. Then CD123 and ABCA1 cell surface expression was evaluated by confocal microscopy analysis. Results from a representative experiment out of 3 using PDC from 3 different donors. (C) Freshly isolated PDC (left panels) or PDC cell line CAL-1 cells (right panel) were treated with 1 µM of T0901317 (T09) or GW3965 (GW) for 24 h, followed by a 18-h stimulation using CpG-ODN2216 (CpG, 2 µM) + R848 (1 µg/mL) (left panels) representing TLR9 and TLR7 ligand, respectively, or each ligand separately (right panel). Supernatants were then collected and assessed for TNF-α and IL-6 concentration by multiplex assays (n=5). Intracellular TNF-α levels in CAL-1 cells were also assessed by cytometry. Cumulated mean fluorescent intensity ratio (MFIR=MFI of treated cells/MFI of untreated vehicle cells) is shown (right panel) as mean±S.E.M. of the 5 independent experiments. (D) Freshly isolated PDC were treated for 24 h with 1 µM of GW3965 (GW), followed by TLR7 ligand, R848 (1 µg/mL) for 45 min. Phosphorylation of the NF-κB p65 (pRelA) subunit and its cellular localization were evaluated by confocal microscopy analysis. Results from a representative experiment out of 3 using PDC from 3 different donors. (E) PDC were treated with 1 µM of T0901317 (T09) or GW3965 (GW), washed and cultured with eFluor-labeled MP for 4 h at a 1/40 PDC/MP ratio. MP uptake by PDC was evaluated by measuring eFluor$^+$ PDC by cytometry (n=3). Left panel shows a representative experiment. Middle panel shows that MP uptake requires PdtSer/PdtSer receptor interactions since blockade of these interactions using unlabeled Annexin-V (AnxV at 10 µg or 20 µg) incubated for 30 min with e-Fluor labeled MP decreases the percentage of eFluor$^+$ PDC (n=3). This shows that free eFluor released from MP was not responsible for PDC labeling. (Right) Cumulative data of 3 independent experiments using LXR agonist-treated PDC from 3 different donors expressed as mean±S.E.M. are shown. (F) PDC were treated with increasing concentrations of T09 (0.1 µM, 1 µM or 10 µM) for 24 h (left panel) or LXR agonists, T0901317 (T09), GW3965 (GW), 22RHC or LXR antagonist 22SHC (for a single dose of 1 µM, then *bai1* gene expression was quantified by qRT-PCR (n=5). (G) PDC were treated 24 h with 1 µM of T0901317 (T09) and GW3965 (GW) and BAI-1 expression was assessed by cytometry (1 representative experiment out of 4, left panel). Numbers represents mean fluorescent intensity (MFI). Data of 4 independent experiments using PDC from 4 different donors expressed as relative PDC BAI expression obtained using the following formula [% of PDC stained with anti-BAI-1 mAb after treatment] / [% of PDC stained with anti-BAI-1 mAb in vehicle condition], bold lines represent the mean of the 4 experiments (mean±SEM;*P<0.05, Wilcoxon) (right panel). (H) PDC were treated with 1 µM of T0901317 (T09) or GW3965 (GW) for 24 h. Then, cells were cultured for 1 h with neutralizing anti-BAI-1 antibody (α-BAI-1) or irrelevant control antibody (Ctrl Ab), before adding eFluor-labeled MP for 4 h and analyzing by cytometry (n=4). Dot plot from one experiment representative of 4 (left panel). Cumulative data of 4 independent experiments expressed as mean±S.E.M. of eFluor$^+$ PDC are shown. Unless specified, all data were expressed as mean±S.E.M. from n independent experiments. *P<0.05, **P<0.001, ***P<0.005 (Mann-Whitney).

activation (*data not shown*). Moreover, Mer-tk blockade in PDC has no effect (*data not shown*). Overall, LXR activation in PDC significantly enhances MP uptake through upregulation of the Ptdser receptor BAI-1. This was observed whatever the MP origin, EMP or PMP (*Online Supplementary Figure S2*).

Since MP contain potential cholesterol-derived LXR ligands,[6] we evaluated LXR activation in PDC after MP co-culture. PMP or EMP were previously reported to exert anti- or pro-inflammatory effects, respectively.[5] We confirmed here that PMP decreased TNF-α and IL-8 secretion in a PMP number-dependent manner (Figure 2A and B). Looking at the LXR pathway, we observed a significant induction of LXR target gene (*lxra, srebp-1c* and *abca1*) and *bai1* transcription, while *tnfa* mRNA levels were significantly diminished in PDC, depending again on the number of PMP (Figure 2C). PDC pre-treatment with the LXR antagonist 22SHC before PMP addition tend to prevent LXR target gene expression upregulation, while significantly increasing *tnfa* mRNA expression (Figure 2D). This identifies a novel anti-inflammatory mechanism of PMP: the activation of the LXR pathway.

Endothelial-derived MP are endowed with pro-inflammatory properties.[5] After having confirmed that TNF-α and IL-8 secretion was increased after EMP incubation, we observed that EMP induced NF-κB activation in PDC

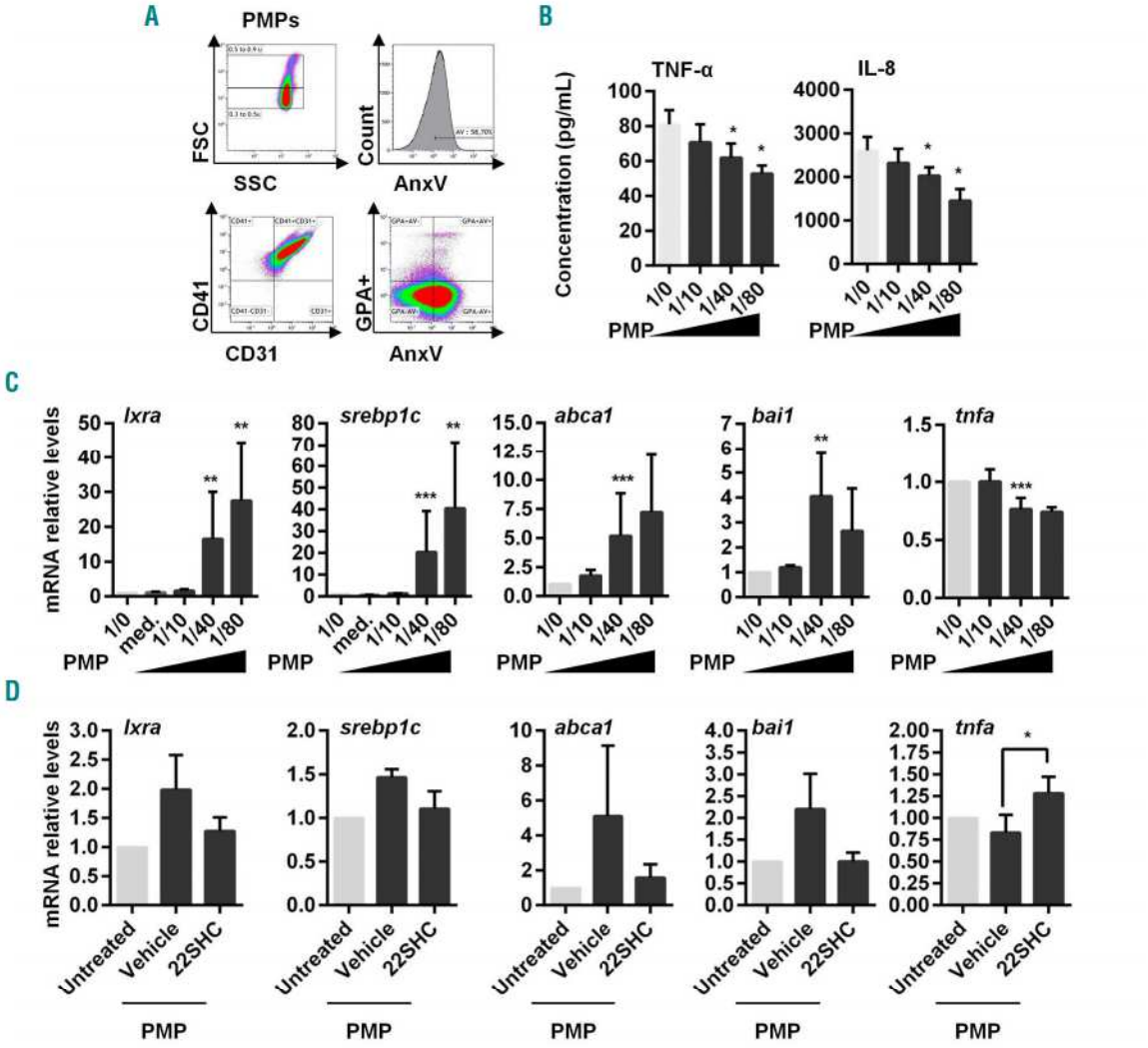

Figure 2. Platelet-derived microparticles reduce PDC pro-inflammatory cytokine secretion and stimulate LXR activation in PDC. (A) **Flow cytometric characterization and quantification of PMP.** MP isolated from platelet concentrates of healthy donors were characterized for PdtSer expression [(annexin V [AnxV] staining)]. In addition, to confirm that PMP are derived from platelets and not red blood cells, expression of CD31, CD41 and CD235a was assessed using Navios cytometer (Beckman Coulter). PMP are positive for CD31 and CD41 but negative for red blood cell marker Glycophorin A (CD235a). Data from one representative experiment out of 7 independent productions of PMP. (B) Freshly isolated PDC were cultured with PMP at different PDC/PMP ratio (i.e. without, 1/0; one PDC for 10 PMP, 1/10; one PDC for 40 PMP, 1/40; 1 PDC for 80 PMP, 1/80) for 18 h. Supernatants from PDC/PMP culture were then collected and assessed for TNF-α and IL-8 using multiplex assays (n=7). (C) LXR target gene (*lxra, srebp1c, abca1*), *bai1* and *tnfa* mRNA transcripts were quantified by qRT-PCR (n=9). The last wash supernatant of PMP preparation in an equivalent volume of PMP suspension was added to PDC culture as control of *lxra* and *srebp1c* mRNA transcript quantification (med. condition). (D) PDC were treated with the LXR antagonist 22SHC (1 μM) or vehicle (DMSO) for 24 h. Then, cells were washed and cultured with PMP at a 1/40 PDC/PMP ratio for 18 h (PMP) or no PMP (Untreated). LXR target gene (*lxra, srebp1c, abca1*), *bai1* and *tnfa* mRNA transcripts were quantified by qRT-PCR (n=4). Data from n independent experiment were expressed as mean±S.E.M. **P*<0.05, ***P*<0.001, ****P*<0.005 (Mann-Whitney).

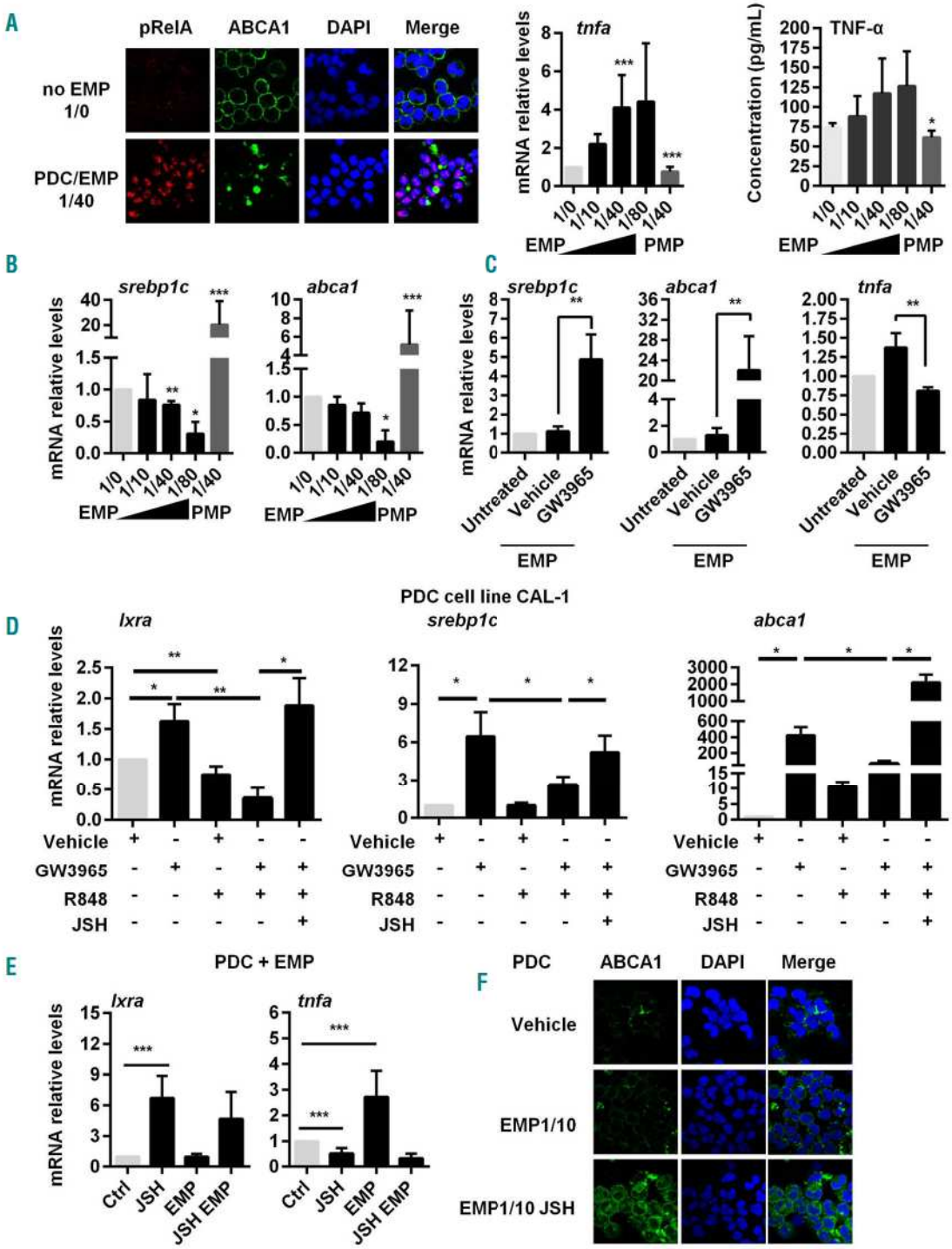

Figure 3. NF-κB triggering by EMP stimulation or TLR7 activation prevents LXR activation in PDC. (A) Freshly isolated PDC were incubated with EMP at different PDC/EMP ratio (i.e. without, 1/0; one PDC for 10 EMP, 1/10; one PDC for 40 EMP, 1/40; one PDC for 80 EMP, 1/80). (Left) Nuclear translocation of phosphorylated NF-κBp65 (pRelA) subunit was determined in PDC cultured at a 1/40 ratio for 2.5 h by confocal microscopy. Nuclei were stained with DAPI. EMP stimulation of PDC decreases also membrane ABCA-1 expression. Results from a representative experiment out of 3. (Middle) *tnfa* mRNA levels from PDC cultured with EMP at the different ratio or with PMP (1/40 ratio) for 18 h, were quantified by qRT-PCR (n=5). (Right) TNF secretion from PDC cultured with EMP at the different ratio or with PMP (1/40 ratio) for 24 h were quantified by multiplex assays (n=5 for EMP and n=3 for PMP). (B) PDC were cultured with EMP at different PDC/EMP ratio (i.e. without, 1/0; one PDC for 10 EMP, 1/10; one PDC for 40 EMP, 1/40; one PDC for 80 EMP, 1/80) for 18 h. LXR target gene (*srebp1c, abca1*) mRNA transcripts were quantified by qRT-PCR (n=5). (C) PDC were treated with the LXR agonist GW3965 (1 μM) or vehicle (DMSO) for 24 h. Then, cells were washed and cultured with EMP at a 1/40 PDC/EMP ratio for 18 h (EMP). Untreated PDC were used as control. Expression of LXR target genes (*lxra, abca1*), and ***tnfa*** gene were quantified by qRT-PCR (n=5). (D) Cells from PDC cell line CAL-1 were treated with GW3965 (1 μM), R848 (1 μg/mL), JSH-23 (JSH, 25 μM), or a combination of these treatments for 18 h. LXR target gene (*lxra, srebp1c, abca1*) mRNA transcripts were quantified by qRT-PCR (n=5). (E) Freshly isolated PDC were treated for 18 h with the NF-κB inhibitor, JSH-23 (JSH), with or without EMP at a PDC/EMP ratio of 1:40. Expression of LXR target gene (*lxra*) and inflammatory cytokine [*tnfa, il6 (not depicted)*] gene mRNA was quantified by qRT-PCR (n=3). (F) PDC were treated with the NF-κB inhibitor JSH-23 (JSH) with or without EMP (at a PDC/EMP ratio of 1/10, EMP/1/10) for 2.5 h. Membrane ABCA1 expression was analyzed by confocal microscopy (one representative experiment out of 3 using PDC from 3 different donors). Data from n independent experiments were expressed as mean±S.E.M. **P*<0.05, ***P*<0.001, ****P*<0.005 (Mann-Whitney).

associated with an increase of *tnfa* mRNA levels (Figure 3A). A downregulation of LXR target gene (*srebp1c* and *abca1*) transcription in PDC in an EMP number-dependent manner was also observed (Figure 3B). This effect of EMP was prevented by the prior LXR activation and associated with a significant decreased *tnfa* mRNA expression (Figure 3C). These data suggest an inhibition of the LXR pathway by NF-κB. To confirm this hypothesis, PDC CAL-1 cells were treated simultaneously with the LXR agonist GW3965 and TLR7 ligand R848 in the presence of the NF-κB inhibitor, JSH-23 or not. R848 treatment down-regulated LXR target gene expression induced by GW3965, while addition of JSH-23 totally reversed this effect (Figure 3D). Thus, the TLR signaling pathway dominates the LXR pathway, and NF-κB blockade is sufficient to restore LXR pathway activation. To translate this observation into EMP, freshly isolated PDC co-cultured with EMP were simultaneously treated with JSH-23. While JSH-23 led to a slight increase in *lxra* mRNA expression, we observed a reduction of *il6* and *tnfa* mRNA levels, statistically significant for *tnfa* mRNA (Figure 3E). Restoration of LXR pathway activation in response to EMP by NF-κB blockade was confirmed by increased ABCA1 membrane expression, assessed by confocal microscopy (Figure 3F). Finally, PDC treatment with R848 simultaneously to PMP significantly decreased *lxra* mRNA expression induced by PMP and increased *il6* mRNA expression (*Online Supplementary Figure S3*). These results confirm the critical role of NF-κB and LXR signaling pathway activation during MP engulfment by PDC, determining the pro- *versus* anti-inflammatory response of these cells.

Overall, this study demonstrates a functional LXR pathway in PDC and a unique LXR/NF-κB balance that controls the non-inflammatory *versus* inflammatory status of MP engulfed by PDC. This remains to be confirmed in pathological settings. However, since increased circulating EMP levels and pro-inflammatory PDC may be implicated in atherosclerosis, we may hypothesize that NF-κB signaling dominates the LXR pathway in this setting. Whether LXR activation could be a potential therapeutic target in atherosclerosis and other pathologies involving PDC and EMP dysregulation[3] (including lupus or psoriasis[9,14,15]) remains to be investigated.

Adam Ceroi,[1-4] Fanny Angelot Delettre,[1-4] Charline Marotel,[1-3] Thierry Gauthier,[1-4] Afag Asgarova,[1-3] Sabéha Biichlé,[1-4] Anne Duperrier,[1-3] Guillaume Mourey,[1-3] Sylvain Perruche,[1-4] Laurent Lagrost,[4-7] David Masson,[4-7] and Philippe Saas[1-4,8]

[1]INSERM, UMR1098, Besançon; [2]EFS Bourgogne Franche-Comté, UMR1098, Besançon; [3]Université Bourgogne Franche-Comté, UMR1098, Besançon; [4]LabEX LipSTIC, ANR-11-LABX-0021, Besançon/Dijon; [5]INSERM, U866, Dijon; [6]Université Bourgogne Franche-Comté, UMR866, Dijon; [7]CHRU Dijon; and [8]CHRU Besançon, INSERM CIC1431, FHU INCREASE, France

Funding: this study was supported by the Etablissement Français du Sang (EFS, grant #2011–11 to PS), the Agence Nationale de la Recherche (Labex LipSTIC, ANR-11-LABX-0021), the Conseil Régional de Franche-Comté ("soutien au LabEX LipSTIC" 2014 & 2015 to PS), and the Fondation de Coopération Scientifique Bourgogne Franche-Comté (BQR BFC to DM & PS).

Acknowledgments: the authors would like to thank Dr Maeda (Nagasaki University, Japan) for kindly providing us with the human PDC line CAL-1, Sarah Odrion for editorial assistance, Yassin Tachikart and Aurore Gaillardet for technical assistance, Prof M de Carvalho Bittencourt (Université de Lorraine, France) for stimulating discussions.

The online version of this letter has a SupplementaryAppendix.

Correspondence: philippe.saas@efs.sante.fr

doi:10.3324/haematol.2015.135459

Key words: LXR, plasmacytoid dendritic cells, ectosomes, extracellular vesicles, microvesicles, inflammation.

Information on authorship, contributions, and financial & other disclosures was provided by the authors and is available with the online version of this article at www.haematologica.org.

References

1. Zeller I, Srivastava S. Macrophage functions in atherosclerosis. Circ. Res. 2014;115(12):e83-85.
2. Döring Y, Zernecke A. Plasmacytoid dendritic cells in atherosclerosis. Front Physiol. 2012;3:230.
3. Reizis B, Bunin A, Ghosh HS, Lewis KL, Sisirak V. Plasmacytoid dendritic cells: recent progress and open questions. Annu Rev Immunol. 2011;29:163-183.
4. Chironi GN, Boulanger CM, Simon A, et al. Endothelial microparticles in diseases. Cell Tissue Res. 2009;335(1):143-151.
5. Angelot F, Seilles E, Biichle S, et al. Endothelial cell-derived microparticles induce plasmacytoid dendritic cell maturation: potential implications in inflammatory diseases. Haematologica. 2009;94(11):1502-1512.
6. Biró É, Akkerman JWN, Hoek FJ, et al. The phospholipid composition and cholesterol content of platelet-derived microparticles: a comparison with platelet membrane fractions. J Thromb Haemost. 2005;3(12):2754-2763.
7. Janowski BA, Grogan MJ, Jones SA, et al. Structural requirements of ligands for the oxysterol liver X receptors LXRα and LXRβ. Proc Natl Acad Sci USA. 1999;96(1):266-271.
8. Kiss M, Czimmerer Z, Nagy L. The role of lipid-activated nuclear receptors in shaping macrophage and dendritic cell function: From physiology to pathology. J Allergy Clin Immunol. 2013;132(2):264-286.
9. A-Gonzalez N, Bensinger SJ, Hong C, et al. Apoptotic cells promote their own clearance and immune tolerance through activation of LXR. Immunity. 2009;31(2):245-258.
10. Canavan M, McCarthy C, Larbi NB, et al. Activation of liver X receptor suppresses the production of the IL-12 family of cytokines by blocking nuclear translocation of NF-κBp50. Innate Immun. 2014;20(7):675-687.
11. Bao M, Liu Y-J. Regulation of TLR7/9 signaling in plasmacytoid dendritic cells. Protein Cell. 2013;4(1):40–52.
12. Ito A, Hong C, Rong X, et al. LXRs link metabolism to inflammation through Abca1-dependent regulation of membrane composition and TLR signaling. Elife. 2015;4:e08009.
13. Saas P, Kaminski S, Perruche S. Prospects of apoptotic cell-based therapies for transplantation and inflammatory diseases. Immunotherapy. 2013;5(10):1055-1073.
14. Pelletier F, Garnache-Ottou F, Angelot F, et al. Increased levels of circulating endothelial-derived microparticles and small-size platelet-derived microparticles in psoriasis. J Invest Dermatol. 2011;131(7):1573-1576.
15. Parker B, Al-Husain A, Pemberton P, et al. Suppression of inflammation reduces endothelial microparticles in active systemic lupus erythematosus. Ann Rheum Dis. 2014;73(6):1144-1150.

Regular Article

blood

MYELOID NEOPLASIA

LXR agonist treatment of blastic plasmacytoid dendritic cell neoplasm restores cholesterol efflux and triggers apoptosis

Adam Ceroi,[1-4] David Masson,[4,5] Anne Roggy,[1-4] Christophe Roumier,[6] Cécile Chagué,[1-4] Thierry Gauthier,[1-4] Laure Philippe,[1-4] Baptiste Lamarthée,[1-4] Fanny Angelot-Delettre,[1-4] Francis Bonnefoy,[1-4] Sylvain Perruche,[1-4] Sabeha Biichle,[1-3] Claude Preudhomme,[6] Elisabeth Macintyre,[7] Laurent Lagrost,[4,5] Francine Garnache-Ottou,[1-4] and Philippe Saas[1-4]

[1]Unité 1098, INSERM, Besançon, France; [2]Université Bourgogne Franche-Comté, Unité Mixte de Recherche 1098, Besançon, France; [3]Etablissement Français du Sang Bourgogne Franche-Comté, Besançon, France; [4]Laboratoires d'Excellence (LabEx) Lipoprotéines et Santé: Prévention et Traitement des Maladies Inflammatoires et du Cancer (LipSTIC), Besançon/Dijon, France; [5]Faculté de Médecine, Université Bourgogne Franche-Comté, INSERM Unité 866, Dijon, France; [6]Laboratoire d'Hématologie, Centre de Biologie Pathologie, Institut de Recherches sur le Cancer de Lille, Centre Hospitalier Régional Universitaire de Lille, INSERM Unité 837, Lille, France; and [7]Laboratoire d'Onco-Hématologie, Hôpital Necker-Enfants Malades, Assistance Publique–Hôpitaux de Paris, Faculté de Médecine Descartes, Université Sorbonne Paris Cité, INSERM Unité 1151, Paris, France

Key Points

- LXR activation inhibits BPDCN cell survival through the increase of cholesterol efflux, the inhibition of NF-κB, and IL-3 signaling.
- Treatment with LXR agonists can be proposed as a new therapeutic approach for BPDCN.

Blastic plasmacytoid dendritic cell (PDC) neoplasm (BPDCN) is an aggressive hematological malignancy with a poor prognosis that derives from PDCs. No consensus for optimal treatment modalities is available today and the full characterization of this leukemia is still emerging. We identified here a BPDCN-specific transcriptomic profile when compared with those of acute myeloid leukemia and T-acute lymphoblastic leukemia, as well as the transcriptomic signature of primary PDCs. This BPDCN gene signature identified a dysregulation of genes involved in cholesterol homeostasis, some of them being liver X receptor (LXR) target genes. LXR agonist treatment of primary BPDCN cells and BPDCN cell lines restored LXR target gene expression and increased cholesterol efflux via the upregulation of adenosine triphosphate–binding cassette (ABC) transporters, ABCA1 and ABCG1. LXR agonist treatment was responsible for limiting BPDCN cell proliferation and inducing intrinsic apoptotic cell death. LXR activation in BPDCN cells was shown to interfere with 3 signaling pathways associated with leukemic cell survival, namely: NF-κB activation, as well as Akt and STAT5 phosphorylation in response to the BPDCN growth/survival factor interleukin-3. These effects were increased by the stimulation of cholesterol efflux through a lipid acceptor, the apolipoprotein A1. In vivo experiments using a mouse model of BPDCN cell xenograft revealed a decrease of leukemic cell infiltration and BPDCN-induced cytopenia associated with increased survival after LXR agonist treatment. This demonstrates that cholesterol homeostasis is modified in BPDCN and can be normalized by treatment with LXR agonists which can be proposed as a new therapeutic approach. (*Blood*. 2016;128(23):2694-2707)

Introduction

Blastic plasmacytoid dendritic cell (PDC) neoplasm (BPDCN) is a rare aggressive malignancy derived from PDCs.[1] This disease is characterized by a heterogeneous presentation at diagnosis (from a disease limited to the skin to a leukemic syndrome with cytopenia and bone marrow involvement), clinical heterogeneity, and manifestations easily changing during disease progression.[2] Currently, there is no consensus regarding the optimal treatment modality.[2] Most BPDCN patients have a very aggressive clinical course with limited median overall survival.[2,3] It has been recently proposed that the frequent relapse after treatment and the poor prognosis can be related to the fact that the involvement of the central nervous system (CNS) is frequently undetected.[4] Recently, BPDCN was classified by the World Health Organization (WHO) as a distinct entity in the group of "acute myeloid leukemia (AML) and related precursor neoplasms."[2,5] Extensive characterization of this malignancy is still limited and diagnosis overlap may exist with immature AML, monoblastic and undifferentiated leukemia. Thus, a better understanding of this leukemia and new therapeutic approaches are urgently needed.

Previous studies have identified a cholesterol metabolism dysregulation in different malignant cells leading to intracellular cholesterol accumulation.[6,7] Cellular cholesterol content results from cholesterol uptake and biosynthesis through the mevalonate pathway, while its

Submitted 27 June 2016; accepted 19 September 2016. Prepublished online as *Blood* First Edition paper, 4 October 2016; DOI 10.1182/blood-2016-06-724807.

The data reported in this article have been deposited in the Gene Expression Omnibus database (accession numbers GSM705329 to GSM705333, and GSE89565).

The online version of this article contains a data supplement.

The publication costs of this article were defrayed in part by page charge payment. Therefore, and solely to indicate this fact, this article is hereby marked "advertisement" in accordance with 18 USC section 1734.

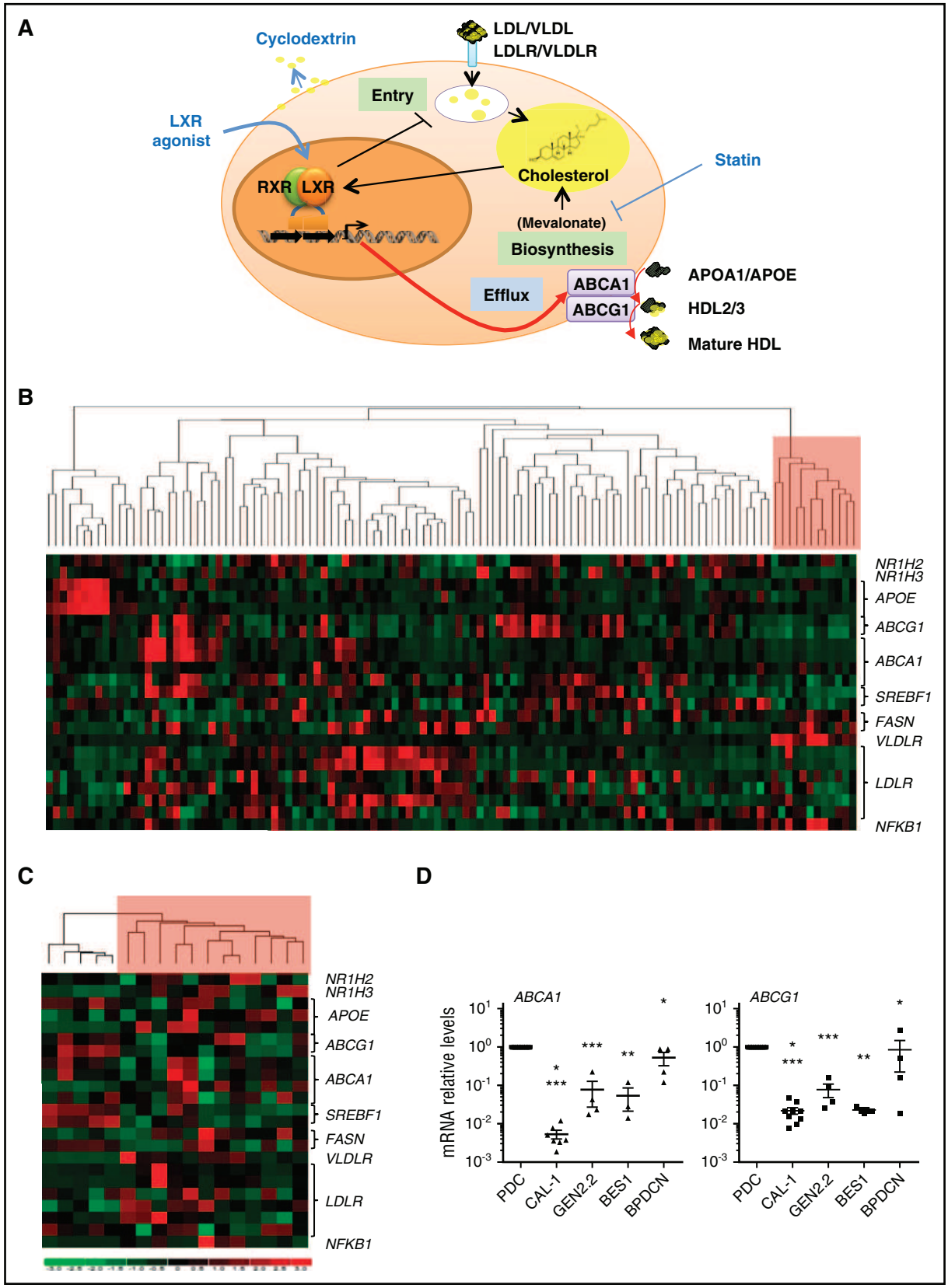

Figure 1. A BPDCN-specific transcriptomic signature with a dysregulation of genes involved in cholesterol homeostasis allows the clustering of BPDCN samples. (A) A schematic representation of cellular cholesterol homeostasis. Mechanisms of cholesterol synthesis and uptake (green boxes) and efflux (blue box) maintain cellular cholesterol homeostasis. The LXR pathway is involved in the regulation of cholesterol homeostasis by inhibiting cholesterol uptake/entry (through the decreased expression of low-density lipoprotein (LDL) and/or very-low-density lipoprotein (VLDL) receptors, LDLR and VLDLR, respectively) and by stimulating cholesterol efflux (through ABC transporters, ABCA1 and ABCG1). This LXR pathway is activated by intermediates from the mevalonate pathway (ie, the cholesterol biosynthesis). Cholesterol efflux also requires cholesterol acceptors, APOA1/APOE, and HDL2/3 to form mature HDL. These cholesterol acceptors can be provided by the cell itself or represent circulating

elimination is mediated by cholesterol efflux (Figure 1A). Cholesterol uptake involves plasma lipoproteins (mainly LDL and VLDL) after interactions with their specific receptors, LDLR and VLDLR, respectively. Cholesterol efflux implicates mainly adenosine triphosphate–binding cassettes (ABCs) A1 and G1 (ABCA1 and ABCG1, respectively) in association with extracellular cholesterol acceptors, including: apolipoprotein A1/E (APOA1 and APOE, respectively) or lipoprotein particles (eg, nascent high-density lipoprotein [HDL] or HDL2).[8]

Leukemic cells (AML and chronic myeloid leukemia) have been shown to increase LDLR expression,[6] decrease LDLR degradation,[7] and stimulate cholesterol biosynthesis resulting in cholesterol accumulation.[6] Cholesterol regulates critical cellular functions, including plasma membrane formation, fluidity, and permeability.[9] These latter functions are implicated in survival signaling pathway activation (eg, Akt)[10] and proliferation.[11,12] For instance, stimulation of cholesterol efflux inhibits interleukin-3 (IL-3)-induced hematological progenitor cell proliferation.[13,14] Interestingly, BPDCN cells express high levels of IL-3 receptor α chain (CD123), and IL-3 is a BPDCN survival factor.[1,15] A targeted therapy directed against IL-3 receptor, called SL-401 associating IL-3 with the catalytic and translocation domains of diphteria toxin, has been tested in a phase 1/2 study with encouraging results.[16,17] Whether cholesterol homeostasis is dysregulated in BPDCN and contributes to its aggressiveness or determines response to therapies remains to be determined.

Cholesterol homeostasis is regulated at least by liver X receptors (LXRs). These nuclear receptors are expressed as 2 isoforms, with LXRβ being the ubiquitous isoform whereas LXRα expression is restricted to cells with high cholesterol turnover (eg, hepatocytes or macrophages).[18,19] The LXR pathway is activated by intermediates from the mevalonate pathway, endogenous oxidized cholesterol derivatives (called oxysterols), and synthetic agonists (eg, T0901317 or GW3965).[19,20] These synthetic compounds are of great interest for therapeutic use because LXR are considered as a promising target in different diseases.[19-21] LXR activation upregulates the expression of several genes involved in cholesterol homeostasis (called LXR target genes), including: *ABCA1*, *ABCG1*,[21] and *APOE* (related to cholesterol efflux),[22] as well as the "inducible degrader of the low-density lipoprotein receptor" preventing cholesterol uptake through LDLR/VLDLR degradation.[23,24] Overall, these mechanisms participate in decreased intracellular cholesterol content. LXRs are functionally expressed in normal PDCs and in a leukemic PDC cell line,[25] but no data are available on the effects of LXR agonists on BPDCN.

The goal of this study was to determine whether BPDCN exhibit a specific gene signature based on genes involved in cholesterol efflux and uptake, in comparison with other leukemic cells (AML and T-acute lymphoblastic leukemia [T-ALL]) and normal PDCs. Because LXR activation controls cholesterol homeostasis via LXR target genes, we studied whether LXR agonist treatment stimulates cholesterol efflux. Effects of LXR activation on cell proliferation and survival were evaluated in vitro, using primary BPDCN samples and 2 established BPDCN cell lines (CAL-1 and GEN2.2). The in vivo LXR agonist therapeutic effect was evaluated using a BPDCN xenograft model treated with the T0901317 LXR agonist.

Methods

BPDCN collection

Twenty-three BPDCN samples were obtained at diagnosis (sample collection authorization number DC-2008-713). BPDCN was diagnosed based on histopathology and immunostaining of cutaneous lesions, blood, or bone marrow samples, as described.[26-28] This study was approved by our local ethics committee (Comité de Protection des Personnes [CPP] Est II, Besançon, France).

Cell lines and culture

Two established BPDCN cell lines (CAL-1 and GEN2.2),[29,30] primary BPDCN cells isolated from a patient and expanded in NOD-SCID IL2Rγc-deficient (NSG) mice (The Jackson Laboratory, Sacramento, CA) (referred to hereafter as BES1), as well as 11 BPDCN samples with different BPDCN infiltration (supplemental Table 1, available on the *Blood* Web site) from newly diagnosed patients were used for in vitro assays. Culture of BPDCN cells and isolation of primary BPDCN samples are described in supplemental Methods.

Transcriptomic analysis

The following samples were submitted to transcriptomic analysis using the GeneChip Human Genome U133 Plus 2.0 Array (Affymetrix, Santa Clara, CA):

- 12 BPDCN samples,
- 65 AML samples (including different French-American-British subtypes: 25 M0, 11 M1, 10 M2, 1 M3, 11 M4, 6 M5, and 1 M6) (Unité 837, Institut de Recherches sur le Cancer de Lille [IRCL], Lille, France),
- 35 T-ALL samples (Unité 1151, Assistance Publique–Hôpitaux de Paris [AP-HP], Hôpital Necker-Enfants Malades, Paris, France) (available at https://www.dropbox.com/sh/v21hg015hf515gw/AAC63OgjzcXXqTM-myca5sjVca?dl=0), and
- 5 primary PDCs (available on the Gene Expression Omnibus [GEO] database, under recording numbers: GSM705329, GSM705330, GSM705331, GSM705332, GSM705333).

Data were analyzed using dChip software (http://www.softpedia.com/get/Science-CAD/dChip.shtml) based on the expression of cholesterol homeostasis and LXR-related genes (*LXRA*, *LXRB*, *ABCA1*, *ABCG1*, *APOE*, *SREBF1*, *FASN*, *LDLR*, and *VLDLR*) plus the *NFKB1* gene.

Quantitative RT-PCR analysis

Transcription of LXR target genes (*ABCA1*, *ABCG1*) and genes coding proteins involved in the intrinsic apoptosis (*BCL2*, *BAK1*, *BAX*) was evaluated by quantitative reverse transcription polymerase chain reaction (qRT-PCR), as described.[25] Details are given in supplemental Methods.

Cholesterol efflux assay

CAL-1 cells were used to assess cholesterol efflux, as described in supplemental Methods and in Ishibashi et al.[31]

Figure 1 (continued) apolipoproteins or lipoprotein particles. Molecules used to modify cholesterol homeostasis in BPDCN are indicated in blue font. (B) Transcriptomic analysis of 65 AML, 35 T-ALL, and 12 BPDCN samples (highlighted in red, right side of the panel) was performed using an Affymetrix U133-2 chip and dChip software. (C) Transcriptomic analysis of the 12 BPDCN samples was compared with 5 primary PDC samples obtained using an Affymetrix U133-2 chip and dChip software. (D) Basal LXR target gene (*ABCA1*, *ABCG1*) transcripts were quantified by qRT-PCR in 2 established BPDCN cell lines, CAL-1 (n = 7) and GEN2.2 cells (n = 4), as well as in a short-term BPDCN cell line, BES1 (n = 3) and 4 primary BPDCN samples (leukemic PDC [LPDC] #2-4, and #7, n = 1). Levels of mRNA were normalized to those of glyceraldehyde-3-phosphate dehydrogenase (GAPDH) for each sample and then expressed as fold change relative to the average value for normal PDCs. Results from n independent experiments with each symbol representing an experiment (*$P < .05$, **$P < .01$, ****$P < .0001$, Mann-Whitney). FASN, fatty acid synthase; RXR, retinoid X receptor.

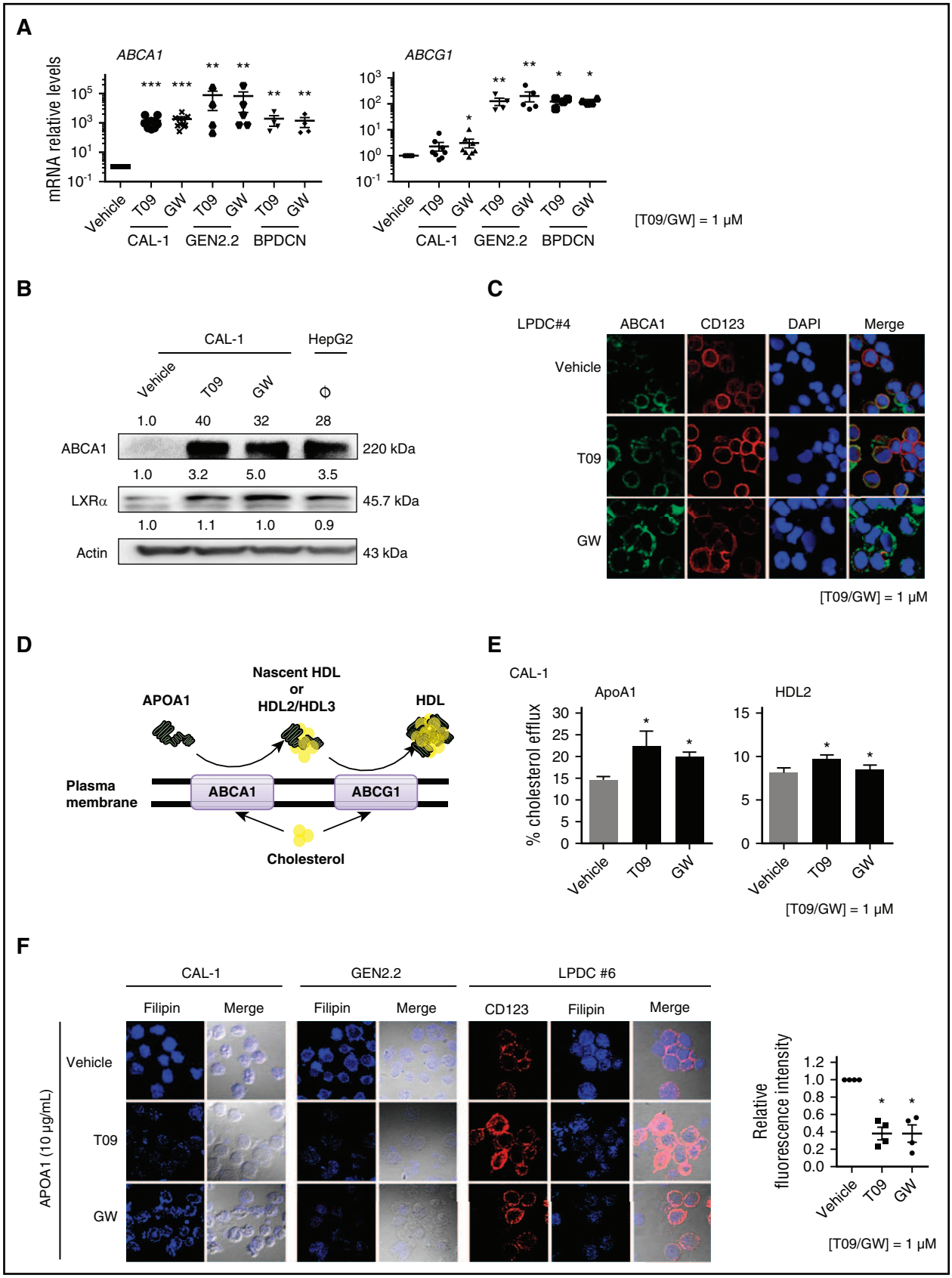

Figure 2. LXR activation restores cholesterol homeostasis-related gene expression and induces cholesterol efflux from BPDCN. (A) BPDCN cell lines (CAL-1, GEN2.2) and blood samples from 4 patients diagnosed with BPDCN (LPDC #4, #7, #8, #10) were treated with 1 μM LXR agonists, T0901317 (T09) or GW3965 (GW), for 24 hours. *ABCA1* and *ABCG1* mRNA levels were determined by qRT-PCR in CAL-1 (n = 8), GEN2.2 (n = 5), and in blood samples containing >75% of leukemic PDCs (n = 4). Levels of mRNA were normalized to those of *GAPDH* for each sample and then expressed as fold change relative to the average value for vehicle-treated cells (*$P < .05$,

Flow cytometry

Cytotoxic effects of LXR agonists were evaluated by staining with Annexin V (AnxV) and 7-amino-actinomycin D (7AAD) (fluorescein isothiocyanate–conjugated AnxV/7AAD; BD Biosciences, Le Pont de Claix, France) or caspase-9 activation (CaspGLOW Fluorescein Active Caspase Staining kit; eBioscience), according to the manufacturer's instructions. Proliferation was assessed on CAL-1 cells after labeling with the cell proliferation dye, eFluor 450 (eBioscience SA, Paris, France). BPDCN gating was performed using antibodies against CD123, CD131, and CD304 (supplemental Table 3). Cell cycle analysis was performed after cell fixation in ethanol 70% (overnight, 4°C), and by propidium iodide staining in a solution containing RNAse (overnight, 4°C). Cell fluorescence was evaluated using a CANTO II cytometer (BD Biosciences, San Jose, CA) and DIVA 6.2 software (BD Biosciences), except for cell cycle analysis where a FC500 cytometer with CXP and WinCycle softwares (Beckman Coulter Immunotech, Miami, FL) were used.

Immunoblotting

Whole-cell protein fraction was obtained by cell lysis in Laemmli buffer (supplemental Methods). Nuclear and cytosolic fractions were separated by cell lysis using a hypotonic, and then hypertonic, buffer solution (for osmosis restauration, supplemental Methods). Cytosolic fraction was isolated by centrifugation while nuclei were lysed in Laemmli buffer. Proteins were separated by electrophoresis on 8.5% or 12% sodium dodecyl sulfate–polyacrylamide gels and transferred to polyvinylidene difluoride membranes (GE Healthcare). Blots were then saturated with 5% milk before incubation with specific antibodies (supplemental Table 3). Blotted proteins were detected and quantified on a bioluminescence imager and BIO-1D advanced software (Vilber-Lourmat, Marne-la-Vallée, France) after blots were incubated with a horseradish peroxidase–conjugated appropriate secondary antibody. Details on blot saturation and quantification are given in supplemental Methods.

Confocal microscopy

Protein expression (CD123 and ABCA1) and phosphorylation (p65, STAT5, and Akt) were evaluated by immunofluorescent staining, as previously described[25] (antibodies used appear in supplemental Table 3). Nuclei were labeled with 4′,6-diamidino-2-phenylindole (DAPI; Sigma-Aldrich) and cholesterol content was investigated using the free cholesterol marker filipin (Sigma-Aldrich), according to the manufacturer's recommendations. Relative fluorescence intensity of filipin staining was measured with the ImageJ application, and determined as: corrected total cell fluorescence = ["integrated density" − ("area of selected cell" × "mean fluorescence of background readings")]/untreated conditions.

Mice and in vivo model

NSG mice were irradiated (2 Gy), inoculated IV 18 hours later with 1×10^6 CAL-1 cells, and treated intraperitoneally 7 days later with 6 injections of T0901317 (total experimental dose, 30 or 60 mg/kg, respectively) or with dimethyl sulfoxide (DMSO)/phosphate-buffered saline (PBS) control solution. Mouse monitoring and quantification of BPDCN cell infiltrate were described in supplemental Methods. Experimentation (#11007R) was approved by our local ethics committee (#58, approved by the French Ministry of Higher Education and Research) and conducted in accordance with the European Union Directive 2010/63.

Statistical analysis

Statistical analyses were performed by GraphPad Prism version 6 (GraphPad Software, San Diego, CA), using the Mann-Whitney, Wilcoxon, or Mantel-Cox test (*$P < .05$, **$P < .01$, ***$P < .001$, ****$P < .0001$). Data are expressed as mean ± standard error of the mean (SEM).

Results

A BPDCN-specific transcriptomic signature identifies a dysregulation of cholesterol homeostasis

Twelve primary BPDCN samples were analyzed using the Affymetrix U133-2 messenger RNA (mRNA) microarray for the expression of cholesterol homeostasis and LXR-related genes (*LXRA*, *LXRB*, *ABCA1*, *ABCG1*, *APOE*, *SREBF1*, *FASN*, *LDLR*, and *VLDLR*) plus the *NFKB1* gene. Comparison with AML and T-ALL samples revealed a specific BPDCN sample clustering, associated with a significant downregulation of LXR target genes *ABCA1* and *ABCG1* (associated with cholesterol efflux) and an upregulation of the *VLDLR* gene (linked to cholesterol entry). *NFKB1* gene upregulation in BPDCN samples was confirmed (Figure 1B; supplemental Figure 1).[32] Comparison of the BPDCN samples with primary PDC samples showed a similar clustering associated with a significant downregulation of LXR target genes, *SREBF1* and *ABCG1*, whereas *VLDLR* and *NFKB1* genes were upregulated (Figure 1C; supplemental Figure 1). This shows that the BPDCN transcriptomic profile is independent of the PDC cell lineage. A significant downregulation of *ABCA1* and *ABCG1* gene transcription was confirmed by qRT-PCR analysis in 2 BPDCN cell lines (GEN2.2 and CAL-1), BES1 cells, and 4 primary BPDCN samples compared with nonleukemic PDC samples (Figure 1D). Overall, these data identify a specific perturbation of cholesterol homeostasis- and LXR-related gene transcription in BPDCN.

LXR activation stimulates cholesterol efflux from BPDCN

Treatment with 2 synthetic LXR agonists (T0901317 and GW3965, 1 μM, 24 hours) upregulated *ABCA1* and *ABCG1* gene transcription in CAL-1, GEN2.2 cell lines, and in 4 primary BPDCN samples (Figure 2A). ABCA1 and LXRα proteins were increased after LXR activation in CAL-1 cells, as assessed by western blot analysis (Figure 2B) and in CAL-1 and GEN2.2 cells, as assessed by confocal

Figure 2 (continued) **$P < .01$, ****$P < .0001$, Mann-Whitney). (B) CAL-1 cells were treated with 1 μM T0901317 (T09) or GW3965 (GW), or vehicle control alone, for 24 hours. LXRα isoform and ABCA1 protein expression were evaluated by western blot. The human hepatocellular carcinoma cell line HepG2 was used as control and reference for LXRα and ABCA1 expression, whereas untreated CAL-1 lysates were used as reference for actin expression. Expression of LXR protein was compared with actin expression with the vehicle condition being considered arbitrary as 1. Results of 1 experiment of 3 are shown. (C) Primary BPDCN cells from 1 patient (LPDC #4) were treated with 1 μM LXR agonists T0901317 (T09) or GW3965 (GW) for 24 hours. Expression of CD123 (as a BPDCN-specific marker) and ABCA1 was assessed by confocal microscopy. Nuclei were stained with DAPI. (D) This cartoon, adapted from Oram and Vaughan,[8] represents 1 of the current accepted models of cholesterol efflux, illustrating cholesterol efflux experiments performed thereafter. Cholesterol is excluded from cells through ABCA1 and/or ABCG1 transporters. Lipid-poor APOA1 accepts cholesterol (yellow symbols) from cells through ABCA1-mediated cholesterol efflux. This induces nascent HDL formation which then accepts supplemental cholesterol loading via ABCG1-mediated efflux. Addition of HDL2 implicates only ABCG1-mediated cholesterol efflux. (E) Cholesterol efflux was assessed using [^{3}H]-cholesterol-acetylated LDL-loaded CAL-1 cells treated with 1 μM T0901317 (T09) or GW3965 (GW) for 24 hours. Cholesterol efflux was triggered by the addition of 20 μg/mL HDL2 (right panel, n = 4) or 10 μg/mL APOA1 (left panel, n = 3). Data were expressed as percentage of cholesterol efflux (mean ± SEM of n experiments), as described in supplemental Methods (*$P < .05$, Mann-Whitney). (F) Cholesterol content of BPDCN cells was assessed after treatment with T0901317 (T09) or GW3965 (1 μM) for 24 hours followed by a 4-hour incubation with APOA1 cholesterol acceptor (10 μg/mL). Cellular cholesterol content was determined using filipin staining analyzed by confocal microscopy. One representative experiment of 3 for CAL-1 cells, 1 of 2 for GEN2.2 cells, is shown. LPDC represents data of a blood sample from 1 BPDCN patient tested of 4 (LPDC #5, #6, #8, #9). The PDC marker CD123 allows the identification of leukemic PDCs in blood samples. Cumulative filipin fluorescence intensity from the 4 different BPDCN samples was expressed as mean ± SEM (bottom right panel, *$P < .05$, Mann-Whitney). Fluorescence intensity of the vehicle condition is considered arbitrary as 1.

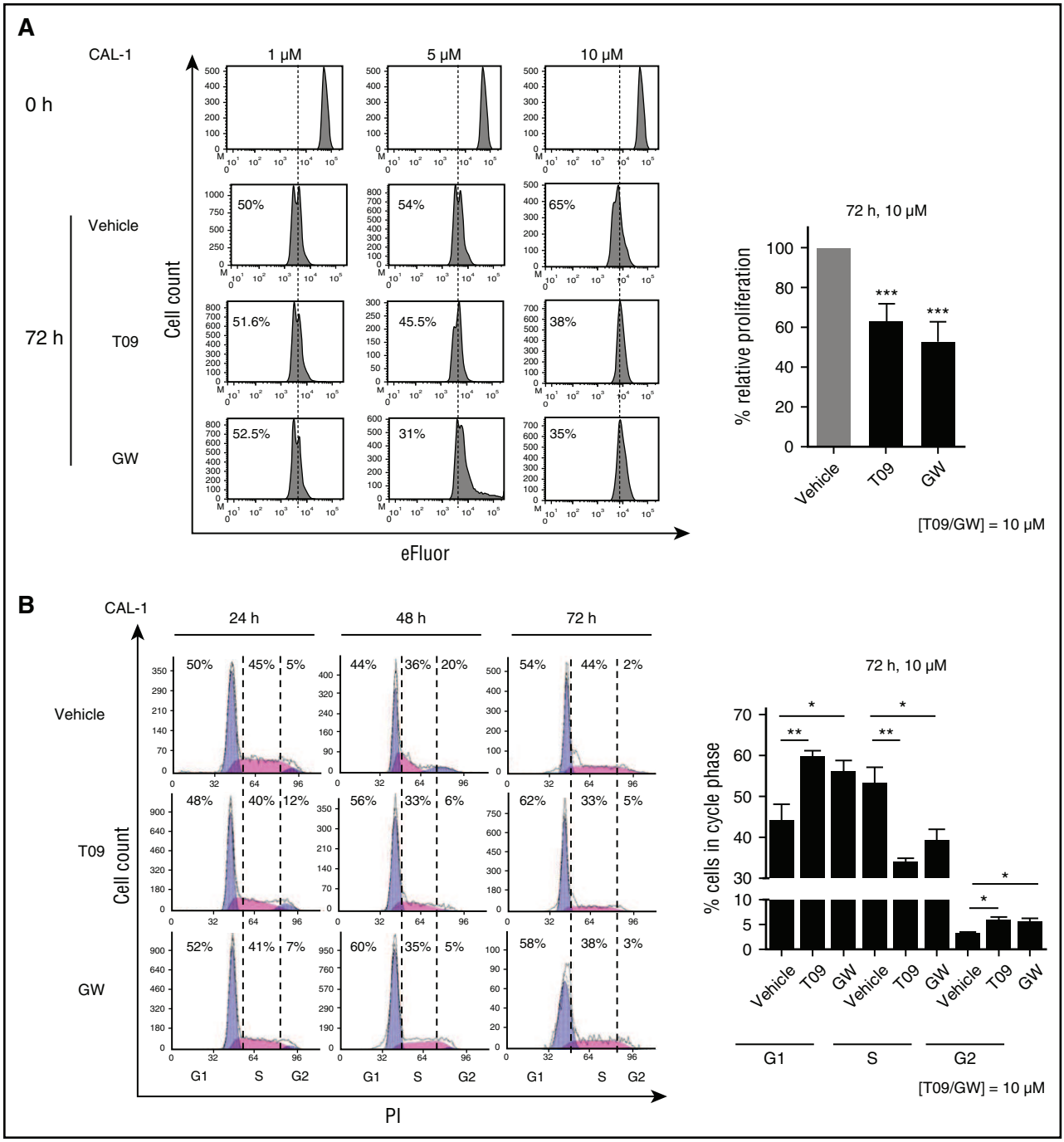

Figure 3. LXR activation inhibits BPDCN cell proliferation. (A) Left panel, eFluor-labeled CAL-1 cells were treated with increasing noncytotoxic concentrations (1 μM, 5 μM, and 10 μM) of LXR agonists, T0901317 (T09) or GW3965 (GW), for 72 hours. Cell proliferation was assessed by eFluor dilution analyzed by flow cytometry. Histograms show 1 representative experiment of 10. Right panel, Cumulative data from the 10 independent experiments are expressed as relative proliferation (mean ± SEM) with the vehicle condition being considered as 100%. Data depicted for LXR agonist treatment illustrate the highest concentration, 10 μM T0901317 (T09) or GW3965 (GW) (***$P < .001$, Wilcoxon). (B) Left panel, CAL-1 cells were treated with 10 μM T09, GW, or vehicle control for 24, 48, or 72 hours. Cell cycle phase distribution was assessed by cytometry (n = 5). Right panel, Cumulative data from 5 independent experiments are expressed as percentage of cells in each cell cycle phase (mean ± SEM) for the highest concentration of LXR agonists, 10 μM (*$P < .05$, **$P < .01$,***$P < .001$, Wilcoxon). PI, propidium iodide.

microscopy (supplemental Figure 2). Increase of ABCA1 expression after LXR activation was analyzed in 1 primary BPDCN sample by confocal microscopy (Figure 2C). Because LXR activation induces cholesterol efflux through ABCA1 and ABCG1 in cooperation with cholesterol acceptors, such as APOA1 and HDL2,[8,21] we then investigated cholesterol efflux using CAL-1 cells preloaded with ^{3}H-cholesterol (1 μCi/mL, 24 hours), and treated with either T0901317 or GW3965 (1 μM, 24 hours) before the addition of APOA1 (10 μg/mL) or HDL2 (20 mg of protein per mL) cholesterol acceptors for 4 hours (Figure 2D). Radioactivity measurement in media and cells demonstrated that LXR agonist treatment significantly increased cholesterol efflux in both conditions (Figure 2E). Intracellular cholesterol staining revealed that LXR agonist treatment followed by APOA1 addition induced a significant diminution of total cholesterol content in CAL-1,

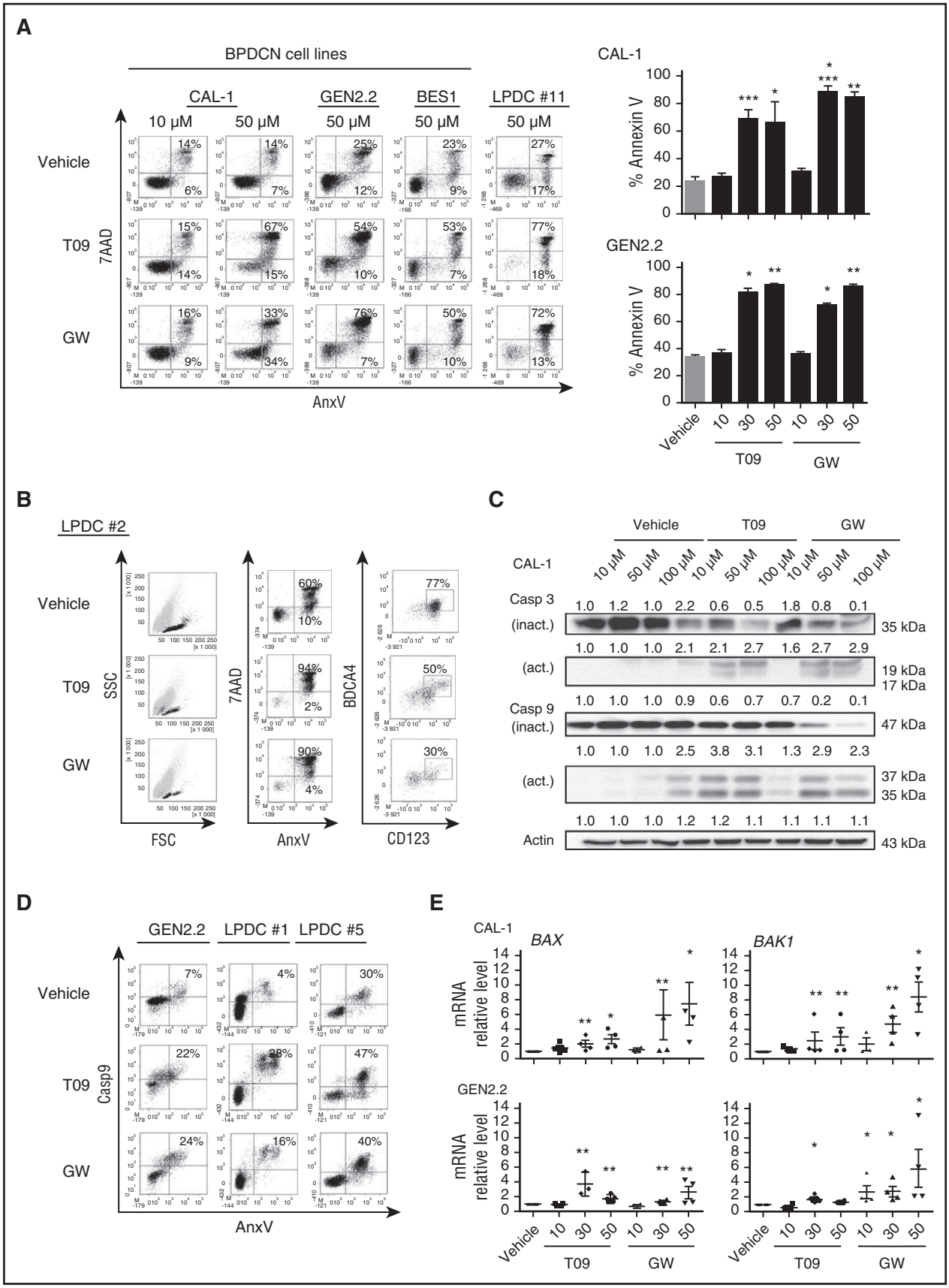

Figure 4. LXR activation in BPDCN cells induces apoptotic cell death. CAL-1, GEN2.2, BES1, and blood samples from 5 patients diagnosed with BPDCN (LPDC #1, #2, #5, #10, #11) were treated with increasing concentrations (10-50 µM) of LXR agonists T0901317 (T09) or GW3965 (GW) for 24 hours. Cell viability was assessed by AnxV and 7AAD staining and cytometry. (A) Left panel, Dot plots illustrate data obtained with cells treated with 50 µM LXR agonists, except for CAL-1 cells that were treated with

GEN2.2 cells, and in 4 primary BPDCN samples (*$P < .05$), as assessed by confocal microscopy (Figure 2F). Overall, these data demonstrated that LXR agonist treatment of BPDCN stimulates cholesterol efflux via ABCA1 and ABCG1 transporters.

LXR activation inhibits BPDCN cell proliferation and induces apoptotic cell death

Because LXR activation regulates cell proliferation and survival,[13,20] we investigated the effects of LXR stimulation on BPDCN cells. CAL-1 cells were treated with increasing concentrations (1 μM, 5 μM, 10 μM) of LXR agonists for 24, 48, or 72 hours. Proliferation analysis of viable cells ($AnxV^-/7AAD^-$) demonstrated a significant decrease of cell proliferation induced by LXR agonist treatment (10 μM, 72 hours, $P < .001$), as assessed by cytometry (Figure 3A). Cell cycle phase analysis demonstrated a significant G1 phase retention associated with a diminution of cells in the S phase in a time-dependent (24 or 72 hours) manner (Figure 3B).

Exposure of CAL-1 and GEN2.2 cells to increasing concentrations of LXR agonists (10 μM, 30 μM, or 50 μM) demonstrated a significant cell death induction for concentrations higher than 10 μM, as assessed by AnxV/7AAD staining and cytometry. The cytotoxic effect of LXR agonists was confirmed in BES1 cells and 5 primary BPDCN samples of 5 tested ($P < .05$; Figure 4A-B). Assessment of viable BPDCN cells ($AnxV^-/7AAD^-/CD123^+/CD304^+$) in 1 blood sample from a BPDCN patient revealed after treatment with LXR agonists, a preferential decrease of viable BPDCN cells (77% vs 50% and 30%, for vehicle- vs T0901317- and GW3965-treated samples, respectively) (Figure 4B). This suggests a specific cytotoxic effect of LXR agonists on BPDCN cells. Western blot analysis of CAL-1 cells treated with LXR agonists for 6 hours showed a caspase-3 and caspase-9 cleavage, suggesting apoptosis induction (Figure 4C). This was confirmed in CAL-1 and GEN2.2 cells by nucleus fragmentation induced by LXR agonists and at morphological levels, as assessed by confocal microscopy (supplemental Figure 3A-B). Caspase-9 activation was confirmed after LXR agonist treatment in GEN2.2 cells and 2 primary BPDCN cells, as assessed by cytometry (Figure 4D). BAX- and BAK1-coding gene upregulation in CAL-1 and GEN2.2 cells after LXR activation was detected (Figure 4E). This suggests the involvement of the intrinsic apoptosis. Overall, this indicated that LXR agonist treatment stimulates apoptotic cell death in BPDCN.

LXR activation interferes with 2 BPDCN survival pathways: the IL-3–induced signaling pathway and NF-κB activation

Because LXR activation inhibits BPDCN survival, we wondered whether LXR stimulation would interfere with the following survival signaling pathways, IL-3 and NF-κB. IL-3 was described to induce STAT5 and Akt activation, both involved in leukemic cell survival.[33-36] NF-κB activation was reported to maintain BPDCN cell survival.[32] To investigate the effects of LXR activation on IL-3–induced STAT5 and Akt activation, CAL-1 cells were treated with increasing noncytotoxic concentrations of LXR agonists (1-10 μM, 24 hours), followed by IL-3 stimulation (10 ng/mL, 30 minutes). Western blot analysis demonstrated a sustained diminution of STAT5 and Akt phosphorylation induced by LXR agonist treatment (Figure 5A). These effects were confirmed by confocal microscopy in 3 primary BPDCN samples (Figure 5B), as well as in CAL-1 and GEN2.2 cells (supplemental Figure 4A).

To demonstrate the involvement of constitutive NF-κB activation in BPDCN cell survival, CAL-1 and GEN2.2 cells were treated with increasing concentrations (12.5-100 μM, 24 hours) of the NF-κB p65 inhibitor, JSH23. A significant increase of BPDCN cell death was revealed by AnxV/7AAD staining (**$P < .01$, Figure 5C). LXR agonists decreased NF-κB p65 phosphorylation in 4 primary BPDCN samples (Figure 5D) and in CAL-1, GEN2.2 cells (supplemental Figure 4B), as assessed by confocal microscopy. Western blot analysis of CAL-1 cells pretreated with LXR agonists (1 μM, 24 hours) demonstrated an inhibition of p50, p65, and c-Rel NF-κB subunit nuclear translocation, induced by a NF-κB activator (R848, 1 μg/mL, 6 hours) (Figure 5E). Overall, these data demonstrated that LXR stimulation in BPDCN cells inhibits IL-3–induced STAT5 and Akt activation, as well as NF-κB activation at phosphorylation and nuclear translocation levels. This may contribute to the cytotoxic effects of LXR agonist treatment on BPDCN.

Stimulation of cholesterol efflux amplifies LXR activation-induced effects

Cholesterol efflux through ABCA1/ABCG1 inhibits IL-3–induced hematopoietic stem cell (HSC) proliferation,[13,14] and LXR activation in BPDCN interferes with the IL-3 signaling pathway. To investigate the contribution of LXR-stimulated cholesterol efflux in these effects, CAL-1 and GEN2.2 cells or a primary BPDCN sample were treated with LXR agonists (1 μM, 24 hours), then with APOA1 (10 μg/mL, 4 hours) followed by IL-3 (10 ng/mL, 30 minutes). Addition of APOA1 markedly diminished IL-3–induced STAT5 and Akt phosphorylation in all LXR-treated BPDCN cells (Figure 6A-B). Treatment of CAL-1 cells with increasing noncytotoxic concentrations of LXR agonists (5-10 μM) in the presence of APOA1 (0-20 μg/mL) showed a significant increase of dead BPDCN cells (Figure 6C). Overall, these data demonstrated that cholesterol efflux increases LXR agonist-mediated effects. To go further on cholesterol dependency of BPDCN, cholesterol was deprived from BPDCN cells by using either an inhibitor of the mevalonate pathway, atorvastatin, or a compound inducing cholesterol removal from cells, methyl-β-cyclodextrin.[37] Cell death analysis 24 hours later by AnxV/7AAD staining and cytometry demonstrated a significant BPDCN cell death (supplemental Figure 5).

Figure 4 (continued) 10 μM and 50 μM. Results from 1 representative experiment of 6 for CAL-1, 1 of 4 for GEN2.2 cells, and 1 representative sample (LPDC#11) of 5 for primary BPDCN samples tested. Right panel, The percentage of $AnxV^+$ dead cells (mean ± SEM from 6 or 4 independent experiments for CAL-1 and GEN2.2, respectively), after LXR agonist treatment (*$P < .05$, **$P < .01$, ***$P < .001$, ****$P < .0001$, Mann-Whitney). (B) One freshly isolated blood sample obtained from a patient diagnosed with BPDCN was treated with 50 μM T0901317 (T09) or GW3965 (GW) for 24 hours. Cytometry dot plots from 1 representative sample of 5 different BPDCN represent the percentage of BPDCN cells (identified by CD123/BDCA4 staining) in the viable cell fraction of blood sample (ie, the $AnxV^-/7AAD^-$ fraction) (*$P < .05$, Mann-Whitney). (C) CAL-1 cells were treated with increasing concentrations of LXR agonists, T0901317 (T09) or GW3965 (GW), for 6 hours. Analysis of full-length inactive (inact.) and cleaved active (act.) forms of caspase-3 and caspase-9 was performed by western blot. Expression of these proteins was compared with actin expression with the vehicle condition being considered as 1. Results from 1 representative experiment of 3. (D) BPDCN cells (GEN2.2 and 2 primary BPDCN samples, LPDC #1 and #5) were treated with 50 μM T0901317 (T09) or GW3965 (GW) for 6 hours. Caspase-9 activation on $7AAD^-$ cell fraction (excluding late apoptotic and necrotic cells) was assessed by cytometry. One dot plot represents 1 representative experiment of 2 for GEN2.2 cells, and the other 2 dot plots represent the experiments performed on 2 BPDCN samples (LPDC #1 and #5). (E) CAL-1 and GEN2.2 cells were treated with increasing concentrations of LXR agonists (10 μM, 30 μM, and 50 μM) for 6 hours. *BCL2*, *BAX*, and *BAK1* gene expression was assessed by qRT-PCR. Levels of mRNA were normalized to those of *GAPDH* for each sample and then expressed as fold change related to the average value for vehicle-treated cells. Cumulative data from 4 independent experiments expressed as mean ± SEM (*$P < .05$, **$P < .01$, Mann-Whitney) are shown. FSC, forward scatter; SSC, side scatter.

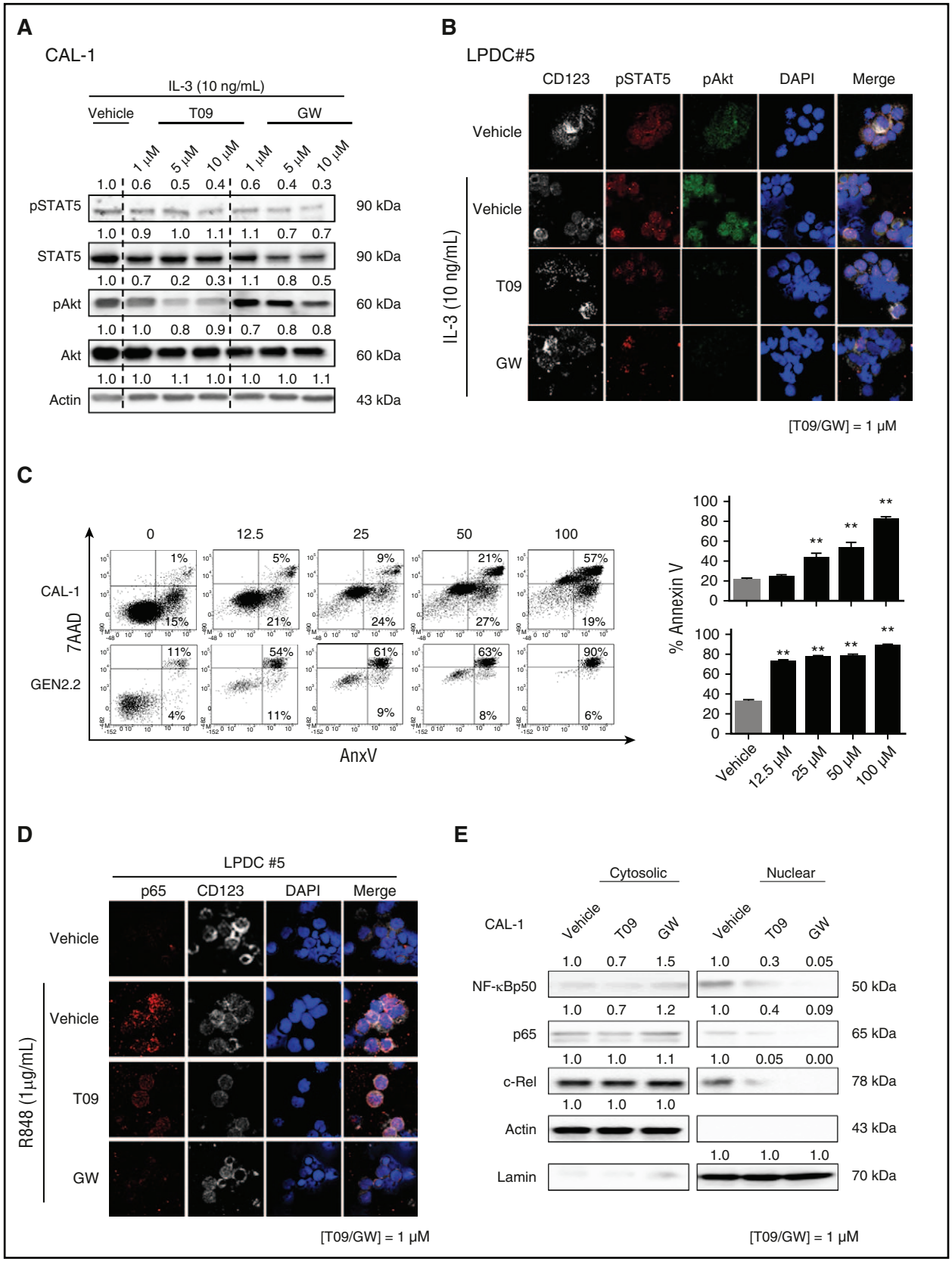

Figure 5. LXR activation in BPDCN cells interferes with IL-3–induced STAT5 and Akt phosphorylation, as well as NF-κB activation. (A) CAL-1 cells were treated with increasing concentrations (1 μM, 5 μM, or 10 μM) of LXR agonists (T09 or GW) for 24 hours, followed by 10 ng/mL of IL-3 for 30 minutes. Phospho-STAT5 (Y694), phospho-Akt (S473), as well as unphosphorylated corresponding protein expression was assessed by western blot. The expression of these proteins was compared with actin with the vehicle condition being considered as 1. Results of 1 representative experiment of 2. (B) BPDCN cells (LPDC #5) were treated with 1 μM LXR agonists for 24 hours. Phospho-STAT5 (Y694) and phospho-Akt (S473) were assessed by confocal microscopy after IL-3 stimulation (10 ng/mL, 30 minutes). Results of 1 representative sample (LPDC #5) of

In vivo LXR agonist treatment prevents cytopenia and BPDCN cell infiltration

To assess LXR therapeutic effects in vivo, sublethally irradiated (2 Gy) NSG mice were grafted with 1 million CAL-1 cells. After 7 days, mice were treated with 2 doses of LXR agonist (T0901317 30 mg/kg or 60 mg/kg) or vehicle, every 2 days until sacrifice. Although CAL-1 cell injection induced a significant persistent decrease of red blood cell (RBC), platelet counts, as well as hemoglobin (Hb) concentration, T0901317-treated mice showed a significant prevention of cytopenia, including RBC counts and Hb concentration (Figure 7A). At sacrifice, a diminution of CAL-1 cell-induced splenomegaly was observed (Figure 7B), supported by a potent decrease of spleen and bone marrow BPDCN cell infiltration, as assessed by flow cytometry (Figure 7C). In an additional experiment, treatment with T0901317 (30 mg/kg or 60 mg/kg) significantly increased the overall survival of NSG mice inoculated with CAL-1 cells compared with CAL-1-inoculated and vehicle-treated mice (Figure 7D-E). Overall, these data provide the in vitro and in vivo demonstration of a therapeutic effect of LXR agonist on BPDCN through different mechanisms, including signaling pathway regulation and cholesterol efflux.

Discussion

Cholesterol is a critical component for cell growth and proliferation, as illustrated by the inhibition of HSC proliferation occurring after cholesterol efflux through ABC transporters.[13,14] In physiological conditions, cholesterol homeostasis is tightly controlled by the LXR signaling pathway. Here, we identified that the aggressive hematological malignancy BPDCN exhibits a specific transcriptomic signature with a downregulation of several LXR target genes involved in cholesterol homeostasis. This may lead to cholesterol accumulation within leukemic cells, responsible for high proliferative properties. We reported that LXR agonist treatment increases LXR target gene expression in BPDCN, stimulates cholesterol efflux from these cells, and is associated with the inhibition of proliferation and survival. These 2 effects may result from the interference of LXR activation with 2 BPDCN survival/proliferative pathways, namely IL-3 and NF-κB signaling pathways. The effects of LXR agonists are amplified by the addition of the lipid acceptor APOA1 known to enhance cholesterol efflux. All of these effects (except cell proliferation) were assessed in vitro in 2 BPDCN cell lines, expanded primary BPDCN cells, and several primary BPDCN samples isolated from 11 different patients. An in vivo therapeutic effect of LXR agonist is also observed in a xenograft model with reduction of BPDCN cell infiltration, prevention of BPDCN-induced cytopenia, and increased mouse survival. These data highlight an unrevealed perturbation of cholesterol homeostasis and LXR activity in BPDCN, and identify a new approach based on LXR agonists to treat this aggressive hematological malignancy.

Treatment of BPDCN with LXR agonists has several effects depending on their concentration. Restoration of LXR target gene expression (inducing cholesterol efflux) and inhibition of IL-3 and NF-κB signaling pathways occurred for concentrations between 1 and 10 μM (ranges usually used in malignant cells[10,38-42]). BPDCN cell proliferation (assessed with the proliferative BPDCN cell line, CAL-1) was significantly inhibited for 10 μM, as reported in several hematological malignancies and solid tumors.[39,42,43] Concentrations higher than 10 μM induced a significant BPDCN cell death, as reported for ovarian, breast, and colon cancer cells.[43-45] All of these data validate the concentrations of LXR agonists used in this study.

LXR activation in BPDCN triggers an apoptotic cell death mechanism based on different features, namely: exposure of phosphatidylserine (assessed by AnxV staining), cleavage of caspase-3 and caspase-9, as well as nucleus fragmentation. Induction of intrinsic apoptosis by LXR agonists was previously described in ovarian carcinoma cells,[45] and confirmed here associated with a significant increase of *BAX* and *BAK1* transcripts (encoding proapoptotic proteins). LXR-induced cell death in breast cancer cells has been demonstrated to implicate BAX upregulation and to be dependent on cholesterol efflux through ABCG1.[43] In our study, a stimulation of ABCA1/ABCG1-dependent cholesterol efflux via the addition of APOA1 increases LXR-mediated cytotoxic effects. APOA1-stimulated cholesterol efflux also potentiates the LXR-induced inhibition of Akt and STAT5 phosphorylation. This is in line with a previous report in prostate cancer cells showing Akt inhibition by increased cholesterol efflux.[10] Although exogenous APOA1 supplementation is required for in vitro assays with BPDCN cells, circulating lipid-free APOA1 (mainly produced by liver and intestine),[8] or APOA1 present in nascent HDL is likely to potentiate the impact of LXR agonist treatment in vivo. Overall, LXR stimulation in BPDCN exerts an antileukemic effect that can be enhanced by increasing cholesterol efflux.

Therapeutic strategies of BPDCN propose to interfere with IL-3[2,16,34,46] because BPDCNs express high levels of CD123,[2,26] and IL-3 is a BPDCN survival factor.[1,15] Here, we explored how LXR activation and LXR-induced cholesterol efflux interact with this pathway. No modification of CD131 and CD123 expression on BPDCN cells after LXR activation is observed (data not shown), whereas LXR agonists inhibit IL-3–induced Akt and STAT5 phosphorylation in BPDCN. Western blot analysis demonstrated that LXR agonists had no effect on STAT5 and Akt protein expression, suggesting a predominant effect at the phosphorylation levels.

BPDCN samples exhibit a specific downregulation of LXR target genes *ABCG1*, *ABCA1*, and *SREBF1*, in favor of repression of LXR transcriptomic activity. However, although LXR target gene transcription is decreased in BPDCN, the transcripts of the 2 LXR coding genes (*LXRA* and *LXRB*) are not and basal LXRβ protein (supplemental Figure 2B) is present. This suggests posttranscriptional regulation of LXR activity in BPDCN. LXR activity in normal PDC is inhibited by prior NF-κB activation.[25] Because NF-κB is constitutively activated in BPDCN,[32] and NF-κB p105 precursor-coding gene (*NFKB1*) is upregulated, LXR repression in BPDCN may be related to NF-κB activation. Restoration of the LXR pathway by agonist treatment in BPDCN inhibits the constitutive NF-κB activation at 3 different levels:

Figure 5 (continued) 3 BPDCN samples tested (LPDC #5, #6, #9). (C) CAL-1 and GEN2.2 cells were treated with increasing concentrations (12.5 μM, 25 μM, 50 μM, and 100 μM) of NF-κB inhibitor JSH23. Cell death was assessed by AnxV/7AAD staining, and analyzed by cytometry. Dot plots from 1 representative experiment of 5 and cumulative data from these 5 experiments expressed as percentage of dead $AnxV^+$ cells are shown (left panel). Cumulative data from 3 experiments expressed as mean ± SEM are shown (right panel) (**$P < .01$, Mann-Whitney). (D) Primary BPDCN cells were treated with 1 μM of LXR agonists for 24 hours, followed by 1 μg/mL of R848 for 45 minutes. P65 phosphorylation (pS536) was assessed by confocal microscopy. Data from 1 representative primary BPDCN sample of 4 (LPDC #5, #6, #8, #9) are shown. (E) CAL-1 cells were treated with 1 μM T0901317 (T09) or GW3965 (GW) for 24 hours, followed by R848 (1 μg/mL) stimulation for 6 hours. Cytosolic and nuclear protein fractions were isolated as described in "Methods". NF-κB1 (p105), p50, p65, and c-Rel proteins were analyzed by western blot and the expression of these proteins was compared with actin and lamin B expression (for cytosolic or nuclear expression, respectively) with the vehicle condition being considered as 1. Results from 1 representative experiment of 3.

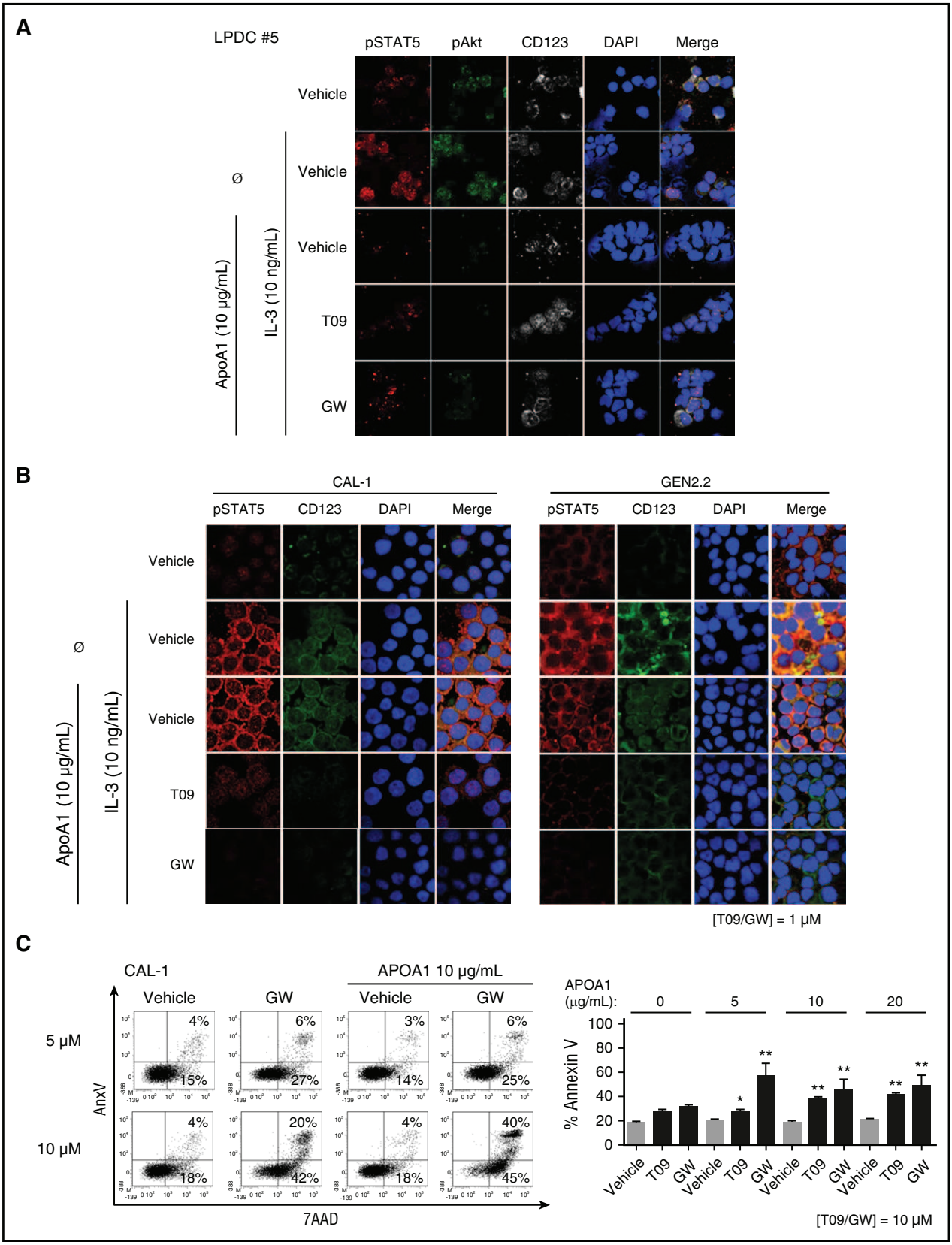

Figure 6. Cholesterol efflux stimulation in BPDCN cells amplifies LXR activation-induced effects. BPDCN CAL-1 and GEN2.2 cells or primary BPDCN samples were treated with 1 μM LXR agonists T0901317 (T09) or GW3965 (GW) for 24 hours. (A-B) Phospho-STAT5 (Y694) and phospho-Akt (S473) were assessed by confocal microscopy after LXR stimulation, followed by APOA1 (10 μg/mL) addition for 4 hours, and then IL-3 stimulation (10 ng/mL for 30 minutes). (A) Data from 1 representative sample of 2 BPDCN samples (LPDC #5, #8) are shown. (B) Data from 1 representative experiment of 3 for CAL-1 and GEN2.2 cells are shown. (C) CAL-1 cells were treated with 10 μM T0901317 or GW3965 simultaneously to increasing concentrations of APOA1 (5, 10, or 20 μg/mL) for 24 hours. Cell death was assessed by AnxV/7AAD staining analyzed by cytometry. Dot plots from 1 representative experiment of 6 are shown (left panel); only data obtained with GW treatment are depicted. Cumulative data from the 6 independent experiments expressed as mean ± SEM of dead $AnxV^+$ cells are shown (right panel, $^*P < .05$, $^{**}P < .01$, Mann-Whitney).

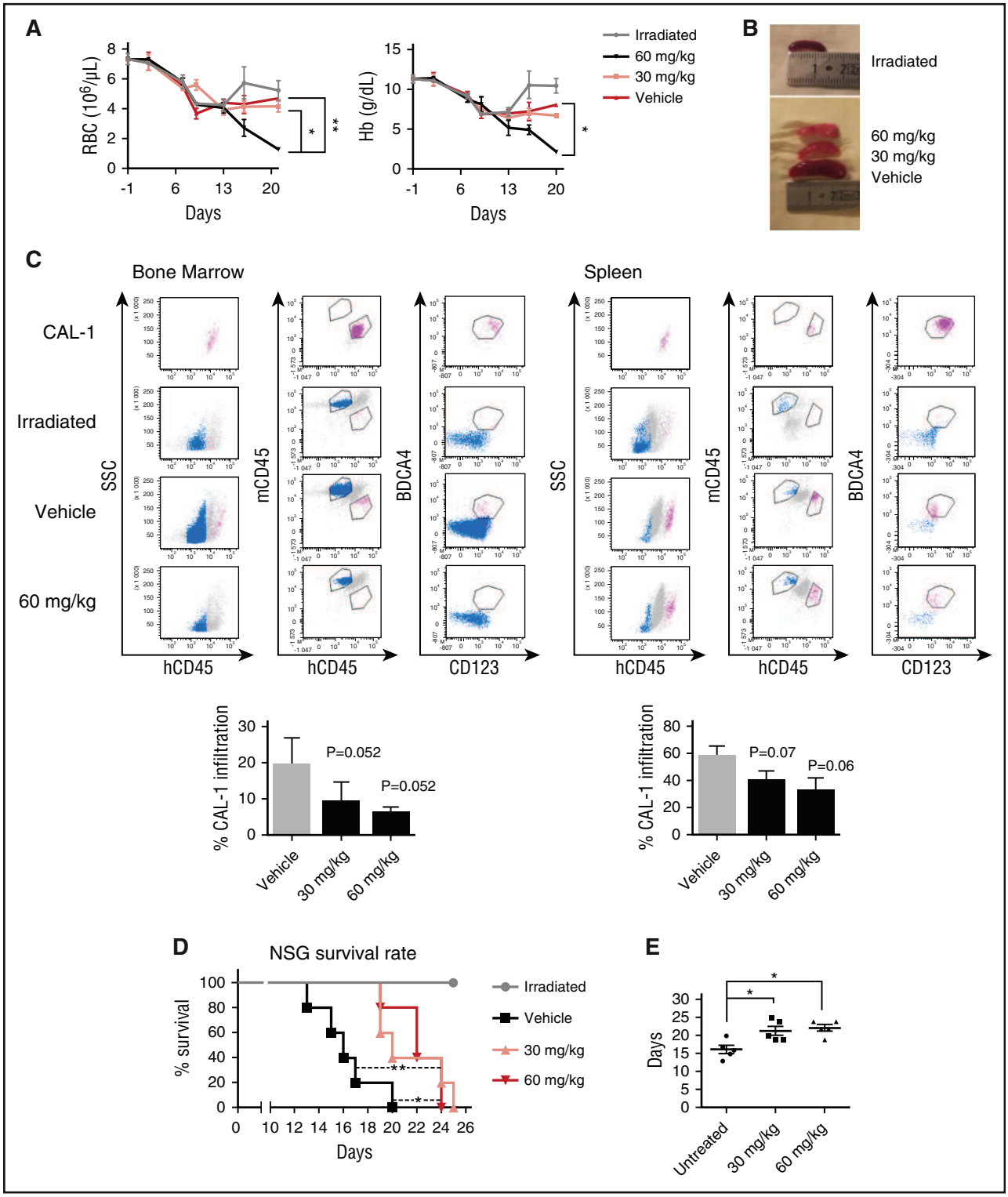

Figure 7. In vivo LXR agonist treatment limits BPDCN-induced cytopenia, spleen and bone marrow infiltration by BPDCN, and also improves overall mouse survival. NSG mice were sublethally irradiated (2 Gy), and then injected IV with 1×10^6 CAL-1 cells. After 7 days, mice were treated with 2 doses of the LXR agonist T0901317 (30 mg/kg or 60 mg/kg) or with vehicle control (PBS/DMSO 50%) every 2 days, until the end of the experiments (4 mice per group, 3 independent experiments). (A) Blood samples were collected every 4 days to assess RBC and Hb concentration. Cumulative data expressed as mean ± SEM are shown (*$P < .05$, **$P < .01$, Mann-Whitney). (B) At the end of the experiments (J20 ± 2), spleens were extracted and measured to evaluate BPDCN spleen involvement. (C) Spleens and bone marrow were collected in order to perform CAL-1 cell quantification. Cells were stained with the following antibodies: human CD45 (hCD45), murine CD45 (mCD45), CD123, and BDCA4 and analyzed by cytometry. Dot plots illustrate the gating strategy with identification of murine cells using mCD45 gating with irradiated mice used as control. Human CAL-1 cells were identified using hCD45, CD123, and BDCA4 staining. Cultured CAL-1 cells were used as control for this staining. Percentage of cell infiltration was calculated as follows: CAL-1 count/(hCD45 + mCD45 counts). Histograms represent cumulative data of 1 experiment of 3 expressed as mean ± SEM of CAL-1 cell infiltration percentage from 5 mice. (D) Overall survival of BPDCN-inoculated mice treated with LXR agonist T0901317 (30 mg/kg, pink triangles; 60 mg/kg, red triangles) or with vehicle (black squares). Irradiated mice (gray circles) were used as control. Statistical comparisons were performed between vehicle and treated groups using the Mantel-Cox test (*$P < .05$, **$P < .001$). (E) Mean overall survival of BPDCN-inoculated mice treated with LXR agonist or vehicle. Bars correspond to the mean of survival time (*$P < .05$, Mann-Whitney). Results from 1 additional experiment with 5 mice per group are shown.

p65 phosphorylation, nuclear translocation of the p50, p65, and cRel subunits, as well as transcription of *NFKB1* (data not shown). Our study confirms constitutive NF-κB activation in BPDCN cells,[32] and demonstrates that inhibition of p65 translocation by JSH-23 is sufficient to induce BPDCN cell death. This suggests that LXR agonist-induced cell death is related to NF-κB inhibition. Interestingly, STAT5 and NF-κB were also reported to promote G1 to S cell cycle phase transition through cyclin D1 induction, and thus cell proliferation.[47,48] In our study, BPDCN cells are retained in G1 phase after LXR activation. This suggests that LXR-induced STAT5 and NF-κB inhibition can be involved in both the inhibition of cell proliferation (through cell cycle arrest) and BPDCN cell death.

LXR agonist treatment of mice grafted with BPDCN cells prevents leukemia-induced cytopenia, reduces BPDCN spleen and bone marrow infiltrations, and slightly but significantly improves mouse survival. To date, the development of LXR agonists in clinical settings has been hampered by unwanted systemic side effects, such as fatty liver disease and LDL elevation.[19] Synthetic LXR agonists have been shown to exert therapeutic effects in mouse models of Alzheimer disease after oral administration.[19] This suggests that these agonists can cross the blood-brain barrier and may target BPDCN cells infiltrating the CNS. The CNS may represent a blast cell sanctuary in BPDCN patients with leukemic presentation both at diagnosis and at relapse.[4] Efforts are currently being made to generate new synthetic agonists with increased specificity for the LXRβ isoform, expressed by BPDCNs, to limit steatosis[19,49] and/or to stimulate LXR specifically in a target tissue.[50,51] Our study supports a new approach for BPDCN treatment using these new synthetic LXR agonists.

Acknowledgments

The authors thank T. Maeda (Nagasaki University, Japan) for kindly providing the BPDCN cell line CAL-1, J. Plumas and L. Chaperot for kindly providing the BPDCN cell line GEN2.2, W. Le Goff (INSERM UMR S1166, University "Pierre et Marie Curie", Paris, France) for helpful discussions on cholesterol metabolism, the Cytology laboratory of the Etablissement Français du Sang Bourgogne Franche-Comté (BFC), for blood cell and platelet counts, Sarah Odrion, and Alexis Varin for editorial assistance.

This work was supported by the Etablissement Français du Sang (grant 2011-11) (P.S.), the Agence Nationale de la Recherche (LabEx LipSTIC, ANR-11-LABX-0021), the Conseil Régional de Franche-Comté (soutien au LabEx LipSTIC 2015 and 2016) (P.S.), and the Fondation de Coopération Scientifique Bourgogne Franche-Comté (A.C., D.M., and P.S. via the Bonus Qualité Recherche BFC).

There are no current or pending patents related to this work. Two material transfer agreements related to the use of CAL-1 cell line and the GEN2.2 cell line are available.

Authorship

Contribution: A.C. performed most of the experiments, collected, assembled, and analyzed data, performed statistical analysis, and wrote the manuscript; D.M. performed cholesterol efflux experiments and helped to write the manuscript; A.R. and C.R. performed transcriptomic experiments and analysis; C.C. performed cell death analysis by flow cytometry, some immunoblotting, and qRT-PCR experiments; T.G. performed some confocal microscopy experiments; L.P. performed cell cycle experiments; B.L., F.A.-D., and F.B. performed and supported in vivo experiments; S.P. commented on the manuscript and helped to write it; S.B., C.P., and E.M. provided leukemia samples and diagnosis; L.L. commented on the manuscript and provided major funding support; F.G.-O. provided study material, collected data, and helped to write the manuscript; and P.S. supervised research, analyzed data, and wrote the manuscript.

Conflict-of-interest disclosure: The authors declare no competing financial interests.

The current affiliation for B.L. is Université Pierre et Marie Curie, UMR 938, INSERM, Paris, France.

ORCID profiles: P.S., 0000-0002-8857-9939.

Correspondence: Philippe Saas, EFS BFC, UMR 1098, INSERM, 8 rue JFX Girod, BP1937, F-25020 Besançon Cedex, France; e-mail: philippe.saas@efs.sante.fr.

References

1. Chaperot L, Bendriss N, Manches O, et al. Identification of a leukemic counterpart of the plasmacytoid dendritic cells. *Blood.* 2001;97(10):3210-3217.
2. Pemmaraju N. Blastic plasmacytoid dendritic cell neoplasm. *Clin Adv Hematol Oncol.* 2016;14(4):220-222.
3. Dalle S, Beylot-Barry M, Bagot M, et al. Blastic plasmacytoid dendritic cell neoplasm: is transplantation the treatment of choice? *Br J Dermatol.* 2010;162(1):74-79.
4. Martín-Martín L, Almeida J, Pomares H, et al. Blastic plasmacytoid dendritic cell neoplasm frequently shows occult central nervous system involvement at diagnosis and benefits from intrathecal therapy. *Oncotarget.* 2016;7(9):10174-10181.
5. Pileri A, Delfino C, Grandi V, Agostinelli C, Pileri SA, Pimpinelli N. Blastic plasmacytoid dendritic cell neoplasm (BPDCN): the cutaneous sanctuary. *G Ital Dermatol Venereol.* 2012;147(6):603-608.
6. Vitols S, Norgren S, Juliusson G, Tatidis L, Luthman H. Multilevel regulation of low-density lipoprotein receptor and 3-hydroxy-3-methylglutaryl coenzyme A reductase gene expression in normal and leukemic cells. *Blood.* 1994;84(8):2689-2698.
7. Tatidis L, Gruber A, Vitols S. Decreased feedback regulation of low density lipoprotein receptor activity by sterols in leukemic cells from patients with acute myelogenous leukemia. *J Lipid Res.* 1997;38(12):2436-2445.
8. Oram JF, Vaughan AM. ATP-binding cassette cholesterol transporters and cardiovascular disease. *Circ Res.* 2006;99(10):1031-1043.
9. Ikonen E. Cellular cholesterol trafficking and compartmentalization. *Nat Rev Mol Cell Biol.* 2008;9(2):125-138.
10. Pommier AJ, Alves G, Viennois E, et al. Liver X receptor activation downregulates AKT survival signaling in lipid rafts and induces apoptosis of prostate cancer cells. *Oncogene.* 2010;29(18):2712-2723.
11. Singh P, Saxena R, Srinivas G, Pande G, Chattopadhyay A. Cholesterol biosynthesis and homeostasis in regulation of the cell cycle. *PLoS One.* 2013;8(3):e58833.
12. Sun Y, Sukumaran P, Varma A, Derry S, Sahmoun AE, Singh BB. Cholesterol-induced activation of TRPM7 regulates cell proliferation, migration, and viability of human prostate cells. *Biochim Biophys Acta.* 2014;1843(9):1839-1850.
13. Yvan-Charvet L, Pagler T, Gautier EL, et al. ATP-binding cassette transporters and HDL suppress hematopoietic stem cell proliferation. *Science.* 2010;328(5986):1689-1693.
14. Murphy AJ, Akhtari M, Tolani S, et al. ApoE regulates hematopoietic stem cell proliferation, monocytosis, and monocyte accumulation in atherosclerotic lesions in mice. *J Clin Invest.* 2011;121(10):4138-4149.
15. Garnache-Ottou F, Chaperot L, Biichle S, et al. Expression of the myeloid-associated marker CD33 is not an exclusive factor for leukemic plasmacytoid dendritic cells. *Blood.* 2005;105(3):1256-1264.
16. Frankel AE, Woo JH, Ahn C, et al. Activity of SL-401, a targeted therapy directed to interleukin-3 receptor, in blastic plasmacytoid dendritic cell neoplasm patients. *Blood.* 2014;124(3):385-392.
17. Pemmaraju N, Lane AA, Sweet KL, et al. Results from phase 2 registration trial of SL-401 in patients with blastic plasmacytoid dendritic cell neoplasm (BPDCN): lead-in completed,

expansion satge ongoing [abstract]. *J Clin Oncol.* 2016;34(15 suppl). Abstract 7006.

18. Im SS, Osborne TF. Liver x receptors in atherosclerosis and inflammation. *Circ Res.* 2011;108(8):996-1001.
19. Hong C, Tontonoz P. Liver X receptors in lipid metabolism: opportunities for drug discovery. *Nat Rev Drug Discov.* 2014;13(6):433-444.
20. Lin CY, Gustafsson JA. Targeting liver X receptors in cancer therapeutics. *Nat Rev Cancer.* 2015;15(4):216-224.
21. Wójcicka G, Jamroz-Wiśniewska A, Horoszewicz K, Bełtowski J. Liver X receptors (LXRs). Part I: structure, function, regulation of activity, and role in lipid metabolism. *Postepy Hig Med Dosw (Online).* 2007;61:736-759.
22. Dove DE, Linton MF, Fazio S. ApoE-mediated cholesterol efflux from macrophages: separation of autocrine and paracrine effects. *Am J Physiol Cell Physiol.* 2005;288(3):C586-C592.
23. Hong C, Duit S, Jalonen P, et al. The E3 ubiquitin ligase IDOL induces the degradation of the low density lipoprotein receptor family members VLDLR and ApoER2. *J Biol Chem.* 2010;285(26): 19720-19726.
24. Zhang L, Reue K, Fong LG, Young SG, Tontonoz P. Feedback regulation of cholesterol uptake by the LXR-IDOL-LDLR axis. *Arterioscler Thromb Vasc Biol.* 2012;32(11):2541-2546.
25. Ceroi A, Delettre FA, Marotel C, et al. The anti-inflammatory effects of platelet-derived microparticles in human plasmacytoid dendritic cells involve liver X receptor activation. *Haematologica.* 2016;101(3):e72-e76.
26. Garnache-Ottou F, Feuillard J, Ferrand C, et al; GOELAMS and GEIL study. Extended diagnostic criteria for plasmacytoid dendritic cell leukaemia. *Br J Haematol.* 2009;145(5):624-636.
27. Angelot-Delettre F, Biichle S, Ferrand C, et al. Intracytoplasmic detection of TCL1–but not ILT7-by flow cytometry is useful for blastic plasmacytoid dendritic cell leukemia diagnosis. *Cytometry A.* 2012;81(8):718-724.
28. Riaz W, Zhang L, Horna P, Sokol L. Blastic plasmacytoid dendritic cell neoplasm: update on molecular biology, diagnosis, and therapy. *Cancer Contr.* 2014;21(4):279-289.
29. Maeda T, Murata K, Fukushima T, et al. A novel plasmacytoid dendritic cell line, CAL-1, established from a patient with blastic natural killer cell lymphoma. *Int J Hematol.* 2005;81(2): 148-154.
30. Chaperot L, Blum A, Manches O, et al. Virus or TLR agonists induce TRAIL-mediated cytotoxic activity of plasmacytoid dendritic cells. *J Immunol.* 2006;176(1):248-255.
31. Ishibashi M, Filomenko R, Rébé C, et al. Knock-down of the oxysterol receptor LXRα impairs cholesterol efflux in human primary macrophages: lack of compensation by LXRβ activation. *Biochem Pharmacol.* 2013;86(1):122-129.
32. Sapienza MR, Fuligni F, Agostinelli C, et al; AIRC 5xMille consortium 'Genetics-driven targeted management of lymphoid malignancies and the Italian Registry on Blastic Plasmacytoid Dendritic Cell Neoplasm. Molecular profiling of blastic plasmacytoid dendritic cell neoplasm reveals a unique pattern and suggests selective sensitivity to NF-kB pathway inhibition. *Leukemia.* 2014; 28(8):1606-1616.
33. Reddy EP, Korapati A, Chaturvedi P, Rane S. IL-3 signaling and the role of Src kinases, JAKs and STATs: a covert liaison unveiled. *Oncogene.* 2000;19(21):2532-2547.
34. Testa U, Pelosi E, Frankel A. CD 123 is a membrane biomarker and a therapeutic target in hematologic malignancies. *Biomark Res.* 2014; 2(1):4.
35. Zhuang J, Hawkins SF, Glenn MA, et al. Akt is activated in chronic lymphocytic leukemia cells and delivers a pro-survival signal: the therapeutic potential of Akt inhibition. *Haematologica.* 2010; 95(1):110-118.
36. Schafranek L, Nievergall E, Powell JA, et al. Sustained inhibition of STAT5, but not JAK2, is essential for TKI-induced cell death in chronic myeloid leukemia. *Leukemia.* 2015;29(1):76-85.
37. Zidovetzki R, Levitan I. Use of cyclodextrins to manipulate plasma membrane cholesterol content: evidence, misconceptions and control strategies. *Biochim Biophys Acta.* 2007;1768(6): 1311-1324.
38. Vedin LL, Lewandowski SA, Parini P, Gustafsson JA, Steffensen KR. The oxysterol receptor LXR inhibits proliferation of human breast cancer cells. *Carcinogenesis.* 2009;30(4):575-579.
39. Vedin LL, Gustafsson JA, Steffensen KR. The oxysterol receptors LXRα and LXRβ suppress proliferation in the colon. *Mol Carcinog.* 2013; 52(11):835-844.
40. Geyeregger R, Shehata M, Zeyda M, et al. Liver X receptors interfere with cytokine-induced proliferation and cell survival in normal and leukemic lymphocytes. *J Leukoc Biol.* 2009;86(5): 1039-1048.
41. Sanchez PV, Glantz ST, Scotland S, Kasner MT, Carroll M. Induced differentiation of acute myeloid leukemia cells by activation of retinoid X and liver X receptors. *Leukemia.* 2014;28(4):749-760.
42. Agarwal JR, Wang Q, Tanno T, et al. Activation of liver X receptors inhibits hedgehog signaling, clonogenic growth, and self-renewal in multiple myeloma. *Mol Cancer Ther.* 2014;13(7): 1873-1881.
43. El Roz A, Bard JM, Huvelin JM, Nazih H. LXR agonists and ABCG1-dependent cholesterol efflux in MCF-7 breast cancer cells: relation to proliferation and apoptosis. *Anticancer Res.* 2012; 32(7):3007-3013.
44. Derangère V, Chevriaux A, Courtaut F, et al. Liver X receptor β activation induces pyroptosis of human and murine colon cancer cells. *Cell Death Differ.* 2014;21(12):1914-1924.
45. Rough JJ, Monroy MA, Yerrum S, Daly JM. Anti-proliferative effect of LXR agonist T0901317 in ovarian carcinoma cells. *J Ovarian Res.* 2010;3:13.
46. Angelot-Delettre F, Roggy A, Frankel AE, et al. In vivo and in vitro sensitivity of blastic plasmacytoid dendritic cell neoplasm to SL-401, an interleukin-3 receptor targeted biologic agent. *Haematologica.* 2015;100(2):223-230.
47. Dagvadorj A, Kirken RA, Leiby B, Karras J, Nevalainen MT. Transcription factor signal transducer and activator of transcription 5 promotes growth of human prostate cancer cells in vivo. *Clin Cancer Res.* 2008;14(5):1317-1324.
48. Hinz M, Krappmann D, Eichten A, Heder A, Scheidereit C, Strauss M. NF-kappaB function in growth control: regulation of cyclin D1 expression and G0/G1-to-S-phase transition. *Mol Cell Biol.* 1999;19(4):2690-2698.
49. Kirchgessner TG, Martin R, Sleph P, et al. Pharmacological characterization of a novel liver X receptor agonist with partial LXRα activity and a favorable window in nonhuman primates. *J Pharmacol Exp Ther.* 2015;352(2):305-314.
50. Hu B, Unwalla RJ, Goljer I, et al. Identification of phenylsulfone-substituted quinoxaline (WYE-672) as a tissue selective liver X-receptor (LXR) agonist. *J Med Chem.* 2010;53(8):3296-3304.
51. Lim RK, Yu S, Cheng B, et al. Targeted delivery of LXR agonist using a site-specific antibody-drug conjugate. *Bioconjug Chem.* 2015;26(11): 2216-2222.

2016 128: 2694-2707
doi:10.1182/blood-2016-06-724807 originally published online October 4, 2016

LXR agonist treatment of blastic plasmacytoid dendritic cell neoplasm restores cholesterol efflux and triggers apoptosis

Adam Ceroi, David Masson, Anne Roggy, Christophe Roumier, Cécile Chagué, Thierry Gauthier, Laure Philippe, Baptiste Lamarthée, Fanny Angelot-Delettre, Francis Bonnefoy, Sylvain Perruche, Sabeha Biichle, Claude Preudhomme, Elisabeth Macintyre, Laurent Lagrost, Francine Garnache-Ottou and Philippe Saas

Blood (print ISSN 0006-4971, online ISSN 1528-0020), is published weekly by the American Society of Hematology, 2021 L St, NW, Suite 900, Washington DC 20036.